

ÉCOLE DOCTORALE DES SCIENCES CHIMIQUES
[Institut de Science et d'Ingénierie Supramoléculaires]

THÈSE présentée par :

[Meixia HE]

soutenue le : 25 Septembre 2020

pour obtenir le grade de : **Docteur de l'université de Strasbourg**
Discipline/ Spécialité : CHIMIE

**DYNAMIC COVALENT PROCESS OF C=N BONDS:
KINETICS AND THERMODYNAMICS, CATALYSIS
AND OUT-OF-EQUILIBRIUM STATES**

THÈSE dirigée par :
M. LEHN Jean-Marie

Professeur Émérite, Université de Strasbourg, France

RAPPORTEURS :

M. ULRICH Sébastien

Professeur, Université de Montpellier, France

Mme. VANTOMME Ghislaine

Professeur, Eindhoven University of Technology, Netherlands

AUTRES MEMBRES DU JURY :

M. CHAMBRON Jean-Claude

Professeur, Université de Strasbourg, France

TABLE OF CONTENT

TABLE OF CONTENT	I
ACKNOWLEDGEMENTS	VII
ABSTRACT.....	IX
ABBREVIATIONS AND SYMBOLS	XII
RESUME EN FRANCAIS.....	XIV
CHAPTER I. GENERAL BIBLIOGRAPY.....	1
1. FROM SUPRAMOLECULAR CHEMISTRY TO CONSTITUTIONAL DYNAMIC CHEMISTRY.....	1
2. ADAPTATION IN CONSTITUTIONAL DYNAMIC CHEMISTRY.....	8
<i>A. Adaptation to light.....</i>	<i>10</i>
<i>B. Adaptation to a change of environment.....</i>	<i>11</i>
<i>C. Adaptation to metal ions.....</i>	<i>11</i>
<i>D. Adaptation to morphological change.....</i>	<i>13</i>
3. DYNAMIC COVALENT REACTIONS USING C=N COMPOUNDS.....	14
<i>A. C=N bond formation.....</i>	<i>16</i>
i. Acid catalysis.....	17
ii. Metal ion catalysis.....	18
iii. Organic amine catalysis.....	18
<i>B. Transimination reaction.....</i>	<i>20</i>
i. Acid catalysis.....	21
ii. Metal ion catalysis.....	21
<i>C. Imine metathesis.....</i>	<i>23</i>
i. Acid catalysis.....	23
ii. Metal ion catalysis.....	25
iii. Organic amine catalysis.....	25
CHAPTER II. CATALYSIS OF IMINE AND HYDRAZONE FORMATION.....	27
1. INTRODUCTION.....	27
2. RESULTS AND DISCUSSIONS	28
<i>A. Imine formation driven by metal salts.....</i>	<i>30</i>
<i>B. Hydrazone formation driven by metal salts.....</i>	<i>42</i>
<i>C. Synergistic effects of metal salts and an auxiliary amine.....</i>	<i>53</i>
i. Synergistic effect for the formation of complex of A1B2	53
ii. Synergistic effect for the formation of complexes of A2B2	63
iii. Synergistic effect for the formation of complex of A3B2	66

iv. Synergistic effect of the three co-factors AgOTf, Zn(OTf) ₂ and B1	69
D. Catalysis of imine and hydrazone formation driven by metal salts and acid.....	71
3. SUMMARY OF CHAPTER II	74
CHAPTER III. CONTROL OF TIME-DEPENDENT SWITCHING OF DCLS.....	76
1. INTRODUCTION.....	76
2. RESULTS AND DISCUSSIONS	80
A. Kinetic switching of a CDL in the absence of metal ions.....	81
i. DCL[1] generated from the four components A3, A4, B4, B5	81
1) The C=N formation from two components	82
2) Component selection in competitive experiment.....	85
3) The kinetic switching of DCL[1]	88
ii. DCL[2] generated from the four components A1, A6, B3, B4	90
1) Component selection in competitive experiment.....	90
2) The kinetic switching of DCL[2]	92
iii. DCL[3] generated from the four components A1, A6, B3, B5	94
1) Component selection in competitive experiment.....	95
2) The kinetic switching of DCL[3]	96
iv. DCL[4] generated from the four components A1, A4, B3, B5	99
B. Kinetic switching of CDLs in the presence of metal ions.....	101
i. DCL[5] generated from the four components A1, A6, B3, B5 in the presence of Cu(I) and Zn(II).....	103
ii. DCL[6] generated from the four components A2, A5, B3, B5 in the presence of two metal ions.....	104
1) DCL[6] generated from the four components A2, A5, B3, B5 on sequential addition of Cu(I) and Zn(II).....	104
2) DCL[6] generated from the four components A2, A5, B3, B5 on sequential addition of Cu(I) and Fe(II); Ag(I) and Zn(II); Ag(I) and Fe(II)	105
iii. DCL[7] generated from the four components A2, A5, B2, B3 in the presence of two metal ions.....	107
1) DCL[7] generated from the four components A2, A5, B2, B3 on sequential addition of Ag(I) and Fe(II)	108
2) DCL[7] generated from the four components A2, A5, B2, B3 on sequential addition of Ag(I) and Zn(II).....	109
iv. DCLs[8] [9] and [10] generated from the four components A1 (A2 or A3), A8, B1, B2 in the presence of two metal ions.....	111
1) DCL[8] generated from the four components A1 (A2 or A3), A8, B1, B2 on simultaneous addition of Ag(I) and Zn(II).....	111

2) DCL[9] generated from the four components A1 (A2 or A3), A8, B1, B2 on simultaneous addition of Ag(I) and Zn(II).....	114
3) DCL[10] generated from the four components A1 (A2 or A3), A8, B1, B2 on simultaneous addition of Ag(I) and Zn(II).....	118
3. SUMMARY OF CHAPTER III.....	120
CHAPTER IV. THE C=N FORMATION FOR GENE REGULATION.....	123
1. INTRODUCTION.....	123
A. <i>Facilitating imine formation in aqueous phase</i>	123
i. The fast-reacting aldehyde for imine formation	123
ii. The increased yield of imine formation.....	125
B. <i>Histones modifications</i>	129
i. The structure of histone and nucleosome.....	129
ii. Gene regulation-acetylation and deacetylation	130
2. RESULTS AND DISCUSSIONS	132
A. <i>Screening of the substrates</i>	132
i. Fast-reacting aldehydes.....	132
ii. Hydrophobic effect of the amines	135
iii. pH dependence.....	136
B. <i>Imine formation driven between PLP and Lysine derivatives</i>	141
i. PLP reacting with mono substituted Lysine	142
ii. PLP reacting with tri-lysine and penta-lysine.....	146
3. SUMMARY OF CHAPTER IV	149
CHAPTER V. CONCLUSION AND PERSPECTIVES	150
CHAPTER VI. EXPERIMENTAL PART	151
1. GENERAL PROCEDURES	151
A. <i>Solvents and Chemicals</i>	151
B. <i>Methods and Instruments</i>	151
i. Chromatography Methods.....	151
ii. Nuclear Magnetic Resonance Spectroscopy.....	151
iii. High resolution electrospray ionization mass spectroscopy.....	152
iv. Elemental Analysis.....	152
v. X-ray crystallography.....	152
vi. pH Measurement.....	152
2. CHAPTER II. CATALYSIS OF IMINE AND HYDRAZONE FORMATION	153
A. <i>Synthesis and characterization</i>	153
i. General procedures for the synthesis.....	153

ii.	Characterization of the newly made compounds.....	155
B. The kinetic analysis of imine/hydrazone formation in absence and in presence of catalysts		
162		
i.	The kinetics of imine formation in the absence of presence of metal salts.....	164
1)	Kinetics of A1 + B1 in absence of metal salts.....	164
2)	Kinetics of A1 + B1 in presence of AgOTf.....	164
3)	Kinetics of A1 + B1 in presence of Zn(OTf) ₂	165
4)	Kinetics of A2 + B1 in absence of metal salts.....	165
5)	Kinetics of A3 + B1 in absence of metal salts.....	166
6)	Kinetics of A2 + B1 in presence of AgOTf.....	166
7)	Kinetics of A3 + B1 in presence of AgOTf.....	167
8)	Kinetics of A2 + B1 in presence of Zn(OTf) ₂	167
9)	Kinetics of A3 + B1 in presence of Zn(OTf) ₂	168
ii.	The kinetics of hydrazone formation in the absence and presence of metal salts	168
1)	Kinetics of A1 + B2 in absence of metal salts.....	168
2)	Kinetics of A1 + B2 in presence of AgOTf.....	169
3)	Kinetics of A1 + B2 in presence of Zn(OTf) ₂	169
4)	Kinetics of A2 + B2 in absence of metal salts.....	170
5)	Kinetics of A3 + B2 in absence of metal salts.....	170
6)	Kinetics of A2 + B2 in presence of AgOTf.....	171
7)	Kinetics of A3 + B2 in presence of AgOTf.....	171
8)	Kinetics of A2 + B2 in presence of Zn(OTf) ₂	172
9)	Kinetics of A3 + B2 in presence of Zn(OTf) ₂	172
C. Kinetics of A1 + B2 in the presence of B1 or metal ion [Ag(I) or Zn(II)] as well as both B1 and metal ion as co-catalysts.....		
173		
1)	Kinetics of A1 + B2 in presence of B1	173
2)	Kinetics of A1 + B2 in presence of both B1 and AgOTf.....	173
3)	Kinetics of A1 + B2 in presence of both B1 and Zn(OTf) ₂	174
4)	Kinetics of A2 + B2 in presence of B1	176
5)	Kinetics of A3 + B2 in presence of B1	176
6)	Kinetics of A2 + B2 in presence of both B1 and AgOTf.....	177
7)	Kinetics of A3 + B2 in presence of both B1 and AgOTf.....	177
8)	Kinetics of A2 + B2 in presence of both B1 and Zn(OTf) ₂	178
9)	Kinetics of A3 + B2 in presence of both B1 and Zn(OTf) ₂	178
D. Catalysis of imine and hydrazone formation by metal salts and acid.....		
179		
1)	Kinetics of A1 + B1 in presence of 0.05 equiv. of AgOTf.....	179
2)	Kinetics of A1 + B1 in presence of 0.05 equiv. of Zn(OTf) ₂	180

3) Kinetics of A1 + B1 in presence of 0.05 equiv. of CF ₃ COOD.....	181
4) Kinetics of A1 + B1 in presence of 0.05 equiv. of Sc(OTf) ₃	182
5) Kinetics of A1 + B2 in presence of 0.05 equiv. of AgOTf.....	183
6) Kinetics of A1 + B2 in presence of 0.05 equiv. of Zn(OTf) ₂	184
7) Kinetics of A2 + B2 in presence of 0.05 equiv. Zn(OTf) ₂	185
8) Kinetics of A1 + B2 in presence of 0.05 equiv. of Sc(OTf) ₃	186
9) Kinetics of A1 + B2 in presence of 0.05 equiv. of CF ₃ COOD.....	187
10) Kinetics of A1 + B2 in presence of 0.05 equiv. B1 and 0.05 equiv. Zn(OTf) ₂ 188	188
3. CHAPTER III. CONTROL OF TIME-DEPENDENT SWITCHING OF DCLS.....	190
A. <i>Synthesis and characterization</i>	190
i. General procedures for the synthesis.....	190
ii. Characterization of the newly made compounds.....	191
B. <i>List of the compounds have been selected in the context.</i>	196
C. <i>The kinetics study of two, three, four-components mixtures</i>	197
i. Two-component reactions.....	197
1) The formation of A4B3 from the same equivalent amount of A4 + B3	197
2) The formation of A4B4 from the same equivalent amount of A4 + B4	197
3) The formation of A5B3 from the same equivalent amount of A5 + B3	198
4) The formation of A5B4 from the same equivalent amount of A5 + B4	198
5) The kinetic data for the formation of A4B3, A4B4, A5B3 and A5B4 from the same equivalent amount of their components.....	199
ii. Three-component reactions.....	199
1) Competitive reactions between A4 + B3 + B4	199
2) Competitive reactions between A5 + B3 + B4	200
3) Competitive reactions between A1 + B3 + B4	200
4) Competitive reactions between A6 + B3 + B4	201
5) Competitive reactions between A3 + B3 + B5	201
iii. Four-component DCLs.....	202
1) DCL generated from A1 + A6 + B3 + B5	203
2) DCL generated from equal amounts of A4 + A5 + B3 + B4	203
3) DCL generated from equal amounts of A4 + A6 + B3 + B4	204
4) DCL generated from equal amounts of A4 + A7 + B3 + B4	206
5) DCL generated from equal amounts of A1 + A6 + B3 + B4	208
6) DCL generated from equal amounts of A1 + A4 + B3 + B5	208
iv. Four-component DCLs in the presence of metal ions.....	208
1) DCL generated from equal amounts of A1 + A8 + B1 + B2 in presence of 0.5 equiv. of AgOTf and Zn(OTf) ₂	209

2) DCL generated from equal amounts of A2 + A8 + B1 + B2 in presence of 0.5 equiv. of AgOTf and Zn(OTf) ₂	210
3) DCL generated from equal amounts of A3 + A8 + B1 + B2 in presence of 0.5 equiv. of AgOTf and Zn(OTf) ₂	211
4) HRMS-ESI spectra of Zinc (II) complex [Zn(B2) ₂] ²⁺ of B2	212
5) ¹ H NMR spectra of all the components and constituents in the absence of presence of metal salts.....	213
4. CHAPTER IV. THE IMINE FORMATION FOR GENE REGULATION	220
A. <i>General procedures for the experiments</i>	220
1) Procedures for preparation of the phosphate buffer	220
2) Procedures for quantitative calculation of the imine yield	220
3) Procedures for titration experiment.....	220
ANNEXES	221
1. CRYSTALLOGRAPHIC DATA FOR DETERMINED CRYSTAL STRUCTURES.....	221
REFERENCES	225

ACKNOWLEDGEMENTS

Firstly, I would like to express my sincere thanks to Prof. Jean-Marie Lehn for giving me this fantastic opportunity to do my Ph.D in his research group. I got enormous inspiration and motivation by his enthusiasm on science, excellent instructions, and amazing personality. I appreciate for his patient guidance, kind support and immense knowledge. It was such great experience working with him and under his guidance which inspires and motivates me a lot towards the scientific research.

I would like to thank Prof. Sebastien Ulrich from Université de Montpellier, Prof. Ghislaine Vantomme from Eindhoven University of Technology, Prof. Jean-Claude Chambron from University of Strasbourg for examination of my work.

Besides, I would also like to express my thank to Prof. Jack Harrowfield for his insightful discussions and suggestions on my research work as well as the carefully correcting my manuscripts both Chemistry and English. I would also like to Dr. Artem Osypenko for his valuable suggestions on my projects as well as correction of my thesis. I must thank the others who helped correcting my thesis, Dr. Youssef Atoini, Aline Chevalier, Dr. Jean-louis Schmidt and Prof. Andrian-Mihail Stadler.

I would like to thank Dr. Jean-Louis Schmitt and Cyril Athenaeums for their help in the laboratory and measurement of nmr. More thanks should give to Dr. Artem Osypenko and Dr. Jean-Francois Ayme, who have stayed in the same lab 515 with me for 4 years and gave me many suggestions and help on the research.

I would like to thank all the current and former lab members in Prof. Lehn's group, particularly Dr. Ruirui Gu and Dr. Chunshuang Liang who has helped me a lot when I first arrived in Strasbourg in late September 2016, and the others: Sirinan, Jan, Martin, Sebastien, Guangwen, Liyuan, Antonio, Chanon, Wissuta, Annia for her help of preparing the documents before I came here, Jacline for her kindness, Stanislav, Bohdan, Michal, Kumar, Chenna, Juan, Zhaozheng, Chengyi, and most of all, Aline Chevalier, who has stayed with me in the lab for three years and always support me in many ways and cheering me up during the hard time.

I am thankful to my former master supervisor Prof. Yu Fang for his support. He was and remains a good scientist and mentor. He inspired me to go to pursue a career in research. His enthusiasm, persistence and love for research is contagious.

There are many friends who I very much appreciate, Xiaoqiao, Zhuo, Xue, Yali, Jia, Gaigai, Yongmei, Thanvy, Xingmao, Rui, Jiayun, Yanyu and Xiaomin for their kindness.

Last but not least, I would like to thank my parents, my sisters and brother for supporting me spiritually throughout my Ph.D life in France. The most special thank I would give to my husband Shaofei Zhang, who is always supporting me and accompanying me.

Finally, I would like to acknowledge the “China Scholarship Council” and Prof. Jean-Marie Lehn, for their financial support on my Ph.D study. Without these, I would not have been here to pursue my research.

ABSTRACT

Supramolecular chemistry deals with the construction of complex systems by interconnected entities through weak non-covalent interactions. Due to the dynamicity, a supramolecular system can undergo self-organization in response to external effectors. Reversible covalent reactions are also dynamic through the formation and breaking of covalent bonds under certain conditions. Constitutional dynamic chemistry (CDC), allows a system to undergo changes in constitution by component recombination through the implementation of reversible covalent reactions and non-covalent linkages. Therefore, many efforts were devoted to facilitation of dynamic covalent reactions (DCR) as well as to construction of dynamic covalent libraries (DCLs) for the applications in catalysis, materials, and biology.

Here we illustrated the study of DCC in several aspects: *a*) kinetics and facilitation of C=N formation in organic phase; *b*) time-dependent switching of DCLs in the absence and in the presence of metal salts; *c*) increasing of imine formation yield in aqueous phase.

As a result of the widely application of DCRs, it is of great importance to develop effective methods to accelerate the corresponding kinetics. We have investigated the formation of imines and hydrazones from their components both in the absence and presence of AgOTf or Zn(OTf)₂. Very large acceleration by factors up to about 10,000 was observed for the formation of the imine complex in presence of Zn(OTf)₂ compared to the formation of the imine itself. Formation of the complexed hydrazone ligand was also moderately accelerated by a factor of 8-14 on addition of Zn(OTf)₂ or AgOTf and notably, organocatalysis of hydrazone formation by a similar factor was induced by the auxiliary amine p-anisidine. Through the synergistic operation of both Zn(OTf)₂ and the p-anisidine, the formation of the zinc complex of the hydrazone ligand was enhanced by a factor of about 630 in comparison to the formation of the hydrazone itself in absence of Zn(OTf)₂. A similar fast reaction is obtained in a three-catalyst setup, combining the two metal salts and the auxiliary amine. Thus, the metal salts and amine together display a strongly synergistic facilitation on the formation of the Zn(II) hydrazone complex.

Combining both metallo- and organo-catalysis, this mode of synergistic effect points to a powerful strategy of co-catalysis of bond-formation in DCC through synergistic interconnected chemical transformations and exemplifies dynamic systems that generate kinetically faster and thermodynamically simpler outputs from mixtures of higher complexity.

The dynamic covalent reactions can be utilized to build up CDLs which adapt to external effectors resulting in component selection through the change in constitution of the DCLs. We have explored the behavior of dynamic covalent libraries (DCLs) of four constituents generated by the reversible formation of C=N bonds between four components, both in the absence and in the presence of metal cations. The $[2 \times 2]$ networks associated to these DCLs undergo time-dependent changes with the variation in the distributions of the constituents. The kinetic network established at the initial generation of the constituents progressively changes to the final thermodynamic one, thus undergoing a switching from a kinetic to the thermodynamic state, involving an orthogonal switching from one diagonal to the other diagonal of the square $[2 \times 2]$ network. The set of DCL constituents could be switched from the kinetic products (imines) to thermodynamic products (oxime or acylhydrazone) based on the reactivities of the components and the thermodynamic stabilities of the constituents without addition of any other external effectors, i.e. solely on the basis of the intrinsic properties of the self-contained system.

Such processes were achieved for purely organic DCLs/DCNs as well as for inorganic ones containing two metal cations, e.g. silver (I) and zinc (II). In the latter inorganic cases, network switching involved changing from the silver(I) complex of an imine (kinetic product) to the zinc complex of a hydrazone (thermodynamic product). Therefore, the DCLs and the associated DCNs could be switched for either organic or inorganic systems. The results also bear relationship to the behavior of out-of-equilibrium systems opening towards kinetic behavior in adaptive chemistry.¹⁰

Imine formation has been extensively studied in mechanism and kinetics, there remains a need for an effective method to increase the yield of imine formation in aqueous phase. We have investigated imine formation from a variety of aldehydes with lysine derivatives to screen the best aldehyde for the highest yield of imine in aqueous phase. Pyridoxal phosphate was first chosen due to its coenzyme role in a variety of enzymatic reactions. The para-N could activate the aldehyde and the ortho-OH could stabilize the generated imine to drive the equilibrium of imine formation. pH titration experiment indicated that the imine forms a higher yield in the pH around 10 to 11. In addition, one also notes that pyridoxal phosphate the most prospective one with 65% imine (pH=11) among all the tested aldehydes. The reaction of **PLP** with monolysine and polylysine provided a model for histone modification since histones are abundant in lysines. This result indicated the possibility of imine formation for dynamic gene regulation. This project is still ongoing, and more experiments still need to be done.

In conclusion, this thesis illustrated several aspects of C=N formation and C/N exchange in dynamic covalent chemistry: catalysis, kinetics and thermodynamics, kinetic switching behavior as well as out-of-equilibrium states.

The present results exemplify the facilitation of dynamic covalent reactions of C=N as well as the construction of DCLs and DCNs to modulate the kinetic behavior of the dynamic system. It is of great importance to understand the relationship of structural differences and the kinetic and thermodynamic properties of the constituents as well as the DCLs. It paves a way to establish high-level, multi-phase systems to generate faster and simpler output in adaptive chemistry. Moreover, these studies indicated the potential applications in biology such as gene regulation.

ABBREVIATIONS AND SYMBOLS

ADA	Acceptor-Donor-Acceptor
Ala	Alanine
CDC	Constitutional Dynamic Chemistry
CDLs	Constitutional Dynamic Libraries
CDNs	Constitutional Dynamic Networks
C=N	Imine Compound
CMC	Critical Micelle Concentration
DNCC	Dynamic Non-Covalent Chemistry
DCRs	Dynamic Covalent Reactions
DNA	Deoxyribonucleic Acid
DAD	Donor-Acceptor-Donor
EDG	Electro-Donating Group
EWG	Electro-Withdrawing Group
Equiv.	Equivalent
ESI	Electro Spray Ionization
Gly	Glycine
h	Hour
HOMO	Highest Occupied Molecular Orbital
HATs	Histone Acetyltransferase
HDAXs	Histone Deacetylase
HMDSO	Hexamethyldisiloxane
HRMS	High Resolution Mass Spectroscopy
His	Histidine
k	Rate Constant
LUMO	Lowest Unoccupied Molecular Orbital
min	Minute
NMR	Nuclear Magnetic Resonance
NBI	Naphthalene Bisimide
mM	Millimolar per Liter
OTf	Trifluoromethanesulfonate
OEG	Oligoethylene Glycol
PLP	Pyridoxal Phosphate
ppm	Part per Million

pH	Potential of Hydrogen
Phe	Phenylalanine
RNA	Ribonucleic Acid
SDS	Sodium Dodecyl Sulfate
μM	Millimolar, $10^{-3} \text{ mol L}^{-1}$
Val	Valine

RESUME EN FRANCAIS

La nature a toujours été une source d'inspiration pour les scientifiques. La capacité des organismes vivants à s'adapter à leurs environnements a inspiré de nombreux chimistes à développer des systèmes chimiques artificiels, capables d'un comportement adaptatif envers des stimuli physiques ou chimiques. La caractéristique commune de tous ces systèmes est leur nature dynamique. Ainsi, la Chimie Adaptative, qui les étudie, repose sur deux piliers principaux : (i) la chimie supramoléculaire, qui enveloppe les interactions non covalentes, intrinsèquement dynamiques; et (ii) la Chimie Covalente Dynamique (DCvC, référant à *Dynamic Covalent Chemistry*), qui enveloppe les liaisons covalentes réversibles. La chimie supramoléculaire et la DCvC établissent ensemble la Chimie Dynamique Constitutionnelle (CDC, référant à *Constitutional Dynamic Chemistry*). La CDC étudie les systèmes qui subissent des changements constitutionnels par échange de composants grâce à la mise en œuvre de réactions covalentes réversibles et/ou d'interactions non covalentes. De tels systèmes sont souvent appelés Bibliothèques Dynamiques Constitutionnelles (CDLs, référant à *Constitutional Dynamic Libraries*) ou Réseaux (CDNs, référant à *Constitutional Dynamic Networks*). Ces dernières années, des nombreuses études ont été effectuées sur les CDLs dans les domaines suivants : la catalyse, la détection, les matériaux adaptatifs, le développement de médicaments, mais aussi en relation avec l'origine de la vie et les systèmes hors-équilibre.

Par conséquent, de nombreux efforts ont été consacrés au développement de nouvelles réactions basées sur la chimie covalente dynamique, ainsi qu'à l'optimisation et à l'étude de celles déjà connues, telles que la formation de bases de Schiff ou de liaisons azométhines (C=N) (comprenant les imines, les acylhydrazones, les hydrazones et les oximes). Entre autres, la formation de cette liaison dans notre corps est présente dans la rhodopsine (molécule photosensible des cellules de la rétine) et dans le métabolisme des acides aminés. Il s'agit de l'une des liaisons dynamiques les plus utilisées dans le domaine de la DCvC. De nombreux groupes l'ont étudié de manière approfondie, y compris le nôtre. Bien que les études cinétiques et thermodynamiques sur les bases de Schiff individuelles soient assez abondantes, seules quelques-unes se focalisent sur le comportement des azométhines dans les CDLs.

Dans cette thèse, notre but est d'élargir nos connaissances sur la liaison imine et à les utiliser pour étudier différents comportements adaptatifs d'un point de vue cinétique et thermodynamique, y compris les commutateurs de CDNs et leurs états hors-équilibre (**Chapitre II et III**). De plus, d'un point de vue thermodynamique, tout en développant des imines pour

des applications biologiques, nous avons également essayé de répondre à une question toujours persistante : “Comment obtenir des imines quantitativement dans l’eau?” (*Chapitre IV*).

Chapitre II. Accélération de la formation de la liaison C=N par des sels métalliques

Du fait des importantes potentielles applications des réactions covalentes dynamiques, il est crucial de développer des méthodes efficaces pour accélérer leur cinétique. Nous avons donc étudié la réaction de formation des imines et des hydrazones à partir de leurs composants correspondants (respectivement aldéhyde/amine ou aldéhyde/hydrazine) d’abord en l’absence, puis en présence des cations de métaux de transition tels que Ag(I) ou Zn(II) (**Schéma 1**).

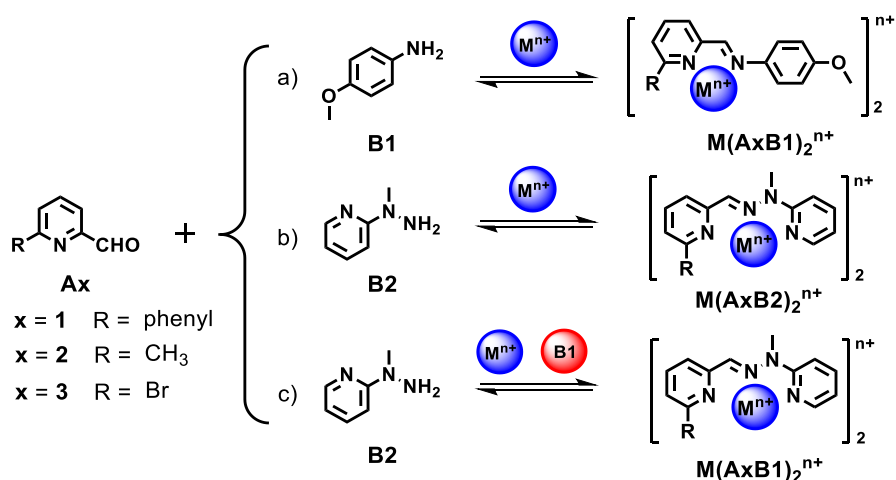


Schéma 1. Formation d'imine et d'hydrazone à partir de pyridine-2-carboxaldéhyde **Ax** et de a) *p*-anisidine (amine auxiliaire) **B1** ou b) 2-N-méthylhydrazino-pyridine **B2** en l'absence et en présence sels de métaux ainsi que c) formation d'hydrazone en présence de sels métalliques et de l'amine auxiliaire **B1**.

Une accélération très importante (par des facteurs allant jusqu'à 10^4) a été observée pour la formation du complexe d'imine en présence de $Zn(OTf)_2$ en comparaison avec la formation de l'imine seul en absence de sel métallique. La formation d'hydrazone complexée a également été modérément accélérée par un facteur de 8 à 14 lors de l'addition de $Zn(OTf)_2$ ou de $AgOTf$. De plus, la formation d'hydrazone a été accélérée par un facteur similaire à l'aide d'une organocatalyse avec l'amine auxiliaire : la *p*-anisidine. Grâce à une contribution mutuelle entre $Zn(OTf)_2$ et la *p*-anisidine, la vitesse de formation du complexe de zinc de l'hydrazone a été augmentée d'un facteur d'environ 630 par rapport à la formation de l'hydrazone sans aucun catalyseur. Une réaction rapide a également été observée dans une configuration à trois catalyseurs, combinant les deux sels métalliques et l'amine auxiliaire. Ainsi, les deux sels métalliques et l'amine induisent une accélération synergique importante de la formation du complexe d'hydrazone du Zn(II).

Combinant à la fois métallo et organocatalyse, cet effet synergique indique que l'utilisation de co-catalyseurs est une stratégie intéressante pour accélérer la formation de liaisons C=N. Il démontre que les systèmes dynamiques peuvent générer des résultats cinétiquement plus rapides et thermodynamiquement plus simples à partir de systèmes dynamiques complexes utilisant la CDC.

Chapitre III. Inversions (transition, permutation) temporaires dans des Bibliothèques Covalentes Dynamiques (DCLs)

Les réactions covalentes dynamiques sont utilisées pour la construction de DCLs capables de s'adapter aux effecteurs externes, ce qui se traduit par des changements dans la constitution de la bibliothèque suite à la sélection des composants. Nous avons exploré le comportement des DCLs composées de quatre constituants générés par la formation réversible de liaisons C=N entre quatre composants (deux aldéhydes **A**, **A'** et deux amines **B**, **B'**), sans et avec cations métalliques (**Figure 1**).

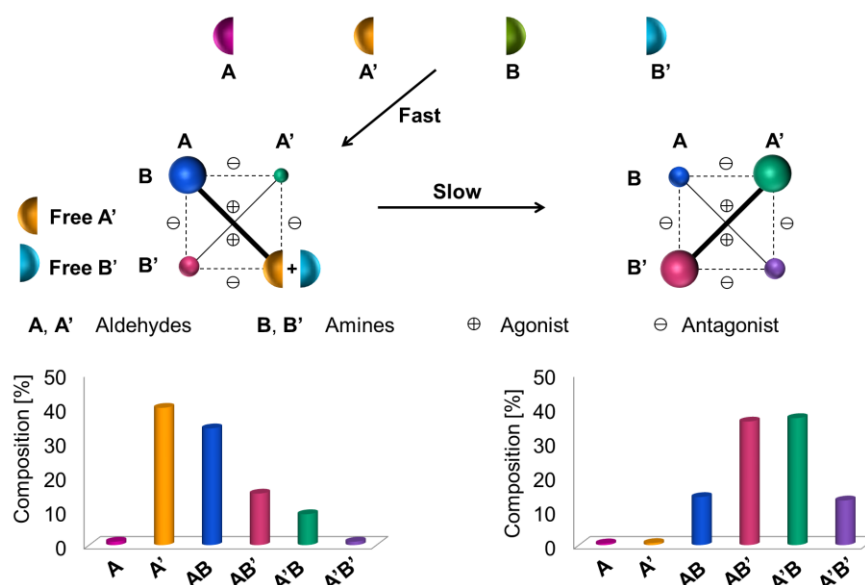


Figure 1. Évolution d'une CDL de quatre constituants subissant une commutation orthogonale en fonction du temps.

Les réseaux $[2 \times 2]$ associés à ces DCLs subissent des variations des distributions des constituants en fonction du temps. Ce réseau passe progressivement de son état initial dit cinétique (formé rapidement après le mélange de tous les composants) à son état thermodynamique final. Ce changement se traduit par une commutation orthogonale du réseau, de la distribution cinétique initiale des constituants à la distribution thermodynamique finale. La possibilité d'une telle commutation constitutionnelle de réseaux dynamiques sans ajout

d'aucun autre effecteur externe réside dans les différentes réactivités intrinsèques des composants sélectionnés (ici, l'imine est le produit cinétique, et l'acylhydrazone ou l'oxime sont les produits thermodynamiques).

Une telle commutation constitutionnelle a été réalisée pour les DCLs/DCNs purement organiques discutés ci-dessus, ainsi que pour ceux contenant deux cations métalliques, par ex. Ag(I) et Zn(II). Dans ces derniers cas, avec des cations métalliques, la commutation de réseau est passée du complexe d'Ag(I) d'une imine (produit cinétique) au complexe de Zn(II) d'une hydrazone (produit thermodynamique). La coopération entre les facteurs cinétiques et thermodynamiques a permis la conception de tels commutateurs constitutionnels, qui sont en quelque sorte liés aux systèmes hors-équilibre.

Chapitre IV. Développement des imines stables dans l'eau

Lors de la formation d'une liaison C=N à partir de carbonyle et d'amine, une molécule d'eau est produite, ce qui limite l'utilisation de cette réaction dynamique dans les systèmes biologiques en raison de l'hydrolyse de l'imine. Un défi important est de trouver un moyen efficace d'augmenter le rendement de formation d'imine dans les conditions aqueuses. Dans la dernière partie de cette thèse, nous avons criblé une variété d'aldéhydes dans une réaction de formation d'imine avec des dérivés de lysine afin de trouver l'aldéhyde donnant la base de Schiff avec le plus haut rendement en solution aqueuse (**Figure 2**).

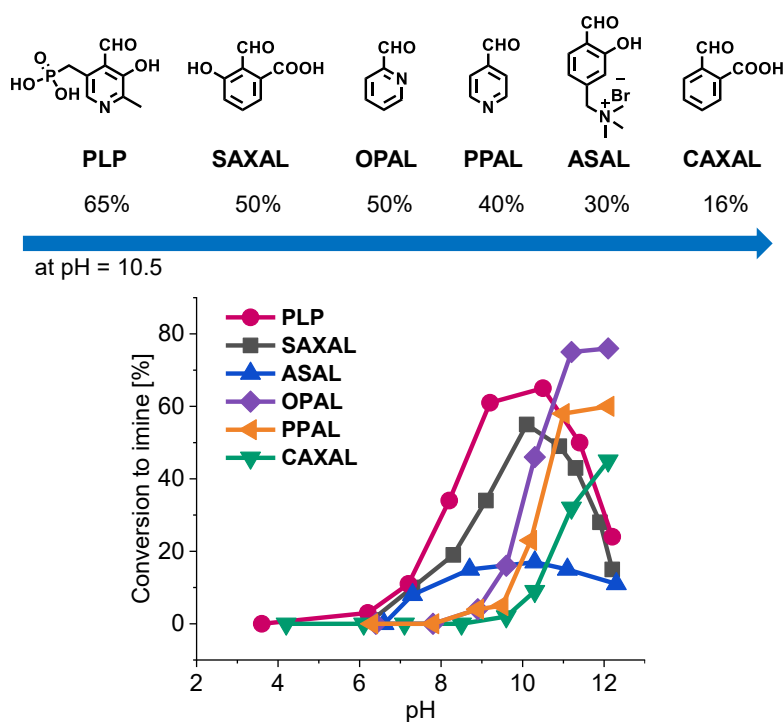


Figure 2. Les aldéhydes sélectionnés pour former l'imine en phase aqueuse (haut), ainsi que les rendements de formation d'imine en fonction du pH (bas).

Pour comprendre les caractéristiques structurales qui augmentent la stabilité de l'imine, nous avons d'abord choisi le phosphate de pyridoxal, car il est connu comme coenzyme de certaines réactions enzymatiques. Ainsi, l'atome d'azote en position para par rapport à un groupement aldéhyde dans un cycle de type pyridine peut activer le carbonyle, et également le groupement hydroxyle en position ortho pourrait stabiliser l'imine formée pour conduire l'équilibre vers la formation d'imine. La variation du pH indique que le rendement en imine le plus élevé est observé au-dessus du pH 10. Jusqu'à présent, le meilleur aldéhyde est le phosphate de pyridoxal avec 65% d'imine formée (à pH 11) parmi tous les aldéhydes testés. Étant donné que les systèmes biologiques fonctionnent à un pH physiologique d'environ 7, il est nécessaire de développer des aldéhydes ayant des propriétés supérieures pour la formation d'imine. Ce projet est toujours en cours et d'autres expériences doivent encore être effectuées.

En conclusion, dans cette thèse, nous avons illustré plusieurs aspects de la formation et de l'échange de liaisons C=N dans la CDC : catalyse, cinétique et thermodynamique, comportement de commutation cinétique et états hors-équilibre.

Pour résumer le présent travail, nous avons élargi nos connaissances et notre compréhension de la CDC d'imines, en particulier du point de vue cinétique, ce qui a longtemps été sous-étudié. La compréhension de l'influence des effets structuraux sur le comportement cinétique et thermodynamique ouvre la voie à l'établissement de systèmes complexes pour générer une production plus rapide et plus simple en chimie adaptative. De plus, ces études ont indiqué des applications potentielles en biologie.

CHAPTER I. GENERAL BIBLIOGRAPY

1. FROM SUPRAMOLECULAR CHEMISTRY TO CONSTITUTIONAL DYNAMIC CHEMISTRY

Supramolecular chemistry has undergone a booming development during the last decades with its wide application in catalysis, sensing, materials, and others. It is defined by J.-M. Lehn as “*chemistry beyond the molecule*” where supramolecular entities are built by linking the molecular components through intermolecular forces. This research field was initially established in the last century based upon the exploitation of non-covalent forces. An important step occurred in the 1960s, when Charles Pedersen^{1,2} successfully synthesized macrocyclic, “crown” ethers. The real burst came in 1987 when the Nobel Prize for chemistry was awarded to three pioneers, C. J. Pedersen,^{1,2} D. J. Cram³⁻⁵ and J.-M. Lehn^{6,7} for their development and use of macro(poly)cyclic molecules with structure-specific interactions of high selectivity.²⁻⁷ Such molecules and their very numerous derivatives were the focus of the rapid development of “host-guest” chemistry, where their interactions with both organic and inorganic species led to the formation of complexes in which the macrocycle was considered the “host” (**Figure 3**).⁸ They can bind specifically with the guests inventing the concept of “molecular recognition”.⁹ Crown ethers and cryptands can form complexes with cations such as such as K^+ and NH_4^+ . Cavitands can encapsulate small organic molecule into its inner cavity. Therefore, this kind of supramolecular interactions has been widely exploited in specific molecular sensing, drug delivery and extraction of hazardous chemical guests.¹⁰

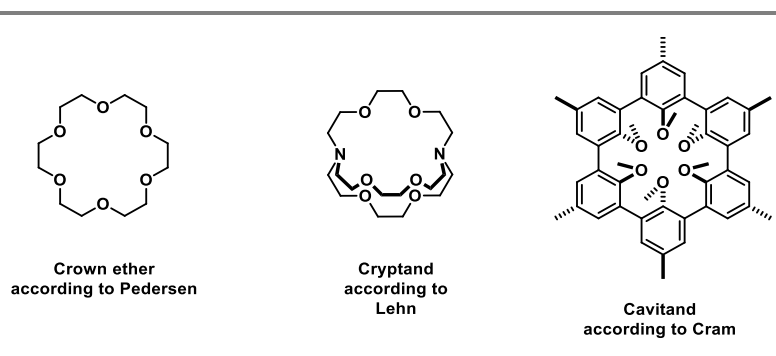


Figure 3. The three early supramolecular host molecules

Supramolecular chemistry can be viewed as Dynamic Non-Covalent Chemistry (DNCC) because of the lability and weak strength energy of most non-covalent interactions such as van

de Waals forces, hydrogen bonding, and metal coordination. This dynamic feature permits supramolecular species to undergo reversibly association and dissociation from their molecular components. The main types of non-covalent interactions are illustrated in **Table 1**.

Table 1. Comparison of different noncovalent interactions.^{11,12}

Interaction	Strength, kJ/mol	Example
Ion-ion	200 – 300	(<i>n</i> -Bu) ₄ N ⁺ Cl ⁻
Ion-dipole	50 – 200	Sodium and [15] crown-5
Dipole-dipole	5 – 50	Acetone
Hydrogen bonding	4 – 120	Nucleotides within DNA
Cation-π	5 – 80	K ⁺ in benzene
π-π	0 – 50	Benzene and graphite
Van der Waals	<5 (but variable depending on surface area)	Liquid gases, packing in molecular crystals
Hydrophobic	Related to solvent-solvent interaction energy	Cyclodextrin inclusion compounds
Metal-ligand	0 – 400	Zn(NH ₃) ₄ ²⁺

Many complex architectures held by non-covalent interactions were developed, thus allowing for the self-organization with selection. The supramolecular systems thus can adapt their structures and constitution to the external effectors.

Such an example is the generation of the circular helicates of different sizes in the presence of anion from the work of Hasenknopf and Lehn (**Figure 4**). They demonstrated the role of counter anions as templates to guide the outcome of the self-organization of the DCL of circular helicates.¹³ By mixing *n* equivalent of tris-bipyridine and Fe(II), they displayed the selective generation of either penta- or hexanuclear architectures depending on the different anions. The addition of FeCl₂ generated the pentanuclear circular helicate [5]**cH**, while the addition of FeSO₄ induced the assembly of the hexanuclear [6]**cH**. Hence, the Fe(II) and the tris-bipy ligands were considered to generate the potential members of the virtual combinatorial library. Addition of the anions either chloride or sulfate induced the selective formation of specific polynuclear architectures. These results indicated that the virtual combinatorial library of supramolecular mixtures can adapt their structures and constitution to the effectors present.

Dynamic Library of Circular Helicates

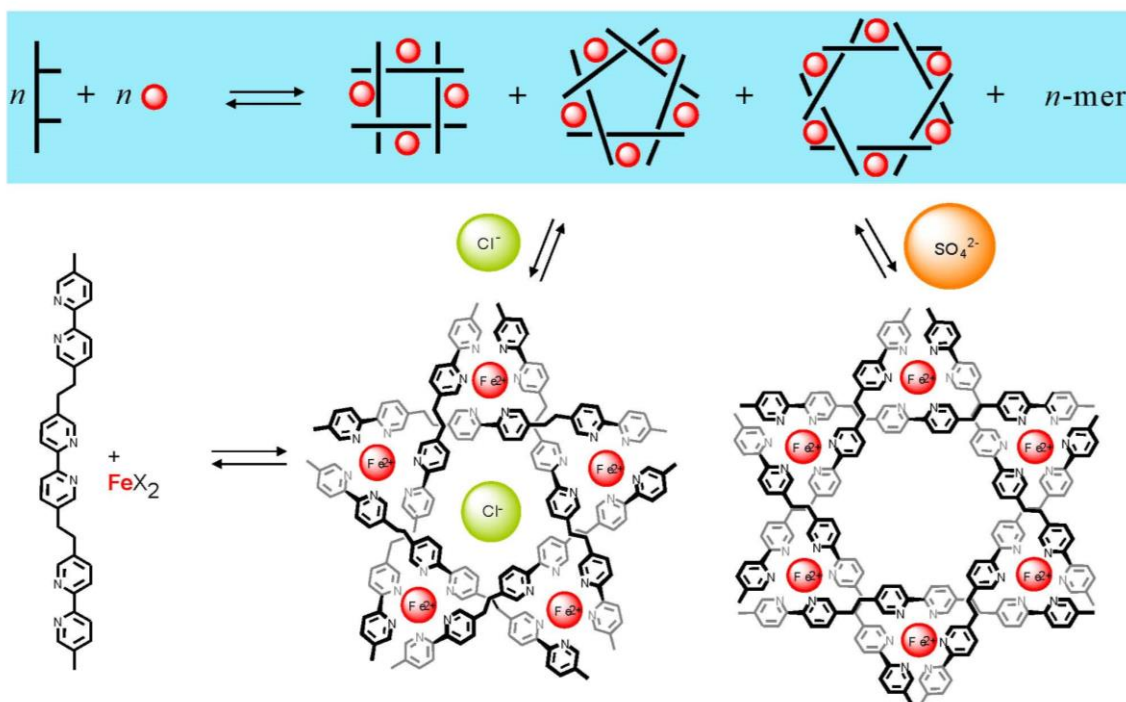


Figure 4. The self-assembly of circular helicates from the ligands and the Fe(II) ions in the presence of different anions (chloride or sulfate anions).¹³

Metal ions were one kind of important effectors to induce the formation of many supramolecular architectures^{14–22} such as two-dimensional (2-D) polygons and three-dimensional (3-D) cages,^{23–26} rotaxane,²⁷ supramolecular trapezoid,^{22,28–31} and more complexed supramolecular structures such as circular helicates and molecular knots.^{32–34}

Lehn and co-workers reported many works on the self-sorting of supramolecular architectures based on metal complexes.^{14,35–40} For example, they investigated the generation of two helicates from a mixture of two types of tris-bipyridine ligands in the presence of two metal ions Cu(I) and Ni(II). With the bipyridine connected by ethylene bridges, penta- and hexanuclear architectures were obtained depending on the anion. With the linker of the bipyridine as oxypropylene, it formed a tetranuclear circular helicate. Through the self-organization of the constituents (tris-bipyridine ligand connected by ethylene bridges) with the two metal ions, only two structures were obtained – the double helicate incorporating copper and the triple helicate incorporating nickel (**Figure 5**).⁴¹ These results implied that the systems composed of mixtures of components could selectively generate well defined architectures through self-organization by adding metal ions.

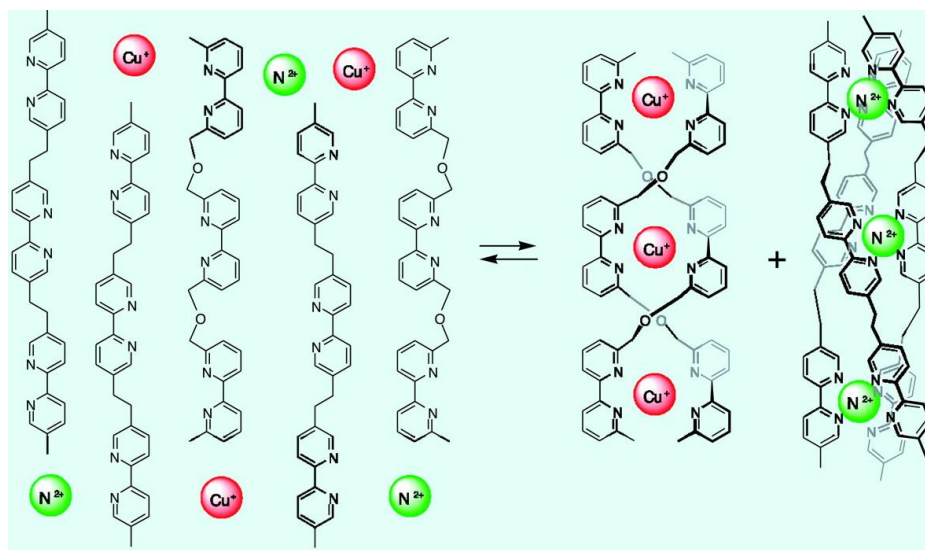


Figure 5. Self-recognition in the self-assembly of the double helicate and the triple helicate from a mixture of the oligobipyridine strands and of CuClO_4 and $\text{Ni}(\text{ClO}_4)_2$.

The adaptation of the supramolecular systems has prompted chemists to consider importing this dynamic feature into molecular chemistry. Accordingly, it required shifting from “static” to “dynamic” covalent bonds to endow molecules with the ability to undergo dynamic exchange and recombination processes passing through the reversible formation and breaking of covalent bonds. This provides a new perspective of considering organic molecules as labile entities, in strong contrast to the conventional view. Many reversible reactions,⁴² for example, imine formation,⁴³ disulfide exchange,⁴⁴ Diels-Alder reactions,⁴⁵ provide instances where covalent chemistry can also be dynamic, with the molecular bond formed and broken rapidly under certain conditions. Thus, the discovery of these dynamic reactions has led to the emergence of dynamic covalent chemistry (DCvC).^{46–54}

Therefore, this constitutional change of the components can exist both at the supramolecular and molecular levels and underlies the field of Constitutional Dynamic Chemistry (CDC).^{50,55–61} CDC gives rise to both the formation and dynamic features of these molecular and supramolecular entities resulting from condensation of the building blocks (*components*) through reversible covalent and non-covalent interactions. In both cases, there is always the recombination of the building blocks, which was also defined as Dynamic Combinatorial Chemistry (DCC) by Sanders.⁵⁹ Therefore, the field of DCvC and DNCC resulted in DCC from the combinatorial point of view and constitutional dynamic chemistry from the compositional point of view (**Figure 6**).⁶² Upon action of chemical effectors or physical stimuli, CDC allows a system to respond to such event by changing the constitution of

the system through component exchange and reorganization, thus generating selection and amplification of one of the products (*constituents*) within the system.^{63–68}

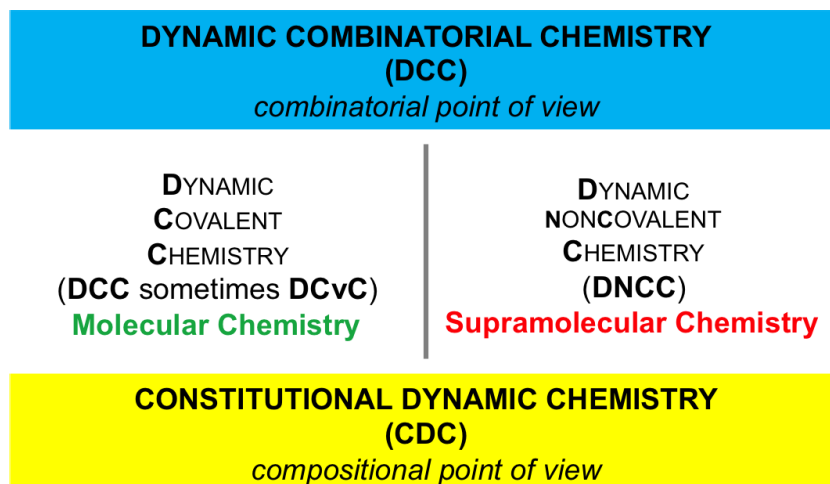


Figure 6. Constitutional dynamic chemistry (CDC) at both molecular and supramolecular level, involving dynamic covalent and supramolecular chemistry for both reversible covalent and non-covalent interactions.⁶²

As noted above, dynamic combinatorial chemistry was first developed by Sanders through macrolactonization¹⁵ and by Lehn through “virtual combinatorial libraries” as well as “dynamic combinatorial libraries (DCLs)” in making the helicates through the self-organization from the mixtures^{13,69} and protein-directed DCC.⁵⁷ The process to generate dynamic diversity resulted in the so-called dynamic combinatorial libraries (DCLs). The following parameters used to describe DCLs are summarized below:⁶¹

- a) *The conversion*, that is, the total amount of constituents generated with respect to the free components.
- b) *The composition*, that is, the distribution or relative amounts of the different constituents that also represents the selectivity of the system.
- c) The product of conversion and selectivity may be considered as defining the *expression of a given constituent*.

The most important feature of DCLs lies in the self-assembly under thermodynamic control. The differences in the thermodynamic stabilities of the constituents (the relative Gibbs free energy) determine the conversion of the components into the constituents, resulting in the final distribution of the DCL. Such a constitutional dynamic library (CDL) or DCL^{70–72} could be illustrated in **Figure 7**. First, the components should be able to form a collection of constituents to generate a CDL via dynamic covalent reactions. Then, the self-organization with

selection will occur on addition of effectors by the specific binding with the fittest constituent (e.g. best binder).⁷³

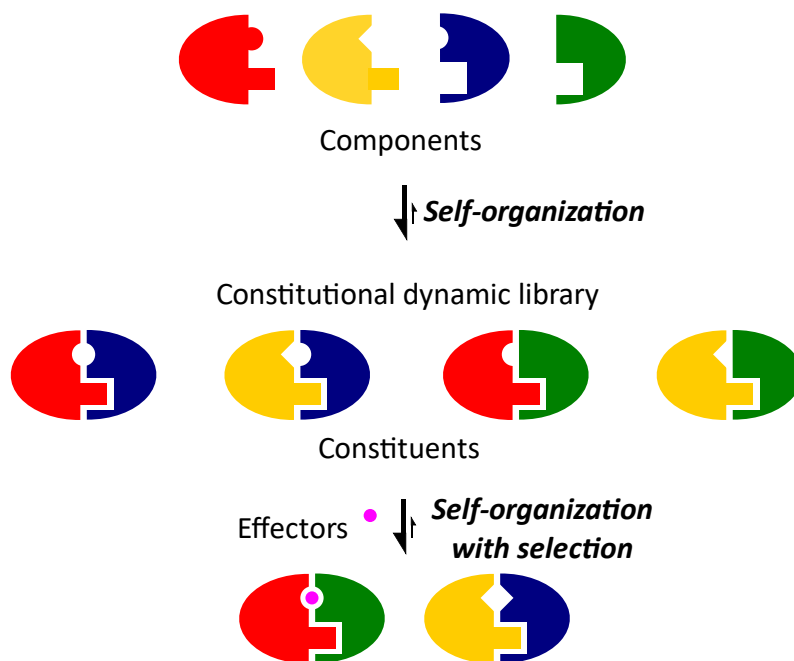


Figure 7. Molecular components spontaneously self-organize into a constitutional dynamic library (CDL) of interconverting supramolecular or molecular constituents. The addition of chemical effectors (perturbation) induces the selective formation of the two constituents providing the best interactions with the effectors.⁷³

The development of the CDC attracted many interests of scientists to explore the use of dynamic covalent bonds to establish DCLs.

A very early example of using transesterification to build up DCLs from macrocycles of esters. Sanders and co-workers developed the DCLs of base-catalyzed transesterification (**Figure 8**). They prepared a series of cholate building blocks. By removal of the methanol from the mixture, the transesterification occurred and led to the formation of macrocycles from the cholic acid under thermodynamic control. They also demonstrated the template effect of metal ions on the generated macrocycles to select the best binder. The reaction was rather slow to reach the equilibrium and only few catalysts were sufficiently active. Afterwards, they developed DCLs of hydrazone formation, further disulfide exchange and studied many DCLs from the exchange of disulfide which proceeded controllable and reversible under mild conditions.^{74–79}

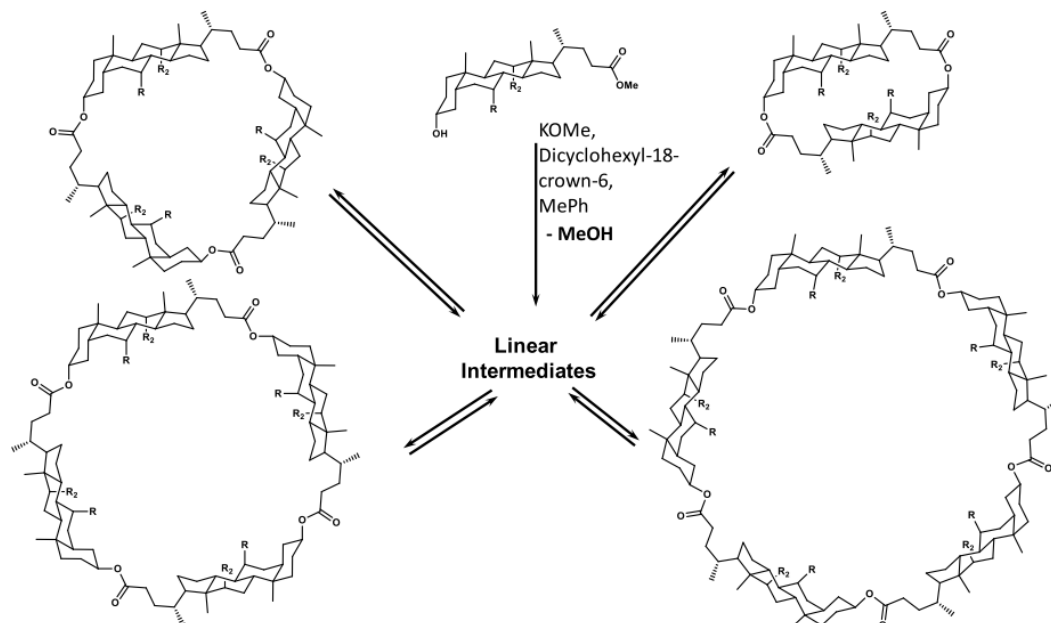


Figure 8. An equilibrium of the dynamic combinatorial library of cyclic steroid oligomers generated from the reversible transesterification.

Lehn and co-workers have also contributed a lot to the development of DCLs. They firstly demonstrated the construction of the DCLs of imines from the components through imine formation (**Figure 9**). Due to the similar structure of one imine to the known inhibitor of carbonic anhydrase, it was found to be selectively amplified from all the possible imine constituents in the DCL on addition of carbonic anhydrase. This work applied the imine constituents into DCLs and indicated the feasibility of imine chemistry for the construction of DCLs due to its fast formation.

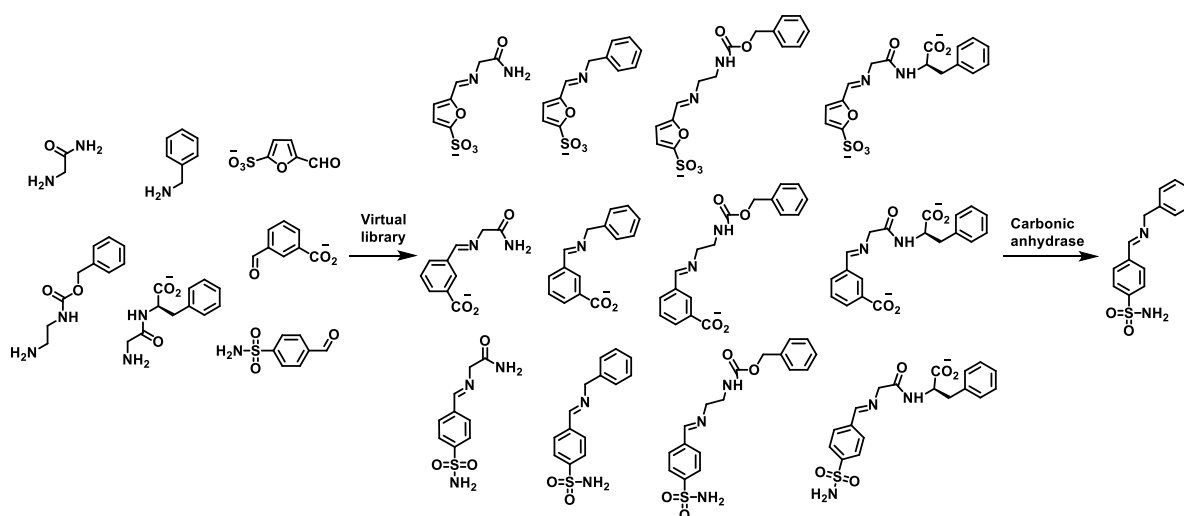


Figure 9. The amplification of the best enzyme inhibitor from the virtual combinatorial library of imine constituents.

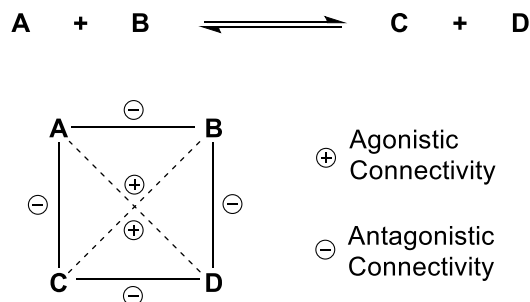
The CDC as well as DCLs underwent a rapid development for their response to different effectors. The response of the effectors resulted in the change of the constitution of the constituents in the DCLs, thus generating adaptation by selecting and amplifying the fittest constituent. A series of dynamic covalent reactions were developed to set up the DCLs. Here, the specific focus for this thesis was on DCLs of imine chemistry. Therefore, other dynamic covalent reactions used for building up DCLs such as aldol formation, Diels-Alder reaction, disulfide formation are not discussed in detail.

2. ADAPTATION IN CONSTITUTIONAL DYNAMIC CHEMISTRY

As mentioned above, CDLs or DCLs are derived from the building blocks which can give rise to multiple library members connected with multiple equilibria through reversible transformations, thus generating diversity. The dynamic transformations involve formation of library members from building blocks, exchange reactions between the library members, and isomerization reactions either covalent or non-covalent, even conformational, if the generated library members are distinguishable from each other. Traditional static chemistry (irreversible) is intended to prepare pure compounds rather than mixtures. The addition of external effectors will lead to the redistribution of the composition of the chemical entities within the system due to the dynamic features of the DCLs. This adaptation behavior of DCLs through the selection and amplification of components leads to the emergence of the higher level of functions such as signal generation, information storage and processing and many other functions.

Constitutional dynamic libraries (CDLs) reflect the dynamic behavior displayed in constitutional changes or variations induced by re-combination of the constituents within a dynamic library under the effect of external factors which initially can be described by the reversible processes between constituents **A**, **B**, **C** and **D**. Originally it was illustrated by the equilibrium between **A** + **B** and **C** + **D** by the reversible equation (top of **Scheme 1**). It was until 2006 Giuseppone and Lehn⁸⁰ proposed for the first time the use of a square graph to represent the relationship of the four constituents **A**, **B**, **C** and **D** in a [2 × 2] DCL (bottom of **Scheme 1**). The constituent **A** shares component with **B** and **C**, so if the concentration of **A** increases, that of **B** and **C** must decrease, they (**A** and **B** or **C**) have antagonistic connectivity where are connected by edges; however, **A** does not share any component with **D**, if the concentration of **A** increases, the concentration of **D** has to increase, thus they (**A** and **D** or **B** and **C**) have the agonistic connectivity, shown by the diagonals. Due to its dynamic features,

the constitution of a DCL can be changed upon exposure to external stimuli, such as temperature, pressure, light, metal cations and active molecules, resulting in a shift of the equilibrium.



Scheme 1. Representation of the connectivities between the constituents **A**, **B**, **C** and **D** of the $[2 \times 2]$ DCL. Antagonists are connected by edges and agonists by the diagonals, the figure was first proposed by Giuseppone and Lehn and it's modified here.⁸⁰

To better establish the $[2 \times 2]$ DCL, It could be presented in **Figure 10** where four components **A**, **A'**, **B** and **B'** could undergo self-organization to generate an equilibrated DCL. The equilibrated DCL in principle should contain four constituents **AB**, **A'B**, **AB'** and **A'B'** with similar composition. This is called statistical distribution. The four constituents have two connectivities: agonistic and antagonistic relationship (see above). On addition of external effectors, the constituent **AB** can bind with the effector to form a fittest product, which will lead to the amplification of its agonist **A'B'**. Adding another effector to interact with **A'B** would induce the amplification of the constituents of **AB'** and **A'B**. This is called enforced distribution.

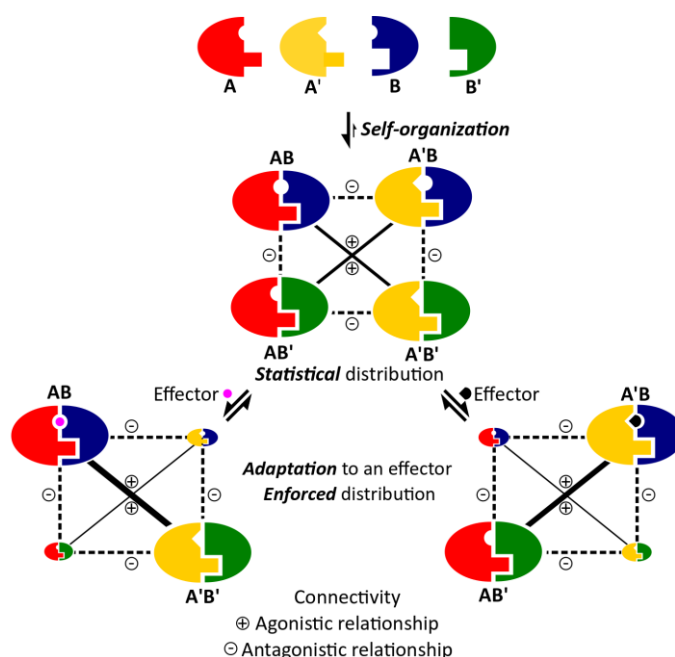


Figure 10. The adaptive behavior of a $[2 \times 2]$ DCL generated from four components on addition of two different effectors.^{65,73}

The effectors that induce the adaptation of DCLs means everything that is not within the DCL but can still affect the composition of the DCL by shifting the equilibrium, such as physical stimuli (light,^{66,81–83} electric field,^{84,85} pressure,⁸⁶ temperature,^{87,88} precipitation⁸⁹ and other purification methods^{49,90–93}) or chemical effectors (metal ions,^{39,40,62,65–67,93–99} the proton,^{87,100–102} active molecules). The specific examples of adaptation of DCLs to different effectors are illustrated selectively in the following in details.

A. Adaptation to light

Light was one of the physical effectors to be employed in DCLs to achieve the adaptation.^{66,67,103,104} It can be used to transform the isomer of one constituent from one configuration to another in the DCL.⁶⁶ Furthermore, the photosensitizer type molecule can be broken to free radicals and formed again in response to light.

One example is that Herder and Lehn⁸³ used sensitized alkoxyamines as “photo-dynamic covalent bonds” because they are stable in the dark at room temperature, while they can dissociate and undergo recombination to the bound state in response to light if there is a photoactive moiety (**Figure 11**). By exploring the photochemical properties of this type of dynamic covalent bond, they found that the nature and efficiency of triplet energy transfer of the sensitizer to the alkoxyamine bond as well as the reversibility of the process depends greatly on the structure of the nitroxide terminus. By screening of the components, they found that dynamic network of a sensitized and a non-sensitized alkoxyamines underwent switching between thermodynamic equilibrium and a kinetically trapped out-of-equilibrium state by temperature variation and photoexcitation. This work is significant for the generation of out-of-equilibrium states of dynamic combinatorial libraries.

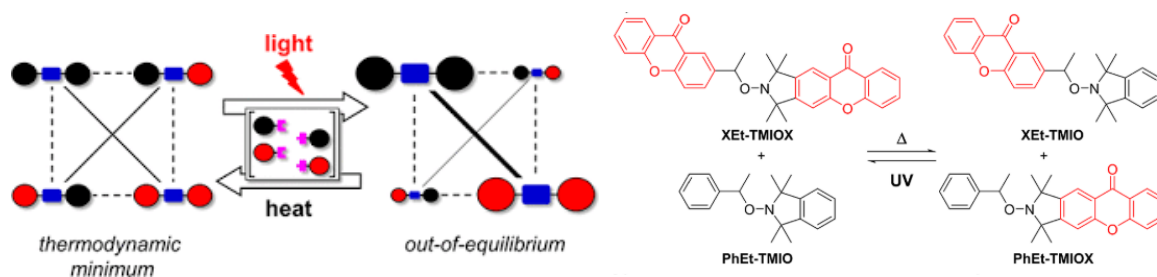


Figure 11. The switching of dynamic covalent reaction network consisting of a sensitized and a non-sensitized photocleavable alkoxyamines between equilibrium and out-of-equilibrium states through Light and heat.⁸³

B. Adaptation to a change of environment

The reaction medium is another important factor for the adaptation behavior of DCLs. By screening the components, the DCL can be set up either in aqueous phase or organic phase and even in multi-phase or mixed solvents. The change of the environment could also induce the adaptive behavior of the DCLs.^{62,64,103}

For example, in 2012, Hafezi and Lehn⁶⁴ established two DCLs of imine constituents in a mixed solvent of acetonitrile/water shown in **Figure 12**. Through screening of the components, one of the two libraries are generated from **1**, **2**, **3** and **4** to form four imines possessing hydrophilic–hydrophilic (**5**), hydrophobic–hydrophobic (**8**), or amphiphilic characteristics (**6** and **7**). The DCL could undergo recombination through component exchange reactions upon phase separation induced by cooling and heating. The phase separation led to amplification of **5** and **8** and down-regulation of **6** and **7**. This adaptive process indicated that the constitution of a DCL can also be changed by a phase change, laying a foundation to development of new effectors for constitution change of a DCL.

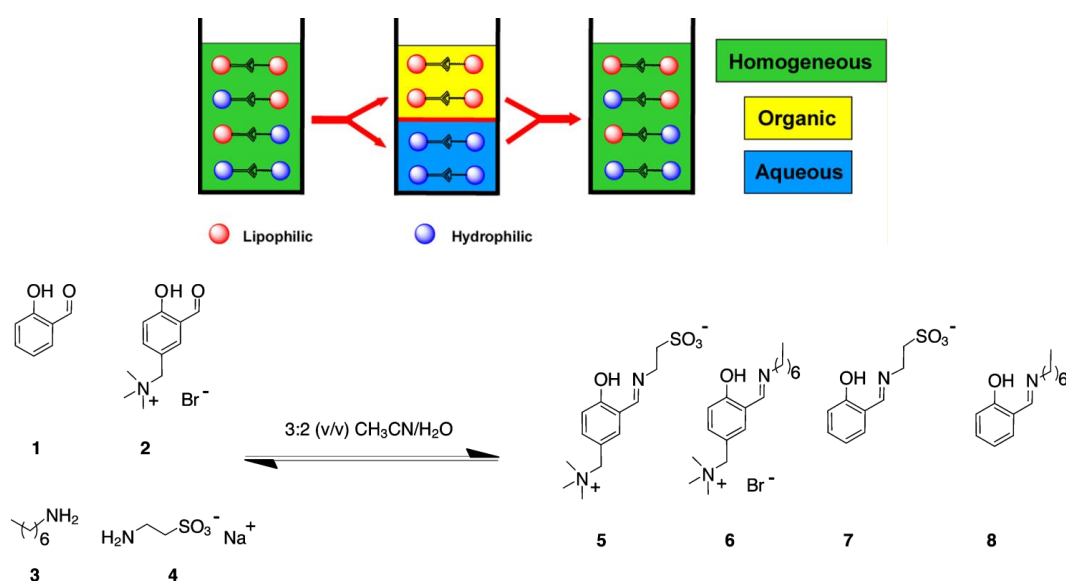


Figure 12. Dynamic covalent library of imines **5-8** generated by reaction of the biogenic amines **1** and **2** with the aldehydes **3** and **4**.

C. Adaptation to metal ions

Metal ions are one of the most common chemical effectors by coordination to donor atoms within the library constituents. So far, many CDLs have been constructed to achieve the adaptation and amplification of the specific constituent which binds the best with metal ions. The metal ions have been combined with other effectors such as light or reaction medium or

even two or three metal ions together to obtain multiple adaptation through addition of different effectors into the CDLs.

One good example of the adaptation to both metal ion and light irradiation of the CDL came from the work of Vantomme and Lehn in 2012.⁶⁶ They reported a CDL of acylhydrazones generated from two aldehydes (^1A , ^2A) and two hydrazides (^1C , ^3C) (**Figure 13**). The set of hydrazones underwent metalloselection on addition of Zn(II), driving the amplification of $\text{Zn}(\text{}^1\text{A}^3\text{C})_2$. While upon irradiation to the system, it caused photoisomerization of $\text{E-}^1\text{A}^1\text{C}$ into $\text{Z-}^1\text{A}^1\text{C}$ with amplification of the latter. Thus, this CDL underwent orthogonal dual adaptation via component exchange in response to two external effectors: metal cation (a chemical effector) and light (a physical stimulus). This paves a way to the development of information storage and processing system through multiple adaptation behavior.

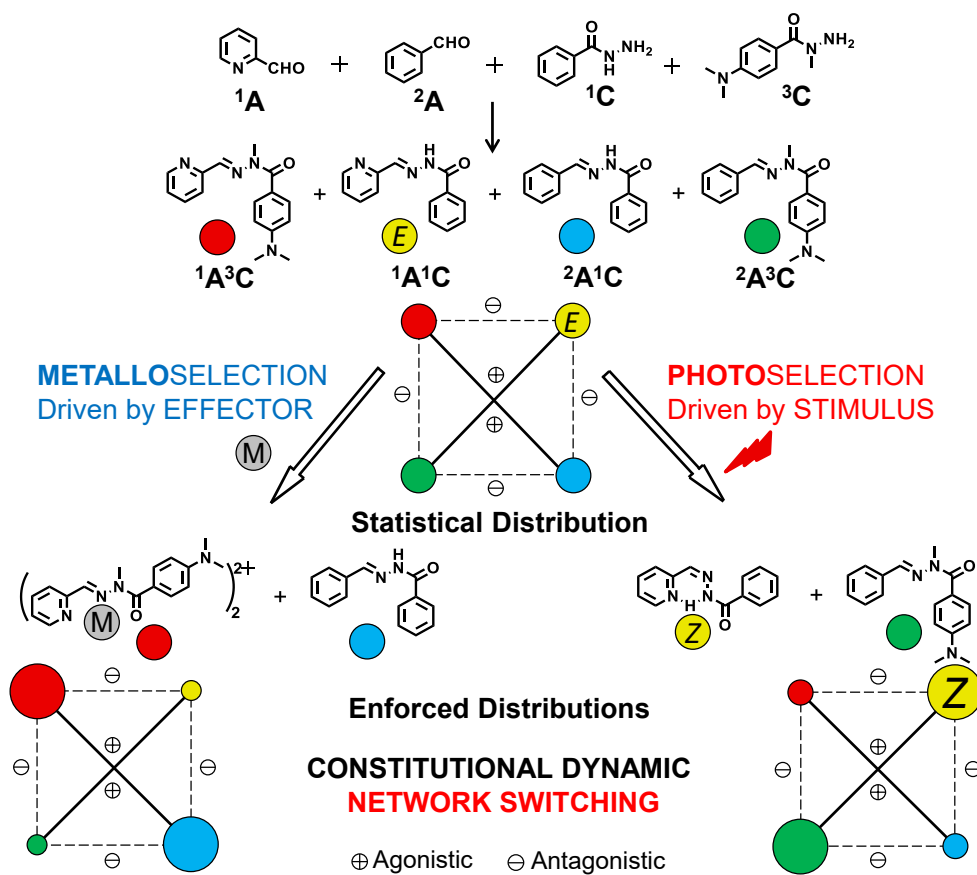


Figure 13. Adaptation of the $[2 \times 2]$ DCL of four constituents $\text{E-}^1\text{A}^1\text{C}$, $^1\text{A}^3\text{C}$, $^2\text{A}^1\text{C}$, and $^2\text{A}^3\text{C}$ by variation of the distributions under (left) metalloselection on addition of zinc(II) and (right) photoselection by photoisomerization of $\text{E-}^1\text{A}^1\text{C}$ into $\text{Z-}^1\text{A}^1\text{C}$ on light irradiation.

Very recently, Ayme and Lehn⁹⁹ reported the parallel selective self-assembly of three complexes of imine type compounds through the self-sorting of a CDL from 3 aldehydes (**2**, **4**

and **5**), 3 amines (**1**, **3** and **6**) and three metal cations Fe(II), Cu(I) and Zn(II) cations (**Figure 14**) in the mixed solvents of CD₃CN/CDCl₃ (4:1). The highly selective self-sorting process of this complicated system can be attributed to the strong differences in the coordination numbers and geometries of the three metals, where Cu(I) has a coordination number of **4**, Zn(II) prefers **5** and Fe(II) favors **6** in this system. The study of the subsystems of the four components **1**, **2**, **5** and **6** in the presence of two metal ions Fe(II) and Zn(II) indicated the formation of the kinetic product [Zn(**1**, **2**)₂]²⁺, which appeared at the beginning and then slowly decreased to form the thermodynamic product [Zn(**5**, **6**)₂]²⁺ and [Fe(**1**, **2**)₂]²⁺. This work demonstrated that a simpler output could be generated through the self-sorting of systems with high complexity by screening of the components and metal ions. And it is important to note that kinetic trapped molecules may be generated in the multiple complex system.

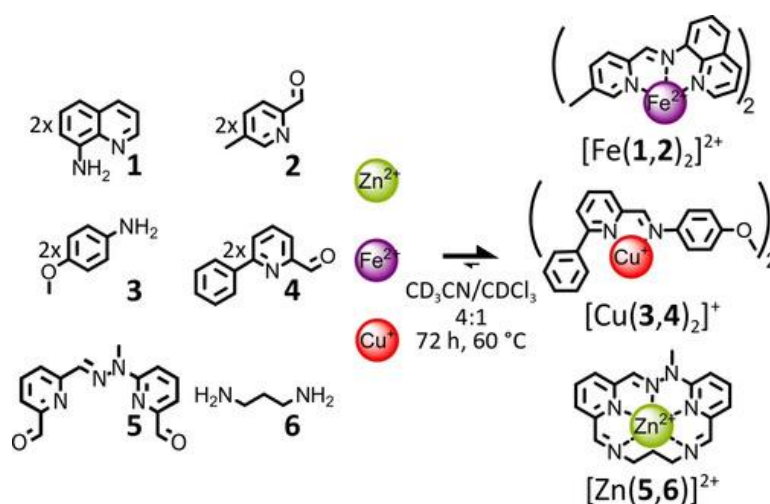


Figure 14. The concomitant formation of complexes [Fe(**1,2**)₂]²⁺, [Cu(**3,4**)₂]⁺, and [Zn(**5,6**)₂]²⁺ through the hetero-self-sorting of their initial reactants.⁹⁹

D. Adaptation to morphological change

A special case of the adaptation was that DCLs can also adapt to the shape switching of the molecules from one configuration to another one in response to the effector.

For instance, Ulrich, Vantomme and Lehn³⁹ reported the use of light and metal cation as the stimuli to trigger the change of the molecular morphology thus leading to the constitution selection in dynamic systems (**Figure 15**). The W-shaped dialdehyde underwent polycondensation with a diamine to form a linear polymer. When the dialdehyde was bound to a metal cation, its configuration changed from W-shape to U-shape to hold the two aldehydes closer to each other, thus favoring the formation of a macrocycle when reacting with a diamine. Thus, this system displayed reversible switching between macrocycle and polymer states upon

addition and removal of metal cations. Moreover, the illumination also induced the shape switching from W to U with the switching of the isomer from E to Z due to the formation of the hydrogen bond.

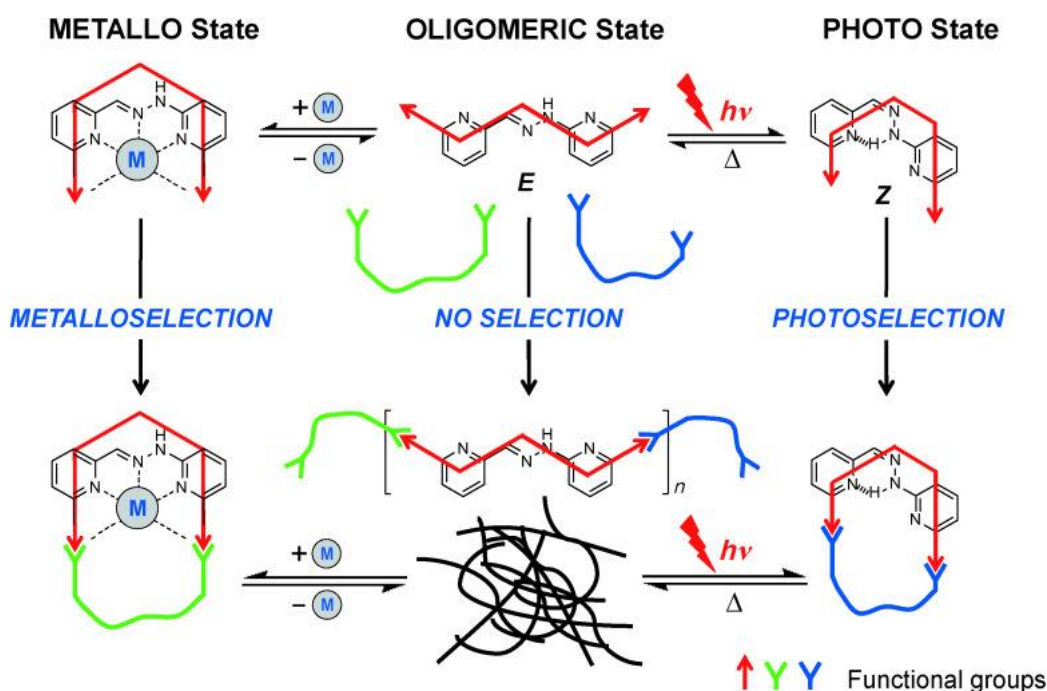


Figure 15. The switching process between a polymer and a metallomacrocycle on interconversion of ligands component between “W” and “U” shapes through binding and removal of a metal ion.³⁹

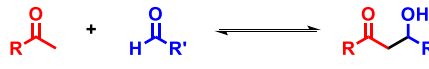
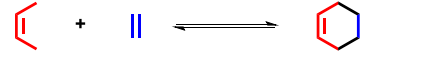
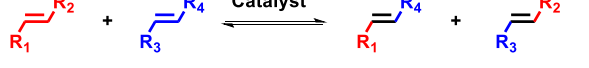
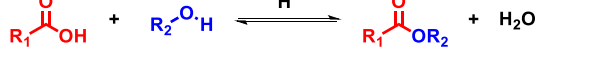
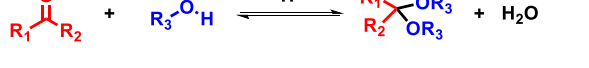
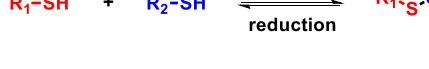
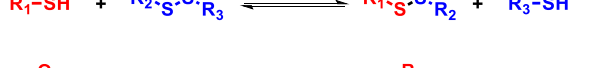

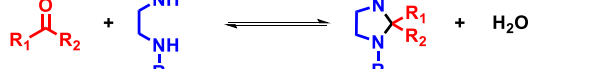
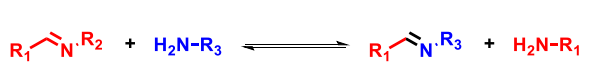
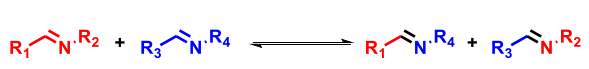
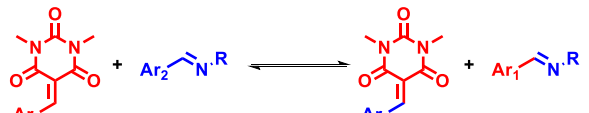
These examples illustrated the adaptation of the DCLs build from the dynamic covalent chemistry in response to the external effectors. Among the dynamic covalent reactions, C=N formation was widely applied in building up DCLs. This prompted the chemists to develop more efficient catalysts to further accelerate dynamic covalent reactions of C=N compounds including C=N formation, transimination, and imine metathesis.

3. DYNAMIC COVALENT REACTIONS USING C=N COMPOUNDS

Dynamic covalent chemistry involves the chemistry of dynamic covalent reactions (DCRs), through which the different constituents could exchange their components with each other. There are currently two main types: the first is formation of dynamic covalent bonds including condensation and addition reactions; the second is exchange reactions of dynamic covalent bonds that include exchange of components from one compound to another, resulting in the recombination and formation of new compounds. The current dynamic covalent reactions

commonly used in DCC are illustrated in **Table 2**. Here, this thesis is mainly focused on the imine chemistry.

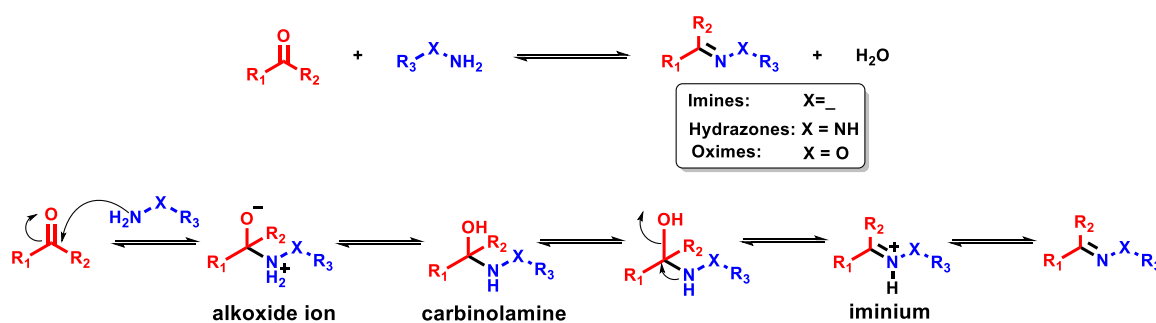
Table 2. The dynamic covalent reactions used in DCC.

Bond type	Reactions	Structure	References
	Aldol formation		105–107
Dynamic C-C bond	Diels-Alder reaction		108–110
	Olefin metathesis		111
Dynamic C-O bond	Ester formation/exchange		15,112,113
	Acetal formation/exchange		114–117
Dynamic S-S bond	Disulfide formation		118–121
	Disulfide exchange		122,123
	C=N formation		124–127
Dynamic C-N bond	Aminal formation		128–130
	Transamination		131–133
	Imine metathesis		67,134–136
	Knoevenagel exchange		137–140

For dynamic C-N bond, it includes: (i) C=N formation; (ii) transamination; (iii) imine metathesis. The mechanism as well as the catalysis of the reactions were discussed in the following in details.

A. C=N bond formation

The C=N (imine, hydrazone, acylhydrazone and oxime) bond formation is one of the most widely used reversible reactions in dynamic covalent chemistry.^{46,127,141–143} It is generally formed from the condensation of an aldehyde and a primary amine, hydrazine, hydrazide or alkoxyamine. When X equals $_$, it is an imine; when X equals NH, it is a hydrazone; when X equals O, it is an oxime. While in the absence of the catalyst, the mechanism includes two important steps: one is nucleophilic attack of the aldehyde by amino group (addition); the other is the removal of water (elimination). So far, the general accepted details of the step by step mechanism are shown in **Scheme 2**.¹⁴⁴ The first step is the nucleophilic attack of the amine on carbonyl group to generate alkoxide ion; after proton transfer, the carbinolamine formed; the next step is removal of hydroxy group to generate iminium ion; the last step is deprotonation of iminium ion to form the final product imine.



Scheme 2. The reversible formation of imines, hydrazones and oxime by the condensation reaction of carbonyl compounds with amine derivatives and the mechanism.

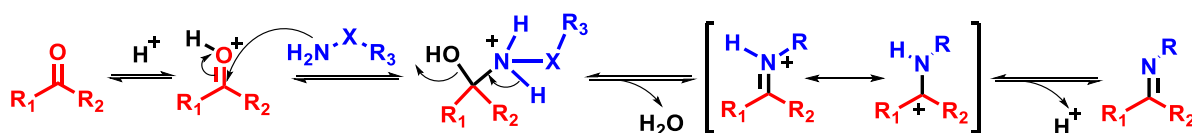
As described above, the reaction of an aldehyde or a ketone with a primary amine is reversible. The presence of water favors the reverse reaction. Due to this dynamic feature, the original method was to use azeotropic distillation by Dean-Stark apparatus to push the reaction towards imine formation. Other studies are devoted to the synthesis of imines through addition of catalysts instead of studying the kinetics in the presence of catalysts. In 1971, Westheim¹⁴⁵ reported that the synthesis of ketimines and enamines is catalyzed by molecular sieves. They calculated that the half-time for the reaction of aniline and acetophenone in the presence of molecular sieves is about 15 min, while in the absence of molecular sieves or other catalysts, the reaction is very slow, with no detectable formation of ketamine in 50 h. Here, the absorbance of water greatly accelerated the kinetics of imine formation. The catalysts included nucleophilic catalysts such as pyrrolidine through iminium activation, metal salts and oxides: P_2O_5/Al_2O_3 ,¹⁴⁶

Nano-tubeTiO₂,¹⁴⁷ CeCl₃•H₂O,¹⁴⁸ Cu(NO₃)₂,⁷⁰ Er(OTf)₃,¹⁴⁹ ZnCl₂,¹⁵⁰ Mg(ClO₄)₂,¹⁵⁰ MgSO₄•Mg(ClO₄)₂,¹⁵⁰ TiCl₄,^[112] and some dehydrate reagents e.g. molecular sieves,¹⁴⁵ CuSO₄¹⁵¹ and even dehydrating solvents such as trimethyl orthoformate.¹⁵² Among these, the Lewis acids activated the nucleophilic attack of the imine on the carbonyl group, while the dehydrating reagents facilitated the removal of water.

Except the synthesis of imines, extensive research has been devoted to exploring the kinetics and mechanism of imine formation and hydrolysis (the reverse reaction) in aqueous phases.^{153–155} Given passage through the two steps of addition followed by elimination, formation can be accelerated by catalysis of either one or both steps. This has led to the identification of a wide variety of catalysts including Brønsted acids,^{156,157} metal salts, aniline and some aniline derivatives,^{132,158,159} secondary amine like pyrrolidine and its derivatives,^{160,161} and amine buffers etc.¹⁶²

i. Acid catalysis

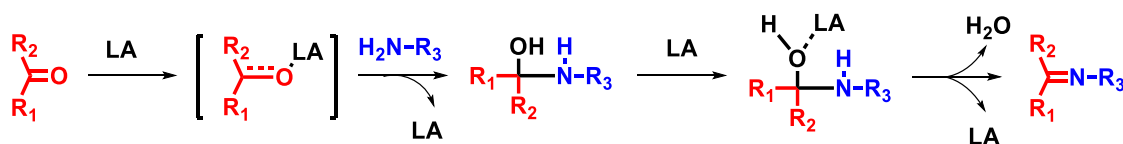
The study of the hydrolysis of Schiff base indicated the susceptibility of this reaction to specific acid catalysis. Willi suggested the addition of water to the imine was rate-determining at neutral pH,¹⁶³ while Kastening et al. obtained the contradictory results which showed the decomposition of carbinolamine was rate-determining.¹⁶⁴ Then Jencks studied the semicarbazone formation at different pH conditions and found that there was a transition of the rate-determining step at neutral pH (water addition) and at acidic conditions (carbinolamine decomposition).^{165,166} Subsequently, after systematically study of Schiff base formation in the presence of different acids as catalysts, they found that a similar result for Schiff base formation. The rate-determining step for Schiff base formation underwent a transition from dehydration of the carbinolamine addition product at neutral pH to amine attack on the carbonyl under acidic conditions. The acid catalysed mechanism of imine formation is shown in **Scheme 3**.



Scheme 3. The imine formation in the presence of Brønsted acid as a catalyst.

ii. Metal ion catalysis

With the discovery of Schiff base by Hugo Schiff, he also studied the catalysis effect of metal ions on this reaction.¹²⁴ In 2004, Chakraborti¹⁵⁰ reported magnesium perchlorate to be an efficient catalyst for the synthesis of imines and hydrazones. As for some other Lewis acid catalysts such as $ZnCl_2$, $TiCl_4$, $CuSO_4 \cdot 5H_2O$ and $Sc(OTf)_3$, the same amount of $Mg(ClO_4)_2$ (5 mol%) accelerated the condensation of less electrophilic carbonyl compounds with poorly nucleophilic amines in dichloroethane (DCE) to give the imines in excellent yields and in short times at room temperature. These results indicated that Lewis acids especially $Mg(ClO_4)_2$ could greatly accelerate the imine formation which activated the nucleophilic attack on the carbonyl group as well as the dehydrating of water. They proposed the mechanism shown in **Scheme 4**.



Scheme 4. The imine formation in the presence of Lewis acid as a catalyst.

iii. Organic amine catalysis

Except acid and metal ion catalysis, the formation of hydrazone and oxime can also be catalyzed by organic amines. Jencks first reported the nucleophilic catalysis of semicarbazone formation by aniline.¹⁵⁹ They demonstrated that the rate-determining step for the semicarbazone formation was the formation of the Schiff base. Dawson and co-workers^{132,167} reported that oxime and hydrazone formation from two unprotected peptide derivatives were both significantly accelerated by using aniline as a catalyst at pH 5.7 (**Figure 16**). The aqueous solubility and otherwise unreactive nature of aniline and derivatives allows for a wide application of this nucleophilic catalysis in bioconjugation and cellular labelling. The possible mechanism for organic amine as nucleophilic catalyst is illustrated in **Scheme 5**.

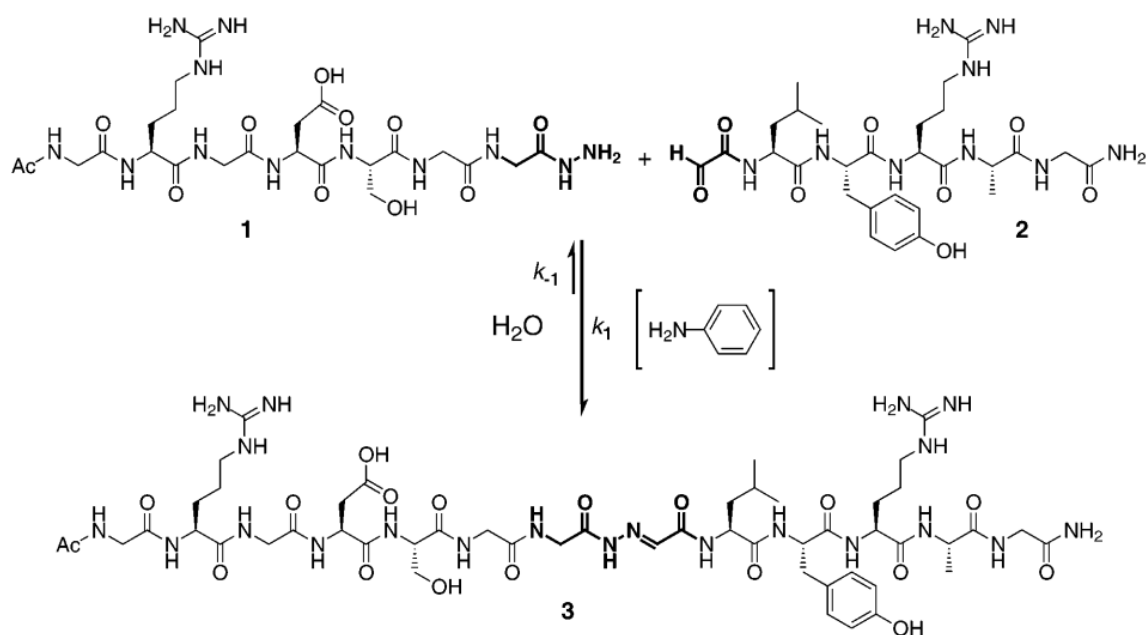
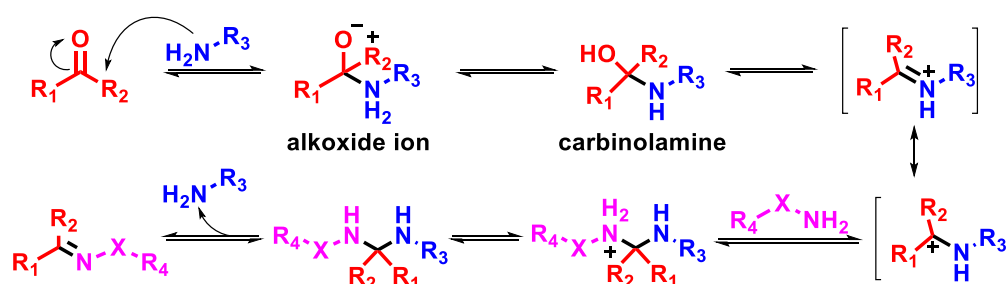


Figure 16. Hydrazone reaction of AcGRGDSGG-Hydrazide **1** and Glyoxylyl-LYRAG **2** in the absence or presence of aniline to form the acylhydrazone **3**.



Scheme 5. The hydrazone (or oxime) formation in the presence of aniline as a catalyst.

Despite the acceleration of imine formation by addition of catalysts, Kool and co-workers^{127,162,168–171} explored structural effects in both aldehydes and amines and developed a series of water soluble and less toxic catalysts for the acceleration of oxime and hydrazone formation in water. Anilines with ortho-proton donors such as carboxylic acid or phosphonic acid groups were shown to give considerable rate enhancements over aniline itself in both hydrazone and oxime formation. This was interpreted as evidence that nucleophilic catalysis is combined with general acid/base catalysis in these cases.

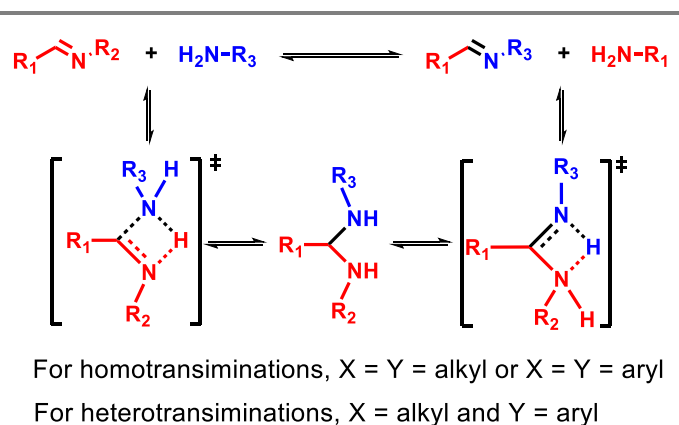
In a summary, the catalysts for C=N formation developed up to now was listed in **Table 3** including both the catalysts for imine synthesis in organic solvents and the acceleration of the kinetics of C=N formation in aqueous phase.

Table 3. catalysis of C=N bond formation (imine, hydrazone, oxime)

Bond type	Catalysts	References
C=N formation (imine, oxime, hydrazone)	acid	156
	aniline and aniline derivatives	159,172–178
	5-aminoindole, 2,4-	179
	Aqueous phase dimethoxyaniline	180,181
	phenylenediamine	157,182
	anthranilic acid	162
	amine buffer	183
	metal salts	150
	pyrrolidine	160,184
	acid	63,185
	Organic phase P ₂ O ₅ /Al ₂ O ₃	146
	molecular sieves	145
	CuSO ₄	151
	trimethyl orthoformate	152

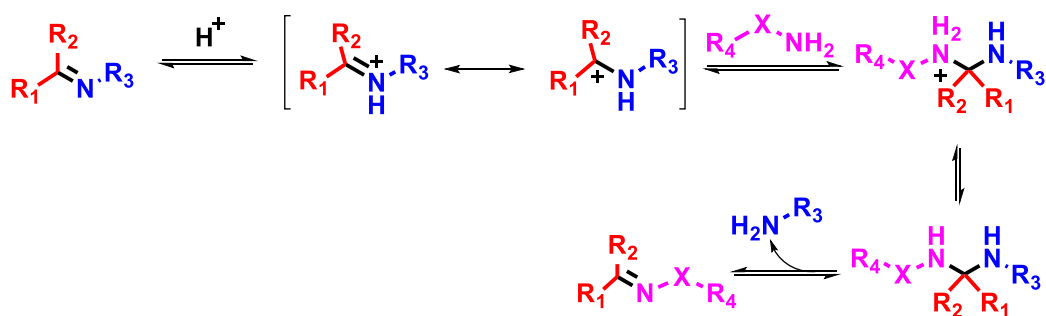
B. Transimination reaction

Transimination occurs originally in the reaction of an amino acid with the imine formed from pyridoxal phosphate and ϵ -amino of lysine in the enzyme. The mechanism was very complicated in enzymatic reactions. For a non-enzymatic transimination, it involves an exchange reaction of an imine with an amine to form another pair of imine and amine.¹⁸⁶ This exchange reaction can occur without breaking the C=N bond to form the carbonyl compound and amine where two protons are removed from the attacking amine and added to the leaving amine (Scheme 6). This reaction proceeds in a two-step pathway involving a gem-diamine as the intermediate: a) the amine directly serves as a nucleophile to attack the imine, and then the other imine is formed by eliminating the original amine.

**Scheme 6.** The general mechanism of transimination.¹⁸⁷

i. Acid catalysis

In 1964, Cordes and co-workers¹⁸⁸ studied the mechanism of hydrolysis and aminolysis (transamination) of Schiff bases with different substituents on the hydroxylamine at different pH in buffers (carbonate, borate, phosphate acetate and chloroacetate). In addition, the aminolysis reaction was very similar to hydrolysis reaction, both of which are subject to general base catalysis which involve the attack of the nucleophilic reagents or amines in the rate-determining step. They indicated that the reaction of substituted benzaldehyde semicarbazones with hydroxylamine are dependent upon acid catalysis. Furthermore, in 1977 Jencks demonstrated the acceleration of the kinetics of the transamination reaction of *N*-*p*-methoxybenzylidenepyrrolidium cation and hydroxylamine by buffer acids and bases. The proposed transamination is shown in **Scheme 7**. The catalysis by acids and base was due to the trapping of the initial cationic addition intermediate by proton transfer. In addition, acids were also used to catalyze transamination in the work of Giuseppone and Lehn⁸⁷ for changing the constitution of the DCL by using CF₃COOD as catalyst and in the work of Armao and Lehn¹⁰⁰ by demonstrating the faster component exchange between the constituent species rather than their formation from the components in the presence of DCl as a catalyst.



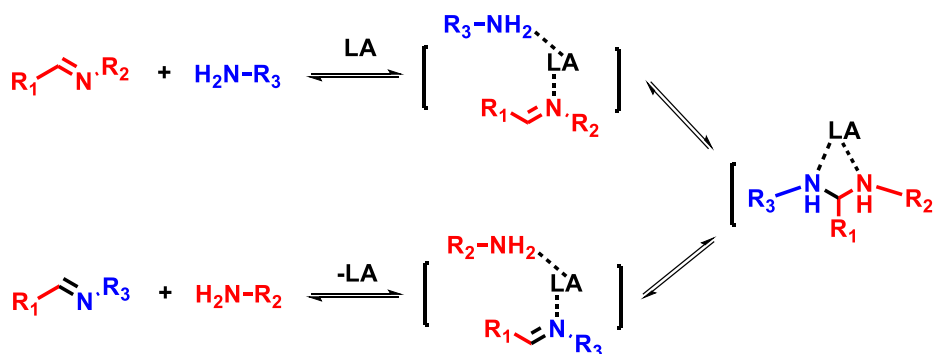
Scheme 7. The general mechanism of transamination in the presence of an acid as a catalyst.^{189,190}

ii. Metal ion catalysis

Boate and co-workers¹⁹¹ reported the efficient catalysis of transamination by metal complexes of thiourea with the exchange of an imine with aniline, while it was inhibited by excess of thiourea and by chelating ligands. In the absence of the catalysts, there was no exchange at room temperature.

Chen and Chu¹⁹² reported the catalysis of transamination with ionic liquid as a catalyst due to its weak Lewis acidity. The presence of the ionic liquid lead to about 100-fold rate enhancement of the transamination. The addition of Sc(OTf)₃ further accelerated the

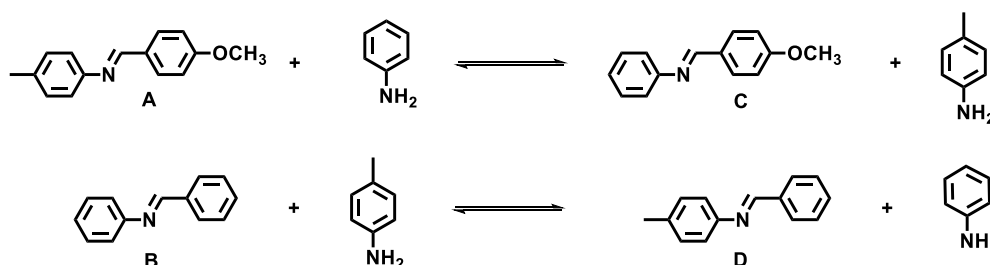
transiminations. The proposed mechanistic hypothesis is shown in **Scheme 8**. These results indicated that the metal ions could coordinate with the imine and thus activating the electrophilicity of the imine, resulting in the increased stabilization of the polar, charged intermediate. This led to the rapid transimination.



Scheme 8. A mechanistic hypothesis for the transimination reaction catalyzed by a Lewis acid (LA).

In 2012, Giuseppone and Lehn¹³¹ reported the efficient catalysis of transimination reaction of various types of C=N bonds in organic solvent by using scandium triflate. Sc(OTf)₃ was acting as a Lewis acid and resulted in the acceleration factor of up to 6×10^5 , with the turnovers up to 3600 h⁻¹. Through analyzing the rates and the distribution of the reaction at equilibrium, the mechanism was proposed by the formation of a ternary intermediate where Sc(III) was simultaneously coordinated to amine and imine (as well as solvent) molecules.

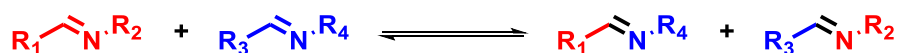
Di Stefano and co-workers¹⁸⁷ reported the fast transimination between aromatic-aromatic or aromatic-aliphatic amines in the absence of catalysts (**Scheme 9**). They carried out a quantitative investigation of rates of amine–imine exchange reactions from primary amines with their benzylidene derivatives in organic solvents at room temperature. The results laid the foundation for the construction of dynamic combinatorial libraries through imine exchange in organic solvents without adding acid or metal salts as catalysts.



Scheme 9. Transimination reactions between **A** and **C**; **B** and **D**.

C. Imine metathesis

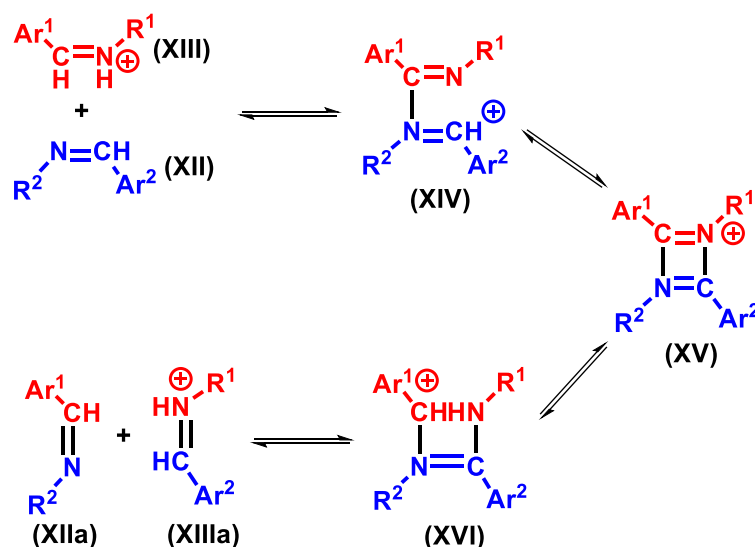
Olefin metathesis proceeds through component exchange between olefins. Similarly, an imine can also react with another imine through exchanging their amino fragment and carbonyl component at the same time, being an imine exchange or imine metathesis reaction (**Scheme 10**). Unlike imine formation and transimination, imine metathesis does not proceed in the absence of a catalyst. So far, there is not a real (associative) imine metathesis. The mechanism of imine metathesis differs depending on the catalysts: acid catalysis, metal salts catalysis and organic amine catalysis.



Scheme 10. The reversible exchange of two imines

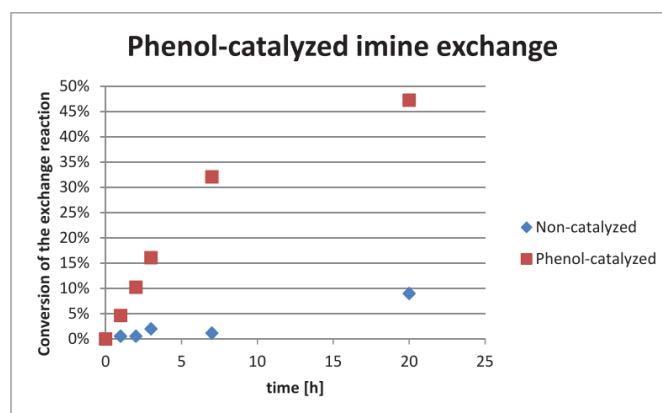
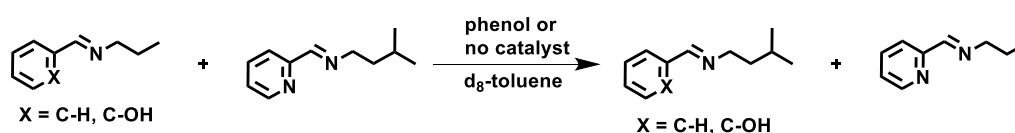
i. Acid catalysis

In 1920s, Ingold and Piggot¹⁹³ proposed the one-step formation of a dimeric intermediate with a 1,3-diazetidene structure for the mechanism. Later Taylor and Buntrock¹⁹⁴ proved that this assumption is incompatible with the orbital symmetry and they isolated methylenedianil intermediates with a trimeric structure. Then in 1974 Messmer and co-workers¹⁹⁵ reconducted the experiments and studied the kinetics using ¹H NMR spectroscopy. They found that the imine exchange reaction proceeds by a stepwise mechanism involving the formation of an ionic intermediate. One imine is protonated in the presence of acid and then attacked by the other imine in its neutral form to give an addition product which, after cyclisation and proton transfer, undergoes elimination to give the exchanged imines. Either the absence or an excess of acid leads to no reaction. The mechanism proposed for imine exchange is shown in **Scheme 11** with acid as catalyst.¹³⁴



Scheme 11. The general mechanism of acid catalysis of imine metathesis.

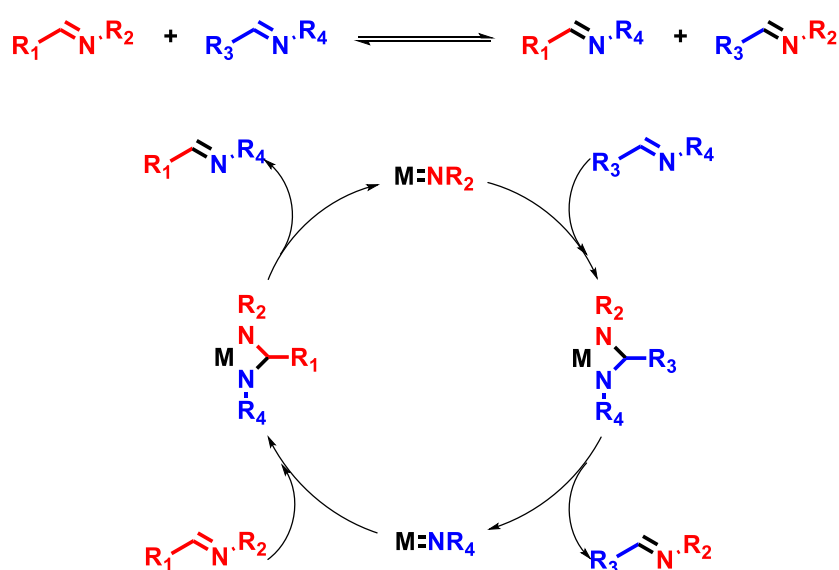
Similar acid catalysis of imine metathesis was developed by Kovaříček and Lehn through addition of phenol serving as the weak acid.¹⁹⁶ They studied the transamination in the absence of phenol and in the presence of 1 equiv. of phenol as catalyst (**Scheme 12**). They found that the imine metathesis was very slow in the absence of catalysts, giving only 10% conversion after 20 hours. While in the presence of 1 equiv. of phenol, the reaction was significantly accelerated. After the same time, the conversion reached equilibrium (47%). The catalysis was due to the acidity of phenolic OH.



Scheme 12. The catalysis of imine metathesis with 1 equiv. of phenol as catalyst in comparison to that in the absence of catalyst.

ii. Metal ion catalysis

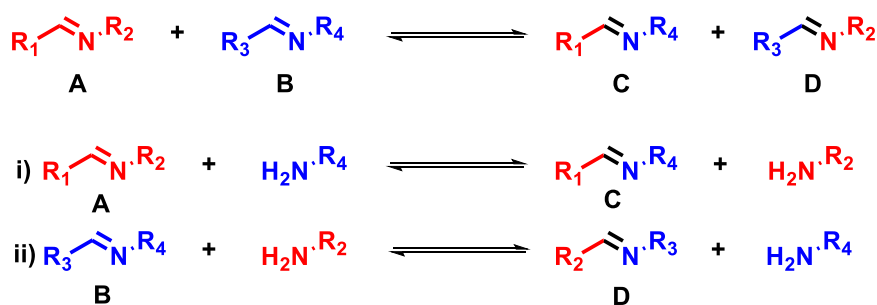
Many efforts have also been devoted to the catalysis of imine metathesis by metal ions, the accepted mechanism being shown in **Scheme 13**.^{135,136} Bergman and co-workers¹⁹⁷ studied the reaction of $\text{Cp}_2\text{Zr}(=\text{N}-t\text{-Bu})(\text{THF})$ with N-phenyl imines to give diazametallacycles through [2 + 2] addition and the addition product could undergo exchange with external imines. This complex is very reactive, and its formation can be inhibited by high concentrations of imines while it is easily deactivated by irreversible dimerization. Meyer and co-workers¹³⁶ reported a new class of bis(imide) complexes $(\text{DME})\text{Cl}_2\text{Mo}(=\text{NR})_2$, initially prepared by Schrock and co-workers¹⁹⁸ which react with an imine to give mixed bis(imide) complexes and a new imine.



Scheme 13. The mechanism of imine metathesis in the presence of transition metal salts as catalysts.^[60]

iii. Organic amine catalysis

For reaction using an organic amine as a nucleophilic catalyst, another mechanism called amine-mediated metathesis has been proposed. It occurs between imine reactants with a sufficient quantity of an amine added to cause transimination reactions. Di Stefano and co-workers¹⁸⁷ have described such reactions for amines (either aromatic or aliphatic) in organic solvents. The amine released in a first step then can undergo transimination with the other imine and so on (**Scheme 14**).



Scheme 14. The mechanism of imine metathesis in the presence of an amine as a catalyst.¹⁸⁷

Thus, the reversible formation of C=N bonds and C/N component exchange reactions can proceed under very mild conditions in the presence of catalysts, indicating a great potential for the construction of dynamic covalent libraries and networks. Moreover, the imine formation in aqueous phase has been extensively studied. It is not only important for the study of the kinetics and mechanism of the reaction, but also for the development of applications in biological processes, especially the modification and influencing proteins folding, such as histones to achieve the regulation of gene expression.

CHAPTER II. CATALYSIS OF IMINE AND HYDRAZONE FORMATION

1. INTRODUCTION

In Chapter I, we described dynamic covalent reactions, especially those based on the formation of the C=N bond. This is a reaction which is considered to pass through two critical steps: (i) nucleophilic addition of an amine to a carbonyl group to give a tetrahedral intermediate and (ii) elimination of water from this intermediate. It is a reversible reaction and many catalysts such as aniline and some aniline derivatives,^{132,157,159,169,174,199–202} protonic acids,^{63,101,156} molecular sieves,^{145,203} metal salts such as ZnCl₂,²⁰⁴ TiCl₄,^{205–207} CeCl₃,¹⁴⁸ MgSO₄-PPTS (PPTS = pyridinium *p*-toluenesulfonate),²⁰⁸ CuSO₄,¹⁵¹ montmorillonite clay K-10 under microwave irradiation,²⁰⁹ and Mg(ClO₄)₂¹⁵⁰ have been developed to accelerate one or both of these steps. Since a catalyst does not change the position of an equilibrium, acceleration of the forward steps must be accompanied by acceleration of the reverse processes, so that catalysis is a means of converting a simple reversible reaction into one that is dynamic. Practical applications of accelerated imine formation include protein ligation in aqueous solution^{175,176,210,211} and synthesis of both C=N compounds and their complexes²¹² as well as building up constitutional dynamic libraries and networks in organic solvents.^{15–23} Studies of the kinetics and catalysis of C=N formation in organic phases are of rather limited extent.²¹³

Based on the assumption that an electron withdrawing substituent would increase the electrophilicity of the carbonyl group, pyridyl-aldehyde derivatives were chosen, because the carbonyl group can be activated not only by electron withdrawing groups due to the pyridyl unit alone but further by protonation of the pyridine-N as well as by metal cation coordination to the carbonyl-O (aided by that to pyridine-N).²¹⁴ The sensitivity of ¹H NMR spectroscopy made it the preferred method for following the reactions but of course limited the choice of metal ions, at least initially, to diamagnetic species, the metal cations Ag(I) and Zn(II) therefore being selected to study their catalysis of C=N formation. Although both these cations can have various coordination numbers,²¹⁵ generally, Ag(I) prefers to form tetrahedral, 4-coordinate complexes with bidentate imines of composition ML₂,²¹⁶ while Zn(II) can expand its coordination number to 6 in octahedral ML₃ species where L is bidentate or ML₂ species where L is tridentate.^{65,66,217} The aldehydes and amino-compounds chosen for our work were therefore

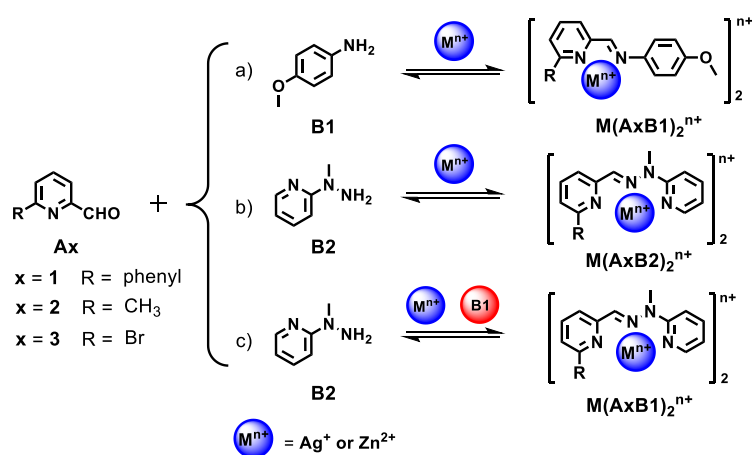
intended to give rise to imines in which the imine-N would be part of either bi- or tri-dentate donor units. Under the reaction conditions employed in acetonitrile solvent, we assumed, on the basis of known equilibrium constants for similar N-donor ligands,²¹⁸ that when either metal ion was present all imine present would be bound in a complex which might have the form $ML(CH_3CN)_n^{x+}$ early in the reaction but which would ultimately attain the form ML_2 . Given the lability of both Ag(I) and Zn(II),²¹⁹ it was expected that formation of the complexes would be effectively instantaneous once the ligand had formed, *i.e.* that the rate of formation of the complexes would not affect the overall rate of the reaction, which would be limited by that of imine formation. Although the reactions in the presence of Ag(I) or Zn(II) were studied under stoichiometric and not catalytic conditions and thus amounted to observations of the rate of formation of the metal ion complexes, comparison of their rates with those of the corresponding reactions without added metal ions enabled it to be judged as to whether or not the metal ion acted as a catalyst of the imine formation.

As noted above, the mechanism proposed for imine formation involves nucleophilic addition of the amine to the carbonyl-C to give a carbinolamine intermediate which must eliminate water to give the imine. Proton transfer processes must intervene to produce this elimination but it is not clear that they are identical in both water and organic solvents.^{32,33} In no case in the present work was any evidence obtained for the presumed carbinolamine intermediate attaining detectable concentrations, indicating that addition, not elimination, was the rate-determining step. Therefore, the results of our work on the kinetics of C=N formation and its catalysis by metal salts and an auxiliary amine in acetonitrile solvent have been interpreted on this basis. The details of these investigations follow.

2. RESULTS AND DISCUSSIONS

A set of three pyridine aldehydes and two compounds bearing an amino group: phenyl (**A1**), methyl (**A2**), bromo (**A3**)-substituted 2-pyridyl aldehyde and **B1** (p-anisidine) or **B2** (*N*-methyl pyridine hydrazine) were selected to study the acceleration of C=N bond formation as shown in **Scheme 15**. The reactions were typically performed with the aldehyde and amino compound in a 1:1 ratio and at moderate concentrations (~0.01 M) to have fast reaction rates and in reactions with catalysis the amine was added in an equimolar amount while the metal ions were added in half-molar amounts assuming that the reaction product would be the ML_2 complex and that this complexation would drive the reactions to completion. To verify the

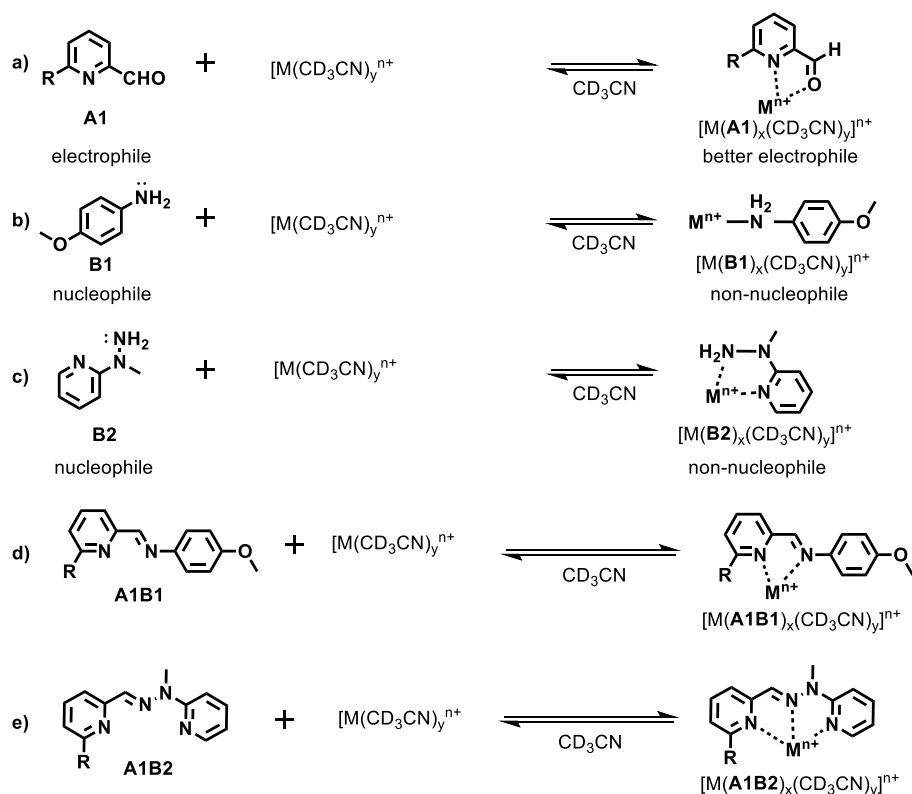
catalyst action, the reactions were also examined with much lower catalyst concentrations more typical of usual catalyzed processes. Complexation of the metal ions by the imine products of course meant that the solvated metal ion catalyst concentration was not constant throughout the reaction, so that an approximate kinetic treatment was applied by assuming that over the first 10 % of reaction conformity to an irreversible second-order process with an effectively constant catalyst concentration would apply and indeed this appeared to be valid. The derived apparent second order rate constants provided a convenient means of comparing the effects of the catalysts in the different imine formation reactions studied.



Scheme 15. Representation of C=N formation from pyridine-2-carboxaldehyde derivatives **A1**, **A2** or **A3** and *p*-anisidine **B1** or hydrazine **B2** catalysed by metal salts alone or in the presence of both metal salts and **B1**.

For the selected components and the metal cations, the possible steps involved in the catalytic processes are shown in **Scheme 16** (taking aldehyde **A1** as an example). The addition of metal cations could have the following effects:²²⁰ a) the metal cation can coordinate with electrophile **A1** through carbonyl-O to activate the carbonyl-C by making it a better electrophile; b) the metal cation can also coordinate with the nucleophiles **B1** and **B2**, making them non-nucleophilic and thus retarding reaction; c) the metal cation can act as a template for reaction by coordinating both **A1** and **B1** or **B2**, though an acceleration of reaction would only occur if the bases are not bound through the nucleophilic N; d) as noted previously, the metal cation can bind to the product, meaning that there could be product inhibition of catalysis, although any 1:1 ML(solvent)_n^{x+} species would still have sites available for substrate binding. The ability of **A1** and **B2** to act as chelate ligands should cause them to be bound more strongly than **B1**, although at the concentrations employed all three should readily displace the bound solvent. For simplicity, the formula given for each complex in the following text shows only the metal

ion and the ligand bound to it, since the possible presence of bound solvent or even bound triflate anions is not relevant to the kinetic analysis (nor detectable in the ^1H NMR spectra).

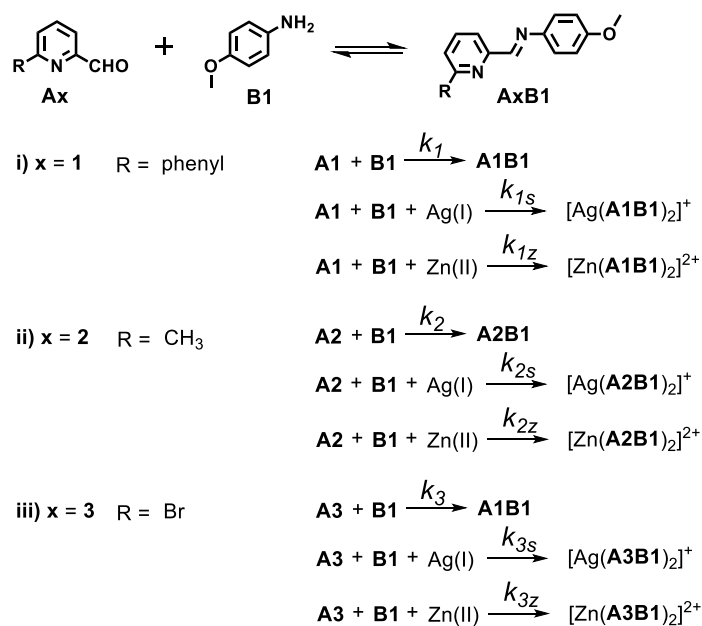


Scheme 16. The possible interactions involved in the processes of C=N formation in the presence of metal ions.

A. Imine formation driven by metal salts

To evaluate the efficiency of metal salts as Lewis acid catalysts in imine formation processes, we studied the condensation between **A1**, **A2** or **A3** and **B1**, leading to the formation of the imine **A1B1**, **A1B2** or **A1B3** (Scheme 17) both in the absence and presence of AgOTf or $\text{Zn}(\text{OTf})_2$.

The ^1H NMR measurements (Figure 17), showed the formation of **A1B1** from the condensation of **A1** with **B1** to be very slow. After about 250 h, the yield of **A1B1** was about 92%, with an initial rate constant k_I of $1.1 \times 10^{-3} \text{ M}^{-1} \text{ s}^{-1}$ (entry 1 in Table 4). The time dependence of the formation of **A1B1** is shown in Figure 20A. This low reactivity is a reflection of the weak nucleophilicity of the aromatic amine **B1** of low basicity ($\text{p}K_a = 5.34$) compared with aliphatic amines ($\text{p}K_a$ between 9 and 11). Note that even so the reaction proceeds to a high degree of completion, further justifying our treatment of the initial phase of reaction as an irreversible second order process.



Scheme 17. Imine formation from a pyridine-2-carboxaldehyde **A1** (**A2** or **A3**) and p-anisidine **B1** in the absence and presence of metal salts [AgOTf or Zn(OTf)₂]. k_1 , k_{1s} , k_{1z} , k_2 , k_{2s} , k_{2z} , k_3 , k_{3s} , k_{3z} are the initial formation rate constants calculated from the formation of 10% product assuming second order kinetics.

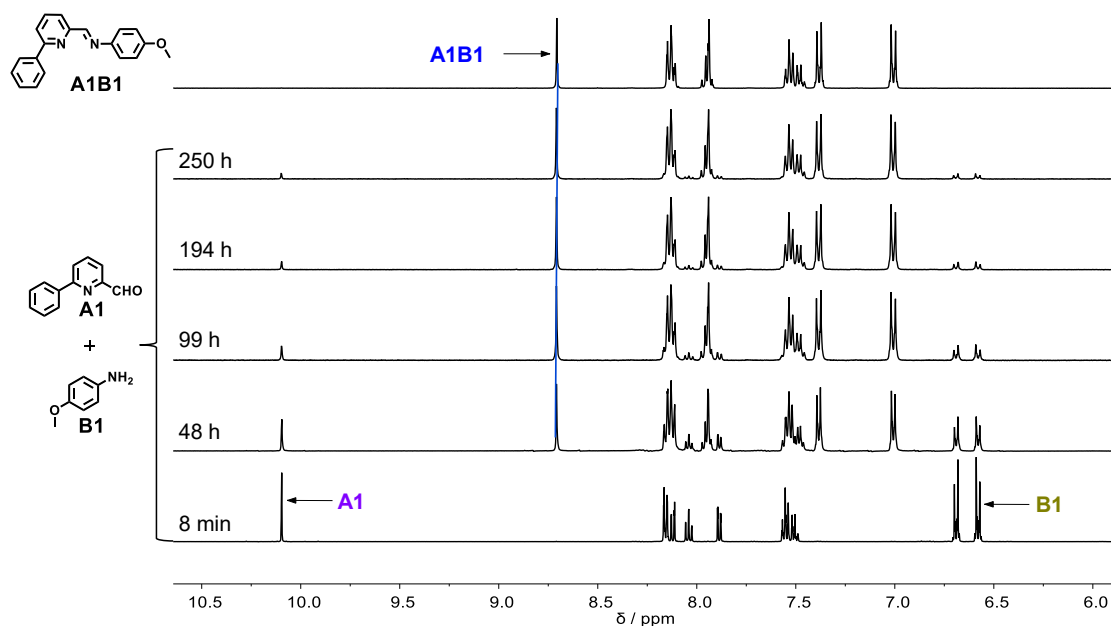


Figure 17. ¹H NMR (500 MHz) spectra of the mixture generated from equal amounts of **A1** + **B1** (10 mM each, CD₃CN, 25°C) after 8 minutes, 48 h, 99 h, 194 h, 250 h (from bottom to top). A reference spectrum of the separately prepared constituent **A1B1** is shown above.

In strong contrast, in the presence of 0.5 equiv. of AgOTf, the silver complex of imine **A1B1** was obtained much more rapidly, meaning that the metal cation considerably accelerates the condensation of **A1** and **B1** to give the imine ligand **A1B1** in its coordinated form. The

initial rate k_{1s} of formation in the presence of AgOTf was $20 \times 10^{-3} \text{ M}^{-1} \text{ s}^{-1}$ (entry 2 in **Table 4**), which is ~ 18 times faster than that in the absence of AgOTf due to the activation of aldehyde **A1** presumably through coordination to Ag(I). The evolution of the ^1H NMR spectrum during the formation of **A1B1** in the presence of Ag(I) is shown in **Figure 18**, the yield being 95% after 45 h. The kinetic plot of this reaction is shown in **Figure 20B**.

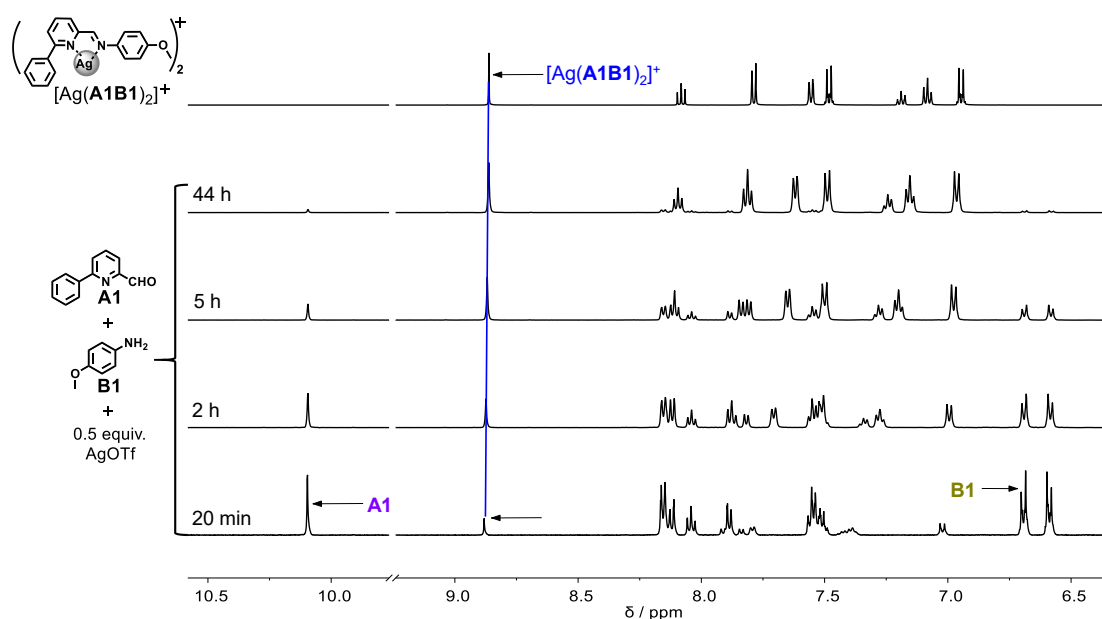


Figure 18. ^1H NMR (500 MHz) spectra of the mixture generated from equal amounts of **A1** + **B1** (10 mM each, CD_3CN , 25°C) in the presence of Ag(OTf) after 20 min, 2 h, 5 h and 44 h (from bottom to top). A reference spectrum of the separately prepared constituent $[\text{Ag}(\text{A1B1})_2]^+$ is shown above.

The formation rate of **A1B1** in the presence of $\text{Zn}(\text{OTf})_2$ was even more strongly accelerated with the almost full formation of product completed within 4 minutes (**Figure 19**). Therefore, the reaction was essentially irreversible in the presence of metal ion, justifying the kinetic treatment. The reaction rate constant k_{1z} was $18.2 \text{ M}^{-1} \text{ s}^{-1}$, amounting to about a 1.65×10^4 times acceleration compared with that in the absence of the Zn(II) salt (entry 3 in **Table 4**, **Figure 20D**).

A similar acceleration is also observed for the formation of **A2B1** or **A3B1** from their components in the presence $\text{Zn}(\text{OTf})_2$ (**Figure 20D**), indicating that $\text{Zn}(\text{OTf})_2$ is a very efficient catalyst of the condensation reactions probably due to the strong activation of the aldehyde **A1** by Zn(II) through coordination.

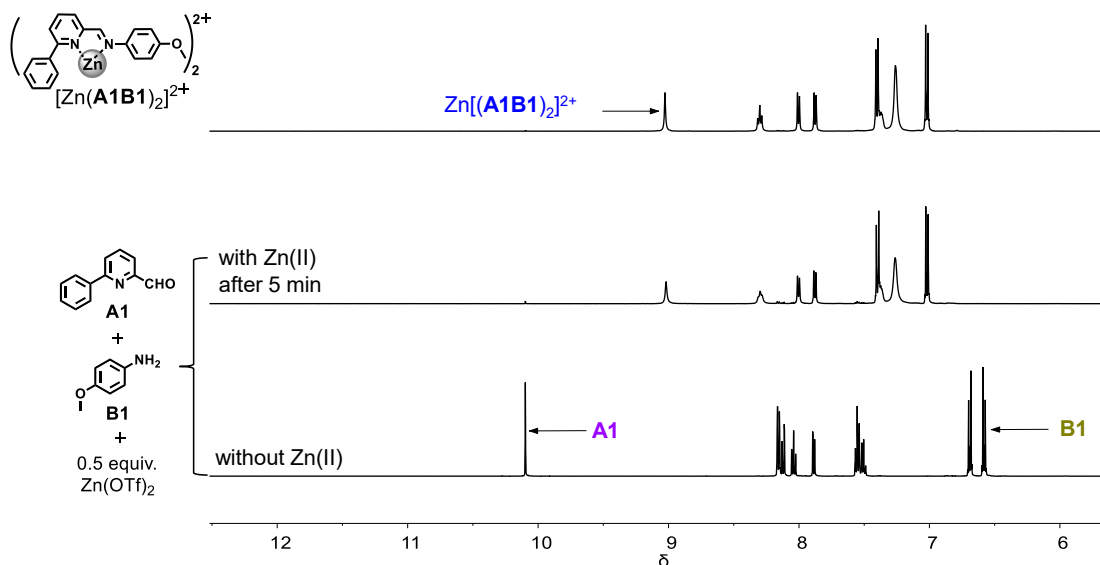


Figure 19. ^1H NMR (500 MHz) spectra of the mixture generated from equal amounts of **A1** + **B1** (10 mM each) and 0.5 equiv. of $\text{Zn}(\text{OTf})_2$ (5 mM) in CD_3CN at 25°C after 5 minutes compared to a reference spectrum of the separately prepared constituent $[\text{Zn}(\text{A1B1})_2]^{2+}$.

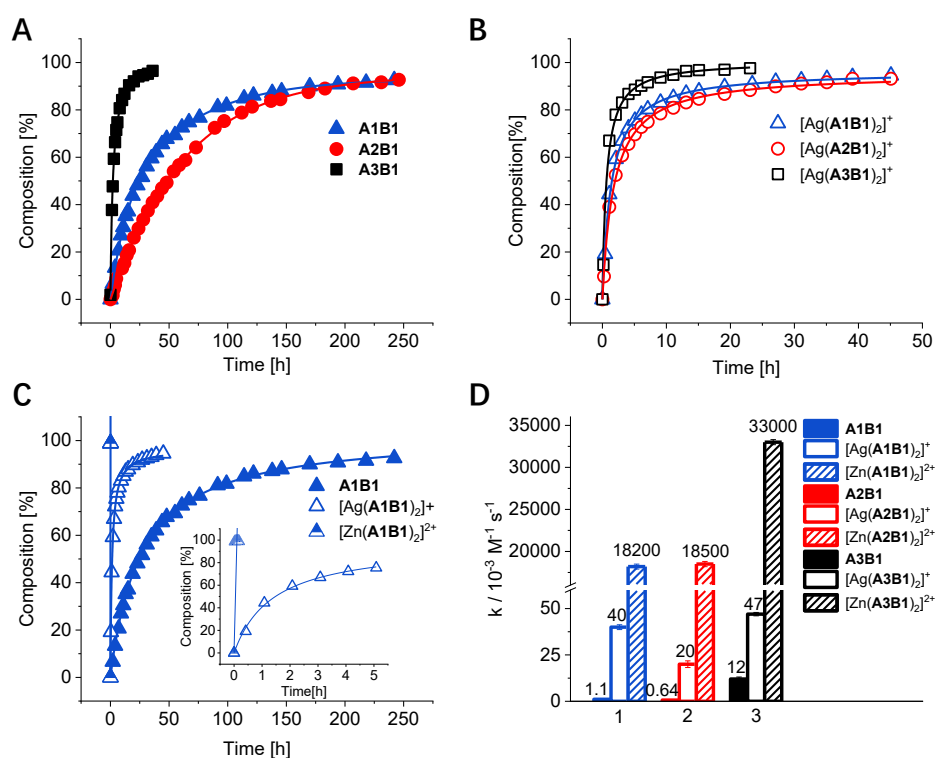


Figure 20. Plots of the evolution of a mixture of equimolar components (A). **A1/A2/A3** + **B1**; (B). **A1/A2/A3** + **B1** + 0.5 equiv. AgOTf ; (C). **A1** + **B1** / **A1** + **B1** + 0.5 equiv. AgOTf / **A1** + **B1** + 0.5 equiv. $\text{Zn}(\text{OTf})_2$ as a function of time as obtained from integration of the imine $\text{CH}=\text{N}$ proton signal in the 500 MHz ^1H NMR spectra (10 mM each, CD_3CN , 25°C); (D). Values of the initial rate constants (k) for the imine formation process between **A1** (**A2** or **A3**) and **B1** in the absence and presence of AgOTf or $\text{Zn}(\text{OTf})_2$, calculated from a fit to a second-order reaction over the first 10% of the reaction. The numbers above the columns correspond to $10^3 k$ for ease of comparison.

To investigate the dependence of the catalysis of the reaction between **A1** and **B1** on the concentration of Zn(II), the reaction was studied with increments in the concentration of Zn(II) starting from a value closer to those of usual catalysis experiments (**Figure 21**).

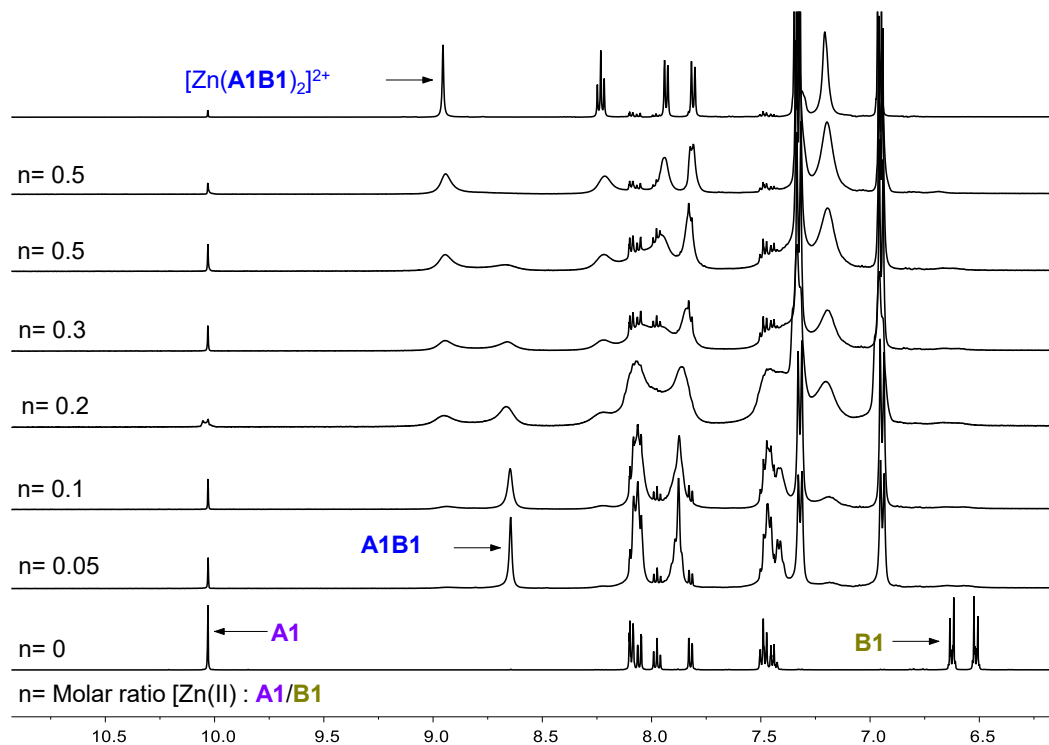


Figure 21. ^1H NMR (500 MHz) spectra for the titration of a mixture of **A1** and **B1** with different equivalents of $\text{Zn}(\text{OTf})_2$ in CD_3CN at 25°C (The initial concentration of **A1** or **B1** was 10 mM each).

The experiment was done in the following way: firstly 0.05 equiv. of Zn(II) was added, it took 4 minutes to obtain the ^1H NMR spectrum and the spectrum didn't change afterwards. It indicated that the kinetics of the catalysis was very fast. Then another 0.05 equiv. of Zn(II) was added and the ^1H NMR spectrum was recorded again. Until the addition of the amount of Zn(II) reached 0.5 equiv., the aldehyde was almost fully transformed to the product. Thus, we found that on addition of only 0.05 equiv. of $\text{Zn}(\text{OTf})_2$, within 4 minutes the imine had formed almost fully both as free **A1B1** (90%) and the remainder as its coordinated form identified by their ^1H NMR imine signals at 8.65 ppm and 9.0 ppm, respectively. In all cases, it appears that the Zn(II) is efficiently bound by the product ligand **A1B1**, meaning that if $[\text{Zn}(\text{CH}_3\text{CN})_6]^{2+}$ is the actual reaction catalyst, its concentration does not stay constant as the reaction proceeds. Furthermore, the ^1H NMR signals became broad after the initial additions of Zn(II), indicating relatively slow exchange reactions between the different Zn(II) species present. On progressively increasing the amount of Zn(II), the two imine-CH signals showed different changes. The peak at 8.65

ppm started to decrease and become broader while the peak at 9.0 ppm start to increase and become sharper. After addition of 0.5 equiv. of Zn(II), the peak at 8.65 ppm had disappeared and the peak at 9.0 ppm had become quite sharp, indicating the exclusive formation of $[\text{Zn}(\mathbf{A1B1})_2]^{2+}$, as verified by the low temperature experiment below. On adding more Zn(II), the complexation equilibria should result in the formation of $[\text{Zn}(\mathbf{A1B1})(\text{CH}_3\text{CN})_4]^{2+}$, but the bound ligand would probably have identical signals to those of $[\text{Zn}(\mathbf{A1B1})_2(\text{CH}_3\text{CN})_2]^{2+}$.

The ligand **A1B1** is an unsymmetrical bidentate species and thus its behavior as a ligand could be complicated by the formation of isomeric complexes of ML_2 composition if M has square planar or octahedral coordination (the latter in $\text{ML}_2(\text{solvent})_2$) or of ML_3 composition if M is octahedrally coordinated. As Zn(II) commonly adopts octahedral 6-coordination, its interaction with **A1B1** was examined by recording the ^1H NMR spectra of mixtures of $\text{Zn}(\text{OTf})_2$ and preformed **A1B1** in the ratios 1:2 and 1:3. Initial measurements at 25°C provided only a very broad and unassignable spectrum for the 1:3 mixture, so that final measurements were made at -35°C in order to obtain better resolution (**Figure 22**). At both 25 and -35°C , the 1:2 mixture showed sharp signals consistent with the presence of a single species, either tetrahedral $[\text{Zn}(\mathbf{A1B1})_2]^{2+}$ or the C_2 -symmetric isomer of $[\text{Zn}(\mathbf{A1B1})_2(\text{CH}_3\text{CN})_2]^{2+}$. At -35°C , the spectrum of the 1:3 mixture still showed some degree of signal broadening and some slight shifting of the coordinated ligand signals but most obvious was the presence of signals due to uncoordinated ligand, all these observations being consistent with at most very limited formation of a $[\text{Zn}(\mathbf{A1B1})_3]^{2+}$ species. To ensure that all product imine was bound to the metal ion, thus simplifying the spectra, all reaction mixtures involving metal ion catalysis were made up with the composition aldehyde: amine: metal in a 1:1:0.5 ratio, the sharp signals observed in the catalysis experiments with Ag(I) confirming that this was a valid procedure for both metal ions. That the species in solution in a 2:1 mixture of **A1B1** and $\text{Zn}(\text{OTf})_2$ is most probably the C_2 -symmetric isomer of octahedral $[\text{Zn}(\mathbf{A1B1})_2(\text{CH}_3\text{CN})_2]^{2+}$ is indicated by the observation that this is the form of $[\text{Zn}(\mathbf{A1B1})_2(\text{CF}_3\text{SO}_3)_2]$ found by an X-ray structure determination on the complex crystallised from acetonitrile by the addition of diethyl ether (**Figure 23**).

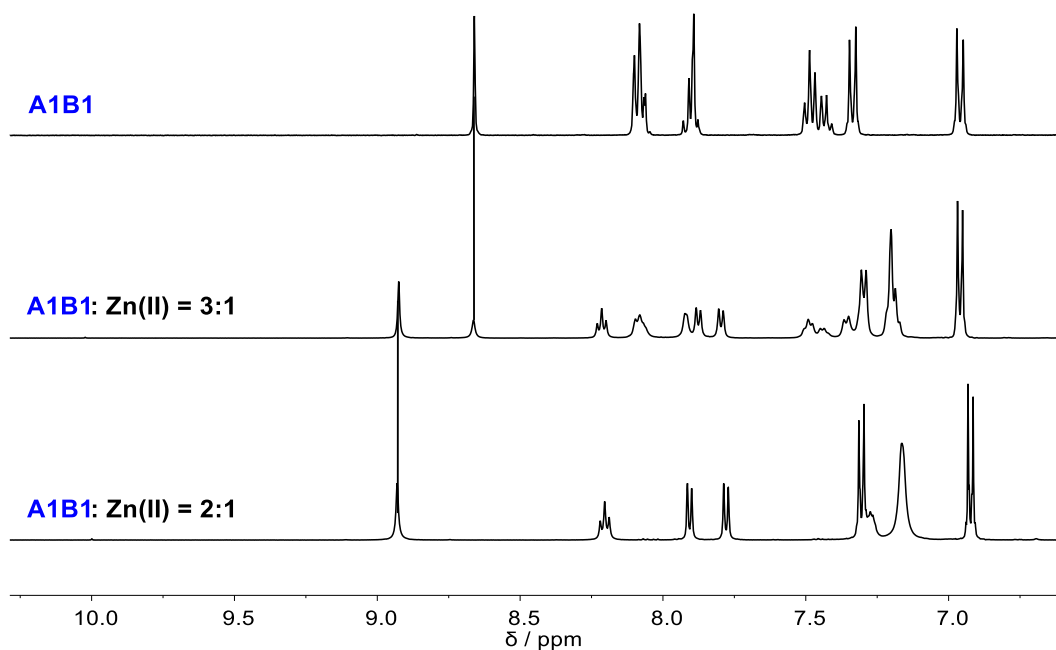


Figure 22. Low temperature (-35°C) ^1H NMR spectra obtained from three experiments: from bottom to top: **A1B1**: $\text{Zn}(\text{OTf})_2 = 2 : 1$; **A1B1**: $\text{Zn}(\text{OTf})_2 = 3 : 1$; **A1B1**. The concentration of **A1B1** is 10 mM.

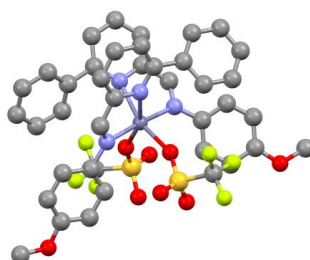


Figure 23. The single crystal structure of $[\text{Zn}(\text{A1B1})_2(\text{CF}_3\text{SO}_3)_2]$ obtained from 1.0 equiv. **A1B1** and 0.5 equiv. $\text{Zn}(\text{II})$ from the system of CH_3CN /diethyl ether.

Table 4. Kinetic features of the reactions between aldehyde **A1**, **A2** or **A3** and p-anisidine **B1** in the absence and presence of metal salts.

Entry ^[a]	Reaction	Catalyst 0.5 equiv.	Product	t ₅₀ [h] ^[c]	t ₁₀ [h] ^[d]	k ^[e] / 10 ⁻³ M ⁻¹ s ⁻¹	Acceleration Factor
1	A1 + B1	— ^[b]	A1B1	23	3	1.1	n.a. ^[f]
2	A1 + B1 + Ag(I)	Ag(I)	[Ag(A1B1) ₂] ⁺	1.4	0.5	20	18
3	A1 + B1 + Zn(II)	Zn(II)	[Zn(A1B1) ₂] ²⁺	≤0.08	≤0.08	≥18200	≥16500
4	A2 + B1	— ^[b]	A2B1	48	6.5	0.64	n.a. ^[f]
5	A2 + B1 + Ag(I)	Ag(I)	[Ag(A2B1) ₂] ⁺	1.9	0.27	14	22
6	A2 + B1 + Zn(II)	Zn(II)	[Zn(A2B1) ₂] ²⁺	≤0.08	≤0.08	≥18500	≥28900
7	A3 + B1	— ^[b]	A3B1	2.1	0.3	12	n.a. ^[f]
8	A3 + B1 + Ag(I)	Ag(I)	[Ag(A3B1) ₂] ⁺	0.80	0.08	44	4
9	A3 + B1 + Zn(II)	Zn(II)	[Zn(A3B1) ₂] ²⁺	≤0.08	≤0.08	≥33000	≥2750

^[a] In all these entries, aldehyde (10 mM), amine (10 mM), AgOTf or Zn(OTf)₂ (5 mM), at 25°C, in CD₃CN, monitored by ¹H NMR. ^[b] No catalyst was added. ^[c] Time for 50% completion of the reaction. ^[d] Time for 10% completion of the reaction. ^[e] The rate constant *k* has been calculated from a fit to a second-order reaction over the first 10% of the reaction. The values are listed as 10³ *k* for ease of comparison. ^[f] Not applicable

To explore the effect of different substituents on the pyridyl aldehyde on the kinetics of the C=N formation, similar experiments involving **A2** or **A3** with **B1** were studied both in the absence and presence of AgOTf and Zn(OTf)₂.

As shown in **Figure 24**, the formation of the **A2B1** from its components **A2** and **B1** is also very slow (95%, 246 h) and similar to that of **A1B1**. The rate constant is 0.64 × 10⁻³ M⁻¹ s⁻¹ (entry 3 in **Table 4**). It indicated that the replacement of phenyl by methyl group did not have great effect on the reactivity of the aldehyde. The formation of **A3B1** is much faster (95%, 12 h, rate constant 12 × 10⁻³ M⁻¹ s⁻¹, **Figure 9**) probably due to the activation of the aldehyde by the electron-withdrawing bromo substituent. The kinetic curves for the formation of **A2B1** and **A3B1** are shown in **Figure 20A**.

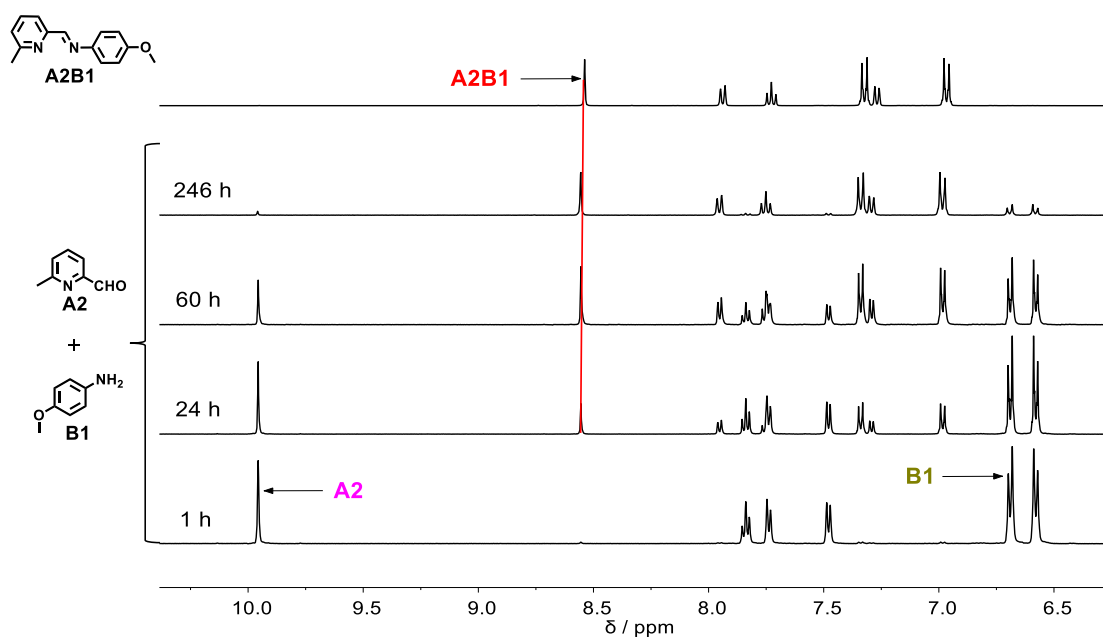


Figure 24. ^1H NMR (500 MHz) spectra of the mixture generated from equal amounts of **A2** + **B1** (10 mM each) in CD_3CN at 25°C after 1 h, 24 h, 60 h, 246 h (from bottom to top). A reference spectrum of the separately prepared constituent **A2B1** is shown above.

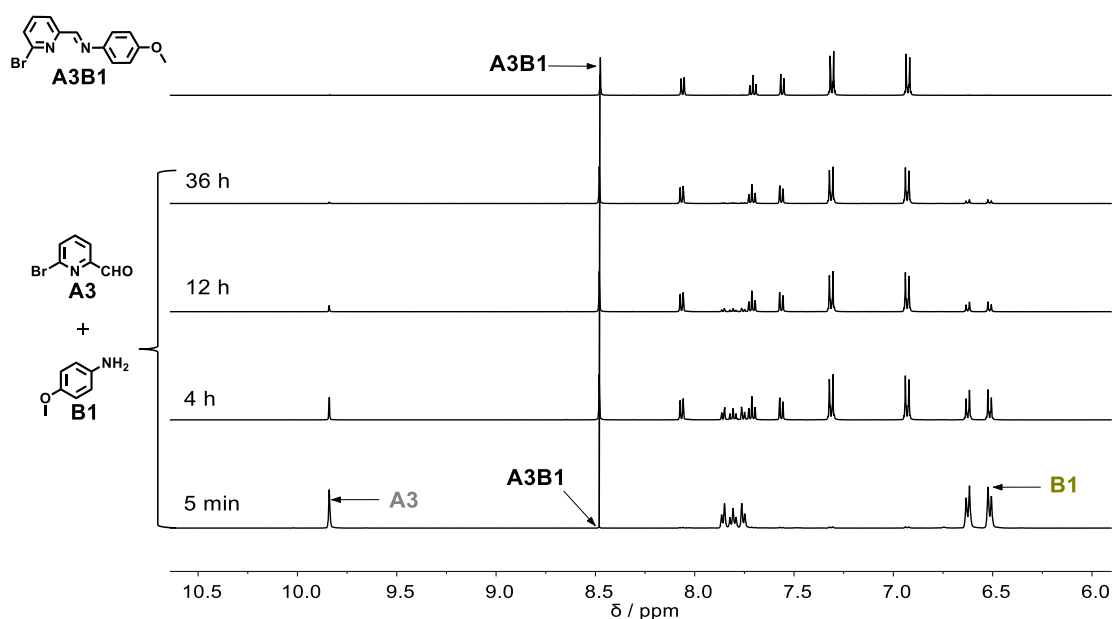


Figure 25. ^1H NMR (500 MHz) spectra of the mixture generated from equal amounts of **A3** + **B1** (10 mM each) in CD_3CN at 25°C after 5 minutes, 4 h, 12 h, 36 h (from bottom to top). A reference spectrum of the separately prepared constituent **A3B1** is shown above.

The ^1H NMR spectra for the $\text{Ag}(\text{I})$ -accelerated formation of **A2B1** are given in **Figure 26**. 5 minutes after addition of 0.5 equiv. of AgOTf , the presence of complexed **A2B1** is

apparent though the signals are slightly shifted from those of the solution of separately prepared $[\text{Ag}(\mathbf{A2B1})_2]\text{CF}_3\text{SO}_3$. Given that at this early stage of the reaction, the concentration of $\text{Ag}(\text{I})$ would considerably exceed that of the imine, this is consistent with the initial formation of the 1:1 complex, $[\text{Ag}(\mathbf{A2B1})(\text{CH}_3\text{CN})_2]^+$. After 44 hours, the reaction was almost complete with a rate constant (k_{2s}) of $14 \times 10^{-3} \text{ M}^{-1} \text{ s}^{-1}$ (entry 5 in **Table 4**). The acceleration factor for the concentration of $\text{Ag}(\text{I})$ used was approximately 22. An X-ray structure determination for the complex $[\text{Ag}(\mathbf{A2B1})_2]^+[\text{CF}_3\text{SO}_3]^-$ (**Figure 27**) shows the cation to have a flattened tetrahedral coordination geometry, which presumably would also be the case for the 1:1 complex.

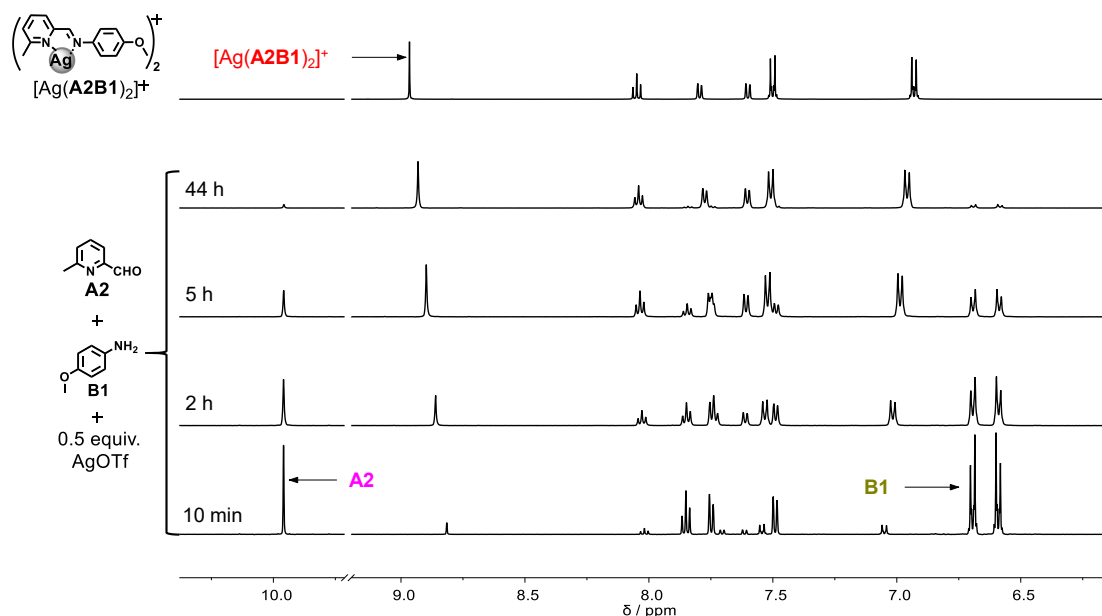


Figure 26. ^1H NMR (500 MHz) spectra of the mixture generated from equal amounts of **A2** + **B1** (10 mM each) + 0.5 equiv. AgOTf (5 mM) in CD_3CN at 25°C after 20 min, 2 h, 5 h and 44 h (from bottom to top). A reference spectrum of the separately prepared constituent $[\text{Ag}(\mathbf{A2B1})_2]^+$ is shown above.

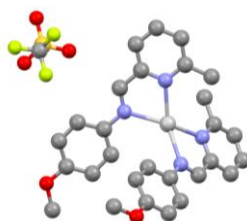


Figure 27. The single crystal structure of $[\text{Ag}(\mathbf{A2B1})_2]$ obtained from 1.0 equiv. **A2B1** and 0.5 equiv. $\text{Ag}(\text{I})$ dissolved in CH_3CN /diethyl ether.

Under the same conditions but with **A3** instead of **A2** as reactant, the acceleration of the condensation due to the presence of $\text{Ag}(\text{I})$ was rather slight. The rate constant was $k_{3s} 44 \times 10^{-3}$

$^3 \text{ M}^{-1} \text{ s}^{-1}$ (entry 8 in **Table 4**), a value which exceeds that of the formation of **A3B1** in the absence of the silver cations ($k_3 = 12 \times 10^{-3} \text{ M}^{-1} \text{ s}^{-1}$) by a factor of only ~ 4 . Once again, small shifts in the ^1H NMR spectral peaks for the coordinated product as the reaction progressed were consistent with the transition from a 1:1 to a 1:2 complex. The single crystal structure of $[\text{Ag}(\text{A3B1})_2] [\text{CF}_3\text{SO}_3]^-$ (**Figure 29**) showed the cation to again have a flattened tetrahedral coordination geometry.

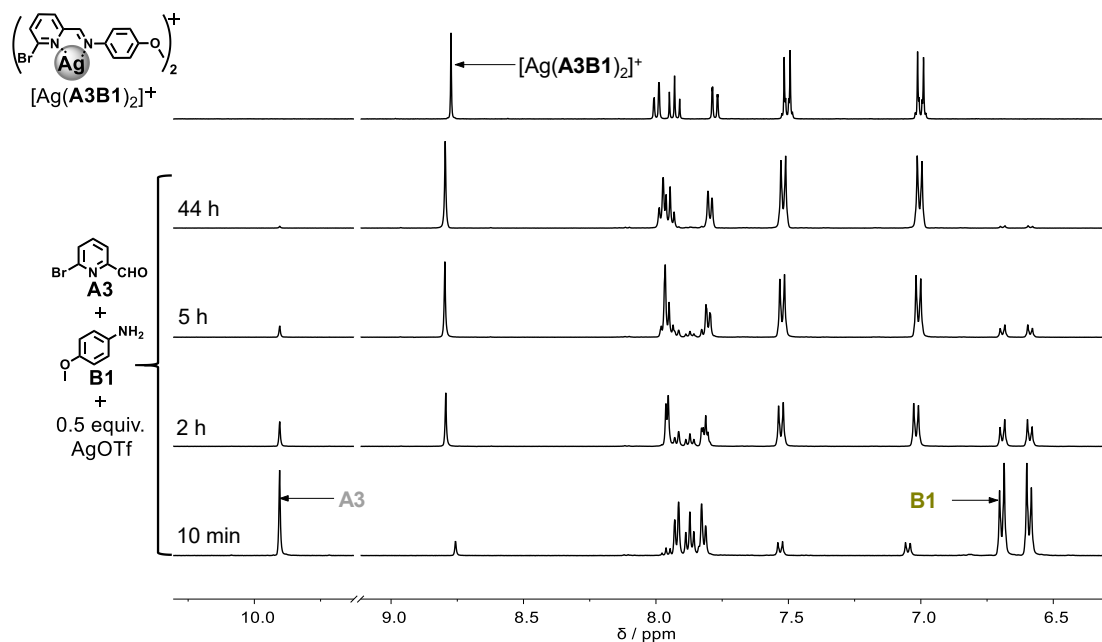


Figure 28. ^1H NMR (500 MHz) spectra of the mixture generated from equal amounts of **A3** + **B1** (10 mM each) + 0.5 equiv. AgOTf (5 mM) in CD_3CN at 25°C after 20 min, 2 h, 5 h, 44 h (from bottom to top). A reference spectrum of the separately prepared constituent $[\text{Ag}(\text{A3B1})_2]^+$ is shown above.

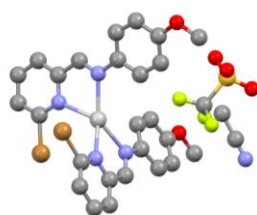


Figure 29. The single crystal structure of $[\text{Ag}(\text{A3B1})_2]$ obtained from 1.0 equiv. **A3B1** and 0.5 equiv. Ag(I) dissolved in CH_3CN /diethyl ether.

Far more effective acceleration of the reactions **A2** + **B1** (**Figure 30**) and **A3** + **B1** (**Figure 31**) was induced by $\text{Zn}(\text{II})$. ^1H NMR signals closely matching those of the separately isolated complexes $[\text{Zn}(\text{A2B1})_2]^{2+}$ and $[\text{Zn}(\text{A3B1})_2]^{2+}$ appeared extremely rapidly, in < 5 minutes in both cases (entries 8 and 9 in **Table 1**). The rate constants for the formation of

$[\text{Zn}(\text{A2B1})_2]^{2+}$ and $[\text{Zn}(\text{A3B1})_2]^{2+}$ were $k_{2z} \geq 18.5 \text{ M}^{-1} \text{ s}^{-1}$ and $k_{3z} = 33 \text{ M}^{-1} \text{ s}^{-1}$, respectively, amounting to acceleration factors of about 2.89×10^4 and 2.75×10^3 . These are in fact minimum values since reaction was almost complete when the first ^1H NMR spectrum was obtained, and the rate constants could not be accurately estimated. No marked dependence of the rates on the nature of the aldehyde substituents was apparent.

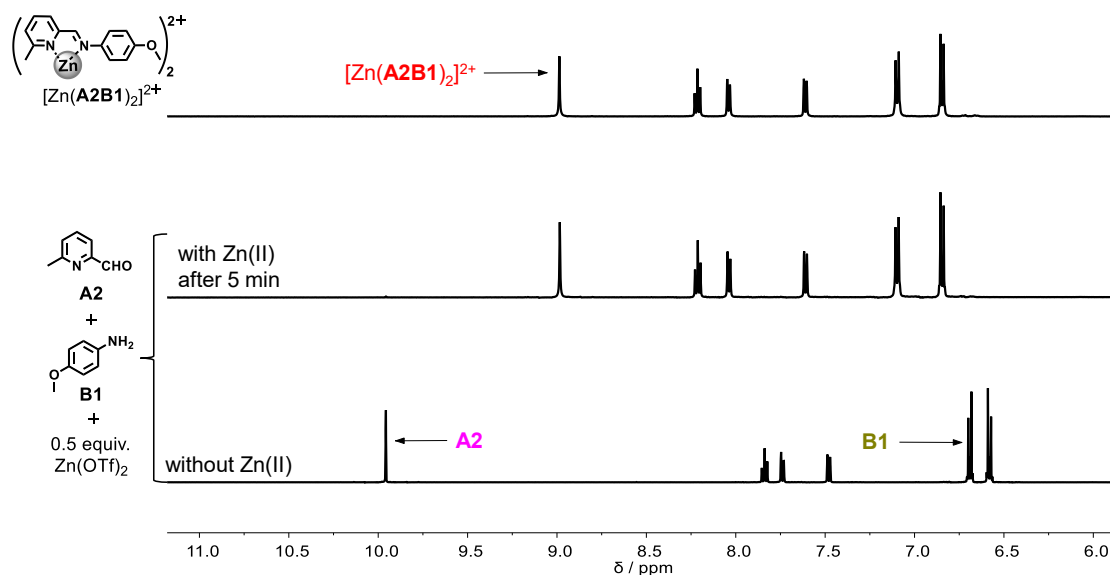


Figure 30. ^1H NMR (500 MHz) spectra of the mixture generated from equal amounts of **A2** + **B1** (10 mM each) + 0.5 equiv. of $\text{Zn}(\text{OTf})_2$ (5 mM) in CD_3CN at 25°C after 5 minutes.

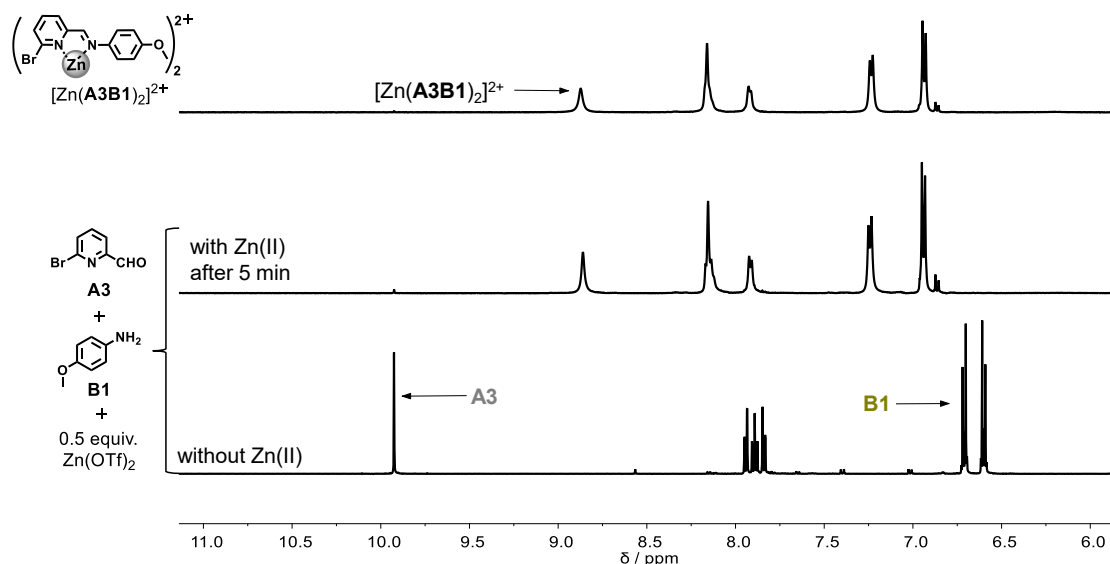
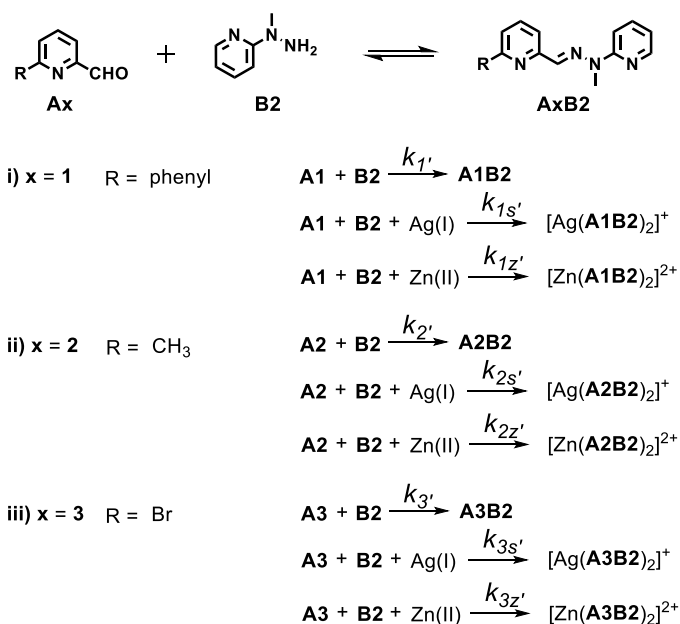


Figure 31. ^1H NMR (500 MHz) spectra of the mixture generated from equal amounts of **A3** + **B1** (10 mM each) + 0.5 equiv. of $\text{Zn}(\text{OTf})_2$ (5 mM) in CD_3CN at 25°C after 5 minutes.

B. Hydrazone formation driven by metal salts

Many efforts have already been made to study the catalysis of hydrazone formation, which is generally a much slower reaction than that of imine formation.¹⁰¹ Catalysts that have been exploited for the acceleration of this reaction include aniline and aniline derivatives,^{132,221,222} Brønsted acids²²³ and amine buffers,²²⁴ metal ion which have been widely applied in biological processes such as fabrication of metal complexes,^{223,225} protein ligation,^{180,211} as well as constitutional dynamic libraries.^{66,67,82,98,226,227} Kinetic studies have been largely focussed on aqueous systems where the reaction is somewhat unfavorable,^{169,221,228,229} so the present work was firstly directed towards the study of its catalysis in organic solvents.

Similar experiments to those just described were performed using the same sets of components **A1** (**A2** or **A3**) and hydrazine **B2** in the absence and presence of metal salts [Ag(I) and Zn(II)] (**Scheme 18**). The evolution of the 9 reactions was followed by ¹H NMR spectroscopy at 25°C in CD₃CN.



Scheme 18. Hydrazone formation from a pyridine-2-carboxaldehyde derivative **A1** (**A2** or **A3**) and 2-N-methylhydrazino-pyridine **B2** in the absence and presence of metal salts [AgOTf or Zn(OTf)₂]. $k_{1'}$, $k_{1s'}$, $k_{1z'}$, $k_{2'}$, $k_{2s'}$, $k_{2z'}$, $k_{3'}$, $k_{3s'}$, $k_{3z'}$ are the initial formation rate constants, their values being estimated from the formation of 10% product using a second order kinetic equation.

The ¹H NMR spectra show that the formation of hydrazone **A1B2** is very slow (**Figure 32**). After 154 hours, the reaction resulted in about 95% **A1B2** formation, showing **B2** to be a weak nucleophile. On addition of 0.5 equiv. of Ag(I), the formation of the hydrazone complex [Ag(**A1B2**)₂]⁺ became much faster (**Figure 33**, 95%, 18 h, entry 2 in **Table 5**) than that of the

ligand **A1B2**. The rate constants were $1.1 \times 10^{-2} \text{ M}^{-1} \text{ s}^{-1}$ and $9.7 \times 10^{-4} \text{ M}^{-1} \text{ s}^{-1}$ in the presence and absence of AgOTf respectively, with a rate acceleration factor of 19 due to the presence of AgOTf. Note that in this system, the coordination of Ag(I) with **B2** was clear from shifts in the NMR spectra when AgOTf was added to a solution of **B2** alone. This would have partially reduced the amount of Ag(**A1**)⁺ that could form and slowed reaction both for this reason and because bound **B2** could not act as a nucleophile. Once again, small shifts in the bound ligand resonances as the reaction proceeded were consistent with the transition from a 1:1 to a 2:1 complex.

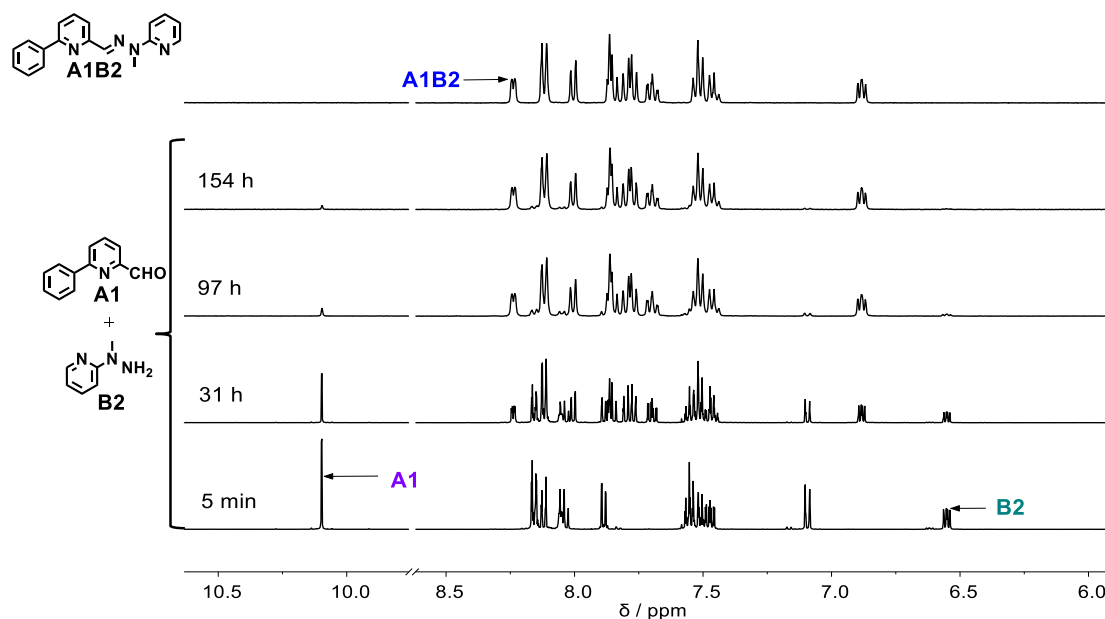


Figure 32. ¹H NMR (500 MHz) spectra of the mixture generated from equal amounts of **A1** + **B2** (10 mM each, CD₃CN, 25°C) after 5 minutes, 31 h, 97 h, 154 h (from bottom to top). A reference spectrum of the separately prepared constituent **A1B2** is shown above.

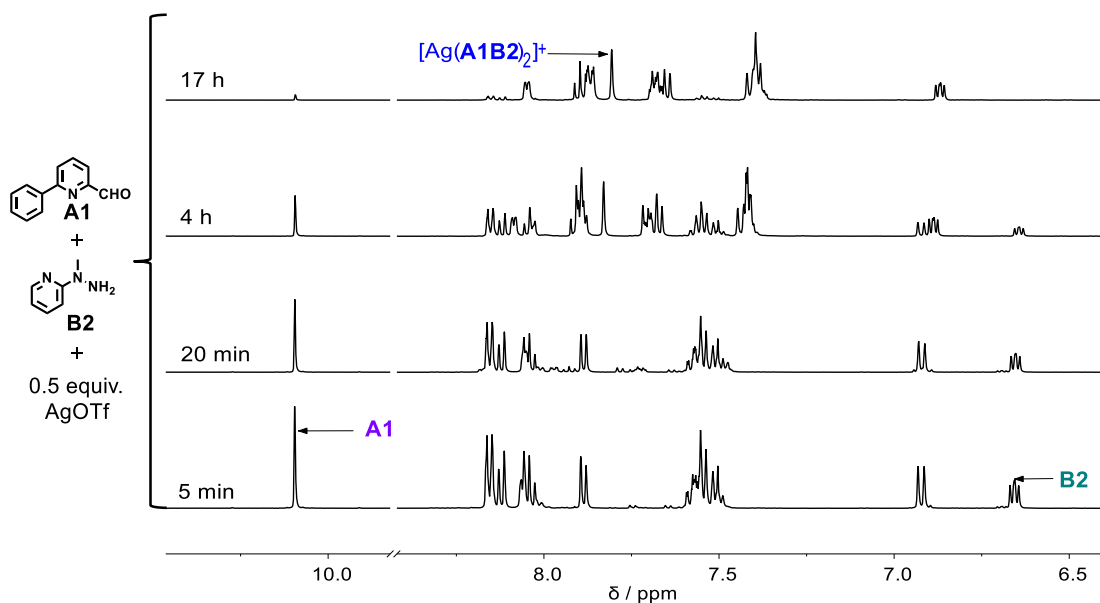


Figure 33. ^1H NMR (500 MHz) spectra of the mixture generated from equal amounts of **A1** + **B2** (10 mM each, CD_3CN , 25°C) + 0.5 equiv. of AgOTf (5 mM) after 5 minutes, 20 min, 4 h, 17 h (from bottom to top).

In the presence of 0.5 equiv. of $\text{Zn}(\text{OTf})_2$, formation of the hydrazone in its complexed forms was again accelerated (**Figure 34**, 95%, 62 h, $k_{2z} = 7.5 \times 10^{-3} \text{ M}^{-1} \text{ s}^{-1}$, entry 3 in **Table 5**) although only 8-fold. As for $\text{Ag}(\text{I})$, NMR spectroscopy showed a clear interaction between $\text{Zn}(\text{II})$ and **B2**, an interaction which presumably diminished acceleration of the overall reaction by $\text{Zn}(\text{II})$ in the same ways as for $\text{Ag}(\text{I})$. An X-ray structure determination on the isolated complex $[\text{Zn}(\text{A1B2})_2](\text{CF}_3\text{SO}_3)_2 \cdot \text{CH}_3\text{CN}$ (**Figure 35**) showed the $\text{Zn}(\text{II})$ to be in octahedral N_6 coordination with each ligand bound in a tridentate mode. The asymmetric unit contains one molecule of the complex, two triflate and one molecule of the acetonitrile solvent. The atoms of one molecule of triflate are disordered over two positions.

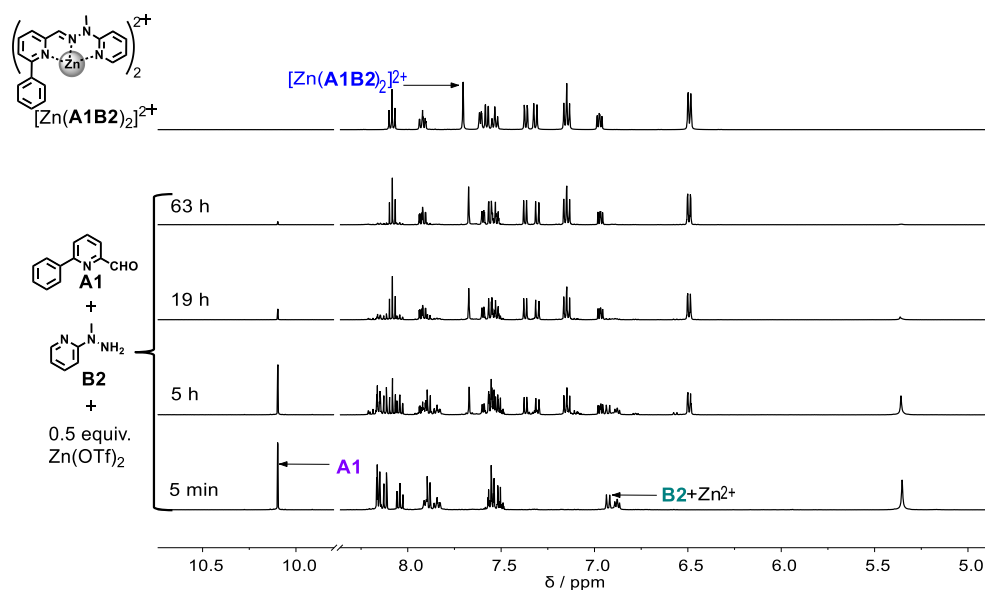


Figure 34. ^1H NMR (500 MHz) spectra of the mixture generated from equal amounts of **A1** + **B2** (10 mM each, CD_3CN , 25°C) + 0.5 equiv. of $\text{Zn}(\text{OTf})_2$ (5 mM) after 5 minutes, 5 h, 19 h, 63 h (from bottom to top). A reference spectrum of the separately prepared constituent $[\text{Zn}(\text{A1B2})_2](\text{CF}_3\text{SO}_3)_2$ is shown above.

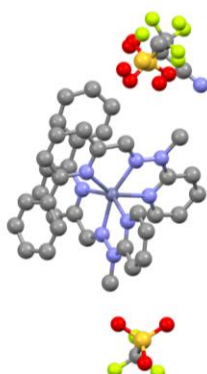


Figure 35. The single crystal structure of $[\text{Zn}(\text{A1B2})_2]$ obtained from 1.0 equiv. of **A1B2** and 0.5 equiv. of $\text{Zn}(\text{II})$ triflate dissolved in CH_3CN /diethyl ether.

In the presence of 0.5 equiv. of $\text{Ag}(\text{OTf})$, the silver complexes $[\text{Ag}(\text{A2B2})_2]^+$ and $[\text{Ag}(\text{A3B2})_2]^+$ formed much more rapidly (entries 5 and 8 in) than did the free ligands **A2B2** and **A3B2** from their components **A2** + **B2** and **A3** + **B2** (entries 4 and 7 in **Table 5**) The evolution of the ^1H NMR spectra during the four experiment is shown below (**Figure 36** to **Figure 42**). The kinetic curves and rate constants are shown in **Figure 43** and **Figure 44**. The accelerations induced by addition of the given amount of $\text{Ag}(\text{I})$ amount to factors of 19 and 2 for the two sets of reactions respectively (**Table 5**).

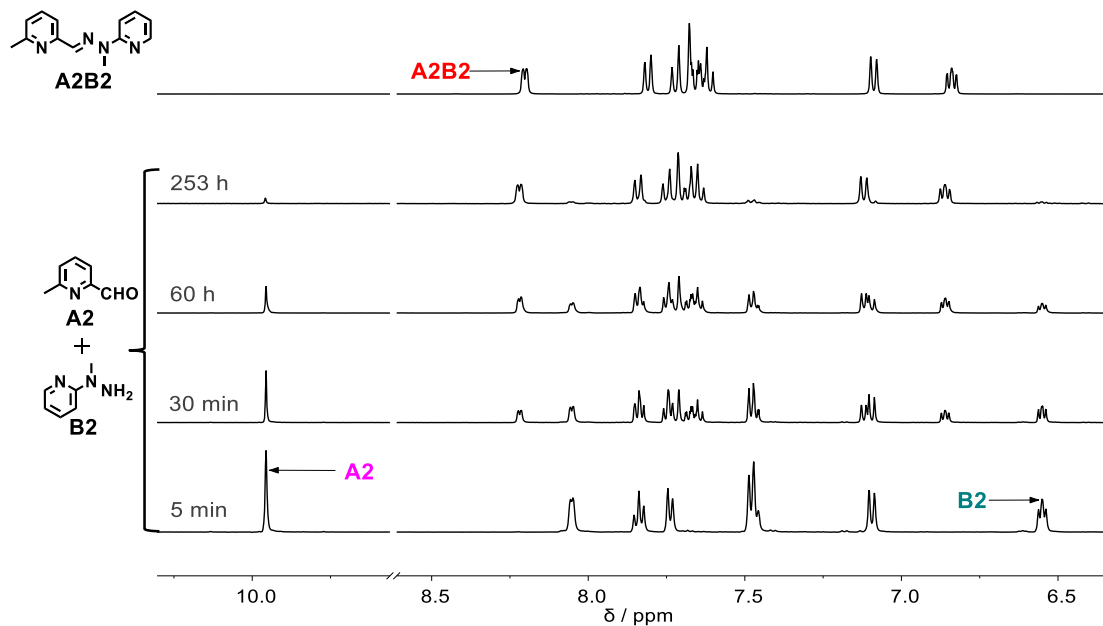


Figure 36. ^1H NMR (500 MHz) spectra of the mixture generated from equal amounts of **A2** + **B2** (10 mM each) in CD_3CN at 25°C after 5 minutes, 30 min, 60 h, 253 h (from bottom to top). A reference spectrum of the separately prepared constituent **A2B2** is shown above.

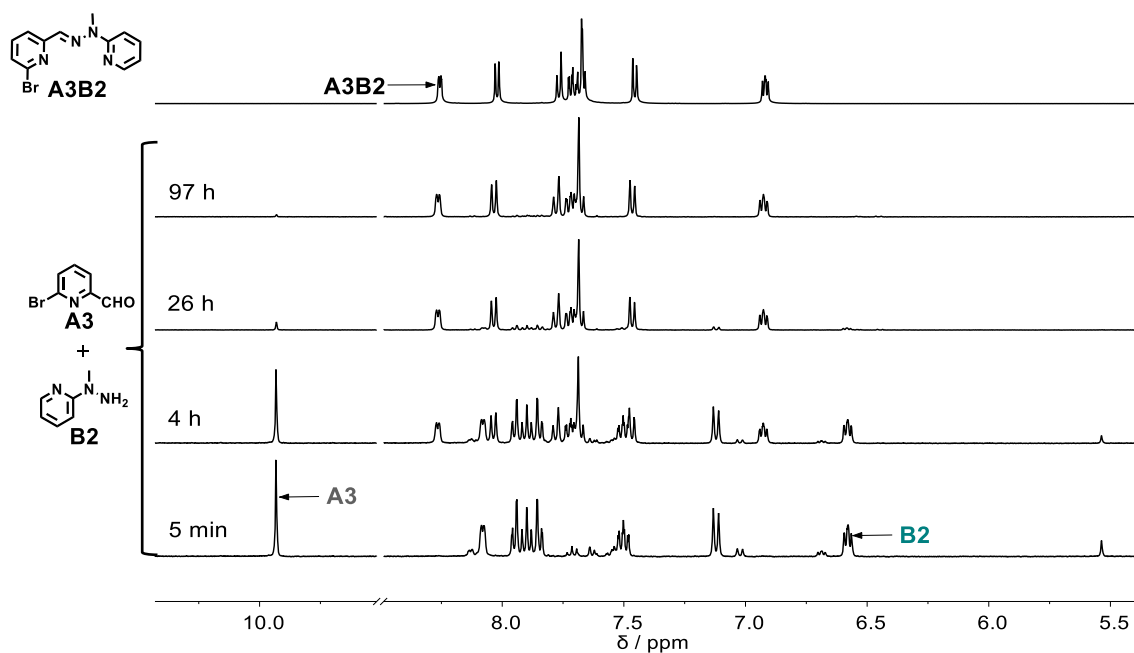


Figure 37. ^1H NMR (500 MHz) spectra of the mixture generated from equal amounts of **A3** + **B2** (10 mM each) in CD_3CN at 25°C after 5 min, 4 h, 26 h and 97 h (from bottom to top). A reference spectrum of the separately prepared constituent **A3B2** is shown above.

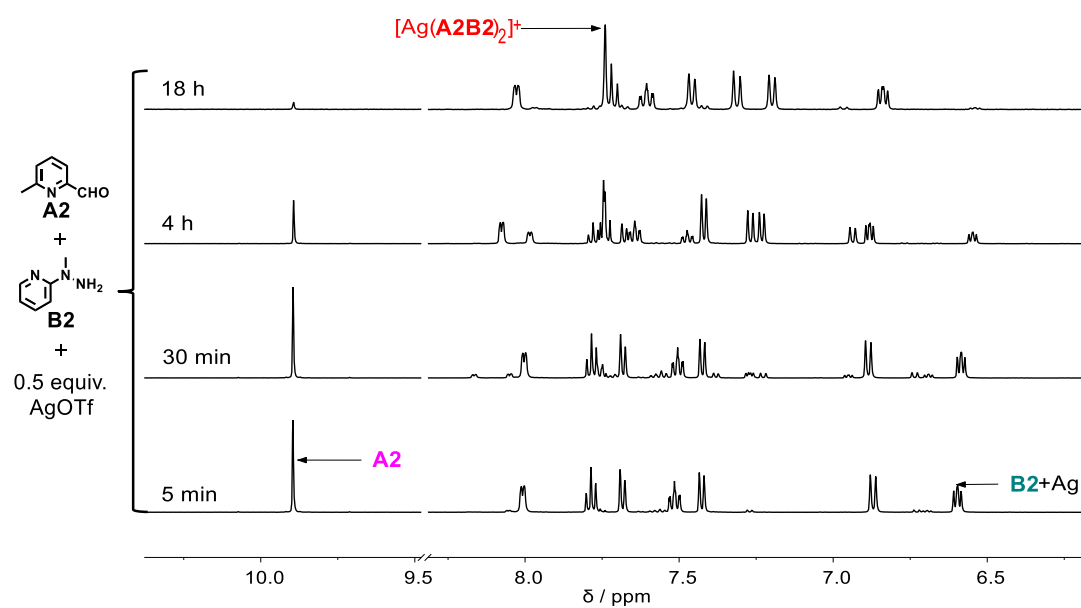


Figure 38. ¹H NMR (500 MHz) spectra of the mixture generated from equal amounts of **A2** + **B2** (10 mM each) + 0.5 equiv. of AgOTf (5 mM) in CD₃CN at 25°C after 5 min, 30 min, 4 h, 18 h (from bottom to top).

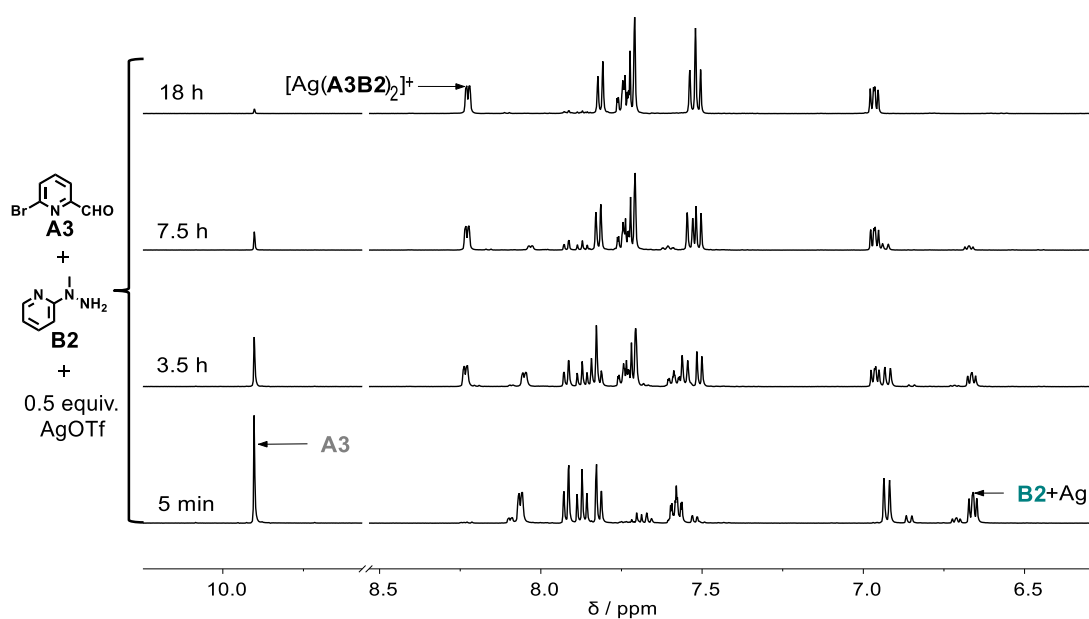


Figure 39. ¹H NMR (500 MHz) spectra of the mixture generated from equal amounts of **A3** + **B2** (10 mM each) + 0.5 equiv. of AgOTf (5 mM) in CD₃CN at 25°C after 5 min, 3.5 h, 7.5 h, 18 h.

To see if similar responses to changes in the aldehyde structure would occur with Zn(II), these experiments were repeated with Zn(OTf)₂ in place of Ag(OTf). The ¹H NMR spectral

monitoring (**Figure 40**) showed $[\text{Zn}(\text{A2B2})_2]^{2+}$ again formed faster (entry 6 in **Table 5**) than did the free ligand (**Figure 36**, entry 4 in **Table 5**), with an acceleration factor of 19 (**Table 5**), the same as found for the same concentration of Ag(I). The single crystal X-ray structure of $[\text{Zn}(\text{A2B2})_2](\text{CF}_3\text{SO}_3)_2 \cdot \text{CH}_3\text{CN}$ (**Figure 41**) again shows the Zn(II) adopts an octahedral 6-coordination.

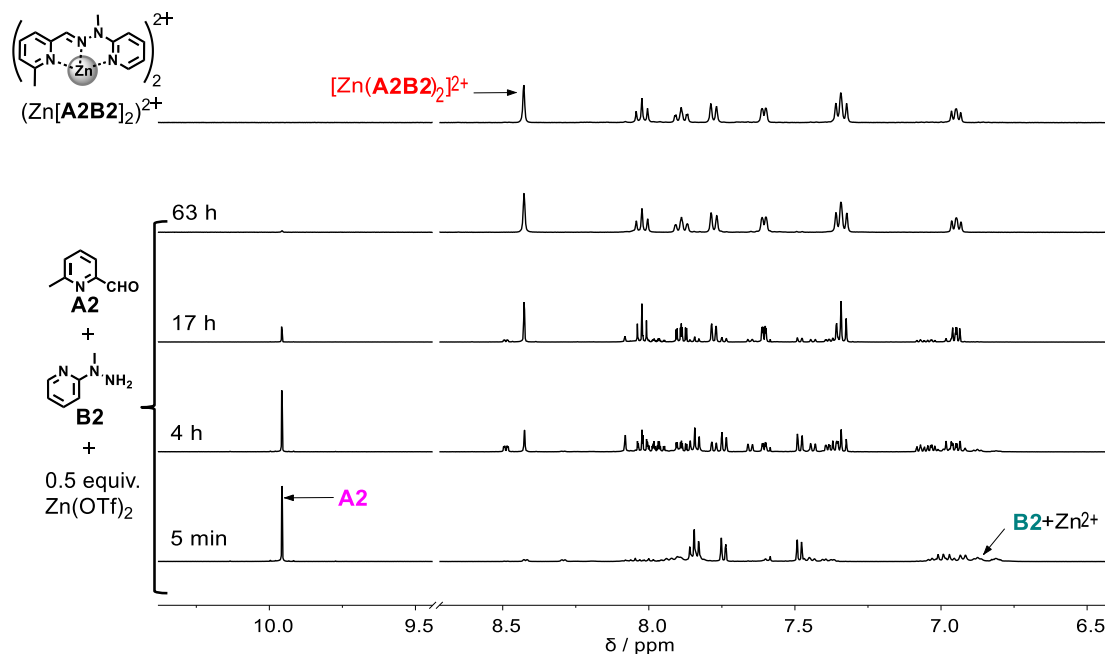


Figure 40. ^1H NMR (500 MHz) spectra of the mixture generated from equal amounts of **A2** + **B2** (10 mM each) + 0.5 equiv. of $\text{Zn}(\text{OTf})_2$ (5 mM) in CD_3CN at 25°C after 5 minutes, 4 h, 17 h, 63 h (from bottom to top). A reference spectrum of the separately prepared constituent $[\text{Zn}(\text{A2B2})_2]^{2+}$ is shown above.

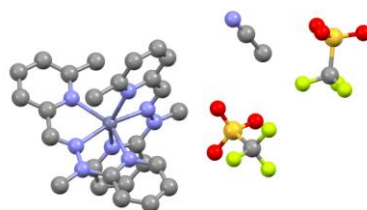


Figure 41. The single crystal structure of $[\text{Zn}(\text{A2B2})_2](\text{CF}_3\text{SO}_3)_2 \cdot \text{CH}_3\text{CN}$ obtained from 1.0 equiv. **A2B2** and 0.5 equiv. Zn(II) from the system of CH_3CN /diethyl ether.

In contrast, the formation of the bound ligand as $[\text{Zn}(\text{A3B2})_2]^{2+}$ (entry 9 in **Table 5**) was slower than that of the free ligand **A3B2** (entry 7 in **Table 5**), as seen from the ^1H NMR spectra (**Figure 37** and **Figure 42**). Suspecting that this inhibitory effect might have been due to coordination of **B2** to Zn(II), the interactions between these two species alone was examined in more detail. The separately prepared complex $[\text{Zn}(\text{B2})_2](\text{CF}_3\text{SO}_3)_2$ gave an NMR spectrum (**Figure 45**) in which the peaks matched those observed immediately after preparing the reaction mixture for the rate study. Titration of $\text{Zn}(\text{OTf})_2$ into a solution of **B2** in acetonitrile (**Figure 46**) provided evidence for the formation of at least two complexes. With 0.1 equiv. of Zn(II) all of the peaks became very broad and new peaks appeared. At 0.2 equiv. added, the peaks became even broader, while peaks assigned to free **B2** decreased in intensity and the new peaks started to increase. Addition of 0.3 equiv. of Zn(II) led to peak sharpening and when the amount of Zn(II) added reached 0.5 equiv., the peaks became very sharp. These observations indicate that it must be possible to form a reasonably stable $[\text{Zn}(\text{B2})_2(\text{CH}_3\text{CN})_2]^{2+}$ species and that presumably a 1:1 complex would form on further additions of Zn(II). The presence of the 2:1 species in solution was confirmed by mass spectroscopy (**Figure 47**).

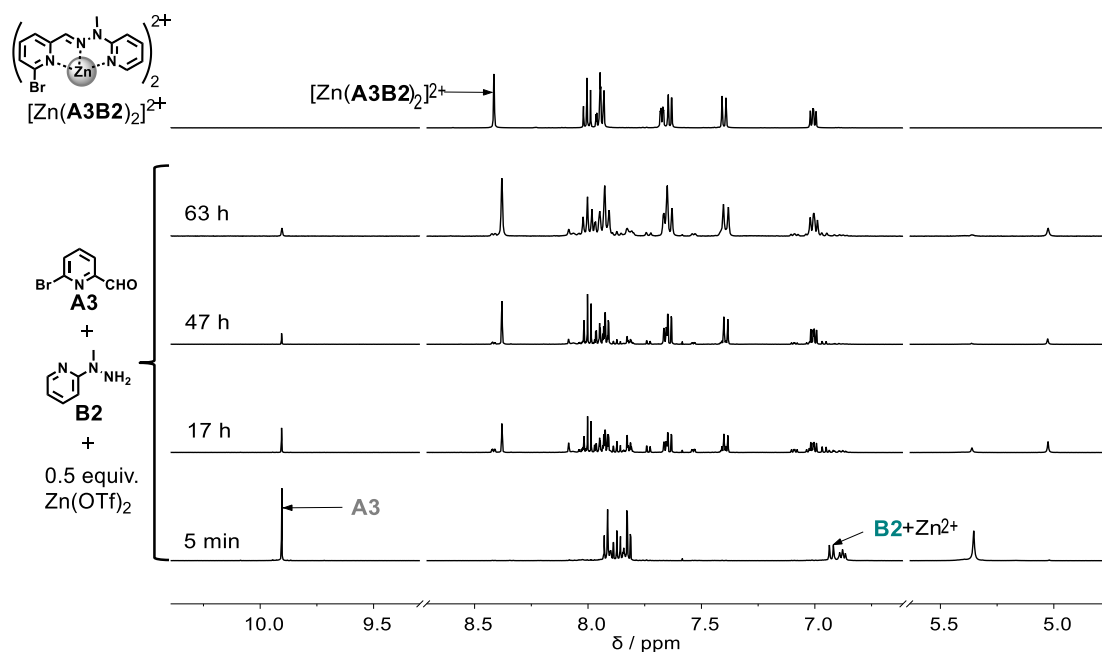


Figure 42. ^1H NMR (500 MHz) spectra of the mixture generated from equal amounts of **A3** + **B2** (10 mM each) + 0.5 equiv. of $\text{Zn}(\text{OTf})_2$ (5 mM) in CD_3CN at 25°C after 5 minutes, 17 h, 47 h, 63 h (from bottom to top). A reference spectrum of the separately prepared constituent $[\text{Zn}(\text{A3B2})_2]^{2+}$ is shown above.

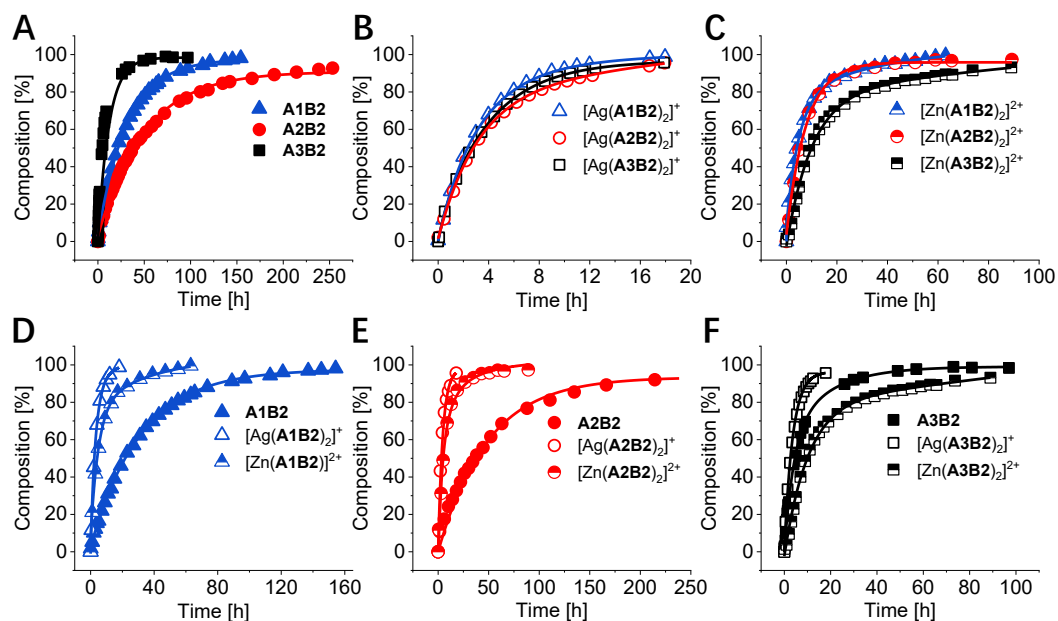


Figure 43. Plots of the evolution of a mixture of equal amounts of components (A). **A1/A2/A3 + B2**; (B). **A1/A2/A3 + B2 + 0.5 equiv. AgOTf**; (C). **A1/A2/A3 + B2 + 0.5 equiv. Zn(OTf)₂**; (D). **A1 + B2, A1 + B2 + 0.5 equiv. AgOTf and A1 + B2 + 0.5 equiv. Zn(OTf)₂**; (E). **A2 + B2, A2 + B2 + 0.5 equiv. AgOTf and A2 + B2 + 0.5 equiv. Zn(OTf)₂**; (F). **A3 + B2, A3 + B2 + 0.5 equiv. AgOTf and A3 + B2 + 0.5 equiv. Zn(OTf)₂** as a function of time as obtained from integration of the imine CH=N proton signal in the 500 MHz ¹H NMR spectra (10 mM each, CD₃CN, 25°C).

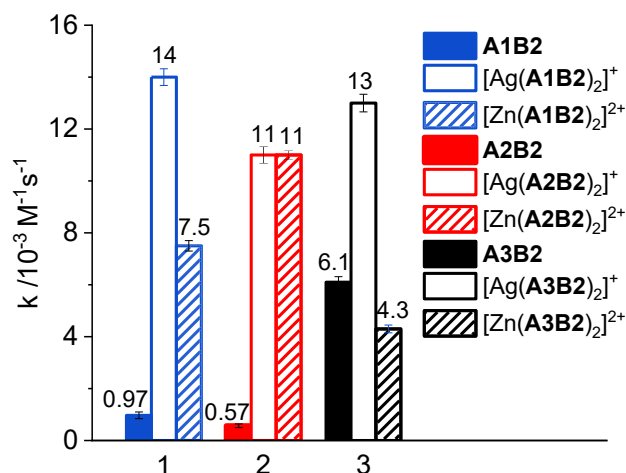
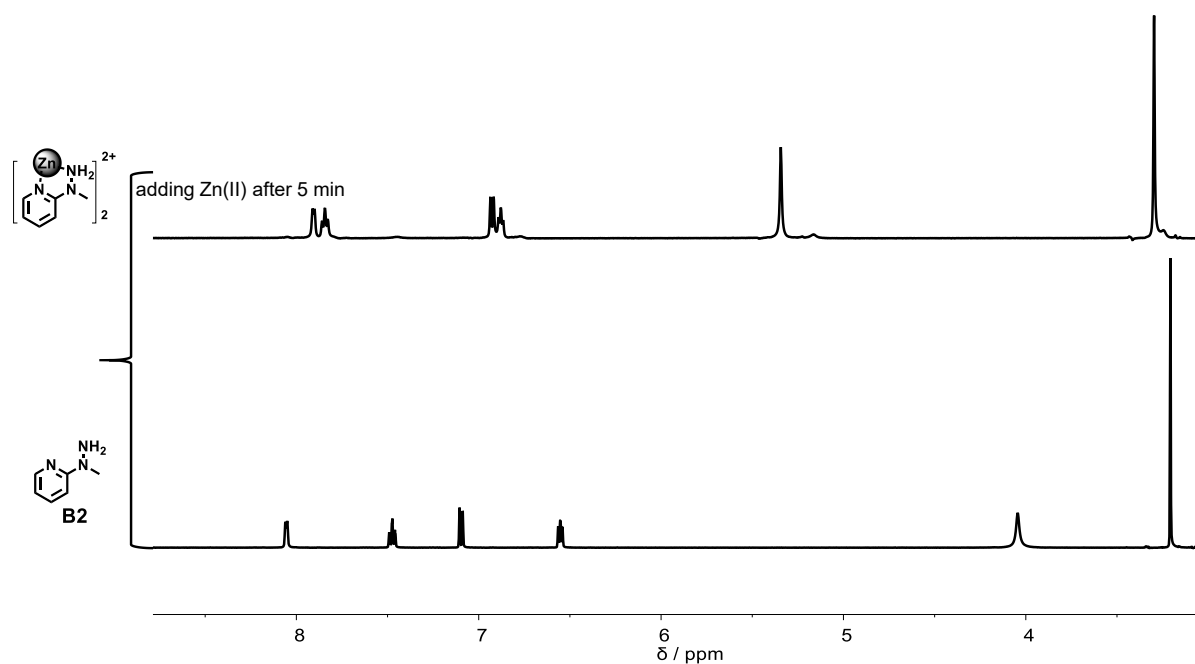


Figure 44. Values of the initial rate constants (k) for the hydrazone formation process between **A1**, **A2** or **A3** and **B2** (Scheme 18) in the absence and presence of metal salts AgOTf or Zn(OTf)₂ in CD₃CN at 25°C, calculated from a fit to a second-order reaction over the first 10% of the reaction. The numbers above the columns correspond to 10³ k for ease of comparison.

Table 5. Kinetic features of the reactions between aldehyde **A1**, **A2** or **A3** and hydrazine **B2** in the absence and presence of metal salts.

Entry ^[a]	Reaction	Catalyst 0.5 equiv.	Product	t ₅₀ [h] ^[c]	t ₁₀ [h] ^[d]	k ^[e] /10 ⁻³ M ⁻¹ s ⁻¹	Acceleration Factor
1	A1 + B2	— ^[b]	A1B2	21	1.94	0.97	n.a. ^[f]
2	A1 + B2 + Ag(I)	Ag(I)	[Ag(A1B2) ₂] ⁺	2.4	0.35	14	14
3	A1 + B2 + Zn(II)	Zn(II)	[Zn(A1B2) ₂] ²⁺	4	0.55	7.5	8
4	A2 + B2	— ^[b]	A2B2	37	3.9	0.57	n.a. ^[f]
5	A2 + B2 + Ag(I)	Ag(I)	[Ag(A2B2) ₂] ⁺	2.8	0.38	11	19
6	A2 + B2 + Zn(II)	Zn(II)	[Zn(A2B2) ₂] ²⁺	5.1	0.98	11	19
7	A3 + B2	— ^[b]	A3B2	4.6	0.63	6.1	n.a. ^[f]
8	A3 + B2 + Ag(I)	Ag(I)	[Ag(A3B2) ₂] ⁺	2.7	0.36	13	2
9	A3 + B2 + Zn(II)	Zn(II)	[Zn(A3B2) ₂] ²⁺	9.4	2.0	4.3	0.7

^[a] In all of these entries, aldehyde (10 mM), hydrazine (10 mM), AgOTf or Zn(OTf)₂ (5 mM), at 25°C, in CD₃CN, monitored by ¹H NMR. ^[b] No catalyst was added. ^[c] Time for 50% completion of the reaction. ^[d] Time for 10% completion of the reaction. ^[e] The rate constant *k* has been calculated from a fit to a second-order reaction over the first 10% of the reaction. The values are listed as 10³ *k* for ease of comparison. ^[f] Not applicable.

**Figure 45.** ¹H NMR spectra of the separately prepared zinc complex from 0.5 equiv. of Zn(II) and 1.0 equiv. of **B2** (10 mM) in CD₃CN at 25°C .

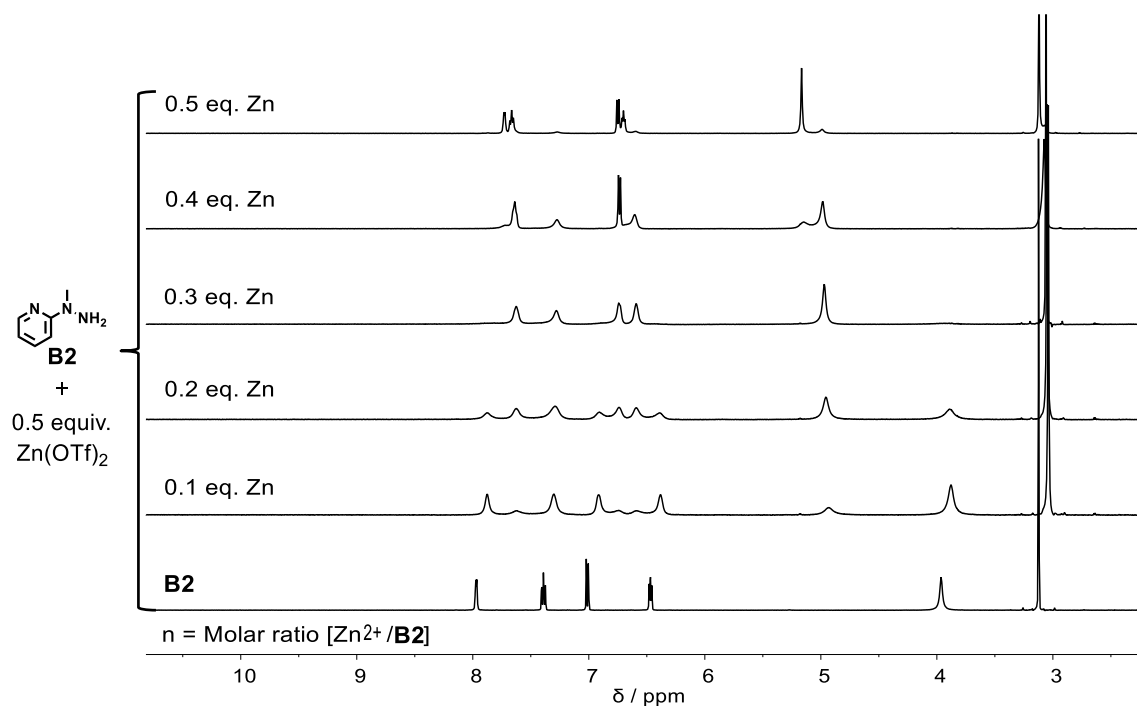


Figure 46. ¹H NMR spectra obtained from ¹H NMR titration experiment of **B2** by addition of Zn(OTf)₂.

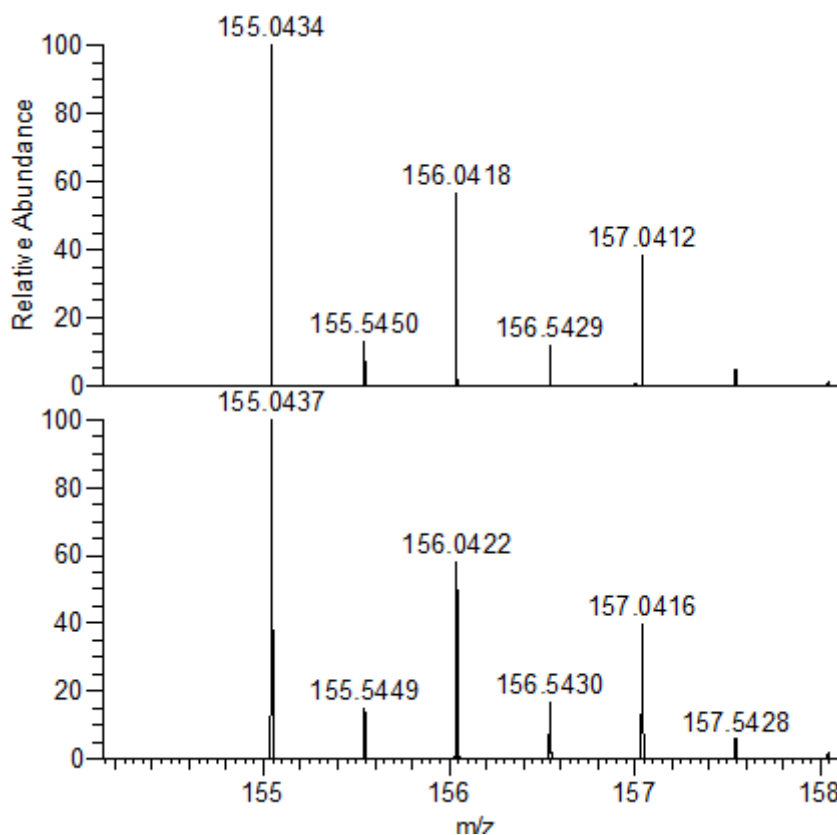
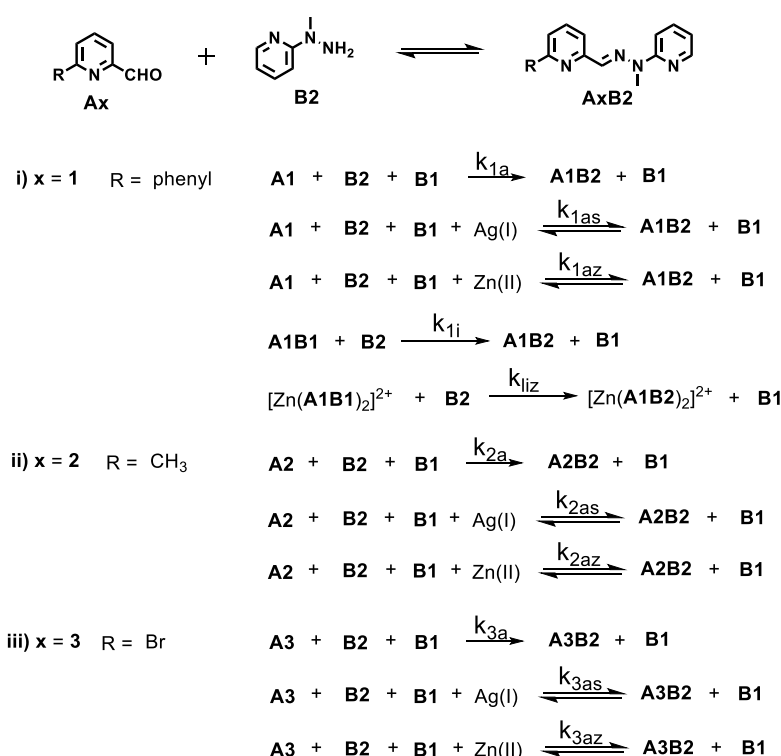


Figure 47. HRMS-ESI spectrum of [Zn(**B2**)₂]²⁺ obtained in situ from 2 equiv. **B2** (20 mM) and 1 equiv. Zn(OTf)₂ (10 mM) in CH₃CN. Measured (top), simulated (bottom).

C. Synergistic effects of metal salts and an auxiliary amine

The results above indicate that metal salts enhanced the rates of both imine and hydrazone formation, the effect being larger on imine formation than on hydrazone formation in the cases investigated. Given also that these reactions are known to be susceptible to nucleophilic catalysis by bases such as aniline, an obvious question was that of whether their conduct in the presence of both metal salts and an aniline derivative (here, *p*-anisidine, **B1**) would provide examples of synergistic catalysis. To answer this, a series of eight experiments were performed (**Scheme 19**). The evolution in time of the concentrations of the compounds in these eight dynamic mixtures and the rate constants are shown in the curves displayed in **Figure 52**.



Scheme 19. Hydrazone formation from pyridine-2-carboxaldehyde **A1** (**A2** or **A3**) and **B2** in the presence of (i) **B1** alone or together with either AgOTf or Zn(OTf)₂ as well as hydrazone formation from **A1B1** and **B2** and [Zn(**A1B2**)₂]²⁺ formation from [Zn(**A1B1**)₂]²⁺ and **B2**. k_{1a} , k_{1as} , k_{1az} , k_{1i} , k_{1iz} , k_{2a} , k_{2as} , k_{2az} , k_{3a} , k_{3as} , k_{3az} are the initial corresponding formation rate constants calculated from the formation of 10% product using a second order kinetic equation. For the structures of **A1B1**, and [Zn(**A1B1**)₂]²⁺ see **Scheme 15**.

i. Synergistic effect for the formation of complex of **A1B2**

The separate reaction of a mixture of the two components **A1** + **B2** (10 mM each) was followed by ¹H NMR either in presence of amine **B1** or metal salt as well as both amine **B1** and metal salt as shown in entries 1 to 8 in **Table 6**. In the presence of only amine **B1** (1.0 equiv.),

A1B2 was formed ($2.4 \times 10^{-3} \text{ M}^{-1}\text{s}^{-1}$, 50 h, entry 2 in **Table 6**, **Figure 48**), with a threefold acceleration of the reaction in comparison to the reaction **A1** + **B2** in the absence of the amine ($0.97 \times 10^{-3} \text{ M}^{-1}\text{s}^{-1}$, 162 h, entry 1 in **Table 6**, **Figure 32**). In the previously described experiments with AgOTf or Zn(OTf)₂ alone as catalysts (at half the concentration of the amine here), accelerations by factors of 14 and 8 were observed, the corresponding rate constants being $14 \times 10^{-3} \text{ M}^{-1}\text{s}^{-1}$ and $7.5 \times 10^{-3} \text{ M}^{-1}\text{s}^{-1}$ respectively (entries 2 and 3 in **Table 6**; 18 h and 62 h, **Figure 33** and **Figure 34**). Here, AgOTf was the slightly better catalyst, perhaps because of differences in the stability of the complexes of **B2** with the two cations.

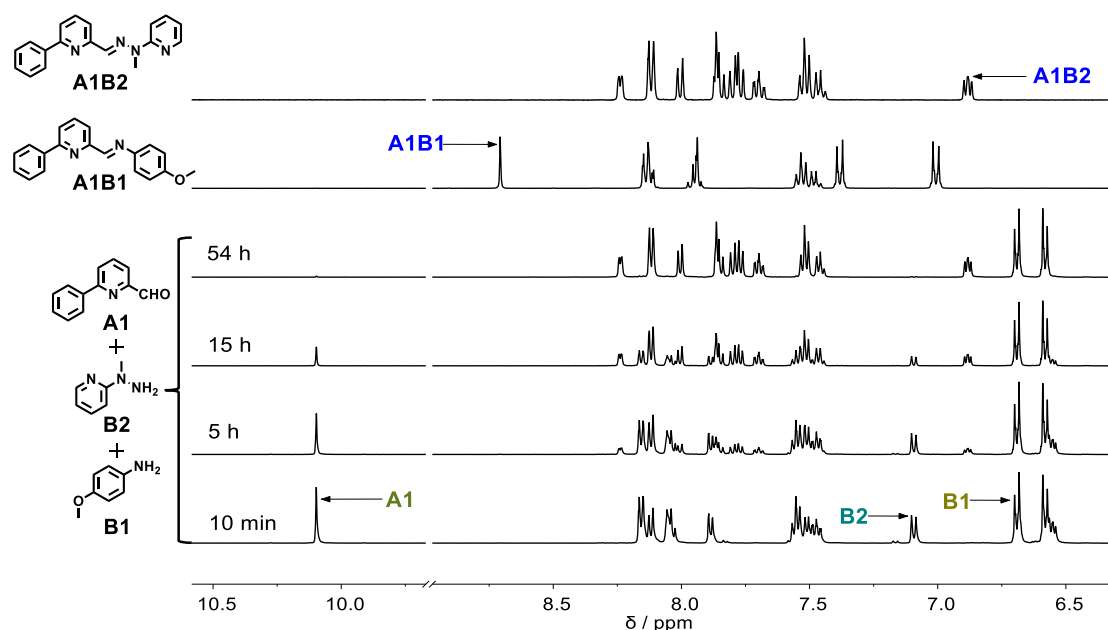


Figure 48. ¹H NMR (500 MHz) spectra of the mixture generated from equal amounts of **A1** + **B2** + **B1** (10 mM each, CD₃CN, 25°C) after 10 min, 5 h, 15 h, 54 h from bottom to top. Reference spectra (top two traces) are of the separately prepared constituents **A1B1**, **A1B2**.

The addition of the amine **B1** to the reaction mixture containing AgOTf had very little effect on the rate of the reaction (entries 3 and 5 in **Table 6**, **Figure 33** and **Figure 49**). The rate constants are $16 \times 10^{-3} \text{ M}^{-1}\text{s}^{-1}$ and $14 \times 10^{-3} \text{ M}^{-1}\text{s}^{-1}$ in the presence and absence, respectively, of **B1** and are essentially identical within experimental error. The kinetic curves are shown in **Figure 52**.

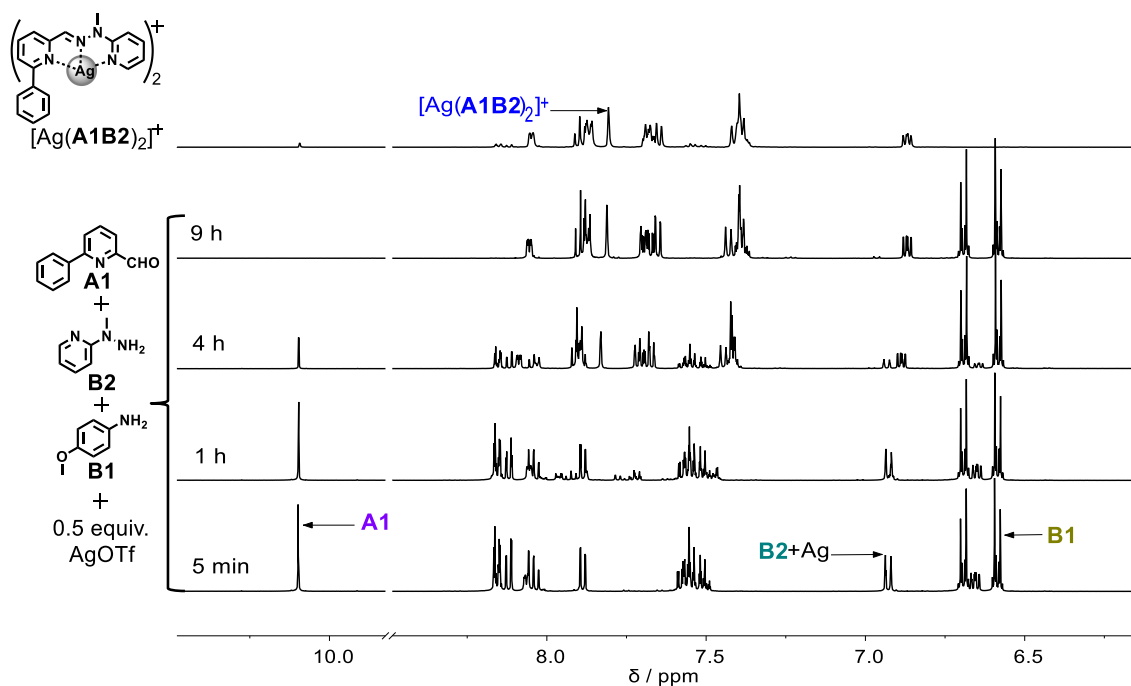


Figure 49. ¹H NMR (500 MHz) spectra of the mixture generated from equal amounts of **A1** + **B2** + **B1** + 0.5 equiv. AgOTf (10 mM each, CD₃CN, 25 °C) after 5 min, 1 h, 4 h, 9 h from bottom to top. A reference spectrum of the separately prepared constituent [Ag(A1B2)₂]⁺ is shown above.

In contrast, a strong effect was observed when **B1** was combined with Zn(OTf)₂ (entry 6 in **Table 6**; **Figure 50**). After just 4 minutes, the mixture contained about 25% of **A1B1** in its complexed form, 29% of free **A1**, 70% of free **B1** and 64% **B2** in its coordinated form together with 26% of [Zn(A1B2)₂]²⁺. Minor signals indicated the presence of other combinations of **A1**, **B1**, **B2** and Zn(II) but the signal broadening seen in several instances during this thesis work with mixtures containing Zn(II) rendered identification of intermediate species difficult. Obviously, rather unsymmetrical species such as [Zn(B2)_x(A1B1)_y(CD₃CN)_z]²⁺ might be present at certain stages. After about 2 hours, the zinc complex [Zn(A1B2)₂]²⁺ was fully formed, leaving free **B1** in the solution. The formation rate constant was about 0.61 M⁻¹ s⁻¹, which is a roughly estimated value calculated with regard to the loss of the aldehyde **A1** for easier comparison of different reactions (98%, 2 h, entry 6 in, **Figure 52**). Thus, the reaction rate was markedly increased when both metal cation and amine were added simultaneously to the reaction of **A1** with **B2**, with an acceleration factor of 630 compared to the formation of **A1B2** from **A1** + **B2** alone.

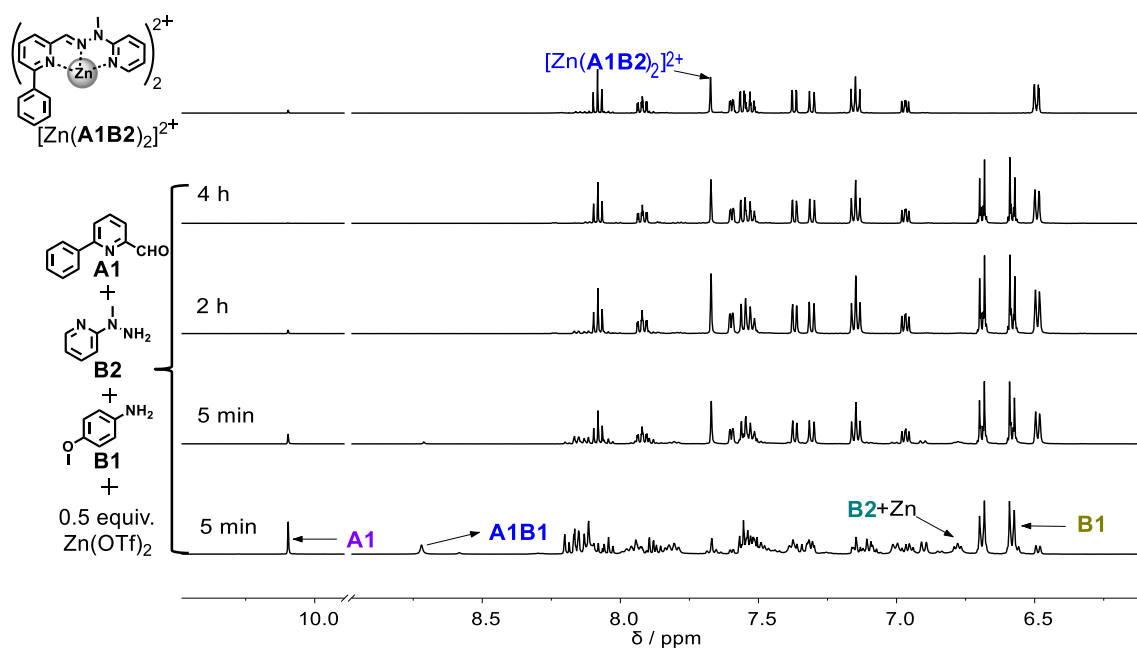


Figure 50. ¹H NMR (500 MHz) spectra of the mixture generated from equal amounts of **A1** + **B2** + **B1** (10 mM each, CD₃CN, 25°C) + Zn(OTf)₂ (5 mM each) after 5 min, 15 min, 2 h, 4 h from bottom to top. Reference spectrum of the separately prepared constituent [Zn(A1B2)₂]²⁺.

In order to slow down the reaction and define the evolution of the reaction especially in the beginning period where the 25°C ¹H NMR spectrum was very broad, the reaction was performed starting at the low temperature of -35°C then incrementing it to +25°C in steps of 10 degrees (**Figure 51**). At each temperature, the ¹H NMR spectrum was recorded 5 minutes after the temperature was attained. At -35°C, the first spectrum recorded showed about 12% **A1**, 14% Zn(II) complex of **A1B1**, 70% **A1B1** with broad signals, 82% **B2** in its coordinated form and 20% free **B1** to be present. **A1B1** reached a maximum of 90% at -25°C. In passing to 15°C, **A1** and [Zn(A1B1)₂]²⁺ decreased progressively and disappeared, while [Zn(A1B2)₂]²⁺ appeared and increased up to complete formation along with the release of free **B1** and the decrease and disappearance of **A1B1** and **B2**. These results indicated that the [Zn(A1B1)₂]²⁺ formed very rapidly at the beginning behaved as an activated species which reacted with **B2** to form [Zn(A1B2)₂]²⁺. Thus, metal salts and an amine together can strongly enhance hydrazone formation.

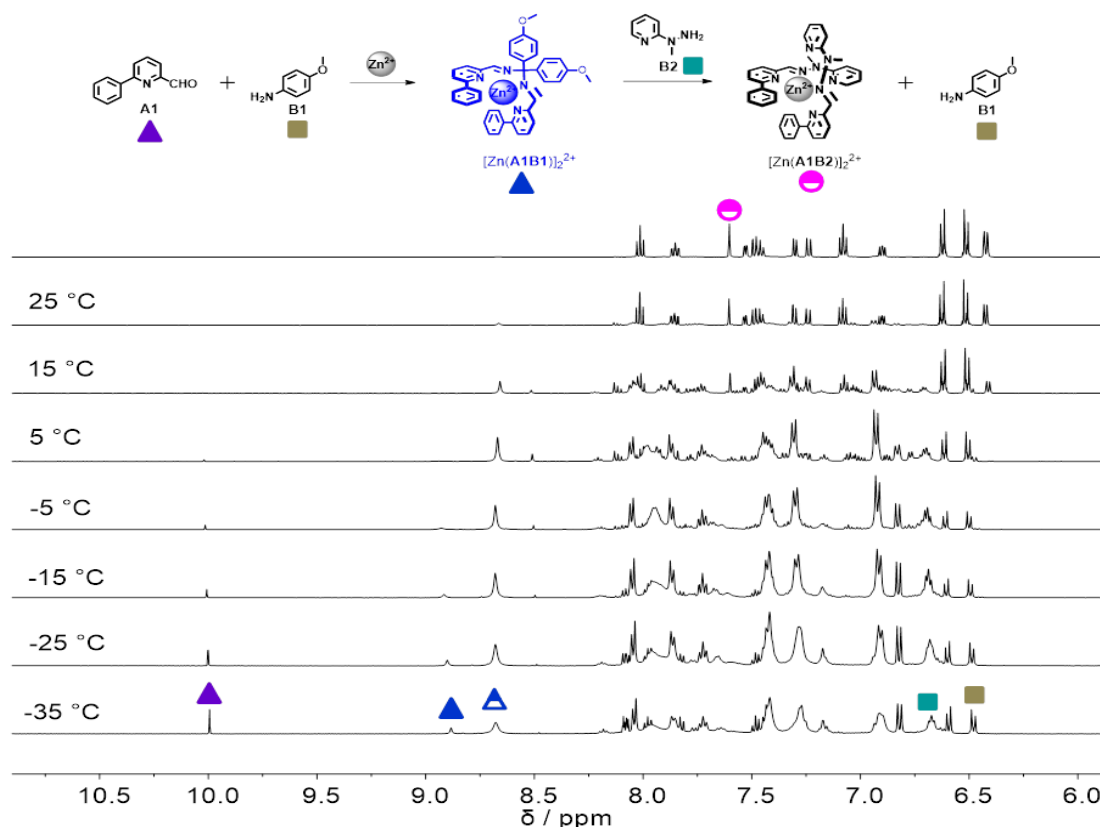


Figure 51. Low temperature ^1H NMR spectra obtained from mixing the same amount of **A1** + **B2** in presence of 1.0 equiv. **B1** and 0.5 equiv. Zn(II) starting from -35°C to +25°C in steps of 10 degrees (10 mM each, CD_3CN).

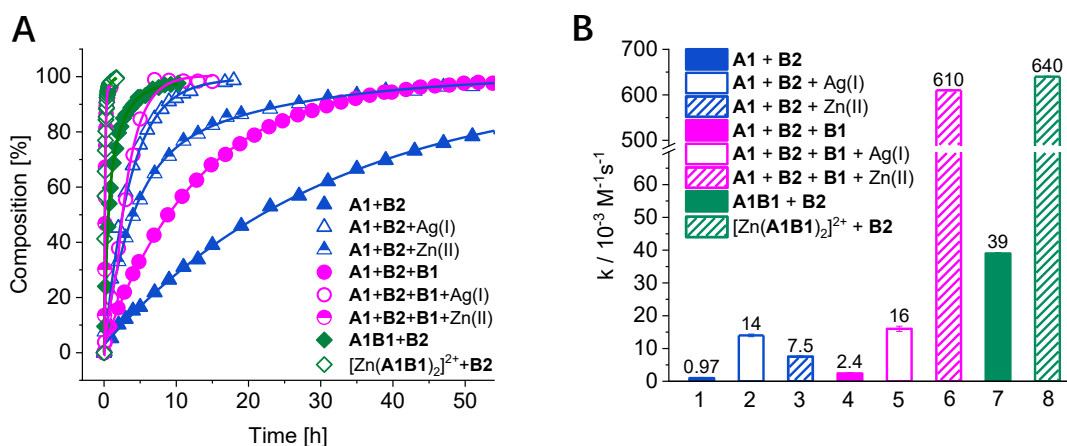


Figure 52. Comparative (A) kinetic curves obtained as a function of time from integration of the imine $\text{CH}=\text{N}$ proton signal in the 500 MHz ^1H NMR spectra (10 mM each, CD_3CN , 25°C) and (B) initial rate constants (k) calculated from a fit to a second-order reaction over the first 10% of the reaction for the hydrazone formation process between **A1** and **B2** (Scheme 19) in the absence of catalyst and in the presence of **B1** or a metal salt, AgOTf or Zn(OTf)_2 separately, as well as **B1** and AgOTf or **B1** and Zn(OTf)_2 together as co-catalysts along with the additional control reactions of **A1B1** with **B2** and $[\text{Zn}(\text{A1B1})_2]^{2+}$ with **B2**. Note that the curves for **A1** + **B2** + **B1** + Zn(II) and for $[\text{Zn}(\text{A1B1})_2]^{2+}$ + **B2** are superimposed.

Table 6. Kinetic features of the reactions between aldehyde **A1** and hydrazine **B2** in the absence and presence of metal salts separately as well as in the presence of both **B1** and metal salts together and control reactions of **A1B1** with **B2** and $[\text{Zn}(\text{A1B1})_2]^{2+}$ with **B2**.

Entry ^[a]	Reaction	Catalyst 0.5 equiv.	Product	$t_{50}[\text{h}]^{[c]}$	$t_{10}[\text{h}]^{[d]}$	$k^{[e]}/10^3 \text{ M}^{-1}\text{s}^{-1}$	Acceleration Factor
1	A1 + B2	No catalyst	A1B2	21	1.94	0.97	n.a. ^[f]
2	A1 + B2 + Ag(I)	Ag(I)	$[\text{Ag}(\text{A1B2})_2]^+$	2.4	0.35	14	14
3	A1 + B2 + Zn(II)	Zn(II)	$[\text{Zn}(\text{A1B2})_2]^{2+}$	4	0.55	7.5	8
4	A1 + B2 + B1	B1 (1.0 equiv.)	A1B2	8.8	0.97	2.4	3
5	A1 + B2 + B1 + Ag(I)	B1 (1.0 equiv.) + Ag(I)	$[\text{Ag}(\text{A1B2})_2]^+$	2.7	0.44	16	16
6	A1 + B2 + B1 + Zn(II)	B1 (1.0 equiv.) + Zn(II)	$[\text{Zn}(\text{A1B2})_2]^{2+}$	0.15	≤ 0.08	≥ 610	630
7	A1B1 + B2	— ^[b]	A1B2	1.0	0.08	39	40 ^[b]
8	$[\text{Zn}(\text{A1B1})_2]^{2+}$ + B2	— ^[b]	$[\text{Zn}(\text{A1B2})_2]^{2+}$	0.16	≤ 0.08	≥ 640	≥ 660 ^[b]

^[a] In all entries, aldehyde (10 mM), amine or hydrazine (10 mM), AgOTf or Zn(OTf)₂ (5 mM), at 25°C, in CD₃CN, monitored by ¹H NMR. ^[b] Transimination experiments; no catalyst added; the acceleration factors correspond to the reaction of **B2** with the imine **A1B1** free (entry 7) or complexed (entry 8) compared to the reaction of **B2** with the aldehyde **A1** (entry 1). ^[c] Time for 50% completion of the reaction. ^[d] Time for 10% completion of the reaction. ^[e] The rate constant *k* has been calculated from a fit to a second-order reaction over the first 10% of the reaction (error on calculated rate constant of about 5%). The values are listed as 10³ *k* for ease of comparison. ^[f] Not applicable.

To analyze the possible origins of this synergistic catalysis, the following experiments were conducted:

a) Starting from the preformed imine **A1B1**, addition of 0.5 equiv. of Zn(OTf)₂, led to the immediate and full formation (99%) of the zinc complex of $[\text{Zn}(\text{A1B1})_2]^{2+}$ as indicated by its imine signal at 9.0 ppm (**Figure 53**). On addition of 1 equiv. **B2**, some of the signals in the ¹H NMR spectrum became broad due to relatively slow exchange reactions of intermediate Zn(II) complexes. Nonetheless signal integrations indicated a composition of about 37% of **B2** coordinated to zinc, 35% complexed imine **A1B1** (imine CH signal at 8.7 ppm), 38% $[\text{Zn}(\text{A1B2})_n]^{2+}$ (imine CH=N signal at 7.6 ppm), 65% of free **B1** and the remainder [about 25% **A1**, 25% **B2** and possibly mixed-ligand complexes of Zn(II)] accounted for other signals in the spectrum. The mixture evolved until after 2 h the zinc complex $[\text{Zn}(\text{A1B2})_2]^{2+}$ was fully (97%) formed with liberation of 1 equiv. of free **B1** (0.64 M⁻¹ s⁻¹).

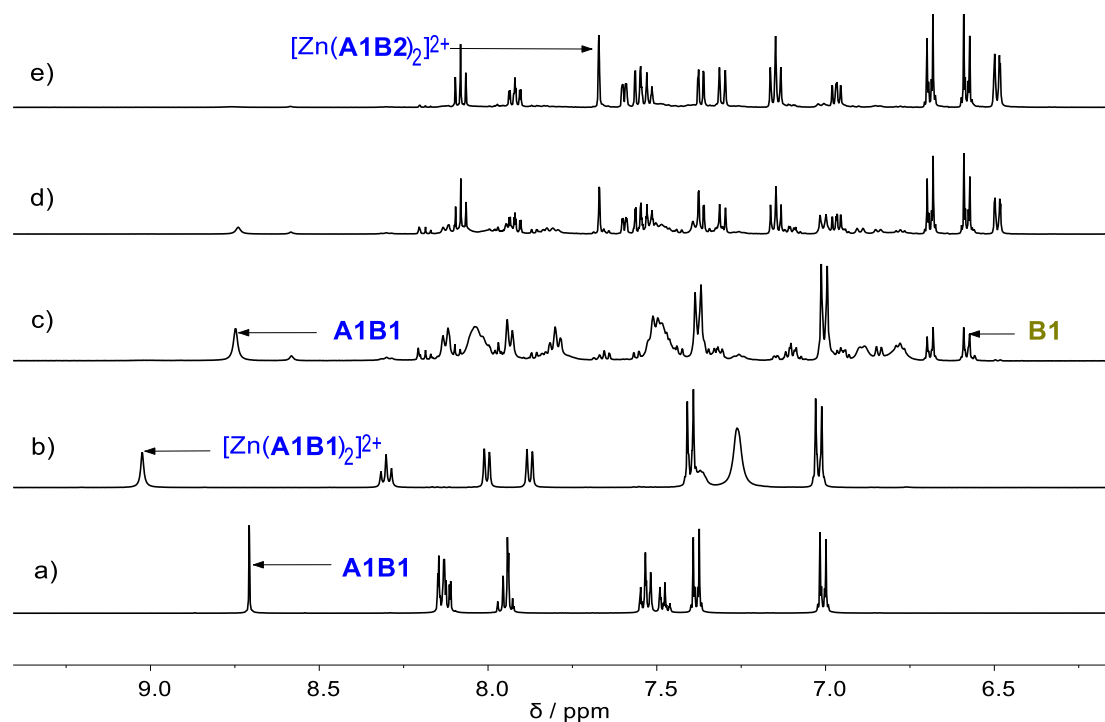


Figure 53. ^1H NMR (500 MHz) spectra from bottom to top: a) **A1B1**; b) **A1B1** (10 mM) + 0.5 equiv. $\text{Zn}(\text{OTf})_2$; c) **A1B1** (10 mM each) + 0.5 equiv. $\text{Zn}(\text{OTf})_2$ + **B2** (10 mM) after 5 min; d) **A1B1** (10 mM each) + 0.5 equiv. $\text{Zn}(\text{OTf})_2$ + **B2** (10 mM) after 20 min; e) **A1B1** (10 mM each) + 0.5 equiv. $\text{Zn}(\text{OTf})_2$ + **B1** (10 mM) after 2 h; e) reference spectrum of the separately constituent $[\text{Zn}(\text{A1B2})_2]^{2+}$.

b) When the same experiment was performed a different order, starting from **A1** + **B2** and adding 0.5 equiv. of $\text{Zn}(\text{OTf})_2$, the signals due to **B2** immediately showed shifts indicative of coordination to $\text{Zn}(\text{II})$ (99%, **Figure 46**) and all **A1** was left free. Thus, essentially all **B2** was converted into a non-nucleophilic species (assuming chelation by pyridine- and hydrazine-N), explaining why no **A1B2** or $[\text{Zn}(\text{A1B2})_2]^{2+}$ was observed at this moment. When **B1** was then added, an imine proton signal due to **A1B1** (46%) at 8.65 ppm (as above) appeared after 5 min, together with 12% of free **A1**, 58% **B2** coordinated to zinc and 4% of $[\text{Zn}(\text{A1B2})_n]^{2+}$, 54% of free **B1**. The remainder (about 38% of **A1** and **B2**) gave rise to other signals in the spectrum but the exact nature of the species involved could not be established. The zinc complex $[\text{Zn}(\text{A1B2})_2]^{2+}$ was fully (98%) formed after about 2 hours (rate constant $180 \text{ M}^{-1} \text{ s}^{-1}$) leaving free **B1** (see **Figure 54**).

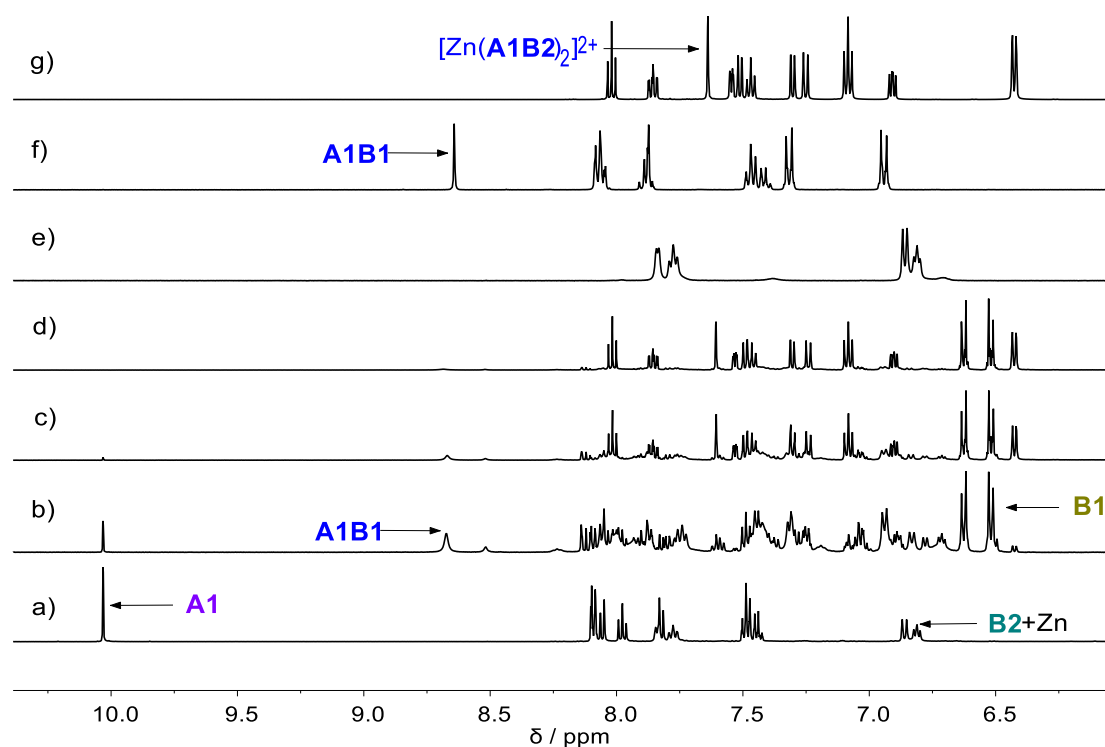


Figure 54. ^1H NMR (500 MHz) spectra from bottom to top: a) **A1** + **B2** (10 mM each) + 0.5 equiv. $\text{Zn}(\text{OTf})_2$; b) **A1** + **B2** (10 mM each) + 0.5 equiv. $\text{Zn}(\text{OTf})_2$ + **B1** (10 mM) after 4 min; c) **A1** + **B2** (10 mM each) + 0.5 equiv. $\text{Zn}(\text{OTf})_2$ + **B1** (10 mM) after 9 min; d) **A1** + **B2** (10 mM each) + 0.5 equiv. $\text{Zn}(\text{OTf})_2$ + **B1** (10 mM) after 30 min; e) reference spectra **B2** (10 mM) + 0.5 equiv. $\text{Zn}(\text{OTf})_2$; f) reference spectrum of the separately prepared constituent **A1B1**; g) reference spectrum of the separately prepared constituent $[\text{Zn}(\text{A1B2})_2]^{2+}$.

c) We then checked if **A1B2** formation was faster from the transamination reaction of **A1B1** with **B2** than from condensation of **A1** and **B2**. As described earlier, when just **A1** and **B2** were mixed, **A1B2** was obtained after about 162 h (entry 1 in **Table 6**). When **B2** was added to **A1B1**, **A1B2** was obtained in about 10 h (99%; entry 7 in **Table 6**; **Figure 55**) with a rate constant of $3.9 \times 10^{-2} \text{ M}^{-1} \text{ s}^{-1}$ amounting to 40-fold acceleration of the formation of **A2B2** from its components **A2**+**B2**. This result indicates that the hydrazone **A1B2** formed more rapidly from the preformed **A1B1** and **B2** than from **A1** + **B2**, implying that **A1B1** is more reactive as an electrophile than **A1**, an interesting result perhaps indicative of differences in proton transfer rates in the aminal addition intermediate than in the carbinolamine.

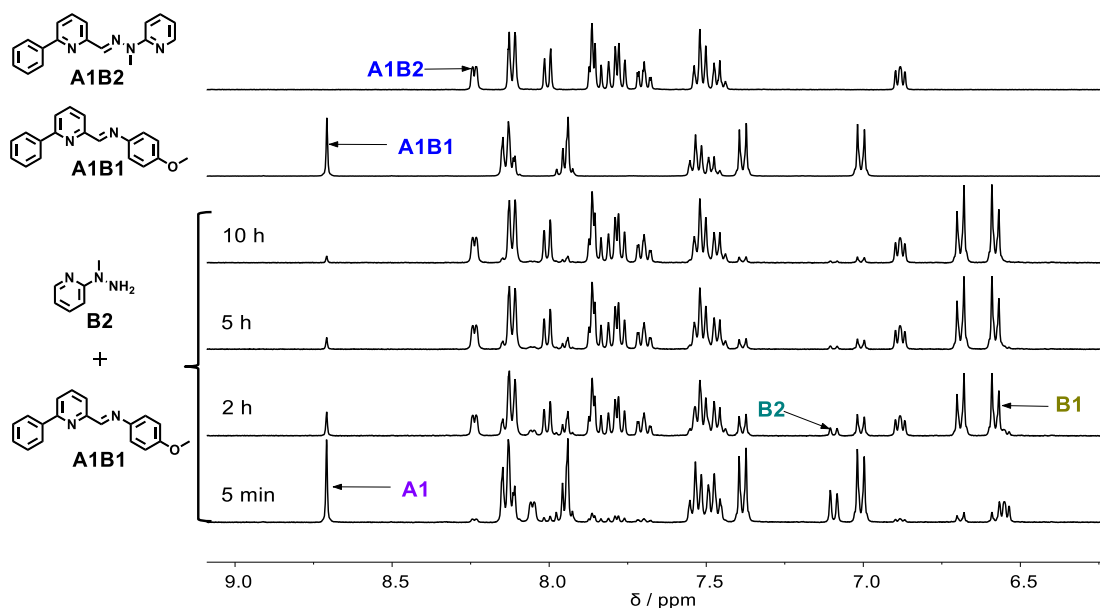


Figure 55. ^1H NMR (500 MHz) spectra of the mixture generated from equal amounts of **A1B1** + **B2** (10 mM each, CD_3CN , 25°C) after 5 min, 2 h, 5 h, 10 h from bottom to top. Two reference spectra of the separately prepared constituents **A1B1**, **A1B2** were shown above.

There is a very marked synergistic co-catalytic effect on simultaneous addition of Zn(II) and **B1** to the **A1** + **B2** mixture which leads to a much faster formation of the $[\text{Zn}(\text{A1B2})_2]^{2+}$ complex than when either Zn(II) or **B1** is added separately (2 h versus 62 h or versus 50 h respectively; see entries 3, 4 and 6 in **Table 6**).

Particular observations which bear upon the mechanism of the co-catalysis described above are:

1) The formation of the imine **A1B1** from **A1** + **B1** is very slow (entry 1 in **Table 4**, $1.1 \times 10^{-3} \text{ M}^{-1} \text{ s}^{-1}$).

2) The formation of the hydrazone **A1B2** is very slow but increases along the sequence: i) **A1** + **B2** (entry 1 in **Table 4**, $0.97 \times 10^{-3} \text{ M}^{-1} \text{ s}^{-1}$); ii) **A1** + **B1** + **B2** (entry 2 in **Table 6**, $3.2 \times 10^{-3} \text{ M}^{-1} \text{ s}^{-1}$) a little faster with no **A1B1** observed; iii) **A1B1** + **B2** (entry 7 in **Table 6**, $16.5 \times 10^{-3} \text{ M}^{-1} \text{ s}^{-1}$).

3) The formation of the imine complex $[\text{Zn}(\text{A1B1})_2]^{2+}$ from **A1** + **B1** + Zn(II) (entry 3 in **Table 4**, $18.2 \text{ M}^{-1} \text{ s}^{-1}$) is much faster than that of the imine **A1B1** in the absence of Zn(II) , being complete when the first spectrum is measured (about 4 min; 98%) giving an acceleration factor at least 1.65×10^4 .

4) The formation of the hydrazone-based zinc complex $[\text{Zn}(\text{A1B2})_2]^{2+}$ from **A1** + **B2** + Zn(II) (entry 3 in **Table 4**, $5.5 \times 10^{-3} \text{ M}^{-1} \text{ s}^{-1}$) is comparable to that of the hydrazone **A1B2** from

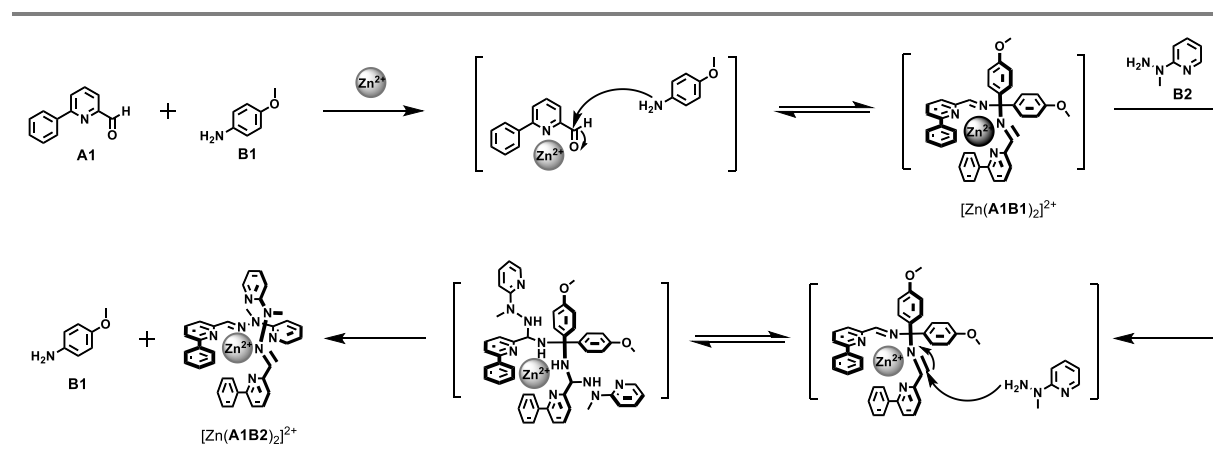
A1 + **B1** + **B2** (2ii above), both being faster (about 6 times and 3 times) than that of the hydrazone **A1B2** from **A1** + **B2** (see 2i).

5) The formation of $[\text{Zn}(\mathbf{A1B2})_2]^{2+}$ from $[\text{Zn}(\mathbf{A1B1})_2]^{2+}$ + **B2** is very fast (entry 8 in **Table 6**, $57 \times 10^{-3} \text{ M}^{-1} \text{ s}^{-1}$).

6) The formation of the hydrazone-based zinc complex $[\text{Zn}(\mathbf{A1B2})_2]^{2+}$ from **A1** + **B1** + **B2** + Zn(II) is very fast (entry 6 in **Table 6**, $54 \times 10^{-3} \text{ M}^{-1} \text{ s}^{-1}$).

The most important aspects of these results are that i) the formation of the imine complex $[\text{Zn}(\mathbf{A1B1})_2(\text{CF}_3\text{SO}_3)_2]$ is by far the fastest reaction of all; ii) **B1** and Zn(II) exert independently a moderate effect on the formation of respectively the ligand **A1B2** itself and of its complex $[\text{Zn}(\mathbf{A1B2})_2]^{2+}$; iii) when BOTH are present, they exert a very strong synergistic catalysis effect on the formation of this same complex.

These observations can be rationalized if i) the complexed imine **A1B1** is the active species in the process, perhaps in the form of $[\text{Zn}(\mathbf{A1B1})_2(\text{CH}_3\text{CN})_2]^{2+}$; ii) the C=N bond of imine **A1B1** is more reactive than the C=O group of aldehyde **A1**; iii) the N of imine **A1B1** is a better binding site for Zn(II) than the O of C=O in **A1**.



Scheme 20. Proposed schematic mechanism for the formation of the zinc complex $[\text{Zn}(\mathbf{A1B2})_2]^{2+}$ from **A1** + **B2** in presence of both $\text{Zn}(\text{OTf})_2$ and **B1** acting in a synergistic co-catalysis pathway. The formation of $[\text{Zn}(\mathbf{A1B2})_2]^{2+}$ could also proceed in two successive steps.

Thus, the proposed mechanism contains three main steps: 1) Zn(II) strongly catalyzes the formation of the imine-based zinc complex $[\text{Zn}(\mathbf{A1B1})_2]^{2+}$; 2) this imine **A1B1** is activated by forming the two ligand complex $[\text{Zn}(\mathbf{A1B1})_2(\text{CF}_3\text{SO}_3)_2]$ which allows easier accessibility of **B2**; 3) **B2** reacts with the activated C=N in the imine-based complex $[\text{Zn}(\mathbf{A1B1})_2]^{2+}$ to form $[\text{Zn}(\mathbf{A1B2})_2]^{2+}$ and release the free **B1**.

ii. Synergistic effect for the formation of complexes of A2B2

To see if synergism applied in catalysis of the formation of the ligand **A2B2**, another set of experiments with **A2** + **B2** in the presence of **B1** alone (**Figure 56**, **Table 7**), and **B1** and 0.5 equiv. of either AgOTf (**Figure 57**) or Zn(OTf)₂ (**Figure 58**) was also conducted. Similar results were obtained. The kinetic curves and rate constants are shown in **Figure 59** and **Table 7**.

In the presence of only **B1** (entry 4 in **Table 7**), the formation of **A2B2** was 3 times faster than for **A2** + **B2** alone (entry 1 in **Table 7**). Reactions of **A2** + **B2** in the presence of Ag(I) or Zn(OTf)₂ both gave 11 times acceleration (entries 2 and 3 in **Table 7**).

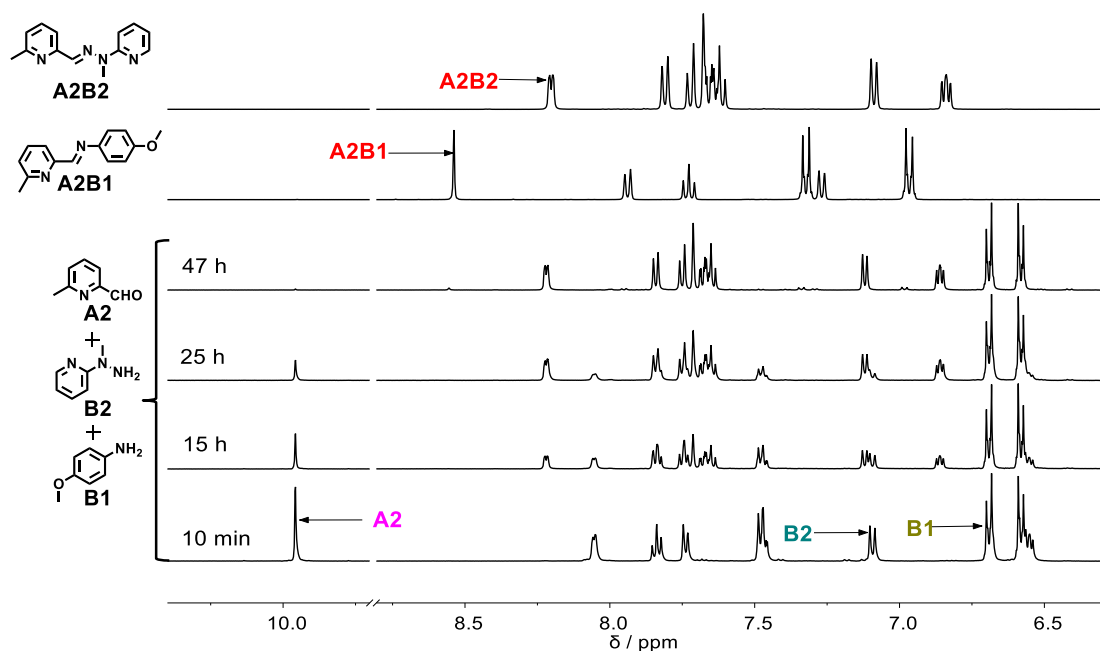


Figure 56. ¹H NMR (500 MHz) spectra of the mixture generated from equal amounts of **A2** + **B2** + **B1** (10 mM each) in CD₃CN at 25°C after 10 min, 15 h, 25 h, 47 h from bottom to top. Two reference spectra (top two traces) of the separately prepared constituents **A2B1**, **A2B2** were shown above.

In the presence of both Ag(I) and **B1** (entry 5 in **Table 7**), the reaction was moderately accelerated in comparison to the formation of **A2B2** alone with 15 times acceleration, a comparable value to that of **A2** + **B2** in the presence of only Ag(I) (entry 2 in **Table 7**).

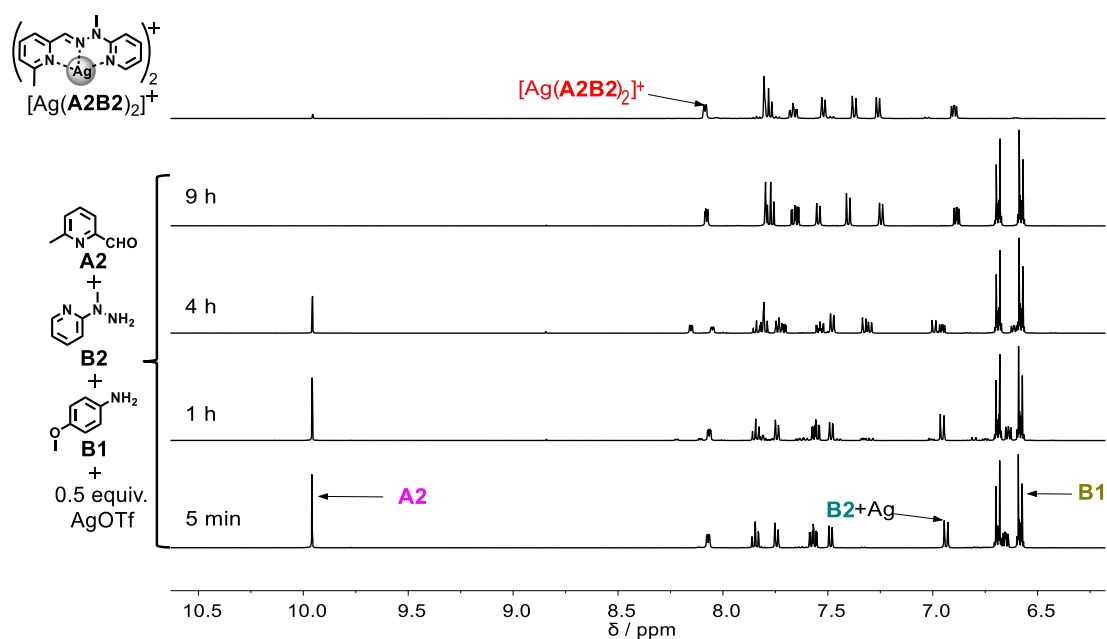


Figure 57. ^1H NMR (500 MHz) spectra of the mixture generated from equal amounts of **A2** + **B2** + **B1** (10 mM each) + 0.5 equiv. AgOTf (5 mM) in CD_3CN at 25°C after 5 min, 1 h, 4 h, 9 h from bottom to top. A reference spectrum of the separately prepared constituent $[\text{Ag}(\text{A2B2})_2]^+$ is shown above.

The formation of hydrazone **A2B2** as its $\text{Zn}(\text{II})$ complex was significantly accelerated in the presence of co-catalysts $\text{Zn}(\text{II})$ and *p*-anisidine (**B1**), with a rate constant of $0.24 \text{ M}^{-1} \text{ s}^{-1}$ (entry 6 in **Table 7**). The acceleration factor of this synergistic catalysis is 421 times that of the formation of **A2B2** alone ($5.7 \times 10^{-4} \text{ M}^{-1} \text{ s}^{-1}$). The ^1H NMR spectra again showed broadened signals in the early stages of reaction, presumably due to relatively slow exchange between different $\text{Zn}(\text{II})$ complexes. After less than 3 hours, $[\text{Zn}(\text{A2B2})_2]^{2+}$ was almost fully formed (**Figure 58**).

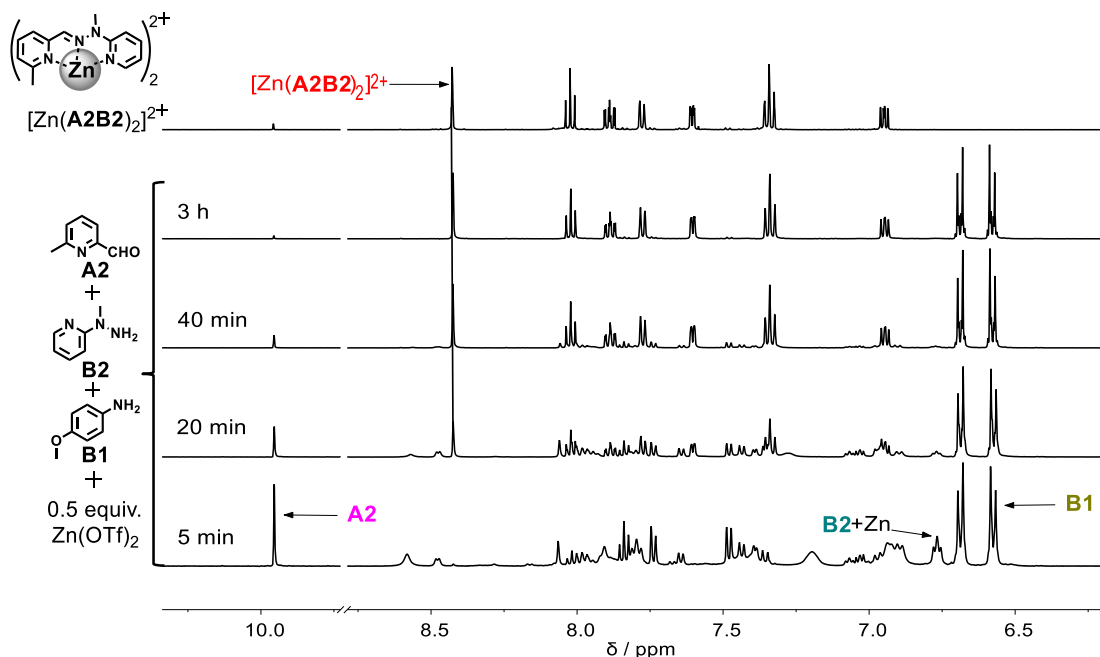


Figure 58. ^1H NMR (500 MHz) spectra of the mixture generated from equal amounts of **A2** + **B2** + **B1** (10 mM each) + $\text{Zn}(\text{OTf})_2$ (5 mM) in CD_3CN at 25°C after 5 min, 20 min, 40 min, 3 h from bottom to top. A reference spectrum of the separately prepared constituent $[\text{Zn}(\text{A2B2})_2]^{2+}$ is shown above.

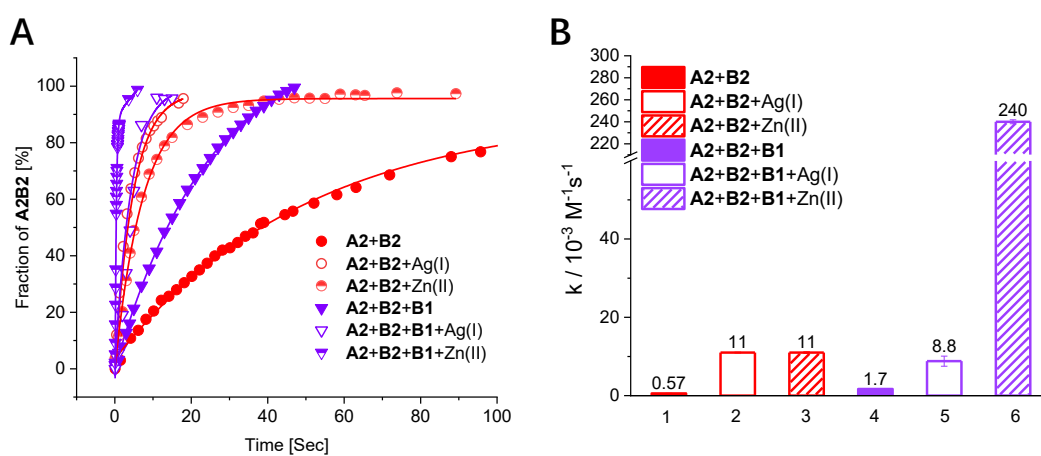


Figure 59. Comparative (A). kinetic curves and (B). initial rate constants for the hydrazone formation process between **A2** and **B2** (Scheme 19) in the absence of catalyst and presence of **B1** or a metal salt, AgOTf or $\text{Zn}(\text{OTf})_2$ separately, as well as **B1** and AgOTf or **B1** and $\text{Zn}(\text{OTf})_2$ together as co-catalysts in CD_3CN at 25°C ; The numbers above the columns correspond to $10^3 k$ for ease of comparison (error on calculated rate constant of about 5%).

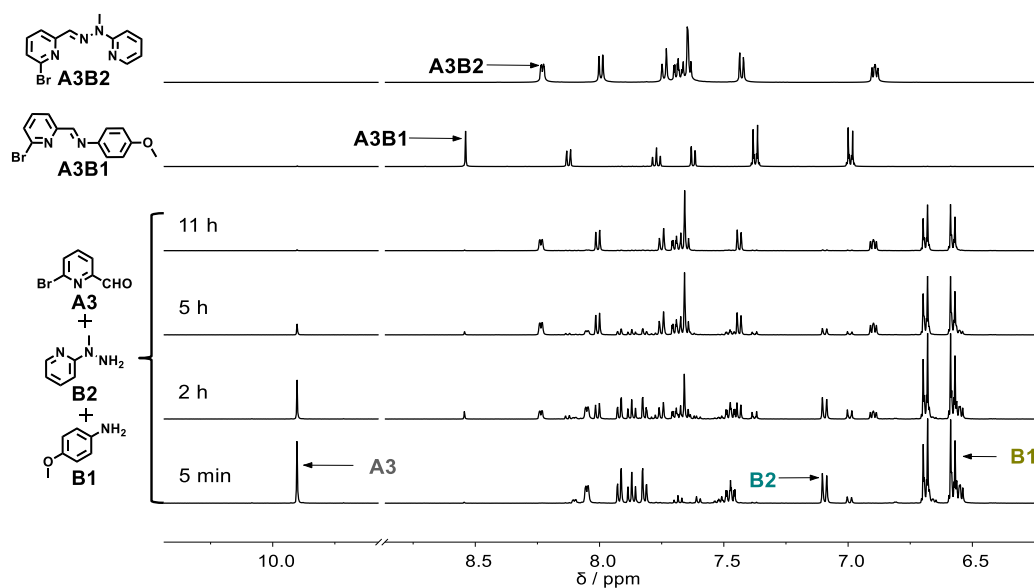
Table 7. Kinetic features of the reactions between aldehyde **A2** and hydrazine **B2** in the absence and presence of metal salts separately as well as in presence of both **B1** and metal salts together

Entry ^[a]	Reaction ^[b]	Catalyst	Product	t ₅₀ [h] ^[c]	t ₁₀ [h] ^[d]	k ^[e] /10 ⁻³ M ⁻¹ s ⁻¹	Acceleration Factor
1	A2 + B2	— ^[b]	A2B2	37	3.9	0.57	n.a. ^[f]
2	A2 + B2 + Ag(I)	Ag(I)	[Ag(A2B2) ₂] ⁺	2.8	0.38	11	19
3	A2 + B2 + Zn(II)	Zn(II)	[Zn(A2B2) ₂] ²⁺	5.1	0.98	11	19
4	A2 + B2 + B1	B1	A1B2	14	2.9	1.7	3
5	A2 + B2 + B1 + Ag(I)	B1 + Ag(I)	[Ag(A1B2) ₂] ⁺	4.1	1.4	8.8	15
6	A2 + B2 + B1 + Zn(II)	B1 + Zn(II)	[Zn(A1B2) ₂] ²⁺	0.26	0.07	240	≥421

^[a] In all these entries, aldehyde (10 mM), amine or hydrazine (10 mM), AgOTf or Zn(OTf)₂ (5 mM), at 25°C, in CD₃CN, monitored by ¹H NMR. ^[b] No catalyst was added. ^[c] Time for 50% completion of the reaction. ^[d] Time for 10% completion of the reaction. ^[e] The rate constant has been calculated from a fit to a second-order reaction over the first 10% of the reaction. The values are listed as 10³ k for ease of comparison. ^[f] Not applicable.

iii. Synergistic effect for the formation of complex of **A3B2**

When **A1** was replaced by **A3**, similar sets of experiments **A3** + **B2**, **A3** + **B2** + **B1**, **A3** + **B2** + **B1** + AgOTf and **A3** + **B2** + **B1** + Zn(OTf)₂ were conducted and the kinetic curves and rate constants are shown in **Figure 63** and **Table 8**.

**Figure 60.** ¹H NMR (500 MHz) spectra of the mixture generated from equal amounts of **A3** + **B2** + **B1** (10 mM each) in CD₃CN at 25°C after 5 min, 2 h, 5 h, 11 h from bottom to top. Two reference spectra (top two traces) of the separately prepared constituents **A3B1**, **A3B2** are shown above.

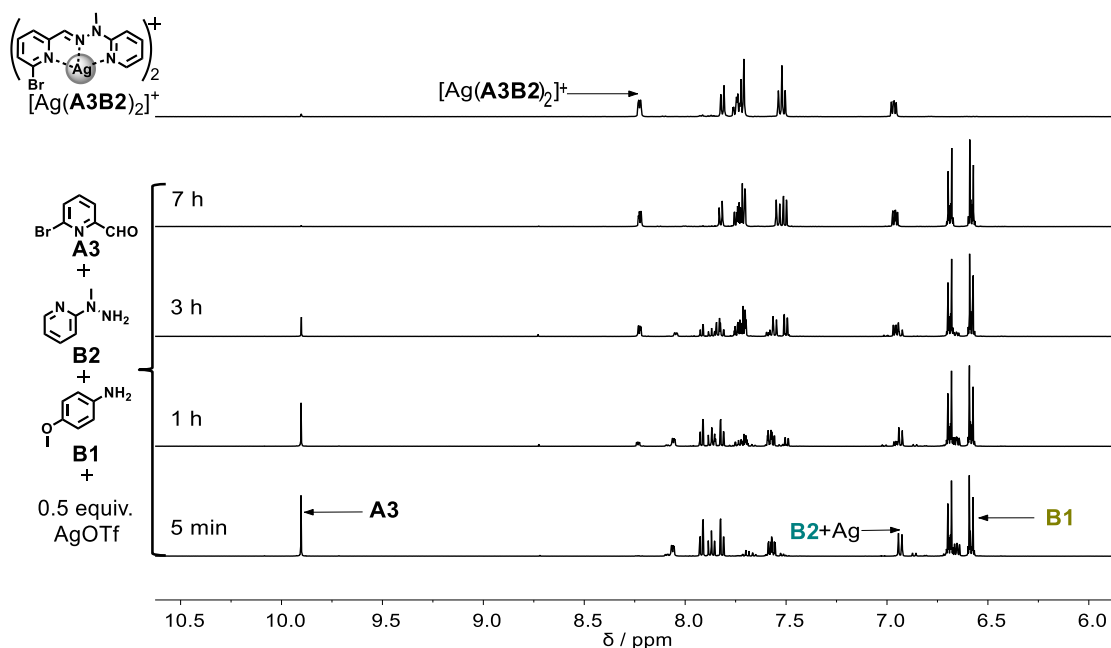


Figure 61. ^1H NMR (500 MHz) spectra of the mixture generated from equal amounts of **A3** + **B2** + **B1** (10 mM each) + AgOTf (5 mM) in CD_3CN at 25°C after 5 min, 1 h, 3 h, 7 h from bottom to top. A reference spectrum of the separately prepared constituent $[\text{Ag}(\text{A3B2})_2]^+$ is shown above.

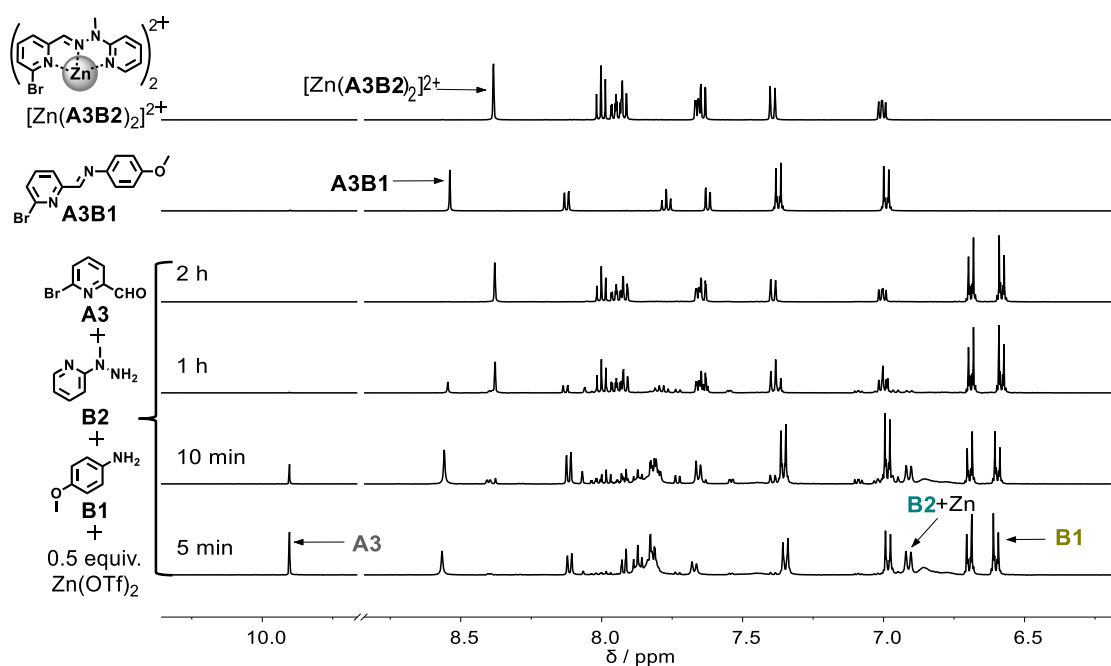


Figure 62. ^1H NMR (500 MHz) spectra of the mixture generated from equal amounts of **A3** + **B2** + **B1** (10 mM each) + $\text{Zn}(\text{OTf})_2$ (5 mM) in CD_3CN at 25°C after 5 min, 10 min, 1 h, 2 h from bottom to top. Reference spectra (top two traces) of the separately prepared constituents **A3B1**, $[\text{Zn}(\text{A3B2})_2]^{2+}$ are shown above.

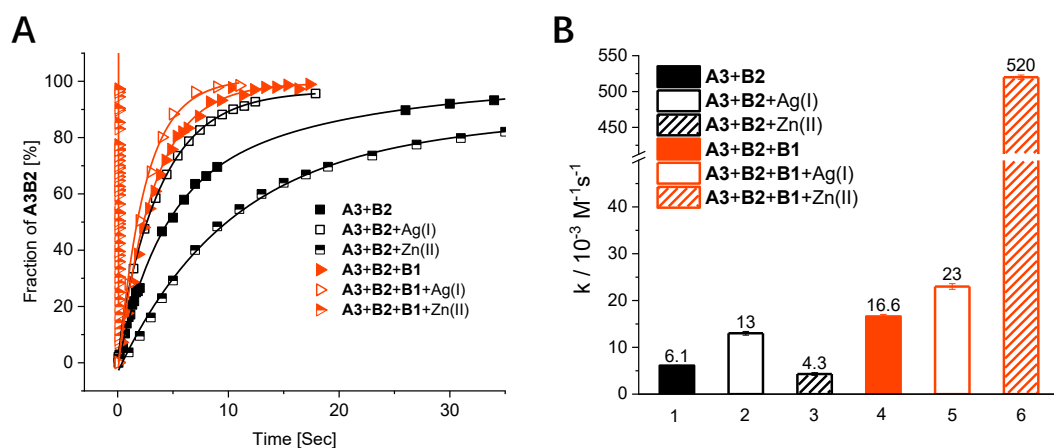


Figure 63. Comparative (A). kinetic curves and (B). initial rate constant (k) for the hydrazone formation process between **A3** and **B2** (Scheme 19) in absence of catalyst and in presence of **B1** or a metal salt, AgOTf or Zn(OTf)₂ separately, as well as **B1** and AgOTf or **B1** and Zn(OTf)₂ together as co-catalysts along in CD₃CN at 25°C. The numbers above the columns correspond to $10^3 k$ for ease of comparison.

Table 8. Kinetic features of the reactions between aldehyde **A3** and hydrazine **B2** in the absence and presence of metal salts separately as well as in the presence of both **B1** and metal salts together

Entry ^[a]	Reaction	Catalyst	Product	t_{50} [h] ^[c]	t_{10} [h] ^[d]	$k^{[e]}$ / 10^{-3} $M^{-1}s^{-1}$	Acceleration Factor
1	A3 + B2	— ^[b]	A3B2	4.6	0.63	6.1	n.a. ^[f]
2	A3 + B2 + Ag(I)	Ag(I)	[Ag(A3B2) ₂] ⁺	2.7	0.36	13	2.1
3	A3 + B2 + Zn(II)	Zn(II)	[Zn(A3B2) ₂] ²⁺	9.4	2.0	4.3	0.7
4	A3 + B2 + B1	B1	A3B2	2.7	0.5	16.6	3
5	A3 + B2 + B1 + Ag(I)	B1 + Ag(I)	[Ag(A3B2) ₂] ⁺	2.0	0.44	23	4
6	A3 + B2 + B1 + Zn(II)	B1 + Zn(II)	[Zn(A3B2) ₂] ²⁺	0.08	≤0.08	≥520	≥85

^[a] In all these entries, aldehyde (10 mM), amine or hydrazine (10 mM), AgOTf or Zn(OTf)₂ (5 mM), at 25°C, in CD₃CN, monitored by ¹H NMR. ^[b] No catalyst was added. ^[c] Time for 50% completion of the reaction. ^[d] Time for 10% completion of the reaction. ^[e] The rate constant has been calculated from a fit to a second-order reaction over the first 10% of the reaction (error on calculated rate constant of about 5%). The values are listed as $10^3 k$ for ease of comparison. ^[f] Not applicable.

The formation of **A3 + B2** in the absence of any catalyst (entry 1 in **Table 8**) is much faster than **A1 + B2** (entry 1 in **Table 6**), possibly due to the electron-withdrawing character of the

bromo group of **A3**. The reaction **A3** + **B2** in the presence of AgOTf gave an acceleration factor of 2.1, while in the presence of Zn(OTf)₂, the formation of zinc complex of **A3B2** is even slower than the formation of **A3B2** from **A3** and **B2**. This is probably an effect of the strong coordination of **B2** by Zn(II). In the presence of co-catalysts **B1** and AgOTf (entry 5 in **Table 8**), the formation of silver complex of **A3B2** is accelerated by a factor of 23 compared to that without any catalyst and 10 compared to that with Ag(I) alone, indicating that there is synergistic effect of **B1** and AgOTf. The simultaneous operation of both **B1** and Zn(OTf)₂ induced a large acceleration by a factor of 85 relative to the uncatalyzed process (entry 6 in **Table 8**), with a rate constant of 0.52 M⁻¹ s⁻¹.

iv. Synergistic effect of the three co-factors AgOTf, Zn(OTf)₂ and B1

When the reaction **A1** + **B2** (10 mM each) was run in presence of the *three* co-factors, **B1** (10 mM) together with both AgOTf (5 mM) and ZnOTf (5 mM), the silver complex of the imine **A1B1** was already formed (92%) after only 10 minutes, with a similar amount of the Zn(II) complex of **B2** being present, in strong contrast to the very slow formation of **A1B1** in the absence of metal cations. The mixture rearranged by component exchange to form the zinc complex [Zn(**A1B2**)₂]²⁺, giving the final distribution of 8% [Ag(**A1B1**)₂]⁺, 92% [Zn(**A1B2**)₂]²⁺ and free **B1** (13 h; **Figure 64**). Thus, in presence of *both* silver and zinc cations, the silver complex of **A1B1**, [Ag(**A1B1**)₂]⁺ is the kinetic product and then the set slowly changes (13 hours) to the zinc complex of **A1B2**, [Zn(**A1B2**)₂]²⁺ as thermodynamic product.

The set of the reactions could proceed as follows: i) Zn(II) was mostly coordinated by **B2** in the beginning; ii) very small amount of free Zn(II) catalyzed the fastest formation of **A1B1**; iii) Ag(I) picked up free **A1B1** to form the silver complex of **A1B1**; iv) the formation of the hydrazone **A1B2** drives the exchange reaction between [Ag(**A1B1**)₂]⁺ and [Zn(**B2**)₂]²⁺, resulting in the final formation of [Zn(**A1B2**)₂]²⁺ and the release of **B1** together with Ag(I). These results display a striking example of a more rapidly formed and simpler *kinetic* output (the silver complex) resulting from competition within a mixture of higher complexity (five entities: three molecular components **A1** + **B2** + **B1** and two metal ions), thus extending to the *kinetic arena* the simplification of behavior noted above on the thermodynamic scene.

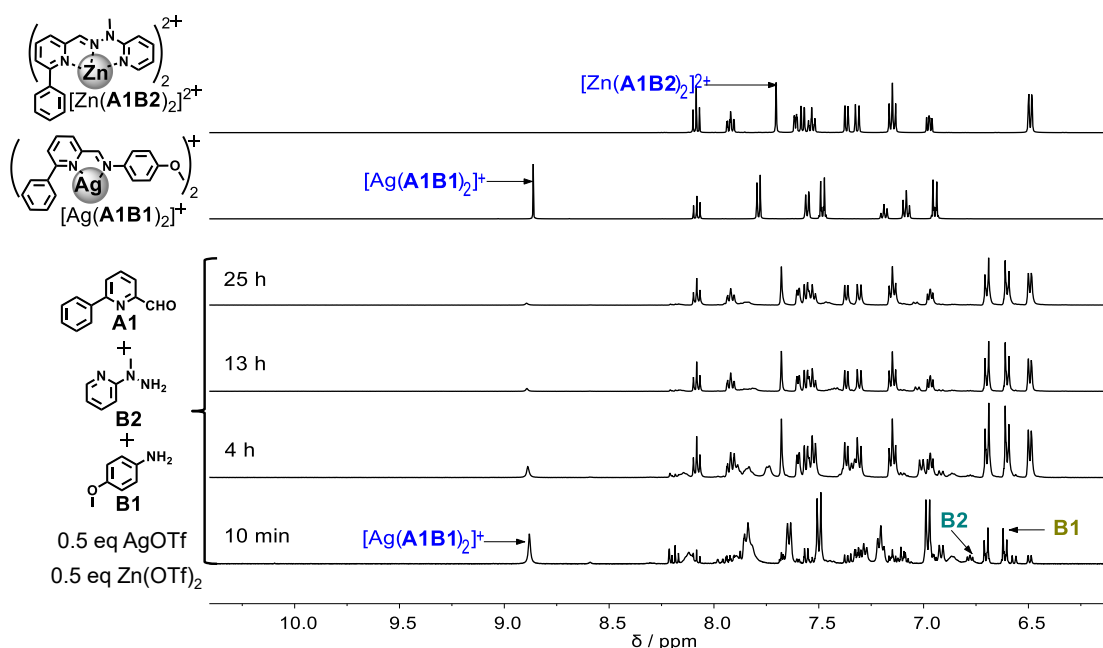


Figure 64. ^1H NMR (500 MHz) spectra of the mixture generated from equal amounts of **A1** + **B2** + **B1** (10 mM each, CD_3CN , 25°C) + AgOTf + $\text{Zn}(\text{OTf})_2$ (5 mM each) after 10 min, 4 h, 13 h, 25 h from bottom to top. Two reference spectra (top two traces) of the separately prepared constituents $[\text{Ag}(\text{A1B1})_2]^+$, $[\text{Zn}(\text{A1B2})_2]^{2+}$ are shown above.

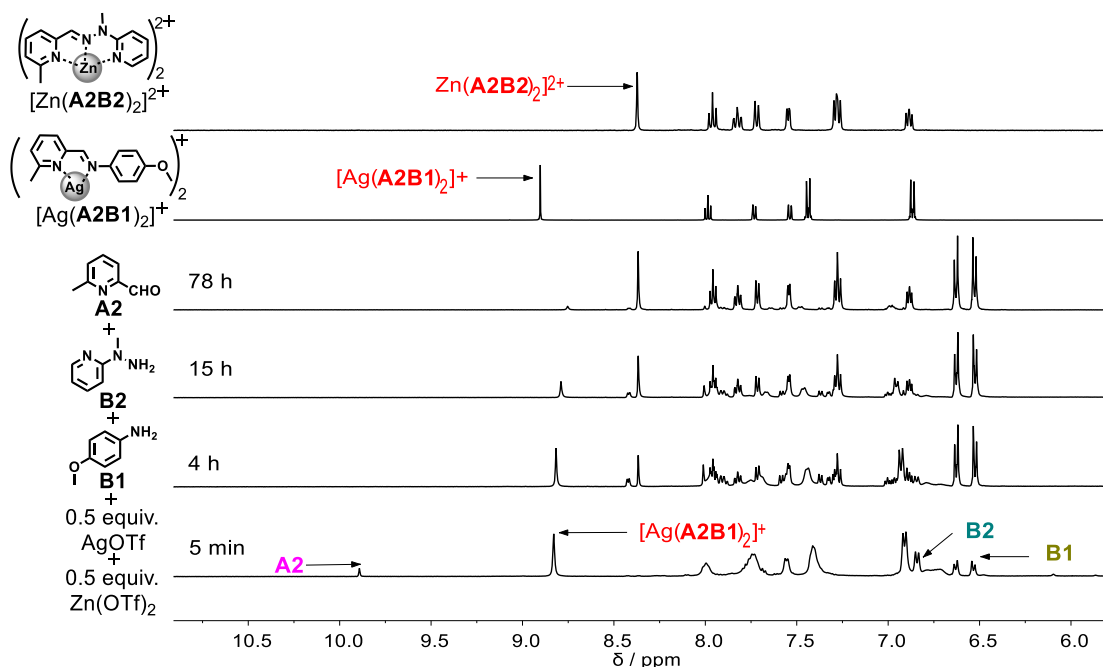


Figure 65. ^1H NMR (500 MHz) spectra of the mixture generated from equal amounts of **A2** + **B2** + **B1** (10 mM each) + AgOTf (5 mM) + $\text{Zn}(\text{OTf})_2$ (5 mM) in CD_3CN at 25°C after 5 min, 4 h, 15 h, 78 h from bottom to top. Two reference spectra (top two traces) of the separately prepared constituents $[\text{Ag}(\text{A2B1})_2]^+$, $[\text{Zn}(\text{A2B2})_2]^{2+}$ are shown above.

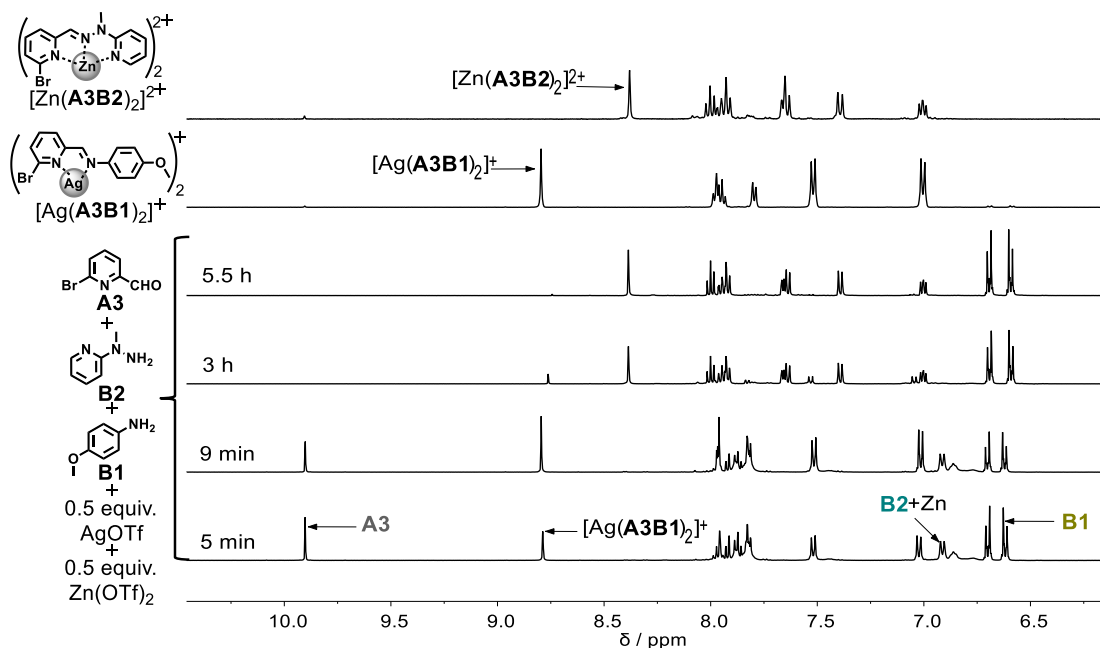


Figure 66. ^1H NMR (500 MHz) spectra of the mixture generated from equal amounts of **A3** + **B2** + **B1** (10 mM each) + AgOTf (5 mM) + Zn(OTf) $_2$ (5 mM) in CD $_3$ CN at 25°C after 5 min, 9 min, 3 h, 5.5 h from bottom to top. Two reference spectra (top two traces) of the separately prepared constituents [Ag(**A3B1**) $_2$] $^+$, [Zn(**A3B2**) $_2$] $^{2+}$ are shown above.

D. Catalysis of imine and hydrazone formation driven by metal salts and acid

The significant accelerations observed for the formation of imine and hydrazone ligands by stoichiometric amounts of metal salts prompted us to explore the effect of catalytic amounts. As is reported earlier, Sc(OTf) $_3$ can effectively catalyze transamination.¹³¹ To evaluate the influence of metal ion catalyst charge on C=N formation with high conversion, the kinetics of the imine **A1B1** and hydrazone **A1B2** formation reactions were investigated in the presence of only 0.05 equiv. (5 mol%) of three metal salts AgOTf, Zn(OTf) $_2$ and Sc(OTf) $_3$, as well as CF $_3$ COOD (**Table 9** and **Figure 67-Figure 68**). Several parameters were determined including the initial rate constant, the turnover frequency (TOF) and the acceleration factor. On addition of 0.05 eq. of Ag(I) (entry 2), the formation of **A1B1** from its components **A1** and **B1** was accelerated by only a factor of 1.5 compared to the rate in the absence of the salt (entry 1), indicating that Ag(I) displayed a very weak catalytic effect on imine formation. In the presence of the same amount of Zn(II), the formation of **A1B1** was greatly accelerated by a factor of 2.6×10^3 (entry 3). The highest rates were found in the presence of 0.05 equiv. of CF $_3$ COOD (entry 5), with a rate enhancement by a factor of 1.2×10^7 times over that in the absence of added acid. The presence of 0.05 eq. of Sc(III) triflate also displayed a remarkable catalytic effect on **A1B1**

formation with an acceleration factor of 5.7×10^6 (entry 4). These results are in line with a study of the effect of different metal ions on the transamination reaction.¹³¹

A similar set of experiments were conducted for the formation of hydrazone **A1B2** (Figure 68 and Table 9). Addition of 0.05 eq. of Ag(I) to **A1** + **B2** produced a catalytic effect with an acceleration by a factor of 3 compared to the reaction in absence of salt (entries 6 and 7 in Table 9), an effect similar to that observed on imine formation. In presence of 0.05 eq. of Zn(II) only a small effect with a rate enhancement of 2 was obtained (entry 8 in Table 9).

Table 9. Kinetic features of the reactions between aldehyde **A1** and p-anisidine **B1** or hydrazine **B2** in absence and in presence of catalysts

Entry ^[a]	Reaction	Catalyst 0.05 eq.	t_{50} [h] ^[c]	t_{10} [h] ^[d]	$k^{[e]}$ / M ⁻¹ s ⁻¹	Acceleration factor	TOF/h ⁻¹
1	A1+B1	— ^[b]	23	3	1.1×10^{-3}	1	n.a. ^[f]
2	A1+B1	Ag(I)	35	2.2	1.6×10^{-3}	1.5	0.005
3	A1+B1	Zn(II)	< 4 min	< 4 min	2.9	2.6×10^3	>8.3
4	A1+B1	Sc(III)	< 4 min	< 4 min	$> 6.3 \times 10^3$	5.7×10^6	>181
5	A1+B1	CF ₃ COOD	< 4 min	< 4 min	$> 1.3 \times 10^4$	1.2×10^7	306
6	A1+B2	— ^[b]	21	1.9	0.97×10^{-3}	1	n.a. ^[f]
7	A1+B2	Ag(I)	6.2	1.5	2.8×10^{-3}	3	0.98
8	A1+B2	Zn(II)	6.4	1.7	2.1×10^{-3}	2	0.54
9	A1+B2	Sc(III)	0.15	< 4 min	> 0.117	>121	6.5
10	A1+B2	CF ₃ COOD	0.17	< 4 min	$> 4.6 \times 10^{-2}$	>47	3.5
11	A1+B2	Zn(II)+ B1	7.7	1.5	6×10^{-3}	6	0.60
12	A2+B2	Zn(II)	5	0.8	2.9×10^{-3}	3	0.44

^[a] Conditions for all these entries: aldehyde (10 mM), amine (10 mM), AgOTf or Zn(OTf)₂ (5 mM), at 25°C, in CD₃CN, monitored by ¹H NMR. ^[b] No catalyst was added. ^[c] Time for 50% completion of the reaction. ^[d] Time for 10% completion of the reaction. ^[e] Rate constant calculated from a fit to a second-order reaction over the first 10% of the reaction, and they are crude estimates values calculated by the loss of aldehyde in the initial stage in order for easier comparison of different reactions.

On changing the aldehyde to **A2**, the initial reaction rate was faster while the reaction conversion time did not change much (entry 12 in Table 9). As in the case of imine formation, Sc(III) or CF₃COOD gave the hydrazone with a significant acceleration by a factor of 121 and 47 respectively (entries 9 and 10 in Table 9). The activity of Sc(III) may reflect its “oxophilic character”, meaning that it forms much more stable complexes with oxygen-containing ligands

than with N-donor species, so that in the mixtures it would be expected to be much less involved in inhibitory coordination of the amine than Zn(II). Finally, when both 0.05 equiv. Zn(II) and 0.05 equiv. auxiliary amine p-anisidine were added (entry 11 in **Table 9**, **Figure 69**), the formation of **A1B2** was 6 times faster than that without catalysts and with Zn(II) or p-anisidine alone (**Figure 68**). This result further verified that Zn(II) and p-anisidine exert synergistic catalysis on hydrazone formation.

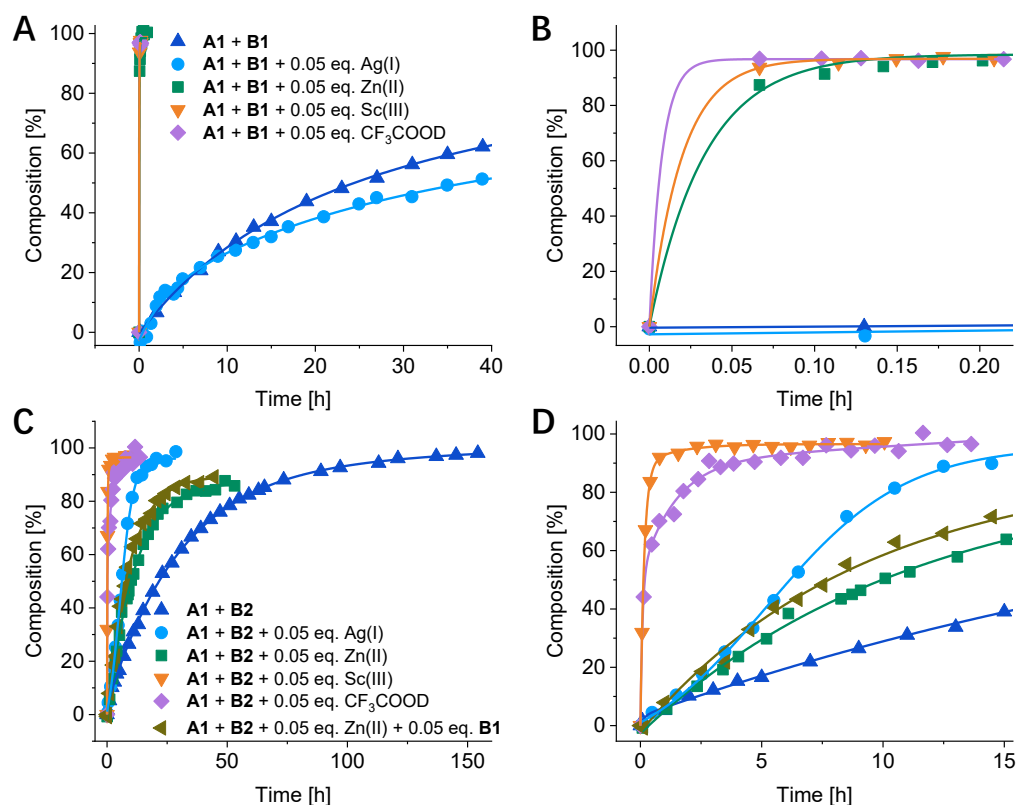


Figure 67. Kinetic plots of the evolution of: **(A)** imine **A1B1** formation from a mixture of equal amounts of components **A1 + B1** in absence of catalyst or in presence of catalysts as indicated; **(B)** zoom of a); **(C)** hydrazone **A1B2** formation from a mixture of equal amounts of components **A1 + B2** in absence of catalyst or in presence of catalysts as indicated; **(D)** zoom of c). Data obtained as a function of time from integration of the CH=N proton signal in the 500 MHz ¹H NMR spectra (10 mM each, CD₃CN, 25°C).

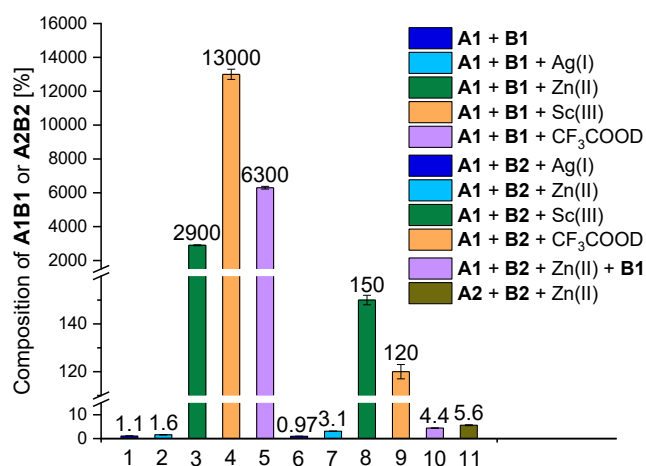


Figure 68. The initial rate constants (k) calculated from a fit to a second-order reaction over the first 10% of the reaction for the imine and hydrazone formation process between **A1** and **B1** or **B2** in absence of catalyst and in presence of 0.05 equiv. catalysts. Note that **A2** + **B2** + Zn(II) was a control experiment.

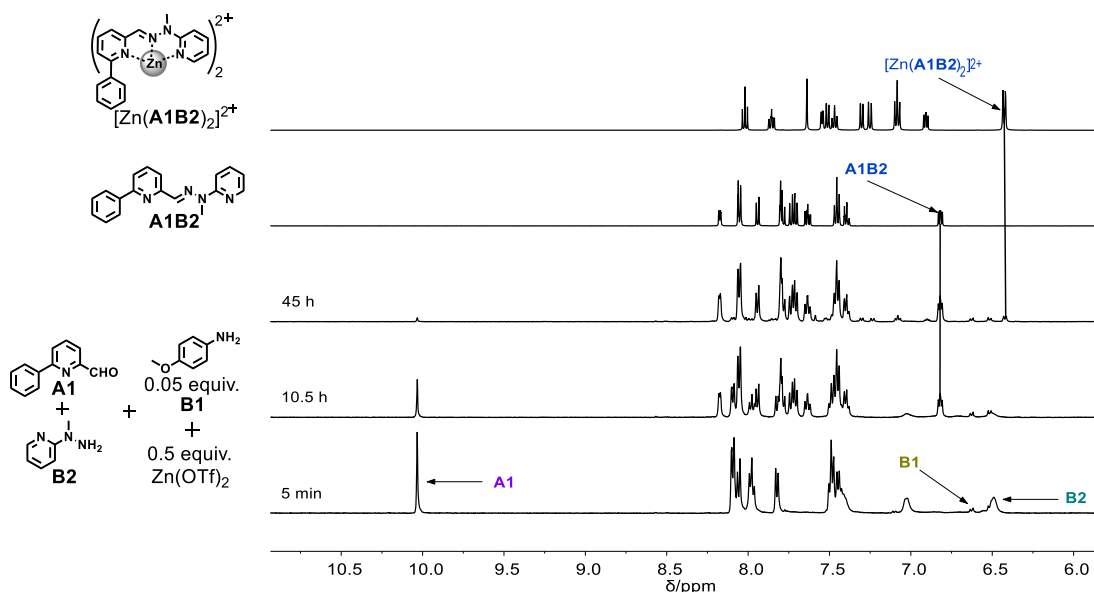


Figure 69. ¹H NMR (500 MHz) spectra of the mixture generated from equal amounts of **A1** + **B2** + 0.05 equiv. **Zn(OTf)₂** (10 mM each, CD₃CN, 25°C) after 5 min, 10.5 h, 45 h from bottom to top. Reference spectra (top two traces) of the separately prepared constituents **A1B2**, **[Zn(A1B2)₂]²⁺**.

3. SUMMARY OF CHAPTER II

We have studied the kinetics and catalysis of a series of C=N (imine and hydrazone) formation in the presence of metal cations as well as the co-operative catalysis by metal cations

and an auxiliary amine. Some of the reactions were conducted both in stoichiometric and catalytic conditions to clarify the role of the metal cations in catalysis

Thus, we have demonstrated a marked enhancement of the efficiency of imine and hydrazone formation by addition of metal cations [Ag(I) and Zn(II)] under stoichiometric conditions where the observed products were the complexes of the imines and hydrazones. Under catalytic conditions, the addition of Ag(I), Zn(II) or Sc(III) metal salts or of CF₃COOD resulted in acceleration of both imine and hydrazone formation. Under both stoichiometric and catalytic conditions, the effect displayed by these catalysts was much more pronounced on the formation of imines than that of hydrazones due probably to inhibitory coordination of the hydrazines by the metal cations. It has been further demonstrated that simultaneous addition of both a metal salt and an aniline derivative as auxiliary amine to the reacting components of a DCL induced a strong acceleration of the formation of the complex of the hydrazone ligand in a synergistic fashion. This was found to be dependent on the very efficient Zn(II) catalysis of imine formation. Further, simultaneous addition of an auxiliary amine as well as both a silver salt and a zinc salt resulted in a synergistic co-catalysis whereby the DCC system undergoes a switching from a kinetic product (the silver complex of an imine) to the thermodynamic product (the zinc complex of a hydrazone). This mode of co-catalysis represents a step in the implementation of two or more catalytic species, in particular in DCC, combining metallo- and organo-catalysis and acting together in a dynamic network through synergistic interconnected chemical transformations. Such effects are of much interest for DCC systems especially [2 × 2] DCLs based on chemical bond formation with differences in formation rates and thermodynamic stabilities. Such behavior shows that increasing system complexity may result in kinetically faster and thermodynamically simpler outputs, an increase in complexity leading thus to simplicity through advanced features such as competition, feedback, and synergy in constitutional dynamic system.

CHAPTER III. CONTROL OF TIME-DEPENDENT SWITCHING OF DCLS

1. INTRODUCTION

In the Chapter II, we discussed the catalysis of imine and hydrazone formation in the presence of metal cations AgOTf and Zn(OTf)₂. Interestingly, the operation of Zn(II) and amine together displayed a synergistic effect on the formation of zinc complex of hydrazone. In addition, upon the simultaneous addition of three co-factors, Ag(I), Zn(II) and amine, the dynamic system underwent a switching from the kinetic product (the silver complex of imine) to the thermodynamic product (the zinc complex of hydrazone). This is a very interesting result, which is worthy to be studied in the [2 × 2] CDL.

As described earlier, a constitutional dynamic library (CDL)^{37,60,230–238} can be generated from the sets of constituents from chemical entities, where the constituents could undergo constitutional variation through reversible formation of covalent and non-covalent linkages. The generated CDL may change the distribution of its constituents in response to physical stimuli (such as light,^{83,103,239–243} temperature,^{63,83} pressure,⁸⁶ and various other factors^{64,85,244,245}) or chemical effectors (metal cations,^{62,65–68,80,98,246} protons,^{247,248} reactive molecules^{249–251} and self-sorting^{92,102,139,252–257}), thus achieving the selection and adaptation. Among these effectors, metal cations are one kind of important effectors which could coordinate with C=N bond ligands, thus driving the formation of the metal complex. To be noted, they can form metal complexes with different geometries due to the specific preference of different metal cations.^{62,65,93,94,99,258} This effector has been applied to achieve multiple mode of adaptation behavior as well as self-sorting of DCLs.^{62,65,66,68,93,98,99,258}

The adaptation of the DCLs were usually performed upon the equilibrium. The generated distribution of the constituents resulted from the thermodynamic control. However, it was very interesting to study the out-of-equilibrium states or far-from equilibrium states of the DCL where the adaptation is under kinetic control. The establishing of such system relies on the variation of the effectors to drive the system towards the out-of-equilibrium states.

One way could be to use light as driving force because the photoisomerization would generate the kinetic product while the heating would lead to the thermodynamic product. As noted by Lehn, such a system could be used to generate the assembly of synthetic receptors

(Figure 70).⁵⁸ The DCL can be utilized in response to binding with a bioactive substance to achieve the selective recognition. This selection can occur in two ways. One is that the photo-responsive receptor would generate a kinetically trapped out-of-equilibrium state to amplify the constituent which would fit the receptor best (kinetic selection). The other is that the receptor amplifies/favors the expression of the constituent/key that binds best to it (thermodynamic selection).²⁴⁹ The out-of-equilibrium state and equilibrium state could also be transformed between each other through light irradiation and high temperature conditions.

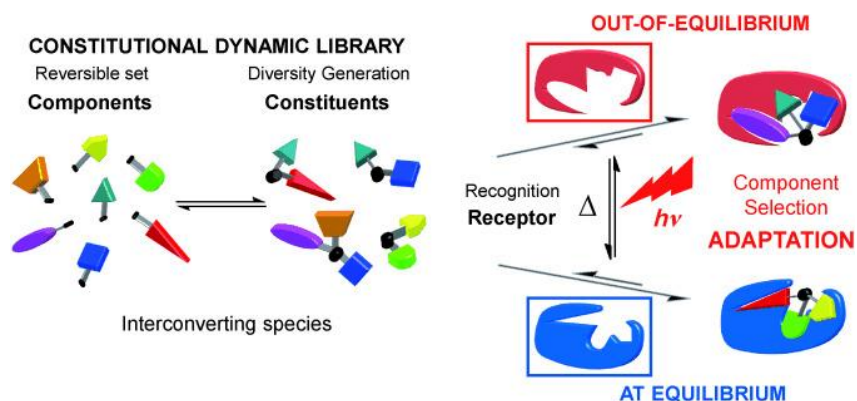


Figure 70. The adaptation of the DCL either to the equilibrium or to photogeneration of the out-of-equilibrium state of the receptor through binding to the best constituent.⁵⁸

The above kinetic behavior of the DCL allows to generate the out-of-equilibrium states. In another way, the kinetic product could also be trapped and thus leaving the DCL to generate the selection of the kinetic product from the DCL. These methods can be, for instance, precipitation-induced organization of DCLs, distillation-induced selection of DCLs, acetylation and other irreversible reactions.⁹²

One example of the kinetic control of the DCLs was from Miljanić and co-workers⁹⁰ who reported the kinetic self-sorting of DCLs by use of the method of distillation (Figure 71). They build up a series of $[2 \times 2]$, $[3 \times 3]$, $[4 \times 4]$, $[5 \times 5]$ DCLs. The main strategy is to screen the aldehydes and amines to generate the imine product with different boiling points. According to the $[2 \times 2]$ DCL, the high molecular mass of the imine also had a higher boiling point. For a $[5 \times 5]$ DCL containing presumably 25 imines from 5 aldehydes (1, 2, 3, 4, 5) and 5 amines (A, B, C, D, E), the first fraction of the distilled product was the **1A** with 77% yield as the lightest imine at the expense of other imines sharing the same component with **1A** including imines **1B-1E**, **2A**, **3A**, **4A** and **5A**. The second observed fraction was **2B** with a yield of 80% between the temperature of 90-120°C. Similarly, the imines shared the components with **2B** was all eliminated during the distillation process including **2C-E**, **3B**, **4B**, and **5B**. Further distillation

of the left DCL generated **3C** (80%, 130-140°C) and **4D** (73%, 240°C) consecutively and **5E** was left in the distillation flask in 80% yield. Through distillation of the [5 × 5] DCL, five imines were generated and separated from the possible 25 imines. In the distillation process, both the rates of the distillation and the thermodynamic equilibration play important roles to achieve this self-sorting behavior. This kinetic control of the self-sorting of the DCLs provided new ways to achieve the selection and amplification of the constituents within the DCLs.

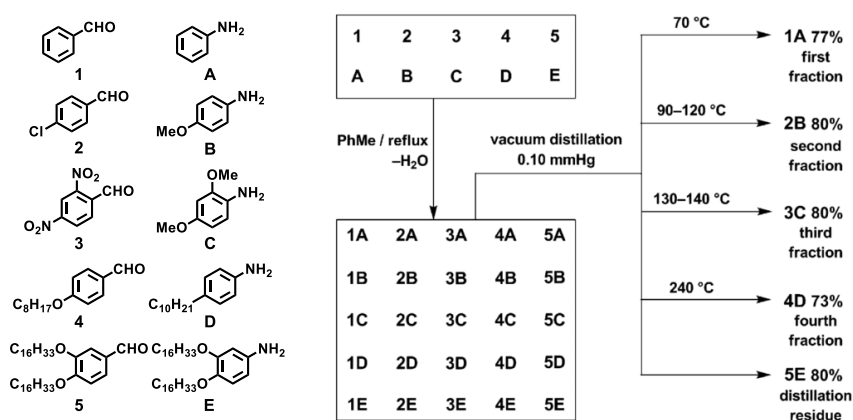


Figure 71. Self-sorting of a dynamic [5 × 5] imine library during a slow vacuum distillation.

Another example to achieve the kinetic control and generate the out-of-equilibrium state of the DCLs of C=N compounds was performed by Holub et al. (Figure 72).⁶⁵ The equilibrated [2 × 2] DCL was generated from 4 components ³A, ⁴A, ¹C and ¹D with the formation of four constituents ³A¹C, ³A¹D, ⁴A¹C, ⁴A¹D with a statistical distribution where the four constituents have similar composition. The addition of one effector CuOTf resulted in the formation of the Cu(I) complex of ³A¹D and the amplification of its agonist ⁴A¹C. On the other hand, the addition of Zn(OTf)₂ led to the formation of the Zn(II) complex of ³A¹C with the amplification of its agonist ⁴A¹D. Both two adaptations are the result of the thermodynamic control. However, by removal of either Zn(II) or Cu(I) from the two equilibrium states, the two corresponding out-of-equilibrium states were generated with only two constituents ³A¹C, and ⁴A¹D (or ³A¹D and ⁴A¹C) in the DCL, which cannot be obtained under thermodynamic conditions. With the readdition of the two metal ions, the DCL can be rapidly transformed back to the two equilibrium states. This work displayed the full circle of the switching between the equilibrium states and out-of-equilibrium states through addition and removal of metal ions to the DCLs of imines. It indicated that the kinetic behavior of the DCLs can be selectively controlled to find

applications of training a CDN for the storage, recall and erasing of information for effector recognition.

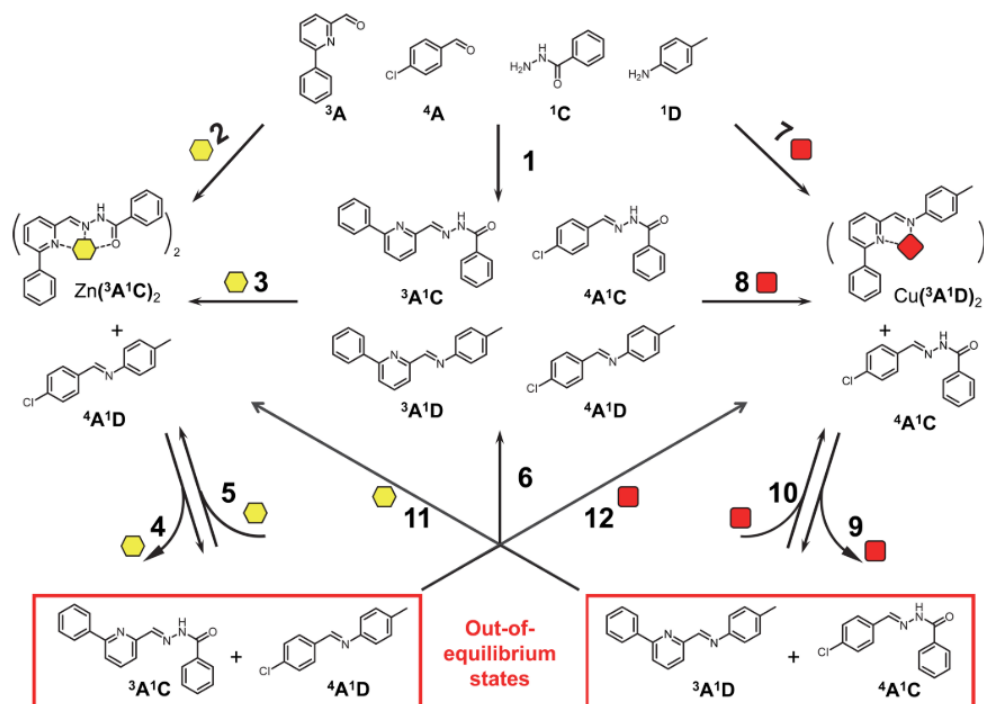
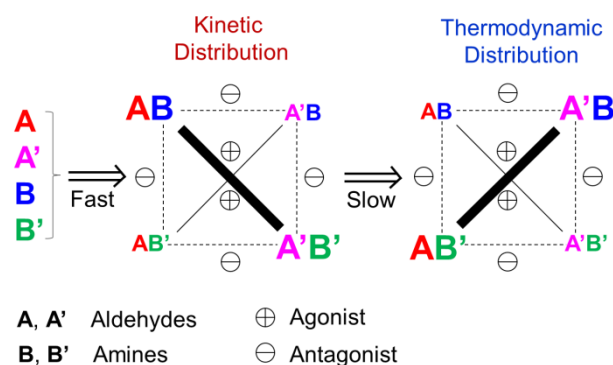


Figure 72. Representation of All of the Transformations Performed by the Dual Responsive Dynamic Covalent System Based on the DCL $3A1C$, $3A1D$, $4A1C$, $4A1D$.

The kinetics study of the reactions within the DCLs especially C-N formation and C/N exchange was thus necessary to control the kinetic behavior of the DCLs. From the previous work,¹⁰¹ it is found that imines¹²⁶ form very fast, while oximes,^{165,167,201,259–263} hydrazones^{158,168,174,264–266} and acylhydrazones^{267,268} form slowly but have higher thermodynamic stabilities at equilibrium.^{143,223} Therefore, the formation of C=N bonds gives out a wide range of reaction rates^{127,132,157,170,175,180,224} and thermodynamic stabilities.^{101,143} Since thermodynamics was the main target for the DCLs studied before, the kinetic aspect of DCLs has rarely been studied and reported.⁶⁵ Here in our cases, by introducing these different C=N bond compounds into a $[2 \times 2]$ DCL, these differences in the relative rates of C=N formation and C/N component exchange would result in a time-dependent variation of the constitution of a DCL.

Based on the switching behavior of the three component with two metal cations [e.g. Ag(I) and Zn(II)], it is very attractive to set up a $[2 \times 2]$ DCL and study the kinetic behavior of such a dynamic system either in the presence or in the absence of metal cations. The above results and considerations prompted us to design systems based on multiple components possessing

different structural and electronic properties to selectively adjust the kinetic and thermodynamic properties of the constituents within the DCL. We thus proposed DCLs of four constituents generated from two aldehydes **A**, **A'** and two amino compounds **B**, **B'**; and investigated the kinetic and thermodynamic properties of the formation of the constituents. This leads to component selection and amplification of the different constituents as a function of time (Scheme 21). When all the constituents **AB**, **AB'**, **A'B**, **A'B'** have similar thermodynamic stabilities, a near-statistical distribution is obtained.⁶⁵ However, by properly designing and selecting the aldehydes and amino compounds, the DCL may be generated to produce at the very beginning of the reaction process, almost exclusively one pair of diagonally located constituents as kinetic products **AB** and **A'B'** and evolve slowly along the time. In terms of distribution, the evolution of such systems means the decrease of **AB** and **A'B'** and consequently the simultaneous increase of the orthogonal constituents **AB'** and **A'B**. Therefore, the evolution of the DCL from a kinetic distribution of the constituents to the thermodynamic distribution was generated, thus achieving in a mode of kinetic network switching of the system.

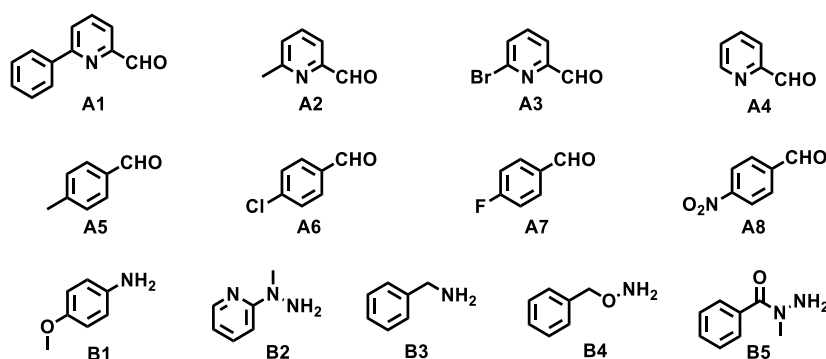


Scheme 21. Evolution of a DCL of four constituents undergoing a time-dependent orthogonal switching of its associated $[2 \times 2]$ CDN from one diagonal to the other one.

2. RESULTS AND DISCUSSIONS

As seen in **Scheme 21**, the main driving forces of this time-dependent switching behavior comes from the exchange reaction of **AB** (kinetic product) with **B'** to form **AB'** (thermodynamic product). Once **AB** is formed, it can undergo the exchange reaction with **B'** to form **AB'** due to its higher stability. As such, the aldehyde **A'** should be less reactive than **A** to allow the fast formation of **AB** and the exchange reaction of **AB** with **B'**. Considering these factors, different types of amines are selected including *p*-anisidine **B1**, *N*-methyl pyridine hydrazine **B2**, benzylamine **B3**, *O*-benzylhydroxylamine **B4** and *N*-methylbenzohydrazide **B5**.

The rates of the formation of these C=N products vary in a large range. In addition, the following aldehydes were selected mainly for two types: the first type is pyridyl-aldehyde which are very reactive including 6-phenyl-2-formyl-pyridine **A1**, 6-methyl-2-formyl-pyridine **A2**, 6-bromo-2-formyl-pyridine **A3**, 2-formyl-pyridine **A4**. The second type is benzaldehyde derivatives including *p*-methyl-benzaldehyde **A5**, *p*-chloro-benzaldehyde **A6**, *p*-fluoro-benzaldehyde **A7** and *p*-nitro-benzaldehyde **A8**. The structure of these selected aldehydes (from **A1** to **A8**) and amines (from **B1** to **B5**) in this chapter is shown in **Scheme 22**. Here, we first studied the DCLs in the absence of metal cations then by involving the latter.



Scheme 22. The structure of the selected aldehydes and amines to set up the [2 x 2] DCLs.

The compositions of the DCLs given below have been determined by integration of characteristic ^1H NMR signals ($-\text{CHO}$, $-\text{CH}=\text{N}$, aromatic $-\text{H}$, $-\text{CH}_2$, $-\text{CH}_3$) with respect to the proton signal (at 0.06 ppm) of hexamethyldisiloxane (HMDSO) as internal standard. The sum of the % for each component in the different entities present in the DCL is equal to 50%, the maximum any constituent can reach. The error in ^1H NMR integration amounts to about 5%.

A. Kinetic switching of a constitutional dynamic library in the absence of metal ions

i. DCL[1] generated from the four components **A3**, **A4**, **B4**, **B5**

The type of pyridine aldehyde (**A1** to **A4**) is known to be more reactive than that of benzaldehyde (**A5** to **A8**) and can also generate an NN bidentate or NNO tridentate coordination site for metal cation binding by reaction with amines or hydrazides. As mentioned above, benzylamines (**B3**), *O*-benzylhydroxylamine (**B4**) or *N*-methylbenzohydrazide (**B5**) were chosen due to the differences in the thermodynamic stabilities of their C=N products. To start with, the four relatively simple components **A4**, **A5**, **B3**, **B4** were selected to set up the first set

of DCL. We were curious to know if the DCL with this combination of the four components would achieve the goal for kinetic switching of CDNs as designed.

1) The C=N formation from two components

Firstly, the sets of *two-component experiments* were studied from the four components **A4**, **A5**, **B3** and **B4**. The separate kinetics of the formation of **A4B3**, **A4B4**, **A5B3** and **A5B4** were followed by ^1H NMR spectroscopy (**Figure 73** to **Figure 76**). The corresponding kinetic curves of these four reactions are displayed in **Figure 77**.

From the ^1H NMR spectra and kinetic curves, we can observe that the formation of **A4B3** from its components **A4** and **B3** was very fast. After 45 minutes, the imine **A4B3** was almost fully formed. While the formation of **A4B4** from its component **A4** and **B4** was very slow, the amount of oxime **A4B4** reached 65% after about 155 hours. These two experiments indicated that the imine formation (**A4B3**) is much faster than the oxime formation (**A4B4**). This is mainly due to the higher nucleophilicity of **B3** compared with **B4**. When similar experiments were run for **A5**, the formation of **A5B3** was slower than the formation of **A4B3** due to the low reactivity of **A5** in comparison with **A4**. As expected, the formation of **A5B4** was also much slower than that of both **A4B4** and **A5B3**. Therefore, these results implied that the imine formation is much faster than oxime formation and the pyridyl-aldehyde is much more reactive than benzaldehyde.

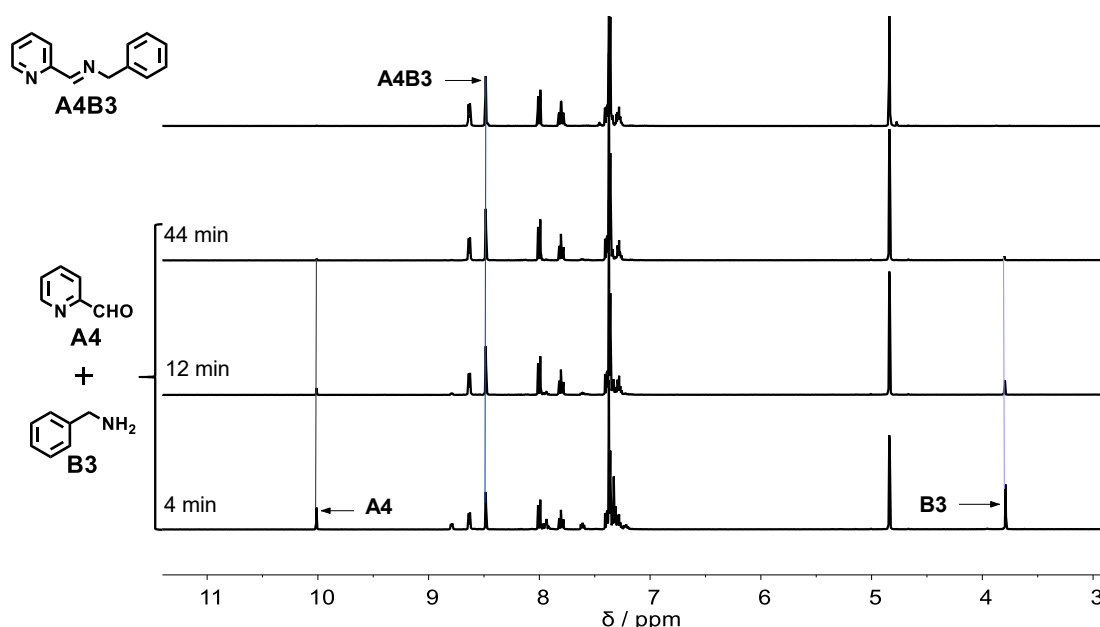


Figure 73. ^1H NMR (400 MHz) spectra of the mixture of equimolar amount **A4** and **B3** (30 mM each, CD_3CN , 25°C) after 4 min, 12 min, 44 min (three bottom traces). A reference spectrum of the separately prepared constituent **A4B3** is shown above.

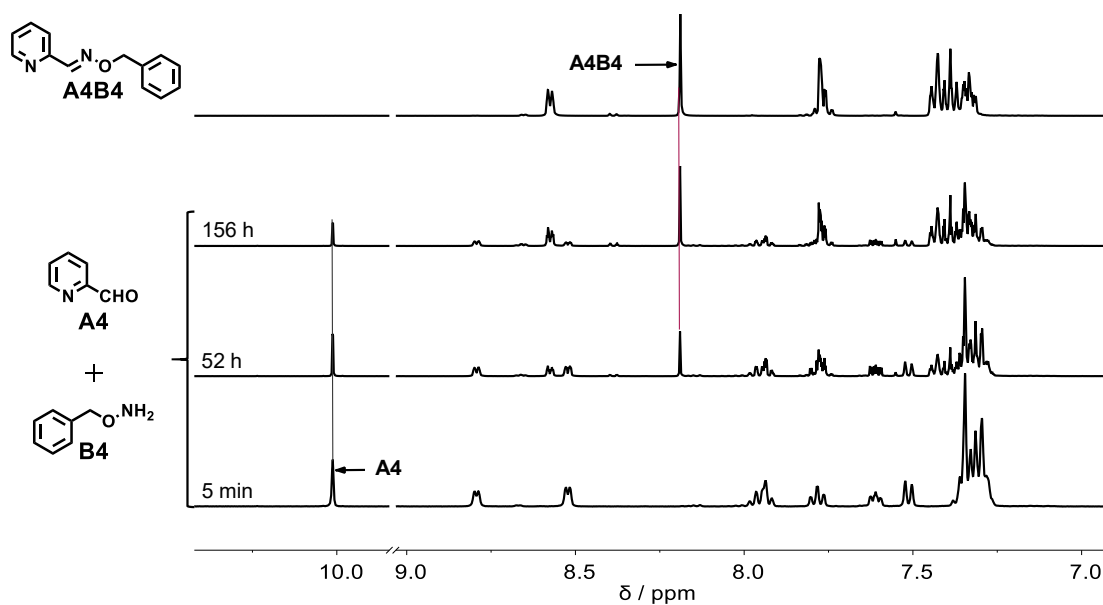


Figure 74. ^1H NMR (400 MHz) spectra of the mixture of equimolar amount of **A4** and **B4** (30 mM each, CD_3CN , 25°C) after 5 min, 52 h, 156 h (three bottom traces). A reference spectrum of the separately prepared constituent **A4B4** is shown above.

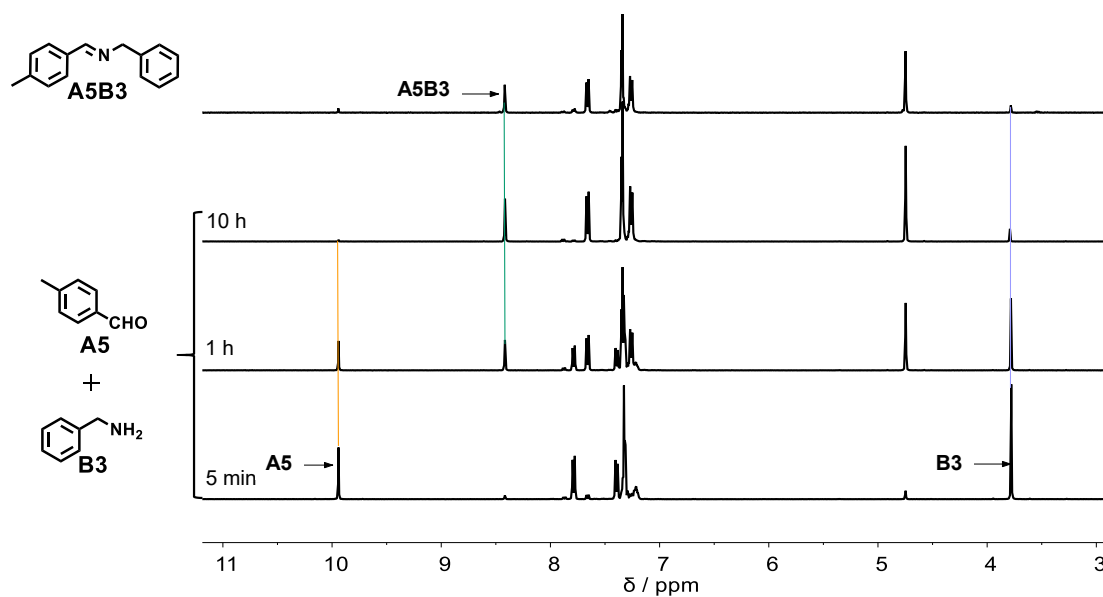


Figure 75. ^1H NMR (400 MHz) spectra of the mixture of equimolar amount of **A5** and **B3** (30 mM each, CD_3CN , 25°C) after 5 min, 1 h, 10 h (three bottom traces). A reference spectrum of the separately prepared constituent **A5B3** is shown above.

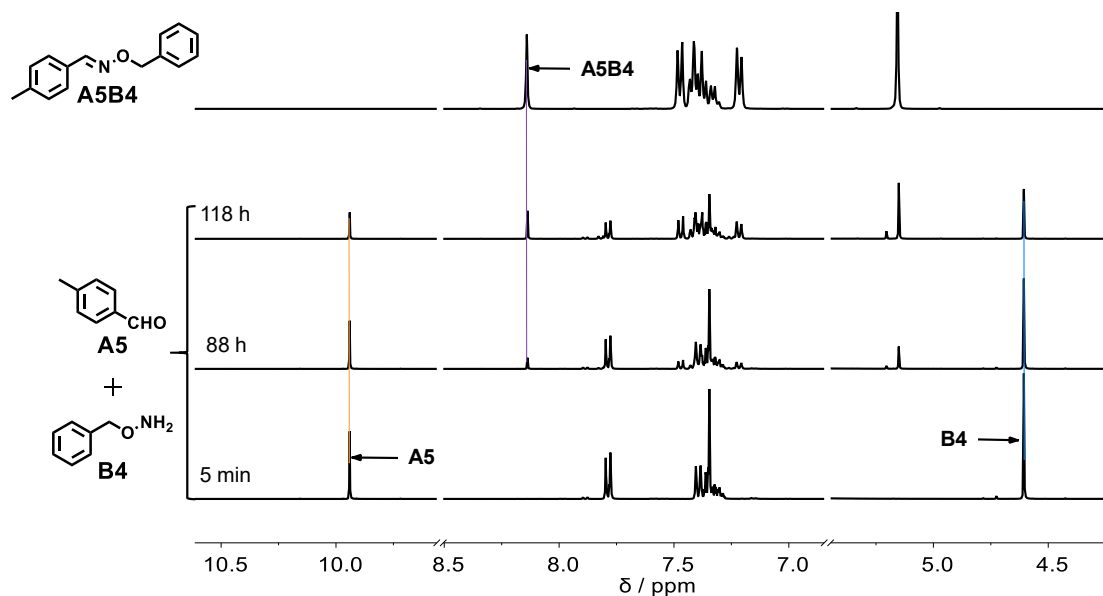


Figure 76. ^1H NMR (400 MHz) spectra of the mixture of equimolar amount of **A5** and **B4** (30 mM each, CD_3CN , 25°C) after 5 min, 88 h, 118 h (from bottom to up). A reference spectrum of the separately prepared constituent **A5B4** is shown above.

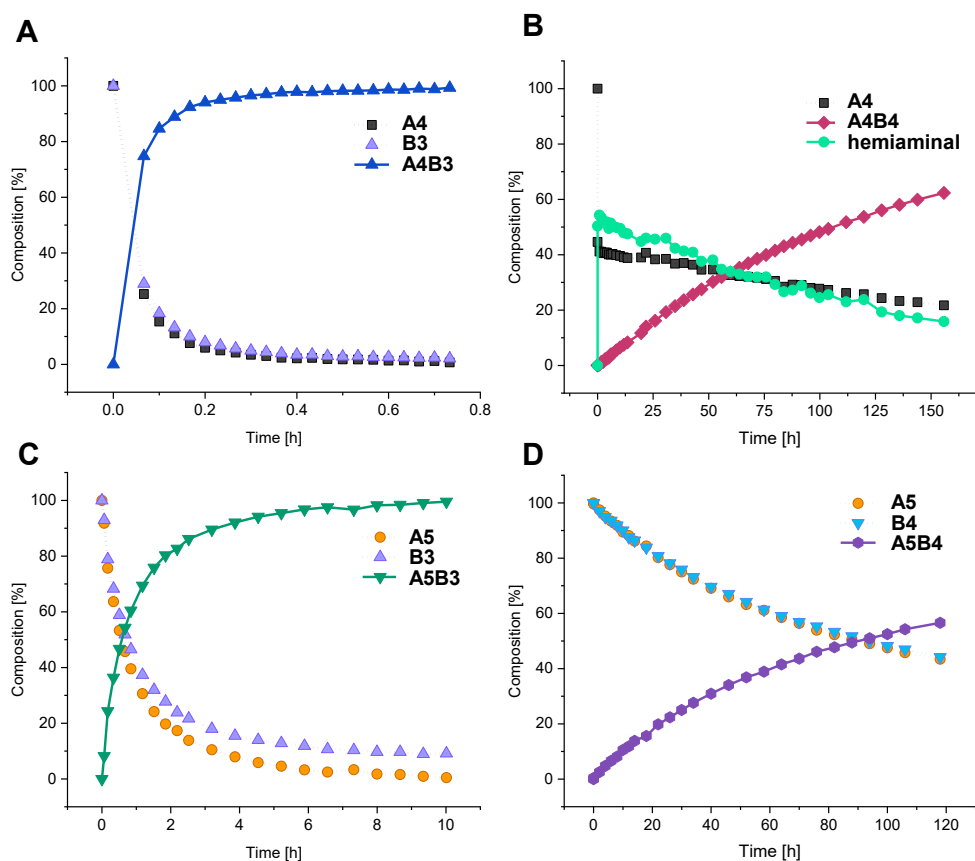


Figure 77. Kinetic plots of the evolution of a mixture of equimolar components (A). **A4** + **B3**; (B). **A4** + **B4**; (C). **A5** + **B3**; (D). **A5** + **B4** as a function of time as obtained from integration of the imine $\text{CH}=\text{N}$ and aldehyde CHO proton signals in the 400 MHz ^1H NMR spectra (30 mM each, CD_3CN , 25°C).

2) Component selection in competitive experiment

To further prove the kinetics observed from the separate experiment of C=N formation, the sets of *three-component competitive experiment* of imine and oxime formation was further investigated from the three components **A4**, **B3** and **B4**. After mixing of equimolar amount of the components, only the imine **A4B3** was observed as the kinetic product within 5 minutes with no formation of oxime **A4B4** at this moment. The reaction thereafter underwent exchange of the component **A4** from imine **A4B3** to form oxime **A4B4**, and a large amount of imine was converted to the oxime **A4B4** as the thermodynamic product after 24 hours. The evolution of the ^1H NMR spectra is depicted in **Figure 78**. The kinetic curve of this reaction is shown in **Figure 81A**.

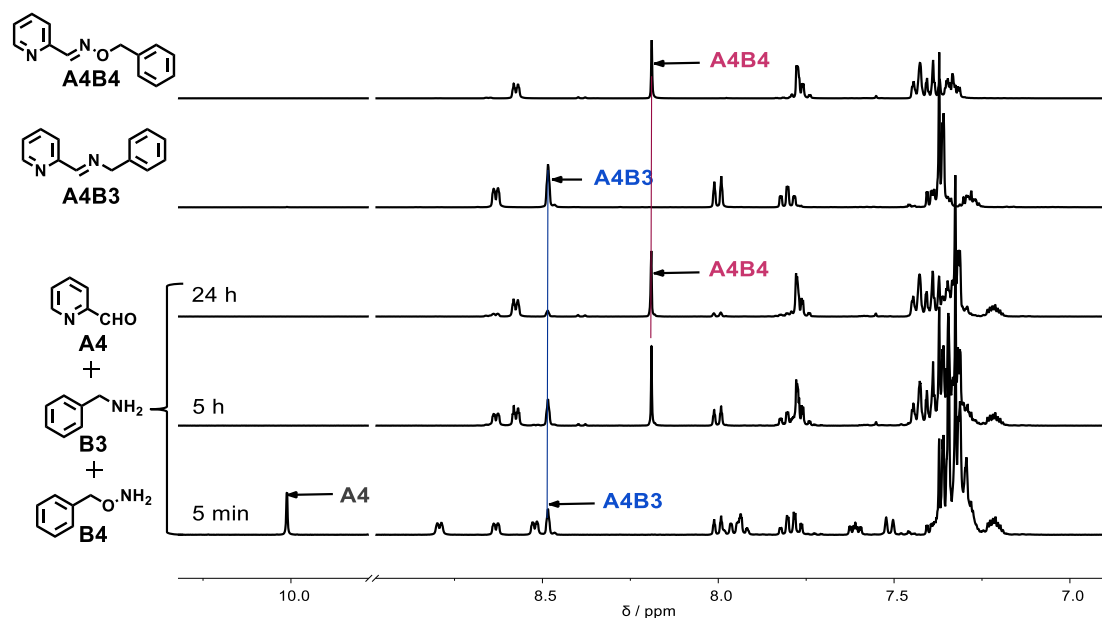


Figure 78. ^1H NMR (400 MHz) spectra of the equimolar mixture of **A4**, **B3** and **B4** (30 mM each, CD_3CN , 25°C) after 5 minutes, 5 h and 24 h (three bottom traces). The two top traces correspond to the isolated constituents **A4B3** and **A4B4**.

To further verify the reactivity of **A5** (less reactive than **A4**), a similar set of experiment [**A5** + **B3** + **B4**] was performed to explore the design and the kinetics (**Figure 79**). As expected, by replacing **A4** by **A5**, the reaction proceeded much more gradually and slower (see **Figure 81B** for the kinetics curve), indicating a clear observation of the reaction behavior within the first hours. In agreement with the set of experiment [**A4** + **B3** + **B4**], the imine **A5B3** formed first as the kinetic product and then transformed to the oxime **A5B4** as the thermodynamic product. This observation indicated that **A4** should be more reactive than **A5** even in the $[2 \times 2]$

DCL where the four components **A4**, **A5**, **B3** and **B4** are all present, which will be discussed later.

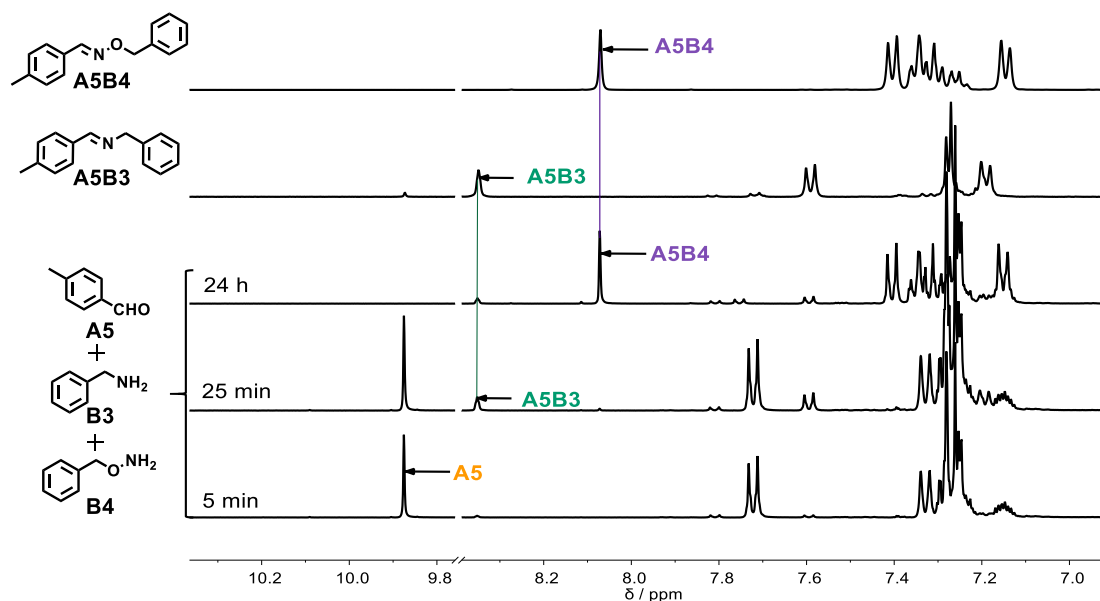


Figure 79. ¹H NMR (400 MHz) spectra of the mixture of the same equivalent of **A5**, **B3** and **B4** (30 mM each, CD₃CN, 25°C) after 5 minutes, 25 min and 24 h (three bottom traces). Two reference spectra of the isolated constituents **A5B3** and **A5B4** are shown above.

As a complementary experiment, the reaction of [**A4** + **A5** + **B3**] with equimolar amount of components was also conducted (**Figure 80**). In the beginning after 5 minutes, only **A4B3** is observed. Then it is very slow for the exchange of **A4B3** with **A5**. After 24 hours, there is less than 10% **A5B3** formation. It proves again **A4** is a much more reactive aldehyde than **A5**. The kinetics curve of this set of reaction is shown in **Figure 81C**. The set of [**A4** + **A5** + **B4**] was also tried but it was too slow to follow the kinetics even for the exchange reaction between **A4B4** with **A5**.

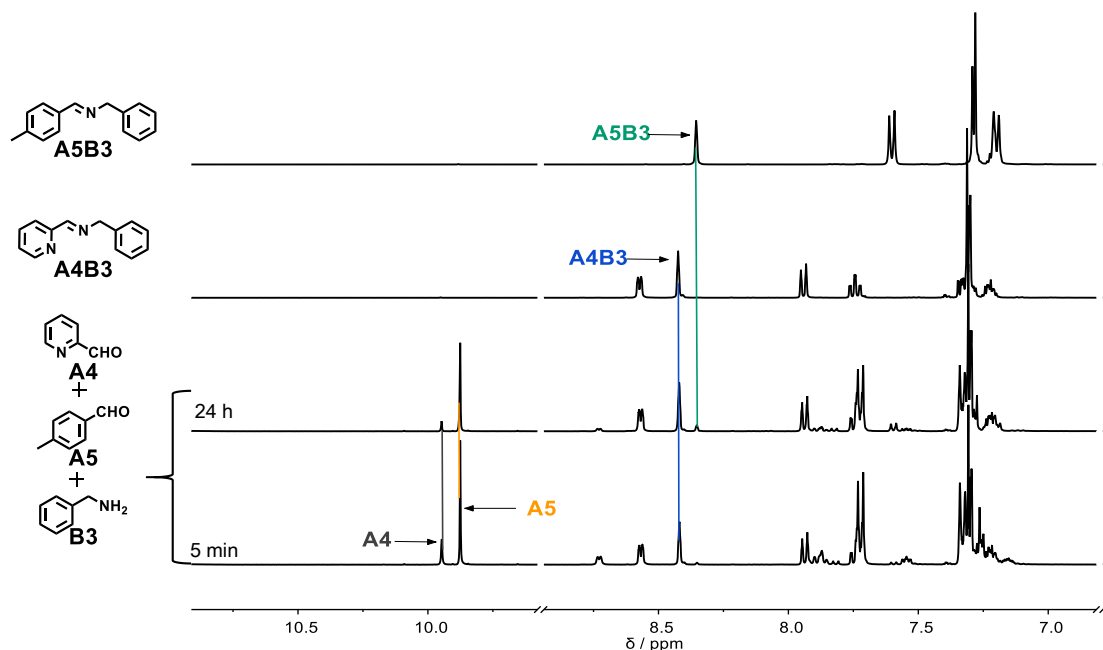


Figure 80. ^1H NMR (400 MHz) spectra of the mixture of equimolar amount of **A4**, **A5** and **B3** (30 mM each, CD_3CN , 25°C) after 5 minutes, 5 h and 24 h (three bottom traces). The two top traces correspond to the isolated constituents **A4B3** and **A5B3**.

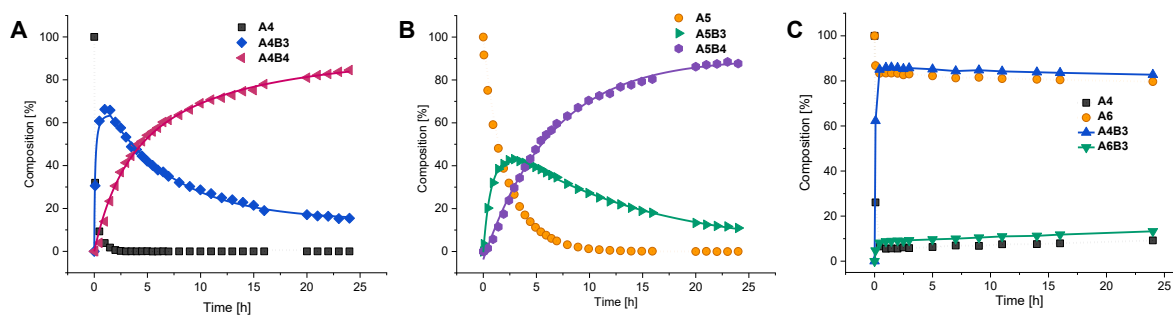


Figure 81. Kinetic plots of the evolution of a mixture of equimolar amount of components (A). **A4** + **B3** + **B4**; (B). **A5** + **B3** + **B4**; (C). **A4** + **A5** + **B3** as a function of time as obtained from integration of the imine $\text{CH}=\text{N}$ and aldehyde CHO proton signals in the 400 MHz ^1H NMR spectra (30 mM each, CD_3CN , 25°C). The kinetic curves are shown for only some of the compounds for clarity.

By comparing the kinetics of the two-component $\text{C}=\text{N}$ formation and the three-component competitive experiments (**Figure 73** to **Figure 81**), the formation of imine is much faster than that of the oxime, so the imine usually forms as the kinetic product while the oxime forms as the thermodynamic one in both cases. Therefore, it is feasible to set up a $[2 \times 2]$ DCL from the four components **A4**, **A5**, **B3** and **B4** to investigate its kinetic behavior.

3) The kinetic switching of **DCL[1]** from of four constituents generated from four components

The **DCL[1]** was thus generated from equimolar amount of the four components **A4**, **A5**, **B3**, **B4** in CD₃CN at room temperature. The evolution of the composition of components and generated constituents of the **DCL[1]** was monitored by ¹H NMR spectroscopy as a function of time (**Figure 82**).

After about half an hour, **A4B3** was detected as the main product with the constituents **A4B4**, **A5B3** and **A5B4** formed in a biased distribution of 36%, 13%, 6%, 1% as well as 44% of free **A5**, 37% of free **B4** and 10% free **B3** respectively (**Scheme 23**). Therefore, **A4B3** was the overwhelming kinetic product of the DCL at the initial stage. Due to the agonist amplification manner of DCLs, the large amount of **A4B3** formation should have amplified its agonist constituent **A5B4**. However, the formation of **A5B4** was not observed at this moment because of the low reactivities of **A5** and **B4** (kept unreacted). This biased kinetic distribution can be attributed to the faster imine **A4B3** formation with respect to the oxime **A4B4** formation. These results were further proven by the results of the competitive reactions above for i) **A4** with **B3** and **B4** (**Figure 81A**); ii) **A5** with **B3** and **B4** (**Figure 81B**) as well as iii) **B3** with **A4** and **A5** (**Figure 81C**). They demonstrated that **A4** is more reactive than **A5** while **B3** is more reactive than **B4**. Then, as the exchange reaction proceeded, the amount of imine **A4B3** decreased, while the oxime product **A4B4** was increased with amplification its agonist constituent **A5B3**. The initial amounts of the components were almost fully consumed after 15 hours and only the four expected constituents were present with the final distribution of 14%/36%/35%/13% for the constituents **A4B3**, **A4B4**, **A5B3**, **A5B4**, with 2% of free **A5** respectively. The kinetic curve of the variation of the constitution of the DCL is presented in **Figure 83**. The whole process displayed a kinetic switching behavior of the CDN associated to **DCL[1]** from the diagonal [**A4B3**, **A5** + **B4**] to the orthogonal diagonal [**A4B4**, **A5B3**] (**Scheme 23**). When replacing **A5** with the more reactive aldehydes *p*-chlorobenzaldehyde **A6** or by *p*-fluorobenzaldehyde **A7**, similar switching behavior were obtained in a relatively shorter time. The corresponding evolution of the ¹H NMR spectra, kinetic curves, and the Schemes for the two DCLs are displayed in experimental section (**Figure III11** to **Figure III 14**, **Scheme III12** and **SchemeIII13**). The evolution of the distributions of the two-component, three-component and four component mixtures were also shown in experiment part in **Table III1** to **Table III7**, **Table III12-Table III15**.

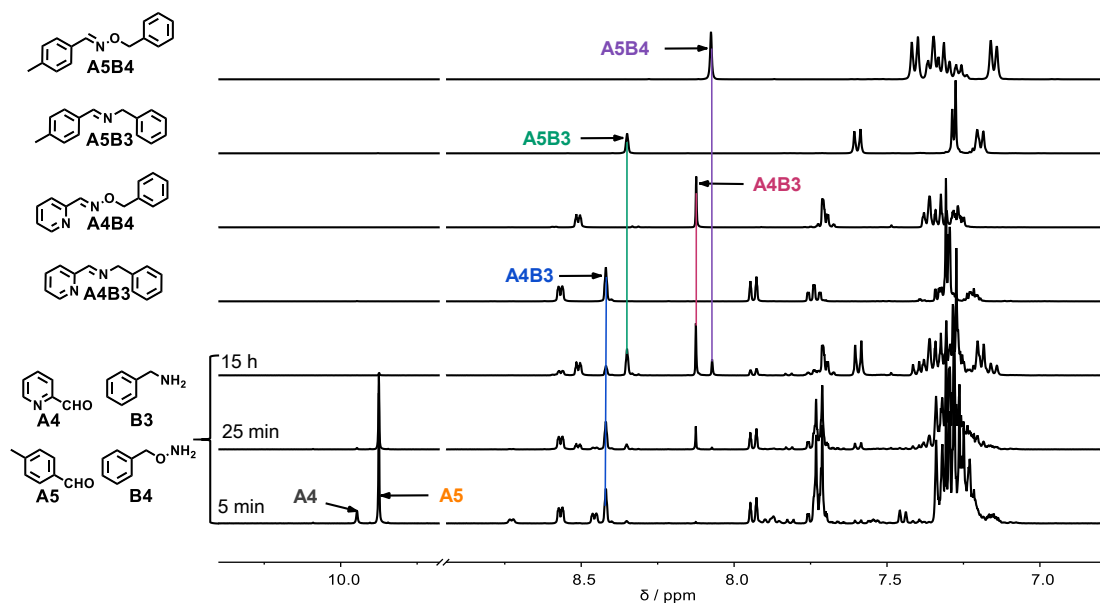


Figure 82. Evolution of ^1H NMR (400 MHz) spectra of the compounds generated from the **DCL[1]** mixture of equal amounts of **A4**, **A5**, **B3**, **B4** (30 mM each in CD_3CN , 25°C) after 5 min, 25 min and 15 h (three bottom traces). The four top traces correspond to the isolated constituents **A4B3**, **A4B4**, **A5B3** and **A5B4**. The arrows indicate the aldehyde CHO proton (9.5-10.0 ppm region) and the imine CH=N proton (8.0-8.5 ppm region) NMR signals of the compounds.

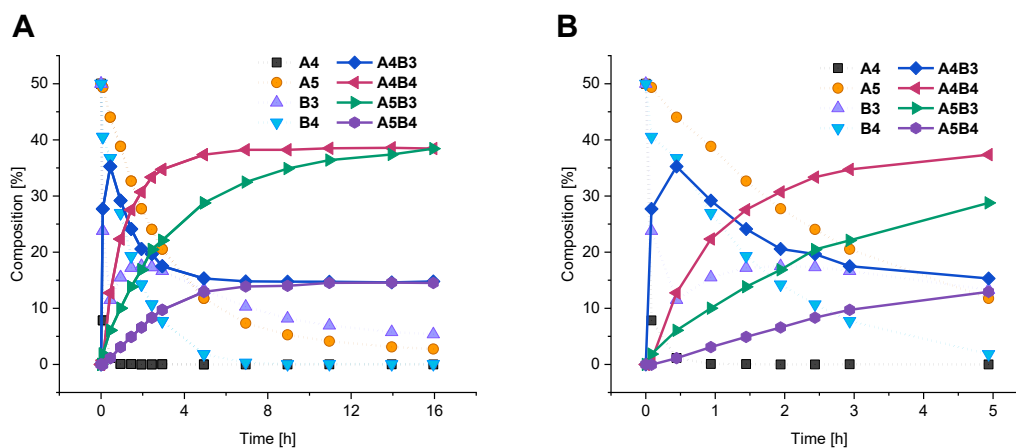
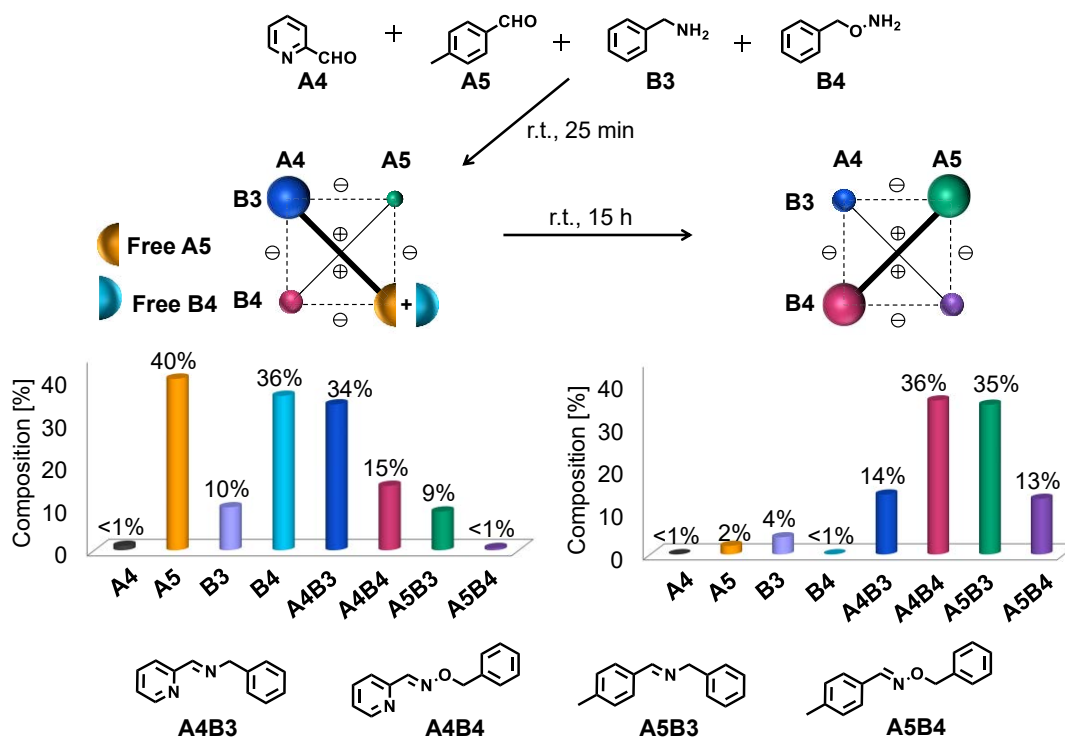


Figure 83. (A). Kinetic curves of the compounds generated from a mixture of equimolar **A4** + **A5** + **B3** + **B4** as a function of time over 16 hours; (B). Zoom of (A). The composition % data have been obtained by integration of the imine CH=N and aldehyde CHO proton signals in the 400 MHz ^1H NMR spectra (30 mM each, CD_3CN , 25°C).



Scheme 23. Kinetic switching of the [2x2] CDN formed by the **DCL[1]** set of components [**A4 + A5 + B3 + B4**] (top) from the [**A4B3, A5 + B4**] state (middle left) to the orthogonal state [**A4B4, A5B3**] (middle right) in CD_3CN at 25°C . The indicated composition % values of the different compounds present correspond to reaction times of 25 min (left) and 16 h (right). Data obtained from the 400 MHz ^1H NMR spectra.

ii. DCL[2] generated from the four components A1, A6, B3, B4

1) Component selection in competitive experiment

The sets of *three-component competition experiments* of [**A1 + B3 + B4**], [**A6 + B3 + B4**] and [**A1 + A6 + B3**] were first studied to confirm the kinetics of the component formation. The experiment for [**A1 + A6 + B4**] were not conducted due to the very low rate of exchange reaction and it is expected to have similar behavior as [**A1 + A6 + B3**]. For both the cases of **A1** and **A6**, the imine **A1B3** and **A6B3** were the kinetic products which formed very fast in the processes and then they exchanged the components to form the oximes **A1B4** and **A6B4** as the thermodynamic products. Further experiment of [**A1 + A6 + B3**] confirmed that **B3** reacted with **A1** rather than **A6**, indicating that **A1** is more reactive in comparison to **A6** (**Figure 84** to **Figure 86**). These results can be observed in the kinetic evolution plots of the three sets of the competition experiments in **Figure 87**.

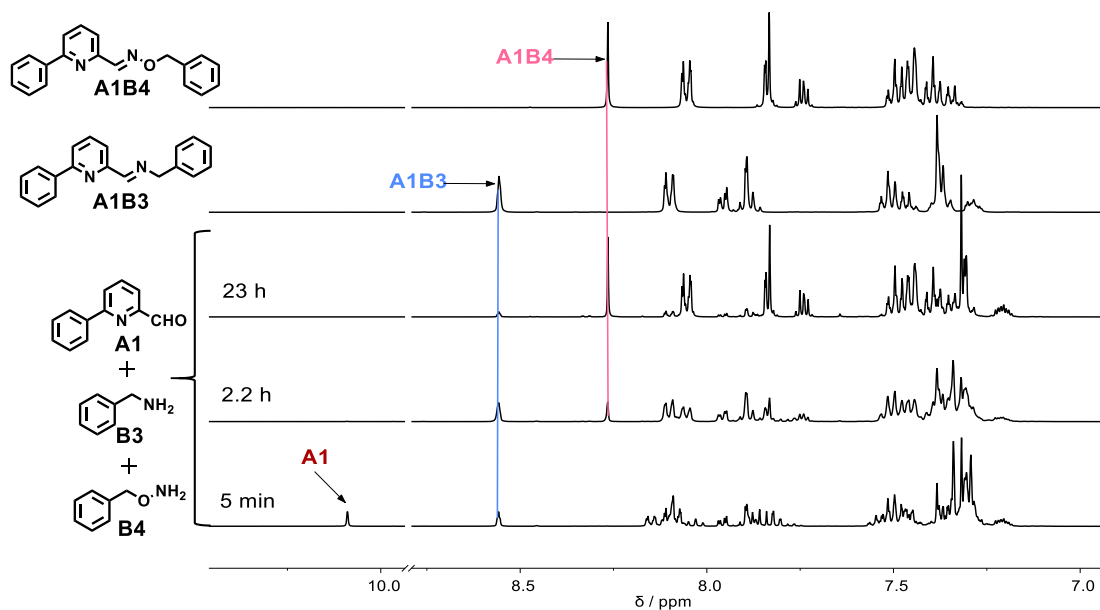


Figure 84. ^1H NMR (400 MHz) spectra of the mixture of equimolar amount of **A1**, **B3** and **B4** (30 mM each, CD_3CN , 25°C) after 5 min, 2.2 h and 23 h (three bottom traces). The reference spectra of the isolated constituents **A1B3** and **A1B4** are shown above.

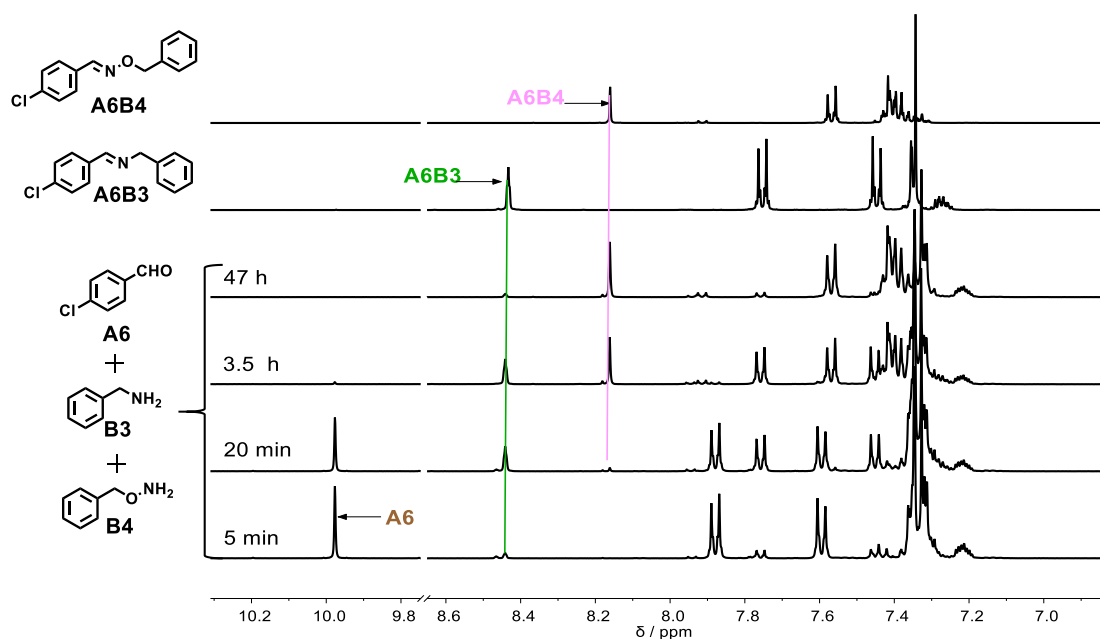


Figure 85. ^1H NMR (400 MHz) spectra of the mixture of equimolar amount of **A6**, **B3** and **B4** (30 mM each, CD_3CN , 25°C) after 5 min, 20 min, 3.5 h and 47 h (four bottom traces). The reference spectra of the isolated constituents **A6B3** and **A6B4** are shown above.

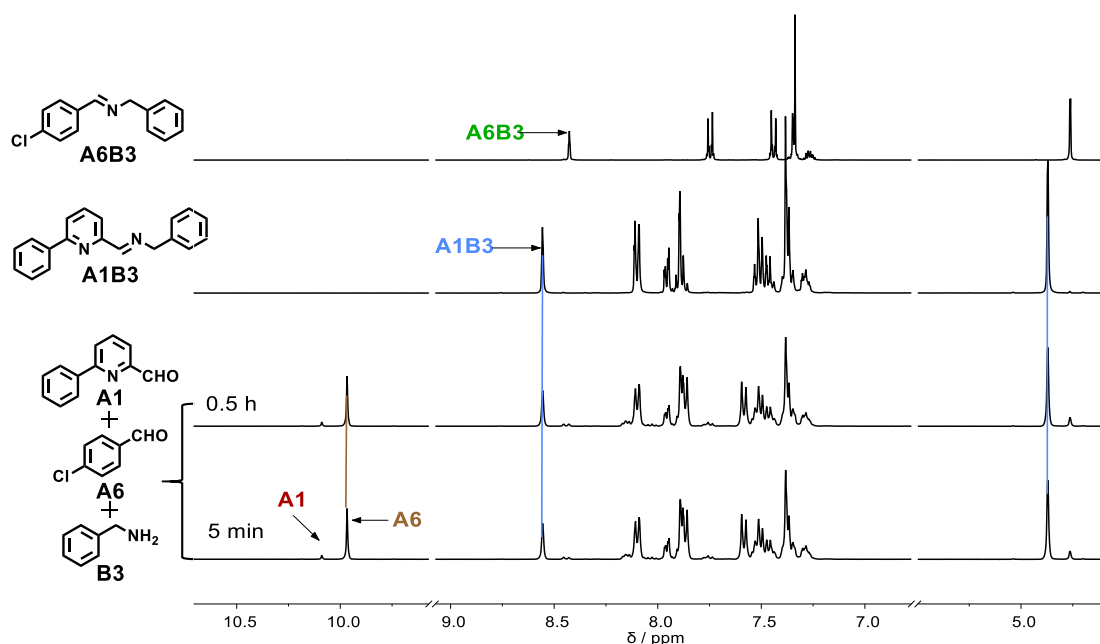


Figure 86. ^1H NMR (400 MHz) spectra of the mixture of the same equivalent of **A1**, **A6** and **B3** (30 mM each, CD_3CN , 25°C) after 5 minutes and 0.5 h (two bottom traces). The reference spectra of the isolated constituents **A1B3** and **A6B3** are shown above.

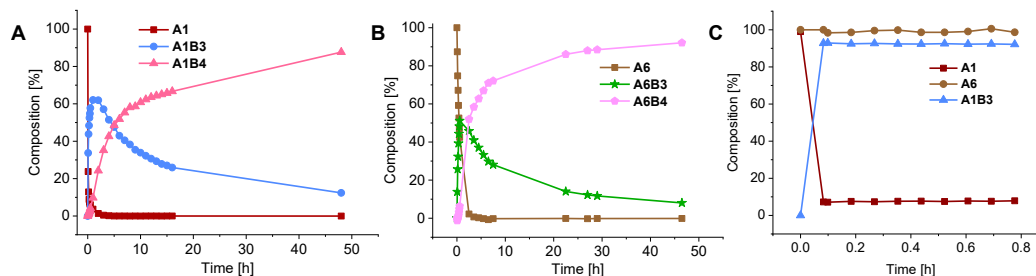
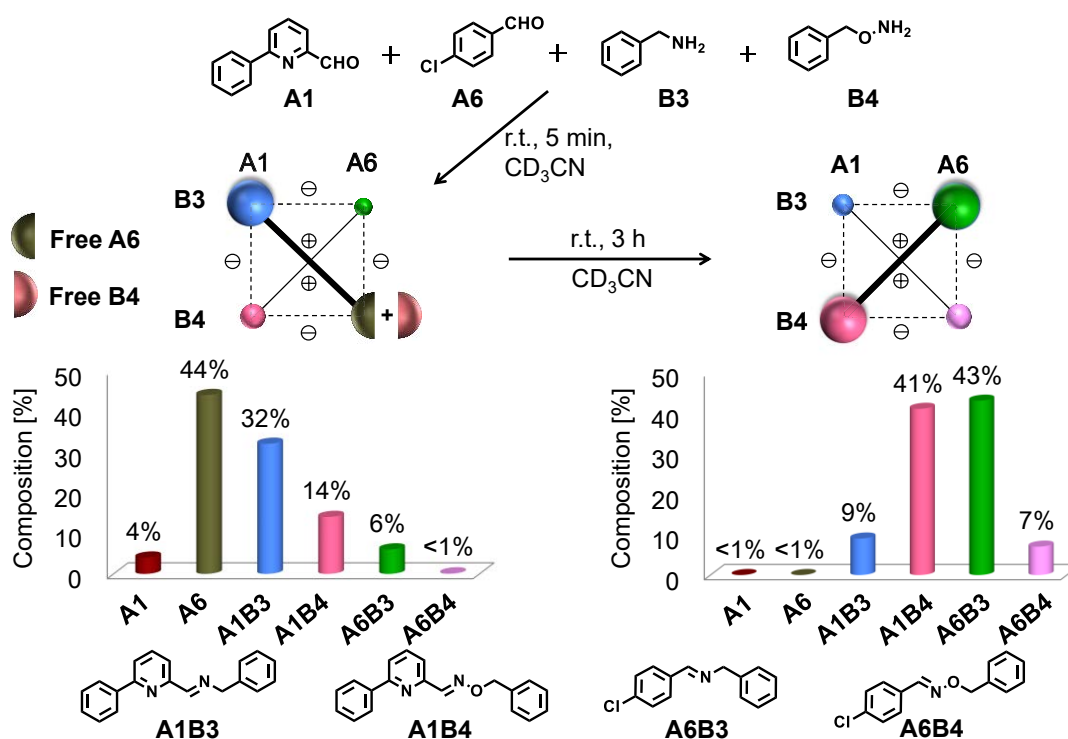


Figure 87. Kinetic plots of the evolution of a mixture of equimolar components (A). **A1** + **B3** + **B4**; (B). **A6** + **B3** + **B4**; (C). **A1** + **A6** + **B3** as a function of time as obtained from integration of the imine $\text{CH}=\text{N}$ and aldehyde CHO proton signals in the 400 MHz ^1H NMR spectra (30 mM each, CD_3CN , 25°C). The kinetic curves are shown for only some of the compounds for clarity.

2) The kinetic switching of **DCL[2]** from four constituents generated from four components

Based on the above explorations, a $[2 \times 2]$ **DCL[2]** was set up from the four components **A1**, **A6**, **B3**, **B4** (Scheme 24). The evolution of ^1H NMR spectra of **DCL[2]** displayed a similar kinetic switching behavior to **DCL[1]** but with a much faster reaction time. After only 4 minutes, a biased distribution was already obtained with the formation of the four constituents with the yield of **A1B3**/32%, **A1B4**/14%, **A6B3**/6%, **A6B4**/ $<1\%$ (Figure 88 and Figure 89) and free **A6**/44% and **B4**/36%. This biased distribution is because **B3** is more reactive than **B4**, and **A1**

is more reactive than **A6**, as verified by the corresponding competitive reactions above (**Figure 87**). Therefore, this **DCL[2]** with **A1B3** as the kinetic product underwent recombination through component formation and exchange reactions with time, shifting to the final equilibrium where the oxime **A1B4** was the thermodynamic product, resulting in the amplification of its diagonal agonist **A6B3**. The final equilibrium state of the **DCL[2]** gave the distribution for the constituents **A1B3**/9%, **A1B4**/41%, **A6B3**/43% and **A6B4**/7%. Thanks to the change to a more reactive aldehydes, the **DCL[2]** produced a faster time-dependent switching of the CDN than **DCL[1]** from the kinetic distribution with the main product of [**A1B3**, **A6** + **B4**] into the thermodynamic distribution in which the main products refer to the diagonal [**A1B4**, **A6B3**].



Scheme 24. Kinetic switching of the [2 x 2] DCL formed by the **DCL[2]** set of components [**A1** + **A6** + **B3** + **B4**] from the [**A1B3**, **A6** + **B4**] state to the orthogonal state [**A1B4**, **A6B3**] in CD_3CN at 25°C. Data obtained from the 400 MHz ^1H NMR spectra.

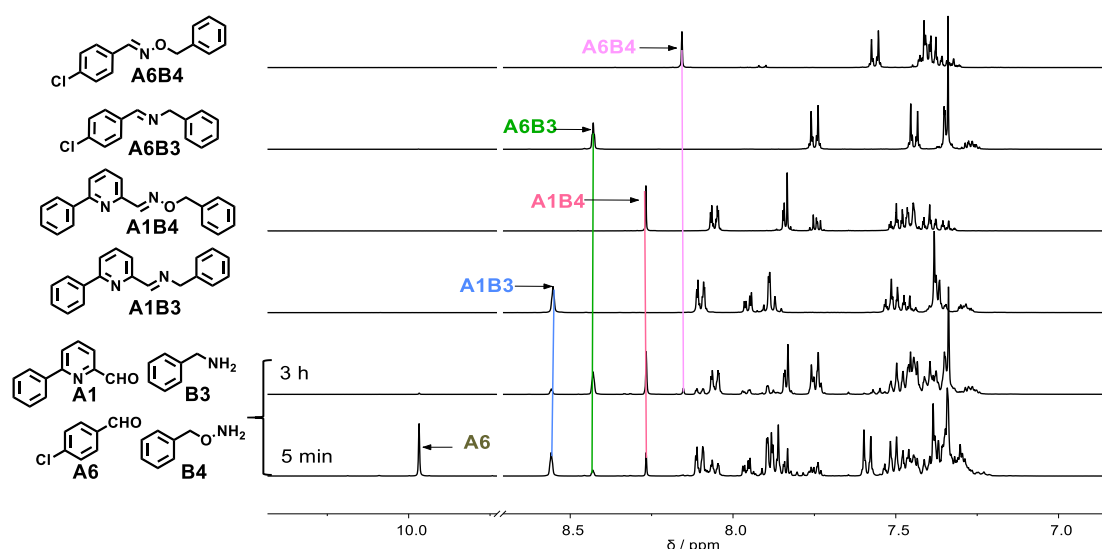


Figure 88. ^1H NMR (400 MHz) spectra of the mixture generated from equimolar amounts of **A1** + **A6** + **B3** + **B4** (30 mM each, CD_3CN , 25°C) after 5 minutes and 3 h (two bottom traces). Four reference spectra of the isolated constituents **A1B3**, **A1B4**, **A6B3** and **A6B4** are shown above.

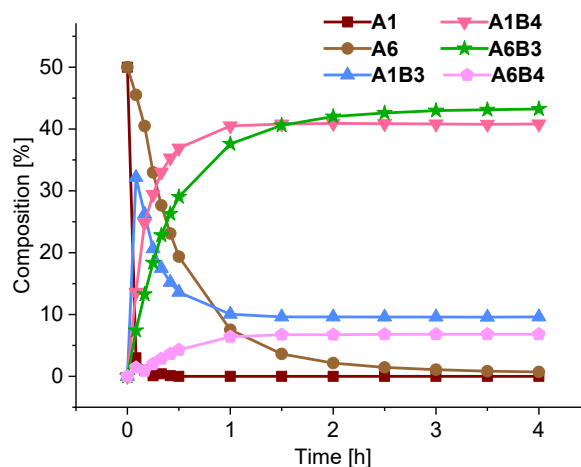


Figure 89. Kinetic plots of the evolution of a mixture of equal amounts of components **A1** + **A6** + **B3** + **B4** as a function of time as obtained from integration of the imine $\text{CH}=\text{N}$ and aldehyde CHO proton signals in the 400 MHz ^1H NMR spectra (30 mM each, CD_3CN , 25°C). For clarity, the kinetic curves are shown for only some of the compounds.

iii. DCL[3] generated from the four components **A1**, **A6**, **B3**, **B5**

From the results above, the design and success of such time-dependent switching system relies to large content on the rates of $\text{C}=\text{N}$ formation where the screening of the aldehydes and amino compounds are of key importance to the kinetic aspects. Since the use of imines and

oximes works well due to the differences in the kinetic and thermodynamic properties, similar behavior should also be observed by use of hydrazones due to the apparent difference in rates and stabilities as imines. We thus envisaged a similar system of **DCL[2]** by replacing alkoxyamine **B4** with hydrazide **B5** to achieve the kinetic switching behavior of the CDNs.

1) Component selection in competitive experiment

Instead of conducting the competitive experiment of the aldehyde **A1** with the benzylamine **B3** and N-methylbenzoylhydrazide **B5**, an easier way is to perform the competition set-up for [**A1** + **B4** + **B5**] to compare the kinetics and thermodynamic stabilities of the oxime **A1B3** and acylhydrazone **A1B5**. Thus, the set-up were conducted in two different ratios with **A1**: **B4**: **B5** = 1: 1: 1 and **A1**: **B4**: **B5** = 2: 1: 1 see in the evolution of the ^1H NMR spectra from **Figure 90** to **Figure 91**. The corresponding kinetic curves are shown in **Figure 92**.

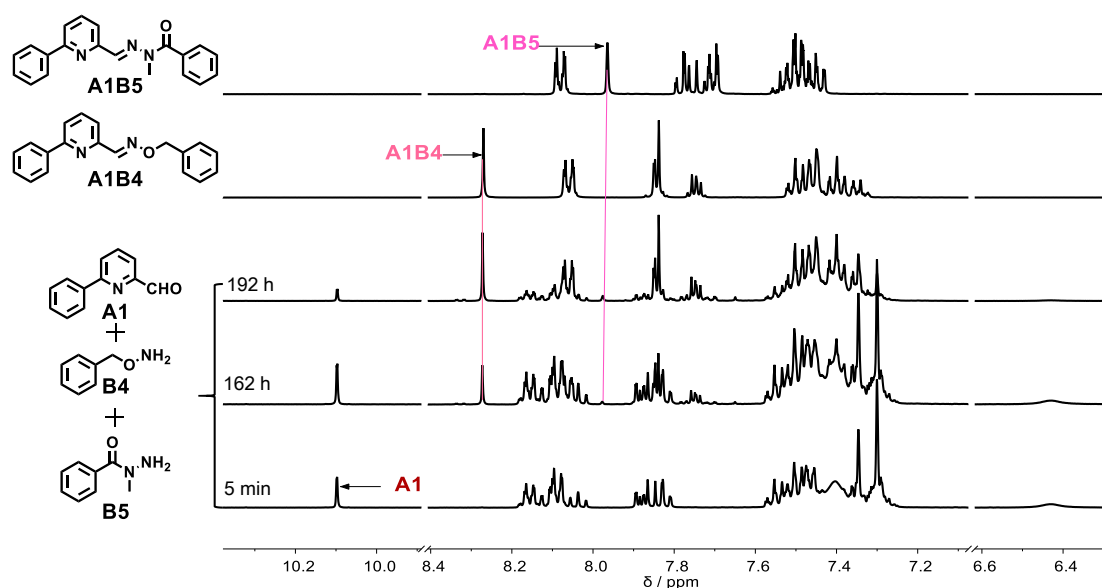


Figure 90. ^1H NMR (400 MHz) spectra of the mixture of the same equivalent of **A1**, **B4** and **B5** (30 mM each, CD_3CN , 25°C) after 5 minutes, 162 h and 192 h (three bottom traces). The two top traces correspond to the isolated constituents **A1B4** and **A1B5**.

The reaction, when performed in a 1: 1: 1 ratio, is very slow with a yield of 21% of **A1B4** and 3% of **A1B5** after 8 days, indicating that **A1B4** is thermodynamically favored over **A1B5**. When the reaction is done in 2: 1: 1 stoichiometry, it gave a distribution of 17% of **A1B4** and 4% **A1B5** after 7 days with many unreacted **A1**. The above two experiment implied that the alkoxyamine **B4** also reacted faster than the hydrazide **B5** and its product **A1B4** is both the kinetic and thermodynamic product compared with **A1B5**.

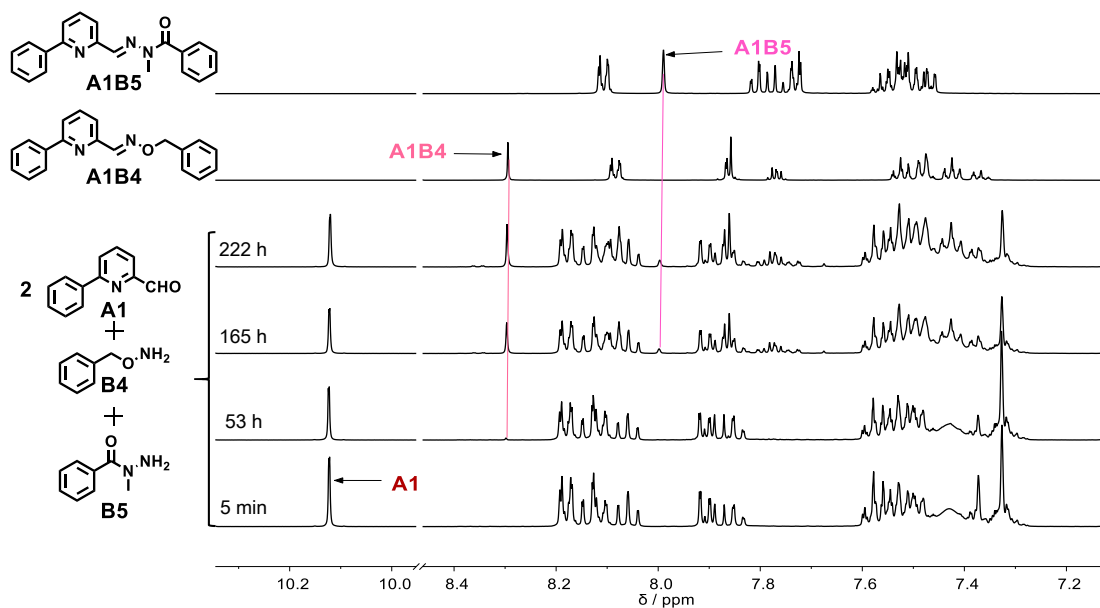


Figure 91. ^1H NMR (400 MHz) spectra of the mixture of 2.0 equiv. **A1** + **B4** + **B5** (1.0 equiv. for **B4** and **B5**) (30 mM each, CD_3CN , 25°C) after 5 minutes, 53 h, 165 h and 222 h (from bottom to top). The reference spectra of the separately prepared constituents **A1B4** and **A1B5** is shown above.

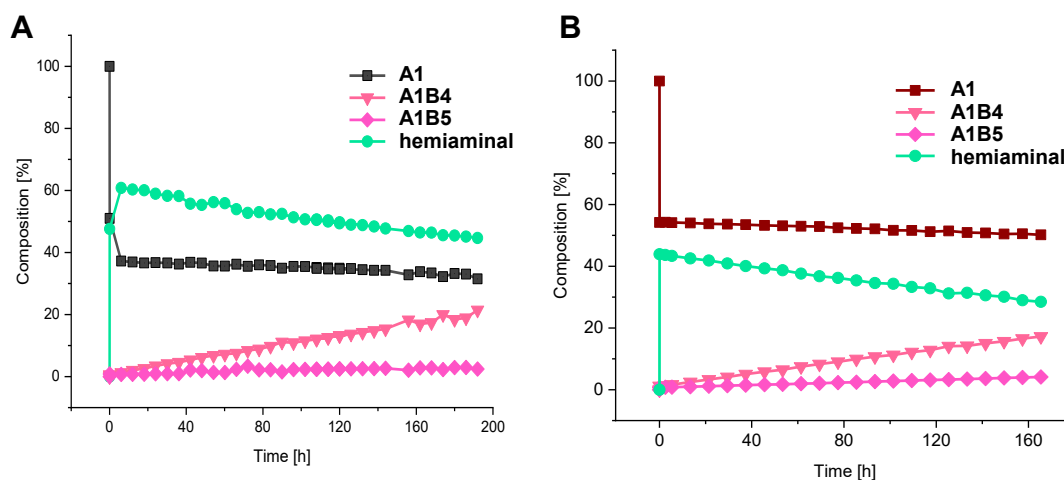
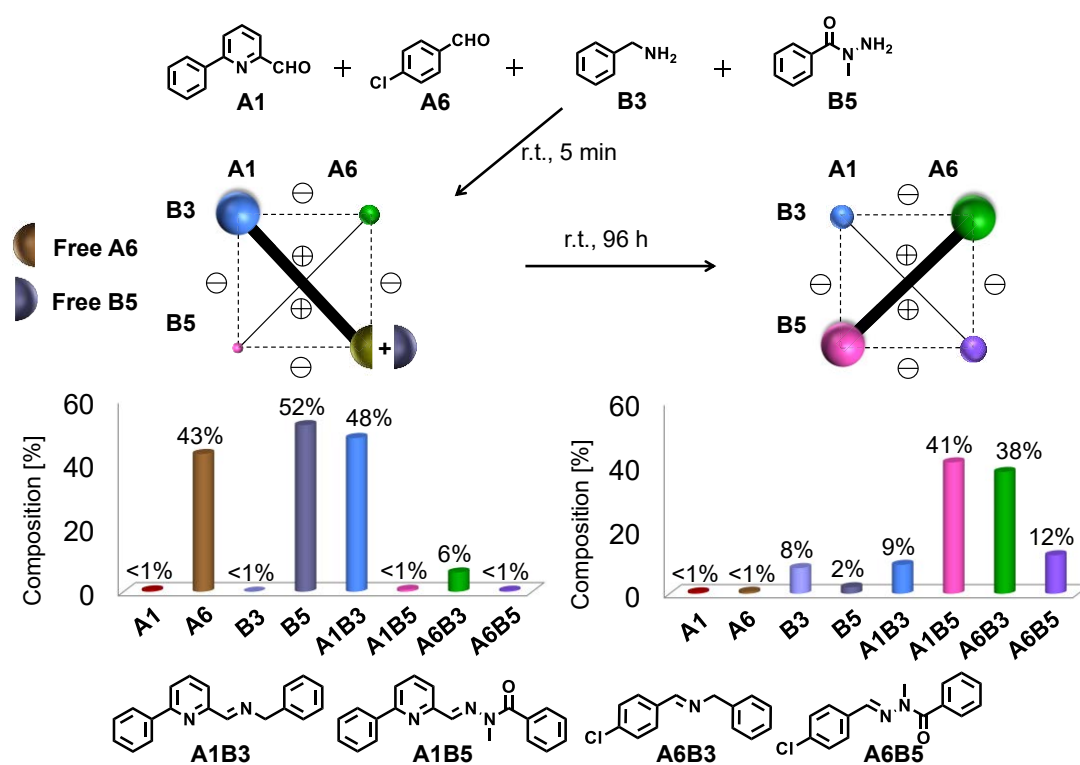


Figure 92. Kinetic plots of the evolution of the mixture of the three components: (A). **A1** + **B4** + **B5** (1.0 equiv. for each); (B) 2.0 equiv. **A1** + **B4** + **B5** (1.0 equiv. for **B4** and **B5**) as a function of time as obtained from integration of the imine $\text{CH}=\text{N}$ and aldehyde CHO proton signals in the 400 MHz ^1H NMR spectra (30 mM each, CD_3CN , 25°C). For clarity, the kinetic curves are shown for only some of the compounds.

2) The kinetic switching of DCL[3] from four constituents generated from four components

Finally a third four component DCL[3] was studied in the same conditions as for DCL[1] and DCL[2] above, based on the components **A1**, **A6**, **B3** and the *N*-methylbenzohydrazide **B5** (Scheme 25). The formation of the four constituents **A1B3**, **A1B5**, **A6B3** and **A6B5** was again

monitored by ^1H NMR as a function of time (**Figure 93**). Like oximes, acylhydrazones are known to be thermodynamically favored products relatively to simple imines.²⁰ **B5** was selected to replace **B4** to investigate the behavior of this new DCL. After 5 minutes, only two products were detected, giving a composition **A1B3**/48%, **A6B3**/6%, together with **A6**/43% and **B5**/50% left unreacted in the solution. After 96 h at room temperature, the reaction reached an equilibrium with a constituent composition of **A1B3**/9%, **A1B5**/41%, **A6B3**/38% and **A6B5**/12%. As seen in the evolution of the ^1H NMR spectra and the kinetic traces, the **DCL[3]** resulted in again an evolution from an initial kinetic distribution to the final thermodynamic distribution with an orthogonal switching of the associated CDN from the diagonal axis [**A1B3**, **A6 + B5**] to the orthogonal [**A1B5**, **A6B3**] one.



Scheme 25. Kinetic switching of the $[2 \times 2]$ CDN formed by the **DCL[3]** set of components [**A1 + A6 + B3 + B5**] (top) from the [**A1B3**, **A6 + B5**] state (middle left) to the orthogonal state [**A1B5**, **A6B3**] (middle right) in CD_3CN at 25°C . The indicated composition % values of the different compounds present correspond to reaction times of 5 min (left) and 96 h (right). Data obtained from the 400 MHz ^1H NMR spectra.

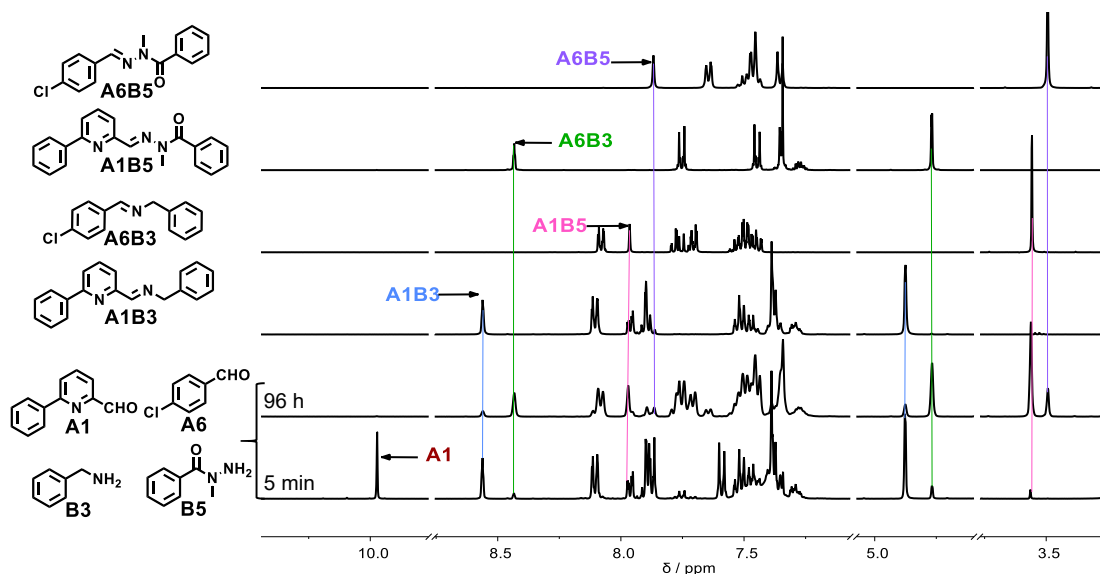


Figure 93. Evolution of ^1H NMR (400 MHz) spectra of the compounds generated from the **DCL[3]** mixture of equimolar amounts of **A1**, **A6**, **B3**, **B5** (30 mM each in CD_3CN , 25°C) after 5 min and 96 h (two bottom traces). The four top traces correspond to the isolated constituents **A1B3**, **A1B5**, **A6B3** and **A6B5**. The arrows indicate the aldehyde CHO proton (9.5-10.0 ppm region) and imine CH=N proton (8.0-9.0 ppm region) NMR signals of the compounds.

Interestingly, the initial distribution turned out $<1\%$ of the acylhydrazone **A1B5** compared to 14% for the corresponding oxime **A1B4** in the **DCL[2]** above, indicating an appreciably lower reactivity of the *N*-methylbenzohydrazide **B5** compared to the alkoxy amine **B4**. This feature is also reflected in the fact that the evolution of the kinetic traces (**Figure 94**) is more gradual than in the previous cases above. This fact that **B4** is more reactive than **B5** has been proven in the competitive experiment described above (**Figure 92**).

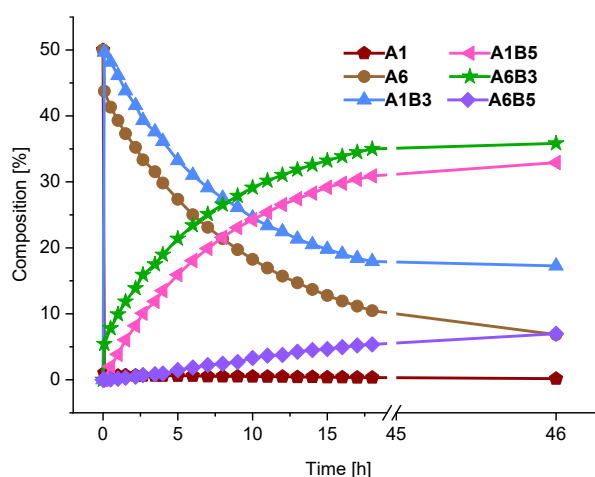
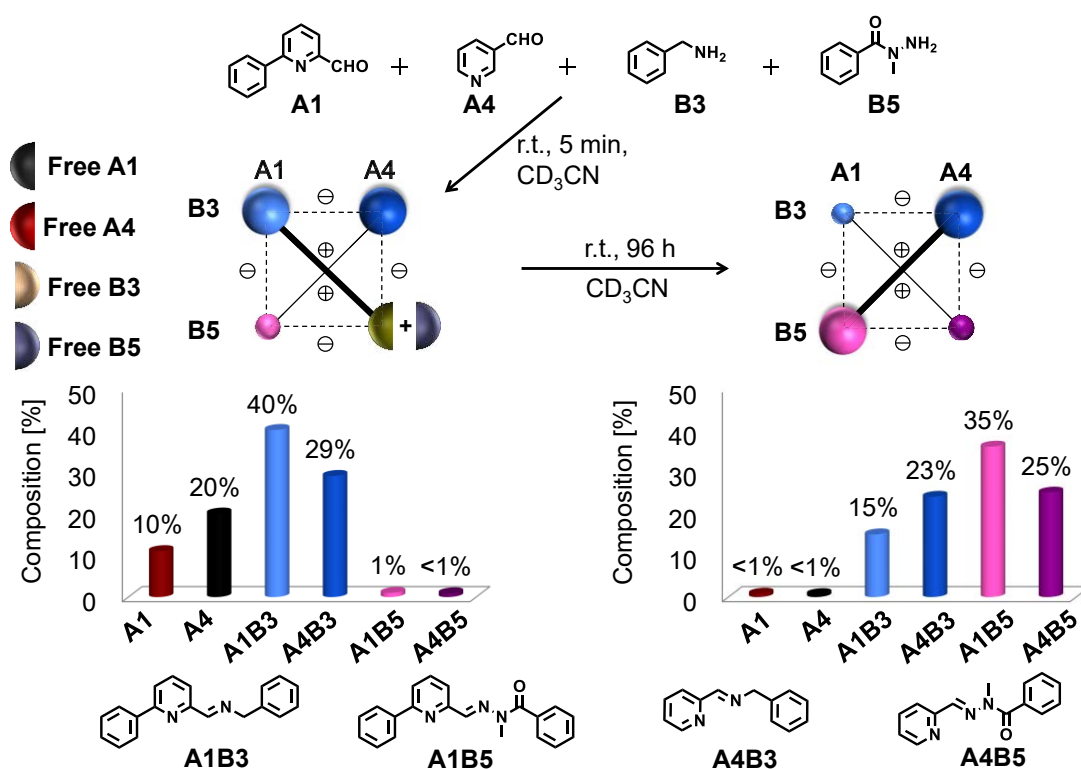


Figure 94. Kinetic plots of the evolution of a mixture of equimolar **A1** + **A6** + **B3** + **B5** as a function of time. The composition % data have been obtained by integration of the imine $-\text{CH}_2-$ (of the benzyl group), hydrazone $\text{N}-\text{CH}_3$ and aldehyde CHO proton signals in the 400 MHz ^1H NMR spectra (30 mM each, CD_3CN , 25°C). For clarity, the kinetic curves are shown for some of the compounds.

iv. DCL[4] generated from the four components A1, A4, B3, B5

In order to try if the reactivities of the two aldehydes influence greatly on the switching behavior, the experiment for the set of components **A1** + **A4** + **B3** + **B5** with **A1** and **A4** having similar reactivities were tested (**Scheme 26**). The differences for **A1** and **A4** is **A1** has a methyl group in the 6-position of **A4** (6-methyl group of 2-formylpyridine). After 5 minutes, the distribution of the DCL was as follows: **A1B3**/40%, **A4B3**/29% together with free **A1**/10% and free **A4**/20% both unreacted in the solution (**Figure 95**). After 96 hours, it reached the equilibrium with a near-statistical distribution for **A1B3**/19%, **A4B3**/25%, **A1B5**/32%, **A4B5**/21%. The kinetic curve of this experiment is shown in **Figure 96**. This experiment further proved that the differences of the reactivities of the two aldehydes has a big effect on the switching behavior of the DCLs.



Scheme 26. The [2 × 2] DCL formed by the DCL set of components [A1 + A4 + B3 + B5] in CD₃CN at 25°C. Data obtained from the 400 MHz ¹H NMR spectra.

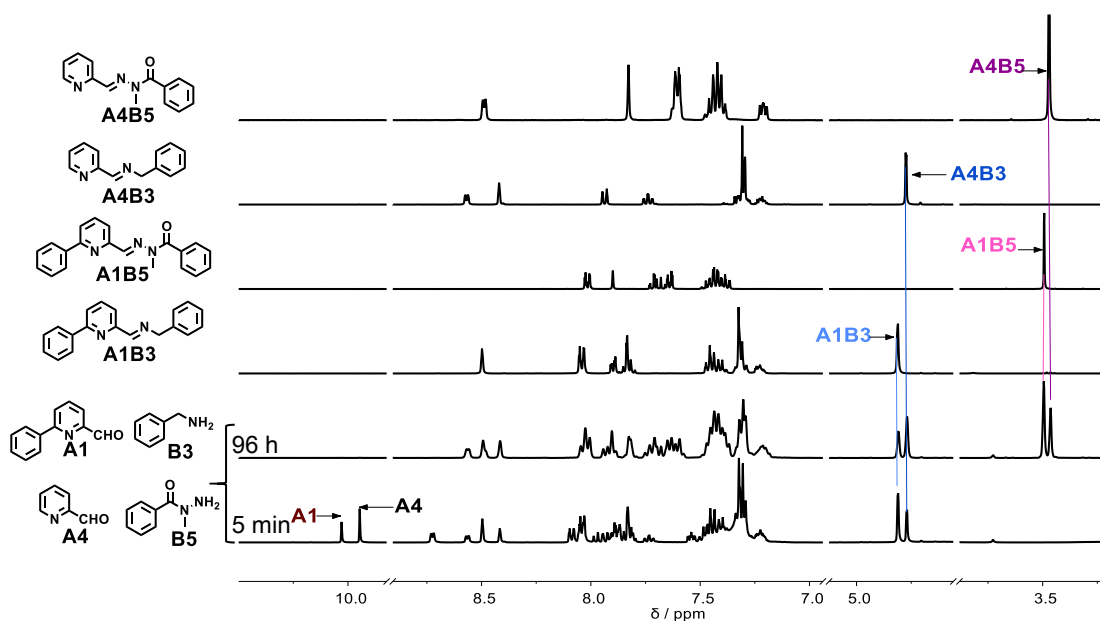


Figure 95. ^1H NMR (400 MHz) spectra of the mixture generated from equimolar amounts of **A1** + **A4** + **B1** + **B3** (30 mM each, CD_3CN , 25°C) after 5 minutes and 96 h (two bottom traces). The reference spectra of the correspond the isolated constituents **A1B3**, **A1B5**, **A4B3** and **A4B5** are shown above.

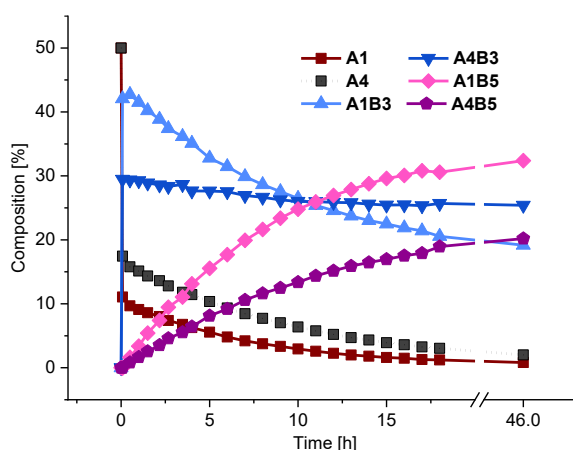


Figure 96. Kinetic plots of the evolution of a mixture of equal amounts of components **A1** + **A4** + **B3** + **B5** as a function of time as obtained from integration of the imine $\text{CH}=\text{N}$ and aldehyde CHO proton signals in the 400 MHz ^1H NMR spectra (30 mM each, CD_3CN , 25°C). For clarity, the kinetic curves are shown for only some of the compounds

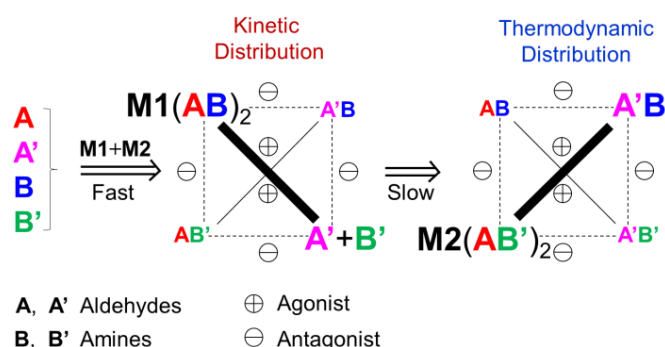
The present DCLs all undergo a network switching from a kinetic distribution to the thermodynamic distribution as a function of time. This process that may be considered as an adaptation to time via component exchange, caused by the internal kinetic and thermodynamic properties of the constituents. It is important to note that network switching achieves a much larger change in distribution (by factors of 3 to 6) than simple amplification from a statistical

distribution, as described previously. Such large changes resulting from kinetic factors represent a very significant feature of the behavior of networks.

B. Kinetic switching of CDNs of ligand constituents driven by metal cations of different coordination geometries

The above results demonstrate the time-dependent switching of the CDNs from the kinetic distribution to the thermodynamic distribution driven by the exchange of the kinetically faster imine to the thermodynamically more stable oximes and hydrazones. It was necessary to explore whether the addition of metal cations would induce a similar switching behavior. As is reported in earlier work,^{65,66,98,99} the presence of metal cations would greatly influence the behavior of a DCL according to the specificity of the metal cation. The adaptation of DCLs in the presence of metal ions were also introduced in Chapter I.

We were thus urged to investigate whether such a switching could also be achieved for a DCL by addition of two different metal cation effectors **M1** and **M2**. Particularly, a CDN underwent switching from the kinetic complex of one metal ion to the thermodynamic complex involving the other metal ion. The achievement of such a switching greatly rely on the difference in both the rate of the ligand formation and relative stabilities of the two generated complexes in the presence of the two metal cations. The evolution of a system undergoing such a CDN switching is represented in **Scheme 27**.

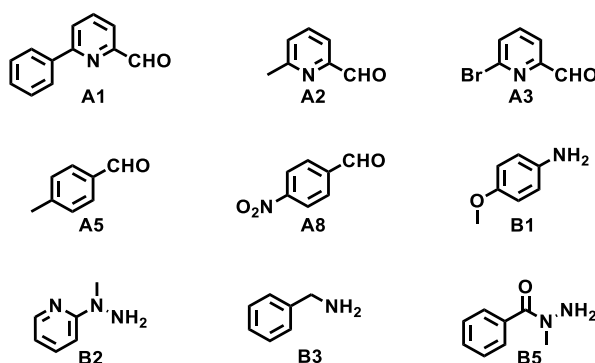


Scheme 27. Evolution of a DCL of four ligand constituents undergoing a time-dependent switch of its associated [2 × 2] CDN driven by the formation of the complexes of two different metal cations **M1** and **M2**.

It is crucial to screen the metal cations according to their different properties, i.e. geometry and stability. As already well known, monovalent metal cations **M1** such as Ag(I) or Cu(I) favors the formation of tetracoordinated metal complexes with bidentate ligands whereas

divalent metal cations **M2** such as Zn(II) or Fe(II) prefer to form hexacoordinated octahedral complexes with tridentate ligands. Considering these conditions above, we envisaged to achieve a kinetic switching of the $[2 \times 2]$ DCL from a tetrahedral complex of an imine to an octahedral complex of hydrazone upon addition of two metal cations. Accordingly, the kinetic behavior of the DCLs with different combination of the metal ions, as well as organic components, were studied in the presence of two metal cations with respect to the coordination characteristics of the metal cations.

Therefore, we selected pyridyl-aldehydes as one kind of the aldehydes since they can form a bidentate imine ligand upon reaction with an amine component and can also generate a tridentate acylhydrazone or pyridyl-hydrazone ligand when reacting with a corresponding acylhydrazine and pyridyl-hydrazine component. The other aldehyde could be less reactive, without any coordination site. The corresponding aldehyde and amine components adopted in this section are depicted in **Scheme 28**.



Scheme 28. The structure of the selected aldehydes and amines to set up the $[2 \times 2]$ DCLs in the presence of metal cations.

In order to find out the system which could achieve this time-dependent switching, we firstly did the experiments for **DCL[5]** to **DCL[7]** with different components by sequential addition of the two metal cations **M1** and **M2**. As such, if the sequential addition of the two metal ions to the $[2 \times 2]$ DCL components could achieve the switching from one metal complex of imine to the other metal complex of another hydrazone, this will make it possible for the DCL to attain the switching on simultaneous addition of the two metal cations together with the components within the DCL. Therefore, the three DCLs {**DCL[5]**, **[6]** and **[7]**} were tested on sequential addition of two metal cations **M1** and **M2**.

i. DCL[5] generated from the four components A1, A6, B3, B5 in the presence of Cu(I) and Zn(II)

By combining previously reported work²⁸ and the switching behavior above for the **DCL[3]**, the imine is the kinetic product which can also act as a bidentate ligand, while the acylhydrazone is the thermodynamic product which can act as a tridentate ligand. Thus, the imine **A1B3** should form a tetrahedral complex with Cu(I) or Ag(I), while the acylhydrazone **A1B5** should form an octahedral complex with Zn(II) or Fe(II). Therefore, the four components **A1**, **A6**, **B3**, **B5** were firstly selected to generate the [2 × 2] DCL in the presence of the two metal cations.

Thus, the **DCL[5]** was set up from an equimolar **A1**, **A6**, **B3**, **B5** (see **Figure 97**). The two metal cations CuOTf and Zn(OTf)₂ were added in sequence. On addition of Cu(I) after 5 minutes, the Cu(I) complex of imine [Cu(**A1B3**)₂]⁺ is almost fully formed with free **A6** which does not react due to the lower reactivity. The ¹H NMR spectrum was very broad due probably to the oxidation of the Cu(I). Addition of Zn(II) to the mixtures after 96 hours, the signal of the [Cu(**A1B3**)₂]⁺ still existed and the signal of the [Zn(**A1B5**)₂]²⁺ was observed. The distribution of [Cu(**A1B3**)₂]²⁺ and [Zn(**A1B5**)₂]²⁺ was 43% and 54% with 3% of free **A1** left. Only slight amount of **A6B3** was observed while the amount of the free **A6** decreased a lot. This could be due to the silver mirror reaction of **A6** with Ag(I) since the silver layer was observed on the inner wall of the nmr tube. From this experiments, the Cu(I) complex of imine [Cu(**A1B3**)₂]²⁺ cannot be largely exchanged to form the Zn(II) complex of hydrazone [Zn(**A1B5**)₂]²⁺ due probably to the very stable coordination of Cu(I) with the imine **A1B3** bearing phenyl substituent on the 6 position of pyridine. The steric hindrance may also inhibit the formation of Zn (II) complex of the hydrazone. The reaction of **A6** with Ag(I) could be due to the relative high reactivity of **A6** in the presence of basic **B3**. This result prompted us to adopt an aldehyde which can form a less stable Cu(I) complex with its imine ligand to allow for the exchange reaction to form the Zn(II) complex of acylhydrazone. At the same time, using a less reactive aldehyde **A5** (*p*-methylbenzaldehyde) instead of **A6** (*p*-chlorobenzaldehyde) or using a less basic aromatic primary amine would avoid the silver mirror reaction. The experiment was first tested for changing the two aldehydes **A1** and **A6** to **A2** and **A5**

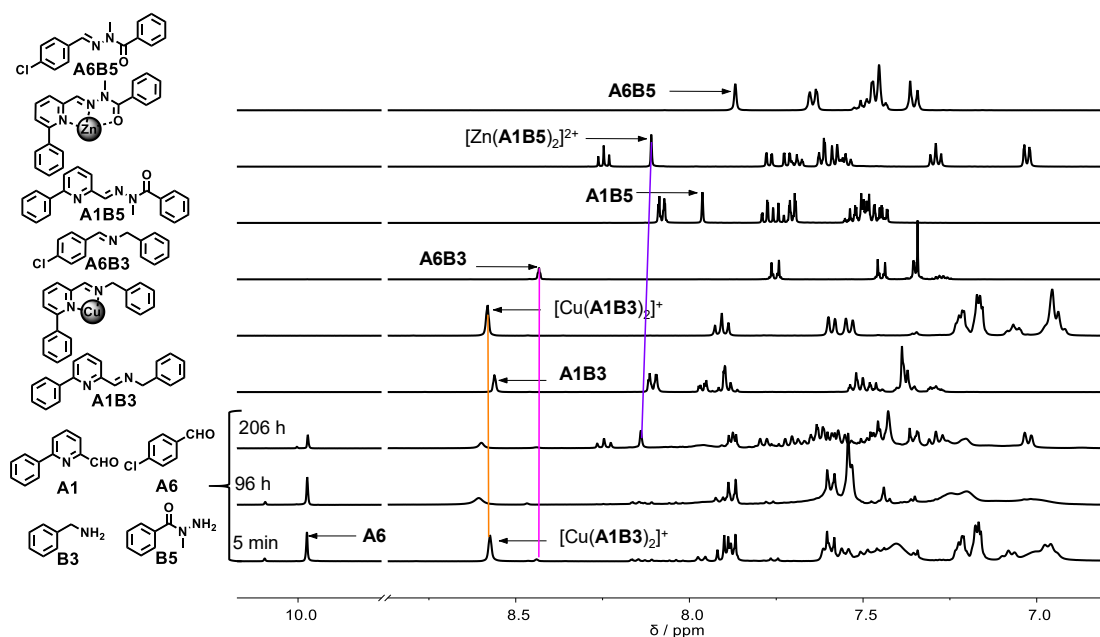


Figure 97. ^1H NMR (400 MHz) spectra of the mixture generated from equal amounts of **A1** + **A6** + **B3** + **B5** (30 mM each, CD_3CN , 25°C) after 5 minutes, 96 h and 206 h (two bottom traces). The four top traces correspond to the isolated constituents **A3B1**, **A3B3**, **A1B1** and **A1B3**.

*ii. DCL[6] generated from the four components **A2**, **A5**, **B3**, **B5** in the presence of two metal ions*

Based on the above result, **A1** (6-phenyl-2-formyl pyridine) was replaced by **A2** (6-methyl-2-formyl pyridine) and **A6** was replaced by a less reactive aldehyde **A5** to leave enough time for the switching of the complexes as well as inhibit the silver mirror reaction. A series of experiments of combination of the four metal cations were tested for generation of the switching behavior of the **DCL[6]** from the four components. The **DCL[6]** of the four components was studied by sequential addition of the two metal salts: first $\text{Cu}(\text{OTf})$ or $\text{Ag}(\text{OTf})$; then $\text{Zn}(\text{OTf})_2$ or $\text{Fe}(\text{OTf})_2$.

1) DCL[6] generated from the four components **A2, **A5**, **B3**, **B5** on sequential addition of $\text{Cu}(\text{I})$ and $\text{Zn}(\text{II})$**

The **DCL[6]** was generated from equimolar **A2**, **A5**, **B3**, **B5** (**Figure 98**). Upon addition of $\text{Cu}(\text{I})$ after 5 minutes, the $\text{Cu}(\text{I})$ complex of imine $[\text{Cu}(\text{A2B3})_2]^+$ already formed in a large amount together with a lot of free **A5** and free **B5**. The spectrum was again a bit broad. On addition of $\text{Zn}(\text{II})$ after 5 minutes, the ^1H NMR spectrum became much broader due probably to the exchange between the complexes. After heating at 60°C for 2 days, the **DCL[6]** reached

equilibrium with the following distribution: $[\text{Cu}(\text{A2B3})_2]^+$ /27% $[\text{Zn}(\text{A2B5})_2]^{2+}$ 22%, and A5B5 /23% with the unreacted A5 /27%. indicating that the Cu(I) complex of imine still cannot be largely transformed to the Zn(II) complex by replacing the aldehyde A1 with A2 . The reason could be due to either the higher stability of the Cu(I) complex of imine or the less coordination ability of the acylhydrazone, which cannot drive the transformation of the Cu(I) complex of imine to Zn(II) complex of acylhydrazone. The key point is to balance these two factors to achieve the switching behavior.

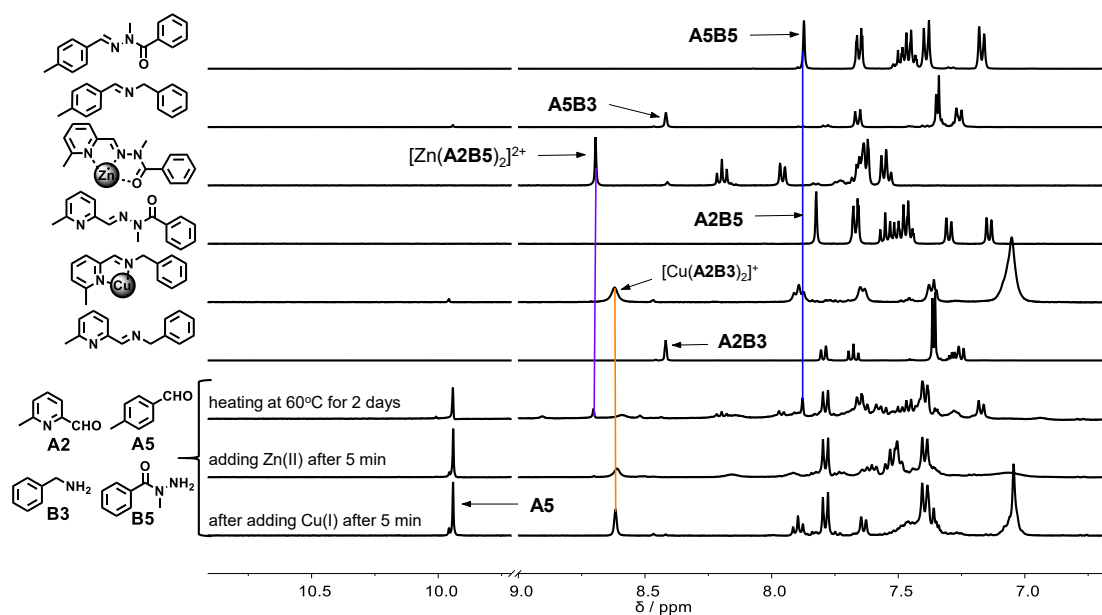


Figure 98. ^1H NMR (400 MHz) spectra of the mixture generated from equimolar amounts of $\text{A2} + \text{A5} + \text{B3} + \text{B5}$ (30 mM each, CD_3CN , 25°C) adding Cu(I) after 5 minutes, adding Zn(II) after 5 minutes and heating at 60°C for 2 days. (three bottom traces). The reference spectra of the isolated constituents A2B3 , $[\text{Cu}(\text{A2B3})_2]^+$, A2B5 , $[\text{Zn}(\text{A2B5})_2]^{2+}$, A5B3 and A5B5 are shown above.

2) DCL[6] generated from the four components A2 , A5 , B3 , B5 on sequential addition of Cu(I) and Fe(II); Ag(I) and Zn(II) or Fe(II)

Apart from Cu(I) and Zn(II), the similar experiment were also conducted for the DCL[6] by sequential addition of Cu(I) and Fe(II) to see if Fe(II) has stronger coordination ability than Zn(II) in the same case.

Seen from **Figure 99**, the formation of the $[\text{Cu}(\text{A2B3})_2]^+$ is very fast. After 5 minutes, it yielded a large amount of $[\text{Cu}(\text{A2B3})_2]^+$ with similar amount of A5 and B5 . After addition of Fe(II), the shape of the spectrum became a bit broad. After the DCL[6] reached the equilibrium (heating at 60°C for 2 days), a sets of broad peaks of the Fe(II) complex $[\text{Fe}(\text{A2B5})_2]^{2+}$ was detected, which is attributed to the high spin complex, together with A5B5 . Nevertheless, a non-negligible amount of $[\text{Cu}(\text{A2B3})_2]^+$ is still present. The ratio of the $[\text{Cu}(\text{A2B3})_2]^+$ and

$[\text{Fe}(\text{A2B5})_2]^{2+}$ is about 1:1. Therefore, the Fe(II) doesn't have stronger coordination with acylhydrazone, leading to the uncomplete transformation from $[\text{Cu}(\text{A2B3})_2]^+$ to $[\text{Fe}(\text{A2B5})_2]^{2+}$.

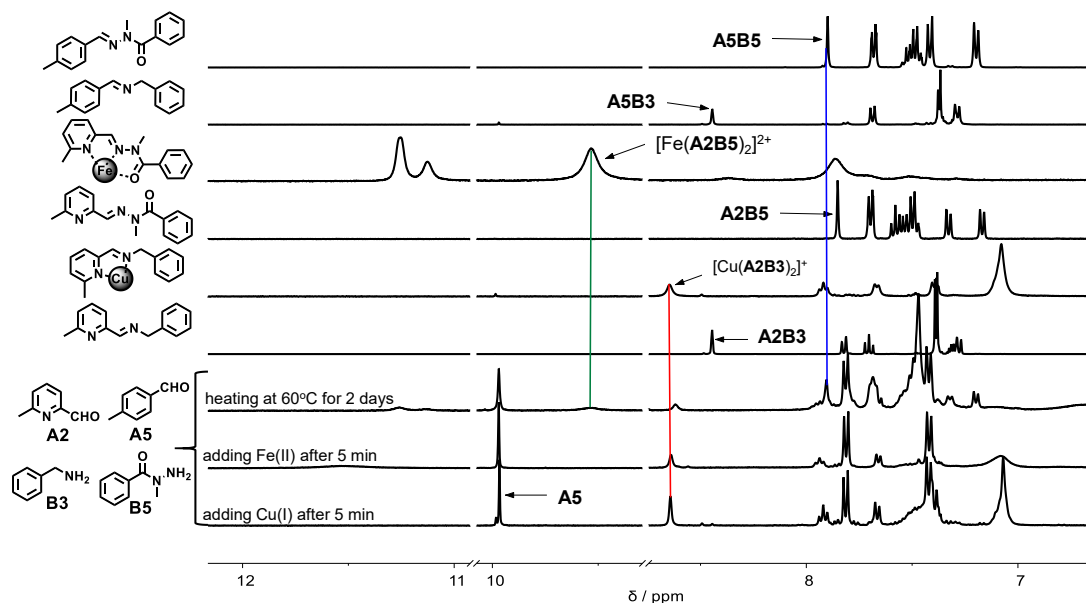


Figure 99. ^1H NMR (400 MHz) spectra of the mixture generated from equal amounts of **A2** + **A5** + **B3** + **B5** (30 mM each, CD_3CN , 25°C) adding Cu(I) after 5 min, adding Fe(II) after 5 minutes and heating at 60°C for 2 days. (three bottom traces). The reference spectra of the isolated constituents **A2B3**, $[\text{Cu}(\text{A2B3})_2]^+$, **A2B5**, $[\text{Fe}(\text{A2B5})_2]^{2+}$, **A5B3** and **A5B5** are shown above.

The same **DCL[6]** were also tested on the sequential addition of Ag(I) and Zn(II) or Ag(I) and Fe(II). Similar results are obtained as above (**Figure 100** and **Figure 101**).

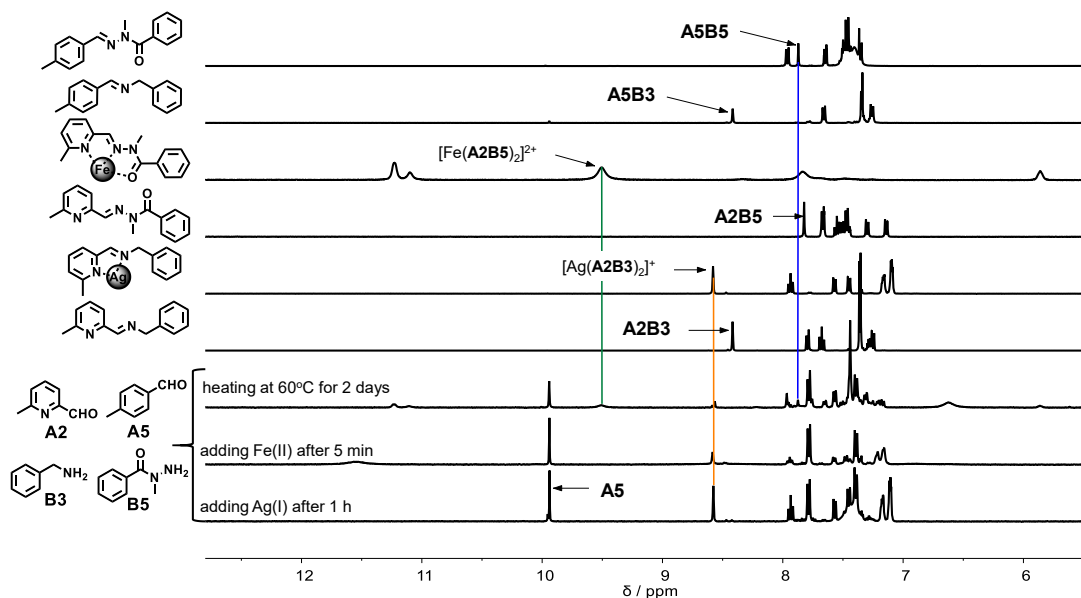


Figure 100. ^1H NMR (400 MHz) spectra of the mixture generated from equal amounts of **A2** + **A5** + **B3** + **B5** (30 mM each, CD_3CN , 25°C) adding Ag(I) after 3 hours, adding Zn(II) after 5 minutes and heating at 60°C for 2 days. (three bottom traces). The reference spectra of the isolated constituents **A2B3**, $[\text{Ag}(\text{A2B3})_2]^+$, **A2B5**, $[\text{Fe}(\text{A2B5})_2]^{2+}$, **A5B3** and **A5B5** are shown above.

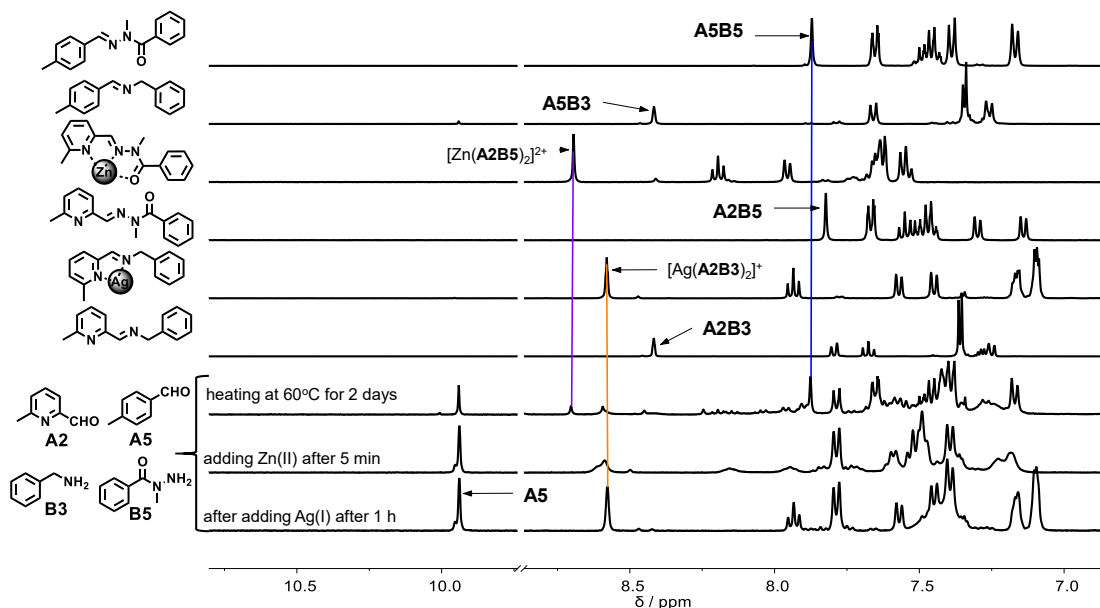


Figure 101. ^1H NMR (400 MHz) spectra of the mixture generated from equal amounts of **A2** + **A5** + **B3** + **B5** (10 mM each, CD_3CN , 25°C) adding Ag(I) after 1 hour, adding Fe(II) after 5 minutes and heating at 60°C for 2 days. (three bottom traces). The reference spectra of the isolated constituents **A2B3**, $[\text{Ag}(\text{A2B3})]^+$, **A2B5**, $[\text{Zn}(\text{A2B5})_2]^{2+}$, **A5B3** and **A5B5** are shown above.

According to these results, the **DCL[6]** with the four components **A1** + **A5** + **B3** + **B5** displayed the uncomplete kinetic switching in principle from the pair of kinetic product, the Cu(I) [or Ag(I)] complex of imine **A2B3** with another acylhydrazone **A5B5**, to the other pair of the thermodynamic product, the Zn(II) (or Fe(II)) complex of acylhydrazone **A2B5** together with another new imine **A5B3**. The most probable reason is due to the less coordination ability of the acylhydrazone with Zn(II) or Fe(II) due to the oxygen on the carbonyl of the acylhydrazone. Hence, we envisaged to use a better ligand instead of acylhydrazone to serve as the final ligand for Fe(II) or Zn(II) and also

iii. **DCL[7] generated from the four components A2, A5, B2, B3 in the presence of two metals**

The above results inspired us to choose a better ligand which is not only thermodynamically more stable than imines but also have better coordination ability than acylhydrazone. The *N*-methyl pyridylhydrazine **B2** was chosen since it can form a tridentate ligand compound with three N coordination sites after reaction with pyridyl-based aldehyde and it is much more stable than imines. The corresponding **DCL[7]** can be established from its components **A2**, **A5**, **B2**, **B3** upon addition of the metal cations. From the previous studies,⁹⁸

Cu(I) can be oxidized thus broadening the ^1H NMR spectra with the presence of **B2**. Therefore, only the two combination of metal cations were tested in the following experiment: 1) Ag(I) and Fe(II), 2) Ag(I) and Zn(II).

1) DCL[7] generated from the four components **A2**, **A5**, **B2**, **B3** on sequential addition of Ag(I) and Fe(II)

Firstly, equal amounts of the four components **A2**, **A5**, **B2**, **B3** were mixed together to build up DCL[7]. Then 0.5 equivalent amount of Ag(I) was added immediately after the mixing. After about 1 hour, the amount of the Ag(I) complex of **A2B3** increased as the main constituent in the DCL together with almost the same amount of the unreacted **A5** and **B2**. Immediately after addition of Fe(II), the color of the solution changed to purple, likely due to the coordination of Fe(II) with **B2**. After heating at 60°C for 2 days, there are some new peaks appearing which could be the hetero complexes of Fe(II) and $[\text{Fe}(\text{A2B2})_2]^{2+}$. The aldehyde **A5** still existed in a large amount indicating the very low reactivity of **A5** with **B2**. This experiment demonstrated that the Fe(II) is still not a very excellent metal cation for coordinating with **A2B2** to drive the formation of itself from the exchange reaction of $[\text{Ag}(\text{A2B3})_2]^+$ with **B2**.

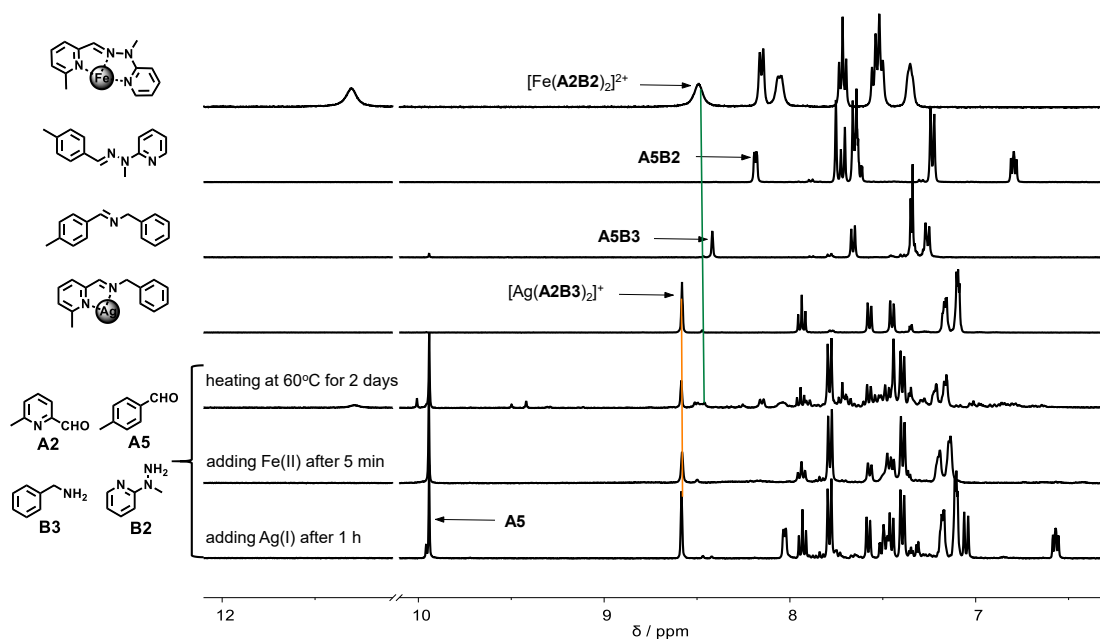


Figure 102. ^1H NMR (400 MHz) spectra of the mixture generated from equal amounts of **A2** + **A5** + **B2** + **B3** (30 mM each, CD_3CN , 25°C) adding Ag(I) after 1 hour, adding Fe(II) after 5 minutes and heating at 60°C for 2 days. (three bottom traces). The four top traces correspond to the isolated constituents $[\text{Ag}(\text{A2B3})_2]^+$, **A5B3**, **A5B2** and $[\text{Fe}(\text{A2B2})_2]^{2+}$.

2) DCL[7] generated from the four components **A2**, **A5**, **B2**, **B3** on sequential addition of Ag(I) and Zn(II)

The same experiment for DCL[7] was also performed with the addition of Ag(I) and Zn(II) in sequence to the mixture of **A2**, **A5**, **B2**, **B3**. The corresponding ^1H NMR spectra of the evolution can be seen in **Figure 103**. Similarly, the large amount of $[\text{Ag}(\text{A2B3})_2]^+$ was formed 1 hour after addition of 0.5 equiv. of Ag(I) with the unreacted **A5** and **B5** in the solution. The ^1H NMR spectrum became broad 5 minutes after addition of 0.5 equiv. of Zn(II). This is due to the exchange $[\text{Ag}(\text{A2B3})_2]^+$ with Zn(II) since Zn(II) and Ag(I) are both labile metal ions. At the same time, Zn(II) can also coordinate with **B2**, resulting in the shift of the peaks of **B2**. The separate titration experiment of **B2** by Zn(II) is shown in **Figure 104**. The formation of $[\text{Zn}(\text{B2})_2]^+$ can also be proven by the HRMS-ESI spectrum (**Figure 105**). After heating at 60°C for 2 days to reach the equilibrium, the $[\text{Ag}(\text{A2B3})_2]^+$ were largely transformed to $[\text{Zn}(\text{A2B2})_2]^+$. However, the agonist compound **A5B3** cannot be clearly attributed while the amount of aldehyde **A5** decreased. In addition, there is a metallic silver layer on the inner wall of the nmr tube probably due to the silver mirror reaction of the Ag(I) with **A5** in the presence of the benzylamine **B3** ($\text{p}K_{\text{a}} = 9.34$). This experiment is of crucial importance for the design of the DCL. It implies that it would be better to choose an appropriate aldehyde which could form the hydrazone much faster than **A5** upon reaction with **B3**, thus avoiding the slow reduction of Ag(I). It is also necessary to choose a less basic amine rather than **B3** (benzylamine).

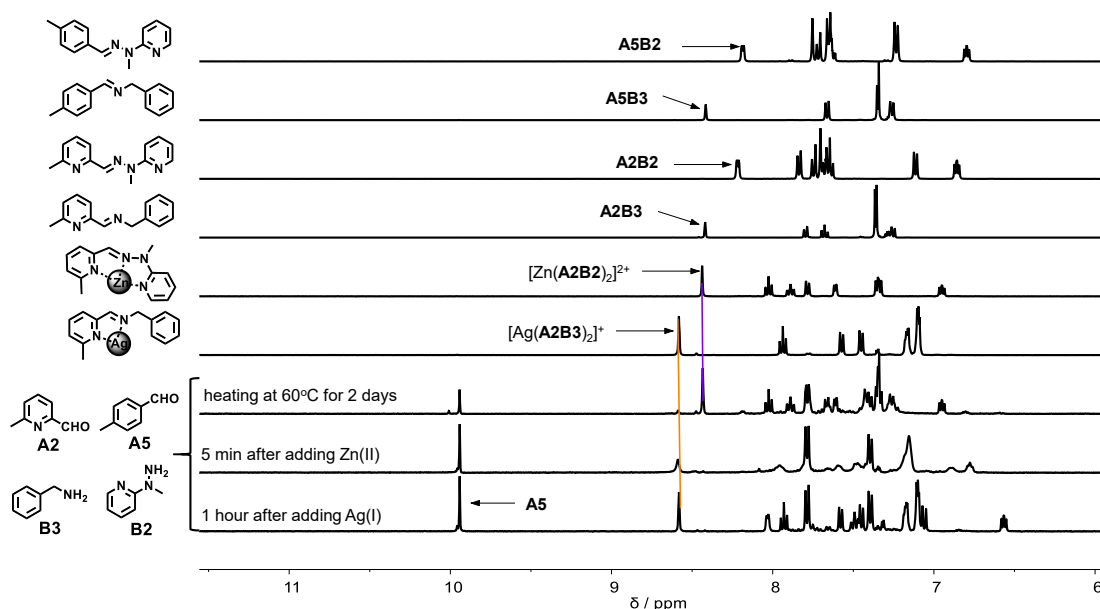


Figure 103. ^1H NMR (400 MHz) spectra of the mixture generated from equal amounts of **A2** + **A5** + **B2** + **B3** (30 mM each, CD_3CN , 25°C) after 5 minutes and 96 h (two bottom traces). The four top traces correspond to the isolated constituents **A2B3**, **A2B2**, **A5B3** and **A5B2**.

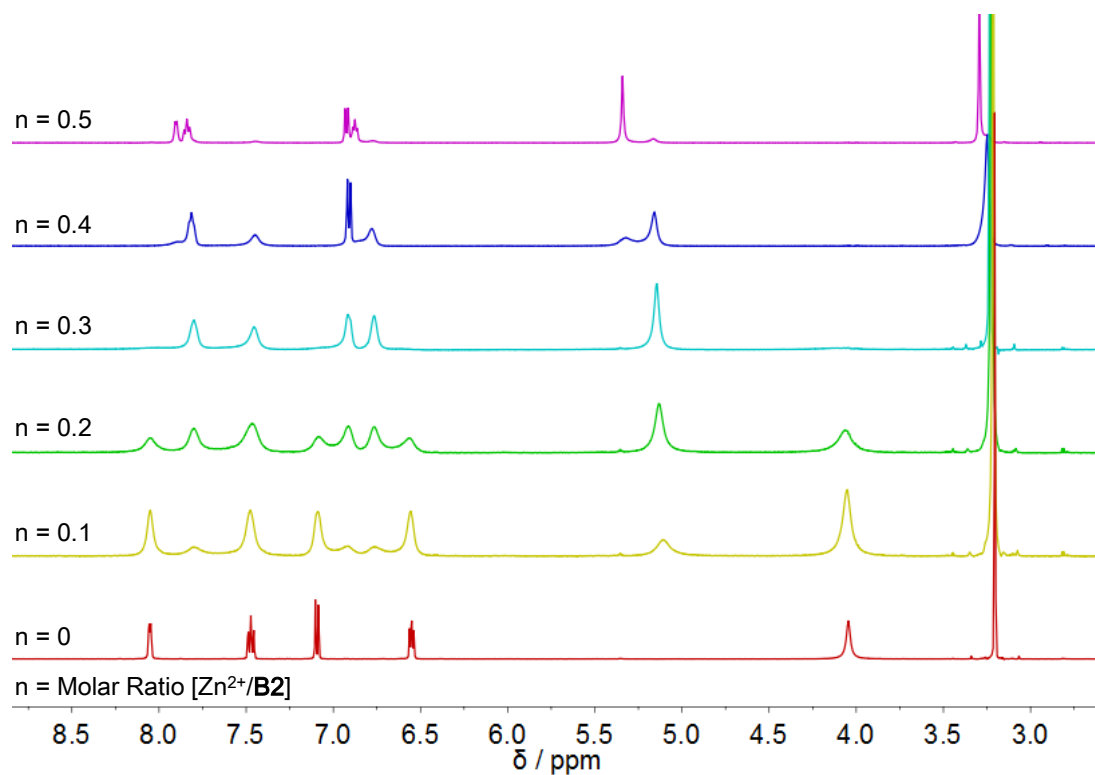


Figure 104. ^1H NMR (400 MHz) spectra obtained from ^1H NMR titration experiment of **B2** with different amounts of $\text{Zn}(\text{OTf})_2$.

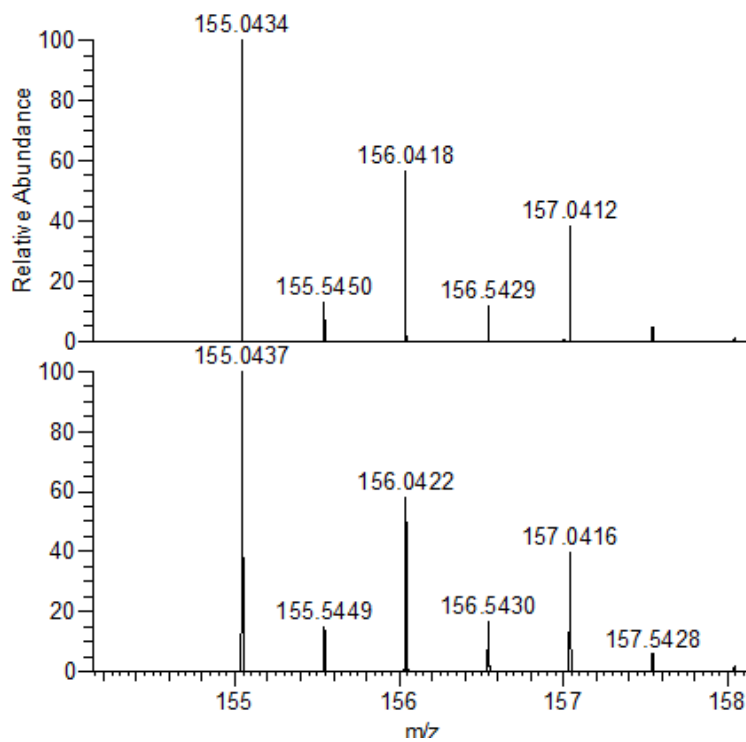


Figure 105. HRMS-ESI spectrum of $[\text{Zn}(\text{B2})_2]^{2+}$ obtained in situ from 2 equiv. **B2** (20 mM) and 1 equiv. $\text{Zn}(\text{OTf})_2$ (10 mM) in CH_3CN . Measured (top), simulated (bottom).

iv. DCLs[8] [9] and [10] generated from the four components A1 (or A2 or A3), A8, B1, B2 in the presence of two metals

After exploration of different component combinations and considering the factors above, we chose much reactive aldehyde *p*-nitrobenzaldehyde **A8** to replace the less reactive aldehyde **A5** and a less basic amine, *p*-anisidine **B1** instead of benzylamine **B3** to avoid the silver mirror reaction. In these cases, the equimolar components **A2** (**A1** or **A3**), **A8**, **B1**, **B2** were mixed together with half equivalent of both Ag(I) and Zn(II). The DCLs including the constituents **A2B1** and **A2B2** presenting different coordination features. The evolution of the reaction was studied in the presence of both AgOTf and Zn(OTf)₂ as a function of time. The details for the kinetic behavior of the three **DCLs**[8], [9] and [10] were shown as follows.

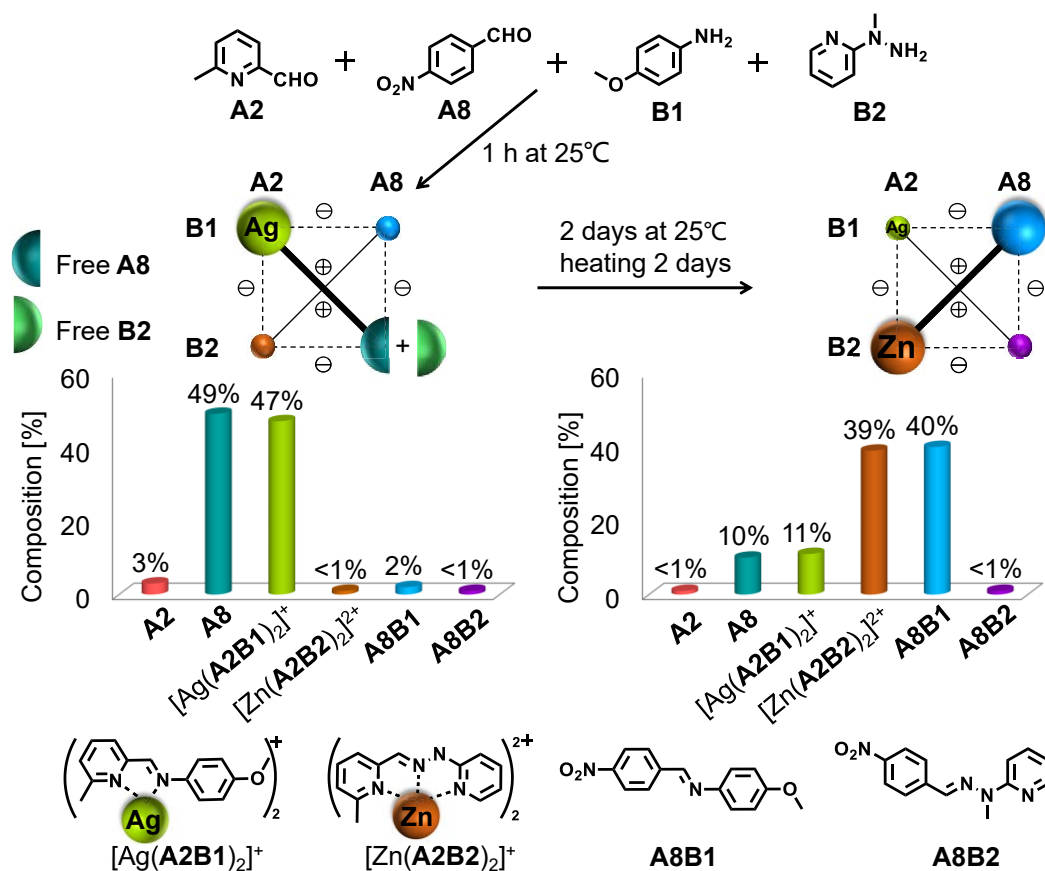
It is to be noted that the coordination of the metal cation by the component may influence the kinetic behavior of that component to form its corresponding constituents. In such a case, in a separate experiment, it was found that Zn(II) coordinates pyridyl-hydrazine **B2** to give [Zn(**B2**)₂]²⁺. Furthermore, addition of metal cations may catalyze the exchange of components between the ligand constituents and thus accelerate the kinetics of the recombination.

In order to be able to identify the entities present in the rather complicated mixtures, the ¹H NMR spectra of all individual components and constituents were measured in the absence and in the presence of the same metal salts AgOTf and Zn(OTf)₂ separately, as well as together. The ¹H NMR spectra of these experiments are shown in experimental part **Figure III19** to **Figure III32**.

1) DCL[8] on simultaneous addition of Ag(I) and Zn(II)

The **DCL**[8] was thus generated from **A2**, **A8**, **B1** and **B2** and its behavior was studied on simultaneous addition of AgOTf and Zn(OTf)₂ (**Scheme 29**). As seen from the ¹H NMR spectra (**Figure 106**), 1 hour after addition of the two metal cations, the silver complex [Ag(**A2B1**)₂]⁺ of imine **A2B1** was almost fully formed (49%) together with unreacted **A6** and **B5** due to the slow rate of hydrazone formation. **B2** was found to be coordinated with Zn(II). As the reaction proceeded for 1 day, the zinc complex [Zn(**A2B2**)₂]²⁺ appeared and its amount increased with amplifying its agonist constituent **A6B4** while the amount of the silver complex [Ag(**A2B1**)₂]⁺ decreased (**Figure 107**). After heating at 60°C for 2 days, the **DCL**[8] reached the equilibrium with the final distribution: [Ag(**A2B1**)₂]⁺ (11%), [Zn(**A2B2**)₂]²⁺ (39%) and **A8B1** (40%) together with 10% of free **A8** and 11% **B2**. Thus, the [2×2] CDN associated to the

DCL[8] had undergone an orthogonal kinetic switching between two metal complexes of different coordination geometries from the kinetic product $[\text{Ag}(\text{A2B1})_2]^+$ together with $[\text{A8} + \text{B2}]$ to the thermodynamic one $[\text{Zn}(\text{A2B2})_2]^{2+}$ and **A8B1**.



Scheme 29. Kinetic switching of a $[2 \times 2]$ **DCL[8]** from the $\{[\text{Ag}(\text{A2B1})_2]^+, \text{A8} + \text{B2}\}$ state to the orthogonal $\{[\text{Zn}(\text{A2B2})_2]^{2+}, \text{A8B1}\}$ state in CD_3CN after 1 h at 25°C and 2 days at 25°C , then 60°C for 2 days (from left to right). Data obtained from the 500 MHz ^1H NMR spectra.

To be noted, the signal of $[\text{Ag}(\text{A2B1})_2]^+$ in the DCL has a large shift and is broadened in comparison with the separately made compound $[\text{Ag}(\text{A2B1})_2]^+$. This could be due to the exchange between the $[\text{Ag}(\text{A2B1})_2]^+$ and $\text{Zn}(\text{II})$. In order to verify this assumption, the titration experiment of $[\text{Ag}(\text{A2B1})_2]^+$ by $\text{Zn}(\text{II})$ was conducted (see in **Figure 108**). Starting with the separately made $[\text{Ag}(\text{A2B1})_2]^+$ which has very sharp peak in the beginning, the signal became broad upon addition of 0.1 equiv. $\text{Zn}(\text{II})$. When more amount of the $\text{Zn}(\text{II})$ salt was added, the signal became broader and broader. With 0.5 equiv. of $\text{Zn}(\text{II})$, a new peak appeared and increased together with the decrease of the original signal. Finally, the original peak disappeared, and the new peak increased but remains broad, similarly to $[\text{Zn}(\text{A2B1})_2]^{2+}$ alone. As we know, both $\text{Ag}(\text{I})$ and $\text{Zn}(\text{II})$ are labile metal cations. The broadening of the spectra is

due to the exchange of the $[\text{Ag}(\text{A2B1})_2]^+$ with $\text{Zn}(\text{II})$. Similar behavior was also observed in the following two DCLs and the corresponding titration experiments below.

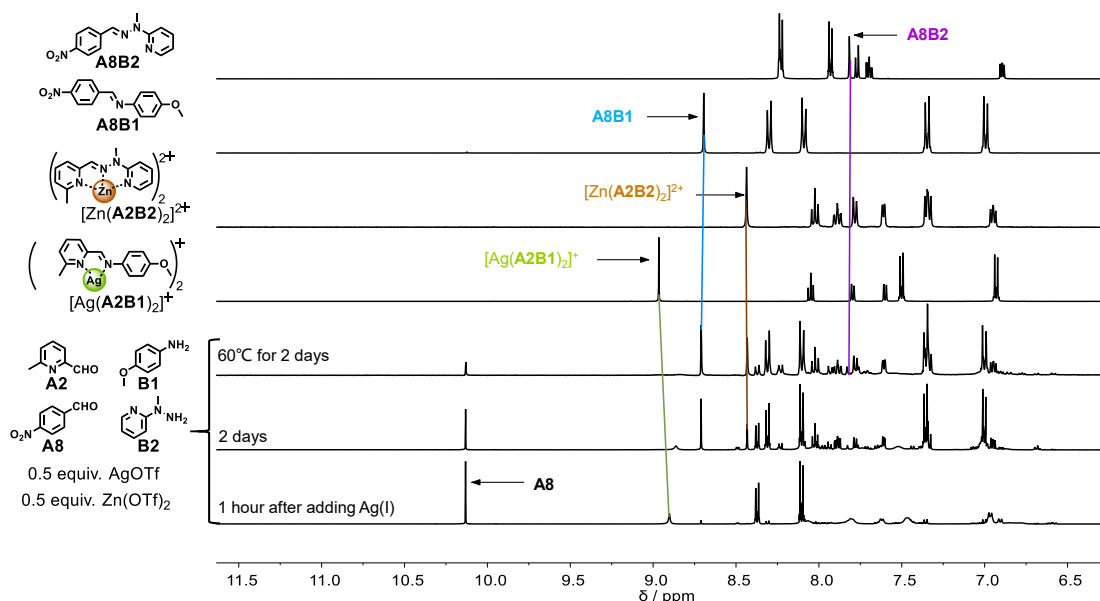


Figure 106. ^1H NMR (500 MHz) spectra of the DCL[8] mixture generated from equal amounts of **A2** + **A8** + **B1** + **B2** (10 mM each, CD_3CN) + 0.5 equiv. AgOTf + 0.5 equiv. $\text{Zn}(\text{OTf})_2$ after 1 h at 25°C , 2 days at 25°C then 2 days at 60°C (three bottom traces). The four top traces correspond to the isolated constituents $[\text{Ag}(\text{A2B1})_2]^+$, $[\text{Zn}(\text{A2B2})_2]^{2+}$, **A8B1** and **A8B2**.

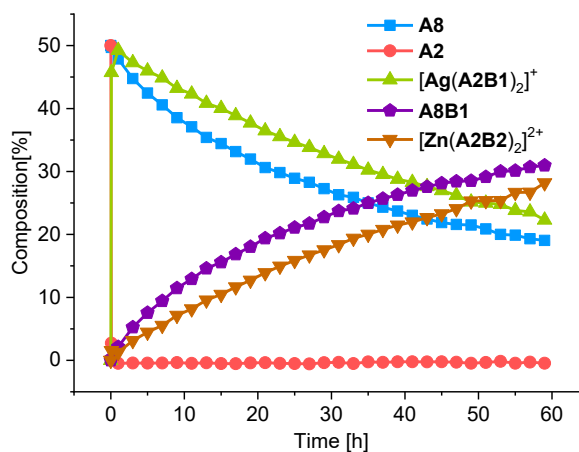


Figure 107. Kinetic plots of the evolution of the DCL[5] mixture of equal amounts of components **A2** + **A8** + **B1** + **B2** + 0.5 equiv. AgOTf + 0.5 equiv. $\text{Zn}(\text{OTf})_2$ as a function of time as obtained from integration of the imine $\text{CH}=\text{N}$ and aldehyde CHO proton signals in the 500 MHz ^1H NMR spectra (10 mM each, CD_3CN , 25°C).

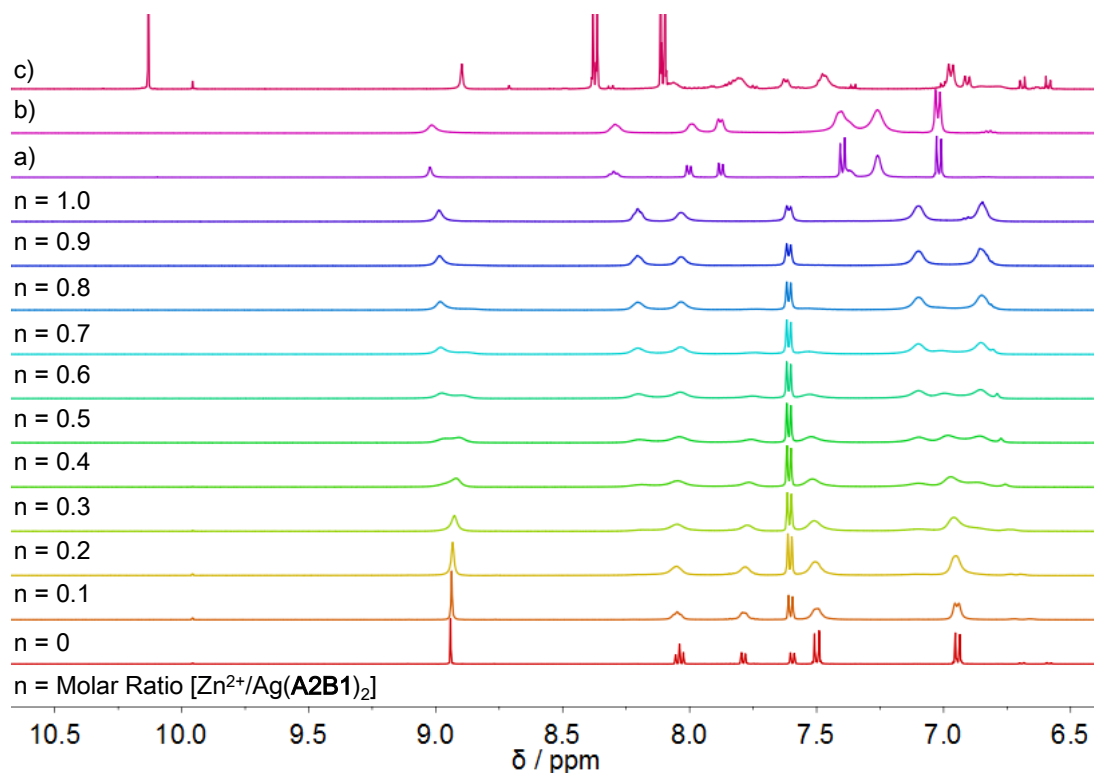
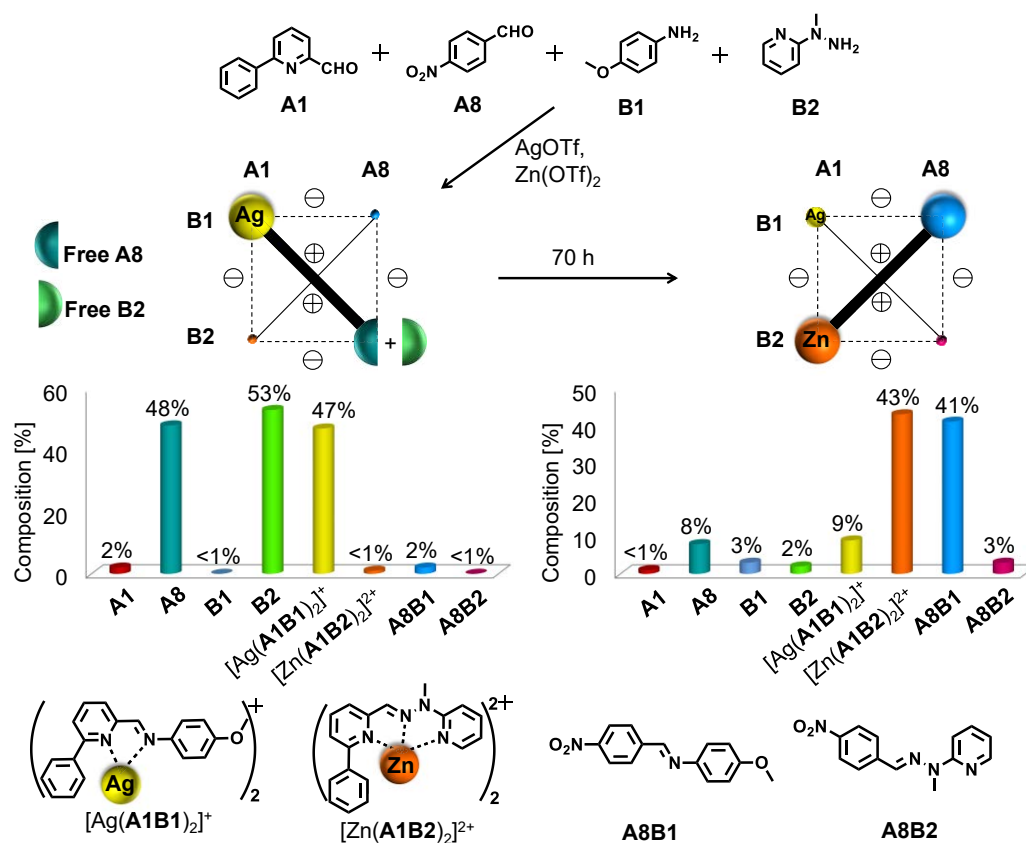


Figure 108. ^1H NMR (500 MHz) spectra obtained from titration experiment of $[\text{Ag}(\mathbf{A2B1})_2]^+$ and $\text{Zn}(\text{OTf})_2$. Reference spectra (top two traces) of the separately prepared constituents (a) $\mathbf{A2} + \mathbf{B1} + 0.5$ equiv. $\text{Zn}(\text{OTf})_2$; (b) $\mathbf{A2} + \mathbf{B1} + 0.5$ equiv. $\text{AgOTf} + 0.5$ equiv. $\text{Zn}(\text{OTf})_2$ c) $\mathbf{A2} + \mathbf{A8} + \mathbf{B1} + \mathbf{B2} + 0.5$ equiv. $\text{AgOTf} + 0.5$ equiv. $\text{Zn}(\text{OTf})_2$ after 1 h.

2) DCL[9] on simultaneous addition of Ag(I) and Zn(II)

To verify if the substituents on the pyridyl-aldehyde have any influence on the switching behavior, the DCL[9] was generated from the components **A1** (6-phenyl-2-formyl pyridine), **A8**, **B1**, **B2** (10 mM, 1.0 equiv. each), AgOTf (5 mM, 0.5 equiv.) and $\text{Zn}(\text{OTf})_2$ (5 mM, 0.5 equiv.) (Scheme 30). The components were mixed together in CD_3CN at room temperature and then were followed by ^1H NMR as a function of time (Figure 109 and Figure 111). After 1 h, the silver complex of imine $[\text{Ag}(\mathbf{A1B1})_2]^+$ formed almost fully together with 48% of unreacted **A8** and 50% of **B2** as its zinc complex. After left at room temperature for 3 days (or 2 days at 60°C), the DCL reached the equilibrium. It is observed that the silver complex $[\text{Ag}(\mathbf{A1B1})_2]^+$ strongly decreased and the formation of the zinc complex $[\text{Zn}(\mathbf{A1B2})_2]^{2+}$ formed in a large amount with amplification of its agonist **A8B1**. Finally the equilibrated DCL gave a distribution of 10% $[\text{Ag}(\mathbf{A1B1})_2]^+$, 41% $[\text{Zn}(\mathbf{A1B2})_2]^{2+}$, 38% **A8B1**, 6% **A8B2** as well as 5% **A8**, 3% **B1** and 2% **B2**, these 3 components staying in their free form. The kinetic curves of the evolution of the experiment is shown in Figure 110. The kinetic switching of the two distributions of the DCL is described in Scheme 30.

Notably, during this process, the ^1H NMR signals become broad 1 hour after adding the metal cations about similarly to the **DCL[8]** above. According to our assumption, the possibility could be due to the interaction of $[\text{Ag}(\text{A1B1})_2]^+$ with zinc cations. The titration experiment was thus conducted with a solution of $[\text{Ag}(\text{A1B1})_2]^+$ by adding different equivalent of $\text{Zn}(\text{OTf})_2$ (**Figure 112**). The peak of $[\text{Ag}(\text{A1B1})_2]^+$ is very sharp in the beginning. It became broad upon addition of 0.1 equiv. $\text{Zn}(\text{OTf})_2$ and then became much broader when more zinc was added. Finally, the spectrum was almost the same as that of the separately prepared $[\text{Zn}(\text{A1B1})_2]^{2+}$ on addition of 1.0 equiv. $\text{Zn}(\text{OTf})_2$ in total. This result demonstrated that initial signal broadening was due to the interaction of $[\text{Ag}(\text{A1B1})_2]^+$ with the $\text{Zn}(\text{II})$ which displaces progressively the silver cation and takes up all the **A1B1** ligand. Therefore, the signal broadening of the DCL is also due to this exchange between $[\text{Ag}(\text{A1B1})_2]^+$ and $\text{Zn}(\text{II})$.



Scheme 30. Kinetic switching of the $[2 \times 2]$ CDN formed by the **DCL[4]** set of components **[A1 + A8 + B1 + B2]** (top) from the $\{[\text{Ag}(\text{A1B1})_2]^+, [\text{A8} + \text{B2}]\}$ state (middle left) to the orthogonal state $\{[\text{Zn}(\text{A1B2})_2]^{2+}, \text{A8B1}\}$ (middle right) (in CD_3CN at 25°C) after 1 h (left) and after 70 h (right). The indicated composition % values of the different compounds present correspond to reaction times of 1 h (left) and 70 h (right). Free anions are not indicated. Data obtained from the 500 MHz ^1H NMR spectra (**Figure 109** and **Figure 111**).

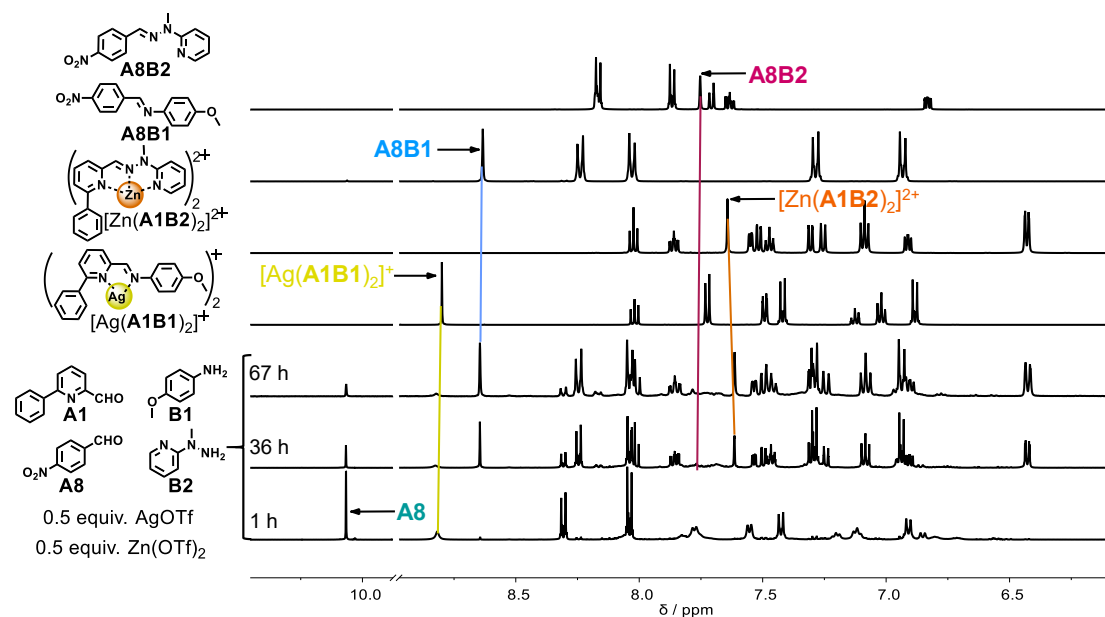


Figure 109. Evolution of ^1H NMR (500 MHz) spectra of the compounds generated from the **DCL[9]** mixture of equal amounts of **A1**, **A8**, **B1**, **B2** (10 mM each in CD_3CN , 25°C) + 0.5 equiv. AgOTf + 0.5 equiv. $\text{Zn}(\text{OTf})_2$ after 1 h, 24 h and 70 h (three bottom traces). The four top traces correspond to the isolated constituents $[\text{Ag}(\text{A1B1})_2]^+$, $[\text{Zn}(\text{A1B2})_2]^{2+}$, **A8B1** and **A8B2**. The arrows indicate the aldehyde CHO proton (9.5-10.0 ppm region) and imine $\text{CH}=\text{N}$ proton NMR signals of the compounds.

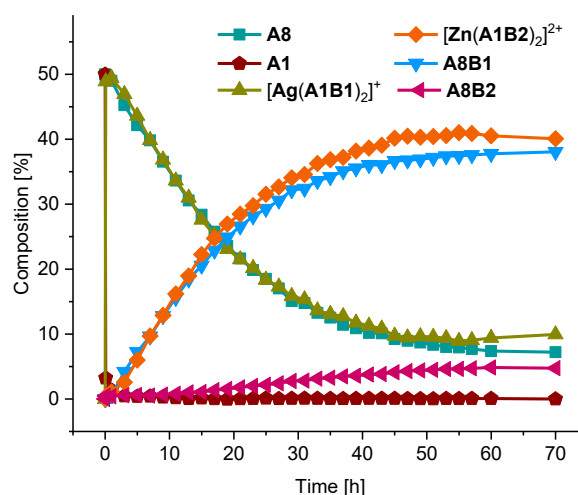


Figure 110. Kinetic plots of the evolution of a mixture of equal amounts of components **A1** + **A8** + **B1** + **B2** (10 mM each) together with 0.5 equiv. AgOTf + 0.5 equiv. $\text{Zn}(\text{OTf})_2$ as a function of time. The composition % data have been obtained by integration of the imine $\text{CH}=\text{N}$ and aldehyde CHO proton signals in the 500 MHz ^1H NMR spectra (CD_3CN , 25°C).

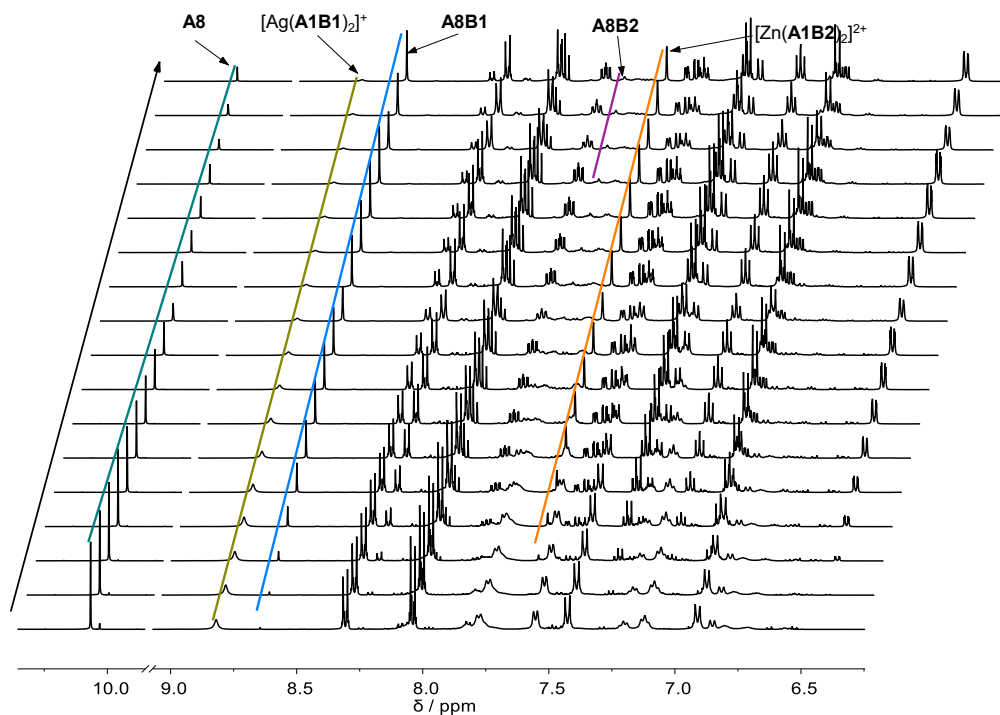


Figure 111. ^1H NMR (500 MHz) spectra of the mixture generated from equal amounts of **A1** + **A8** + **B1** + **B2** (1.0 equiv., 10 mM each, CD_3CN , 25°C) + 0.5 equiv. AgOTf + 0.5 equiv. $\text{Zn}(\text{OTf})_2$ (5 mM) as a function of time at room temperature (from 5 min, bottom, to 64 h, top). The time between successive spectra is 4 hours.

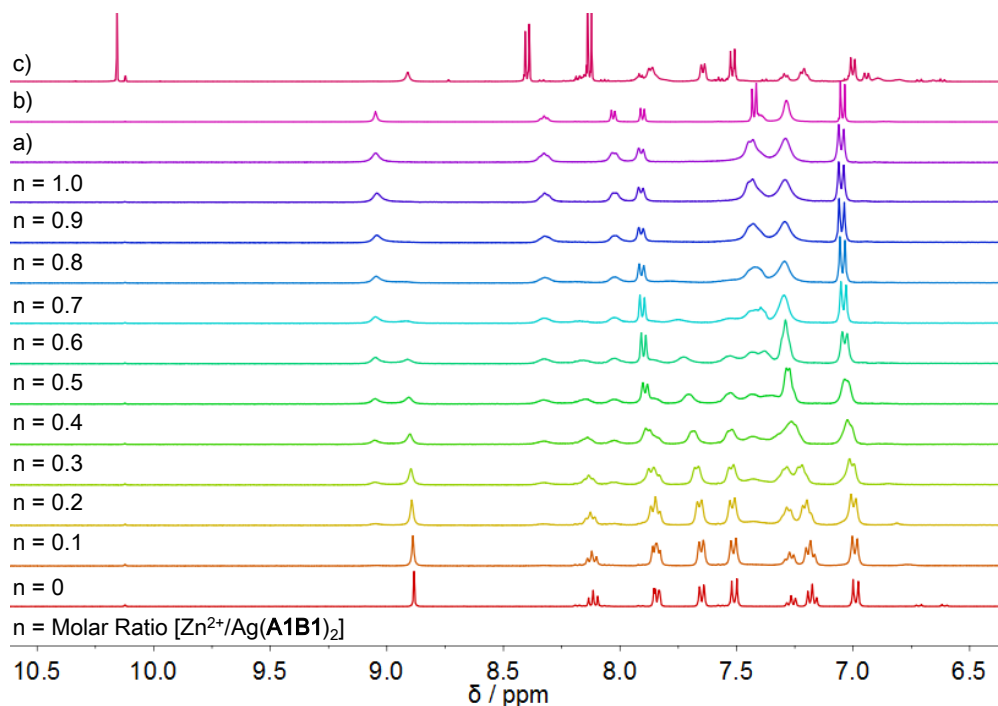


Figure 112. ^1H NMR (500 MHz) spectra obtained from titration experiment of $[\text{Ag}(\mathbf{A1B1})_2]^+$ and $\text{Zn}(\text{OTf})_2$. Reference spectra (top two traces) of the separately prepared constituents a) **A1** + **B1** + 0.5 equiv. $\text{Zn}(\text{OTf})_2$; b) **A1** + **B1** + 0.5 equiv. AgOTf + 0.5 equiv. $\text{Zn}(\text{OTf})_2$ c) **A1** + **A8** + **B1** + **B2** + 0.5 equiv. AgOTf + 0.5 equiv. $\text{Zn}(\text{OTf})_2$ after 1 h.

3) DCL[10] on simultaneous addition of Ag(I) and Zn(II)

By using a much more reactive aldehyde **A3** (6-bromo-2-formyl pyridine), similar kinetic switching behavior was achieved by following the kinetics of the ^1H NMR spectrum of the **DCL[10]** from the equimolar amount of components **A3**, **A8**, **B1**, **B2**, 0.5 equiv. AgOTf and 0.5 equiv. Zn(OTf) $_2$ (**Figure 113** and **Figure 114**). The schematic figure for the orthogonal switching from the kinetic state $\{[\text{Ag}(\text{A3B1})_2]^+, \text{A8} + \text{B2}\}$ to the orthogonal state $\{[\text{Zn}(\text{A3B2})_2]^{2+}, \text{A8B1}\}$ (**Scheme 31**). Similar broad peaks were observed for the **DCL[10]** 1 hour after addition of the metal cations see in the titration experiment of $[\text{Ag}(\text{A3B1})_2]^+$ by Zn(II) (**Figure 115**).

Therefore, the three **DCLs**[8], [9] and [10] described here present orthogonal network switching of the corresponding CDNs from one diagonal to the other diagonal of the $[2 \times 2]$ square, from a non-equilibrium state to an equilibrium state under the action of the two metal cation effectors, Ag(I) and Zn(II) as a function of time. The kinetic up-regulation amounts to a factor of at least 20 for the constituents **A8B1** and $[\text{Zn}(\text{A1B2})_2]^{2+}$.

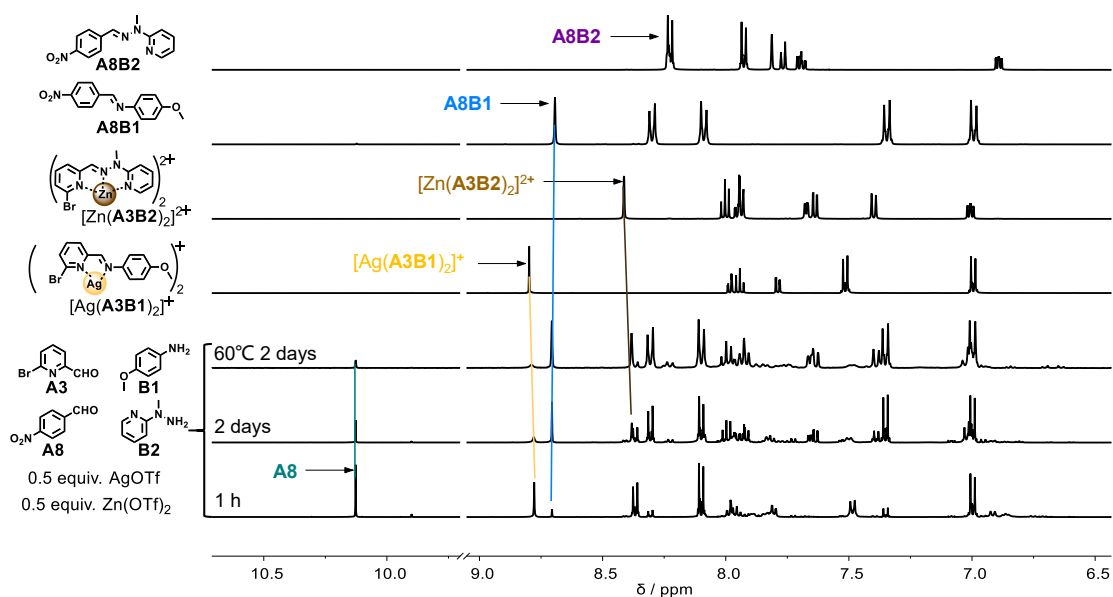


Figure 113. Evolution of ^1H NMR (500 MHz) spectra of the compounds generated from the **DCL[10]** mixture of equal amounts of **A3**, **A8**, **B1**, **B2** (10 mM each in CD_3CN , 25°C) + 0.5 equiv. AgOTf (5 mM) + 0.5 equiv. Zn(OTf) $_2$ (5 mM) after 1 h at 25°C , 2 days at 25°C and heating at 60°C for 2 days (three bottom traces). The four top traces correspond to the isolated constituents $[\text{Ag}(\text{A3B1})_2]^+$, $[\text{Zn}(\text{A3B2})_2]^{2+}$, **A8B1** and **A8B2**. The arrows indicate the aldehyde CHO proton (9.5-10.0 ppm region) and imine $\text{CH}=\text{N}$ proton (8.0-8.5 ppm region) NMR signals of the compounds.

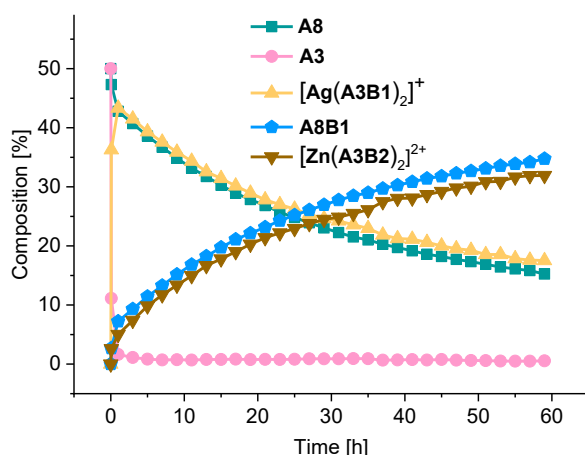
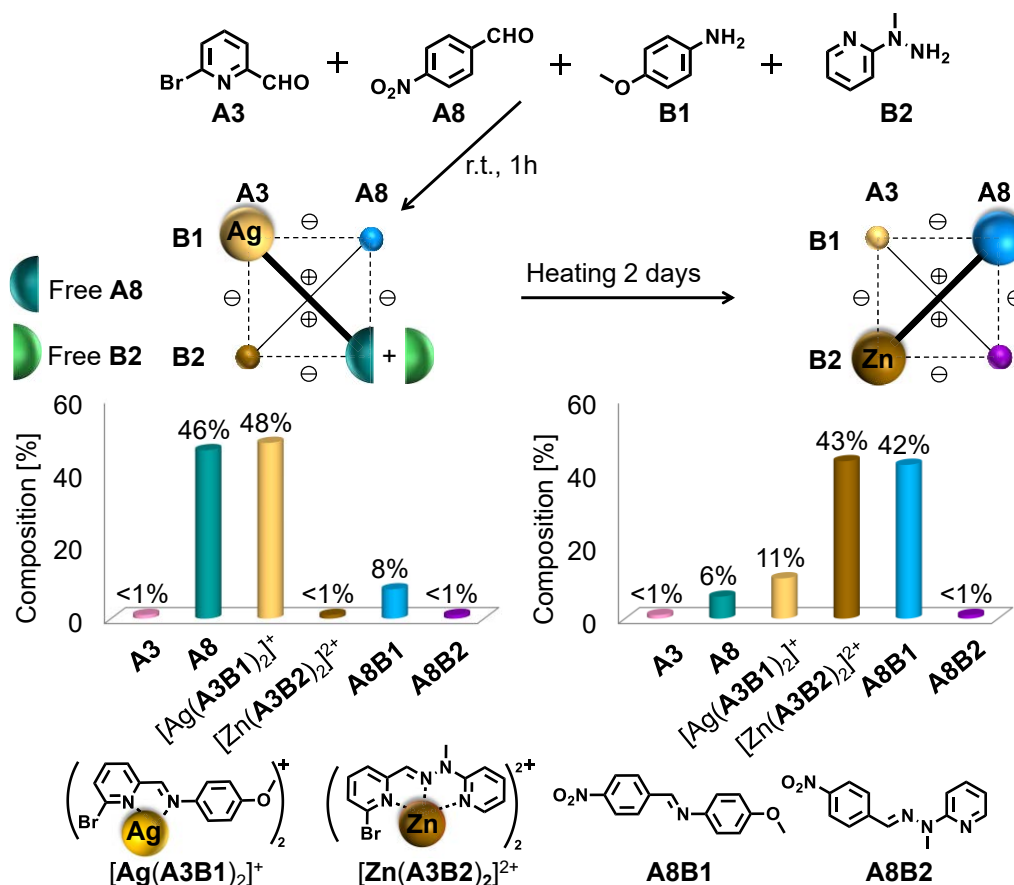


Figure 114. Kinetic plots of the evolution of the **DCL[10]** mixture of equal amounts of components **A3** + **A8** + **B1** + **B2** (10 mM each) + 0.5 equiv. AgOTf (5 mM) + 0.5 equiv. Zn(OTf)₂ (5 mM) as a function of time as obtained from integration of the imine CH=N and aldehyde CHO proton signals in the 500 MHz (¹H NMR spectra, CD₃CN, 25°C).



Scheme 31. Kinetic switching of a [2 × 2] **DCL[10]** from the {[Ag(A3B1)₂]⁺, A8 + B2} state to the orthogonal state {[Zn(A3B2)₂]²⁺, A8B1} in CD₃CN after 1 h at 25°C, and 2 days at 25°C then 60°C 2 days (from left to right). Data obtained from the 500 MHz ¹H NMR spectra.

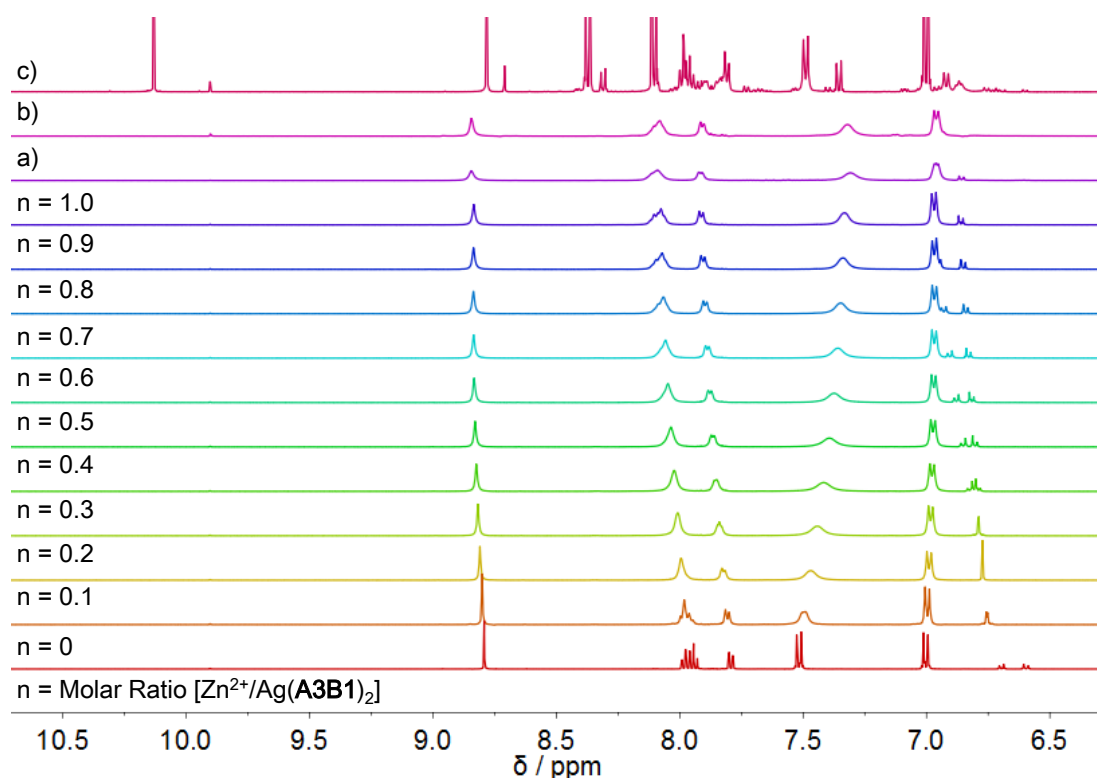


Figure 115. ^1H NMR (500 MHz) spectra obtained from titration experiment of $[\text{Ag}(\text{A3B1})_2]^+$ and $\text{Zn}(\text{OTf})_2$. Reference spectra (top two traces) of the separately prepared constituents (a) **A3** + **B1** + 0.5 equiv. $\text{Zn}(\text{OTf})_2$; (b) **A3** + **B1** + 0.5 equiv. AgOTf + 0.5 equiv. $\text{Zn}(\text{OTf})_2$ c) **A3** + **A8** + **B1** + **B2** + 0.5 equiv. AgOTf + 0.5 equiv. $\text{Zn}(\text{OTf})_2$ after 1 h.

In the previous studies, starting from a statistical distribution (about 25% of each of the four constituents) of the initial equilibrated state of the DCL, the maximum amplification achievable for a given constituent was at most twice that in the initial distribution, i.e., from 25% to a maximum of 50% (together with 50% of its agonist). The processes described here display much larger changes in distributions: they amount to a network switching from an initial state where one pair of diagonally linked agonistic constituents is almost absent to a final state where this same pair is strongly dominant and conversely for the other pair of constituents. For example, in **DCL[9]**, the constituents $[\text{Zn}(\text{A1B2})_2]^{2+}$ and **A8B1** are amplified from 1% and 2%, respectively, in the initial kinetic distribution to 41% and 38% in the final thermodynamic distribution, a change by more than a factor of 20.

3. SUMMARY OF CHAPTER III

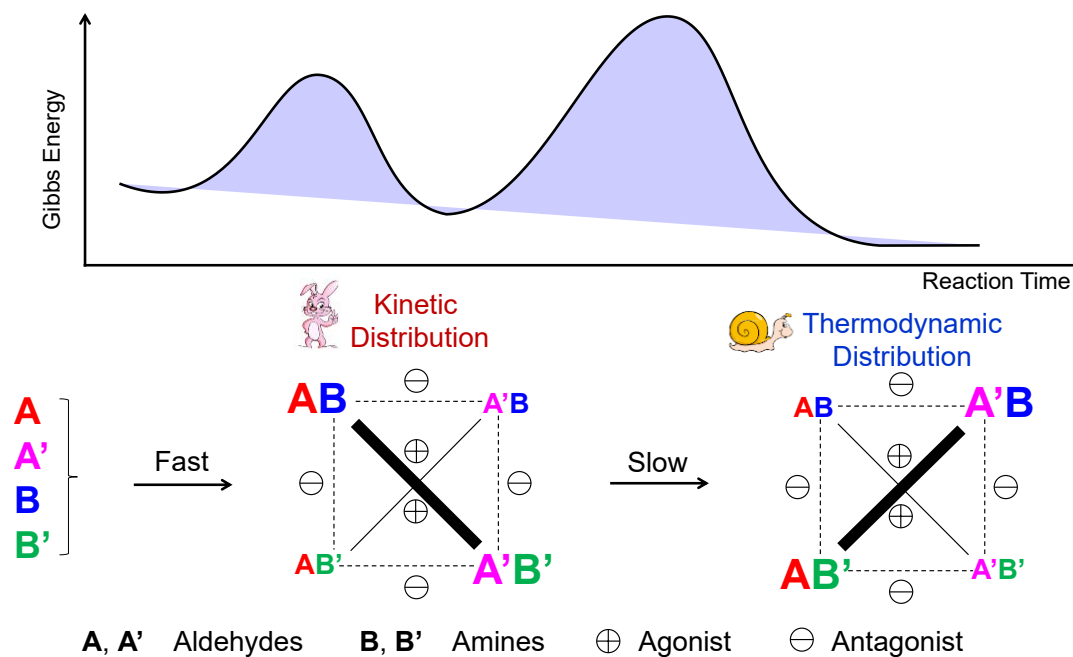
To summarize, we studied and controlled the time-dependent switching of the $[2 \times 2]$ DCLs from the kinetic distribution of constituents to the thermodynamic one (**Scheme 32**)

either in the absence (section 2A) or in the presence of metal cations (section 2B). Such kinetic switching of the DCLs is achieved by selective screening of the appropriate aldehyde and amino components (amine, hydroxylamine, hydrazine, hydrazide), as well as the metal cations. The determining factors for the screening of the components are as follows:

1) The formation rates usually decrease, and the thermodynamic stabilities increase along the sequence of (aliphatic) imine, acylhydrazone, hydrazone and oxime, leading to the possibility of the generation of the time-dependent distributions for a network switching.

2) In the presence of metal cations, it is important to adjust the kinetics of ligand formation for the complex, the thermodynamic stabilities of the two complexes and even the exceptional interaction of the metal cation with the component:

a) the formation of the hydrazone-based zinc complex is much slower than the formation of imine-based silver complex, allowing the fast formation of the silver complex of imine;



Scheme 32. Schematic time-dependent switching of a $[2 \times 2]$ DCL from kinetic distribution to the thermodynamic distribution with an orthogonal switching from one diagonal $\{AB, A'B\}$ to the other diagonal $\{AB', A'B'\}$ of the square.

b) the zinc complex of the tridentate hydrazone is thermodynamically more stable than the silver complex of the bidentate imine, which makes possible the exchange of the common component, i.e. pyridyl-aldehyde, from the silver complex of the imine to the zinc complex of the hydrazone;

c) The trapping of Zn(II) by coordination with the pyridyl-hydrazine **B2** by the formation of $[\text{Zn}(\text{B2})_2]^{2+}$ may slow down the formation of the zinc complex of hydrazone thus allowing the silver complex with the imine constituent to form first.

3) For both cases, in the absence and presence of metal cations, the switching behavior of the DCLs was obtained by simply mixing the components together and following the kinetics by ^1H NMR spectra, indicating that it's determined only by the internal kinetic and thermodynamic properties of the whole system.

The present work explicitly implements networks switching driven by internal kinetic and thermodynamic properties in the self-contained CDNs. In terms of the constituent's amount, the very large amplification (from 3 to about 40 times) represents an adaptation to time, a significant step in the adaptive behavior of dynamic covalent systems. It paves the way to further exploration of kinetically adaptive behavior in CDC. The results described also bear relationship to the behavior of out-of-equilibrium systems opening towards higher level of kinetic behavior (for instance in training processes) in adaptive chemistry.

CHAPTER IV. THE C=N FORMATION FOR GENE REGULATION

1. INTRODUCTION

As described in Chapter I, the mechanism of C=N formation consists of nucleophilic attack of amine on the carbonyl group and the removal of water from the tetrahedral intermediate proposed by Jencks in the 1960s.²⁶⁹ He further indicated that at acidic condition the rate-determining step for C=N formation was the nucleophilic attack of the amine on carbonyl group, while at neutral and basic condition the rate-determining step is the dehydration.¹⁵⁶ Scientists have made great efforts to study and accelerate the kinetics of the imine formation in aqueous phase.²⁷⁰⁻²⁷⁵ In 1960s Jencks demonstrated both the acid catalysis¹⁵⁶ and nucleophilic catalysis¹⁵⁹ of semicarbazone formation in aqueous phase. Here we are focused on the facilitating of imine formation in aqueous phase to find more application in biological process.

A. Facilitating imine formation in aqueous phase

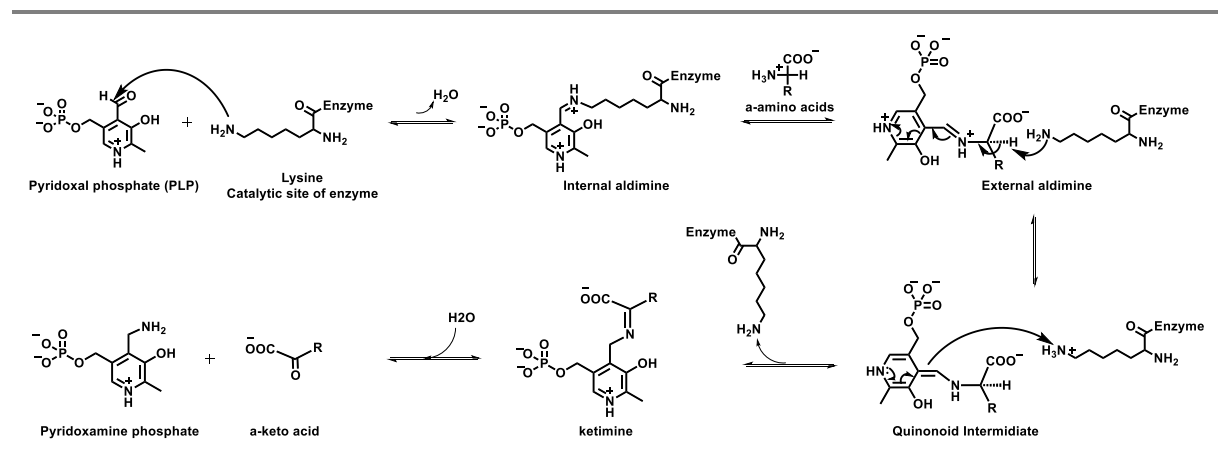
There are many factors which could influence the imine formation. To facilitate imine formation included both to accelerate the kinetics of imine formation and to increase the yield of imine formation. Considering the two steps of imine formation: the nucleophilic addition of the amine on the carbonyl and elimination of water. From structural factors, the fast-reacting aldehyde would accelerate the nucleophilic addition on the carbonyl which is the rate-determining step at acidic conditions. To increase the yield of imine formation, both the structural factor and the environment factor would act. They are discussed as follows.

i. The fast-reacting aldehyde for imine formation

Jencks and co-workers pointed out that the *o*-substituted aryl aldehyde reacted somehow more rapidly than *p*-substituted aldehyde with methoxy, hydroxy, chloride and nitro groups.²⁷⁶ Similar phenomenon was found by Wang and Li for the reaction of ortho-halobenzaldehyde derivatives with peptides especially *o*-chloro benzaldehyde.²⁷⁷ Bane and coworkers reported on the findings of the *o*-phosphate group of the aryl aldehyde strongly accelerates the kinetics of hydrazone formation through the intramolecular general acid catalysis.²⁷⁸ Moreover,

Gillingham and co-workers demonstrated the fast formation of oxime from phthaldehyde through the generation of the intermediate cyclic hemiaminal.²⁷⁹ They also introduced a boronic acid group in the ortho position of benzaldehyde, which in the first step participated in the formation of the tetrahedral intermediate very rapidly.²⁶² Kool and co-workers systematically studied the structure effect on the reactivity of aldehyde with acylhydrazines.¹²⁷ They found that: 1) the electron-deficient carbonyl groups react much faster on average; 2) steric hindrance plays moderate to small effect on hydrazone formation; 3) alkyl aldehydes react much faster than aryl ones; 4) aldehydes with nearby basic group (such as 2-formyl pyridine) react much rapidly due probably to the internal acid-base catalysis.

Pyridoxal phosphate (**PLP**), as a co-enzyme in the transamination reactions, can form an internal aldimine with the ϵ -amino group of a specific lysine group of the aminotransferase enzyme.^{280–282} The transamination includes three steps (**Scheme 33**): i) The addition of an α -amino acid would induce the transamination reaction of the internal aldimine with it, resulting the formation of external aldimine. b) The formed external aldimine would undergo tautomerization to form quinonoid intermediate and a ketimine product. c) The ketimine would hydrolyze to form pyridoxamine and α -keto acid.

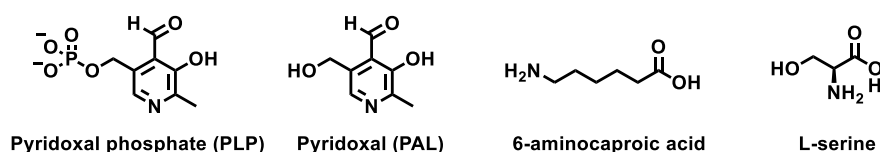


Scheme 33. Representation of the imine formation from **PLP** and Lysine (in enzyme) and the subsequent transamination processes.

Because **PLP** has four functional groups, it can exist in different protonation and tautomer states in water.^{283,270} Therefore, the imine formation from **PLP** and amino acids in aqueous media have been widely studied^{274,284–288} such as **PLP** with hexylamine²⁸⁹ and dodecylamine^{273,290} as well as amino acids.^{154,291–294} Chan-Huot and Limbach studied the protonated states of **PLP**,²⁹⁵ the pH dependence of aldimine formation from **PLP** and ^{15}N -labelled diaminopropane, ^{15}N - α -labelled L-lysine, ^{15}N - ϵ -labelled L-lysine,²⁸⁶ hydrogen bonds

of **PLP** in polar solution,^{296,297} and the stability, protonation and tautomer states of the aldimine.²⁹⁸ They found that: 1) only the free aldehyde and the hydrate forms existed at low pH; 2) all of the protonated species were present at neutral conditions; and 3) the zwitterionic form was favored before deprotonation at high pH. These studies provided the possibilities to tune the imine formation through changing the protonation states.

Hinz and co-workers studied the kinetics and thermodynamics of imine formation from pyridoxal phosphate (**PLP**) and pyridoxal (**PAL**) with 6-aminocaproic acid and L-serine (**Scheme 34**).²⁹⁹ They found that the reaction rate increased with the increasing of the pH of **PLP** reaction with 6-aminocaproic acid due to the decrease of the activation energy. This was because the rate-determining step under the studied pH (6.6-8) was the attack of the deprotonated amino acids on the carbonyl. While for **PAL** reaction with 6-aminocaproic acid, the activation energy was much higher. This is because for **PAL**, there was the equilibrium between free aldehyde and the cyclic hemiacetal formed. Therefore, the activation energy also required the dissociation of the hemiacetal to generate the free aldehyde. In addition, the phosphate group played an important role in preventing the hemiacetal formation. This experiment indicated that **PLP** had much faster and low activation energy for imine formation with amino acids. Similar results were obtained by the work of Blanco and co-workers²⁷⁰, in which they indicated **PLP** has the largest rate constant for imine formation and the lowest constants for imine hydrolysis. In addition, the role of pyridine nitrogen in pyridoxal phosphate was also studied by Grisword and Toney.³⁰⁰ By selectively adjusting the protonation states of pyridine nitrogen, the electrophilic strength of **PLP** could be modulated to increase the desired product while decrease the unwanted side product.



Scheme 34. Representation of the structures of the **PLP**, **PAL**, 6-aminocaproic acid and L-serine.

ii. The increased yield of imine formation

Systematic studies of the influence of structural factors as well as the external effectors on imine formation in aqueous solution, however, have been less frequent.³⁰¹ While accelerating the kinetics of C=N formation, it is challenging to increase the yield of imine formation since

it is a reversible reaction and the presence of water would always induce the hydrolysis of the imine.

Godoy-Alcántar and Lehn³⁰² studied structure-stability correlations for imine formation from 25 aldehydes and 13 primary amines in water (**Figure 116A**). The involvement of considerable amounts of hydrated species for pyridyl aldehydes and most aliphatic aldehydes was taken as an indication that these should be the most reactive carbonyl compounds. The reactions of imine formation were carried out in three different buffers of pD 7.5 (D₃PO₄ + NaOD), pD 8.5 (ND₄OD + DCl) and pD 11 (NaHCO₃ + NaOD), separately. To obtain high yield of imine an excess of amines was needed. From these observations, a three-parameter linear equation correlating the logarithms of imine formation constants with pK_a values and HOMO energies of the amines and LUMO energies of the aldehydes was obtained (**Figure 116B**). This is particularly useful for the study of imine formation and exchange as well as for the construction of dynamic covalent libraries.

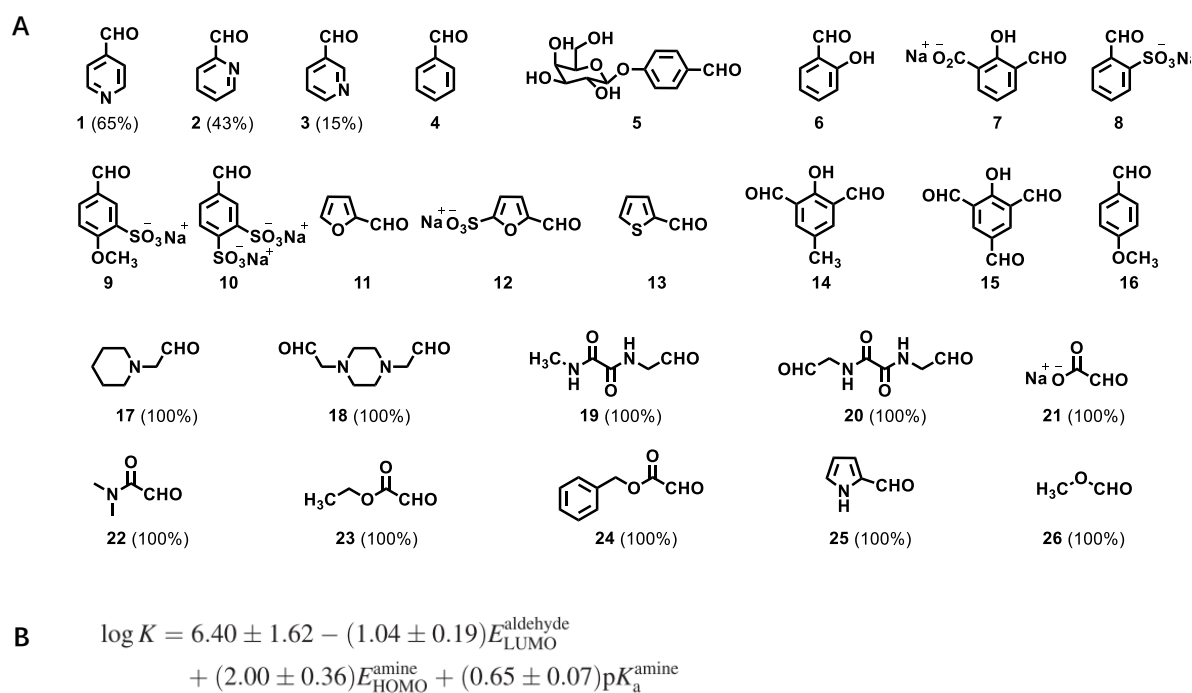


Figure 116. Structures of aldehydes tested for imine formation. The fraction of hydrated aldehyde is given in parentheses when it was detectable by ¹H NMR. Aldehydes **17–26** did not form detectable amounts of imines with aniline.

Martínez and Godoy-Alcántar³⁰³ further studied imine formation in aqueous solution from *km*(kanamycin) and **PLP** (pyridoxal phosphate) as well as other aldehydes by NMR spectroscopy, potentiometry and calculations (**Figure 117**). They demonstrated that imines formed nearly 100% at pH 7 with equimolar reactant ratio of *km* and **PLP**. The reason was

found to be the anion recognition properties of the *km* which lead to the high yield of imine formation. The titration of **PLP** by *km* at pH 7 and the pH dependence of imine *km*-**PLP** formation showed that the imine formation required only 1 equivalent of *km* to reach full formation of imine only in the range of pH 7.0-8.7. The reasons were i) the complete protonation occurred at acidic pH; ii) the imine formation was not complete at higher pH because *km* was almost neutral in these conditions and didn't have any attractive effect for **PLP**; iii) *km* provided an ionic environment through the charges of the amine groups at pH 7.0-8.7, which can organize together to stabilize the generated imine and offered a hydrophobic surface to prevent the imine hydrolysis.

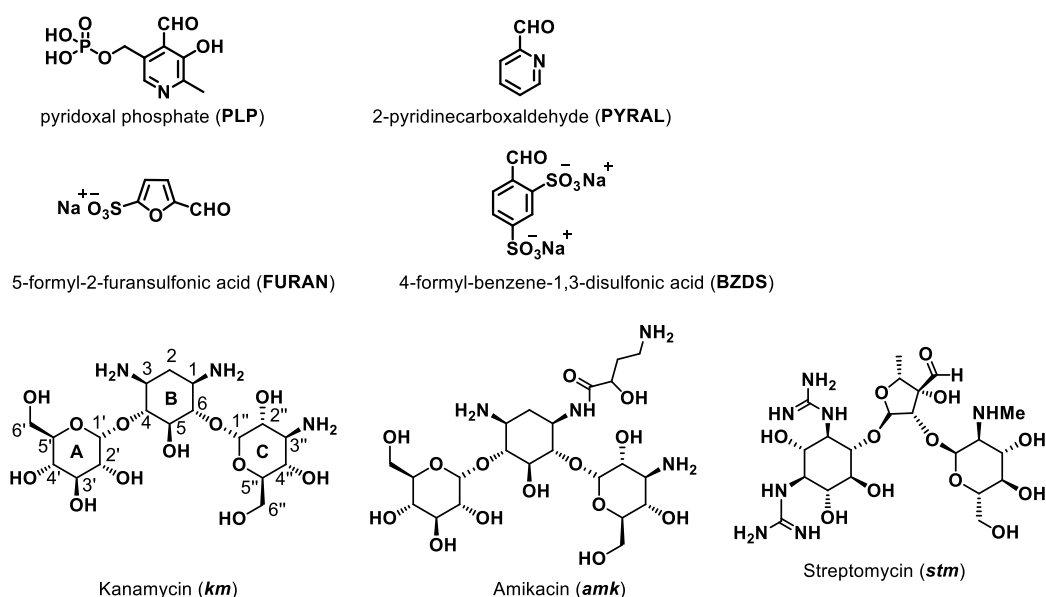
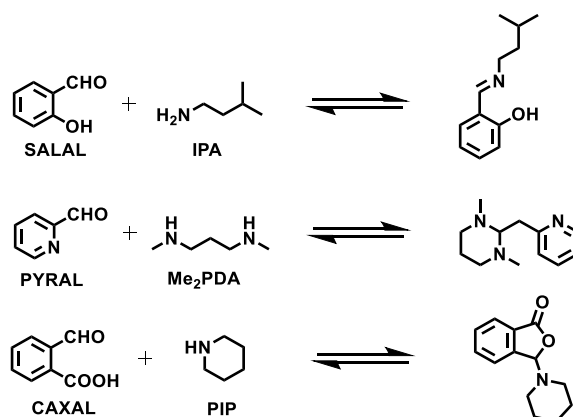


Figure 117. Representation of the structures of aminoglycosides and aldehydes used for imine formation.

Another method of dynamic modifications of amines in water with high yields is the amination. Kovaříček and Lehn¹³⁰ studied the reactions of aldehydes and amines (primary amines and secondary amines) (**Scheme 35**). The salicylaldehyde reacted with isopentylamine to generate imine driven by the hydrogen bond formation. While pyridine aldehyde reacted with *N,N'*-dimethyl-1,3-diaminopropane, it generated a six-member-ring amination. Interestingly, by introducing the carboxylic group in the alpha position of benzaldehyde, a five or six member-ring amino-lactone was generated from reacting with piperidine. This work prompts us to make multi-functional aldehyde with OH or carboxyl group in the alpha position in the 2-carbonyl-pyridine, which would also be a good candidate to achieve a higher yield of conversion.



Scheme 35. Representation of the reactions of different aldehydes and amines to form imine from **SALAL** with **IPA**, cyclic aminal with **PYRAL** and diamine **Me₂PDA** and lactone with **CAXAL** and a cyclic secondary amine **PIP**

In addition, Griffiths and Ladame³⁰⁴ demonstrated a novel method of enhanced imine formation in water by adding either surfactants or double-stranded DNA (**Figure 118**). Their study showed that anionic surfactants (e.g. SDS) below the CMC act as true catalysts by stabilizing the reaction transition state by interaction with the polar head groups of the surfactant. Above the CMC they can shift the equilibrium in favor of imine formation, via increase of local concentrations within micellar compartments. By adding a double-stranded DNA, a large enhancement of reaction was also observed, possibly due to the stabilization of the fluorescent imine **3** upon binding into the DNA minor groove like the equivalent trimethine cyanine dye. This example demonstrates that by changing the microenvironment of the reaction in aqueous phase, the imine formation can be enhanced, which offers a new way to increase the efficiency of this dynamic reaction.

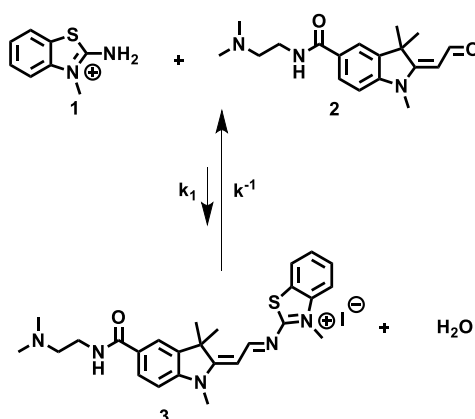


Figure 118. Reversible synthesis of fluorescent imine **3** from non-fluorescent amine **1** and weakly fluorescent aldehyde **2**.

The above strategy indicated that it is promising to find or make the aldehydes which could have high yields of imine formation. Considering the multiple application of imine formation from PLP and amino acids in enzymatic reactions in biology, we were curious if the formation and breaking of imine bond from the aldehyde and lysines could realize the reversible regulation of genes since histones are abundant in lysine. The details of the introduction histones and its modification as well as gene regulation are as follows.

B. Histones modifications

i. The structure of histone and nucleosome

Histones are highly basic proteins in eukaryotic cell nuclei which play a crucial role in packing the DNA molecule in an orderly way into the highly ordered structure unit – nucleosome (**Figure 119A**). They are relatively small proteins with a very high ratio of positively charged amino acids, mainly lysine and arginine.

There are five types of histones in humans are: **H1/H5**, **H2A**, **H2B**, **H3**, and **H4**. Among them, histones **H2A**, **H2B**, **H3** and **H4** are known as the core histones or nucleosomes histones, while histones **H1/H5** are the linker histones (**Figure 119B**). The core histones all exist as dimers. The four distinct dimers then come together to form one octameric nucleosome core. **H1** is involved with the packing of the “beads on a string” sub-structures into a high order structure, and its details have not yet been solved. Histones are the main structural proteins of chromatin and play an important role in regulation of gene expression.

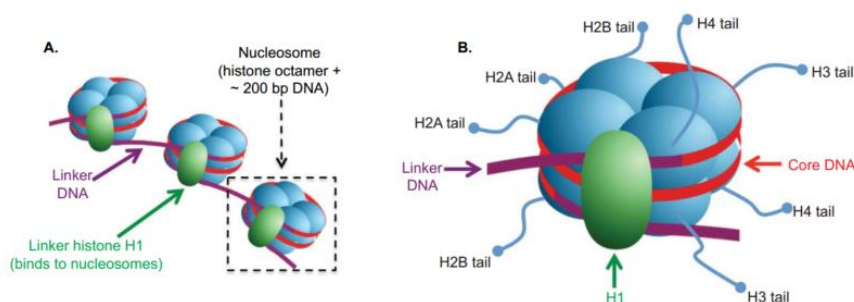


Figure 119. (A). The beads on a string structure composed of nucleosomes; (B). The general composition structure unit of an octamer.

In 1974, the major progress came in understanding the structure of chromatin structure with the discovery of the fundamental packing unit known as the nucleosome, which gives a beads-on-a-string appearance in electron micrographs taken after the treatments that unfold higher-order packing. The DNA string can be broken into nucleosome beads by digestion with

enzymes that degrade DNA (deoxyribonuclease). After the digestion, only the DNA between the nucleosome beads is degraded. The rest remain as double helix fragments 146 nucleotide pairs long bound to a specific complex of eight nucleosomal histones (the histone octamer). The crystal structure of the nucleosome was obtained in 1997 by Richmond.^{305,306}

The core histones are among the most highly conserved of all known proteins. This evolutionary conservation indicates that a change in any position of the chain is deleterious to the cell. (N.B. a nucleosome = a histone octamer + DNA, Histone **H1** can connect two nucleosome).

ii. Gene regulation-acetylation and deacetylation

Generally, gene expression is the process where information from a gene is used in the synthesis of a functional gene product. The products are proteins in most cases, whereas in non-protein-coding genes, it is a functional RNA. Virtually the regulation can occur in any step of the gene expression including the transcription, RNA splicing, translation, and post-translational modification of a protein. Thus, it is very important for all the living organisms as it increases the versatility and adaptability of an organism by allowing the cell to express protein when needed. This is of great importance for the evolution of the species.

One of the strategies is to alter the chromatin structure of DNA by modification of its histones. The free N-terminal of lysine and arginine in histones can be modified in various ways such as methylation, acetylation, phosphorylation, ubiquitination and other modification processes under the action of related enzymes. Among these processes, the methylation of histone modification is the most stable method, so it is most suitable for stable epigenetic information. The acetylation modification is a highly dynamic process, and the others are unstable modifications. Through the modification of histone, the affinity of histones and DNA double-strands can be affected, thereby changing the looseness or agglutination state of chromatin, or affecting the affinity of other transcription factors and structural gene promoters to play a role in gene regulation. Herein, we are mainly interested in the acetylation of histones to influence the gene expression due to the highly dynamic feature.

The discovery of the fact that acetylation of histones caused changes in the transcription activity dated back to the work of Allfrey and co-workers in 1964.^{307,308} Acetylation and deacetylation are the processes in which the N-terminus tail of lysine protruding out from the chromatin are acetylated and deacetylated under the corresponding enzymes histone acetyltransferase (HATs) and histone deacetylase (HDACs) (**Figure 120**).

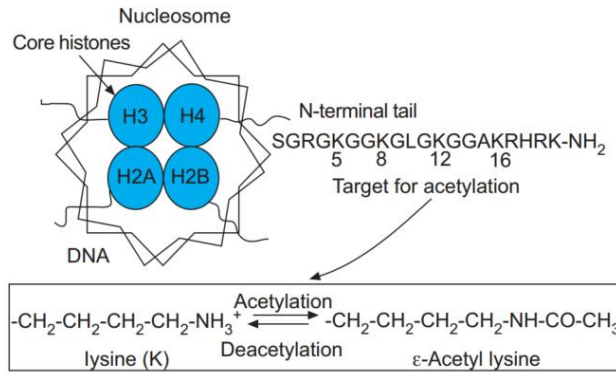


Figure 120. The modification of histones through acetylation.

Originally, the chromatin has a highly condensed structure. Acetylation of histones can remove the positive charges of histones, thus decreasing the elastic attractive interaction between the N-terminus tail and the negatively charged phosphate groups of the DNA (**Figure 121**). Consequently, the chromatin forms a loose, relaxed structure, resulting in more transcriptional factors to access to the DNA, thus increasing the gene expression through the activation of transcription. By deacetylation of histone tails, the relaxed DNA can be converted back to tightly wrapped structure under the function of HDACs, leading to the decrease of gene expression (or gene silencing). In this way, gene expression is regulated by acetylation of core histones through the action of coactivators, such as CREB-binding protein, with intrinsic histone acetyltransferase (HAT) activity. Conversely, gene repression is mediated via histone deacetylases (HDACs) and other corepressors (**Figure 121**).

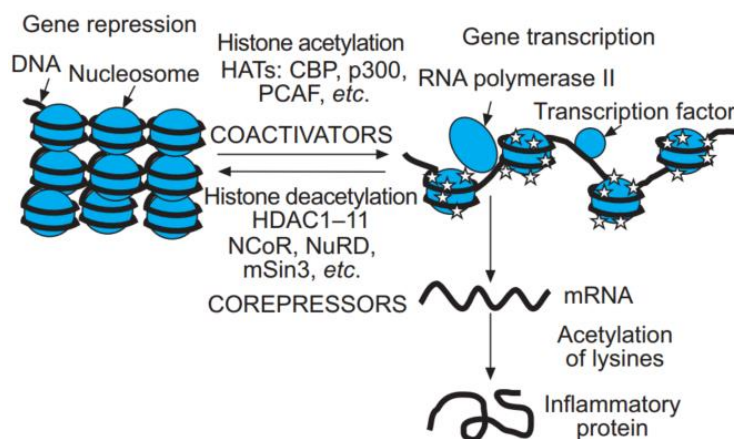


Figure 121. Gene activation and repression are regulated by acetylation and deacetylation of core histones. Histone acetylation by coactivators that have intrinsic HAT activity, opened up the chromatin structure to allow binding of RNA polymerase II and transcription factors that were unable to bind DNA in the closed chromatin configuration. This is reversed by corepressors, which include HDACs that reverse this acetylation, causing gene silencing.

Many diseases were found to be relevant to the acetylation of the lysines in histones such as inflammatory lung diseases. For example, in asthma, there is an increase in HAT activity and some reduction in HDAC activity, which is restored by corticosteroid therapy. Therefore, we are interested to see whether a simple imine formation with N-terminus of lysines in histones could generate reversible control of gene expression. Therefore, it is of great importance to search for the aldehyde which could form high yield of imine in aqueous phase.

In this part of the present work, we envisage to generate the imines with high yields in aqueous phase. The factors of the reactivities of aldehydes, hydrophobic environment of the reaction (here mainly the hydrophobicity of amines) as well as the medium acidity were investigated. The imine formation from a series of aldehydes and amines was explored especially with the derivatives of lysine. Considering the abundance of lysine in histones, we further studied the imine formation from an aldehyde and a poly-lysine such as tri-lysine as a model for modification of histones, which might give us the possibility to regulate the gene expression with dynamic covalent reactions.

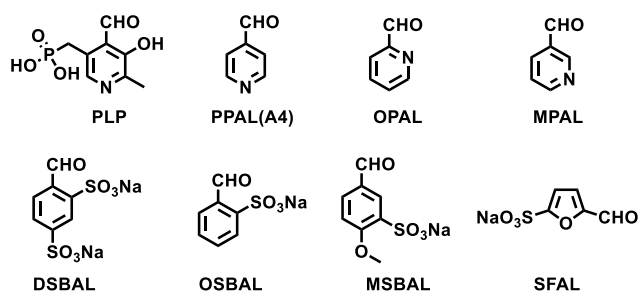
2. RESULTS AND DISCUSSIONS

A. Screening of the substrates

i. Fast-reacting aldehydes

Combining the factors discussed above with the good solubility in aqueous phase, some aldehydes were chosen to find the one which could generate the product (such as imine, aminal or lactone) with the highest yield in aqueous phase (**Scheme 36**).

The selected aldehydes were mainly of three types: 1) pyridyl-aldehyde derivatives, which have basic pyridine nitrogen and have been proven to have higher reactivity; 2) electron-deficient aldehydes which have higher reactivities; 3) *o*-substituted aldehydes which showed higher reactivities before. The imine formation of the aldehydes and N- α -acetyl lysine were studied in aqueous phase at different pH. The corresponding yields of imine formation is shown in **Table 10**.



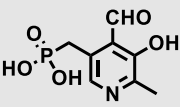
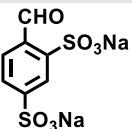
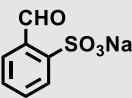
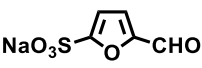
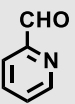
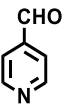
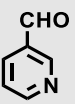
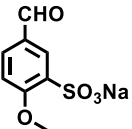
Scheme 36. The structures of the aldehydes tested for imine formation in aqueous phase.

As seen from **Table 4**, most of the aldehyde can form hydrates in different buffers except **DSBAL** (entry 8). In addition, the imine formed in a very low yield (less than 10%) at lower pH (pH 7.4 and pH 8.1) due to the protonation of the ϵ -amino group in the N- α acetyl lysine. With the increase of pH to 11, the yield of imine increased and the amount of the free aldehyde (or the free amine) as well as the aldehyde hydrates decreased. Among all the tested aldehydes, **PLP** formed imine with the highest yield (up to nearly 70%) at basic condition (entry 1, pH = 11.0). There are two reasons for this: *i*) the pyridine nitrogen activate the carbonyl group and makes it a fast-reacting aldehyde; *ii*) the ortho-hydroxy group could stabilize the imine through the formation of the intramolecular hydrogen bond.

In comparison with **PLP**, other aldehydes have much lower yield of imine formation. The **DSBAL** yielded 56% of imine which is a bit less than **PLP** but much better than the rest of the aldehydes (entry 2). It is due to the two electron-withdrawing groups, which greatly activated the carbonyl group. Similarly, the ortho-sulfonate substituted aldehyde **OSBAL** also generated a comparable 51% imine compare to **DSBAL** (entries 2 and 3). Moreover, **SFAL** formed 49% of imine. For the three pyridyl aldehydes, the yields of imine are 46%, 44% and 37% for 2, 3 and 4-pyridinecarboxaldehydes, respectively. This means that introducing the electron-deficient group in the ortho and para-position plays a more important role than meta position.

The above experiments indicated that the aldehyde with electron-deficient group produced imines in the yield range of 17% to 69% at pH 11. Due to the existence of hydrolysis, which competed with imine formation, it is important to develop reactive aldehyde which can also stabilize the generated imine by more interactions like hydrogen bonding through introduction of other substituents.

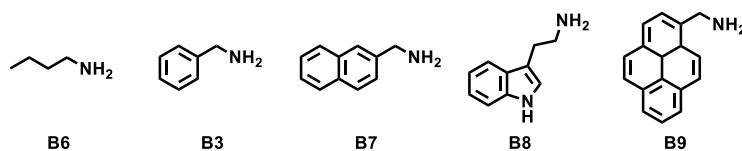
Table 10. Distribution of imines generated by reaction of different aldehydes with N- α -acetyl lysine at pH values of 7.4, 8.1, 11.0 at 25°C in D₂O (in phosphate buffer), using an initial concentration of 20 mM for all reactants at 25°C.

Entry	Aldehyde	Product	pH = 7.4	pH = 8.1	pH = 11.0
1	 PLP	Aldehyde or amine	58%	n.d.	15%
		Imine	29%	n.d.	69%
		Hydration	13%	n.d.	17%
2	 DSBAL	Aldehyde or amine	85%	81.7%	38%
		Imine	1%	4.3%	56%
		Hydration	14%	14.0%	6%
3	 OSBAL	Aldehyde or amine	97%	95.7%	49%
		Imine	_ ^[a]	_ ^[a]	51%
		Hydration	3%	3.3%	_ ^[a]
4	 SFAL	Aldehyde or amine	95%	92%	49%
		Imine	_ ^[a]	3%	49%
		Hydration	5%	5%	2%
5	 OPAL	Aldehyde or amine	60%	59%	34%
		Imine	_ ^[a]	1.0%	46%
		Hydration	40%	40%	19%
6	 PPAL	Aldehyde or amine	n.d.	38%	26%
		Imine	n.d.	8%	44%
		Hydration	n.d.	54%	29.8%
7	 MPAL	Aldehyde or amine	n.d.	88%	58%
		Imine	n.d.	_ ^[a]	37%
		Hydration	n.d.	12%	5%
8	 MSBAL	Aldehyde or amine	100%	100%	83%
		Imine	_ ^[a]	_ ^[a]	17%
		Hydration	_ ^[a]	_ ^[a]	_ ^[a]

^[a] _ represents no imine or hydration was found. n.d. not determined. From the table, only in basic condition the imine formation is good because the N- α -acetyl lysine has free amino group. We draw a conclusion of the reactivity among the different aldehyde:

ii. Hydrophobic effect of the amines

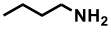
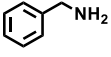
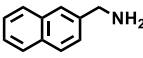
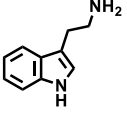
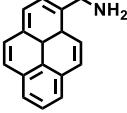
Along with the reactivities of the aldehydes, the properties of the amines could also influence the imine formation. As mentioned earlier, hydrophobic effect are very important driving force in biological processes such as protein folding.³⁰⁹ As such, they are always used to adjust the self-assembly behavior of the supramolecular polymers.³¹⁰ Inspired also by the enhanced imine formation through the addition of double-stranded DNA,³⁰⁴ we were curious to know if introducing of amines with more hydrophobic substituents would yield imines efficiently through the hydrophobic interactions in aqueous phase. Therefore, the following aliphatic amines with different size of hydrophobic groups were selected to study the imine formation with **PLP** in aqueous phase (**Scheme 37**). The experiments were conducted in phosphate buffer at pH 8 at the final concentration of 5 mM.



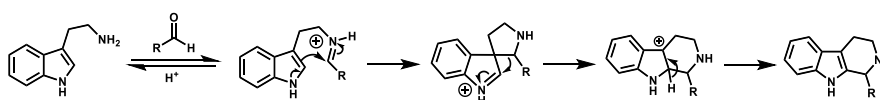
Scheme 37. The structures of the amines with hydrophobic groups tested for imine formation in aqueous phase.

As seen from **Table 11**, the yield of imine increased with the size of the hydrophobic group on the amine. For n-butylamine, the yield of imine was 39% together with 29% of unreacted aldehyde and hydrate of **PLP**. The benzylamine yielded 55% of imine. 1-naphthylmethylamine resulted, in 64% of imine product in the same condition. The tryptamine didn't generate higher yield probably due to the Pictet–Spengler reaction, to form the cyclic product (**Scheme 38**). These results indicated that the hydrophobic effect indeed influenced the yield of imine formation in aqueous phase through decreasing the concentration of water by creating a relative hydrophobic environment for the reactants. The more hydrophobic groups included in the reactants, the higher yield of imine was generated.

Table 11. Distribution of the reactions of imine formation generated from equimolar **PLP** and amines with different hydrophobic groups at pH 8.1 at 25 °C in D₂O (in phosphate buffer), using an initial concentration of 5 mM for all reactants at 25 °C.

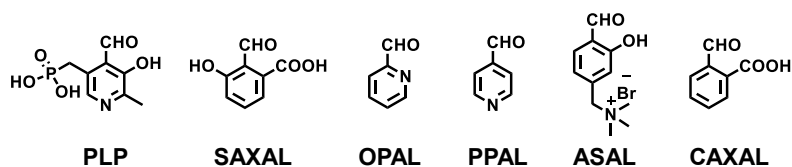
Entry ^[a]	Amine	pKa	Imine	Aldehyde	Other side products (hydrate + hemiaminal)
1		10.78	32%	29%	39%
2		9.33	55%	35%	10%
3		-	64%	27%	9%
4		10.2	10%	12%	78%
5		n.d.	n.d.	n.d.	n.d.

^[a] The experiment of imine formation from equimolar **PLP** and amine in phosphate buffer at pH 8. n.d. not determined.

**Scheme 38.** The mechanism of the Pictet–Spengler reaction from a β -arylenylamine and an aldehyde or ketone to form a tetrahydroisoquinoline in the presence of acid catalysis.³¹¹

iii. pH dependence

For imine formation in aqueous phase, pH is another important factor. There are several points to be noted: a) an acid could protonate the carbonyl group of the aldehyde, which would activate the carbonyl and make it a better electrophile; b) an acid could also protonate the amine, making them non-nucleophilic any more, which would inhibit the its addition to the carbonyl. Thus, the following fast-reacting aldehydes were selected to find the best pH range for imine formation with N- α acetyl lysine in water (**Scheme 39**). The pH titration curves for the imine formation from different aldehydes and N- α acetyl lysine were shown in **Figure 122**.



Scheme 39. The structures of the aldehydes for imine formation in aqueous phase.

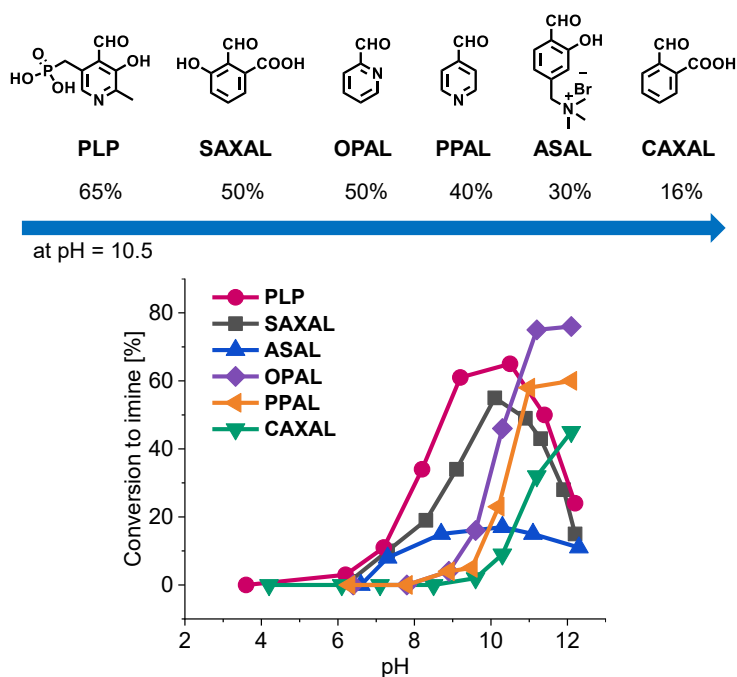


Figure 122. The schematic catalysis of C=N formation from a pyridine-2-carboxaldehyde **A1** (**A2** or **A3**) and p-anisidine **B1** in presence of metal salts catalyst.

As seen in **Figure 123**, no imine is formed at pH 3.6 and only the free aldehyde and the hydrate of the aldehyde were observed, which was the same as reported by Limbarch and co-workers.²⁹⁷ This is because the amine is fully protonated at this pH. By increasing the pH to 6.2, the hydrate of **PLP** decreased with the appearance of the imine peak at around 9 ppm. The yield of imine increased with the increase of the pH. This is because the amine was less protonated when the pH was increased. Moreover, for **PLP**, the pyridine nitrogen was protonated, which makes the electron-withdrawing properties even stronger. When the pH was further increased to 10.5, the imine reached the highest yield of 65% with almost no hydrate observed. On continuously increasing the pH, the yield of imine decreased. This could be due to the difficulty of the protonation of the carbonyl group at higher pH. And also, the phenol group was deprotonated, making **PLP** more electron-rich, resulting its low reactivity.

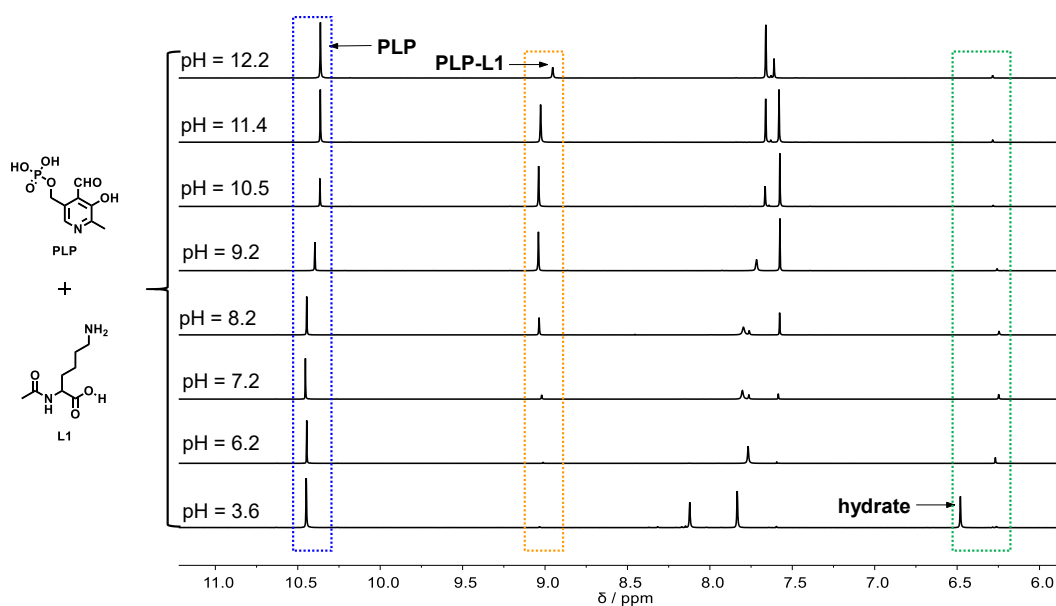


Figure 123. The pH titration experiment of **PLP** with **L1** in D_2O at 25°C (5 mM each).

When using a simple 4-pyridinecarboxyaldehyde (**PPAL**) (**Figure 124**), there are only the signals of free aldehyde (50%) and hydrate of aldehyde (50%) below pH 7.8. On increasing the pH to 8.9, the signal of imine was observed. The yield of imine continuously with the increase of pH. The imine was almost fully formed at pH 12.1. The use of 2-pyridine-carboxyaldehyde (**OPAL**) displayed the similar behavior here where it presented a bit higher yield of imine under the same conditions, which can be seen in **Figure 125**.

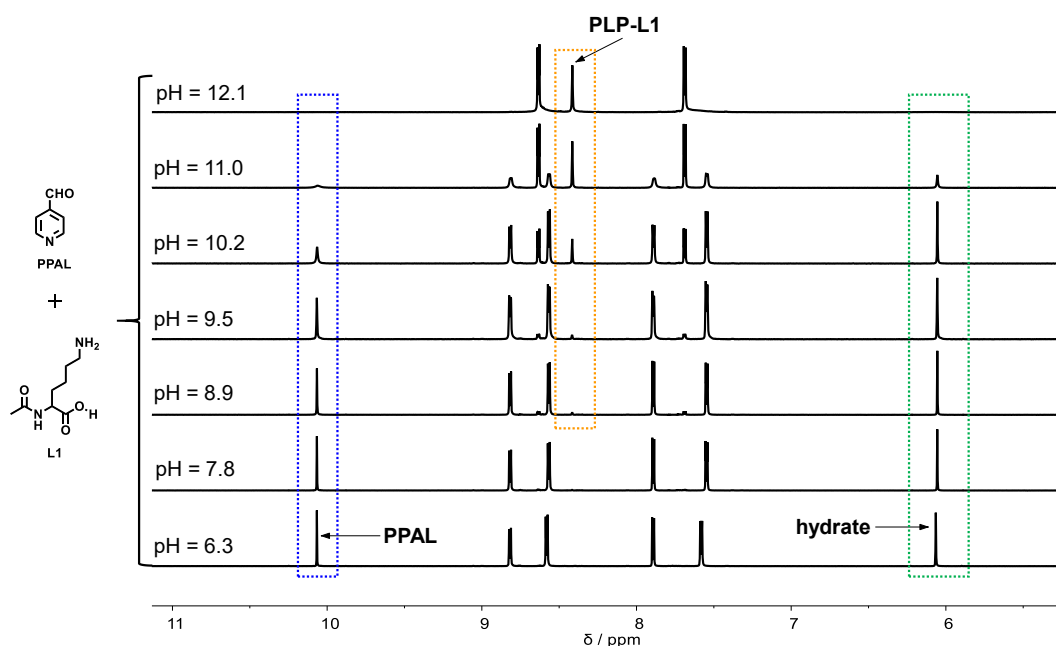


Figure 124. The pH titration experiment of **PPAL (A4)** with **L1** in D_2O at 25°C (5 mM each).

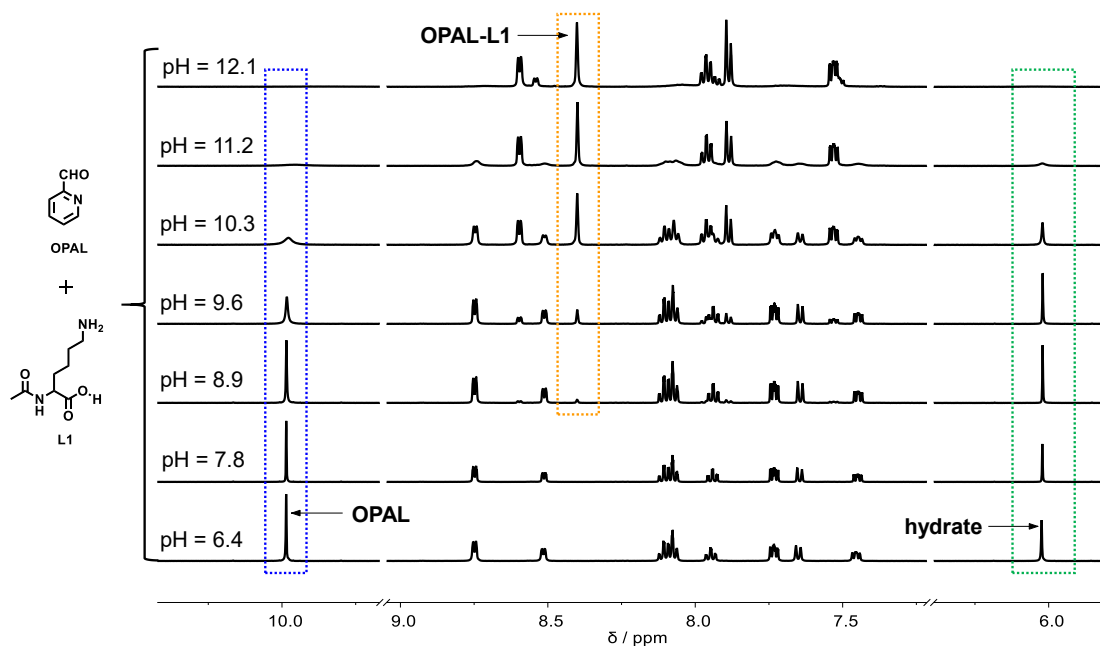


Figure 125. The pH titration experiment of **OPAL** with **L1** in D_2O at $25^\circ C$ (5 mM each).

For **CAXAL**, the imine signal was detected clearly at pH 10.3, but no imine was detected at lower pH. Like the above experiments, the yield of imine increased with the increase of pH. The yield of imine reached 45% at pH 12.1 (**Figure 126**).

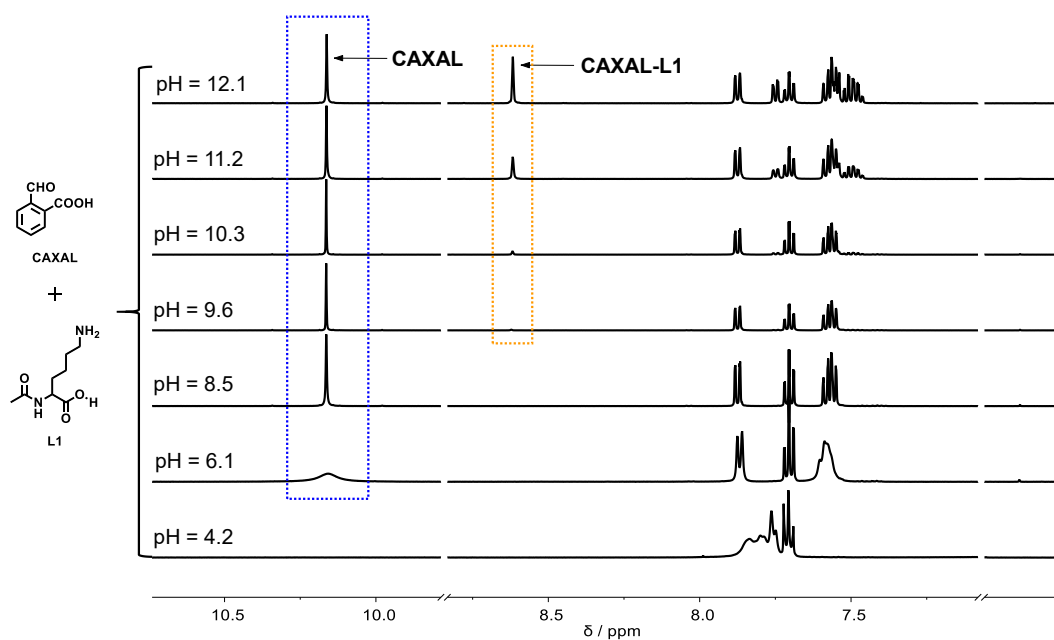


Figure 126. The pH titration experiment of **CAXAL** with **L1** in D_2O at $25^\circ C$ (5 mM each).

For a derivative of salicylaldehyde (**ASAL**), the imine signal was detected at pH 6.6 and no hydrate was observed. The yield of imine also increased with the increase of pH 6.6 to 10.3 in a gradual trend. When pH was above 10.3, the yield of imine decreased due probably to the deprotonation of the hydroxy group, thus the imine cannot be stabilized by the hydrogen bonding. Therefore, the amount of the imine decreased. The evolution of this ^1H NMR spectra was shown in **Figure 127**.

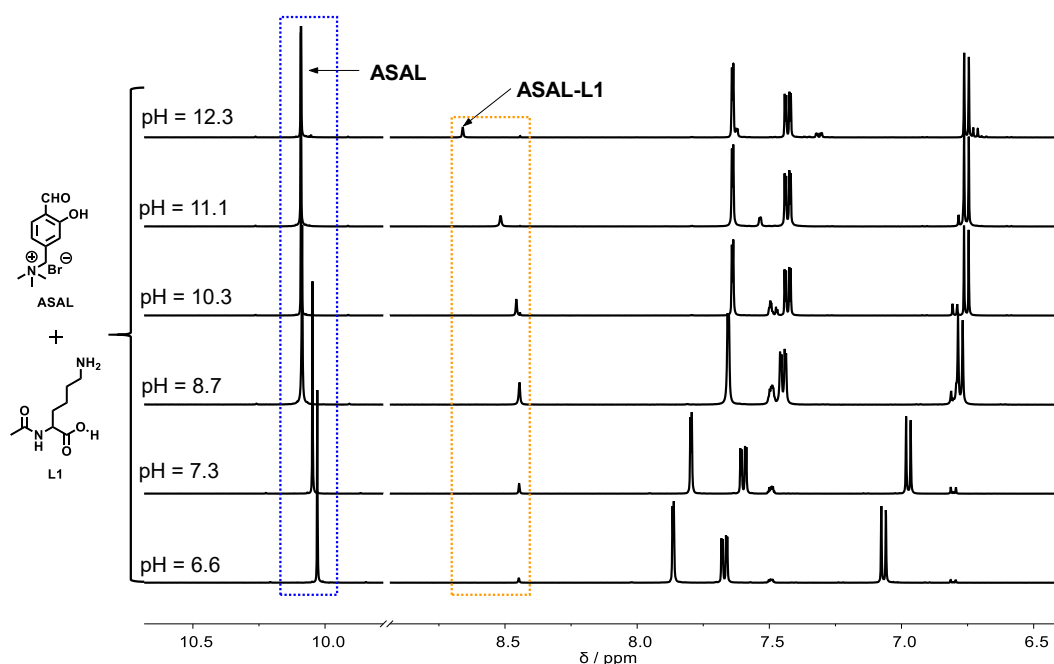


Figure 127. The pH titration experiment of **ASAL** with **L1** in D_2O at 25°C (5 mM each).

Finally, the aldehyde bearing both the carboxyl group and hydroxy group (**SAXAL**) in the ortho position was chosen to study the imine formation. As seen in **Figure 128**, there wasn't imine formed at pH 6.3 due to the full protonation of the amine at this pH. The imine signal appeared at pH 7.3 and kept increasing with the increasing of the basicity of the solution. The amount of imine reached its maximum (57%) at pH 10.1. Thereafter, the yield of imine declined with the increase of pH. The reason could be the less stability of the formed imine due to the disappearance of the hydrogen bonding from the hydroxy group at highly basic conditions.

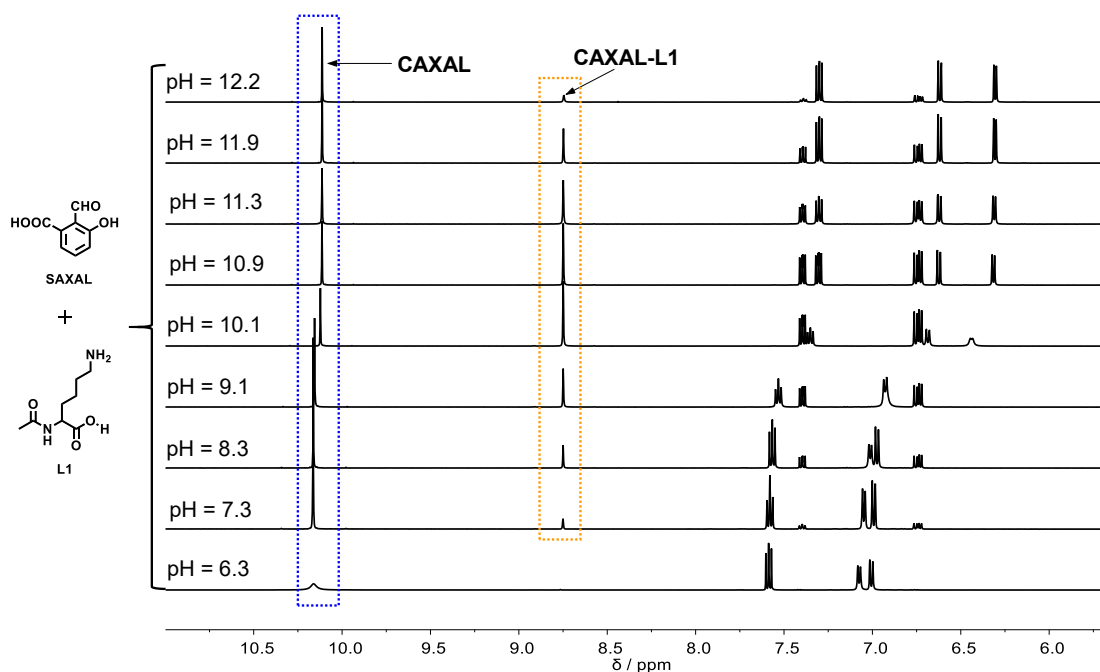


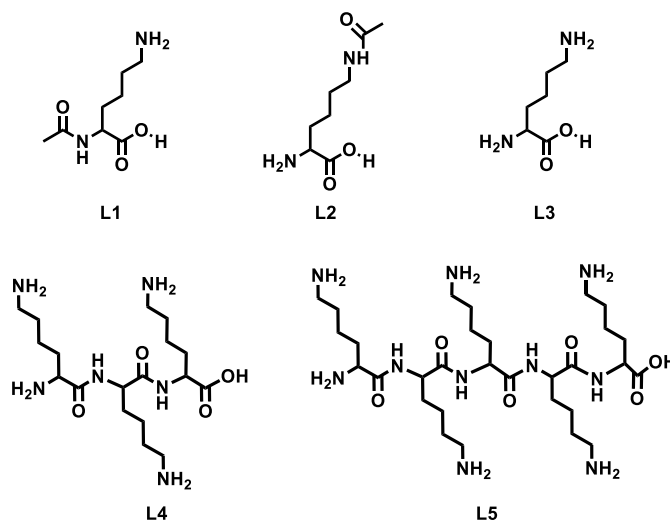
Figure 128. The pH titration experiment of **SAXAL** with **L1** in D_2O at $25^\circ C$ (5 mM each).

From the above experiments, the yield of imine differs depending on the pH of the aqueous medium. The corresponding pH titration curves for the reaction of imine formation from the aldehydes and N- α acetyl lysine are shown in **Scheme 15** above. For the tested aldehydes, the best range for the efficient imine formation is between 10 to 11. The reason lies in the fact that the pK_a of the ϵ -amino group of the N- α acetyl lysine is about 10.5. At pH below 10.5, there are always some amines protonated which cannot react with the aldehyde, leading to the lower yield of imines. While at higher pH above 11, the ortho hydroxy group of some aldehydes has lower yield of imine due to the deprotonation of the hydroxy group at these conditions, resulting in the disappearance of the hydrogen bonding. In addition, the deprotonated hydroxy group served as the electro-donating group, which decreased the reactivity of the aldehyde.

B. Imine formation driven between PLP and Lysine derivatives

From the above experiments, **PLP** is the aldehyde which could generate the higher yield of imine at pH between 10 and 11. Therefore, it was chosen to test the imine formation with different lysine derivatives in order to figure out the efficiency of the reaction of **PLP** with different amino sites and identifying the differences for the α -amino of lysine and ϵ -amino of lysine in imine formation. The experiments were conducted at the concentration of 5 mM in

phosphate buffer at 25°C. The structures of the lysine derivatives **L1** to **L5** are shown below in **Scheme 40**.



Scheme 40. The structures of the lysine derivatives.

i. PLP reacting with mono substituted Lysine

The imine formation from **PLP** and **L1** was firstly studied and followed by the ^1H NMR spectroscopy (**Figure 129**). It was found that the imine formed very fast from **PLP** and **L1**. Within 5 minutes, there were about 38% of imine **PLP-L1** formed together with less than 2% of hydrate of **PLP** observed in the spectra. After less than 1 hour, the composition of the reaction did not change any more, giving 62% of imine **PLP-L1**. The relative kinetic curves of the imine formation are shown in **Figure 130A**.

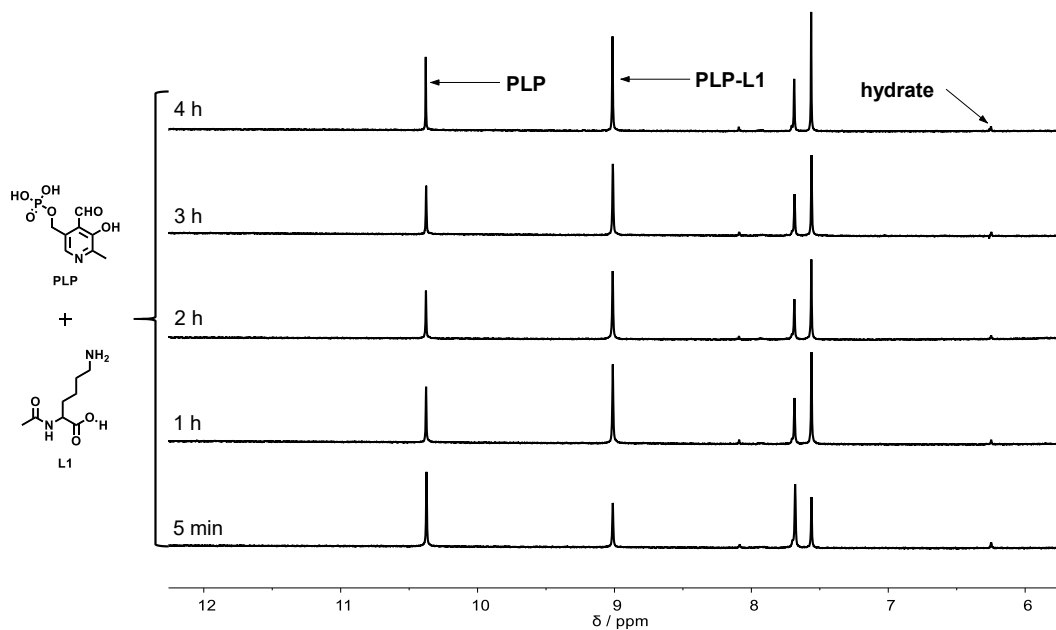


Figure 129. ¹H NMR (500 MHz) of the evolution of the imine formation from **PLP** and **L1** (5 mM each, phosphate buffer, pH 11.0) at 25°C .

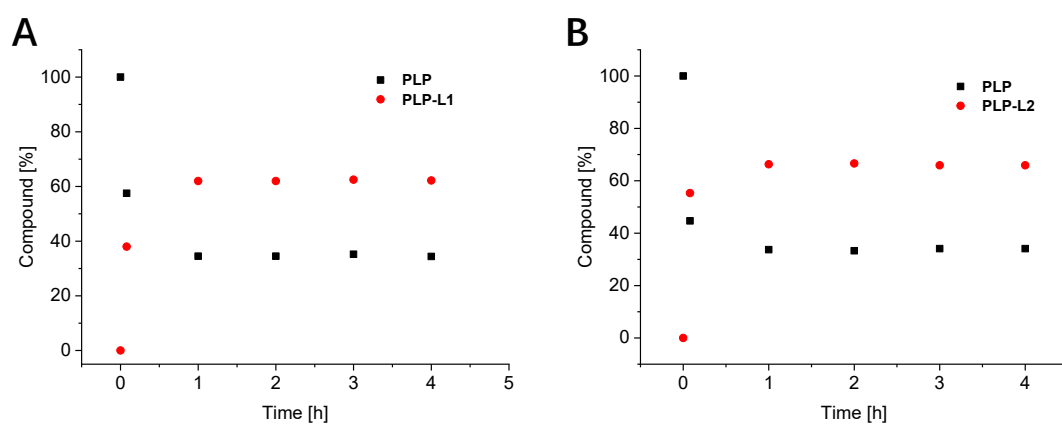


Figure 130. The kinetic plot of the imine **PLP-L1** and **PLP-L2** formation from its components **PLP** and **L1** or **L2** (5 mM each, phosphate buffer, pH 11.0) at 25°C .

For N-ε-acetyl-lysine (**L2**), the similar experiment was conducted in the ratio of 1 : 1 ratio, the amount of **PLP** decreased to 45% after 5 minute with the appearing of the imine signal at 7.6 ppm which took up 55%. After 1 hour, there is still 34% of free **PLP** left unreacted. The final yield of the imine **PLP-L2** was 66%. The kinetic curve is shown in **Figure 130B**.

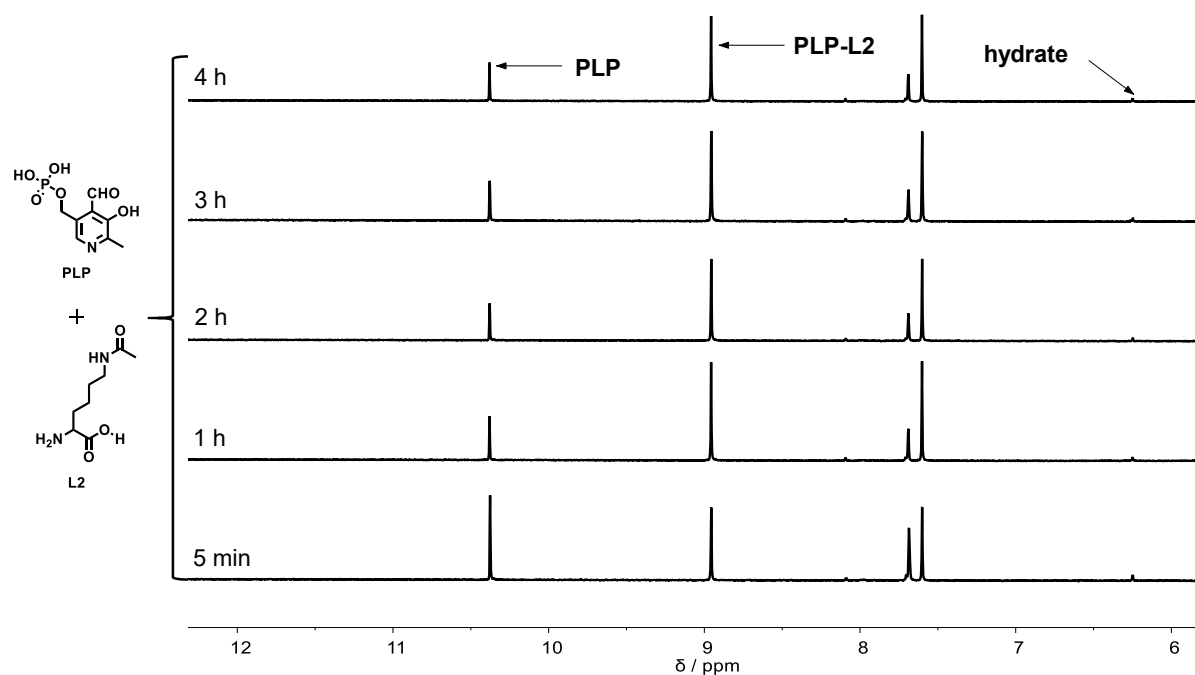


Figure 131. ^1H NMR (500 MHz) of the evolution of imine formation from **PLP** and **L2** (5 mM each, phosphate buffer, pH 11.0) at 25°C .

In the following, the experiment was conducted for the reaction of **PLP** with lysine (**L3**) (with both α -amino and ϵ -amino groups) in the ratios of 1:1, 2:1 and 4:1 to generate the full conversion of lysine to the imine product.

As seen in **Figure 132**, the **PLP** and **L3** were mixed in the ratio of 1:1 in phosphate buffer (pH = 11.0) at 25°C. After 20 minutes, the reaction reached the equilibrium. Lysine has two types of amino groups: α -amino and ϵ -amino groups. It could generate three imines with four imine peaks on reacting with **PLP**: mono imine **PLP- α -L1**, mono imine **PLP- ϵ -L1** and the bisimine **PLP- α,ϵ -L3**. The composition of the imines did not change after 20 minutes. The final composition of the reaction mixture/outcome was 47% **PLP**, 33% **PLP- ϵ -L3**, 10% **PLP- α -L3** and 4% of bisimine product **PLP- α,ϵ -L3** with 2% of hydrate of **PLP**. The higher yield of **PLP- ϵ -L3** in comparison with **PLP- α -L3** is due to the higher pK_a of ϵ -amino ($pK_a = 10.5$) than α -amino of lysine ($pK_a = 9.0$). The total amount of imine formed added up to about 51% including the two mono imines and the bisimine together.

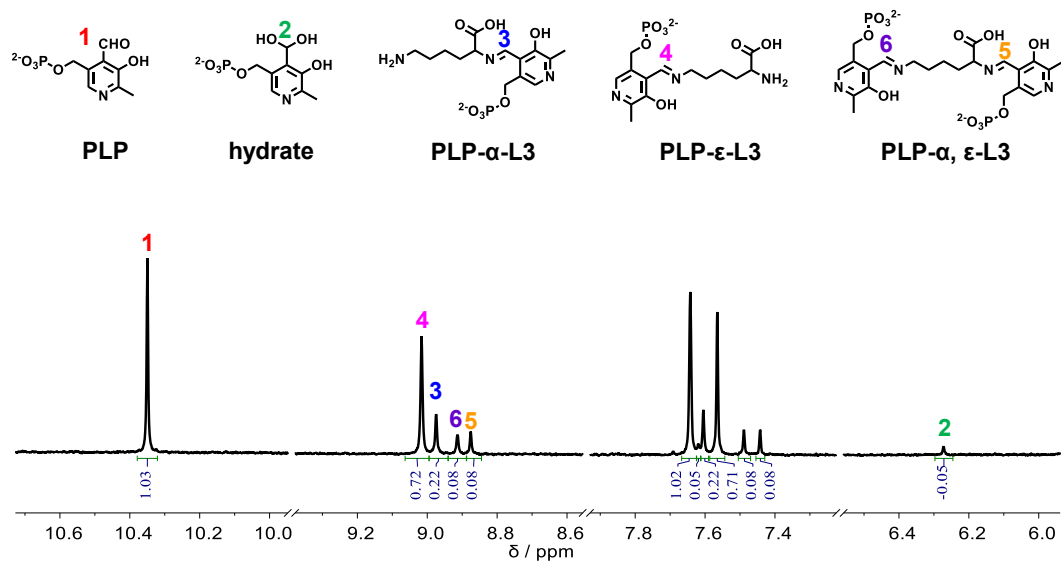


Figure 132. ^1H NMR (500 MHz) of the imine formation from **PLP** and **L3** with the ratio of 1:1 (5 mM each, phosphate buffer, pH 11.0) at 25°C.

The experiment of **PLP** and **L3** were also conducted in the ratio of 2:1 in phosphate buffer (pH = 11.0) at 25°C seen in **Figure 133**. Similarly, the composition of the reaction did not change after 20 minutes. By adding one more equivalent of **PLP**, the yields of imines also increased. The final composition of the mixture included 21% **PLP- ϵ -L3**, 36% **PLP- α -L3** and 22% of bisimine product **PLP- α, ϵ -L3** together with free **PLP** and its hydrate. The total yield of imine according to the conversion of amino group is 79%.

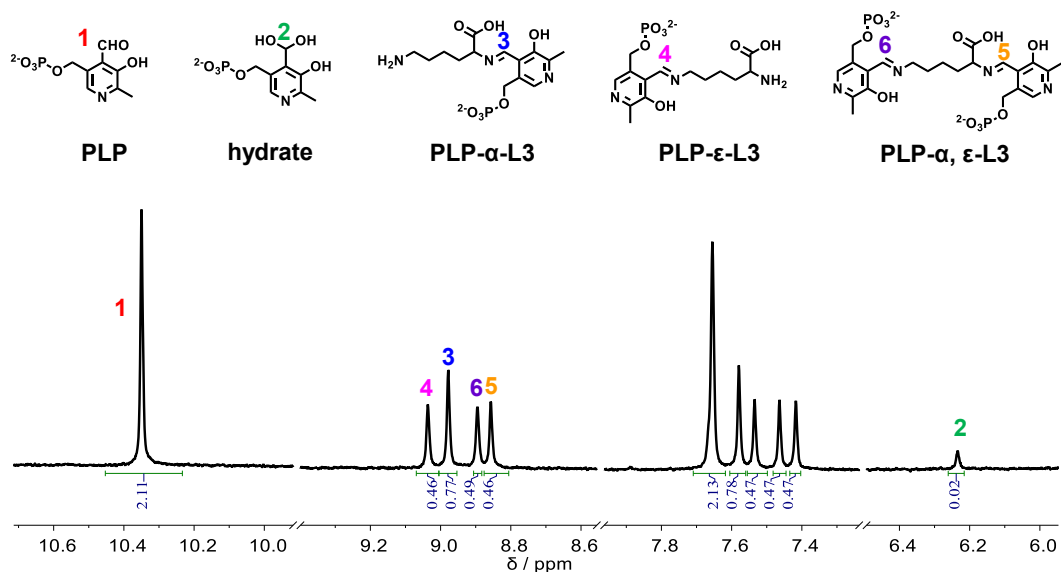


Figure 133. ^1H NMR (500 MHz) of the imine formation from **PLP** and **L3** with the ratio of 2:1 (5 mM each, phosphate buffer, pH 11.0) at 25°C.

While the experiment of **PLP** with **L3** in the ratio of 4:1 (**Figure 134**), it resulted in the final distribution of the mixture: 22% **PLP- ϵ -L3**, 40% **PLP- α -L3** and 19% of bisimine product **PLP- α,ϵ -L3** together with the access of free aldehyde **PLP** and its hydrate. The total amount of imine added up to 81% considering the conversion of the amino groups of **L3**.

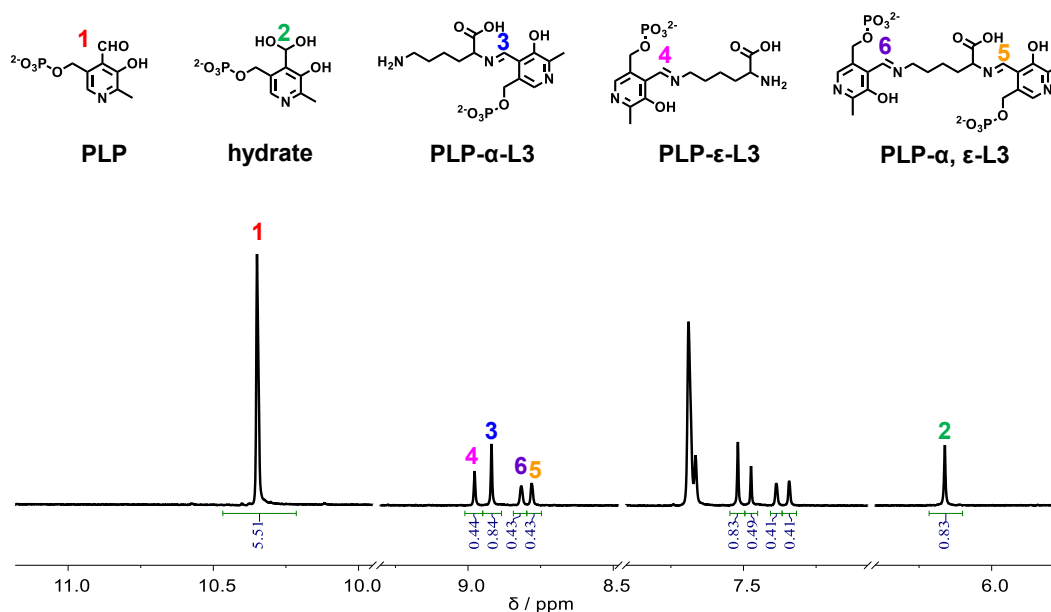


Figure 134. ^1H NMR (500 MHz) of the imine formation from **PLP** and **L3** with the ratio of 4:1 (5 mM each, phosphate buffer, pH 11.0) at 25°C .

ii. PLP reacting with tri-lysine and penta-lysine

To mimic the reaction between histones (abundant in lysines) and **PLP**, the imine formation from the polylysine and **PLP** was firstly investigated in different ratios. Therefore, the tri-lysine **KKK** (**L4**) were used to study the imine formation under the same condition. The experiments were also conducted in different ratios to get higher conversion of the amino groups to imines.

As seen in **Figure 135**, on mixing the equal amount of **PLP** and **L4**, a series of imine peaks were observed at around 9 ppm due to the presence of many species as there are 3 ϵ -amino and 1 α -amino groups within one **L4**, which can generate different monoamine, bis-imine, tris-imine and tetra-imine products. The total yield of amine conversion was about 57%.

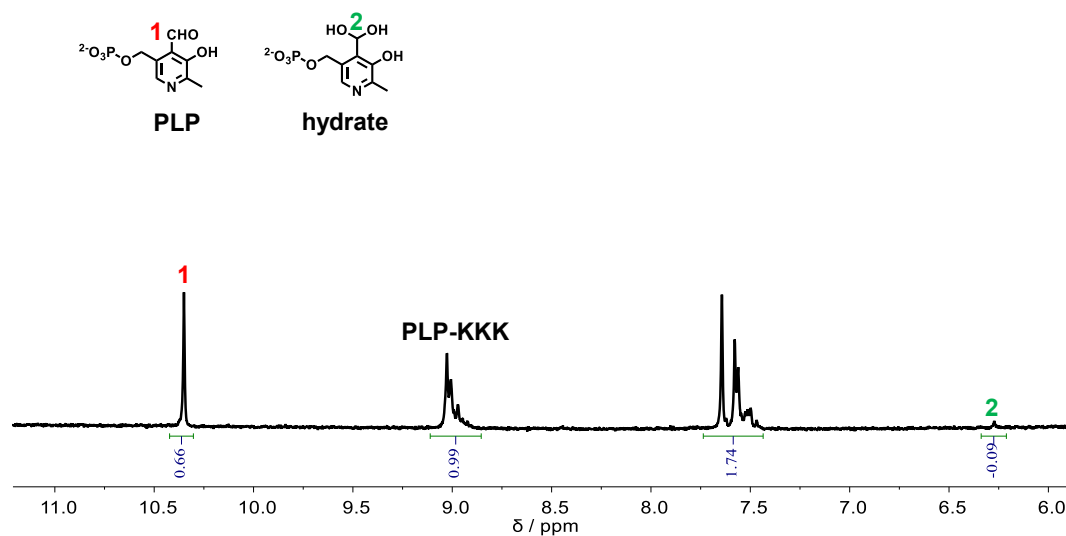


Figure 135. ^1H NMR (500 MHz) of the imine formation from **PLP** and **L4** (KKK) (5 mM each, phosphate buffer, pH 11.0) at 25°C .

On addition of 3 equivalents of **PLP** relative to **L4** (**Figure 136**), it gave out 83% of imine product at equilibrium relative to the initial amount of **L4**. While the experiment with 6 equivalents of **PLP** (**Figure 137**) generated almost the same amount of imine product (84%). Therefore, by using 3 equivalents or 4 equivalents of **PLP**, a similar yield of imine was obtained. The current results indicated that **PLP** gave higher yield of imine up to 83% with polylysine in the presence of 3 equiv. of **PLP**. The reason could also be due to the presence of the hydrophobic effect from the alkyl chain of the polylysine. Thus, it becomes very interesting for the further investigation of imine formation from **PLP** and **L5** as well as the histones which are abundant in lysine and play important roles in the process of gene expression.

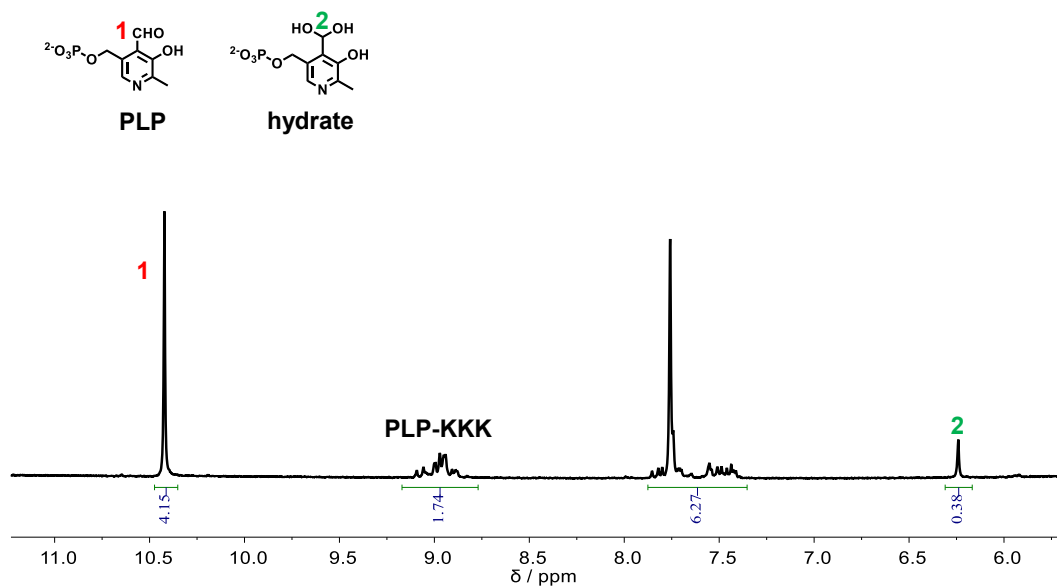


Figure 136. ^1H NMR (500 MHz) of the imine formation from (5 mM) and L4 (15 mM) in phosphate buffer, at pH 11.0 at 25°C .

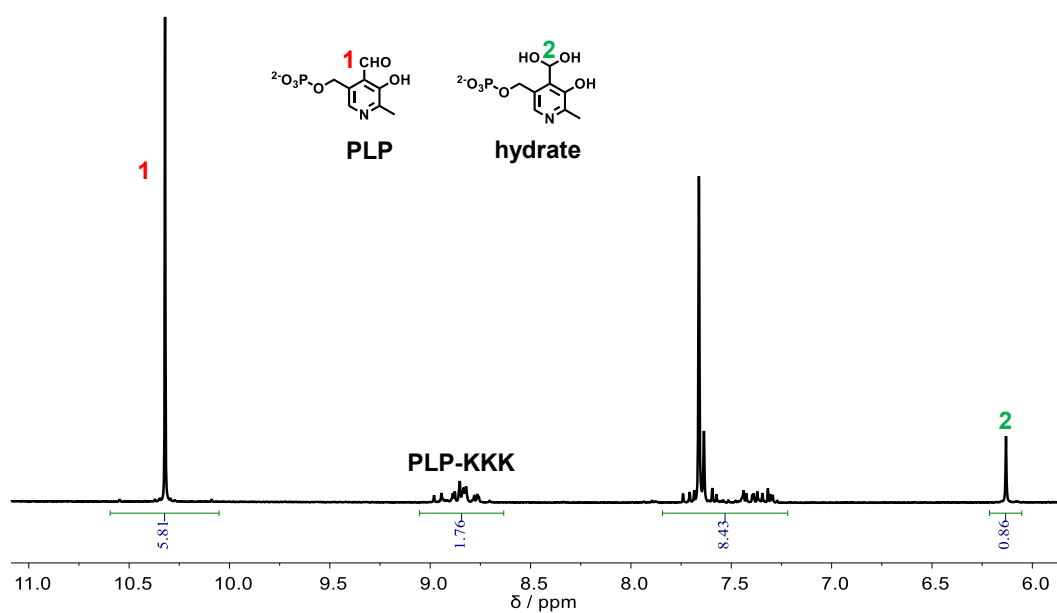


Figure 137. ^1H NMR (500 MHz) of the imine formation from PLP (5 mM) and L4 (20 mM) in phosphate buffer at pH 11.0 at 25°C .

3. SUMMARY OF CHAPTER IV

In this chapter, we investigated the yield of imine formation in aqueous phase influenced by several factors. The results have shown that the reactivity of the aldehydes, the hydrophobic effect of reactants as well as the pH could greatly influence the yield of imine formation. It was found that the aldehyde which generated higher yield of imine included not only the electron-withdrawing group to activate the aldehyde, but also the ortho-substituent to stabilize the generated imine. The selected **PLP**, which is a co-enzyme of the transamination reactions, have shown higher yield of imine formation up to 84% with **KKK** at basic pH conditions.

Further studies will be oriented to determine the imine formation of **PLP** with oligo-lysine such as **KKKKK** and histones. The exploration of more reversible chemical reactions which could convert amino groups of lysine to a new product in a higher yield will also be continued, especially for those products which can be formed stable at physiological conditions.

CHAPTER V. CONCLUSION AND PERSPECTIVES

This thesis was based on dynamic combinatorial chemistry of imine bonds and used them to study different adaptive behaviors from a kinetic and thermodynamic point of view, including the catalysis of imine and hydrazone formation (Chapter II), CDNs switches in organic phase and their out-of-equilibrium states (Chapter III). In addition, from a thermodynamic point of view, the imine formation in aqueous phase was studied to achieve the increased yield of imine formation for potential application in gene regulation through modification of histones.

In the first chapter, we gave a general introduction of the development from supramolecular chemistry to constitutional dynamic chemistry, the adaptive behavior of CDLs as well as the dynamic imine chemistry used in CDLs.

In the second Chapter, we have demonstrated the acceleration of the imine and hydrazone formation by the addition of metal salts such as Ag (I) and Zn (II). The simultaneous addition of metal salt and auxiliary amine resulted in remarkably faster formation of the hydrazone complex. By adding three catalysts, the dynamic system evolves from the formation of the kinetic product (the silver complex of imine) to a thermodynamic product (the zinc complex of hydrazone), and this prompted us to examine kinetic switching behavior of CDLs.

In the third Chapter, we used the dynamic imine formation to establish CDNs [2 × 2] and its associated CDLs and applied the kinetic switching behavior of the second chapter into DCLs, thus realizing a time-dependent network switching from a kinetic distribution to a thermodynamic distribution both in the absence and presence of metal cations.

Finally, in the fourth Chapter, from the thermodynamic point of view, we discovered the rapid and quantitative formation of imine from different aldehydes and lysine derivatives in a phosphate buffer, indicating that pyridoxal phosphate has much higher yield of imine formation in basic pH 10-11. This gives it great potential for use in certain applications such as the modification of proteins in biology.

To sum up, in the present work, we have broadened our knowledge and understanding of the CDC of imines, in particular from the kinetic point of view, which has long been neglected. Understanding the influence of structural effects on kinetic and thermodynamic behavior opens the way to the establishment of complex multiphase systems to generate faster and simpler production in adaptive chemistry. In addition, these studies have indicated potential applications in biological activities such as protein modification to regulate gene expression.

CHAPTER VI. EXPERIMENTAL PART

1. GENERAL PROCEDURES

A. Solvents and Chemicals

All the reagents and solvents were purchased from Sigma-Aldrich, Alfa Aesar, Fluorochem and Adamas and were used without further purification. Deuterated solvents were purchased from Fluorochem or Sigma-Aldrich and used without further purification. Deionized water was obtained from a milli-gradient system (Millipore, France). Dry deuterated CD_3CN was treated with 4Å molecular sieves. The molecular sieves were activated by heating at 550°C for 3 hours, then cool down progressively until 200°C, move the molecular sieves to a desiccator filled with argon.

B. Methods and Instruments

i. Chromatography Methods

Thin Layer Chromatography was performed using silica on TCL Aluminium foils (silica gel matrix with fluorescent indicator 254 nm, thickness: 500 μm , sigma-Aldrich). The visual detection of the TLC was performed using UV-lamp and iodine vapor. The flash column chromatography was performed using silica gel (60Å, 230-400 mesh, 40-63 μm , Sigma-Aldrich). The reverse phase column (C18 column) was performed with a water/ CH_3CN gradient as the eluent.

ii. Nuclear Magnetic Resonance Spectroscopy

NMR spectra were recorded on Bruker Avance III plus 400 (400 MHz for ^1H and 100 MHz for ^{13}C) and Bruker Ascend Spectroscopy Avance Neo-500 MHz (500 MHz for ^1H and 125 MHz for ^{13}C). All the collected spectra using CD_3CN as the solvent were referenced on residual CD_3CN signal as 1.94 ppm, others were referenced on residual solvent signal according to Nudelman et al. The CD_3CN used for kinetics measurements of NMR was passed through molecular sieves to remove water and was preserved in a brown glass vial to keep out of the light. The quantitative ^1H NMR was measured by using HMDSO (hexamethyldisiloxane) as internal standard. The stock solution of HMDSO and components in CD_3CN were prepared and added to the set of the experiments.

iii. High resolution electrospray ionization mass spectroscopy

High resolution electrospray ionization mass spectroscopy (HR-ESI-MS) analysis were performed on a ThermoFisher Exactive Plus EMR Orbitrap mass spectrometer.

iv. Elemental Analysis

Elemental analysis was performed on a ThermoFischer Scientific Flash 200 with absolute precision of 0.3% at the service de Microanalyse, University of Strasbourg. The data were given by the percentage of the elements C, H and N.

v. X-ray crystallography

X-ray crystallography was performed at the service de radiocristallographie, university of Strasbourg.

vi. pH Measurement

All pH and pD were measured directly after calibration of pH meter in aqueous pH 2, pH 4.1, pH 7, and pH 10 buffer (Fluka) on a *SEVENCOMPACTTM pH/Ion meter S220* using a Hamilton Spintrode mini-probe.

2. CHAPTER II, CATALYSIS OF IMINE AND HYDRAZONE FORMATION

A. Synthesis and characterization

i. General procedures for the synthesis

6-Phenylpyridine-2-carbaldehyde²

6-bromo-2-pyridinecarboxaldehyde (930 mg, 5.0 mmol) and phenylboronic acid (856 mg, 6.25 mmol) were dissolved in dioxane (36 mL) and water (4 mL) and flushed with nitrogen. Pd(PPh₃)₄ (290 mg, 0.25 mmol) and Cs₂CO₃ (8.1 g, 25 mmol) were added. After refluxing overnight, water (100 mL) and CH₂Cl₂ (100 mL) were added to the solution after cooling to room temperature. The aqueous phase was separated and extracted with CH₂Cl₂ (25 mL), and the combined organic extracts were dried overnight using Na₂SO₄. Further purification by a silica gel column chromatography gave the title compound as a pale yellow oil, yield 68%. (pentane: CH₂Cl₂ = 2:1). ¹H NMR (400 MHz, CD₃CN): δ 10.11 (d, *J* = 0.78, 1H); 8.18-8.15 (m, 2H); 8.13 (dd, *J* = 1.2, *J* = 7.8, 1H); 8.05 (dt, 1H); 7.89 (dd, *J* = 1.2, *J* = 7.4, 1H); 7.58-7.49 (m, 3H).

General methods for preparation of imines and hydrazones

Aryl aldehydes **Ax** (1 equiv.) and 4 Å MS were added to ethanol solutions of amines, hydrazines **By** (1 equiv.) respectively. After the mixtures were heated under reflux for 6 hours, the mixture was filtrated to remove 4 Å MS and washed by CH₂Cl₂ (20 mL) The solution was then dried with Na₂SO₄. After evaporation of the volatile materials under reduced pressure, the desired imines were afforded in a quantitative yield. Purer imine products could be obtained via vacuum distillation. all of the relevant imines and hydrazones were reported before. The characterizations were consistent with the literature values.

General methods for preparation of the relative complexes

0.5 equiv. of metal ions were added to the CD₃CN solutions of 1 equiv. of the ligand constituents. The mixtures were heated overnight at 70 °C. The complexes were always freshly prepared prior to every new experiment. The complexes were never isolated, all the present experiments and analysis were done in CD₃CN solution. Nevertheless, all of the relevant imines, hydrazones and complexes were reported before. The characterizations were consistent with the literature values.^[1]

General methods for imine and hydrazone formation in the absence of metal salts

In a typical experiment, the stock solution of aryl aldehydes **Ax** (60 mM), the amine or hydrazine **By** (60 mM) and the internal standard (hexamethyldisiloxane, 33.3 mM) was

prepared in advance. And then the same volume (100 μL) of **Ax** and **By** were mixed together with addition of internal standard (10 μL) in CD_3CN (600 μL). After vigorous shaking, the resulting mixture was monitored at 25°C by ^1H NMR as a function of time.

General methods for imine and hydrazone formation in the presence of metal salts

In a typical experiment, the stock solution of aryl aldehydes **Ax** (60 mM), the amine or hydrazine **By** (60 mM), metal salt (60 mM) and the internal standard (hexamethyldisiloxane, 33.3 mM) was prepared in advance. And then the same volume (100 μL) of **Ax** and **By** were mixed together with 50 μL metal salt (or 5 μL for catalysis experiment) and the internal standard (10 μL) in CD_3CN (600 μL). After vigorous shaking, the resulting mixture was monitored at 25°C by ^1H NMR as a function of time.

General methods for hydrazone formation in presence of B1 or metal salts

In a typical experiment, the stock solution of aryl aldehydes **Ax** (60 mM), hydrazine **B2** (60 mM), the internal standard (hexamethyldisiloxane, 33.3 mM) and amine **B1** (60 mM) or metal salt (60 mM) was prepared in advance. And then the same volume (100 μL) of **Ax** and **By** were mixed together with the internal standard (10 μL) and 100 μL **B1** (or 5 μL for catalysis experiment) or 50 μL metal salt (or 5 μL for catalysis experiment) in CD_3CN (600 μL). After vigorous shaking, the resulting mixture was monitored at 25°C by ^1H NMR as a function of time.

General methods for hydrazone formation in presence of both B1 and metal salts

In a typical experiment, the stock solution of aryl aldehydes **Ax** (60 mM), the amine **B1** (60 mM), hydrazine **B2** (60 mM), metal salt (60 mM) and the internal standard (hexamethyldisiloxane, 33.3 mM) was prepared in advance. And then the same volume (100 μL) of **Ax**, **B2** and **B1** (or 5 μL for catalysis experiment) were mixed together with 50 μL metal salt (or 5 μL for catalysis experiment) and the internal standard (10 μL) in CD_3CN (600 μL). After vigorous shaking, the resulting mixture was monitored at 25°C by ^1H NMR as a function of time.

General methods for hydrazone formation in presence of catalytical amount of acid or metal salts

In a typical experiment, the stock solution of aryl aldehydes **Ax** (60 mM), the amine **B1** (60 mM) or hydrazine **B2** (60 mM), metal salt (30 mM) and the internal standard (hexamethyldisiloxane, 33.3 mM) was prepared in advance. And then the same volume (100 μL) of **Ax**, **B1** or **B2** were mixed with 10 μL metal salt and the internal standard (10 μL) in

CD₃CN (600 μL). After vigorous shaking, the resulting mixture was monitored at 25°C by ¹H NMR as a function of time.

ii. Characterization of the newly made compounds

A3B1: ¹H NMR (500 MHz, CD₃CN): δ = 8.54 (s, 1H, H⁶), 8.13–8.11 (d, *J* = 10.0 Hz, 1H, H²), 7.79–7.75 (t, *J* = 10.0 Hz, 1H, H³), 7.63–7.61 (d, *J* = 10.0 Hz, 1H, H⁴), 7.39–7.35 (m, 2H, H^{8,8'}), 7.01–6.97 (m, 2H, H^{9,9'}), 3.82 (s, 3H, H¹¹); ¹³C NMR (126 MHz, CD₃CN): δ 160.06 (C¹⁰), 157.05 (C⁶), 156.79 (C⁵), 143.65 (C⁷), 142.05 (C¹), 140.39 (C³), 129.96 (C⁴), 123.66 (C^{8,8'}), 120.82 (C²), 115.12 (C^{9,9'}), 55.87 (C¹¹); ESI-MS: calculated for [C₁₃H₁₁BrN₂O+H]⁺ 291.0128, found: 291.0123; Elemental analysis calculated (%) for C₁₃H₁₁BrN₂O: : C, 53.63; H, 3.81; Br, 27.44; N, 9.62; O, 5.50; found: C, 53.53; H, 3.85; N, 9.55.

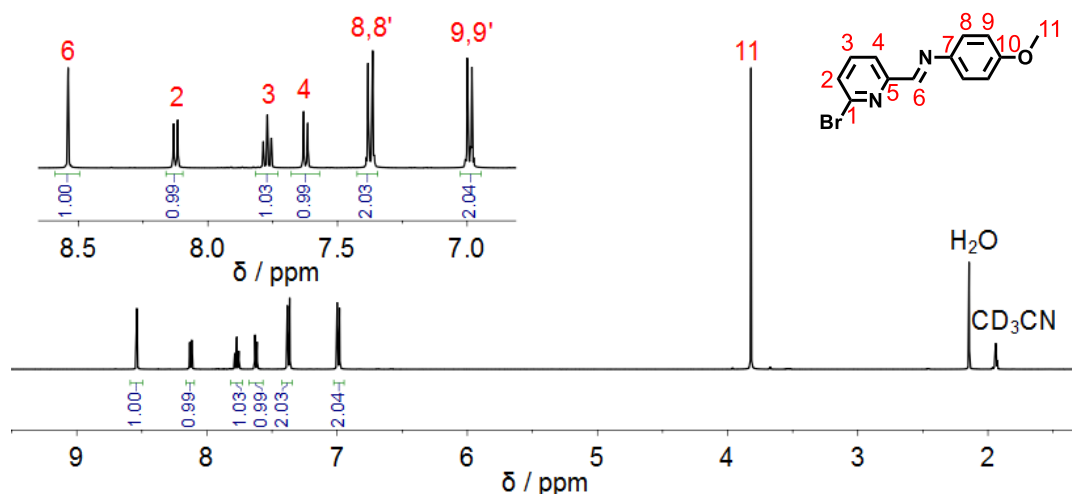


Figure II.1. ¹H NMR spectrum of **A3B1** (125 MHz, 298 K, CD₃CN).

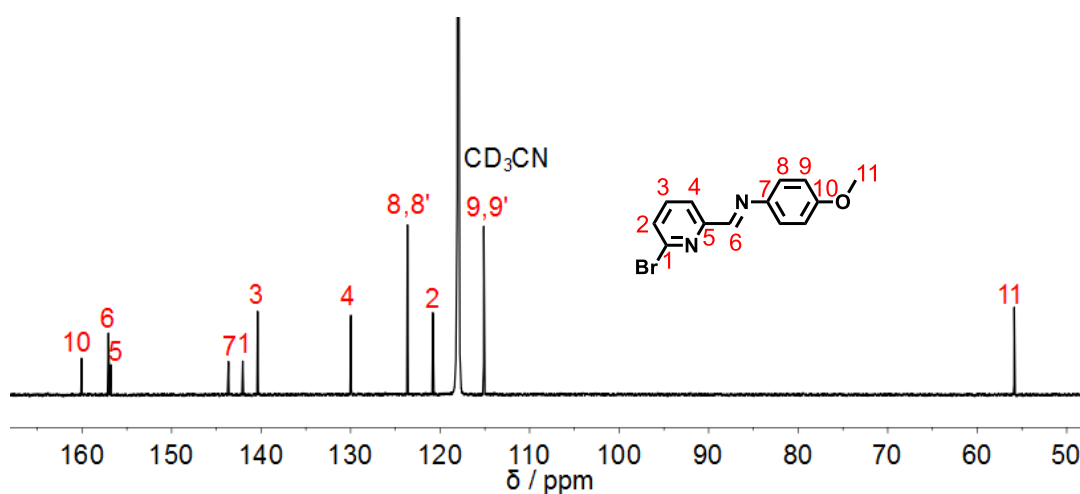
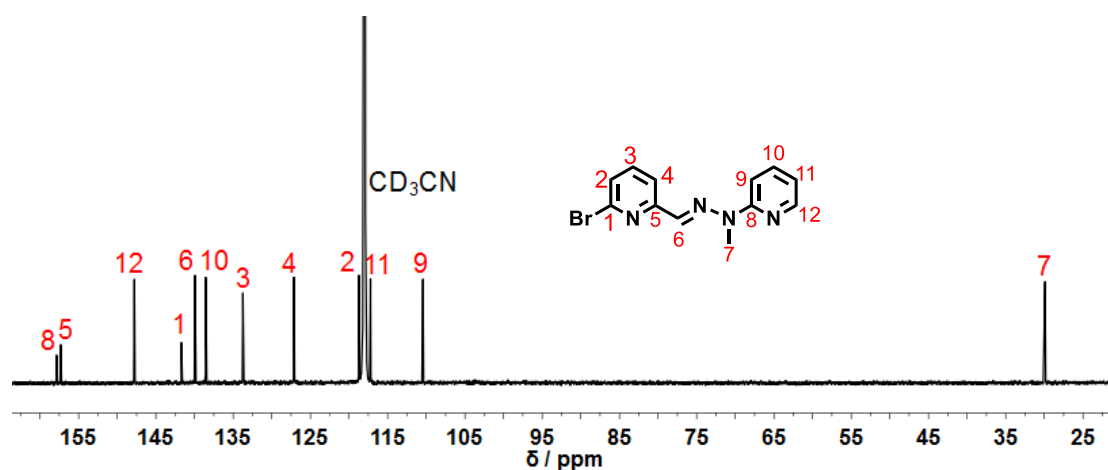
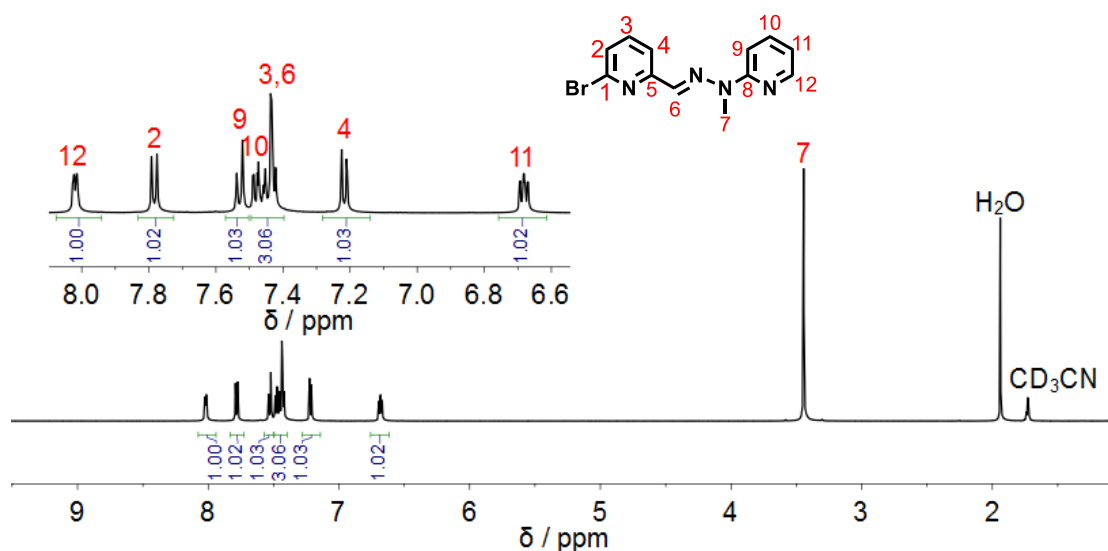


Figure II.2. ¹³C NMR spectrum of **A3B1** (125 MHz, 298 K, CD₃CN).

A3B2: ^1H NMR (500 MHz, CD_3CN): δ 8.23 (d, $J = 5.0$ Hz, 1H, H^{12}), 8.00–7.98 (d, $J = 5.0$ Hz, 1H, H^2), 7.74 (d, $J = 8.6$ Hz, 1H, H^9), 7.71–7.60 (t, 3H, H^{10+3+6}), 7.43 (m, $J = 7.7, 0.9$ Hz, 1H, H^4), 6.89 (d, $J = 7.0, 1.2$ Hz, 1H, H^{11}), 3.66 (s, 3H, H^7); ^{13}C NMR (126 MHz, CD_3CN): δ 157.85 (C^8), 157.32 (C^5), 147.78 (C^{12}), 141.69 (C^1), 139.94 (C^6), 138.55 (C^{10}), 133.73 (C^3), 127.12 (C^4), 118.71 (C^2), 117.22 (C^{11}), 110.43 (C^9), 29.91 (C^7); ESI-MS: calculated for $[\text{C}_{12}\text{H}_{11}\text{BrN}_4+\text{H}]^+$ 291.0240, found: 291.0232; Elemental analysis calculated (%) for $\text{C}_{12}\text{H}_{11}\text{BrN}_4$: C, 49.50; H, 3.81; Br, 27.44; N, 19.24; found: C, 49.44; H, 3.86; N, 19.18.



$[\text{Ag}(\text{A1B1})_2]^+$: ^1H NMR (500 MHz, CD_3CN): $\delta = 8.86$ (s, 1H, H^{10}), 8.08 (t, $J = 7.8$ Hz, 1H, H^7), 7.83–7.74 (m, 2H, H^{6+8}), 7.59–7.52 (m, 2H, $H^{3,3'}$), 7.51–7.45 (m, 2H, $H^{12,12'}$), 7.22–7.16 (m, 1H, H^1), 7.13–7.05 (m, 2H, $H^{2,2'}$), 6.98–6.91 (m, 2H, $H^{13,13'}$), 3.80 (s, 3H, H^{15}); ^{13}C NMR (126 MHz, CD_3CN): $\delta = 161.03$ (C^{14}), 159.34 (C^5), 157.18 (C^{10}), 150.42 (C^9), 140.87 (C^{11}), 140.46 (C^4), 140.33 (C^7), 130.20 (C^1), 129.01 ($C^{2,2'}$), 127.78 ($C^{3,3'}$), 126.83 (C^{6+8}), 124.87 ($C^{12,12'}$), 115.39 ($C^{13,13'}$), 56.02 (C^{15}); ESI-MS: calculated for $[\text{C}_{38}\text{H}_{32}\text{N}_4\text{O}_2 + \text{Ag}]^+$ 683.1571, found: 683.1563.

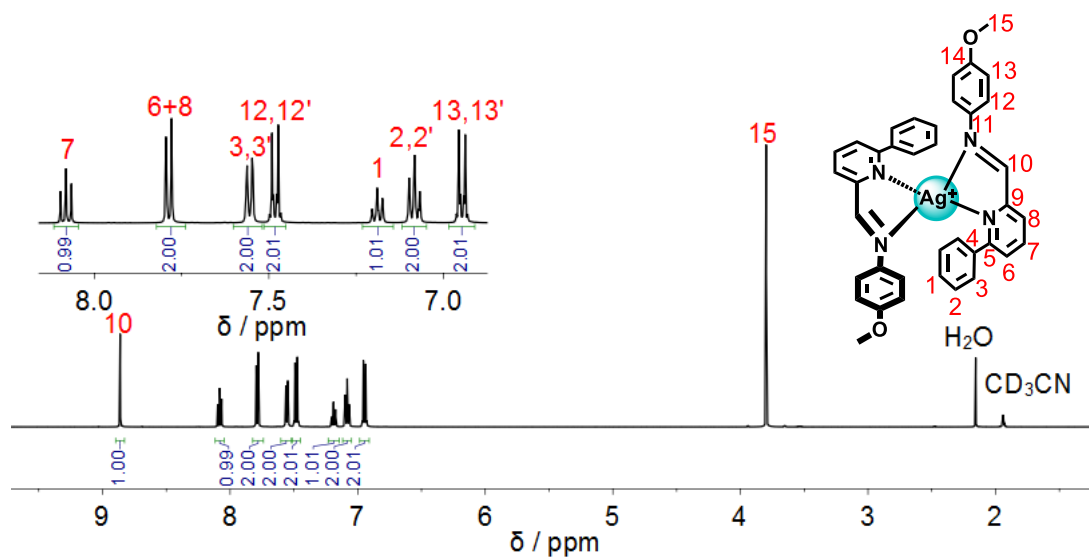


Figure II5. ^1H NMR spectrum of $[\text{Ag}(\text{A1B1})_2]^+$ (125 MHz, 298 K, CD_3CN).

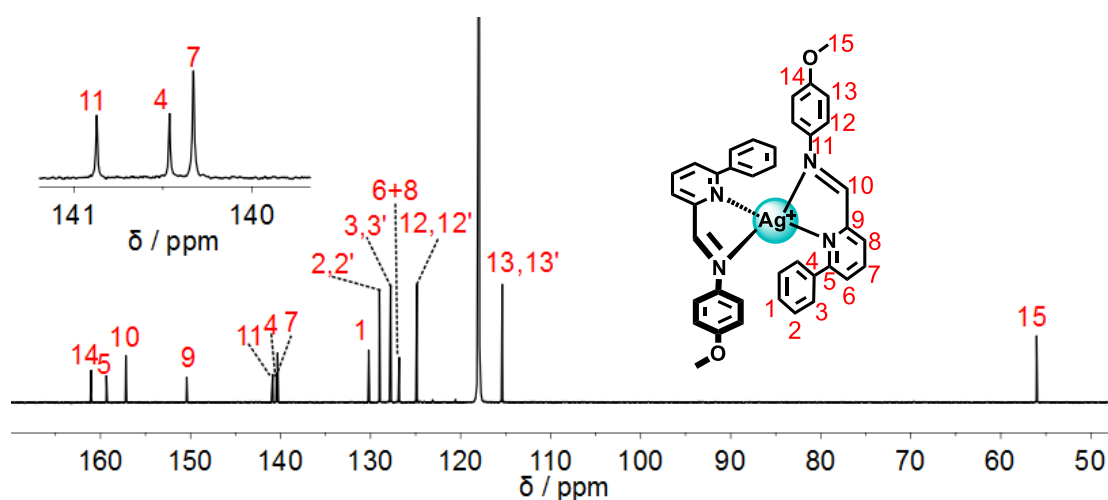


Figure II6. ^{13}C NMR spectrum of $[\text{Ag}(\text{A1B1})_2]^+$ (125 MHz, 298 K, CD_3CN).

$[\text{Zn}(\text{A1B2})_2]^{2+}$: ^1H NMR (500 MHz, CD_3CN): $\delta = 8.08$ (t, $J = 10.0$ Hz, 1H, H^7), 7.92 (t, $J = 8.8, 7.2, 1.8$ Hz, 1H, H^{14}), 7.70 (s, 1H, H^{10}), 7.61 (d, $J = 1.0$ Hz, 1H, H^{16}), 7.58 (d, $J = 1.0$ Hz, 1H, H^8), 7.53 (t, $J = 7.5, 1.3$ Hz, 1H, H^1), 7.37 (d, $J = 1.0$ Hz, 1H, H^6), 7.32 (d, $J = 1.0$ Hz, 1H, H^{13}), 7.15 (m, $J = 8.6, 7.0$ Hz, 2H, $H^{2,2'}$), 6.97 (t, $J = 10.0$ Hz, 1.0 Hz, 1H, H^1), 6.61–6.35 (m, 2H, $H^{3,3'}$), 3.57 (s, 3H, H^{11}); ^{13}C NMR (126 MHz, CD_3CN): δ 161.05 (C^5), 151.92 (C^{12}), 148.53 (C^9), 146.02 (C^{16}), 142.95 (C^{14}), 141.84 (C^7), 139.06 (C^4), 133.22 (C^{10}), 130.51 (C^1), 129.12 ($C^{2,2'}$), 128.23 ($C^{3,3'}$), 128.19 (C^6), 126.42 (C^8), 119.73 (C^{15}), 110.50 (C^{13}), 33.42 (C^{11}); ESI-MS: calculated for $[\text{C}_{36}\text{H}_{32}\text{N}_8 + \text{Zn}]^{2+} [\text{CF}_3\text{SO}_3]^-$ 789.1556, found: 789.1546. $[\text{C}_{36}\text{H}_{32}\text{N}_8 + \text{Zn}]^{2+}$, found: 320.10.

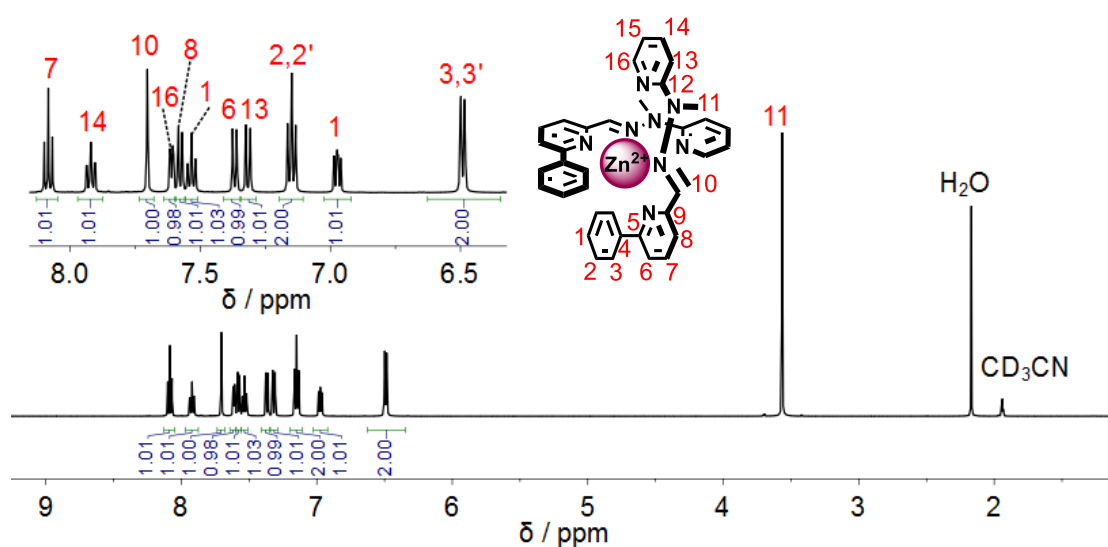


Figure II7. ^1H NMR spectrum of $[\text{Zn}(\text{A1B2})_2]^{2+}$ (125 MHz, 298 K, CD_3CN).

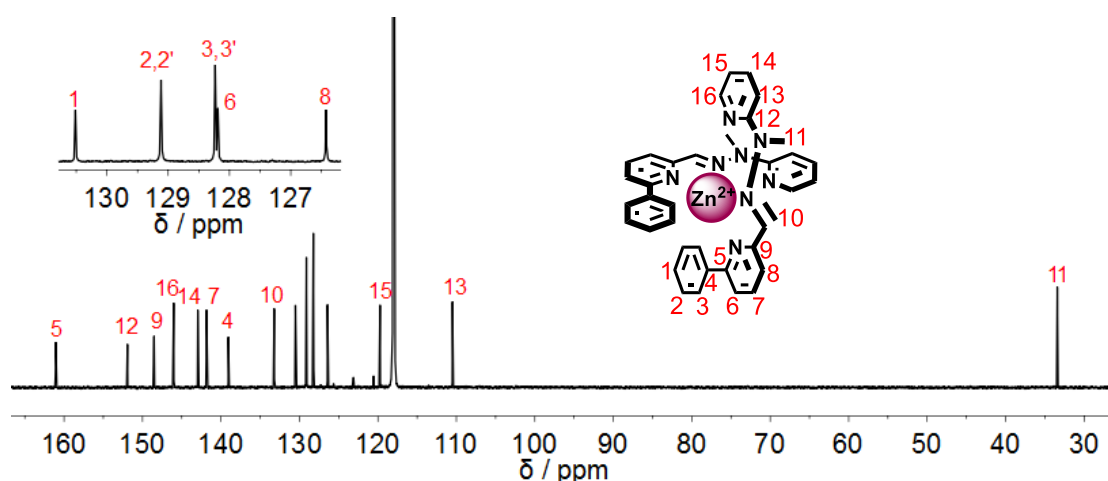


Figure II8. ^{13}C NMR spectrum of $[\text{Zn}(\text{A1B2})_2]^{2+}$ (125 MHz, 298 K, CD_3CN).

$[\text{Ag}(\text{A2B1})_2]^+$: ^1H NMR (500 MHz, CD_3CN): $\delta = 8.97$ (s, 1H, H^7), 8.05 (t, $J = 10.0$ Hz, 1H, H^4), 7.80 (d, $J = 10.0$ Hz, 1H, H^5), 7.60 (d, $J = 10.0$ Hz, 1H, H^3), 7.55–7.45 (m, 2H, $H^{9,9'}$), 6.99–6.86 (m, 2H, $H^{10,10'}$), 3.78 (s, 3H, H^{12}), 2.54 (s, 3H, H^1); ^{13}C NMR (126 MHz, CD_3CN): δ 161.02 (C^{11}), 160.13 (C^2), 156.96 (C^7), 150.17 (C^6), 140.78 (C^8), 140.27 (C^4), 128.41 (C^3), 127.00 (C^5), 124.80 ($C^{9,9'}$), 115.40 ($C^{10,10'}$), 55.98 (C^{12}), 26.47 (C^1). ESI-MS: calculated for $[\text{C}_{28}\text{H}_{28}\text{N}_4\text{O}_2+\text{Ag}]^+$ 559.1258, found: 559.1254.

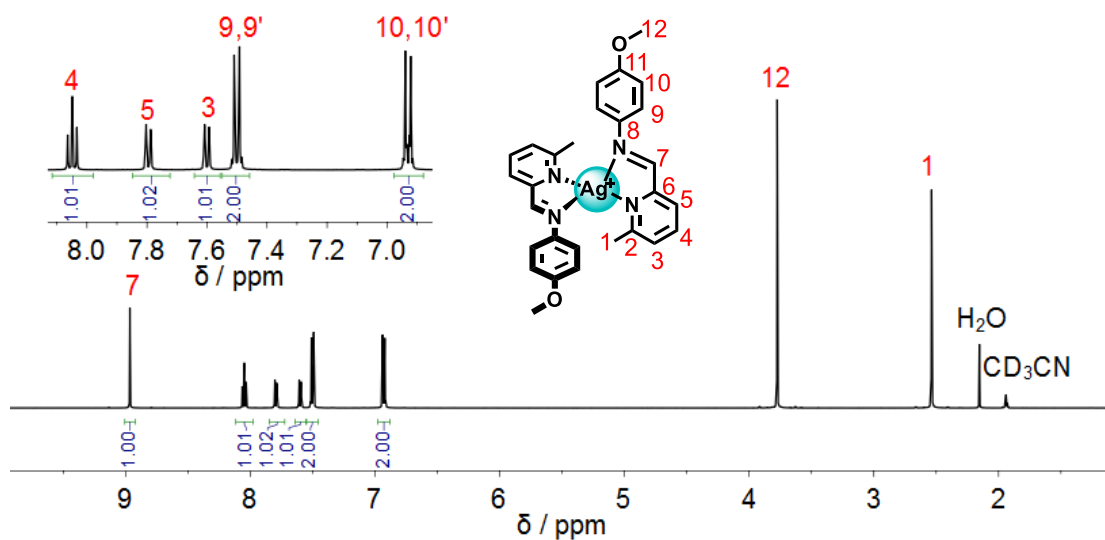


Figure II9. ^1H NMR spectrum of $[\text{Ag}(\text{A2B1})_2]^+$ (125 MHz, 298 K, CD_3CN).

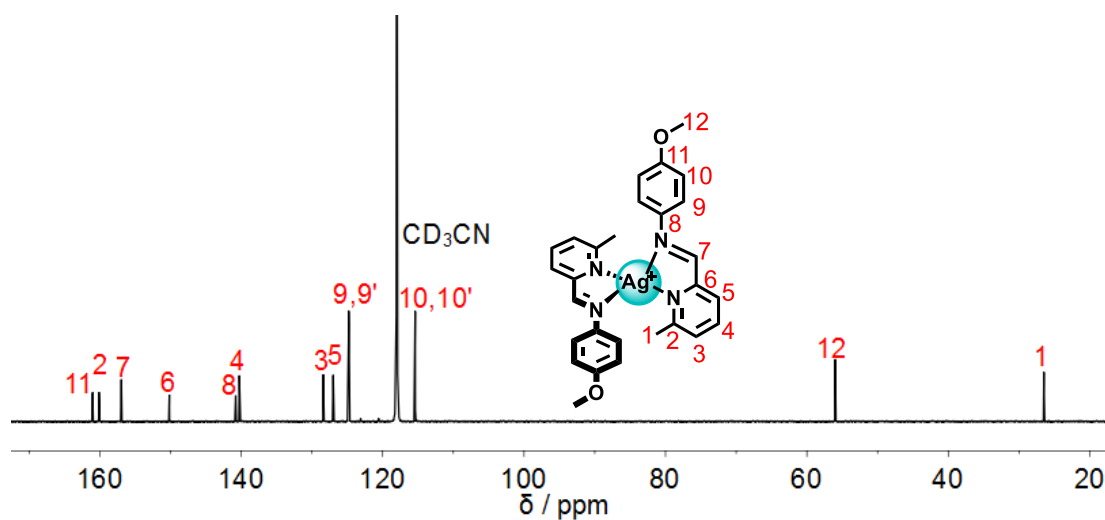


Figure II10. ^{13}C NMR spectrum of $[\text{Ag}(\text{A2B1})_2]^+$ (125 MHz, 298 K, CD_3CN).

$[\text{Ag}(\text{A3B1})_2]^+$: ^1H NMR (500 MHz, CD_3CN): 8.88 (s, 1H, H^6), 8.06–7.90 (m, 2H, H^{4+3}), 7.83–7.81 (d, $J = 10.0$ Hz, 1H, H^2), 7.63–7.48 (m, 2H, $H^{8,8'}$), 7.06–6.91 (m, 2H, $H^{9,9'}$), 3.81 (s, 3H, H^{11}); ^{13}C NMR (126 MHz, CD_3CN): δ 161.24 (C^{10}), 155.80 (C^6), 152.51 (C^1), 143.59 (C^5), 142.28 (C^3), 140.86 (C^7), 132.01 (C^4), 127.27 (C^2), 125.01 ($C^{8,8'}$), 115.45 ($C^{9,9'}$), 56.03 (C^{11}); ESI-MS: calculated for $[\text{C}_{26}\text{H}_{22}\text{Br}_2\text{N}_4\text{O}_2 + \text{Ag}]^+$ 686.9155, found: 686.9153.

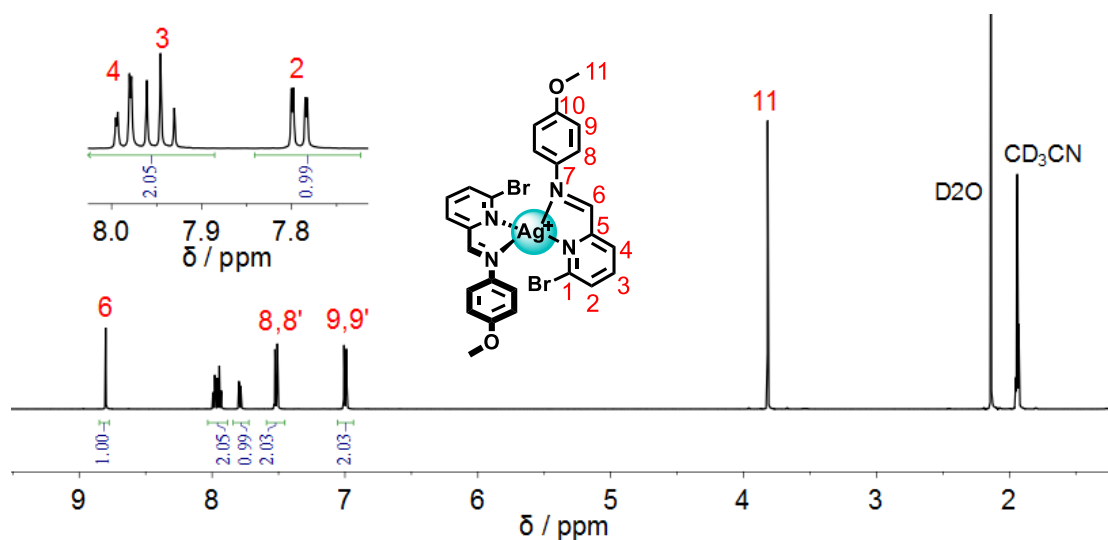


Figure II11. ^1H NMR spectrum of $[\text{Ag}(\text{A3B1})_2]^+$ (125 MHz, 298 K, CD_3CN).

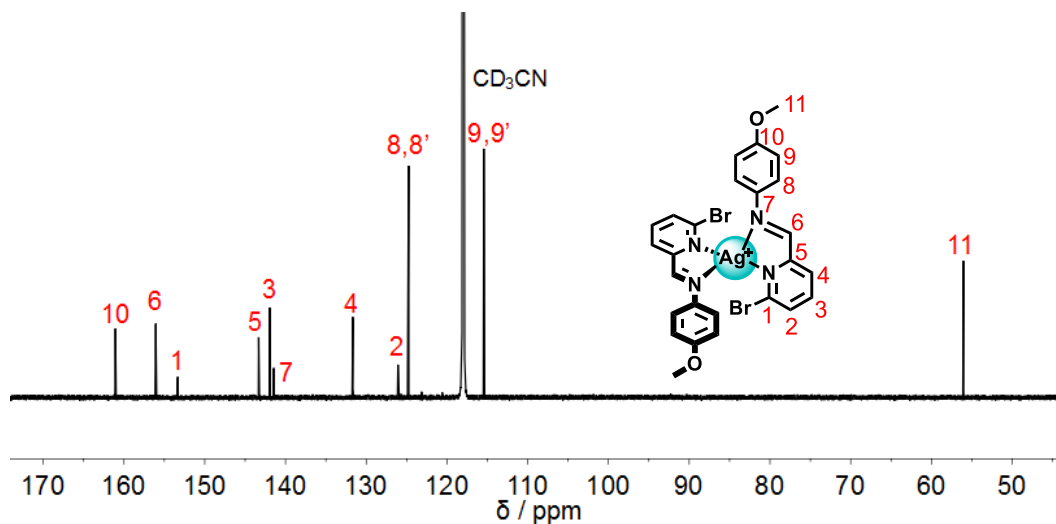


Figure II12. ^{13}C NMR spectrum of $[\text{Ag}(\text{A3B1})_2]^+$ (125 MHz, 298 K, CD_3CN).

$[\text{Zn}(\text{A3B2})_2]^{2+}$: ^1H NMR (500 MHz, CD_3CN): $\delta = 8.41$ (s, 1H, H^6), 8.01 (t, $J = 7.8$ Hz, 1H, H^3), 7.95 (td, $J = 8.2, 1.6$ Hz, 2H, H^{11+4}), 7.67 (d, $J = 5.4, 1.8, 0.8$ Hz, 1H, H^9), 7.64 (d, $J = 7.9, 1.1$ Hz, 1H, H^2), 7.40 (dd, $J = 8.7, 0.9$ Hz, 1H, H^{12}), 7.01 (t, $J = 7.3, 5.4, 0.9$ Hz, 1H, H^{10}), 3.86 (s, 3H, H^7); ^{13}C NMR (126 MHz, CD_3CN): $\delta = 152.51$ (C^8), 150.73 (C^5), 146.01 (C^9), 144.07 (C^3), 143.39 (C^{11}), 143.36 (C^1), 134.29 (C^6), 132.39 (C^2), 126.76 (C^4), 120.07 (C^{10}), 110.93 (C^{12}), 34.32 (C^7); ESI-MS: calculated for $[\text{C}_{24}\text{H}_{22}\text{Br}_2\text{N}_8 + \text{Zn}]^{2+} [\text{CF}_3\text{SO}_3]^-$ 792.9140, found: 792.9130.

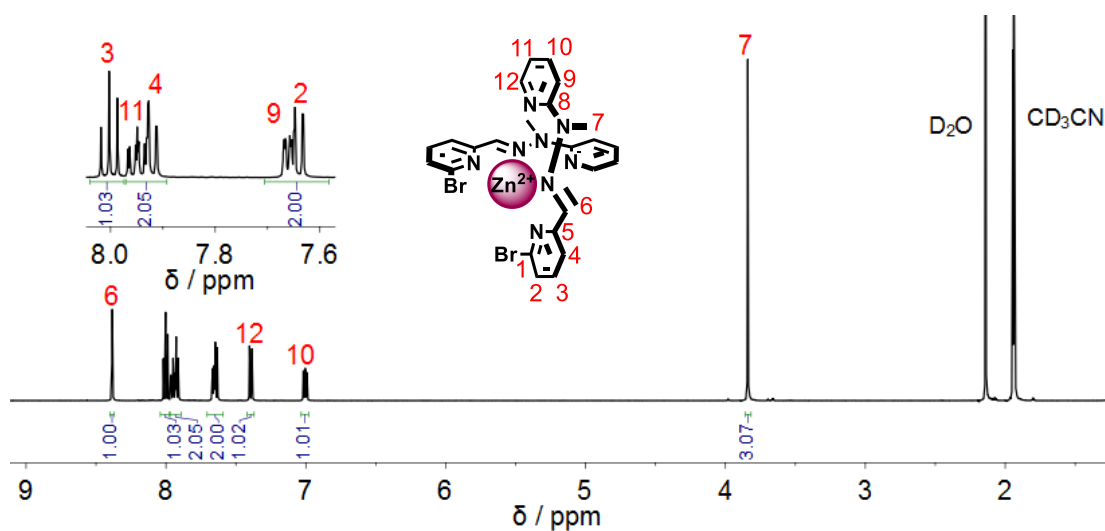


Figure II13. ^1H NMR spectrum of $[\text{Zn}(\text{A3B2})_2]^{2+}$ (125 MHz, 298 K, CD_3CN).

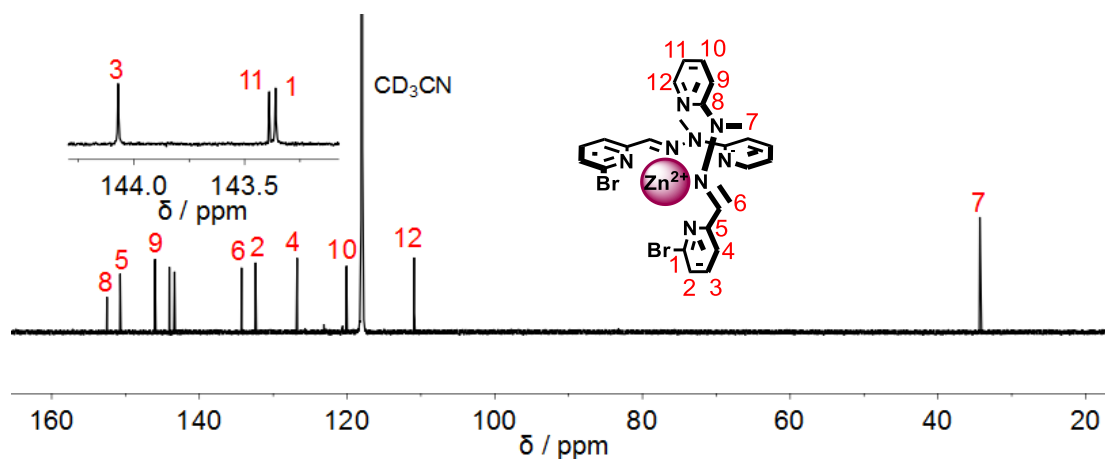


Figure II14. ^{13}C NMR spectrum of $[\text{Zn}(\text{A3B2})_2]^{2+}$ (125 MHz, 298 K, CD_3CN).

B. The kinetic analysis of imine/hydrazone formation in absence and in presence of catalysts



$$\text{at } t = 0 \quad [A_0] = [B_0], [AB_0] = 0$$

$$\text{at any } t \quad [A_t] = [B_t], [AB_t] = [A_0] - [A_t]$$

Integration of second-order rate law yields

$$1/[A_t] = 1/[A_0] + kt, \text{ where the slope is the rate constant}$$

For an irreversible, bimolecular reaction between **Ax** and **By** subject to catalysis by a species **C** (**AxB_y**), the rate of the reaction, *R*, is given by

$$R_u = k_1[\mathbf{Ax}][\mathbf{By}] \text{ for the uncatalysed pathway and}$$

$$R_c = k_1[\mathbf{Ax}][\mathbf{By}] + k_{\text{cat}}[\mathbf{Ax}][\mathbf{By}][\mathbf{C}] \text{ when under catalysis.}$$

Since, by definition, a catalyst is a species which appears in the rate equation but not in the overall reaction, its concentration does not change, *i.e.* it is constant, so that the second equation can be written as

$$R_c = k_1[\mathbf{Ax}][\mathbf{By}] + k_2[\mathbf{Ax}][\mathbf{By}], \text{ where } k_2 = k_{\text{cat}}[\mathbf{C}], \text{ and so}$$

$$R_c = (k_1 + k_2)[\mathbf{Ax}][\mathbf{By}] = k_{\text{obs}}[\mathbf{Ax}][\mathbf{By}], \text{ where } k_{\text{obs}} = (k_1 + k_2).$$

If there is a second catalyst, **D**, which independently of **C**, also affects the reaction rate, then it makes a contribution to the overall reaction rate of $k'_{\text{cat}}[\mathbf{Ax}][\mathbf{By}][\mathbf{D}]$, where again **[D]** must be constant, meaning $k_3 = k'_{\text{cat}}[\mathbf{C}]$, so that now

$$R'_c = (k_1 + k_2 + k_3)[\mathbf{Ax}][\mathbf{By}] = k'_{\text{obs}}[\mathbf{Ax}][\mathbf{By}], \text{ where } k'_{\text{obs}} = (k_1 + k_2 + k_3).$$

Where catalytic effects are large, k_1 may be considered negligible and rate measurements on the catalysed reaction can therefore provide k_2 (and k_3) directly. However, this is not necessarily the case and if, for example, a rate acceleration by a factor of 5 were to be observed under catalysis, then $k_{\text{obs}} = k_1 + k_2 = 5k_1$ and thus $k_2 = 4k_1$.

For a reaction where two catalysts are effective and have been studied separately so that k_2 and k_3 are known, the value of the observed rate constant when both catalysts are present in the reaction mixture should be $k'_{\text{obs}} = (k_1 + k_2 + k_3)$ if there is NO synergy between the catalysts. If there is a positive synergy, then k'_{obs} should be greater than this sum.

In a practical sense, catalyst synergy is a useful phenomenon but whether the simple analysis above can be applied to metal ion and amine catalysis of imine and hydrazone

formation seems unlikely, since its basic premise that the catalyst concentration is constant cannot hold. If, for example, it is assumed that $\text{Zn}(\text{OTf})_2$ dissolves in CH_3CN to give $[\text{Zn}(\text{NCCH}_3)_6]^{2+}$ and that on addition of pyridine-2-aldehyde and anisidine, this extremely labile cation is chelated to a small degree by the aldehyde in a "pre-equilibrium" to give the activated species with carbonyl-O bound to Zn(II) which then undergoes rate-determining nucleophilic attack by the amine to give an addition product that very rapidly undergoes elimination to the imine, I, then the rate of the reaction would be given by $R_t = k[\text{aldehyde chelate}][\text{amine}] = kK_{\text{eq}}[\text{aldehyde}][\text{Zn}(\text{NCCH}_3)_6^{2+}][\text{amine}]$, where K_{eq} is the equilibrium constant for the preliminary complexation of the aldehyde. This is a rate law of the form $R = k[\mathbf{Ax}][\mathbf{By}][\mathbf{C}]$ given above where $\mathbf{C} = [\text{Zn}(\text{NCCH}_3)_6]^{2+}$ remains at an essentially constant concentration provided the chelation equilibrium is very unfavorable, so that the observed kinetics would be that of a simple second-order reaction. Note that the Zn(II) could also coordinate the amine but this would be less extensive than that of the aldehyde (since there is no chelation) and in any case would inhibit reaction because the bound amine is not nucleophilic. A real complication arises from the fact that the product imine is a good chelating agent, so that, as seen by NMR spectroscopy, the Zn(II) is ultimately bound to this ligand and not to CH_3CN . Whether or not $[\text{Zn}(\text{imine})(\text{CH}_3\text{CN})_2]^{2+}$ (which presumably would form during the early stages of the reaction where the zinc concentration would be much greater than that of the imine) or $[\text{Zn}(\text{imine})_2]^{2+}$ could bind and activate the aldehyde and therefore act as catalysts themselves, the catalyst concentration must vary and at most it might be argued that the rate law $R = k[\mathbf{Ax}][\mathbf{By}][\mathbf{C}]$ could provide an approximate treatment of the initial stages of reaction.

For easy comparison of the initial rate constant, the corresponding rate constants were calculated from a fit to a second-order reaction rate equation ($1/[A_t] = 1/[A_0] + kt$) over the initial 10% of the product (t_{10}). In some cases, it was calculated from integration of the first ^1H NMR spectrum as the yield of the product is already above 10%.

i. The kinetics of imine formation in the absence of presence of metal salts

1) Kinetics of **A1 + B1** in absence of metal salts

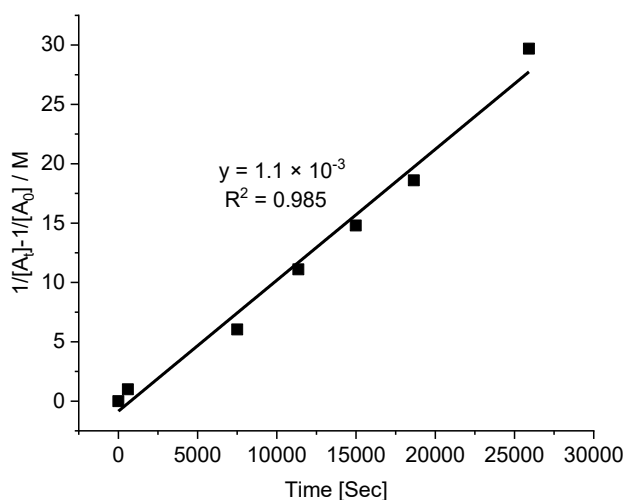


Figure II15. Representative linear least-squares fit ($1/[A]_t - 1/[A]_0$ vs. t) of the imine **A1B1** formation from **A1 + B1** (10 mM each) in CD_3CN at $25^\circ C$ over about 10% of the imine **A1B1** formation. The slope of the fit corresponds to the second order rate constant; R^2 values shown.

2) Kinetics of **A1 + B1** in presence of AgOTf

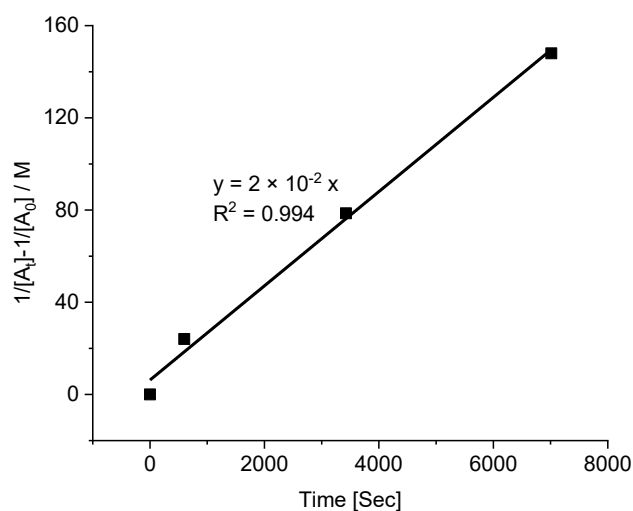


Figure II16. Representative linear least-squares fit ($1/[A]_t - 1/[A]_0$ vs. t) of the silver complex of imine $[Ag(A1B1)]_2^+$ formation from **A1 + B1** (10 mM each) + 0.5 equiv. Ag (5 mM) in CD_3CN at $25^\circ C$ over about 10% of the silver complex of imine $[Ag(A1B1)]_2^+$ formation. The slope of the fit corresponds to the second order rate constant; R^2 values shown.

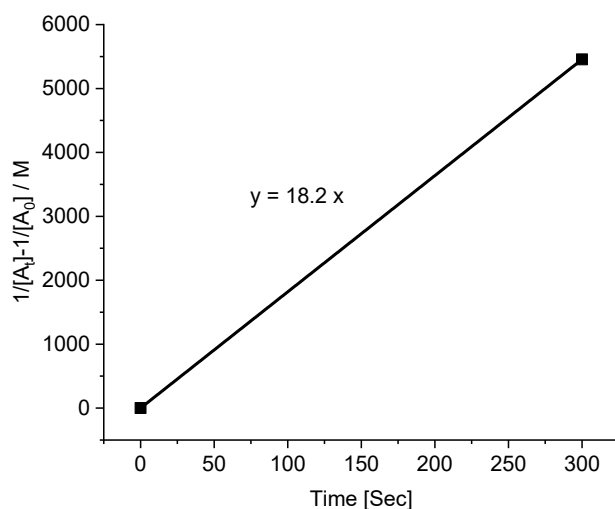
3) Kinetics of **A1 + B1** in presence of $\text{Zn}(\text{OTf})_2$ 

Figure II17. Representative linear least-squares fit ($1/[A]_t - 1/[A]_0$ vs. t) of zinc complex of imine $[\text{Zn}(\text{A1B1})_2]^{2+}$ formation from **A1 + B1** (10 mM each) + 0.5 equiv. of $\text{Zn}(\text{OTf})_2$ (5 mM) in CD_3CN at 25°C over the first ^1H NMR spectrum was obtained. The slope of the fit corresponds to the second order rate constant. **NOTE:** The reaction of **A1 + B1** in presence of 0.5 equiv. $\text{Zn}(\text{OTf})_2$ is already complete within 5 minutes (the time to insert the tube, lock, shim and run the acquisition), the rate constant ($k \geq 18.2 \text{ M}^{-1}\text{s}^{-1}$) is the lowest value, which is calculated from the first ^1H NMR spectrum obtained.

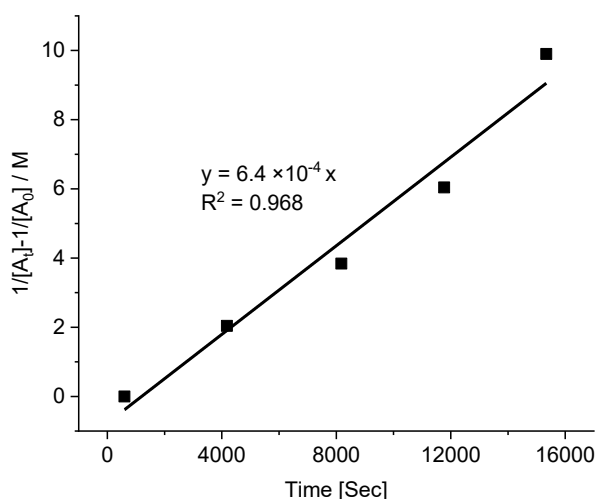
4) Kinetics of **A2 + B1** in absence of metal salts

Figure II18. Representative linear least-squares fit ($1/[A]_t - 1/[A]_0$ vs. t) of the imine **A2B1** formation from **A2 + B1** (10 mM each) in CD_3CN at 25°C over about 10% of the imine **A2B1** formation. The slope of the fit corresponds to the second order rate constant; R^2 values shown.

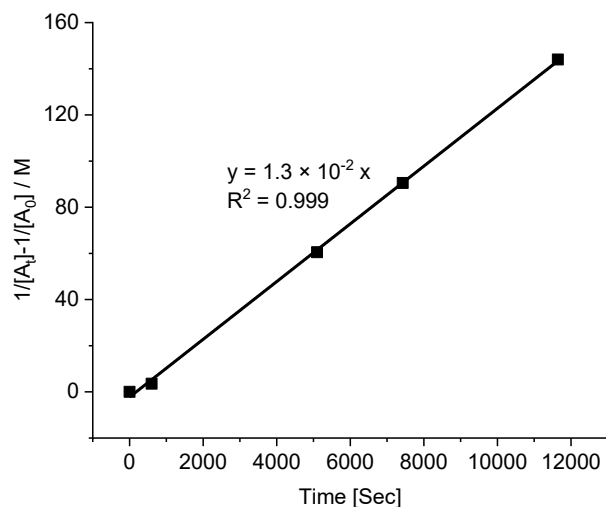
5) Kinetics of **A3 + B1** in absence of metal salts

Figure II19. Representative linear least-squares fit ($1/[A]_t - 1/[A]_0$ vs. t) of the imine formation **A3B1** from **A3** and **B1** in CD_3CN at $25^\circ C$ over about 10% of the imine **A3B1** formation. The slope of the fit corresponds to the second order rate constant; R^2 values shown.

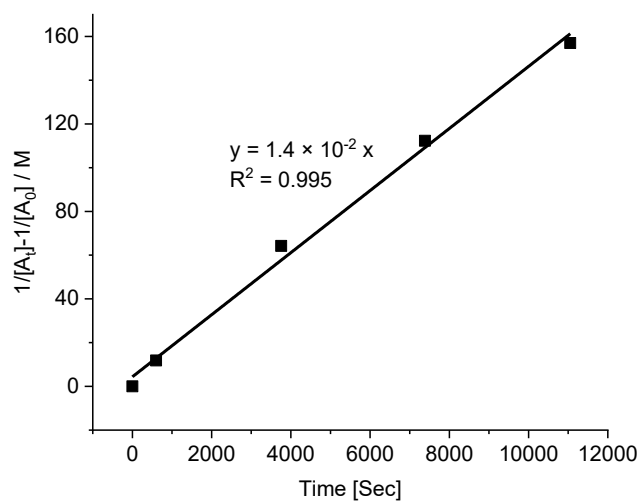
6) Kinetics of **A2 + B1** in presence of AgOTf

Figure II20. Representative linear least-squares fit ($1/[A]_t - 1/[A]_0$ vs. t) of the silver complex of imine $[Ag(A2B1)]_2^+$ formation from **A2 + B1 + 0.5 equiv. AgOTf** in CD_3CN at $25^\circ C$ over about 10% of the silver complex of imine $[Ag(A2B1)]_2^+$ formation. The slope of the fit corresponds to the second order rate constant; R^2 values shown.

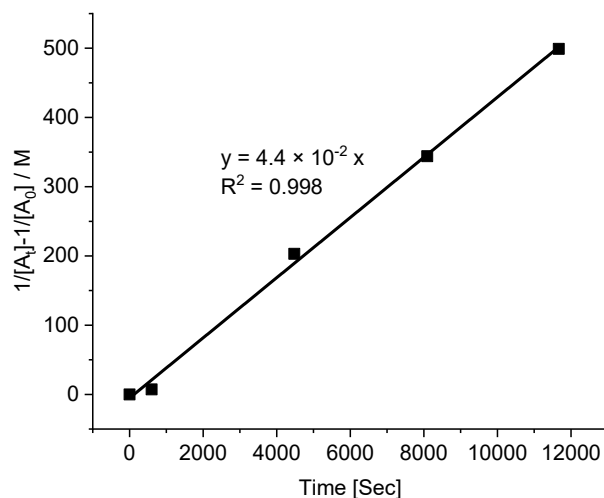
7) Kinetics of **A3 + B1** in presence of AgOTf

Figure II21. Representative linear least-squares fit ($1/[A]_t - 1/[A]_0$ vs. t) of the silver complex of imine $[Ag(A3B1)]_2^+$ formation from **A3 + B1** (10 mM each) + 0.5 equiv AgOTf (5 mM) in CD_3CN at $25^\circ C$ over about 10% of the silver complex of imine $[Ag(A3B1)]_2^+$ formation. The slope of the fit corresponds to the second order rate constant; R^2 values shown.

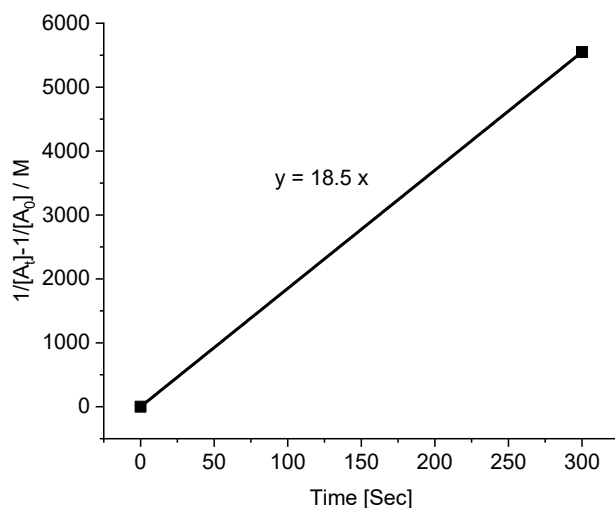
8) Kinetics of **A2 + B1** in presence of $Zn(OTf)_2$ 

Figure II22. Representative linear least-squares fit ($1/[A]_t - 1/[A]_0$ vs. t) of the zinc complex of imine formation from **A2 + B1** (10 mM each) + 0.5 equiv. of $Zn(OTf)_2$ (5 mM) in CD_3CN at $25^\circ C$ over the first 1H NMR spectrum was obtained. The slope of the fit corresponds to the second order rate constant. **NOTE:** The reaction of **A2 + B1** in presence of 0.5 equiv. $Zn(OTf)_2$ is already complete within 5 minutes (the time to insert the tube, lock, shim and run the acquisition), the rate constant ($k \geq 18.5 M^{-1}s^{-1}$) is the lowest value, which is calculated from the first 1H NMR spectrum obtained.

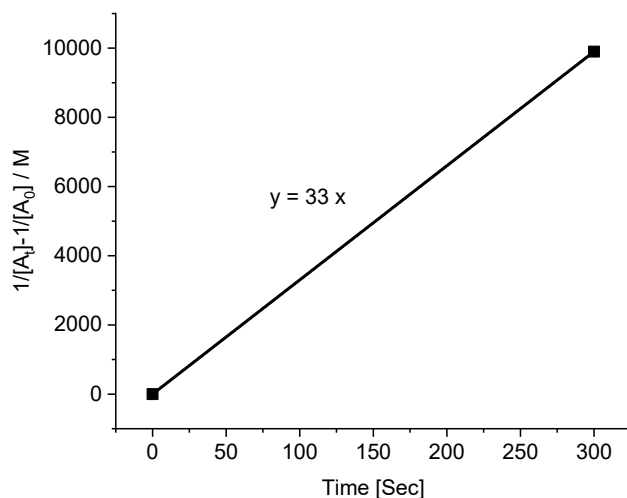
9) Kinetics of **A3** + **B1** in presence of $\text{Zn}(\text{OTf})_2$ 

Figure II23. Representative linear least-squares fit ($1/[A]_t - 1/[A]_0$ vs. t) of the zinc complex of imine $[\text{Zn}(\text{A3B1})]_2^{2+}$ formation from **A3** + **B1** (10 mM each) + 0.5 equiv. of $\text{Zn}(\text{OTf})_2$ (5 mM) in CD_3CN at 25°C over the first ^1H NMR spectrum was obtained. The slope of the fit corresponds to the second order rate constant. **NOTE:** The reaction of **A3** + **B1** in presence of 0.5 equiv. $\text{Zn}(\text{OTf})_2$ is already complete within 5 minutes (the time to insert the tube, lock, shim and run the acquisition), the rate constant ($k \geq 33 \text{ M}^{-1}\text{s}^{-1}$) is the lowest value, which is calculated from the first ^1H NMR spectrum obtained.

ii. **The kinetics of hydrazone formation in the absence and presence of metal salts**

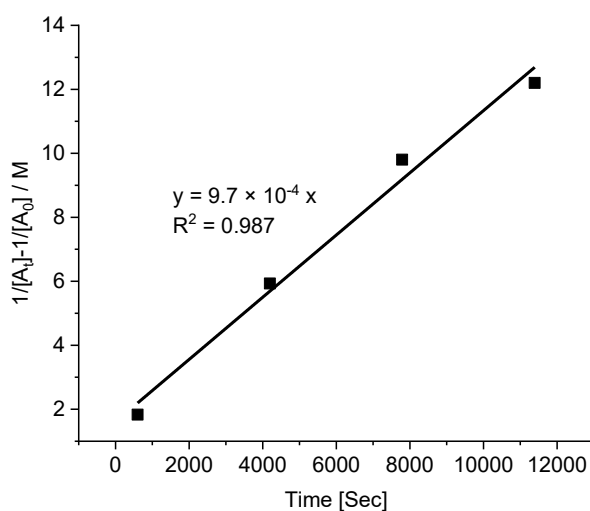
1) Kinetics of **A1** + **B2** in absence of metal salts

Figure II24. Representative linear least-squares fit ($1/[A]_t - 1/[A]_0$ vs. t) of the hydrazone **A1B2** formation from **A1** + **B2** (10 mM each) in CD_3CN at 25°C over about 10% of the hydrazone **A1B2** formation. The slope of the fit corresponds to the second order rate constant; R^2 values shown.

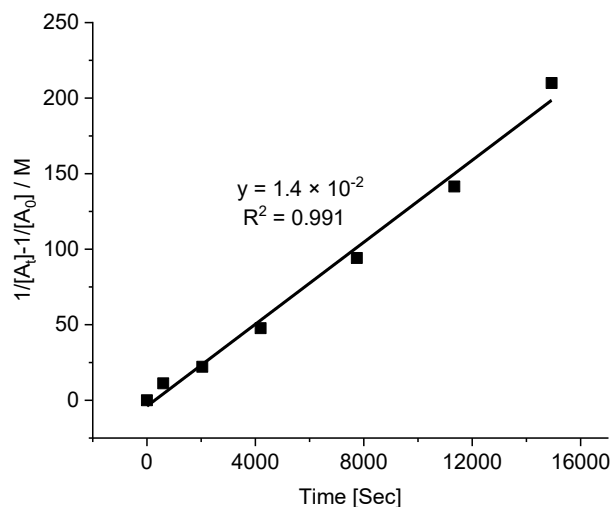
2) Kinetics of **A1** + **B2** in presence of AgOTf

Figure II25. Representative linear least-squares fit ($1/[A]_t - 1/[A]_0$ vs. t) of the silver complex of hydrazone $[Ag(A1B2)_2]^{2+}$ formation from **A1** + **B2** (10 mM each) + 0.5 equiv. of AgOTf (5 mM) in CD_3CN at 25°C over about 10% of the silver complex of hydrazone $[Ag(A1B2)_2]^{2+}$ formation. The slope of the fit corresponds to the second order rate constant; R^2 values shown.

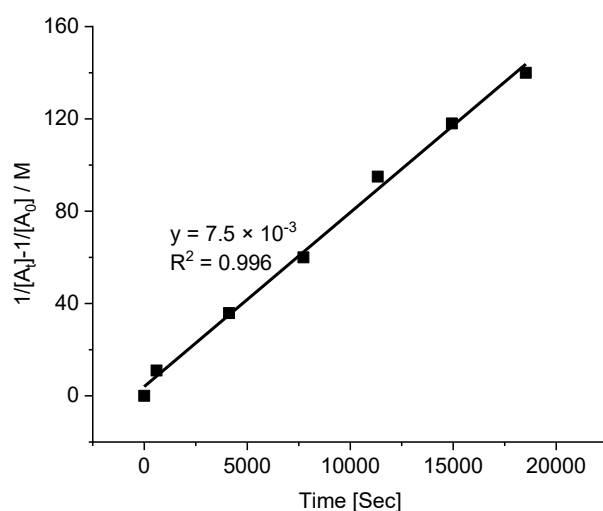
3) Kinetics of **A1** + **B2** in presence of $Zn(OTf)_2$ 

Figure II26. Representative linear least-squares fit ($1/[A]_t - 1/[A]_0$ vs. t) of the zinc complex of hydrazone $[Zn(A1B2)_2]^{2+}$ formation from (10 mM each) + 0.5 equiv. of $Zn(OTf)_2$ (5 mM) in CD_3CN at 25°C over about 10% of the zinc complex of hydrazone $[Zn(A1B2)_2]^{2+}$ formation. The slope of the fit corresponds to the second order rate constant; R^2 values shown.

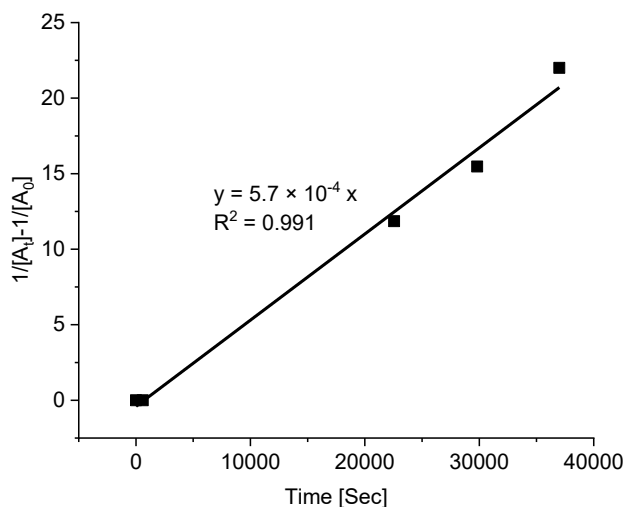
4) Kinetics of **A2 + B2** in absence of metal salts

Figure II27. Representative linear least-squares fit ($1/[A]_t - 1/[A]_0$ vs. t) of the hydrazone **A2B2** formation from **A2 + B2** (10 mM each) in CD_3CN at $25^\circ C$ over about 10% of the hydrazone **A2B2** formation. The slope of the fit corresponds to the second order rate constant; R^2 values shown.

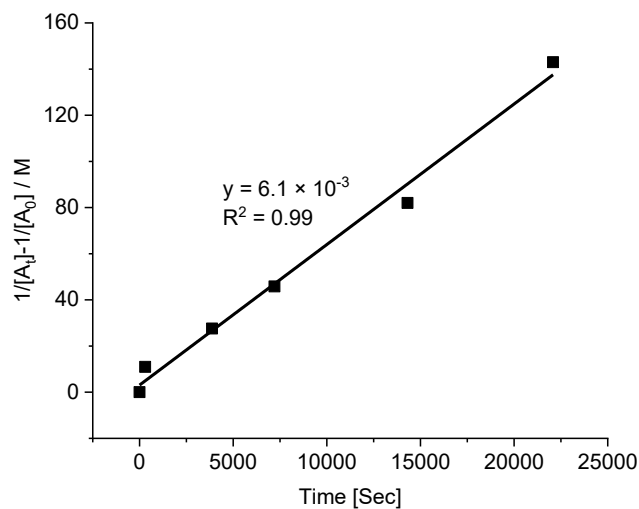
5) Kinetics of **A3 + B2** in absence of metal salts

Figure II28. Representative linear least-squares fit ($1/[A]_t - 1/[A]_0$ vs. t) of the hydrazone **A3B2** formation from **A3 + B2** (10 mM each) in CD_3CN at $25^\circ C$ over about 10% of the hydrazone **A3B2** formation. The slope of the fit corresponds to the second order rate constant; R^2 values shown.

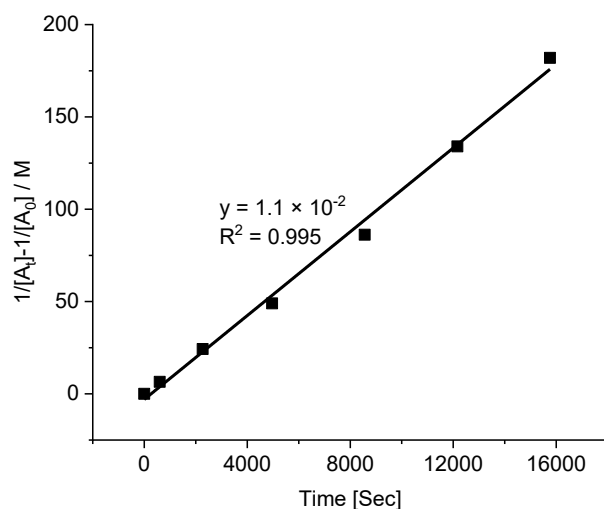
6) Kinetics of **A2 + B2** in presence of AgOTf

Figure II29. Representative linear least-squares fit ($1/[A]_t - 1/[A]_0$ vs. t) of the silver complex of hydrazone $[\text{Ag}(\mathbf{A2B2})_2]^+$ formation from **A2 + B2** (10 mM each) + 0.5 equiv. of AgOTf (5 mM) in CD_3CN at 25°C over about 10% of the silver complex of hydrazone $[\text{Ag}(\mathbf{A2B2})_2]^+$ formation. The slope of the fit corresponds to the second order rate constant; R^2 values shown.

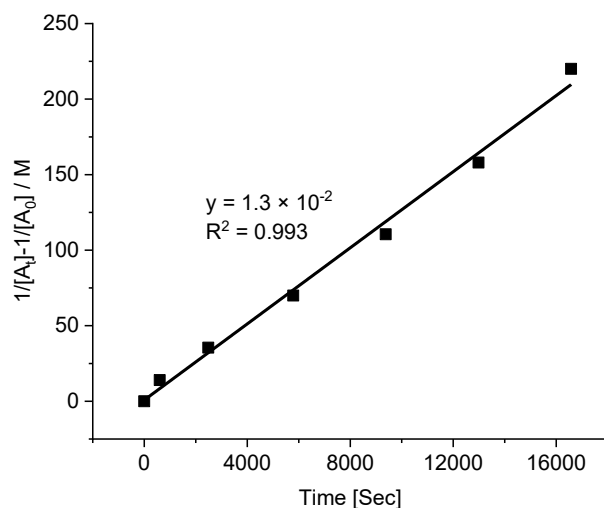
7) Kinetics of **A3 + B2** in presence of AgOTf

Figure II30. Representative linear least-squares fit ($1/[A]_t - 1/[A]_0$ vs. t) of the silver complex of hydrazone $[\text{Ag}(\mathbf{A3B2})_2]^+$ formation from **A3 + B2** (10 mM each) + 0.5 equiv. of AgOTf (5 mM) in CD_3CN at 25°C over about 10% of the silver complex of hydrazone $[\text{Ag}(\mathbf{A3B2})_2]^+$ formation. The slope of the fit corresponds to the second order rate constant; R^2 values shown.

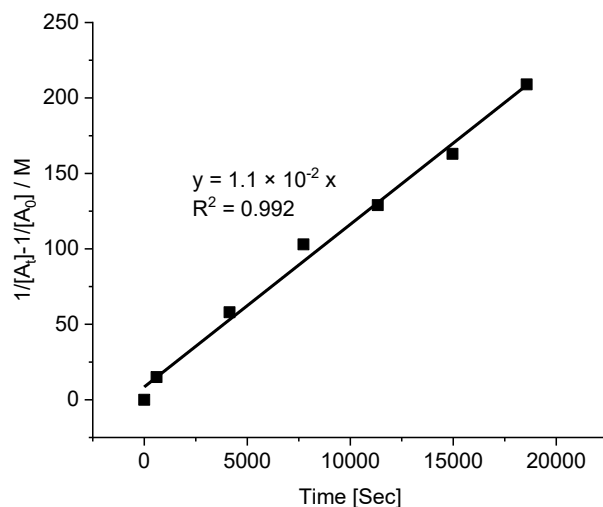
8) Kinetics of **A2 + B2** in presence of $\text{Zn}(\text{OTf})_2$ 

Figure II31. Representative linear least-squares fit ($1/[A]_t - 1/[A]_0$ vs. t) of the zinc complex of hydrazone $[\text{Zn}(\mathbf{A2B2})_2]^{2+}$ formation from **A2 + B2** (10 mM each) + 0.5 equiv. of $\text{Zn}(\text{OTf})_2$ (5 mM) in CD_3CN at 25°C over about 10% of the zinc complex of hydrazone $[\text{Zn}(\mathbf{A2B2})_2]^{2+}$ formation. The slope of the fit corresponds to the second order rate constant; R^2 values shown.

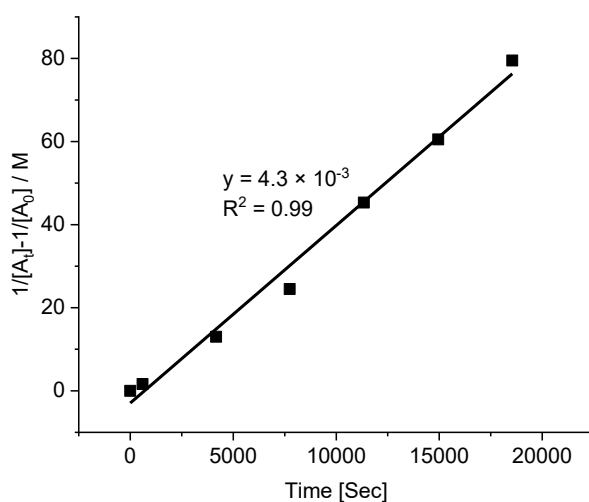
9) Kinetics of **A3 + B2** in presence of $\text{Zn}(\text{OTf})_2$ 

Figure II32. Representative linear least-squares fit ($1/[A]_t - 1/[A]_0$ vs. t) of the zinc complex of hydrazone $[\text{Zn}(\mathbf{A3B2})_2]^{2+}$ formation from **A3 + B2** (10 mM each) + 0.5 equiv. of $\text{Zn}(\text{OTf})_2$ (5 mM) in CD_3CN at 25°C over about 10% of the zinc complex of hydrazone $[\text{Zn}(\mathbf{A3B2})_2]^{2+}$ formation. The slope of the fit corresponds to the second order rate constant; R^2 values shown.

C. Kinetics of A1+B2 in the presence of B1 or metal ion [Ag(I) or Zn(II)] as well as both B1 and metal ion as co-catalysts.

1) Kinetics of A1 + B2 in presence of B1

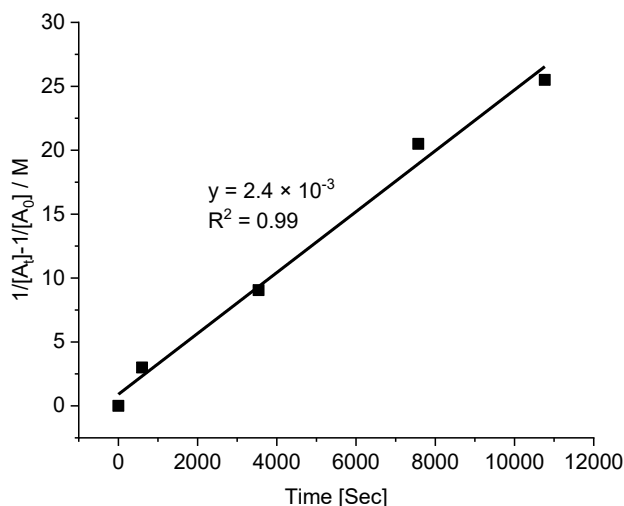


Figure II33. Representative linear least-squares fit ($1/[A]_t - 1/[A]_0$ vs. t) of the hydrazone **A1B2** formation from **A1 + B2 + B1** (10 mM each) in CD_3CN at $25^\circ C$ over about 10% of the hydrazone **A1B2** formation. The slope of the fit corresponds to the second order rate constant; R^2 values shown.

2) Kinetics of A1 + B2 in presence of both B1 and AgOTf

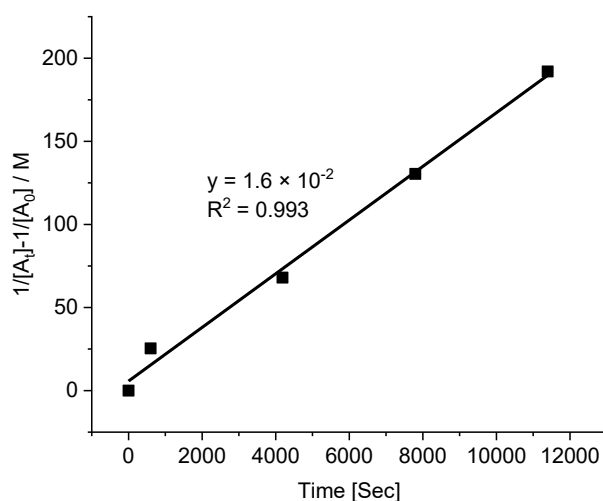


Figure II34. Representative linear least-squares fit ($1/[A]_t - 1/[A]_0$ vs. t) of the hydrazone-based silver complex $[Ag(A1B2)_2]^+$ formation from **A1 + B2 + B1** (10 mM each) + 0.5 equiv. AgOTf (5 mM) in CD_3CN at $25^\circ C$ over about 10% of the silver complex of hydrazone $[Ag(A1B2)_2]^+$ formation. The slope of the fit corresponds to the second order rate constant; R^2 values shown.

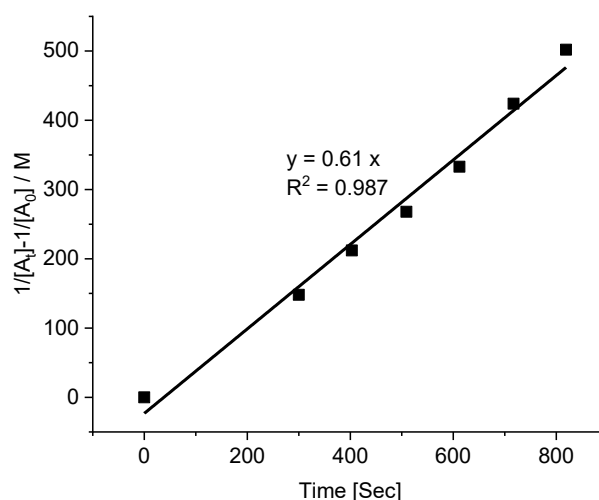
3) Kinetics of **A1 + B2** in presence of both **B1** and $\text{Zn}(\text{OTf})_2$ a) $\text{A1} + \text{B2} + \text{B1} + 0.5 \text{ equiv. Zn}(\text{OTf})_2$ 

Figure II35. Representative linear least-squares fit ($1/[A]_t - 1/[A]_0$ vs. t) of the hydrazone-based zinc complex $[\text{Zn}(\text{A1B2})_2]^{2+}$ formation from **A1 + B2 + B1** (10 mM each) + $\text{Zn}(\text{OTf})_2$ (5 mM each) in CD_3CN at 25°C over about 10% of the zinc complex of hydrazone $[\text{Zn}(\text{A1B2})_2]^{2+}$ formation. The slope of the fit corresponds to the second order rate constant; R^2 values shown.

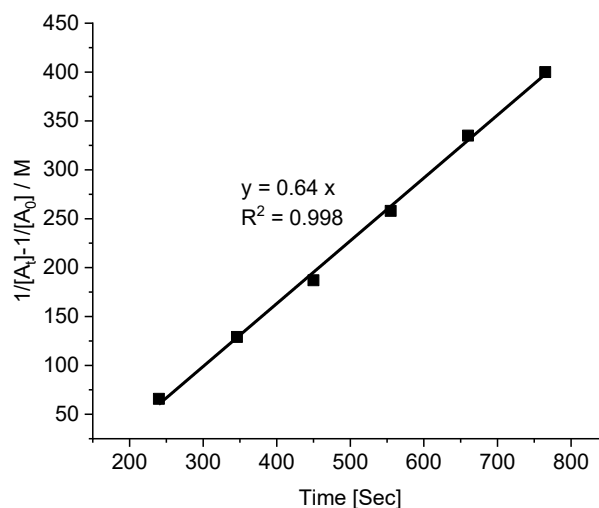
b) $[\text{Zn}(\text{A1B1})_2]^{2+} + \text{B2}$ 

Figure II36. Representative linear least-squares fit ($1/[A]_t - 1/[A]_0$ vs. t) of the zinc complex of hydrazone $[\text{Zn}(\text{A1B2})_2]^{2+}$ formation from $[\text{Zn}(\text{A1B1})_2]^{2+} + \text{B2}$ in CD_3CN at 25°C over about 10% of the zinc complex of hydrazone $[\text{Zn}(\text{A1B2})_2]^{2+}$ formation. The final solution is 10 mM. The slope of the fit corresponds to the second order rate constant; R^2 values shown.

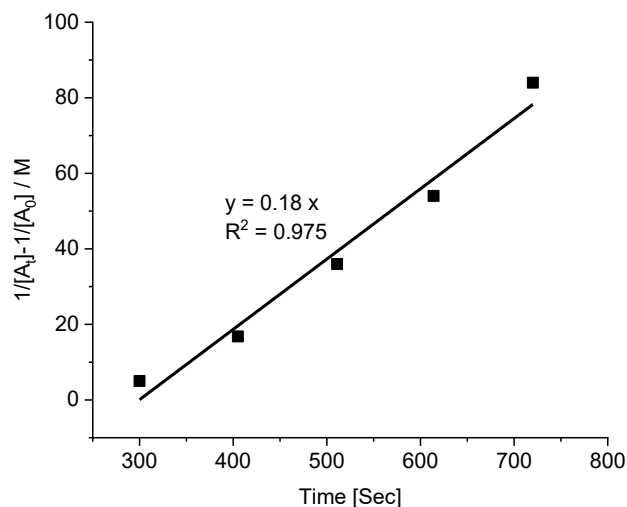
b) $[\text{Zn}(\text{A1B1})_2]^{2+} + \text{B2}$ 

Figure II37. Representative linear least-squares fit ($1/[A]_t - 1/[A]_0$ vs. t) of the zinc complex of hydrazone $[\text{Zn}(\text{A1B2})_2]^{2+}$ formation from $[\text{Zn}(\text{B2})_2]^{2+} + \text{A1} + \text{B1}$ in CD_3CN at 25°C over about 10% of the zinc complex of hydrazone $[\text{Zn}(\text{A1B2})_2]^{2+}$ formation. The slope of the fit corresponds to the second order rate constant; R^2 values shown.

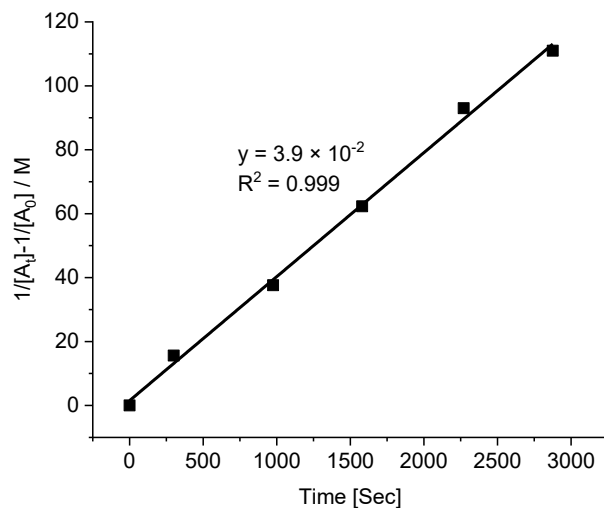
c) $\text{A1B1} + \text{B2}$ 

Figure II38. Representative linear least-squares fit ($1/[A]_t - 1/[A]_0$ vs. t) of the hydrazone **A1B2** formation from **A1B1** + **B2** (10 mM each) in CD_3CN at 25°C over about 10% of the hydrazone **A1B2** formation. The slope of the fit corresponds to the second order rate constant; R^2 values shown.

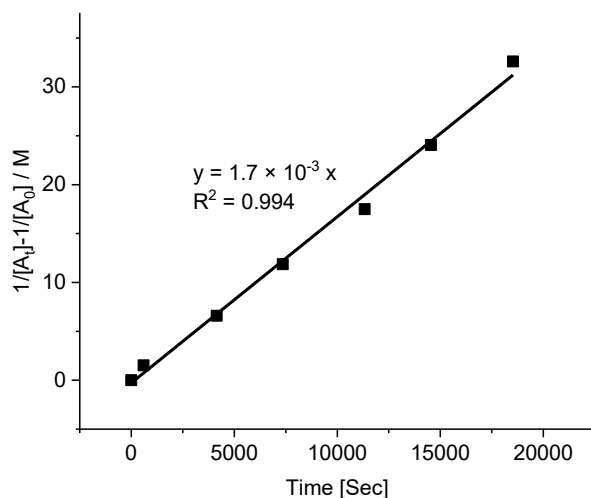
4) Kinetics of **A2 + B2** in presence of **B1**

Figure II39. Representative linear least-squares fit ($1/[A]_t - 1/[A]_0$ vs. t) of the hydrazone **A2B2** formation from **A2 + B2 + B1** (10 mM each) in CD_3CN at $25^\circ C$ over about 10% of the hydrazone **A2B2** formation. The slope of the fit corresponds to the second order rate constant; R^2 values shown.

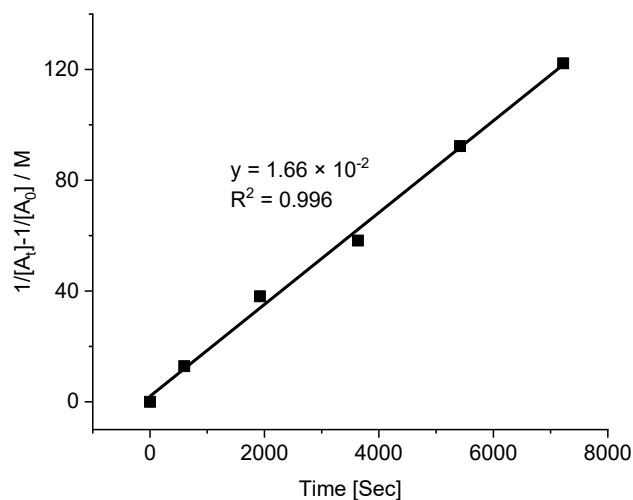
5) Kinetics of **A3 + B2** in presence of **B1**

Figure II40. Representative linear least-squares fit ($1/[A]_t - 1/[A]_0$ vs. t) of the hydrazone **A3B2** formation from **A3 + B2 + B1** (10 mM each) in CD_3CN at $25^\circ C$ over about 10% of the hydrazone **A3B2** formation. The slope of the fit corresponds to the second order rate constant; R^2 values shown.

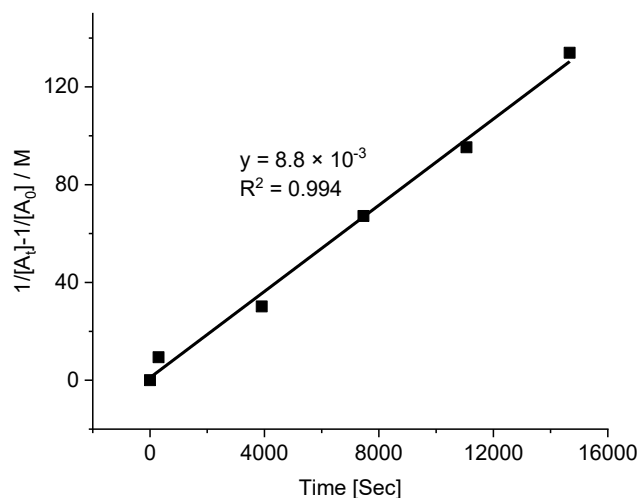
6) Kinetics of **A2 + B2** in presence of both **B1** and AgOTf

Figure II41. Representative linear least-squares fit ($1/[A]_t - 1/[A]_0$ vs. t) of the silver complex of hydrazone $[\text{Ag}(\mathbf{A2B2})_2]^+$ formation from $\mathbf{A2} + \mathbf{B2} + \mathbf{B1}$ (10 mM each) + 0.5 equiv. AgOTf (5 mM) in CD_3CN at 25°C over about 10% of the silver complex of hydrazone $[\text{Ag}(\mathbf{A2B2})_2]^+$ formation. The slope of the fit corresponds to the second order rate constant; R^2 values shown.

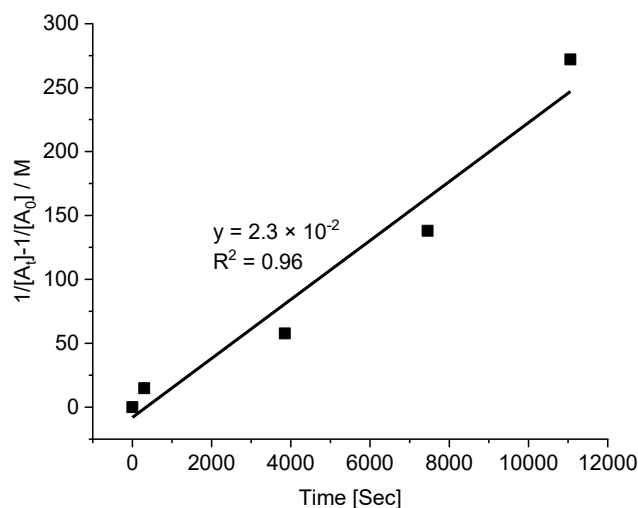
7) Kinetics of **A3 + B2** in presence of both **B1** and AgOTf

Figure II42. Representative linear least-squares fit ($1/[A]_t - 1/[A]_0$ vs. t) of the silver complex of hydrazone $[\text{Ag}(\mathbf{A3B2})_2]^+$ formation from $\mathbf{A3} + \mathbf{B2} + \mathbf{B1}$ (10 mM each) + AgOTf (5 mM) in CD_3CN at 25°C over about 10% of the silver complex of hydrazone $[\text{Ag}(\mathbf{A3B2})_2]^+$ formation. The slope of the fit corresponds to the second order rate constant; R^2 values shown.

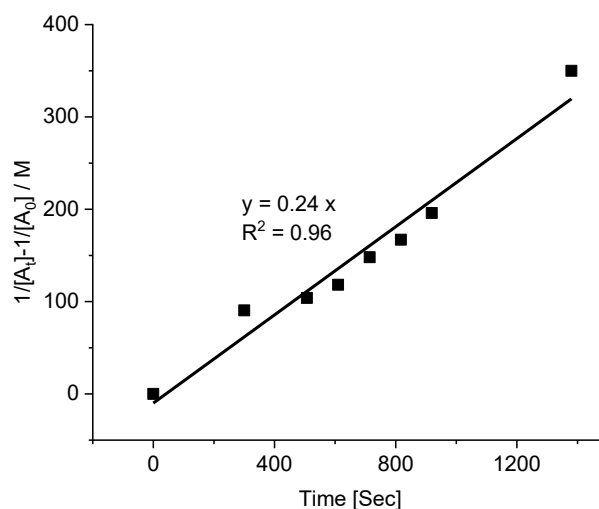
8) Kinetics of **A2** + **B2** in presence of both **B1** and $\text{Zn}(\text{OTf})_2$ 

Figure II43. Representative linear least-squares fit ($1/[A]_t - 1/[A]_0$ vs. t) of the zinc complex of hydrazone $[\text{Zn}(\text{A2B2})_2]^{2+}$ formation from **A2** + **B2** + **B1** (10 mM each) + $\text{Zn}(\text{OTf})_2$ (5 mM) in CD_3CN at 25°C over about 10% of the zinc complex of hydrazone $[\text{Zn}(\text{A2B2})_2]^{2+}$ formation. The slope of the fit corresponds to the second order rate constant; R^2 value shown.

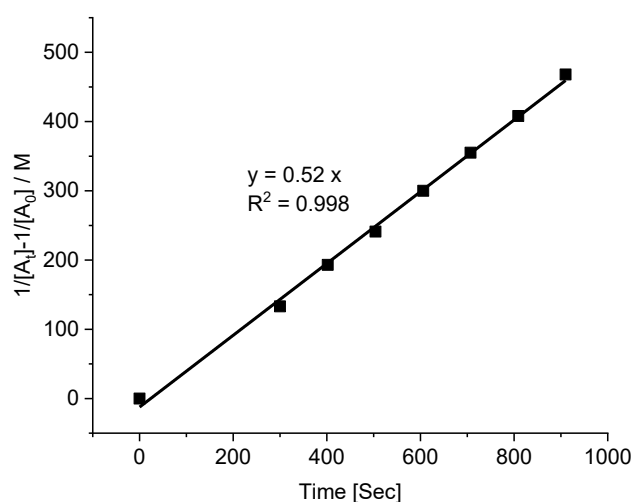
9) Kinetics of **A3** + **B2** in presence of both **B1** and $\text{Zn}(\text{OTf})_2$ 

Figure II44. Representative linear least-squares fit ($1/[A]_t - 1/[A]_0$ vs. t) of the zinc complex of hydrazone $[\text{Zn}(\text{A3B2})_2]^{2+}$ formation from **A3** + **B2** + **B1** (10 mM each) + $\text{Zn}(\text{OTf})_2$ (5 mM) in CD_3CN at 25°C over about 10% of the zinc complex of hydrazone $[\text{Zn}(\text{A3B2})_2]^{2+}$ formation. The slope of the fit corresponds to the second order rate constant; R^2 values shown.

D. Catalysis of imine and hydrazone formation by metal salts and acid

1) Kinetics of **A1** + **B1** in presence of 0.05 equiv. of AgOTf

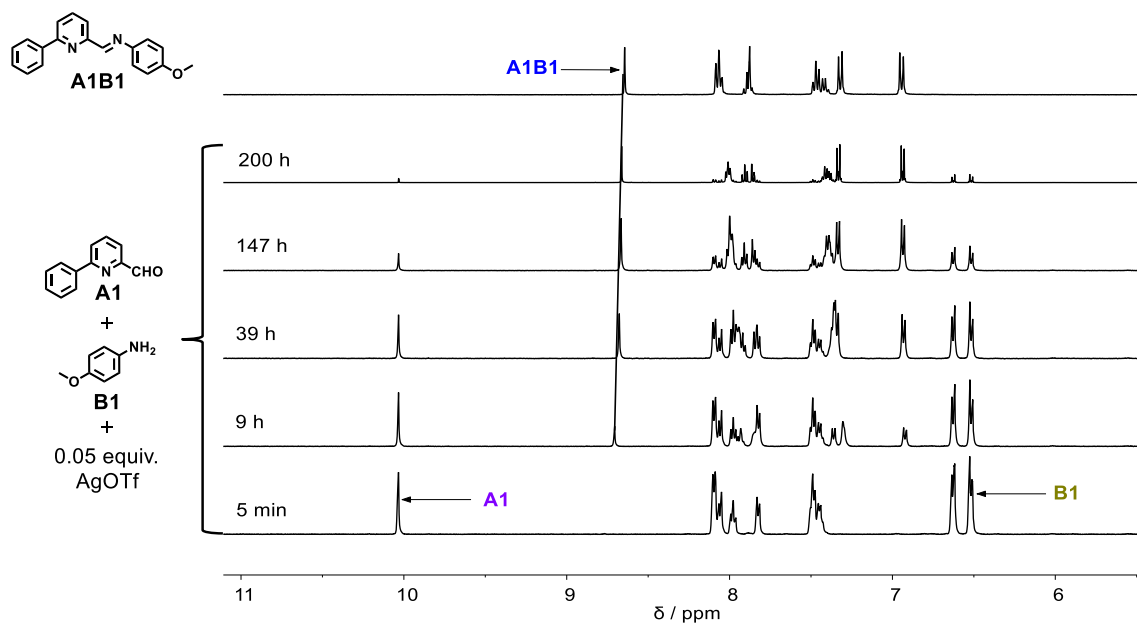


Figure II45. ^1H NMR (500 MHz) spectra of the mixture generated from equal amounts of **A1** + **B1** (10 mM each) + 0.05 equiv. AgOTf (0.5 mM) in CD_3CN at 25°C after 5 min, 9 h, 39 h, 147 h, 200 h from bottom to top. Reference spectrum (top one trace) of the separately prepared constituent **A1B1**.

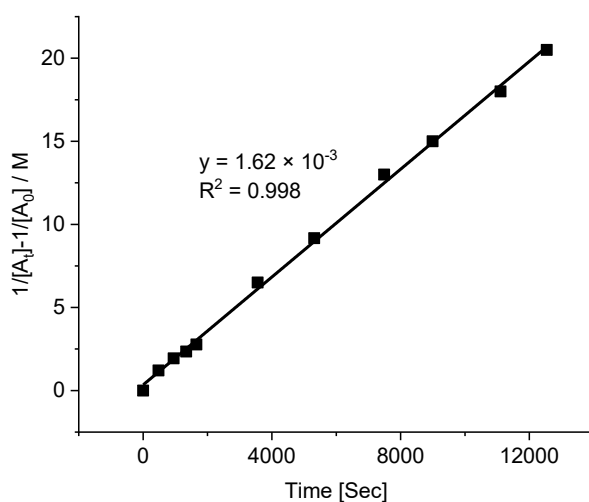


Figure II46. Representative linear least-squares fit ($1/[\text{A}]_t - 1/[\text{A}]_0$ vs. t) of the imine **A1B1** formation from **A1** + **B1** (10 mM each) + 0.05 equiv. AgOTf (0.5 mM) in CD_3CN at 25°C over about 10% of the imine **A1B1** formation. The slope of the fit corresponds to the second order rate constant; R^2 values shown.

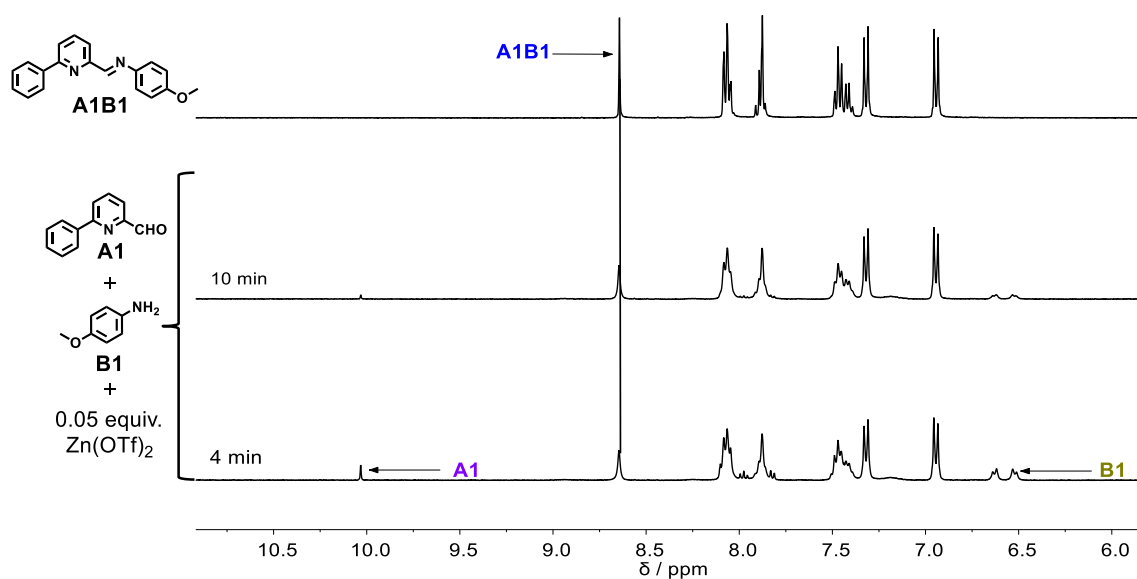
2) Kinetics of **A1** + **B1** in presence of 0.05 equiv. of Zn(OTf)₂

Figure II47. ¹H NMR (500 MHz) spectra of the mixture generated from equal amounts of **A1** + **B1** (10 mM each) + 0.05 equiv. Zn(OTf)₂ (0.5 mM) in CD₃CN at 25°C after 4 min, 10 min from bottom to top. Reference spectrum (top one trace) of the separately prepared constituent **A1B1**.

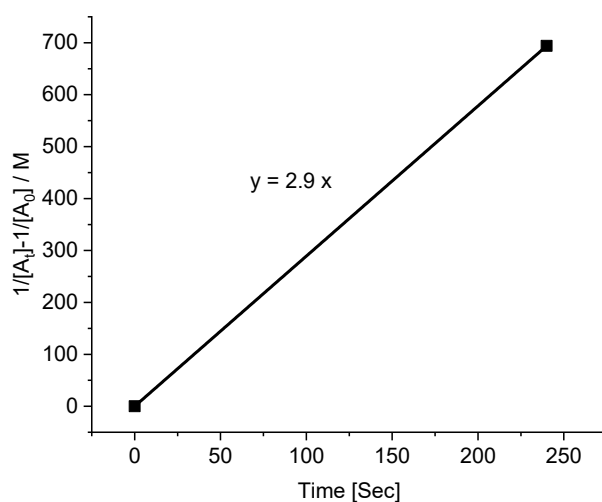


Figure II48. Representative linear least-squares fit ($1/[A]_t - 1/[A]_0$ vs. t) of the imine **A1B1** formation from **A1** + **B1** (10 mM each) + 0.05 equiv. Zn(OTf)₂ (0.5 mM) in CD₃CN at 25°C over the first ¹H NMR spectrum was obtained. The final solution is 10 mM. The slope of the fit corresponds to the second order rate constant; R² values shown. **NOTE: The reaction of **A1** + **B1** in presence of 0.05 equiv. Zn(II) is almost finished within 4 minutes, the rate constant ($k \geq 2.9 \text{ M}^{-1}\text{s}^{-1}$) is the lowest value, which is calculated from the first ¹H NMR spectrum obtained.**

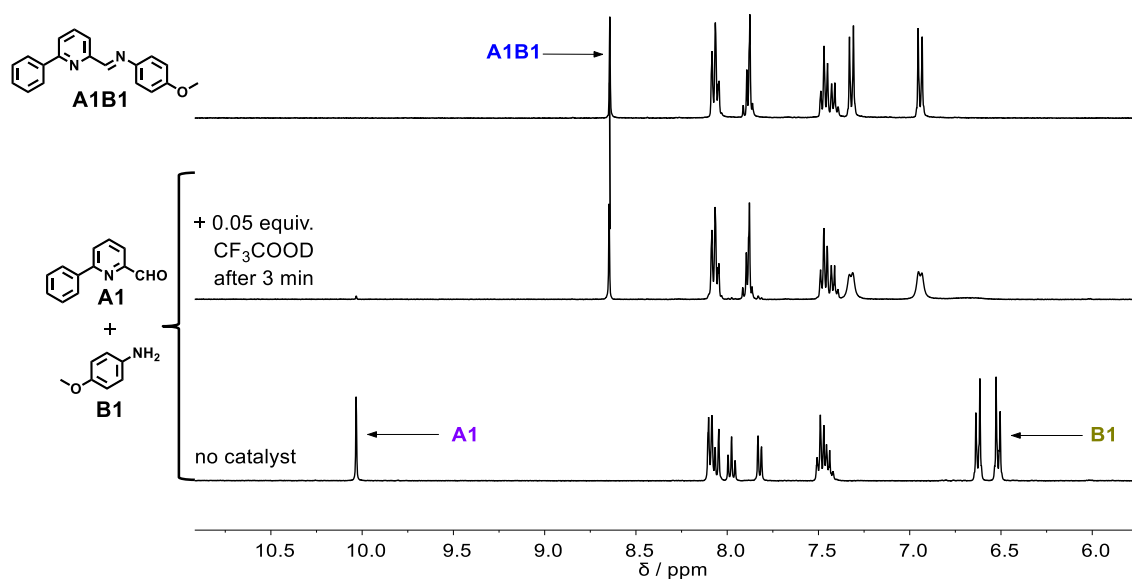
3) Kinetics of **A1** + **B1** in presence of 0.05 equiv. of CF_3COOD 

Figure II49. ^1H NMR (500 MHz) spectra of the mixture generated from equal amounts of **A1** + **B1** (10 mM each) before and after addition of 0.5 equiv. CF_3COOD (0.5 mM) in CD_3CN at 25°C for 3 min from bottom to top. Reference spectrum (top one trace) of the separately prepared constituent **A1B1**.

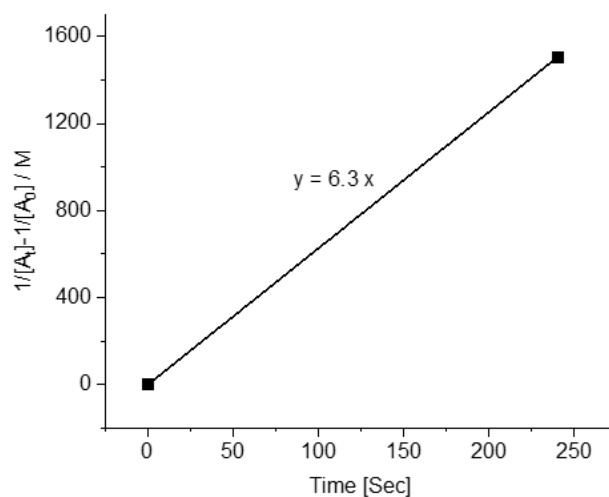


Figure II50. Representative linear least-squares fit ($1/[\text{A}]_t - 1/[\text{A}]_0$ vs. t) of the imine **A1B1** formation from **A1** + **B1** (10 mM each) + 0.05 equiv. CF_3COOD (0.5 mM) in CD_3CN at 25°C over the first ^1H NMR spectrum was obtained. The slope of the fit corresponds to the second order rate constant; R^2 values shown. **NOTE:** The reaction of **A1** + **B1** in presence of 0.05 equiv. CF_3COOD is already finished in 3 minutes, the rate constant ($k \geq 6.3 \text{ M}^{-1}\text{s}^{-1}$) is the lowest value, which is calculated from the first ^1H NMR spectrum obtained.

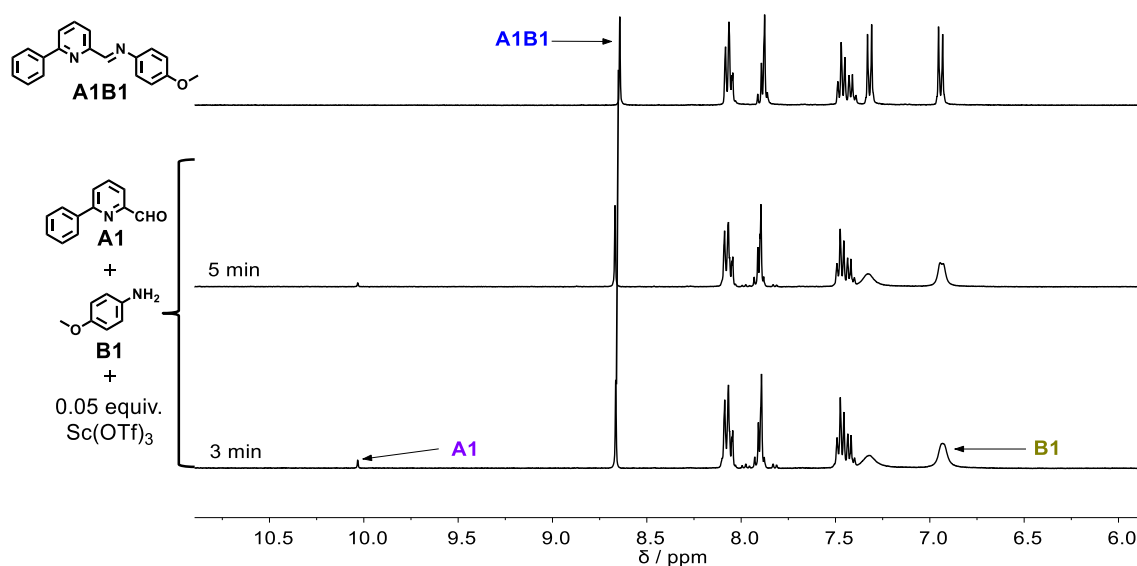
4) Kinetics of **A1** + **B1** in presence of 0.05 equiv. of $\text{Sc}(\text{OTf})_3$ 

Figure II51. ^1H NMR (500 MHz) spectra of the mixture generated from equal amounts of **A1** + **B1** (10 mM each) + 0.05 equiv. $\text{Sc}(\text{OTf})_3$ (0.5 mM) in CD_3CN , 25°C after 3 min, 5 min from bottom to top. Reference spectrum (top one trace) of the separately prepared constituent **A1B1**.

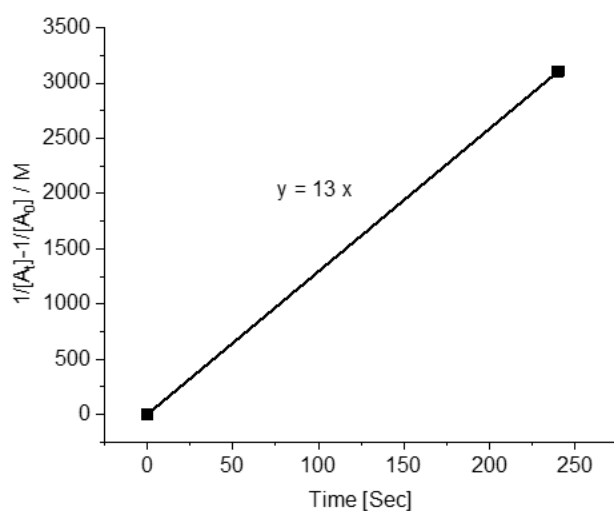


Figure II52. Representative linear least-squares fit ($1/[\text{A}]_t - 1/[\text{A}]_0$ vs. t) of the imine **A1B1** formation from **A1** + **B1** (10 mM each) + 0.05 equiv. $\text{Sc}(\text{OTf})_3$ (0.5 mM) in CD_3CN , 25°C over the first ^1H NMR spectrum was obtained. The slope of the fit corresponds to the second order rate constant; R^2 values shown. **NOTE:** The reaction of **A1** + **B1** in presence of 0.05 equiv. $\text{Sc}(\text{III})$ is already finished in 3 minutes, the rate constant ($k \geq 13 \text{ M}^{-1} \text{ s}^{-1}$) is the lowest value, which is calculated from the first ^1H NMR spectrum obtained.

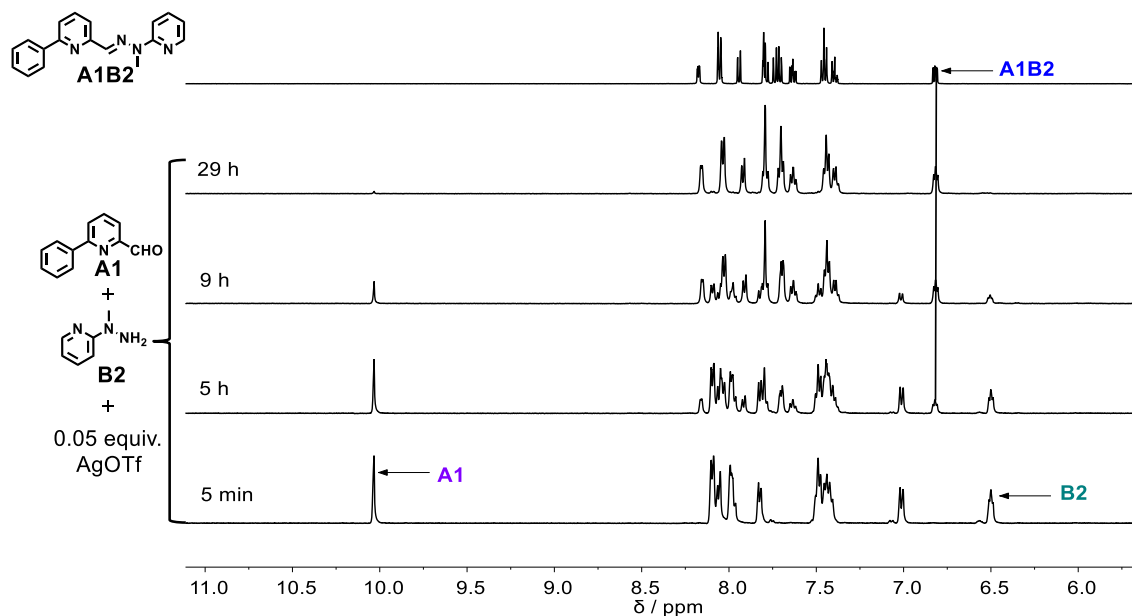
5) Kinetics of **A1** + **B2** in presence of 0.05 equiv. of AgOTf

Figure II53. ¹H NMR (500 MHz) spectra of the mixture generated from equal amounts of **A1** + **B2** (10 mM each) + 0.5 equiv. AgOTf (0.5 mM) in CD₃CN at 25°C after 5 min, 5 h, 9 h, 29 h from bottom to top. Reference spectrum (top one trace) of the separately prepared constituent **A1B2**.

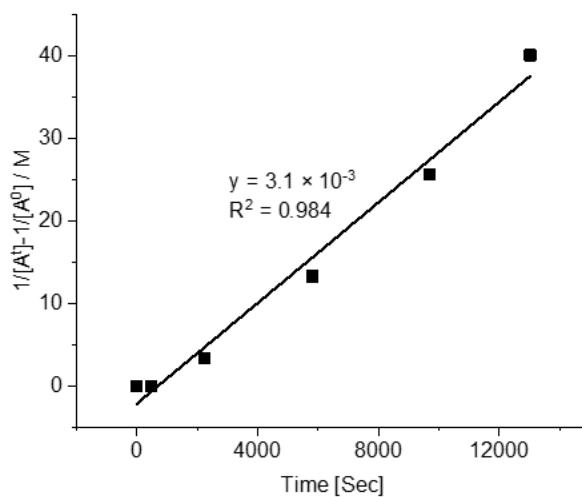


Figure II54. Representative linear least-squares fit ($1/[A]_t - 1/[A]_0$ vs. t) of the hydrazone **A1B2** formation from **A1** + **B2** (10 mM each) + 0.5 equiv. AgOTf (0.5 mM) in CD₃CN at 25°C over about 10% of the hydrazone **A1B2** formation. The slope of the fit corresponds to the second order rate constant; R^2 values shown.

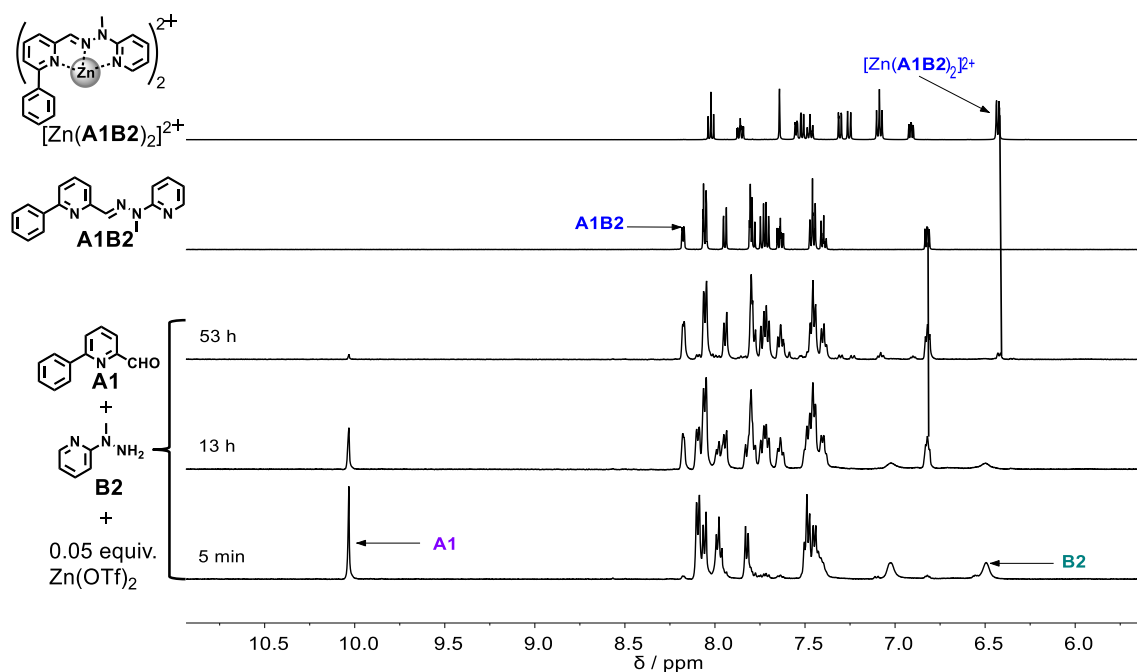
6) Kinetics of **A1** + **B2** in presence of 0.05 equiv. of $\text{Zn}(\text{OTf})_2$ 

Figure II55. ^1H NMR (500 MHz) spectra of the mixture generated from equal amounts of **A1** + **B2** (10 mM each) + 0.5 equiv. $\text{Zn}(\text{OTf})_2$ (0.5 mM) in CD_3CN at 25°C after 5 min, 13 h, 53 h from bottom to top. Reference spectra (top two traces) of the separately prepared constituents **A1B2**, $[\text{Zn}(\text{A1B2})_2]^{2+}$.

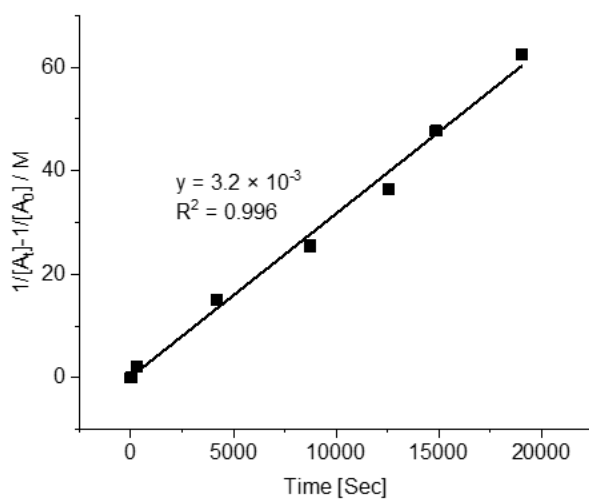


Figure II56. Representative linear least-squares fit ($1/[\text{A}]_t - 1/[\text{A}]_0$ vs. t) of the zinc complex of hydrazone **A1B2** formation from **A1** + **B2** (10 mM each) + 0.5 equiv. $\text{Zn}(\text{OTf})_2$ (0.5 mM) in CD_3CN at 25°C over about 10% of the hydrazone **A1B2** formation. The slope of the fit corresponds to the second order rate constant; R^2 values shown.

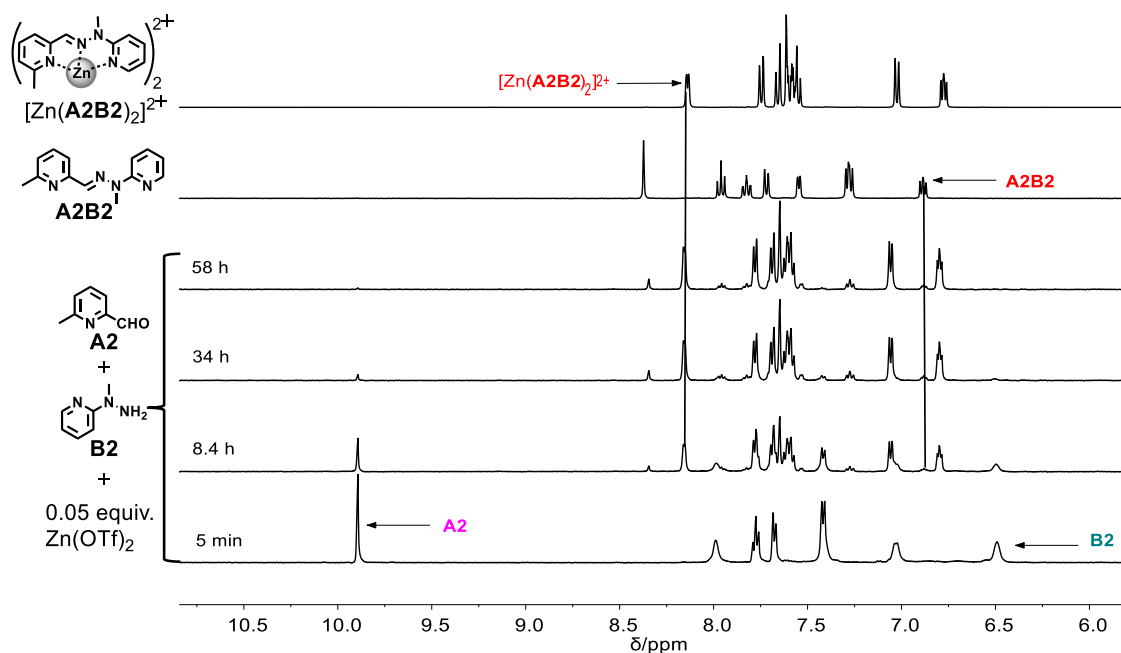
7) Kinetics of **A2** + **B2** in presence of 0.05 equiv. $\text{Zn}(\text{OTf})_2$ 

Figure II57. ^1H NMR (500 MHz) spectra of the mixture generated from equal amounts of **A2** + **B2** (10 mM each) + 0.5 equiv. $\text{Zn}(\text{OTf})_2$ (0.5 mM) in CD_3CN at 25°C after 5 min, 8.4 h, 34 h, 58 h from bottom to top. Reference spectra (top two traces) of the separately prepared constituents **A2B2**, $[\text{Zn}(\text{A2B2})_2]^{2+}$.

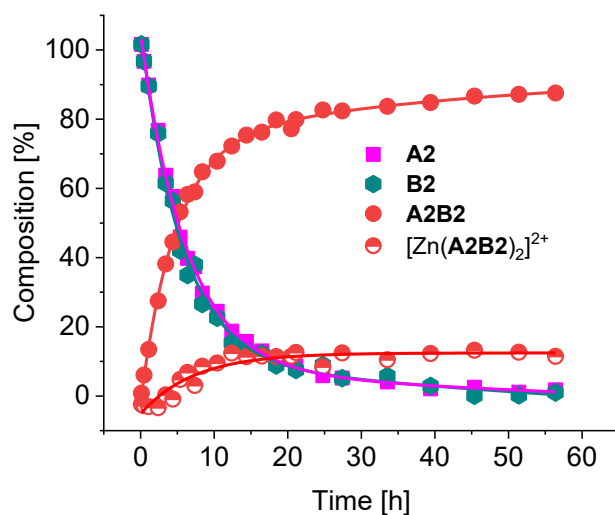


Figure II58. Formation of hydrazone **A2B2** from a mixture of equal amounts of components **A2** + **B2** (10 mM each) + 0.5 equiv. $\text{Zn}(\text{OTf})_2$ (0.5 mM) in CD_3CN at 25°C as a function of time as obtained from integration of the imine $\text{CH}=\text{N}$ proton signal in the 500 MHz ^1H NMR spectra.

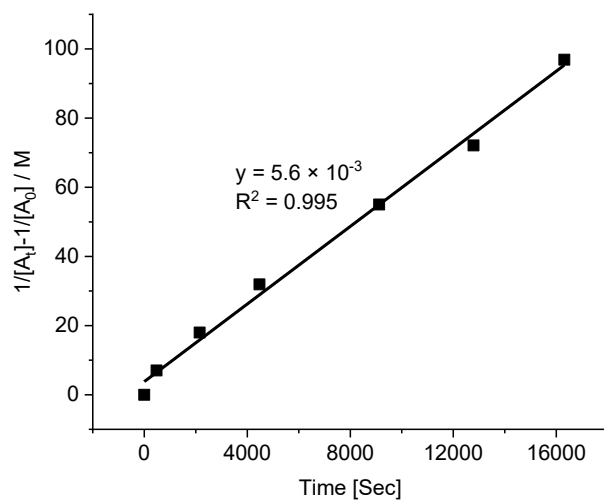


Figure II59. Representative linear least-squares fit ($1/[A]_t - 1/[A]_0$ vs. t) of the zinc complex of hydrazone **A2B2** formation from **A1** + **B2** (10 mM each) + 0.5 equiv. $\text{Zn}(\text{OTf})_2$ (0.5 mM) in CD_3CN at 25°C over about 10% of the hydrazone **A2B2** formation. The slope of the fit corresponds to the second order rate constant; R^2 values shown.

8) Kinetics of **A1** + **B2** in presence of 0.05 equiv. of $\text{Sc}(\text{OTf})_3$

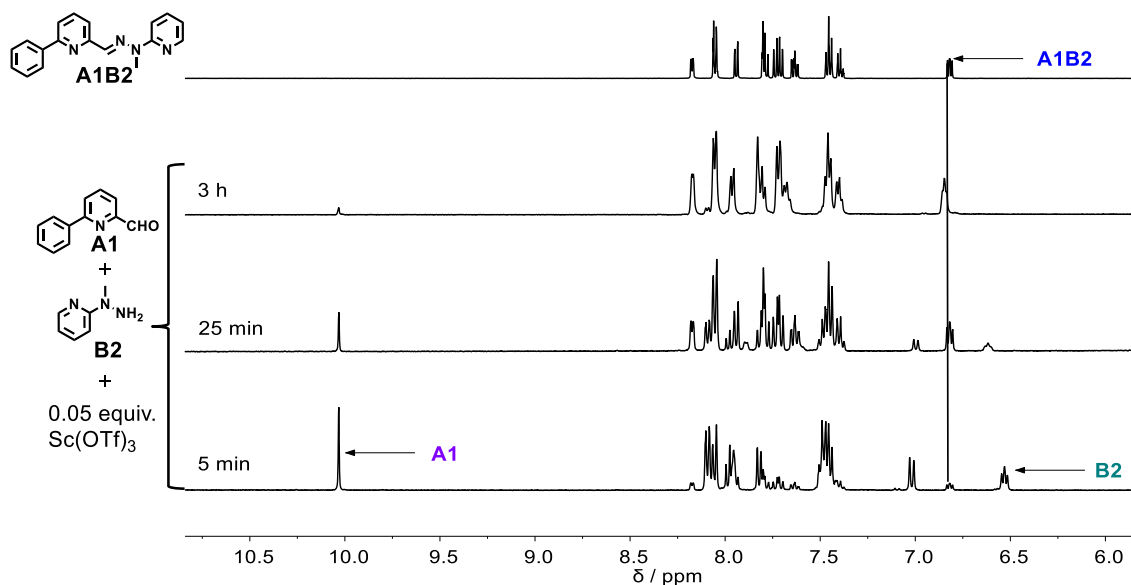


Figure II60. ^1H NMR (500 MHz) spectra of the mixture generated from equal amounts of **A1** + **B2** (10 mM each) + 0.05 equiv. $\text{Sc}(\text{OTf})_3$ (0.5 mM) in CD_3CN at 25°C after 5 min, 25 min, 3 h from bottom to top. Reference spectrum of the separately prepared constituent **A1B2**.

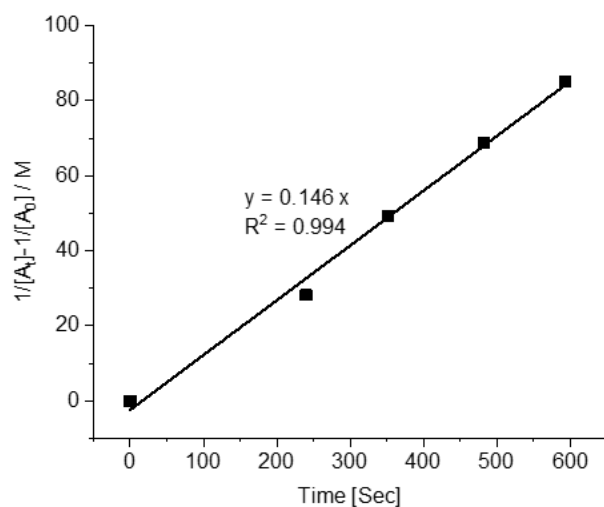


Figure II61. Representative linear least-squares fit ($1/[A]_t - 1/[A]_0$ vs. t) of the zinc complex of hydrazone **A1B2** formation from **A1** + **B2** (10 mM each) + 0.5 equiv. $\text{Sc}(\text{OTf})_3$ (0.5 mM) in CD_3CN at 25°C over the first ^1H NMR spectrum was obtained. The slope of the fit corresponds to the second order rate constant; R^2 values shown.

9) Kinetics of **A1** + **B2** in presence of 0.05 equiv. of CF_3COOD

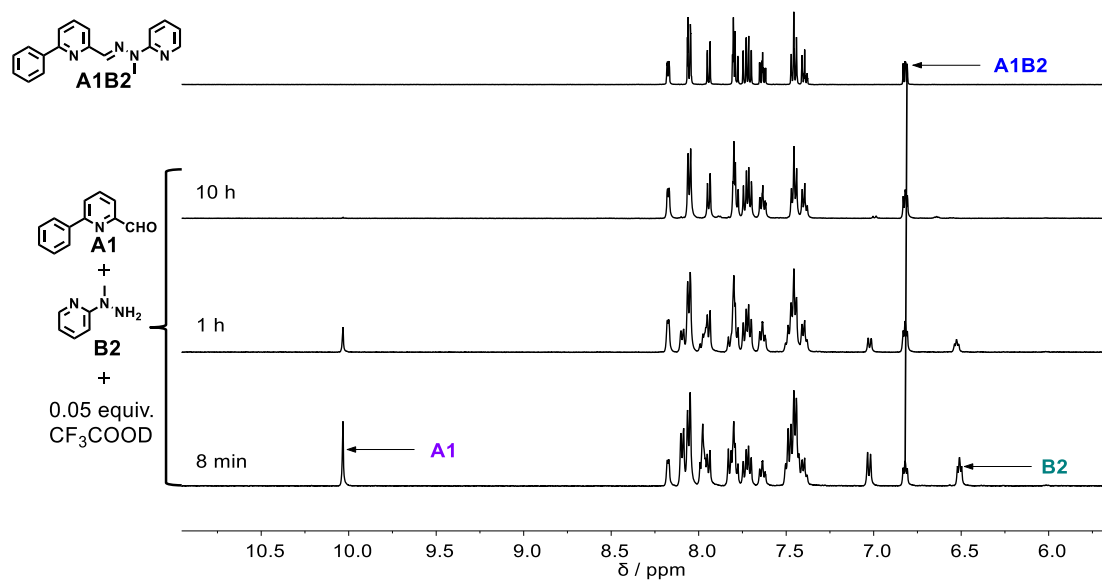


Figure II62. ^1H NMR (500 MHz) spectra of the mixture generated from equal amounts of **A1** + **B2** (10 mM each) + 0.5 equiv. CF_3COOD (0.5 mM) in CD_3CN at 25°C after 8 min, 1 h, 10 h from bottom to top. Reference spectrum of the separately prepared constituent **A1B2**.

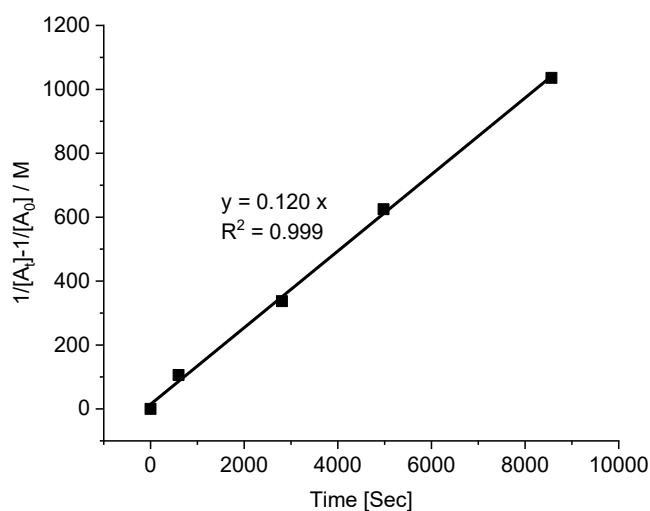


Figure II63. Representative linear least-squares fit ($1/[A]_t - 1/[A]_0$ vs. t) of the zinc complex of hydrazone A1B2 formation from **A1** + **B2** (10 mM each) + 0.5 equiv. CF_3COOD (0.5 mM) in CD_3CN at 25°C over the first ^1H NMR spectrum was obtained. The slope of the fit corresponds to the second order rate constant; R^2 values shown.

10) Kinetics of **A1** + **B2** in presence of 0.05 equiv. **B1** and 0.05 equiv. $\text{Zn}(\text{OTf})_2$

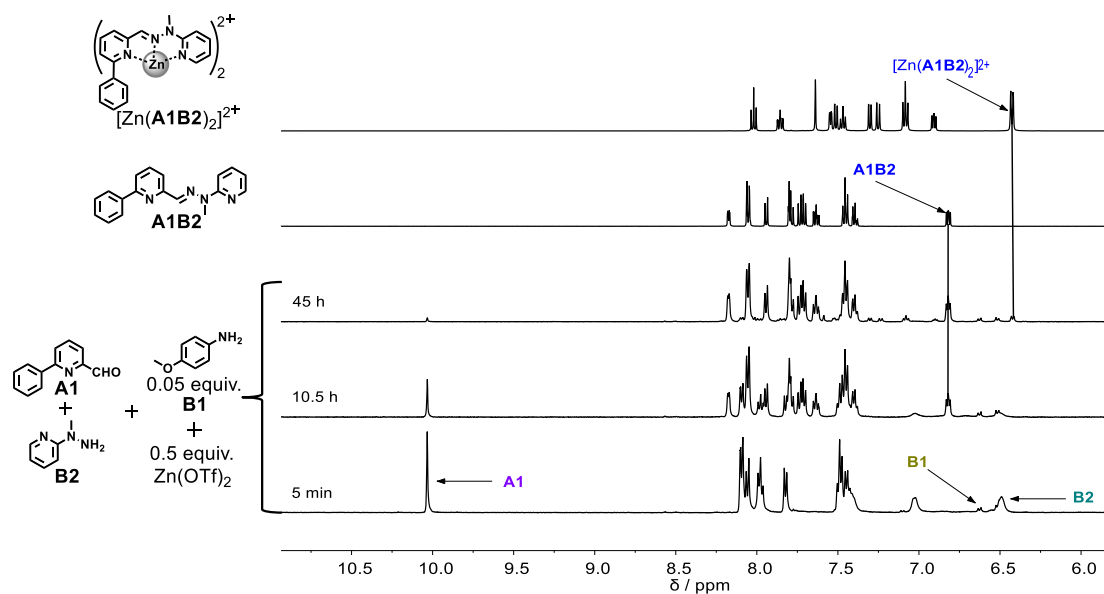


Figure II64. ^1H NMR (500 MHz) spectra of the mixture generated from equal amounts of **A1** + **B2** (10 mM each) + 0.05 equiv. $\text{Zn}(\text{OTf})_2$ (0.5 mM) + 0.05 equiv. **B1** (0.5 mM) after in CD_3CN at 25°C after 5 min, 10.5 h, 45 h from bottom to top. Reference spectra (top two traces) of the separately prepared constituents **A1B2**, $[\text{Zn}(\text{A1B2})_2]^{2+}$.

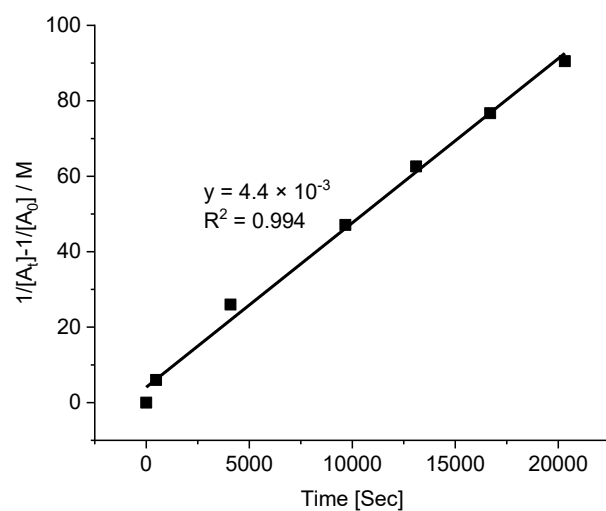


Figure II65. Representative linear least-squares fit ($1/[A]_t - 1/[A]_0$ vs. t) of hydrazone **A1B2** formation from **A1** + **B2** (10 mM each) + 0.05 equiv. $Zn(OTf)_2$ (0.5 mM) + 0.05 equiv. B1 (0.5 mM) after in CD_3CN at $25^\circ C$ over about 10% of the hydrazone **A1B2** formation. The slope of the fit corresponds to the second order rate constant; R^2 values shown.

3. CHAPTER III. CONTROL OF TIME-DEPENDENT SWITCHING OF DCLS

A. Synthesis and characterization

i. General procedures for the synthesis

General methods for preparation of imines, acylhydrazones and hydrazones

Aryl aldehydes Ax (1 equiv.) and 4 Å MS were added to ethanol solutions of amines, hydrazines or acylhydrazides (1.0 equiv.) respectively. After the mixtures were heated under reflux for 6 hours, the mixture was filtrated to remove 4 Å MS and washed by CH₂Cl₂ (20 mL). The solution was then dried with Na₂SO₄. After evaporation of the volatile materials under reduced pressure, the desired imines were afforded in a quantitative yield. Purer imine products could be obtained via vacuum distillation.

General methods for preparation of oximes³

Pyridine (1.1 equiv.) was added dropwise to a stirred solution of *o*-benzylhydroxylamine hydrochloride (1.3 equiv.) and aldehyde (1.0 equiv.) in methanol or ethanol (4 mL/mmol) and the mixture was heated at reflux for 4 h. The solvent was removed under reduced pressure, and the remaining solid residue was dissolved in CH₂Cl₂ (20 mL/mmol) and washed with water (20 mL/mmol). The aqueous layer was extracted with CH₂Cl₂ (20 mL/mmol×3) and the combined organic layers were dried over Na₂SO₄. The solvent was removed under reduced pressure and the crude product was purified by flash column chromatography.

General procedure for preparation of the relevant complexes:

0.5 equiv. of metal salt were added to the CD₃CN solutions of 1 equiv. of the ligand constituents. The complexes were always freshly prepared prior to every new experiment. The complexes were never isolated, all the present experiments and analysis were done in CD₃CN solution. Nevertheless, several relevant components, constituents and complexes were reported before; the characterizations were consistent with the literature values.⁴⁻¹⁶ The new compounds are described below.

ii. Characterization of the newly made compounds

A1B1: ^1H NMR (500 MHz, CD_3CN , 298 K): $\delta = 8.55$ (s, 1H, H^{10}), 8.14–8.06 (m, 2H, $H^{3,3'}$), 7.96–7.95 (t, 1H, H^7), 7.93–7.82 (m, 2H, H^{6+8}), 7.56–7.49 (m, 2H, $H^{2,2'}$), 7.49–7.43 (m, 1H, H^1) 7.42–7.33 (m, 4H, $H^{13,13'+14,14'}$), 7.33–7.25 (m, 1H, H^{15}), 4.87 (s, 2H, H^{11}); ^{13}C NMR (126 MHz, CD_3CN): δ 163.62 (C^{10}), 157.22 (C^5), 155.24 (C^9), 140.06 (C^{12}), 139.39 (C^4), 138.38 (C^6), 129.89 (C^1), 129.46 ($C^{2,2'}$), 129.12 ($C^{14,14'}$), 128.84 ($C^{13,13'}$), 127.69 (C^{15}), 127.40 ($C^{3,3'}$), 65.03 (C^{11}) ESI-MS: calculated for $[\text{C}_{19}\text{H}_{16}\text{N}_2+\text{H}]^+$ 273.1392, found, 273.1382; Elemental analysis calculated (%) for $\text{C}_{19}\text{H}_{16}\text{N}_2$: C, 83.79; H, 5.92; N, 10.29; found: C, 83.34; H, 5.93; N, 10.25.

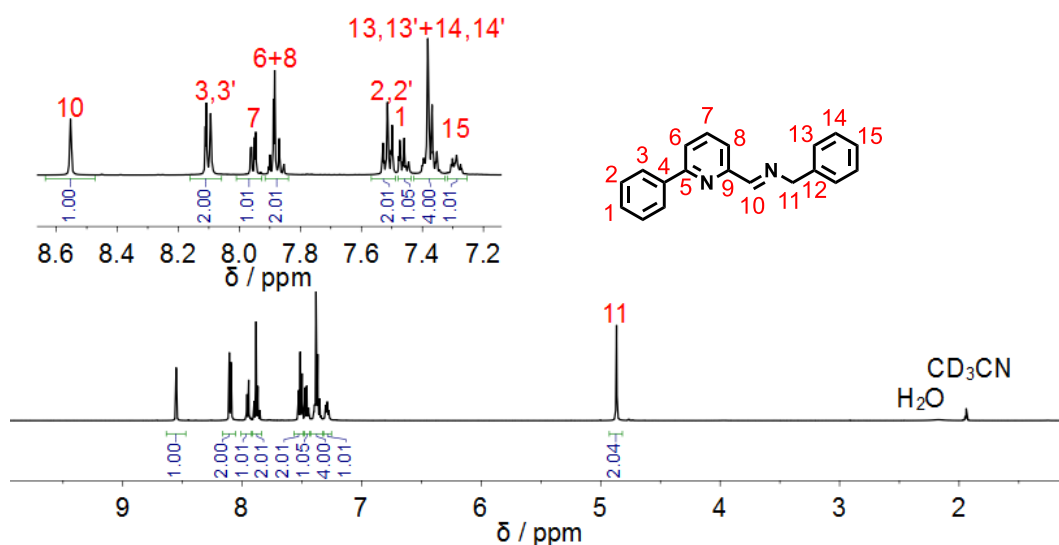


Figure III.1. ^1H NMR spectrum of **A1B3** (500 MHz, 298 K, CD_3CN).

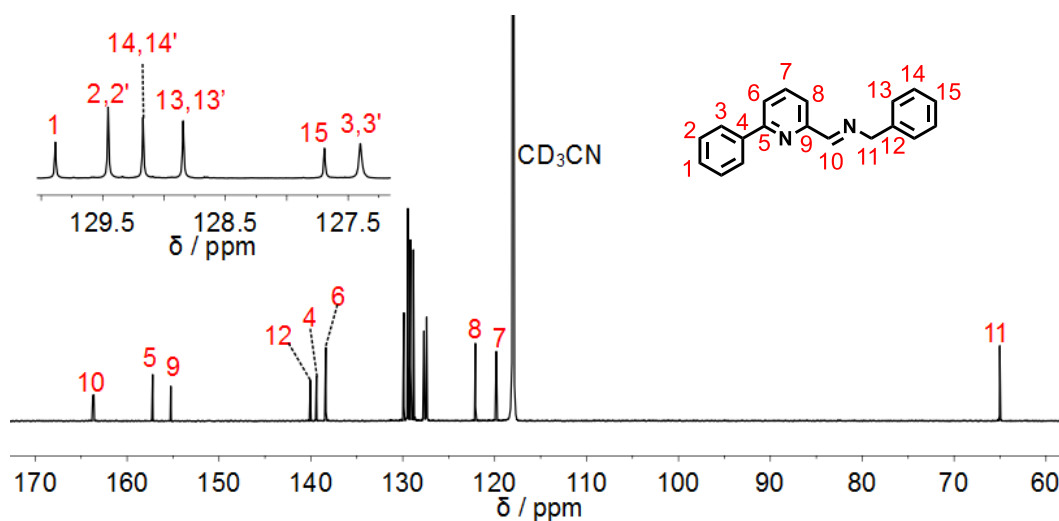


Figure III.2. ^{13}C NMR spectrum of **A1B3** (125 MHz, 298 K, CD_3CN).

A1B4: ^1H NMR (500 MHz, CD_3CN): $\delta = 8.27$ (s, 1H, H^{10}), 8.10–8.01 (m, 2H, $H^{3,3'}$), 7.88–7.80 (m, 2H, H^{6+8}), 7.79–7.70 (m, 1H, H^7), 7.53–7.47 (m, 2H, $H^{2,2'}$), 7.47–7.43 (m, 3H, $H^{1+13,13'}$), 7.42–7.37 (m, 2H, $H^{14,14'}$), 7.37–7.30 (m, 1H, H^{15}), 5.25 (s, 2H, H^7). ^{13}C NMR (126 MHz, CD_3CN): δ 157.44 (C^5), 152.11 (C^9), 150.78 (C^{10}), 139.29 (C^4), 138.37 (C^{12}), 138.36 (C^6), 129.93 (C^1), 129.43 ($C^{2,2'}$), 129.14 ($C^{14,14'}$), 129.09 ($C^{13,13'}$), 128.70 (C^{15}), 127.38 ($C^{3,3'}$), 121.41 (C^8), 119.61 (C^7), 77.01 (C^{11}). ESI-MS: calculated for $[\text{C}_{19}\text{H}_{16}\text{N}_2\text{O}+\text{H}]^+$ 289.1341, found, 289.1335; Elemental analysis calculated (%) for $\text{C}_{19}\text{H}_{16}\text{N}_2\text{O}$: C, 79.14; H, 5.59; N, 9.72; O, 5.55; found: C, 79.07; H, 5.60; N, 9.72.

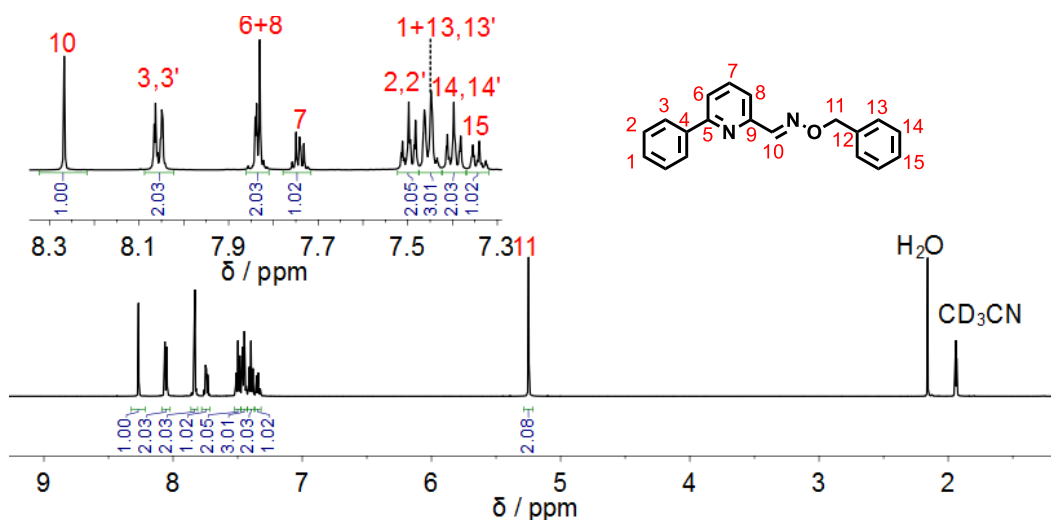


Figure III.3. ^1H NMR spectrum of **A1B4** (500 MHz, 298 K, CD_3CN).

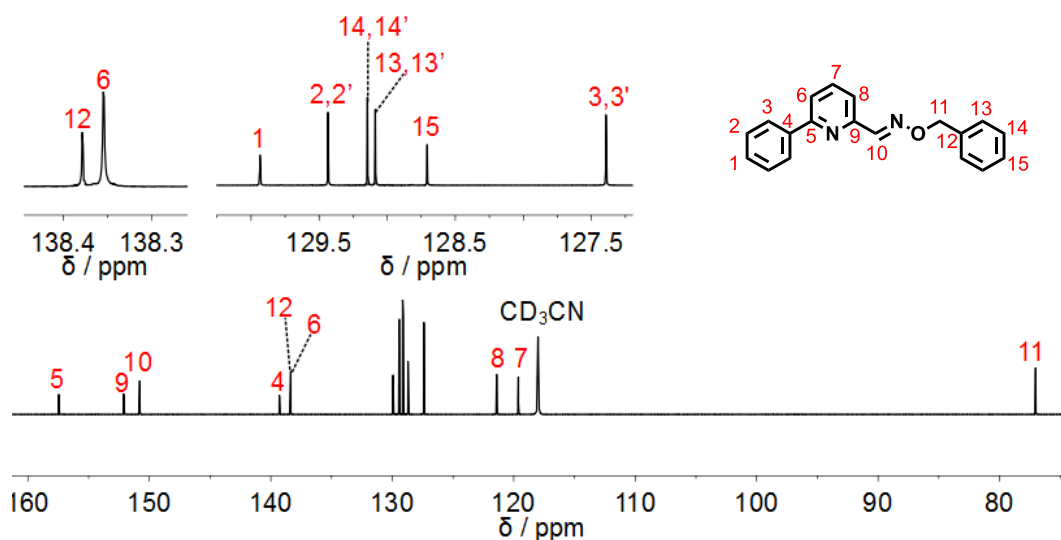


Figure III.4. ^{13}C NMR spectrum of **A1B4** (125 MHz, 298 K, CD_3CN).

A1B5: ^1H NMR (500 MHz, CD_3CN): $\delta = 8.12\text{--}8.05$ (m, 2H, $H^{3,3'}$), 7.96 (s, 1H, H^{10}), 7.79-7.77 (dd, $J = 10.0, 5.0$ Hz, 1H, H^6), 7.74 (t, $J = 7.7$ Hz, 1H, H^7), 7.72-7.66 (m, 2H, $H^{14,14'}$), 7.59-7.39 (m, 7H, $H^{16,6,2+2',15,+15',1,8}$), 3.56 (s, 3H, H^{11}); ^{13}C NMR (126 MHz, CD_3CN): δ 171.36 (C^{12}), 157.13 (C^5), 154.59 (C^9), 140.95 (C^{10}), 139.36 (C^4), 138.27 (C^7), 136.29 (C^{13}), 130.82 (C^{16}), 130.22 ($C^{14,14'}$), 129.88 (C^1), 129.43 ($C^{15,15'}$), 128.16 ($C^{2,2'}$), 127.33 ($C^{3,3'}$), 120.78 (C^6), 118.99 (C^8), 29.09 (C^{11}); ESI-MS: calculated for $[\text{C}_{20}\text{H}_{17}\text{N}_3\text{O}+\text{H}]^+$ 316.1444, found, 316.1438; Elemental analysis calculated (%) for $\text{C}_{20}\text{H}_{17}\text{N}_3\text{O}$: C, 76.17; H, 5.43; N, 13.32; O, 5.07; found: C, 75.89; H, 5.42; N, 13.29.

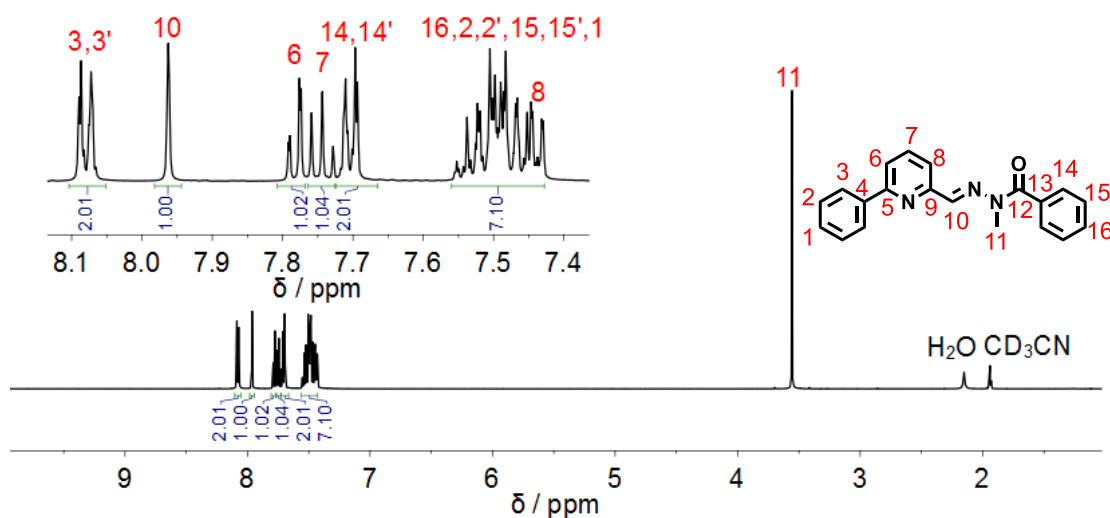


Figure III.5. ^1H NMR spectrum of **A1B5** (500 MHz, 298 K, CD_3CN).

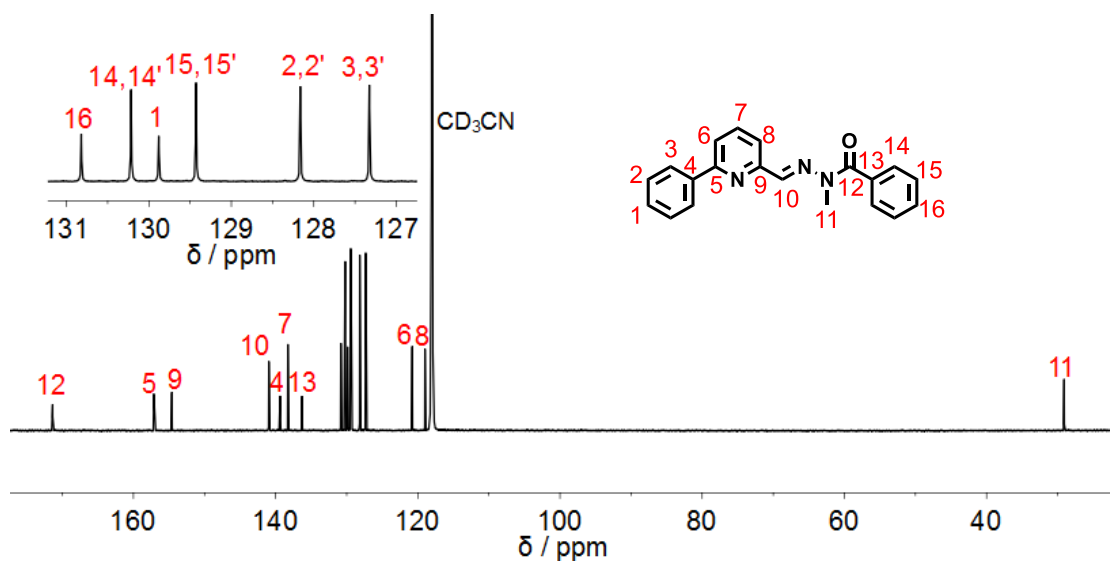


Figure III.6. ^{13}C NMR spectrum of **A1B5** (125 MHz, 298 K, CD_3CN).

A7B4: ^1H NMR (500 MHz, CD_3CN): δ = 8.16 (s, 1H, H^5), 7.66–7.54 (m, 2H, $H^{3,3'}$), 7.48–7.41 (m, 2H, $H^{8,8'}$), 7.41–7.21 (m, 2H, $H^{9,9'}$), 7.21–6.88 (m, 1H, H^{10}), 5.17 (s, 2H, H^6); ^{13}C NMR (125 MHz, CD_3CN): δ 165.26 (C^4), 163.29 (C^1), 148.62 (C^5), 138.65 (C^7), 129.67 (C^3), 129.61 ($C^{3'}$), 129.11 ($C^{9,9'}$), 129.06 ($C^{8,8'}$), 128.61 (C^{10}), 116.53 (C^2), 116.35 ($C^{2'}$), 76.62 (C^6); ESI-MS: calculated for $[\text{C}_{14}\text{H}_{12}\text{FNO}+\text{H}]^+$ 230.0976, found, 230.0971; Elemental analysis calculated (%) for $\text{C}_{14}\text{H}_{12}\text{FNO}$: C, 73.35; H, 5.28; F, 8.29; N, 6.11; O, 6.98; found : C, 72.99; H, 5.30; N, 6.25.

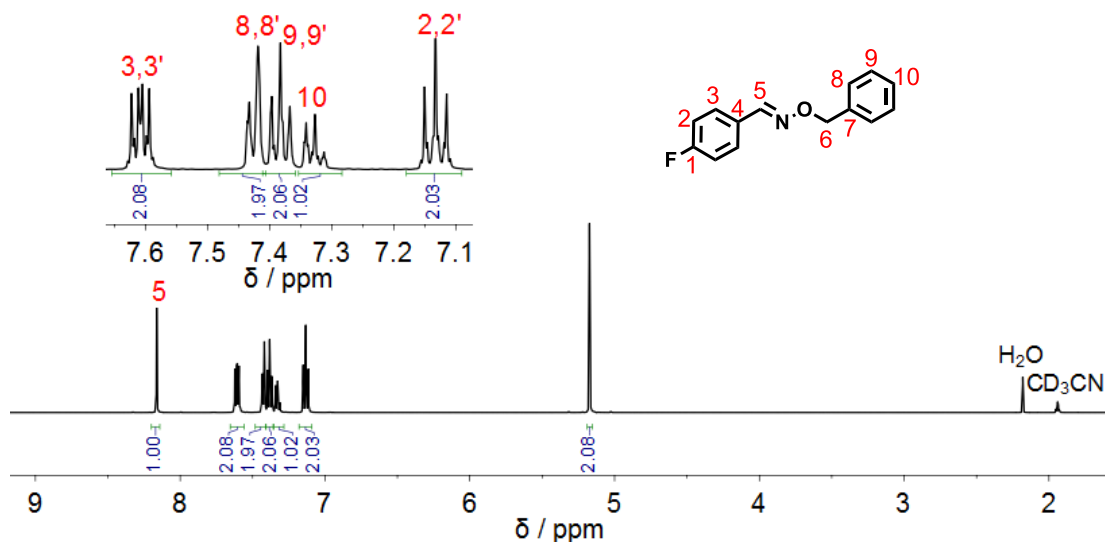


Figure III.7. ^1H NMR spectrum of **A7B4** (500 MHz, 298 K, CD_3CN).

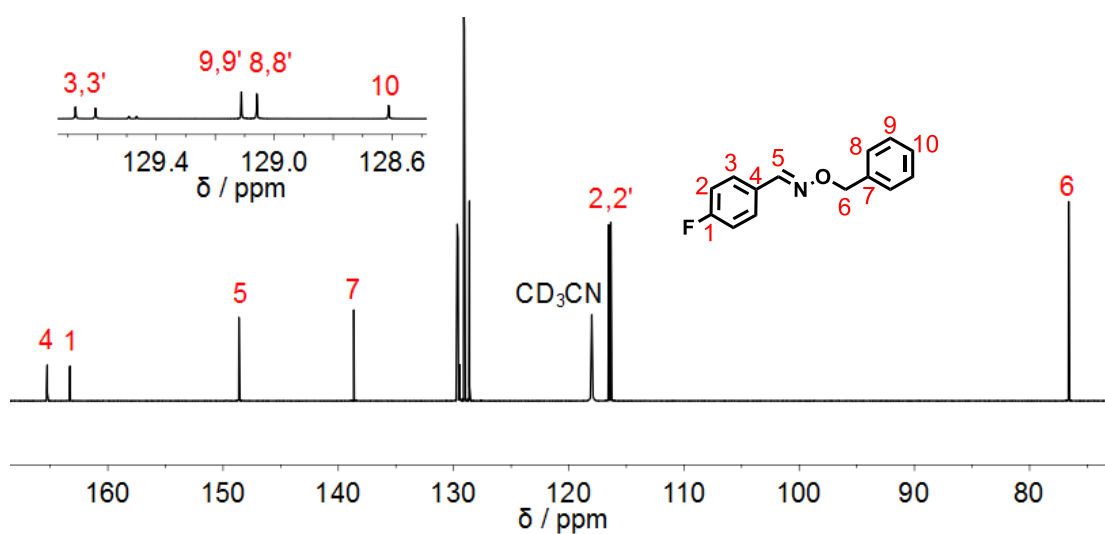


Figure III.8. ^{13}C NMR spectrum of **A7B4** (125 MHz, 298 K, CD_3CN).

A8B2: ^1H NMR (500 MHz, CD_3CN): $\delta = 8.28\text{--}8.17$ (m, 3H, $H^{2,2'+,11}$), 7.97–7.88 (d, 2H, $H^{3,3'}$), 7.82 (s, 1H, H^5), 7.78–7.76 (d, $J = 10.0$ Hz, 1H, H^8), 7.70 (t, 1H, H^9), 6.89 (t, 1H, H^{10}), 3.67 (s, 3H, H^6); ^{13}C NMR (126 MHz, CD_3CN): δ 157.98 (C^7), 147.79 (C^{11}), 147.70 (C^1), 143.59 (C^4), 138.55 (C^9), 132.74 (C^5), 127.20 ($C^{3,3'}$), 124.73 ($C^{2,2'}$), 117.13 (C^{10}), 110.48 (C^8), 29.93 (C^6). ESI-MS: calculated for $[\text{C}_{14}\text{H}_{12}\text{N}_2\text{O}_3+\text{H}]^+$ 257.1039, found: 257.1026; Elemental analysis calculated (%) for $\text{C}_{14}\text{H}_{12}\text{N}_2\text{O}_3$: C, 60.93; H, 4.72; N, 21.86; O, 12.49; found: C, 60.75; H, 4.79; N, 21.75.

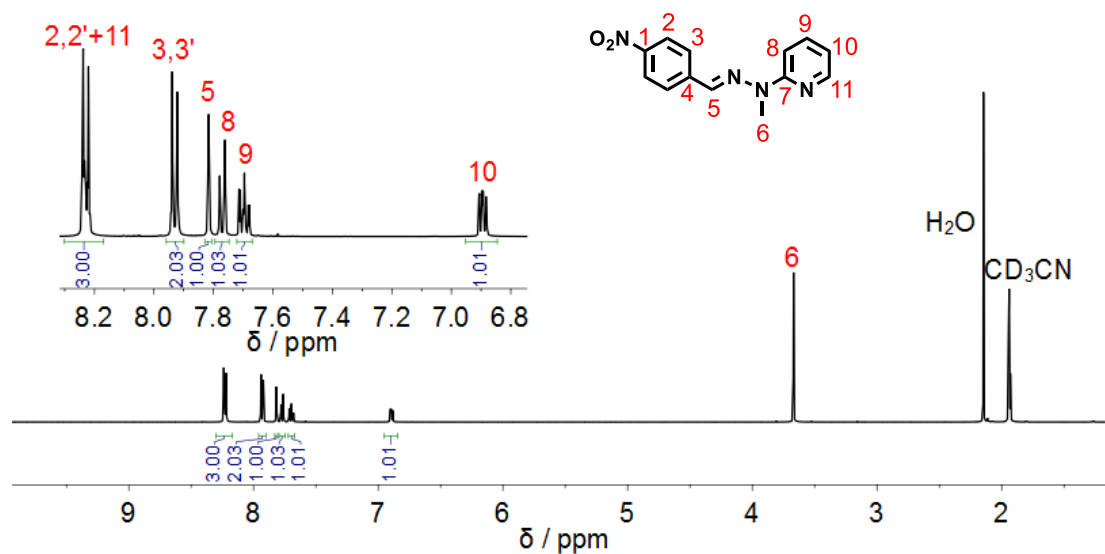


Figure III.9. ^1H NMR spectrum of **A8B2** (500 MHz, 298 K, CD_3CN).

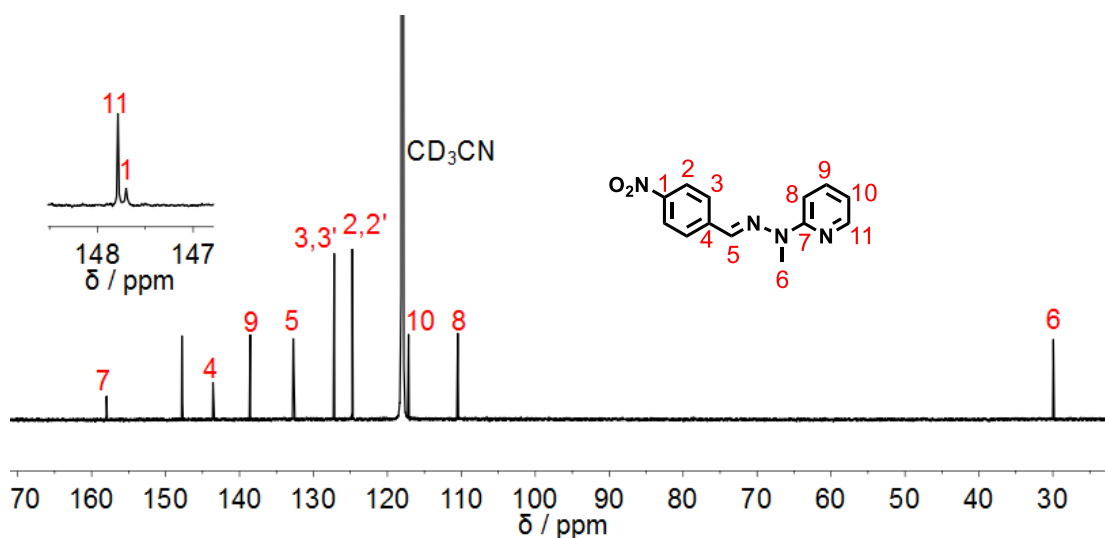
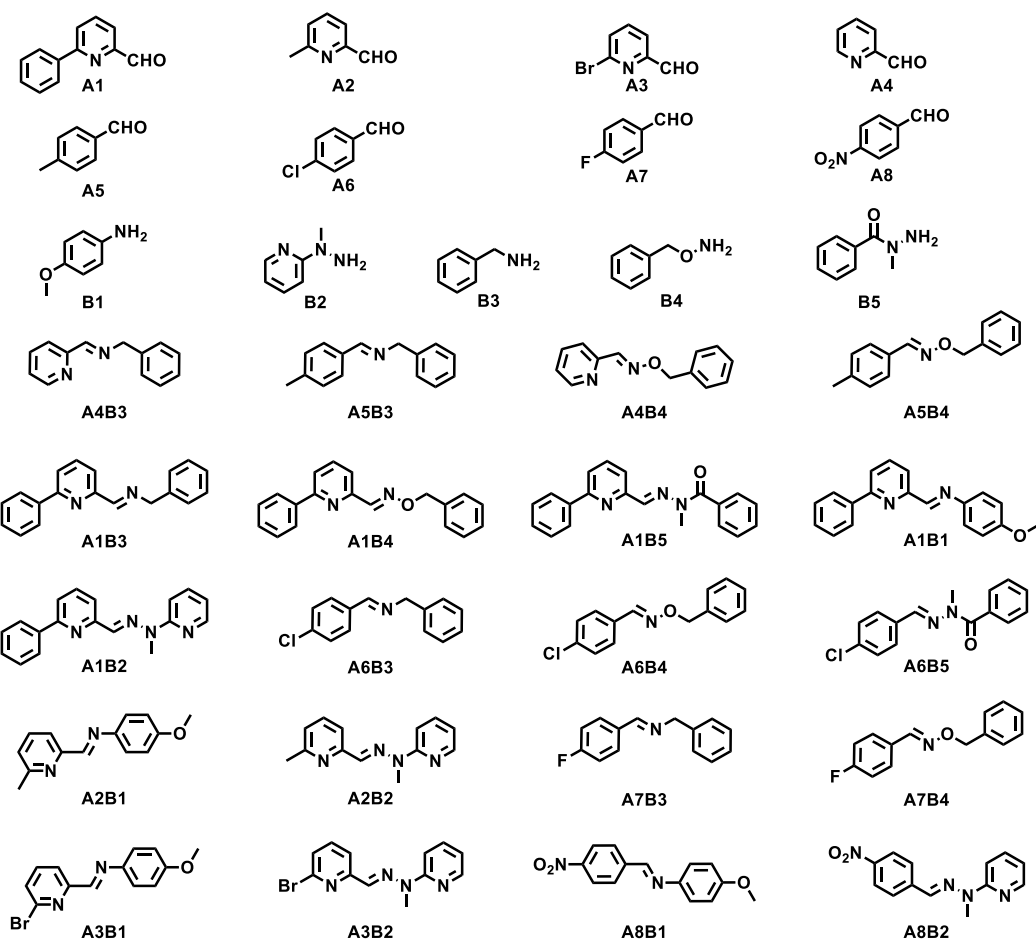


Figure III.10. ^{13}C NMR spectrum of **A8B2** (125 MHz, 298 K, CD_3CN).

B. List of the aldehydes, amines and imines have been selected in the context.



Scheme III1 All of aldehydes, amines and imine compounds that have been used in Chapter III.

C. The kinetics study of two, three, four-components mixtures

i. Two-component reactions

General procedure for the two-component and three components reactions

All the components were added in the same equivalent and the composition of the DCL was calculated according to the internal standard. In all of the libraries in organic part (in the absence of metal cations), the same equivalent of four components (100 μ L, 180 mM for each) were mixed together in CD_3CN , the composition of the DCL was monitored by 1H NMR as a function of time.

1) The formation of **A4B3** from the same equivalent amount of **A4** + **B3**

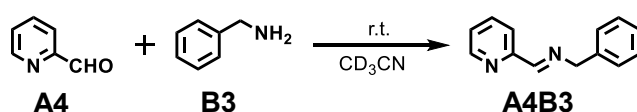


Table III1. Time-dependent of the evolution of distributions generated from equal amounts of **A4** + **B3**.

Entry	t [h] ^[b]	Compound Distribution [%] ^[c]		
		A4	B3	A4B3
1 ^[a]	0.07	25%	26%	75%
2 ^[a]	0.2	6%	7%	94%
3 ^[a]	0.7	1%	2%	99%

^[a] The reaction was performed in CD_3CN , 30 mM each, r.t. ^[b] Reaction times indicate the time at which distribution data were collected. ^[c] Error in 1H -NMR signal integration: 5%.

2) The formation of **A4B4** from the same equivalent amount of **A4** + **B4**

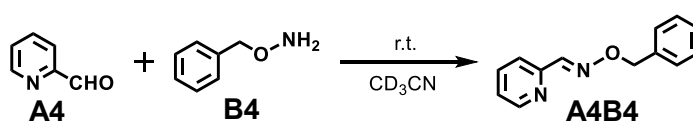
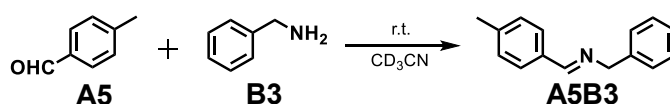


Table III2. Time-dependent of the evolution of distributions generated from equal amounts of **A4** + **B4**.

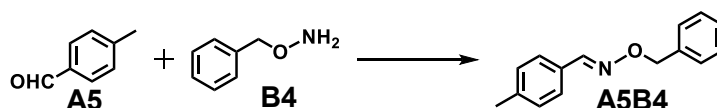
Entry	t [h] ^[b]	Compound Distribution [%] ^[c]		
		A4	A4B4	hemiaminal
1 ^[a]	0.07	45	<1%	55
2 ^[a]	52	33	30	37
3 ^[a]	156	22	62	16

^[a] The reaction was performed in CD_3CN , 30 mM each, r.t. ^[b] Reaction times indicate the time at which distribution data were collected. ^[c] Error in 1H -NMR signal integration: 5%.

3) The formation of **A5B3** from the same equivalent amount of **A5** + **B3****Table III3.** Time-dependent of the evolution of distributions generated from equal amounts of **A5** + **B3**.

Entry	t [h] ^[b]	Compound Distribution [%] ^[c]		
		A5	B3	A5B3
1 ^[a]	0.08	92%	93%	8%
2 ^[a]	1	31%	34%	69%
3 ^[a]	10	3%	8%	97%

^[a] The reaction was performed in CD₃CN, 30 mM each, r.t. ^[b] Reaction times indicate the time at which distribution data were collected. ^[c] Error in ¹H-NMR signal integration: 5%.

4) The formation of **A5B4** from the same equivalent amount of **A5** + **B4****Table III4.** Time-dependent of the evolution of distributions generated from equal amounts of **A5** + **B4**.

Entry	t [h] ^[b]	Compound Distribution [%] ^[c]		
		A5	B4	A5B4
1 ^[a]	0.08	100%	100%	0%
2 ^[a]	88	51%	52%	49%
3 ^[a]	118	43%	44%	57%

^[a] The reaction was performed in CD₃CN, 30 mM each, r.t. ^[b] Reaction times indicate the time at which distribution data were collected. ^[c] Error in ¹H-NMR signal integration: 5%.

5) The kinetic data for the formation of **A4B3**, **A4B4**, **A5B3** and **A5B4** from the same equivalent amount of their components

Table III5. The formation rates between **A4** or **A5** and **B3** or **B4**.

Entry ^[a]	reaction	product	t ₅₀ [h] ^[b]	t ₁₀ [h] ^[c]	k (×10 ⁻³ M ⁻¹ s ⁻¹) ^d
1	A4 + B3	A4B3	0.04	n.d.	409
2	A4 + B2	A4B4	104	16	12.3
3	A5 + B3	A5B3	0.6	0.08	1.1
4	A5 + B2	A5B4	91	10	0.11

^[a] In all of these entries, Aldehyde (30 mM), Amine (30 mM), at room temperature, in CD₃CN, monitored by ¹H NMR. ^[b] Time for 50% completion of the reaction. ^[c] Time for 10% completion of the reaction. ^[d] Rate constant calculated from a fit to a second-order reaction over the first 10% of the reaction, reached when the first spectrum recorded. n.d. The reaction is too fast, not calculated.

ii. **Three-component reactions**

1) **Competitive reactions between A4 + B3 + B4**

General procedure for the two-component and three components reactions

All the components were added in the same equivalent and the composition of the DCL was calculated according to the internal standard. In all of the reactions in organic part (in the absence of metal cations), the same equivalent of four components (100 μL, 180 mM for each) were mixed together in CD₃CN, the composition of the DCL was monitored by ¹H NMR as a function of time.

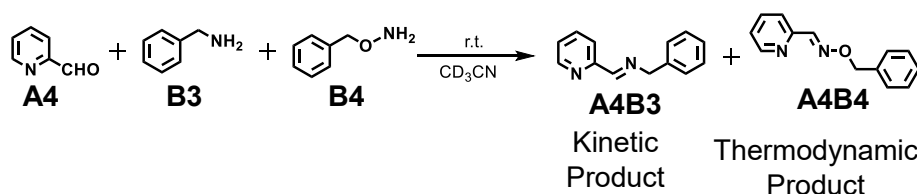
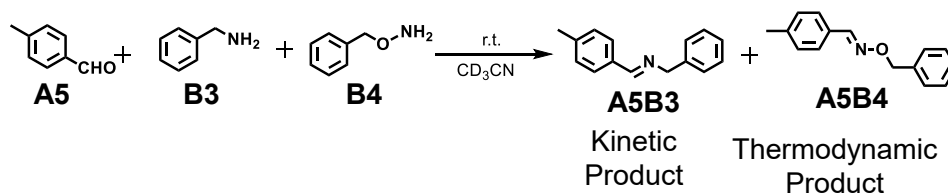


Table III6. Time-dependent of the evolution of distributions generated from equal amounts of **A4 + B3 + B4**.

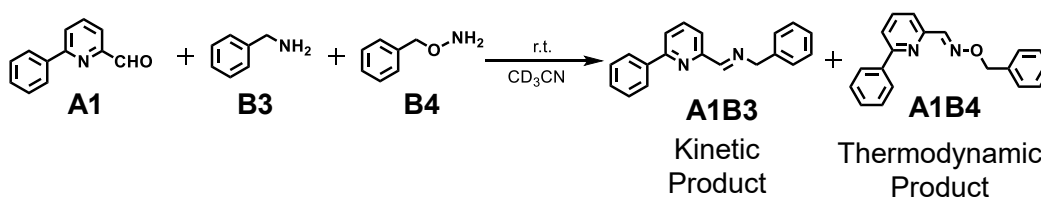
Entry	t [h] ^[b]	Compound Distribution [%] ^[c]		
		A4	A4B3	A4B4
1 ^[a]	0.08	30%	70%	<1%
2 ^[a]	3	6%	53%	41%
3 ^[a]	24	0%	10%	90%

^[a] The reaction was performed in CD₃CN, 30 mM each, r.t.. ^[b] Reaction times indicate the time at which distribution data were collected. ^[c] Error in ¹H-NMR signal integration: 5%.

2) Competitive reactions between **A5** + **B3** + **B4****Table III7.** Time-dependent of the DCL distributions generated from equal amounts of **A5** + **B3** + **B4**.

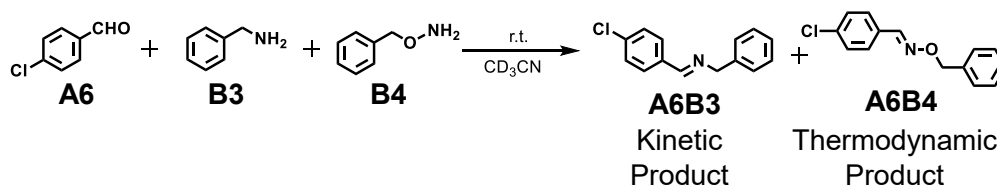
Entry	t [h] ^[b]	Compound Distribution [%] ^[c]		
		A5	A5B3	A5B4
1 ^[a]	0.08	96%	3%	0%
2 ^[a]	3	27	43%	30%
3 ^[a]	24	1%	11%	88%

^[a] The reaction was performed in CD₃CN, 30 mM each, r.t. ^[b] Reaction times indicate the time at which distribution data were collected. ^[c] Error in ¹H-NMR signal integration: 5%.

3) Competitive reactions between **A1** + **B3** + **B4****Table III8.** Time-dependent of the evolution of distributions generated from equal amounts of **A1** + **B3** + **B4**.

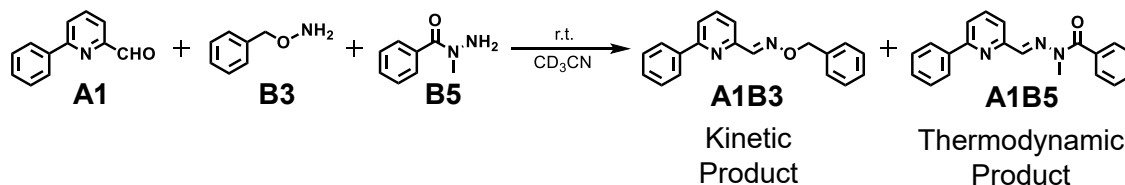
Entry	t [h] ^[b]	Compound Distribution [%] ^[c]			
		A1	A1B3	A1B4	aminal
1 ^[a]	0.07	11%	43%	<1%	45%
2 ^[a]	2.5	<1%	45%	51%	6%
3 ^[a]	23	<1%	8%	92%	0%

^[a] The reaction was performed in CD₃CN, 30 mM each, r.t. ^[b] Reaction times indicate the time at which distribution data were collected. ^[c] Error in ¹H-NMR signal integration: 5%.

4) Competitive reactions between **A6 + B3 + B4****Table III9.** Time-dependent of the evolution of distributions generated from equal amounts of **A6 + B3 + B4**.

Entry	t [h] ^[b]	Compound Distribution [%] ^[c]		
		A4	A4B1	A4B2
1 ^[a]	0.4	<1%	87%	13%
2 ^[a]	5	<1%	46%	54%
3 ^[a]	29	<1%	12%	88%

^[a] The reaction was performed in CD₃CN, 30 mM each, r.t. ^[b] Reaction times indicate the time at which distribution data were collected. ^[c] Error in ¹H-NMR signal integration: 5%.

5) Competitive reactions between **A3 + B3 + B5****Table III10.** Time-dependent of the evolution of distributions generated from equal amounts of **A1 + B3 + B5**.

Entry	t [h] ^[b]	Compound Distribution [%] ^[c]			
		A3	A3B2	A3B3	hemiaminal
1 ^[a]	0.07	51%	<1%	<1%	48%
2 ^[a]	162	34%	17%	3%	46%
3 ^[a]	192	31%	21%	3%	45%

^[a] The reaction was performed at 25°C. ^[b] Reaction times indicate the time at which distribution data were collected. ^[c] Error in ¹H-NMR signal integration: 5%.

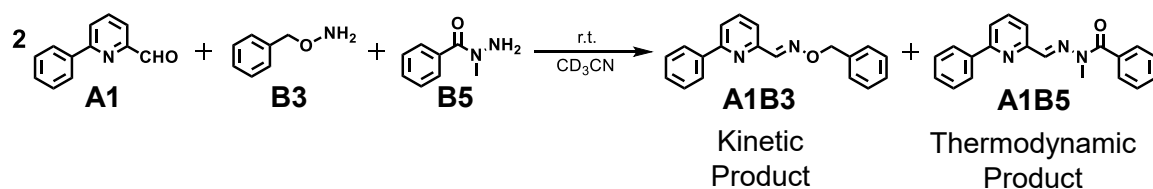


Table III11. Time-dependent of the evolution of distributions generated from equal amounts of **B3** and **B5** with 2 equiv. **A1**.

Entry	t [h] ^[b]	Compound Distribution [%] ^[c]			
		A3	A3B2	A3B3	hemiaminal
1 ^[a]	0.07	54%	1%	<1%	44%
2 ^[a]	93	52%	11%	3%	36%
3 ^[a]	165	50%	17%	4%	28%

^[a] The reaction was performed at 25°C. ^[b] Reaction times indicate the time at which distribution data were collected. ^[c] Error in ¹H-NMR signal integration: 5%.

iii. Four-component DCLs

General procedure for the experiments of the switching of the DCLs

For all of the quantitative measurements hexamethyldisiloxane (HMDSO) was added as internal standard, T1 relaxation times were determined, and the d1 delay parameter was set to obtain full signal by adjusting d1 to three times the longest T1 relaxation constant in the sample. All the components were added in the same equivalent and the composition of the DCL was calculated according to the internal standard. In all of the libraries in organic part (in the absence of metal cations), the same equivalent of four components (30 mM for each) were mixed together in CD_3CN , the composition of the DCL was monitored by ¹H NMR as a function of time.

1) DCL generated from **A1 + A6 + B3 + B5**.**Table III12.** Time-dependent of the evolution of DCL distributions generated from equal amounts of **A1 + A6 + B3 + B5**.

Entry	t [h] ^[b]	Compound Distribution [%] ^[c]					
		A1	A6	A1B3	A1B5	A6B3	A6B5
1 ^[a]	0.083	<1%	44%	50%	<1%	6%	<1%
2 ^[a]	14	<1%	14%	21%	28%	37%	5%
3 ^[a]	96	<1%	<1%	9%	41%	38%	12%

^[a] The reaction was performed at 25°C. ^[b] Reaction times indicate the time at which distribution data were collected. ^[c] Error in ¹H-NMR signal integration: 5%.

2) DCL generated from equal amounts of **A4 + A5 + B3 + B4****Table III13.** Time-dependent of the evolution of DCL distributions generated from equal amounts of **A4 + A5 + B3 + B4**.

Entry	t [h] ^[b]	Compound Distribution [%] ^[c]					
		A4	A5	A4B3	A4B4	A5B3	A5B4
1 ^[a]	0.4	1%	44%	36%	13%	6%	1%
2 ^[a]	5	<1%	11%	15%	35%	29%	12%
3 ^[a]	15	<1%	2%	14%	36%	35%	14%

^[a] The reaction was performed in CD₃CN, 30 mM each, r.t. ^[b] Reaction times indicate the time at which distribution data were collected. ^[c] Error in ¹H-NMR signal integration: 5%.

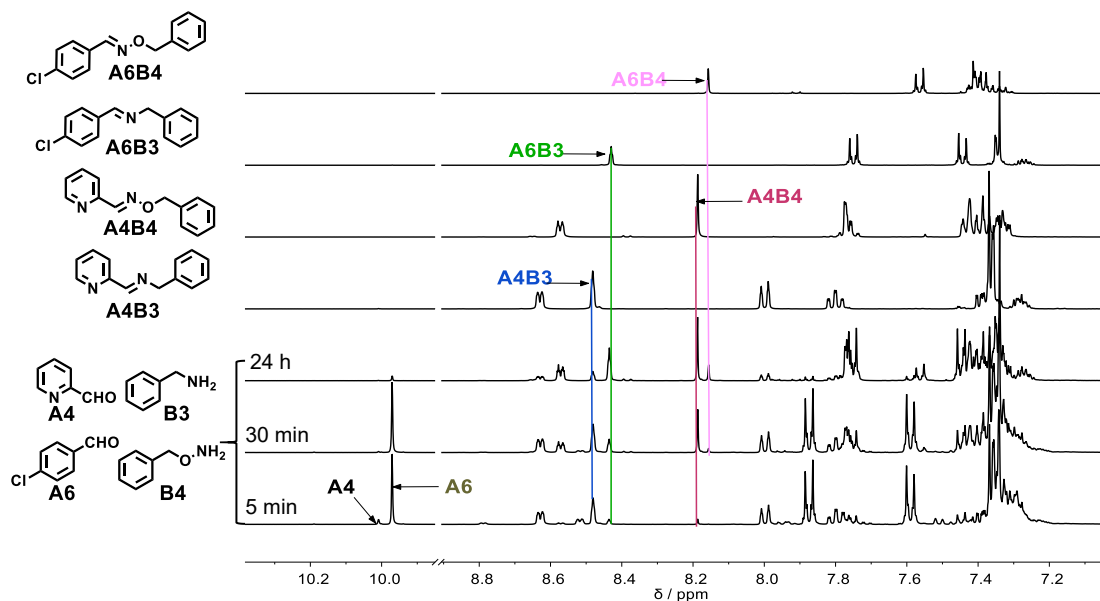
3) DCL generated from equal amounts of **A4 + A6 + B3 + B4**.

Figure III11. ^1H NMR (400 MHz) spectra of the mixture generated from equal amounts of **A4 + A6 + B3 + B4** (30 mM each, CD_3CN , r.t.) after 5 minutes, 30 minutes and 24 h (from bottom to up). The top four traces are the reference spectra of the separately prepared constituents **A4B3**, **A4B4**, **A6B3** and **A6B4**.

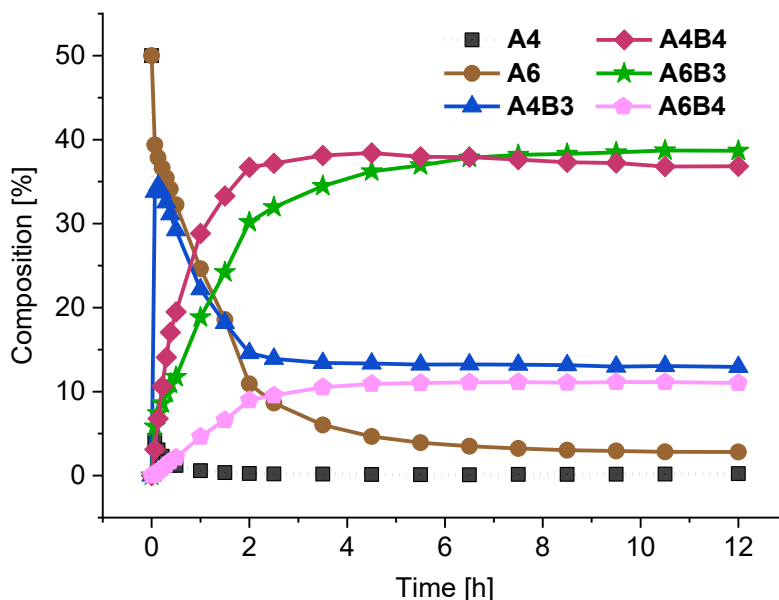
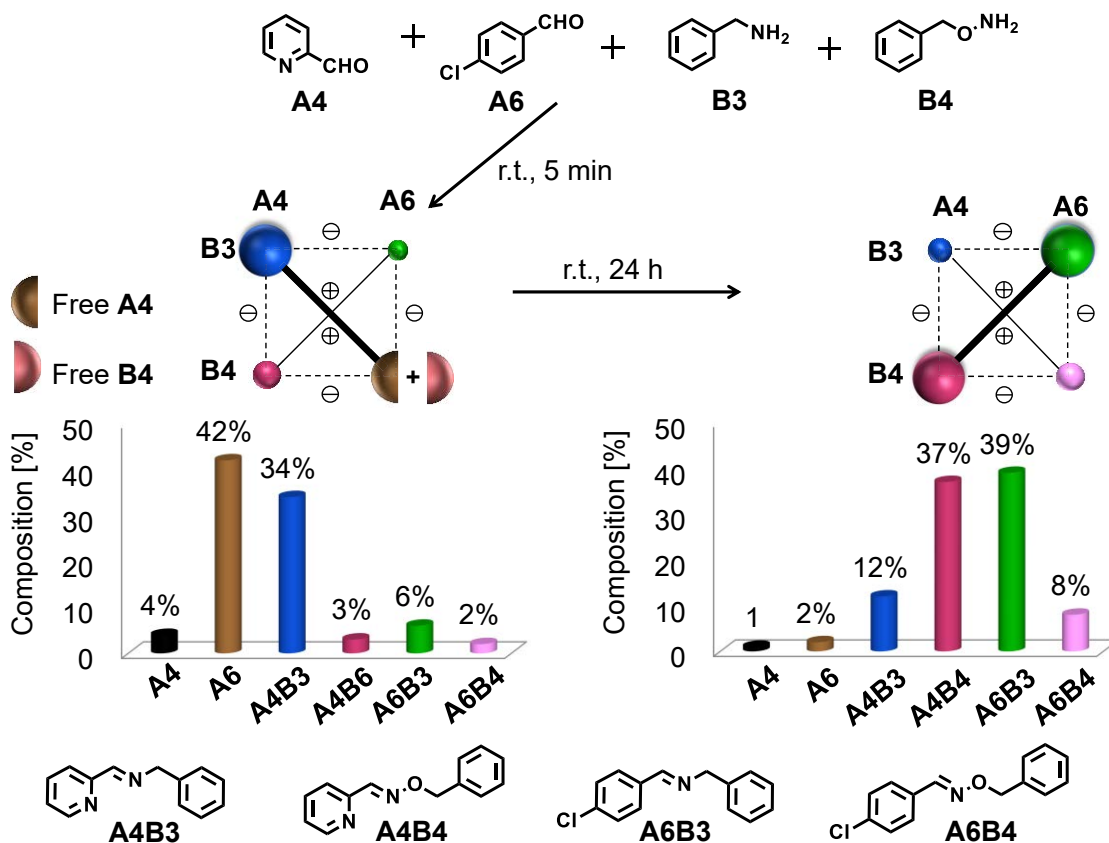


Figure III12. Kinetic plots of the evolution of a mixture of equal amounts of components **A4 + A6 + B3 + B4** as a function of time as obtained from integration of the imine $\text{CH}=\text{N}$ and aldehyde CHO proton signals in the 400 MHz ^1H NMR spectra (30 mM each, CD_3CN , r.t.). For clarity, the kinetic curves are shown for only some of the compounds.



Scheme III2. Kinetic switch of a [2 x 2] DCL from the [A4B3, A6 + B4] state to the orthogonal state [A4B4, A6B3] in CD₃CN at room temperature. Data obtained from the 400 MHz ¹H NMR spectra.

Table III14. Time-dependent of the evolution of DCL distributions generated from equal amounts of A4 + A6 + B3 + B4.

Entry	t [h] ^[b]	Compound Distribution [%] ^[c]					
		A4	A6	A4B3	A4B4	A6B3	A6B4
1 ^[a]	0.083	4%	42%	34%	3%	6%	2%
2 ^[a]	3.5	2%	6%	13%	34%	35%	11%
3 ^[a]	12	0%	4%	12%	39%	37%	8%

^[a] The reaction was performed in CD₃CN, 30 mM each, r.t. ^[b] Reaction times indicate the time at which distribution data were collected. ^[c] Error in ¹H-NMR signal integration: 5%.

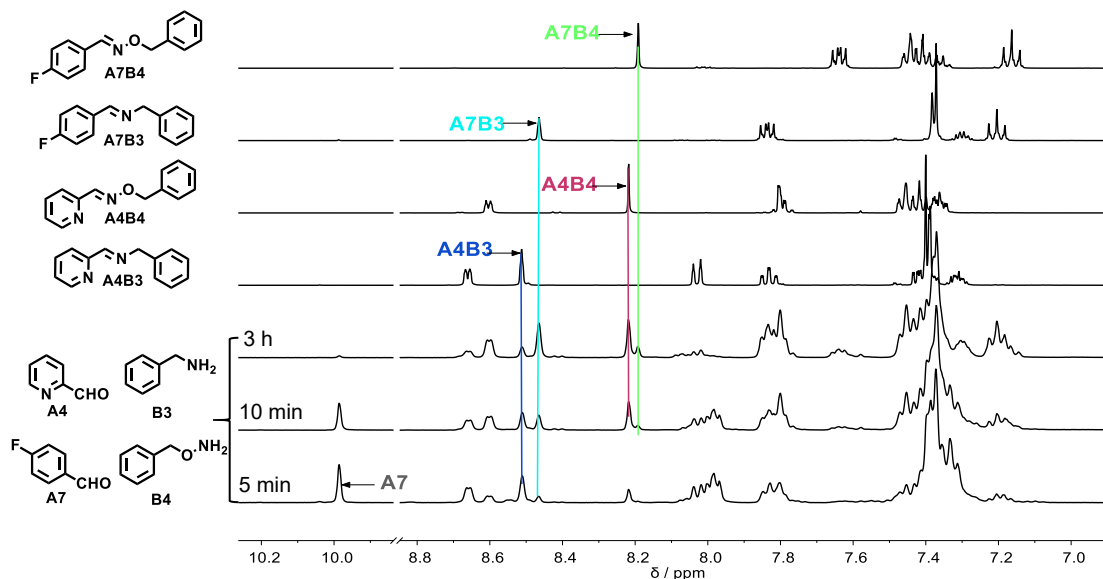
4) DCL generated from equal amounts of **A4** + **A7** + **B3** + **B4**

Figure III13. ^1H NMR (400 MHz) spectra of the mixture generated from equal amounts of **A4** + **A7** + **B3** + **B4** (30 mM each, CD_3CN , r.t.) after 5 min, 10 min, 3 h (from bottom to up). The top four traces are the reference spectra of the separately prepared constituents **A4B3**, **A4B4**, **A7B3** and **A7B4**.

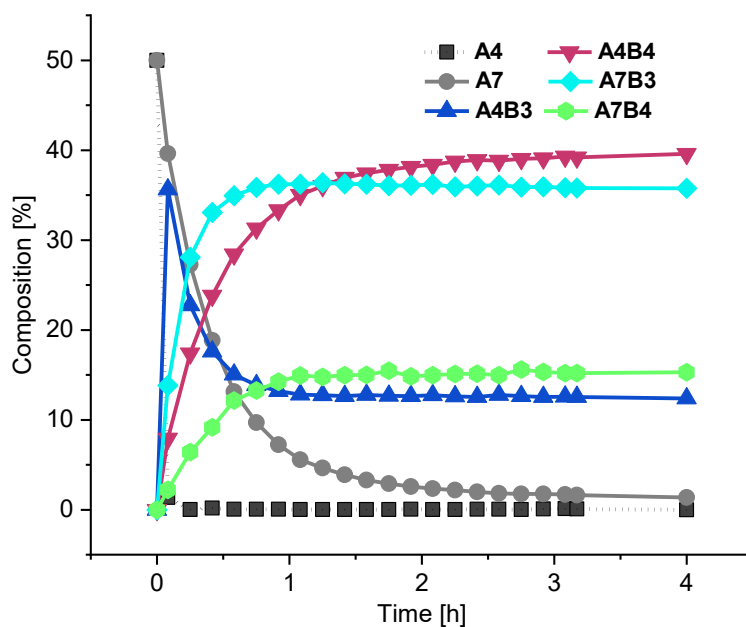
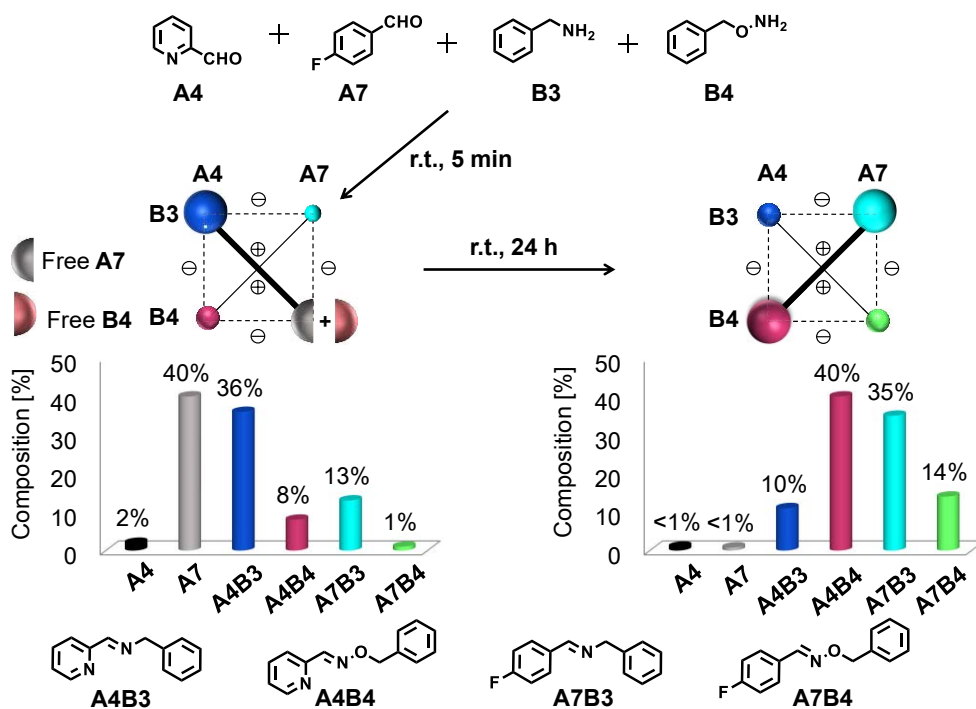


Figure III14. Kinetic plots of the evolution of the mixture of equal amounts of components **A4** + **A7** + **B3** + **B4** as a function of time obtained from integration of the imine $\text{CH}=\text{N}$ and aldehyde CHO proton signals in the 400 MHz ^1H NMR spectra (30 mM each, CD_3CN , r.t.). For clarity, the kinetic curves are shown for only some of the compounds.



Scheme III3. Kinetic switch of a $[2 \times 2]$ DCL from the $[A4B3, A7 + B4]$ state to the orthogonal state $[A4B4, A7B3]$ in CD_3CN at room temperature. Data obtained from the 400 MHz 1H NMR spectra.

Table III15. Time-dependent evolution of DCL distributions generated from equal amounts of **A4** + **A7** + **B3** + **B4**

Entry	t [h] ^[b]	Compound Distribution [%] ^[c]					
		A4	A7	A4B3	A4B4	A7B3	A7B4
1 ^[a]	0.08	1%	40%	36%	8%	14%	2%
2 ^[a]	0.75	0%	10%	14%	31%	36%	13%
3 ^[a]	2.3	0%	2%	13%	39%	36%	15%

^[a] The reaction was performed in CD_3CN , 30 mM each, r.t. ^[b] Reaction times indicate the time at which distribution data were collected. ^[c] Error in 1H -NMR signal integration: 5%.

5) DCL generated from equal amounts of **A1 + A6 + B3 + B4****Table III16.** Time-dependent of the evolution of DCL distributions generated from equal amounts of **A1 + A6 + B3 + B4**.

Entry	t [h] ^[b]	Compound Distribution [%] ^[c]					
		A1	A6	A1B3	A1B4	A6B3	A6B4
1 ^[a]	0.083	3%	44%	32%	14%	6%	1%
2 ^[a]	0.5	0%	19%	14%	37%	29%	4%
3 ^[a]	4	0%	1%	9%	41%	43%	7%

^[a] The reaction was performed at 25°C. ^[b] Reaction times indicate the time at which distribution data were collected. ^[c] Error in ¹H-NMR signal integration: 5%.

6) DCL generated from equal amounts of **A1 + A4 + B3 + B5****Table III17.** Time-dependent of the evolution of DCL distributions generated from equal amounts of **A1 + A4 + B3 + B5**.

Entry	t [h] ^[b]	Compound Distribution [%] ^[c]					
		A1	A4	A1B3	A1B5	A4B3	A4B5
1 ^[a]	0.5	10%	20%	40%	1%	29%	<1%
2 ^[a]	10	2%	8%	26%	25%	27%	14%
3 ^[a]	46	0%	2%	19%	32%	25%	21%

^[a] The reaction was performed in CD₃CN, 30 mM each, r.t. ^[b] Reaction times indicate the time at which distribution data were collected. ^[c] Error in ¹H-NMR signal integration: 5%.

iv. Four-component DCLs in the presence of metal ions

For the experiments in inorganic part (in the presence of **AgOTf** and **Zn(OTf)₂**), the same equivalent of four components (10 mM) (because of the solubility) together with 0.5 equiv. **AgOTf** (5 mM) and 0.5 equiv. **Zn(OTf)₂** (5 mM) were mixed at the same time in CD₃CN, the composition of the DCL was monitored by ¹H NMR as a function of time. The composition of the DCLs was determined by comparison with the internal standard.

1) DCL generated from equal amounts of **A1 + A8 + B1 + B2** in presence of 0.5 equiv. of AgOTf and Zn(OTf)₂

Table III18. Time-dependent of the evolution of DCL distributions generated from equal amounts of **A1 + A8 + B1 + B2** (10 mM each) in the presence of both AgOTf (0.5 equiv., 5 mM) and Zn(OTf)₂ (0.5 equiv., 5 mM).

Entry	t [h] ^[b]	Compound Distribution [%] ^[c]					
		A8	A1	[Ag(A1B1) ₂] ⁺	[Zn(A1B2) ₂] ²⁺	A8B4	A8B5
1 ^[a]	1	50%	<1%	48%	<1%	<1%	0%
2 ^[a]	70	5%	<1%	10%	41%	38%	6%

^[a] The reaction was performed in CD₃CN, r.t. ^[b] Reaction times indicate the time at which distribution data were collected. ^[c] Error in ¹H-NMR signal integration: 5%.

Quantitative integration of DCL[5] (A1 + A8 + B1 + B2) in presence of AgOTf and Zn(OTf)₂ after 1 h and 70 h.

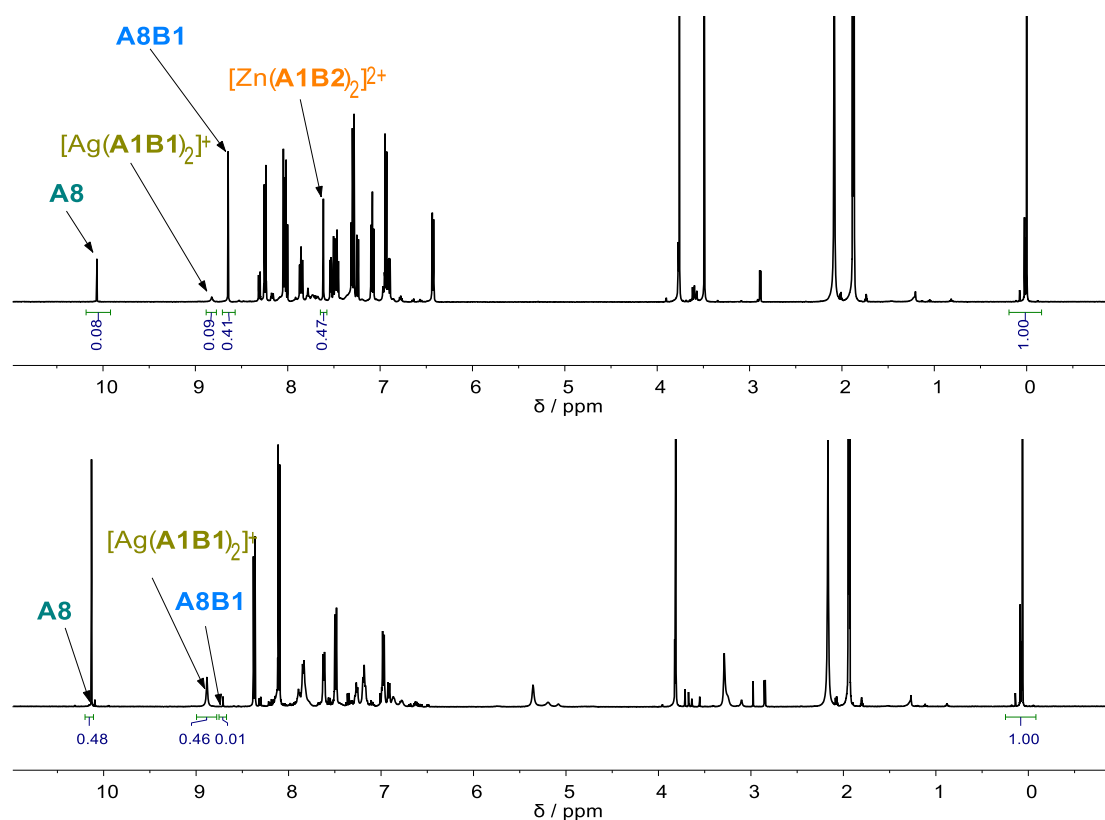


Figure III15. ¹H NMR (600 MHz) spectra of the mixture generated from equal amounts of **A1 + A8 + B1 + B2** (10 mM each, CD₃CN) + 0.5 equiv. AgOTf + 0.5 equiv. Zn(OTf)₂ after 1 h (bottom) and 70 hours (top) at 25°C.

2) DCL generated from equal amounts of **A2 + A8 + B1 + B2** in presence of 0.5 equiv. of AgOTf and Zn(OTf)₂

Table III19. Time-dependent of the evolution of DCL[5] distributions generated from equal amounts of **A2 + A8 + B1 + B2** (10 mM each) in the presence of both AgOTf (0.5 equiv., 5 mM) and Zn(OTf)₂ (0.5 equiv., 5 mM).

Entry	t [h] ^[c]	Compound Distribution [%] ^[d]					
		A8	A2	[Ag(A2B1) ₂] ⁺	[Zn(A2B2) ₂] ²⁺	A8B1	A8B2
1 ^[a]	1	49%	3%	47%	<1%	1%	<1%
2 ^[b]	2 days	10%	<1%	11%	39%	40%	<1%

^[a] The reaction was performed in CD₃CN, r.t. ^[b] The reaction was performed at 60°C. ^[c] Reaction times indicate the time at which distribution data were collected. ^[d] Error in ¹H-NMR signal integration: 5%.

Quantitative integration of DCL[6] (A2+A8+B1+B2) in presence of AgOTf and Zn(OTf)₂ after 1 h and heating for 2 days

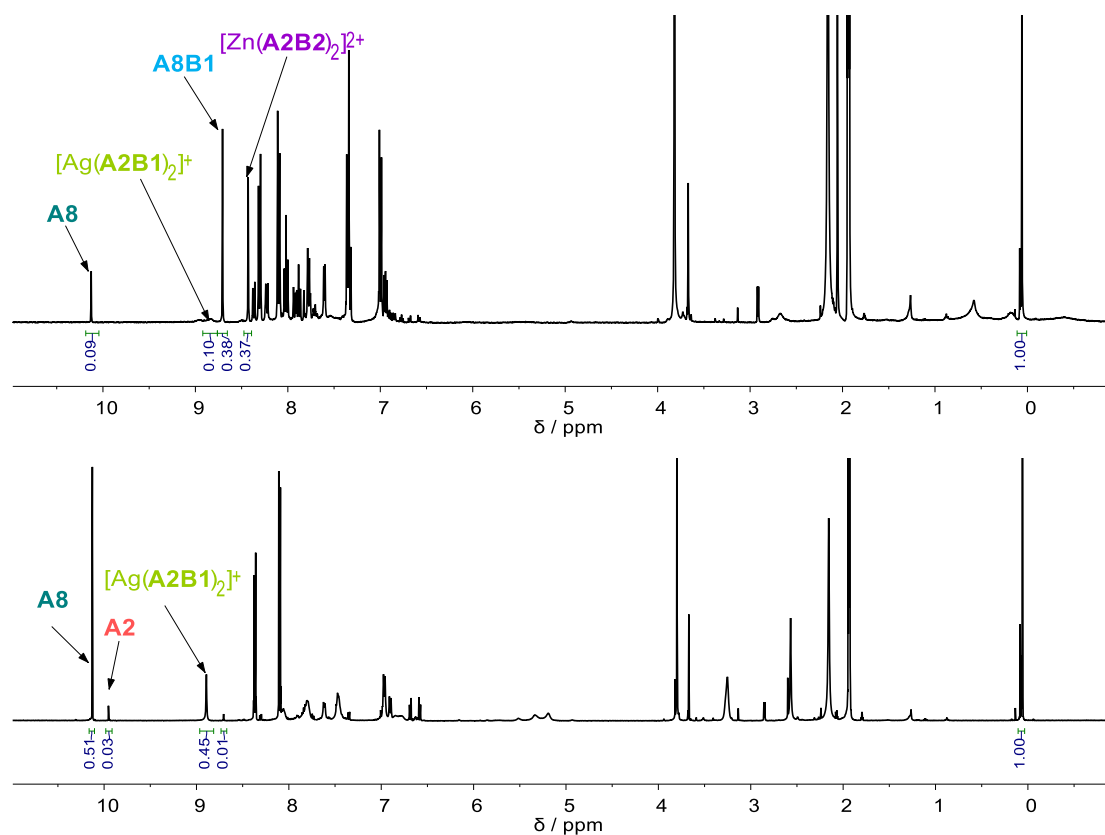


Figure III16. ¹H NMR (600 MHz) spectra of the mixture generated from equal amounts of **A2 + A8 + B1 + B2** (10 mM each, CD₃CN) + 0.5 equiv. AgOTf + 0.5 equiv. Zn(OTf)₂ after 1 h (bottom) and after heating for 2 days (top).

3) DCL generated from equal amounts of **A3** + **A8** + **B1** + **B2** in presence of 0.5 equiv. of AgOTf and Zn(OTf)₂

Table III20. Time-dependent of the evolution of **DCL[6]** distributions generated from equal amounts of **A8+A6+B4+B5** (10 mM) in the presence of both AgOTf (0.5 equiv., 5 mM) and Zn(OTf)₂ (0.5 equiv., 5 mM).

Entry	t [h] ^[c]	Compound Distribution [%] ^[d]					
		A8	A3	[Ag(A3B1) ₂] ⁺	[Zn(A3B2) ₂] ²⁺	A8B1	A8B2
1 ^[a]	1	46%	1%	48%	<1%	1%	8%
2 ^[b]	2 days	6%	<1%	11%	43%	2%	<1%

^[a] The reaction was performed at 25°C. ^[b] The reaction was performed at 60°C. ^[c] Reaction times indicate the time at which distribution data were collected. ^[d] Error in ¹H-NMR signal integration: 5%.

Quantitative integration of DCL[7] (A3+A8+B1+B2) in presence of AgOTf and Zn(OTf)₂ after 1 h and 2 days (heating).

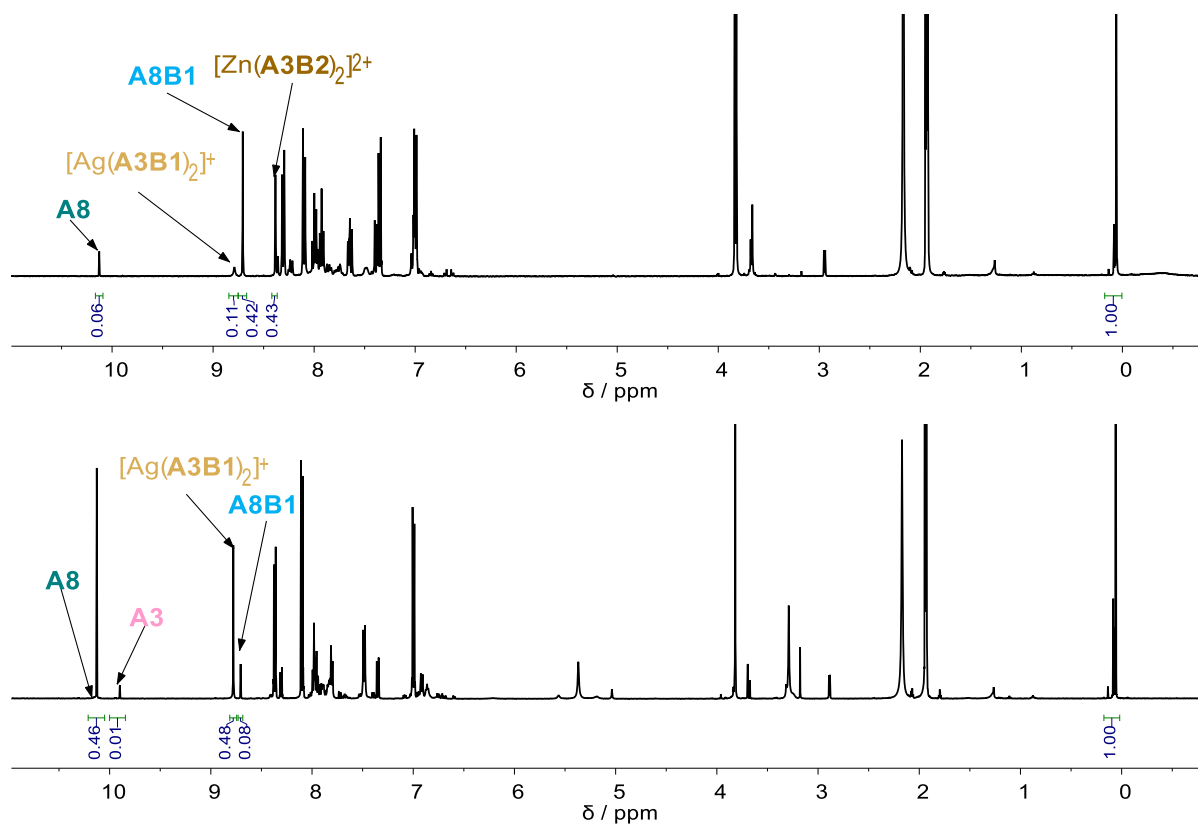


Figure III17. ¹H NMR (600 MHz) spectra of the mixture generated from equal amounts of **A3** + **A8** + **B1** + **B2** (10 mM each, CD₃CN) + 0.5 equiv. AgOTf + 0.5 equiv. Zn(OTf)₂ after 1 hour (bottom), and after heating 2 days (top).

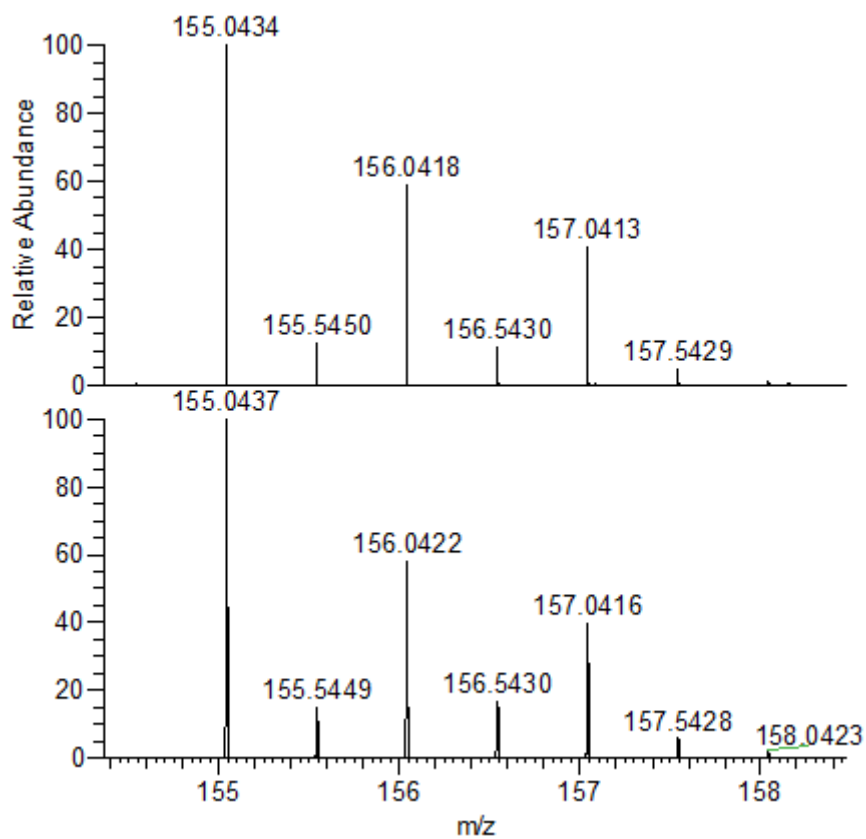
4) HRMS-ESI spectra of Zinc (II) complex $[\text{Zn}(\text{B2})_2]^{2+}$ of **B2**.

Figure III18. HRMS-ESI spectrum of $[\text{Zn}(\text{B2})_2]^{2+}$ obtained in situ from 3 equiv. **B2** (30 mM) and 1 equiv. $\text{Zn}(\text{OTf})_2$ (10 mM) in CH_3CN . Measured (top), simulated (bottom).

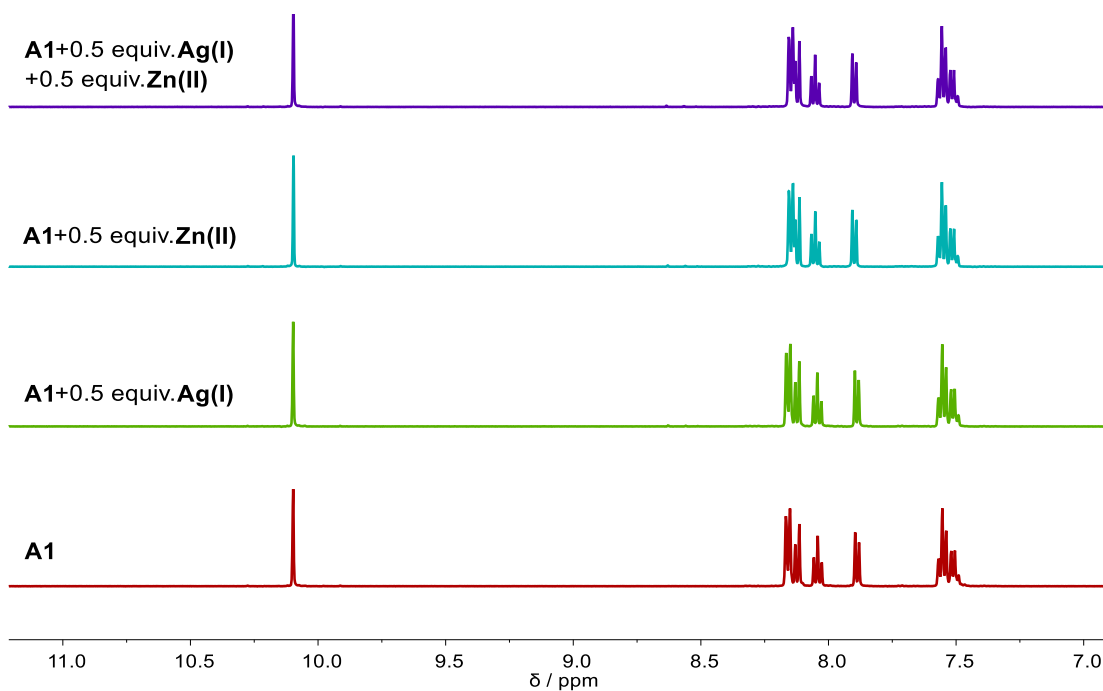
5) ^1H NMR spectra of all the components and constituents in the absence of presence of metal salts

Figure III19. ^1H NMR (500 MHz) spectra of **A1**, **A1**+0.5 equiv. AgOTf , **A1**+0.5 equiv. $\text{Zn}(\text{OTf})_2$ and **A1**+0.5 equiv. AgOTf +0.5 equiv. $\text{Zn}(\text{OTf})_2$ obtained from freshly mixing the components in CD_3CN at r.t. The concentration for **A1** is 10 mM and for AgOTf or $\text{Zn}(\text{OTf})_2$ is 5 mM.

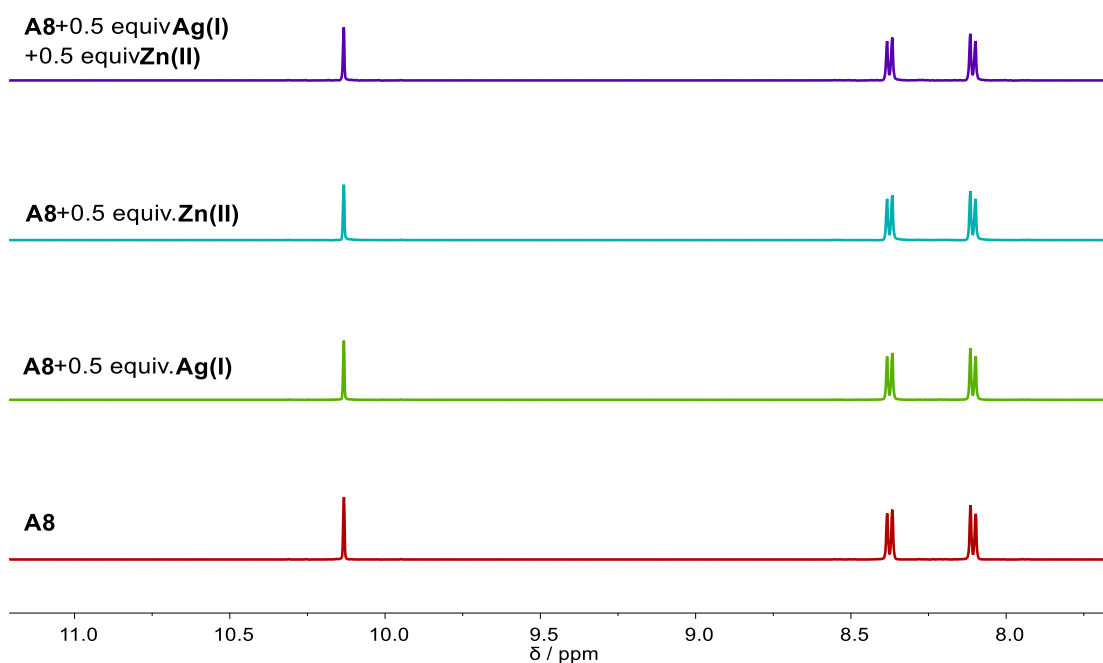


Figure III20. ^1H NMR (500 MHz) spectra of **A8**, **A8**+0.5 equiv. AgOTf , **A8**+0.5 equiv. $\text{Zn}(\text{OTf})_2$ and **A8**+0.5 equiv. AgOTf +0.5 equiv. $\text{Zn}(\text{OTf})_2$ obtained from freshly mixing the components in CD_3CN at r.t. The concentration for **A8** is 10 mM and for AgOTf or $\text{Zn}(\text{OTf})_2$ is 5 mM.

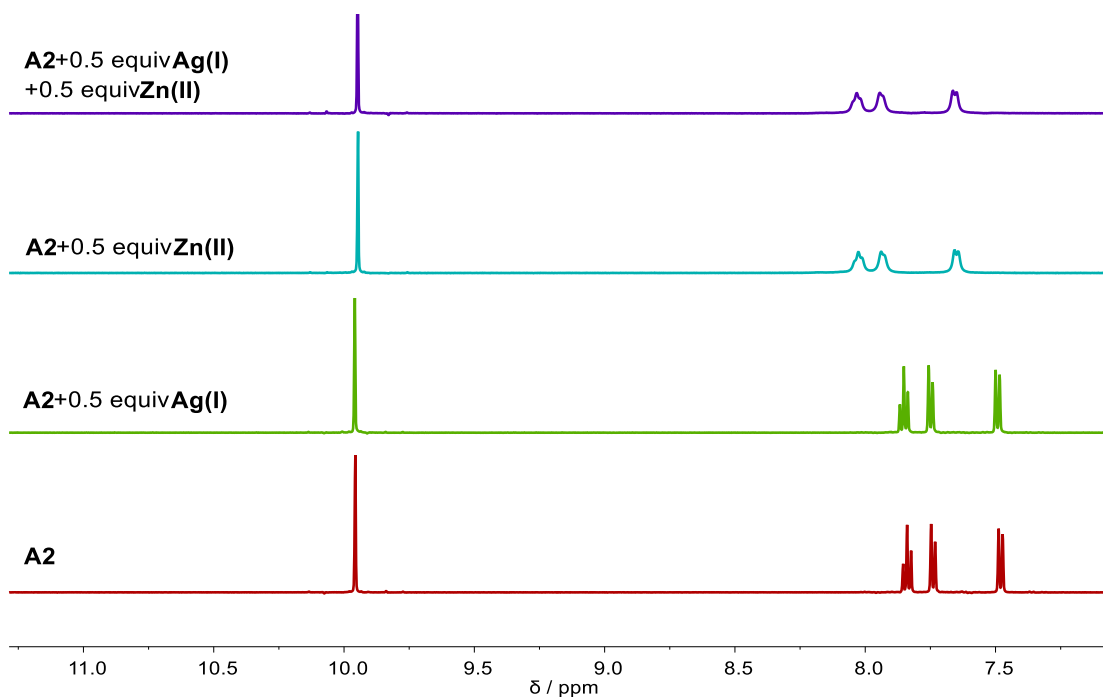


Figure III21. ¹H NMR (500 MHz) spectra of **A2**, **A2**+0.5 equiv. AgOTf, **A2**+0.5 equiv. Zn(OTf)₂ and **A2**+0.5 equiv. AgOTf +0.5 equiv. Zn(OTf)₂ obtained from freshly mixing the components in CD₃CN at r.t. The concentration for **A2** is 10 mM and for AgOTf or Zn(OTf)₂ is 5 mM.

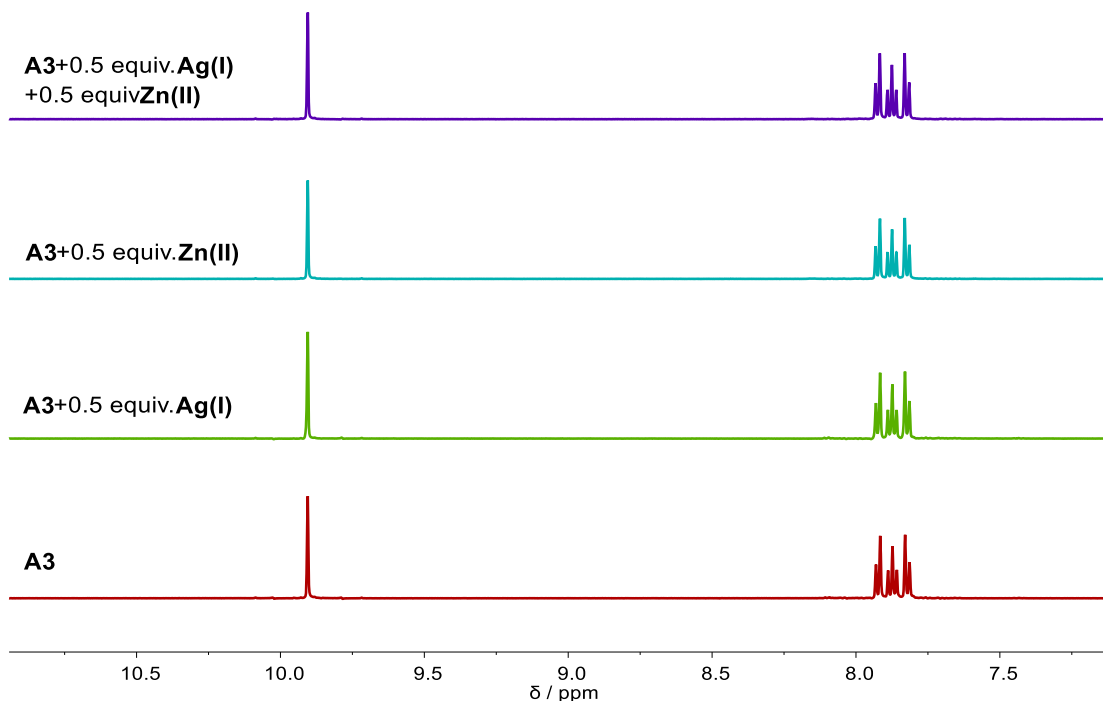


Figure III22. ¹H NMR (500 MHz) spectra of **A3**, **A3**+0.5 equiv. AgOTf, **A3**+0.5 equiv. Zn(OTf)₂ and **A3**+0.5 equiv. AgOTf +0.5 equiv. Zn(OTf)₂ obtained from freshly mixing the components in CD₃CN at r.t. The concentration for **A3** is 10 mM and for AgOTf or Zn(OTf)₂ is 5 mM.

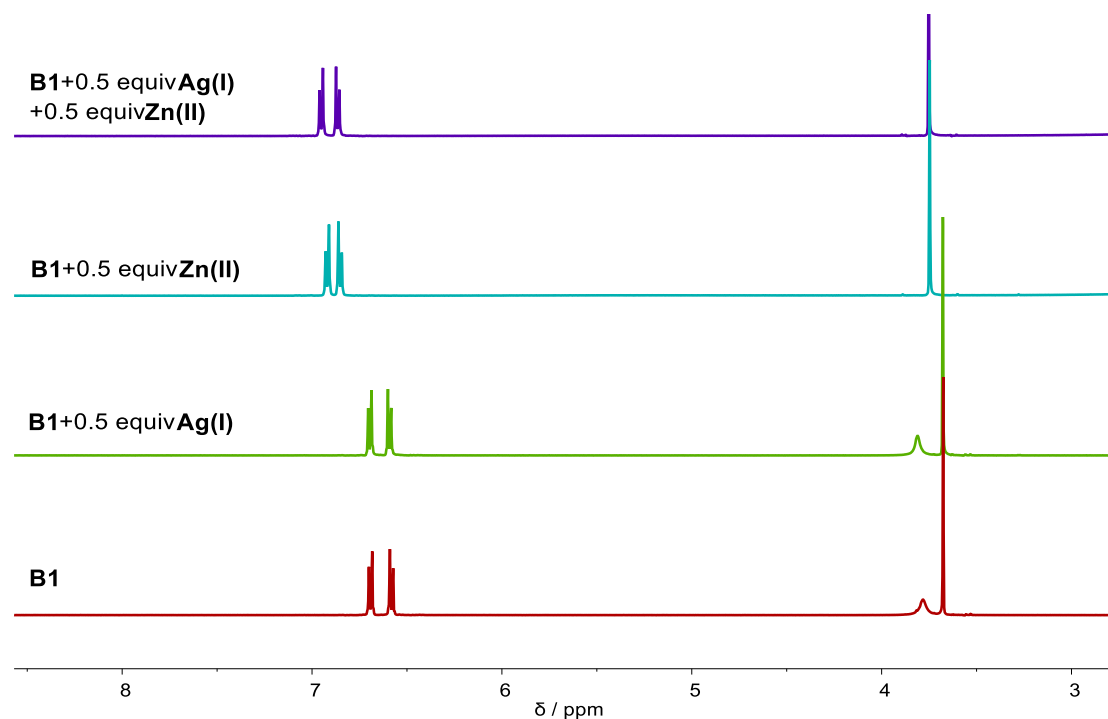


Figure III23. ¹H NMR (500 MHz) spectra of **B1**, **B1**+0.5 equiv. AgOTf, **B1**+0.5 equiv. Zn(OTf)₂ and **B1**+0.5 equiv. AgOTf +0.5 equiv. Zn(OTf)₂ obtained from freshly mixing the components in CD₃CN at r.t. The concentration for **B1** is 10 mM and for AgOTf or Zn(OTf)₂ is 5 mM.

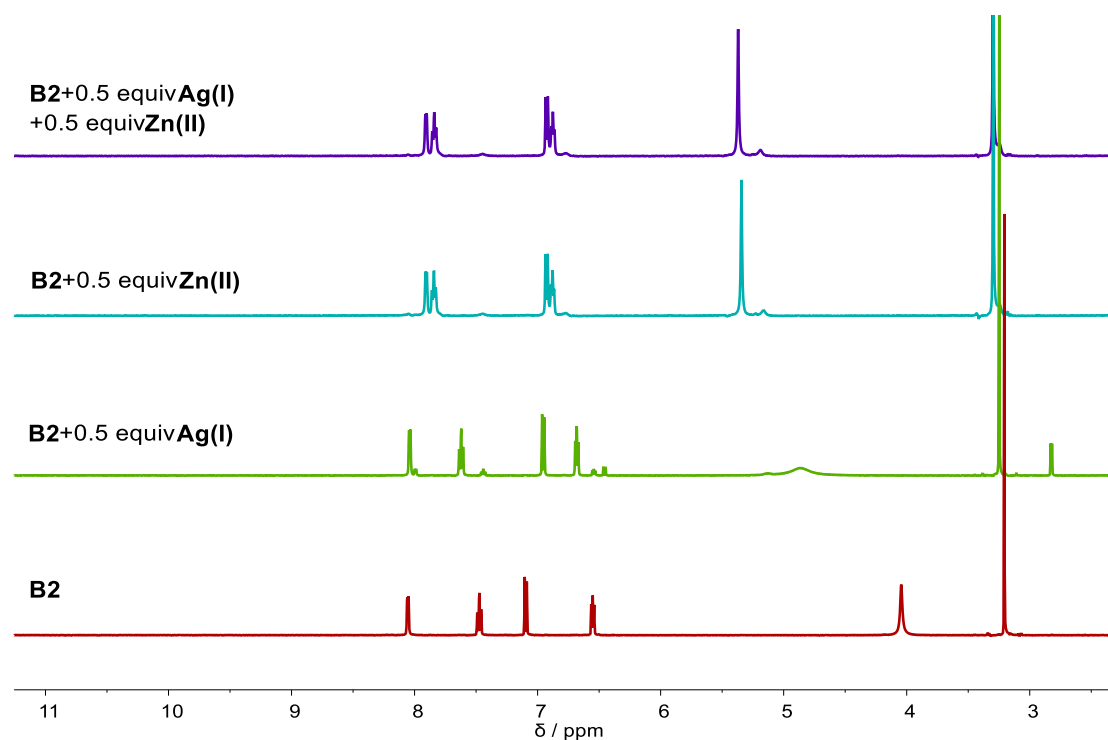


Figure III24. ¹H NMR (500 MHz) spectra of **B2**, **B2**+0.5 equiv. AgOTf, **B2**+0.5 equiv. Zn(OTf)₂ and **B2**+0.5 equiv. AgOTf +0.5 equiv. Zn(OTf)₂ obtained from freshly mixing the components in CD₃CN at r.t. The concentration for **B2** is 10 mM and for AgOTf or Zn(OTf)₂ is 5 mM.

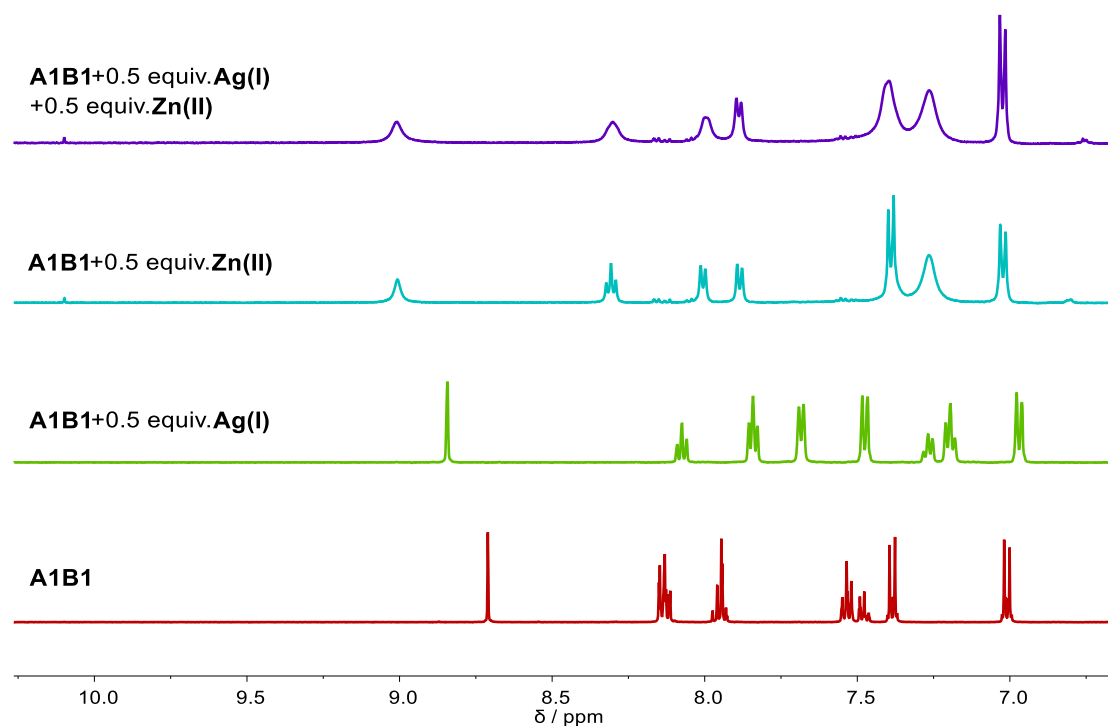


Figure III25. ¹H NMR (500 MHz) spectra of **A1B1**, **A1B1**+0.5 equiv. AgOTf, **A1B1**+0.5 equiv. Zn(OTf)₂ and **A1B1**+0.5 equiv. AgOTf +0.5 equiv. Zn(OTf)₂ obtained from freshly mixing the components in CD₃CN at r.t. The concentration for **A1B1** is 10 mM and for AgOTf or Zn(OTf)₂ is 5 mM.

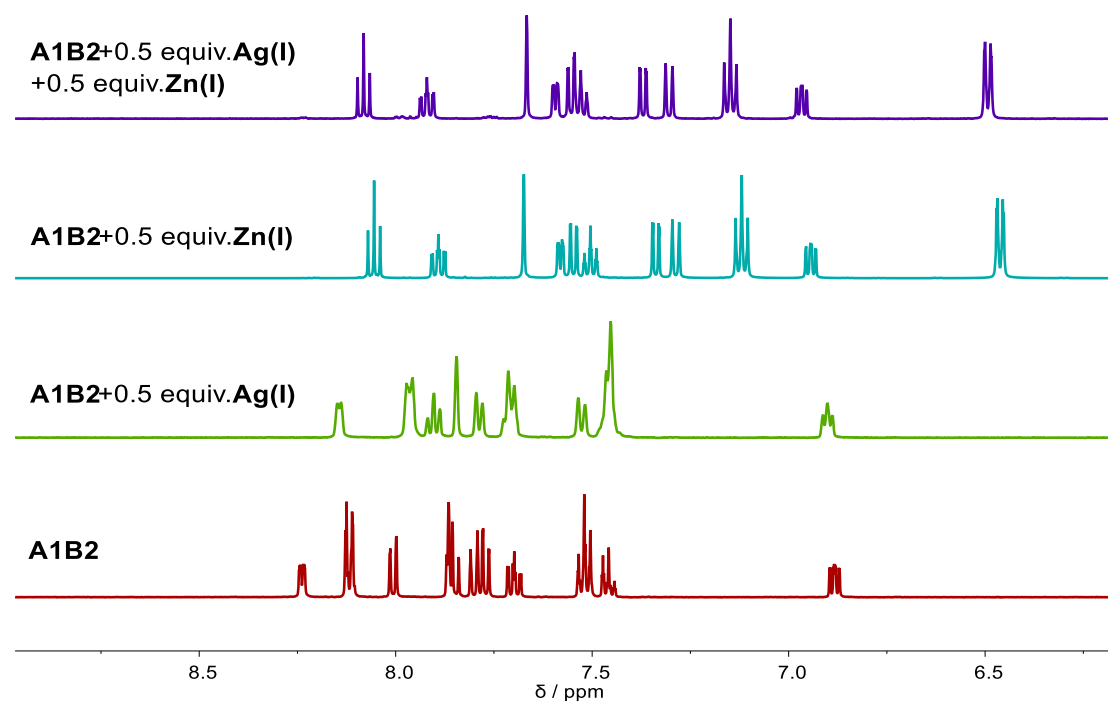


Figure III26. ¹H NMR (500 MHz) spectra of **A1B2**, **A1B2**+0.5 equiv. AgOTf, **A1B2**+0.5 equiv. Zn(OTf)₂ and **A1B2**+0.5 equiv. AgOTf +0.5 equiv. Zn(OTf)₂ obtained from freshly mixing the components in CD₃CN at r.t. The concentration for **A1B2** is 10 mM and for AgOTf or Zn(OTf)₂ is 5 mM.

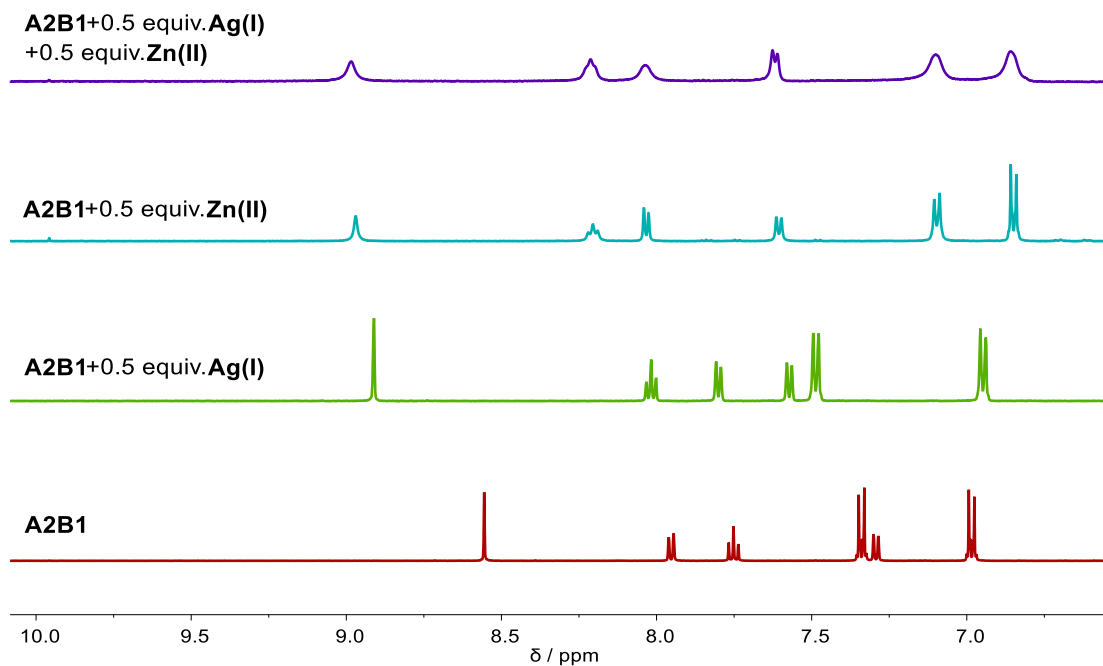


Figure III27. ¹H NMR (500 MHz) spectra of **A2B1**, **A2B1**+0.5 equiv. AgOTf, **A2B1**+0.5 equiv. Zn(OTf)₂ and **A2B1**+0.5 equiv. AgOTf +0.5 equiv. Zn(OTf)₂ obtained from freshly mixing the components in CD₃CN at r.t. The concentration for **A2B1** is 10 mM and for AgOTf or Zn(OTf)₂ is 5 mM.

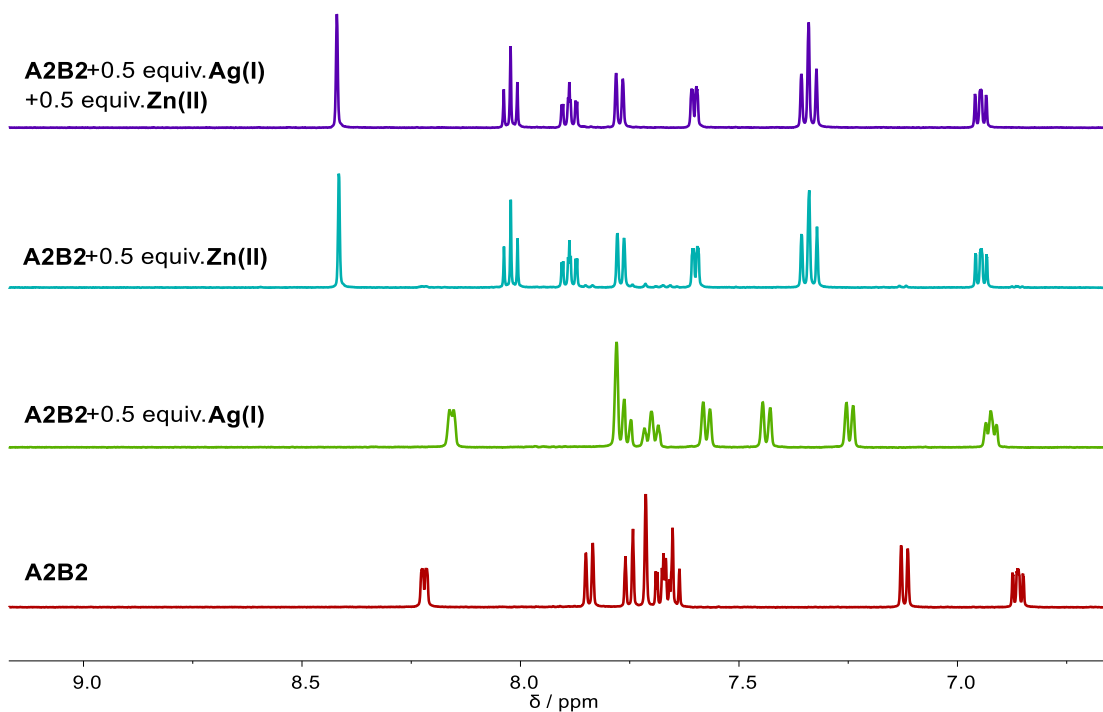


Figure III28. ¹H NMR (500 MHz) spectra of **A2B2**, **A2B2**+0.5 equiv. AgOTf, **A2B2**+0.5 equiv. Zn(OTf)₂ and **A2B2**+0.5 equiv. AgOTf +0.5 equiv. Zn(OTf)₂ obtained from freshly mixing the components in CD₃CN at r.t. The concentration for **A2B2** is 10 mM and for AgOTf or Zn(OTf)₂ is 5 mM.

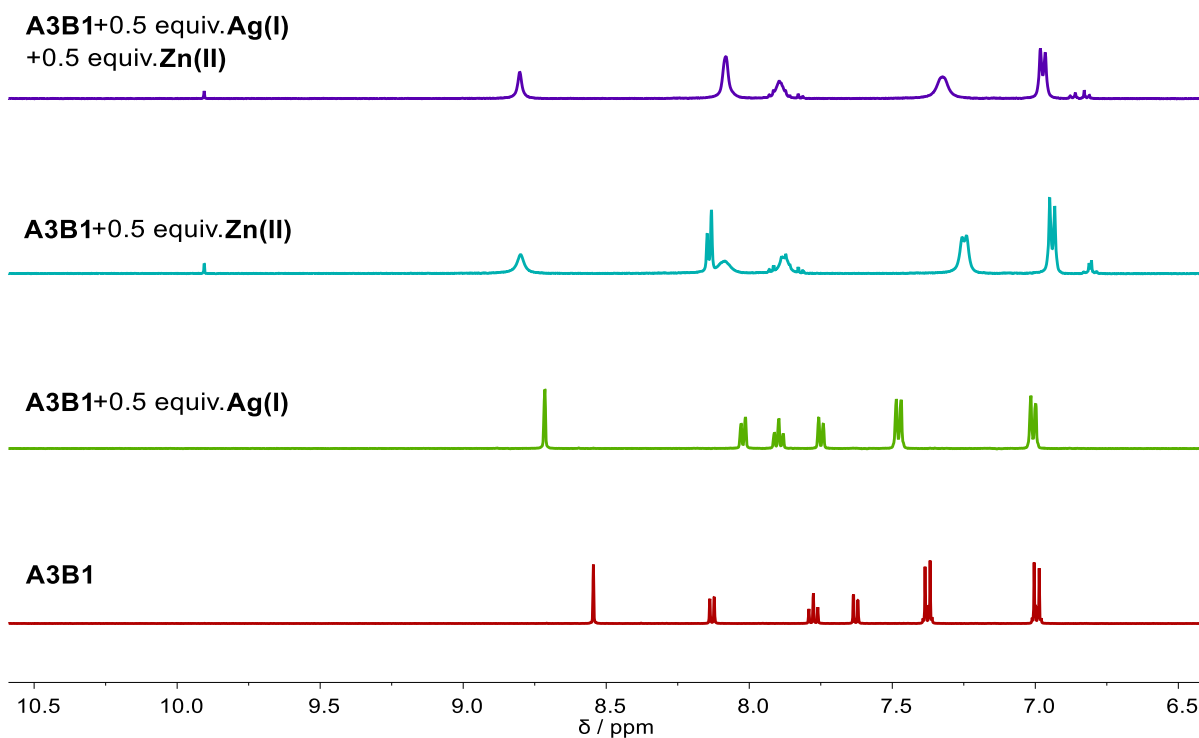


Figure III29. ¹H NMR (500 MHz) spectra of **A3B1**, **A3B1**+0.5 equiv. AgOTf, **A3B1**+0.5 equiv. Zn(OTf)₂ and **A3B1**+0.5 equiv. AgOTf +0.5 equiv. Zn(OTf)₂ obtained from freshly mixing the components in CD₃CN at r.t. The concentration for **A3B1** is 10 mM and for AgOTf or Zn(OTf)₂ is 5 mM.

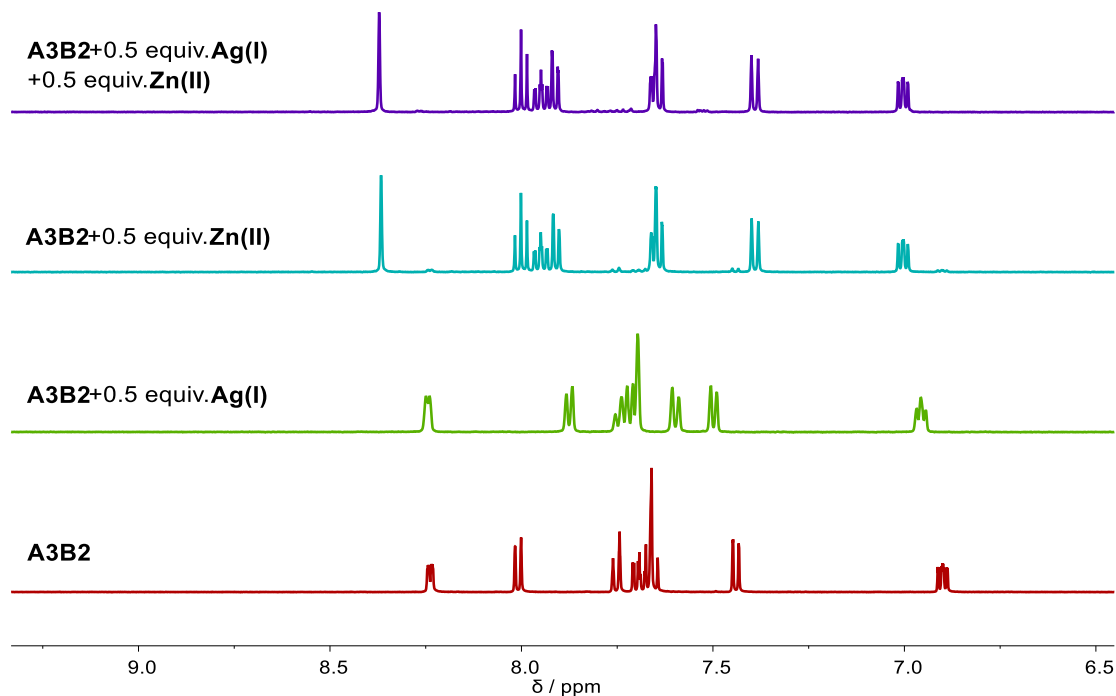


Figure III30. ¹H NMR (500 MHz) spectra of **A3B2**, **A3B2**+0.5 equiv. AgOTf, **A3B2**+0.5 equiv. Zn(OTf)₂ and **A3B2**+0.5 equiv. AgOTf +0.5 equiv. Zn(OTf)₂ obtained from freshly mixing the components in CD₃CN at r.t. The concentration for **A3B2** is 10 mM and for AgOTf or Zn(OTf)₂ is 5 mM.

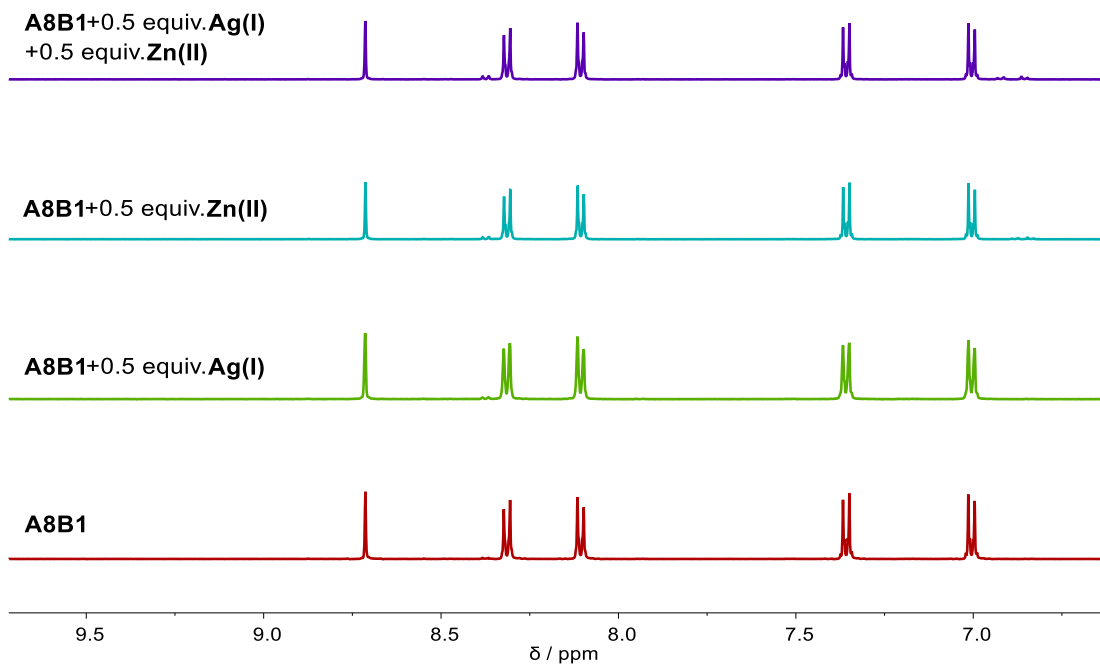


Figure III31. ¹H NMR (500 MHz) spectra of **A8B1**, **A8B1+0.5 equiv. AgOTf**, **A8B1+0.5 equiv. Zn(OTf)₂** and **A8B1+0.5 equiv. AgOTf +0.5 equiv. Zn(OTf)₂** obtained from freshly mixing the components in CD₃CN at r.t. The concentration for **A8B1** is 10 mM and for AgOTf or Zn(OTf)₂ is 5 mM.

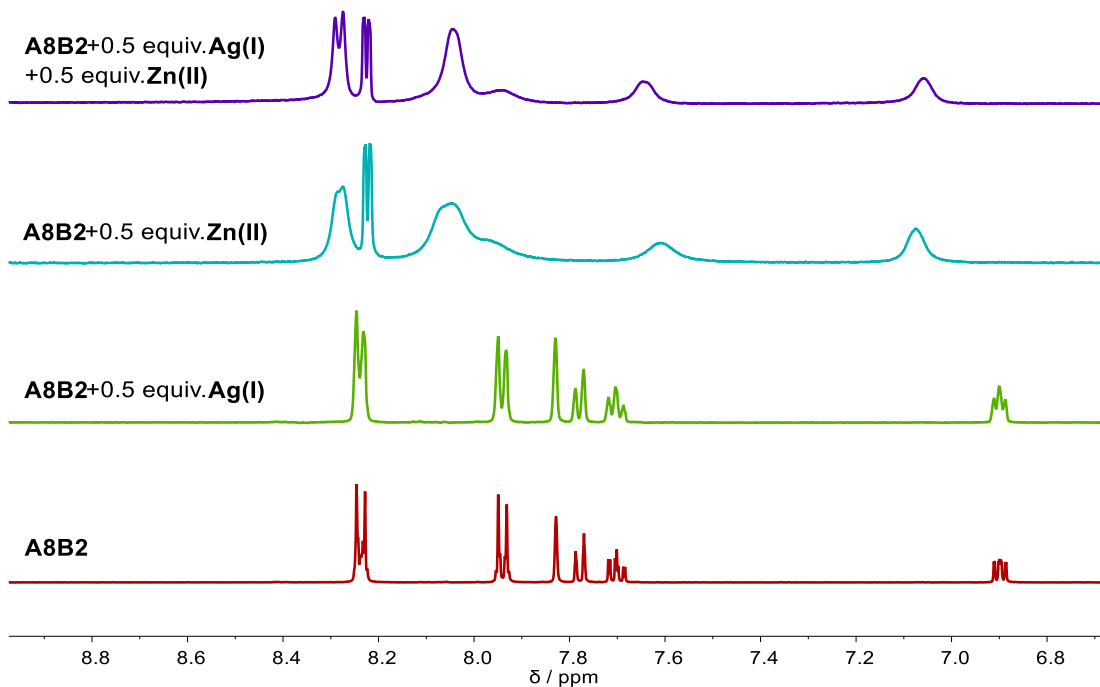


Figure III32. ¹H NMR (500 MHz) spectra of **A8B2**, **A8B2+0.5 equiv. AgOTf**, **A8B2+0.5 equiv. Zn(OTf)₂** and **A8B2+0.5 equiv. AgOTf +0.5 equiv. Zn(OTf)₂** obtained from freshly mixing the components in CD₃CN at r.t. The concentration for **A8B2** is 10 mM and for AgOTf or Zn(OTf)₂ is 5 mM.

4. CHAPTER IV. THE C=N FORMATION FOR GENE REGULATION

A. General procedures for the experiments

1) Procedures for preparation of the phosphate buffer

0.134 g of $\text{Na}_2\text{HPO}_4 \cdot 7\text{H}_2\text{O}$ ($M = 268.07$) was dissolved in approx. 9 ml of D_2O and then titrated to pH 11.39 at the lab temperature of 25°C with monovalent strong base (NaOD) or acid (DCI) as needed. The volume of D_2O was made up to 10 ml with pure water, the buffer was ready with pH 11.4 at 25°C .

2) Procedures for quantitative calculation of the imine yield

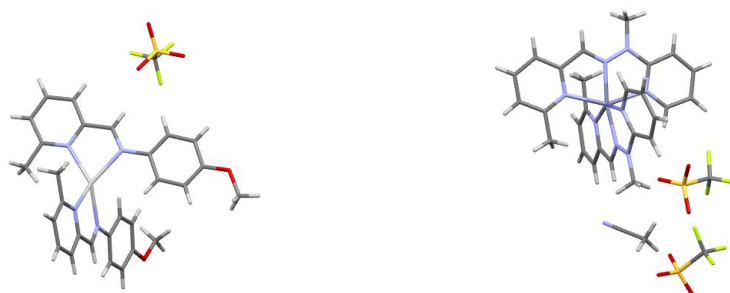
In a typical experiment, the stock solution of aldehydes (30 mM), the amine or hydrazine **By** (30 mM), and the internal standard (sodium trimethylsilylpropylsulfonate) (20 mM) was prepared in advance. And then the same volume (100 μL) of **Ax** and **By** were mixed together with the internal standard (10 μL) in phosphate buffer (600 μL). After vigorous shaking and 10 minutes, the resulting mixture was monitored at 25°C by ^1H NMR.

3) Procedures for titration experiment

The equimolar amount of the aldehyde and N- α -Lysine (5mM) was mixed together in 20 mL acidic D_2O . The generated solution was titrated with strong base to generate solutions with different pH consecutively. The prepared solution was waited for 30 minutes to reach equilibrium and the ^1H NMR spectra were measured for each of the solution at 25°C , respectively.

ANNEXES

1. CRYSTALLOGRAPHIC DATA FOR DETERMINED CRYSTAL STRUCTURES

Figure S1. Crystal structure for $[\text{Ag}(\text{A2B1})_2]^+$ and $[\text{Zn}(\text{A2B2})_2]^{2+}$.Table S1. Crystal data and structure refinement for $[\text{Ag}(\text{A2B1})_2]^+$ and $[\text{Zn}(\text{A2B2})_2]^{2+}$

Compound	$[\text{Ag}(\text{A2B1})_2]^+$	$[\text{Zn}(\text{A2B2})_2]^{2+}$
Empirical formula	$\text{C}_{29}\text{H}_{28}\text{AgF}_3\text{N}_4\text{O}_5\text{S}$	$\text{C}_{30}\text{H}_{31}\text{F}_6\text{N}_9\text{O}_6\text{S}_2\text{Zn}$
Formula weight/ $\text{g}\cdot\text{mol}^{-1}$	709.48	857.13
Temperature/K	120(2)	120(2)
Wavelength/ \AA	0.71073	0.71073
Crystal system	Triclinic	Monoclinic
space group	P -1	P 2 ₁ /c
Unit cell dimensions/ \AA	a = 7.4188(4)	a = 17.3605(6)
	b = 14.6012(6)	b = 9.0875(3)
	c = 14.6512(7)	c = 23.7855(9)
Unit cell angles/ $^\circ$	α = 98.563(2)	α = 90
	β = 104.430(2)	β = 106.9770(10)
	γ = 103.554(2)	γ = 90
Volume/ \AA^3	1457.52(12)	3589.0(2)
Z	2	4
Calculated density/ $\text{Mg}\cdot\text{m}^{-3}$	1.617	1.586
Absorption coefficient/ mm^{-1}	0.829	0.888
$F(000)$	720	1752

Annexes

Crystal size/mm ³	0.180 × 0.150 × 0.120	0.160 × 0.140 × 0.080
θ range for data collection/°	2.298 to 30.095	2.413 to 29.030
Limiting indices	-10 ≤ h ≤ 10	-23 ≤ h ≤ 23
	-16 ≤ k ≤ 20	-12 ≤ k ≤ 10
	-20 ≤ l ≤ 20	-32 ≤ l ≤ 32
Reflections collected	101550	107770
Independent reflections	8560 [R(int) = 0.0346]	9560 [R(int) = 0.0283]
Completeness to $\theta = 25.242$	99.9 %	100.0 %
Absorption correction	Semi-empirical from equivalents	Semi-empirical from equivalents
Max. and min. transmission	0.7460 / 0.7019	0.7458 / 0.6963
Refinement method	Full-matrix least- squares on F^2	Full-matrix least- squares on F^2
Data / restraints / parameters	8560 / 0 / 392	9560 / 0 / 492
Goodness-of-fit on F^2	1.043	1.019
Final R indices [$I > 2\sigma(I)$]	R ₁ = 0.0385, wR ₂ = 0.0925	R ₁ = 0.0374, wR ₂ = 0.0962
R indices [all data]	R ₁ = 0.0432, wR ₂ = 0.0963	R ₁ = 0.0410, wR ₂ = 0.0990
Largest diff. peak and hole/e. Å ⁻³	3.045 / -0.952	0.951 / -0.796

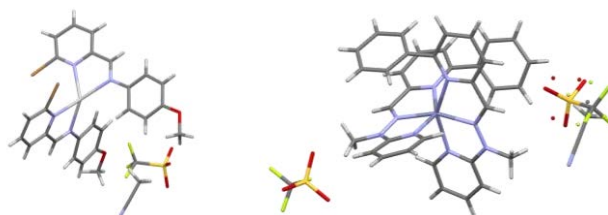


Figure S2. Crystal structure for [Ag(A3B1)₂]⁺ and [Zn(A1B2)₂]²⁺.

Table S2. Crystal data and structure refinement for [Ag(A3B1)₂]⁺ and [Zn(A1B2)₂]²⁺

Compound	[Ag(A3B1) ₂] ⁺	[Zn(A1B2) ₂] ²⁺
Empirical formula	C ₂₉ H ₂₅ AgBr ₂ F ₃ N ₅ O ₅ S	C ₄₀ H ₃₅ F ₆ N ₉ O ₆ S ₂ Zn
Formula weight/g.mol ⁻¹	880.29	981.26
Temperature/K	173(2)	173(2)

Annexes

Wavelength/Å	0.71073	0.71073
Crystal system	Monoclinic	Monoclinic
space group	P 2 ₁ /c	P 2 ₁ /c
Unit cell dimensions/Å	a = 8.0188(2)	a = 21.6809(9)
	b = 16.5325(6)	b = 12.2832(5)
	c = 24.7696(9)	c = 15.8865(7)
Unit cell angles/°	α = 90	α = 90
	β = 93.9960(10)	β = 98.780(2)
	γ = 90	γ = 90
Volume/Å ³	3275.74(19)	4181.2(3)
Z	4	4
Calculated density/Mg.m ⁻³	1.785	1.559
Absorption coefficient/mm ⁻¹	3.182	0.774
F(000)	1736	2008
Crystal size/mm ³	0.340 × 0.120 ×	0.260 × 0.240 ×
	0.080	0.120
θ range for data collection/°	1.482 to 30.043	0.950 to 28.116
Limiting indices	-11 ≤ h ≤ 7	-28 ≤ h ≤ 28
	-23 ≤ k ≤ 23	-12 ≤ k ≤ 16
	-34 ≤ l ≤ 34	-21 ≤ l ≤ 21
Reflections collected	57399	68058
Independent reflections	9568 [R(int) =	10155 [R(int) =
	0.0381]	0.0856]
Completeness to θ = 25.242	100.0%	100.0 %
Absorption correction	Semi-empirical from equivalents	Semi-empirical from equivalents
Max. and min. transmission	0.7460 / 0.6184	0.7456 / 0.6545
Refinement method	Full-matrix least- squares on F ²	Full-matrix least- squares on F ²
Data / restraints / parameters	9568 / 0 / 406	10155 / 5 / 592
Goodness-of-fit on F ²	1.016	1.039
Final R indices [I > 2σ (I)]	R ₁ = 0.0483, wR ₂ =	R ₁ = 0.0549, wR ₂ =
	0.1225	0.1283
R indices [all data]	R ₁ = 0.0651, wR ₂ =	R ₁ = 0.1049, wR ₂ =
	0.1328	0.1602
Largest diff. peak and hole/e. Å ⁻³	2.702/ -2.110	1.256 / -1.030

REFERENCES

- (1) Pedersen, C. J. Cyclic Polyethers and Their Complexes. *J. Am. Chem. Soc.* **1967**, *2*, 209.
- (2) Pedersen, C. J. Crystalline Salt Complexes of Macrocyclic Polyethers *J. Am. Chem. Soc.* **1970**, *92*, 386–391.
- (3) Gokel, G. W.; Cram, D. J. Molecular Complexation of Arenediazonium and Benzoyl Cations by Macrocyclic Polyethers. *J. Chem. Soc. Chem. Commun.* **1973**, *1*, 481–482.
- (4) Kyba, E. P.; Sousa, L. R.; Sogah, G. D. Y.; Siegel, M. G.; Cram, D. J. Chiral, Hinged, and Functionalized Multiheteromacrocycles. *J. Am. Chem. Soc.* **1973**, *95*, 2691–2692.
- (5) Jane, M. Host-Guest Chemistry: Complexes between Organic Compounds Simulate the Substrate Selectivity of Enzymes. *Science* **1974**, *183*, 803–809.
- (6) Dietrich, B.; Lehn, J. M.; Sauvage, J. P. Diaza-Polyoxa-Macrocycles et Macrobicycles. *Tetrahedron Lett.* **1969**, *10*, 2885–2888.
- (7) Dietrich, B.; Lehn, J. M.; Sauvage, J. P. Les Cryptates. *Tetrahedron Lett.* **1969**, *10*, 2889–2892.
- (8) Cram, D. J. International Edition in English. *Angew. Chem. Int. Ed.* **1985**, *24*, 799–810.
- (9) J.-M. Lehn. Supramolecular Chemistry-Scope and Perspectives Molecules, Supermolecules, and Molecular Devices (Nobel Lecture). *Angew. Chem. Int. Ed.* **1988**, *27*, 89–112.
- (10) Ma, X.; Zhao, Y. Biomedical Applications of Supramolecular Systems Based on Host-Guest Interactions. *Chem. Rev.* **2015**, *115*, 7794–7839.
- (11) Hoeben, F. J. M.; Jonkheijm, P.; Meijer, E. W.; Schenning, A. P. H. J. About Supramolecular Assemblies of π -Conjugated Systems. *Chem. Rev.* **2005**, *105*, 1491–1546.
- (12) Artem Osypenko (2016) Supramolecular Self-assemblies of Triarylaminines: Fundamental Studies and Applications. [University of Strasbourg]
- (13) Hasenknopf, B.; Lehn, J. M.; Boumediene, N.; Dupont-Gervais, A.; Van Dorsselaer, A.; Kneisel, B.; Fenske, D. Self-Assembly of Tetra- and Hexanuclear Circular Helicates. *J. Am. Chem. Soc.* **1997**, *119*, 10956–10962.
- (14) Kramer R. Lehn, J.-M. Marquis-Rigault, A. Self-recognition in Helicate Self-assembly: Spontaneous Formation of Helical Metal Complexes from Mixtures of Ligands and Metal Ions. *Proc. Natl. Acad. Sci.* **1993**, *90*, 5394–5398.
- (15) Brady, P. A.; Sanders, J. K. M. Thermodynamically-Controlled Cyclisation and Interconversion of Oligocholates: Metal Ion Templated “living” Macrolactonisation. *J. Chem. Soc. Perkin Trans. 1.* **1997**, No. 21, 3237–3253.
- (16) Stadler, A.-M.; Ramírez, J.; Lehn, J.-M.; Vincent, B. Supramolecular Reactions of Metallo-architectures: Ag₂-Double-Helicate/Zn₄-Grid, Pb₄-Grid/Zn₄-Grid Interconversions, And Ag₂-Double-Helicate Fusion. *Chem. Sci.* **2016**, *7*, 3689–3693.
- (17) Hsu, C. W.; Miljanić, O. Š. Self-Sorting through Dynamic Covalent Chemistry; Zhang, W., Jin, Y., Eds.; John Wiley & Sons Ltd: Chichester, UK, 2018; pp 253–284.

- (18) Black, S. P.; Wood, D. M.; Schwarz, F. B.; Ronson, T. K.; Holstein, J. J.; Stefankiewicz, A. R.; Schalley, C. A.; Sanders, J. K. M.; Nitschke, J. R. Catenation and Encapsulation Induce Distinct Reconstitutions within a Dynamic Library of Mixed-Ligand Zn_4L_6 Cages. *Chem. Sci.* **2016**, *7*, 2614–2620.
- (19) Lal Saha, M.; Schmittel, M. Degree of Molecular Self-Sorting in Multicomponent Systems. *Org. Biomol. Chem.* **2012**, *10*, 4651–4684.
- (20) Ji, Q.; Lirag, R. C.; Miljanić, O. Š. Kinetically Controlled Phenomena in Dynamic Combinatorial Libraries. *Chem. Soc. Rev.* **2014**, *43*, 1873–1884.
- (21) Chambron, J.-C. *Perspect. Supramol. Chem.* **1999**, *5*, 225.
- (22) Mahata, K.; Saha, M. L.; Schmittel, M. From an Eight-Component Self-Sorting Algorithm to a Trisheterometallic Scalene Triangle. *J. Am. Chem. Soc.* **2010**, *132*, 15933–15935.
- (23) Addicott, C.; Das, N.; Stang, P. J. Self-Recognition in the Coordination Driven Self-Assembly of 2-D Polygons. *Inorg. Chem.* **2004**, *43*, 5335–5338.
- (24) Zheng, Y. R.; Yang, H. B.; Ghosh, K.; Zhao, L.; Stang, P. J. Multicomponent Supramolecular Systems: Self-Organization in Coordination-Driven Self-Assembly. *Chem. - A Eur. J.* **2009**, *15*, 7203–7214.
- (25) Sepehrpour, H.; Saha, M. L.; Stang, P. J. Fe-Pt Twisted Heterometallic Bicyclic Supramolecules via Multicomponent Self-Assembly. *J. Am. Chem. Soc.* **2017**, *139*, 2553–2556.
- (26) Zhou, Z.; Hauke, C. E.; Song, B.; Li, X.; Stang, P. J.; Cook, T. R. Understanding the Effects of Coordination and Self-Assembly on an Emissive Phenothiazine. *J. Am. Chem. Soc.* **2019**, *141*, 3717–3722.
- (27) Jiang, W.; Winkler, H. D. F.; Schalley, C. A. Integrative Self-Sorting: Construction of a Cascade-Stoppered Hetero[3]Rotaxane. *J. Am. Chem. Soc.* **2008**, *130*, 13852–13853.
- (28) Mahata, K.; Schmittel, M. From 2-Fold Complete to Integrative Self-Sorting: A Five-Component Supramolecular Trapezoid. *J. Am. Chem. Soc.* **2009**, *131*, 16544–16554.
- (29) Saha, M. L.; Schmittel, M. From 3-Fold Complete Self-Sorting of a Nine-Component Library to a Seven-Component Scalene Quadrilateral. *J. Am. Chem. Soc.* **2013**, *135*, 17743–17746.
- (30) Saha, M. L.; Mittal, N.; Bats, J. W.; Schmittel, M. A Six-Component Metallosupramolecular Pentagon via Self-Sorting. *Chem. Commun.* **2014**, *50*, 12189–12192.
- (31) Gaikwad, S.; Lal Saha, M.; Samanta, D.; Schmittel, M. Five-Component Trigonal Nanoprism with Six Dynamic Corners. *Chem. Commun.* **2017**, *53*, 8034–8037.
- (32) Ayme, J. F.; Beves, J. E.; Campbell, C. J.; Leigh, D. A. The Self-Sorting Behavior of Circular Helicates and Molecular Knots and Links. *Angew. Chem. Int. Ed.* **2014**, *53*, 7823–7827.
- (33) Campbell, C. J.; Leigh, D. A.; Vitorica-Yrezabal, I. J.; Woltering, S. L. A Simple and Highly Effective Ligand System for the Copper I-Mediated Assembly of Rotaxanes. *Angew. Chem. Int. Ed.* **2014**, *53*, 13771–13774.
- (34) Ayme, J. F.; Beves, J. E.; Leigh, D. A.; McBurney, R. T.; Rissanen, K.; Schultz, D. A Synthetic Molecular Pentafoil Knot. *Nat. Chem.* **2012**, *4*, 15–20.
- (35) Baxter, P.; Lehn, J. -M.; DeCian, A.; Fischer, J. Multicomponent Self-Assembly: Spontaneous Formation of a Cylindrical Complex from Five Ligands and Six Metal Ions. *Angew. Chem. Int. Ed.* **1993**, *32*, 69–72.
- (36) Chow, C. F.; Fujii, S.; Lehn, J. M. Metallodynamers: Neutral Dynamic Metallosupramolecular Polymers Displaying Transformation of Mechanical and Optical Properties on Constitutional Exchange. *Angew. Chem. Int. Ed.* **2007**, *46*, 5007–5010.

- (37) Fujii, S.; Lehn, J. M. Structural and Functional Evolution of a Library of Constitutional Dynamic Polymers Driven by Alkali Metal Ion Recognition. *Angew. Chem. Int. Ed.* **2009**, *48*, 7635–7638.
- (38) Ulrich, S.; Lehn, J. M. Reversible Switching between Macrocyclic and Polymeric States by Morphological Control in a Constitutional Dynamic System. *Angew. Chem. Int. Ed.* **2008**, *47*, 2240–2243.
- (39) Lehn, J.; Ulrich, S. Adaptation to Shape Switching by Component Selection in a Constitutional Dynamic System. *J. Am. Chem. Soc.* **2009**, *131*, 5546–5559.
- (40) Ulrich, S.; Buhler, E.; Lehn, J. M. Reversible Constitutional Switching between Macrocycles and Polymers Induced by Shape Change in a Dynamic Covalent System. *New J. Chem.* **2009**, *33*, 271–292.
- (41) Kramer, R.; Lehn, J. M.; Marquis-Rigault, A. Self-Recognition in Helicate Self-Assembly: Spontaneous Formation of Helical Metal Complexes from Mixtures of Ligands and Metal Ions. *Proc. Natl. Acad. Sci.* **1993**, *90*, 5394–5398.
- (42) Jin, Y.; Yu, C.; Denman, R. J.; Zhang, W. Recent Advances in Dynamic Covalent Chemistry. *Chem. Soc. Rev.* **2013**, *42*, 6634–6654.
- (43) Rowan, S. J.; Cantrill, S. J.; Cousins, G. R. L.; Sanders, J. K. M.; Stoddart, J. F. Dynamic Covalent Chemistry. *Angew. Chem. Int. Ed.* **2002**, *41*, 898–952.
- (44) Nagy, P. Kinetics and Mechanisms of Thiol-Disulfide Exchange Covering Direct Substitution and Thiol Oxidation-Mediated Pathways. *Antioxidants Redox Signal.* **2013**, *18*, 1623–1641.
- (45) Whiting, A.; Windsor, C. M. What Makes a Neutral Imino Dieneophile Undergo a Thermal, Non-Catalysed, Diels-Alder Reaction? *Tetrahedron* **1998**, *54*, 6035–6050.
- (46) Belowich, M. E.; Stoddart, J. F. Dynamic Imine Chemistry. *Chem. Soc. Rev.* **2012**, *41*, 2003–2024.
- (47) Black, S. P.; Sanders, J. K. M.; Stefankiewicz, A. R. Disulfide Exchange: Exposing Supramolecular Reactivity through Dynamic Covalent Chemistry. *Chem. Soc. Rev.* **2014**, *43*, 1861–1872.
- (48) Herrmann, A. Dynamic Combinatorial/Covalent Chemistry: A Tool to Read, Generate and Modulate the Bioactivity of Compounds and Compound Mixtures. *Chem. Soc. Rev.* **2014**, *43*, 1899–1933.
- (49) Meguellati, K.; Ladame, S. Reversible Covalent Chemistries Compatible with the Principles of Constitutional Dynamic Chemistry: New Reactions to Create More Diversity; 2011; pp 291–314.
- (50) Jin, Y.; Yu, C.; Denman, R. J.; Zhang, W. Recent Advances in Dynamic Covalent Chemistry. *Chem. Soc. Rev.* **2013**, *42*, 6634–6654.
- (51) Sadownik, J. W.; Ulijn, R. V. Dynamic Covalent Chemistry in Aid of Peptide Self-Assembly. *Curr. Opin. Biotechnol.* **2010**, *21*, 401–411.
- (52) Rowan, S. J.; Cantrill, S. J.; Cousins, G. R. L.; Sanders, J. K. M.; Stoddart, J. F. *Dynamic Covalent Chemistry*; 2002; Vol. 41.
- (53) Gasparini, G.; Dal Molin, M.; Lovato, A.; Prins, L. J. Dynamic Covalent Chemistry. In *Supramolecular Chemistry*; John Wiley & Sons, Ltd: Chichester, UK, 2012.
- (54) Lehn, J.-M. From Supramolecular Chemistry towards Constitutional Dynamic Chemistry and Adaptive Chemistry. *Chem. Soc. Rev.* **2007**, *36*, 151–160.
- (55) Lehn, J.-M. Dynamic Combinatorial Chemistry and Virtual Combinatorial Libraries. *Chem. - Eur. J.* **1999**, *5*, 2455–2463.
- (56) Barboiu, M.; Aastrup, T. (Teodor). *Constitutional Dynamic Chemistry*; Springer, 2012.

- (57) Huc, I.; Lehn, J. M. Virtual Combinatorial Libraries: Dynamic Generation of Molecular and Supramolecular Diversity by Self-Assembly. *Proc. Natl. Acad. Sci.* **1997**, *94*, 2106–2110.
- (58) Lehn, J. M. Perspectives in Chemistry - Aspects of Adaptive Chemistry and Materials. *Angew. Chem. Int. Ed.* **2015**, *54*, 3276–3289.
- (59) Corbett, P. T.; Leclaire, J.; Vial, L.; West, K. R.; Wietor, J.-L.; Sanders, J. K. M.; Otto, S. Dynamic Combinatorial Chemistry. *Chem. Rev.* **2006**, *106*, 3652–3711.
- (60) Hunt, R. A. R.; Otto, S. Dynamic Combinatorial Libraries: New Opportunities in Systems Chemistry. *Chem. Commun.* **2011**, *47*, 847–858.
- (61) Schaufelberger, F.; Timmer, B. J. J.; Ramström, O. Principles of Dynamic Covalent Chemistry. In *Dynamic Covalent Chemistry*; John Wiley & Sons, Ltd: Chichester, UK, 2017; pp 1–30.
- (62) Osypenko, A.; Dhers, S.; Lehn, J. M. Pattern Generation and Information Transfer through a Liquid/Liquid Interface in 3D Constitutional Dynamic Networks of Imine Ligands in Response to Metal Cation Effectors. *J. Am. Chem. Soc.* **2019**, *141*, 12724–12737.
- (63) Giuseppone, N.; Lehn, J. M. Protonic and Temperature Modulation of Constituent Expression by Component Selection in a Dynamic Combinatorial Library of Imines. *Chem. - Eur. J.* **2006**, *12*, 1715–1722.
- (64) Hafezi, N.; Lehn, J. M. Adaptation of Dynamic Covalent Systems of Imine Constituents to Medium Change by Component Redistribution under Reversible Phase Separation. *J. Am. Chem. Soc.* **2012**, *134*, 12861–12868.
- (65) Holub, J.; Vantomme, G.; Lehn, J. M. Training a Constitutional Dynamic Network for Effector Recognition: Storage, Recall, and Erasing of Information. *J. Am. Chem. Soc.* **2016**, *138*, 11783–11791.
- (66) Vantomme, G.; Jiang, S.; Lehn, J. M. Adaptation in Constitutional Dynamic Libraries and Networks, Switching between Orthogonal Metalloselection and Photoselection Processes. *J. Am. Chem. Soc.* **2014**, *136*, 9509–9518.
- (67) Men, G.; Lehn, J. M. Multiple Adaptation of Constitutional Dynamic Networks and Information Storage in Constitutional Distributions of Acylhydrazones. *Chem. Sci.* **2019**, *10*, 90–98.
- (68) Ayme, J.-F.; Lehn, J.-M. Self-Sorting of Two Imine-Based Metal Complexes: Balancing Kinetics and Thermodynamics in Constitutional Dynamic Networks. *Chem. Sci.* **2020**, *11*, 1114–1121.
- (69) Hasenknopf, B.; Lehn, J. M.; Kneisel, B. O.; Baum, G.; Fenske, D. Self-Assembly of a Circular Double Helicate. *Angew. Chem. Int. Ed.* **1996**, *35*, 1838–1840.
- (70) Huc, I.; Lehn, J.-M. Virtual Combinatorial Libraries: Dynamic Generation of Molecular and Supramolecular Diversity by Self-Assembly. *Proc. Natl. Acad. Sci.* **1997**, *94*, 2106–2110.
- (71) Li, J.; Nowak, P.; Otto, S. Dynamic Combinatorial Libraries: From Exploring Molecular Recognition to Systems Chemistry. *J. Am. Chem. Soc.* **2013**, *135*, 9222–9239.
- (72) Coughon, F. B. L.; Sanders, J. K. M. Evolution of Dynamic Combinatorial Chemistry. *Acc. Chem. Res.* **2012**, *45*, 2211–2221.
- (73) Ayme, J.-F.; Lehn, J.-M. Chapter One - From Coordination Chemistry to Adaptive Chemistry. *Supramol. Chem.* **2018**, *71*, 3–78.
- (74) Otto, S.; Furlan, R. L. E.; Sanders, J. K. M. Dynamic Combinatorial Libraries of Macrocyclic Disulfides in Water. *J. Am. Chem. Soc.* **2000**, *122*, 12063–12064.

- (75) Leclaire, J.; Vial, L.; Otto, S.; Sanders, J. K. M. Expanding Diversity in Dynamic Combinatorial Libraries: Simultaneous Exchange of Disulfide and Thioester Linkages. *Chem. Commun.* **2005**, No. 15, 1959–1961.
- (76) Corbett, P. T.; Otto, S.; Sanders, J. K. M. What Are the Limits to the Size of Effective Dynamic Combinatorial Libraries? *Org. Lett.* **2004**, *6*, 1825–1827.
- (77) Beeren, S. R.; Sanders, J. K. M. History and Principles of Dynamic Combinatorial Chemistry. *Dyn. Comb. Chem.* **2010**, 1–22.
- (78) Cousins, G. R. L.; Poulsen, S. A.; Sanders, J. K. M. Dynamic Combinatorial Libraries of Pseudo-Peptide Hydrazone Macrocycles. *Chem. Commun.* **1999**, *16*, 1575–1576.
- (79) Simpson, M. G.; Pittelkow, M.; Watson, S. P.; Sanders, J. K. M. Dynamic Combinatorial Chemistry with Hydrazones: Libraries Incorporating Heterocyclic and Steroidal Motifs. *Org. Biomol. Chem.* **2010**, *8*, 1181–1187.
- (80) Giuseppone, N.; Schmitt, J. L.; Lehn, J. M. Driven Evolution of a Constitutional Dynamic Library of Molecular Helices toward the Selective Generation of [2 × 2] Gridlike Arrays under the Pressure of Metal Ion Coordination. *J. Am. Chem. Soc.* **2006**, *128*, 16748–16763.
- (81) Ingerman, L. A.; Waters, M. L. Photoswitchable Dynamic Combinatorial Libraries: Coupling Azobenzene Photoisomerization with Hydrazone Exchange. *J. Org. Chem.* **2009**, *74*, 111–117.
- (82) Vantomme, G.; Hafezi, N.; Lehn, J.-M. A Light-Induced Reversible Phase Separation and Its Coupling to a Dynamic Library of Imines. *Chem. Sci.* **2014**, *5*, 1475–1483.
- (83) Herder, M.; Lehn, J.-M. The Photodynamic Covalent Bond: Sensitized Alkoxyamines as a Tool To Shift Reaction Networks Out-of-Equilibrium Using Light Energy. *J. Am. Chem. Soc.* **2018**, *140*, 7647–7657.
- (84) Herrmann, A.; Ghiseppe, N.; Lehn, J. M. Electric-Field Triggered Controlled Release of Bioactive Volatiles from Imine-Based Liquid Crystalline Phases. *Chem. - A Eur. J.* **2009**, *15*, 117–124.
- (85) Giuseppone, N.; Lehn, J.-M. Electric-Field Modulation of Component Exchange in Constitutional Dynamic Liquid Crystals. *Angew. Chem. Int. Ed.* **2006**, *45*, 4619–4624.
- (86) Sobczak, S.; Drożdż, W.; Lampronti, G. I.; Belenguer, A. M.; Katrusiak, A.; Stefankiewicz, A. R. Dynamic Covalent Chemistry under High-Pressure: A New Route to Disulfide Metathesis. *Chem. - A Eur. J.* **2018**, *24*, 8769–8773.
- (87) Giuseppone, N.; Lehn, J. M. Protonic and Temperature Modulation of Constituent Expression by Component Selection in a Dynamic Combinatorial Library of Imines. *Chem. - A Eur. J.* **2006**, *12*, 1715–1722.
- (88) Niu, Y.; Yuan, X.; Zhao, Y.; Zhang, W.; Ren, L. Temperature and pH Dual-Responsive Supramolecular Polymer Hydrogels Hybridized with Functional Inorganic Nanoparticles. *Macromol. Chem. Phys.* **2017**, *218*, 1–8.
- (89) Puangsamlee, T.; Miljanić, O. Š. Precipitation-driven self-sorting of imines. *Org. Biomol. Chem.*, 2012, *10*, 4847–4850
- (90) Lirag, R.C.; Osowska, K.; Miljanić, O. Š. Oxidative Kinetic Self-Sorting of a Dynamic Imine Library. *J. Am. Chem. Soc.* **2011**, *133*, 724–727.
- (91) Hsu, C. W.; Miljanić, O. Adsorption-Driven Self-Sorting of Dynamic Imine Libraries. *Angew. Chem. Int. Ed.* **2015**, *54*, 2219–2222.

- (92) Ji, Q.; Lirag, R. C.; Miljanić, O. Š. Kinetically Controlled Phenomena in Dynamic Combinatorial Libraries. *Chem. Soc. Rev.* **2014**, *43*, 1873–1884.
- (93) Ayme, J. F.; Lehn, J. M.; Bailly, C.; Karmazin, L. Simultaneous Generation of a $[2 \times 2]$ Grid-Like Complex and a Linear Double Helicate: A Three-Level Self-Sorting Process. *J. Am. Chem. Soc.* **2020**, *142*, 5819–5824.
- (94) Ayme, J. F.; Lehn, J. M. Self-Sorting of Two Imine-Based Metal Complexes: Balancing Kinetics and Thermodynamics in Constitutional Dynamic Networks. *Chem. Sci.* **2020**, *11*, 1114–1121.
- (95) He, M.; Lehn, J.-M. Time-Dependent Switching of Constitutional Dynamic Libraries and Networks from Kinetic to Thermodynamic Distributions. *J. Am. Chem. Soc.* **2019**, *141*, 18560–18569.
- (96) Ulrich, S.; Lehn, J. M. Adaptation and Optical Signal Generation in a Constitutional Dynamic Network. *Chem. - A Eur. J.* **2009**, *15*, 5640–5645.
- (97) Giuseppone, N.; Schmitt, J. L.; Lehn, J. M. Generation of Dynamic Constitutional Diversity and Driven Evolution in Helical Molecular Strands under Lewis Acid Catalyzed Component Exchange. *Angew. Chem. Int. Ed.* **2004**, *43*, 4902–4906.
- (98) Men, G.; Lehn, J. M. Higher Order Constitutional Dynamic Networks: $[2 \times 3]$ and $[3 \times 3]$ Networks Displaying Multiple, Synergistic and Competitive Hierarchical Adaptation. *J. Am. Chem. Soc.* **2017**, *139*, 2474–2483.
- (99) Ayme, J. F.; Dhers, S.; Lehn, J. M. Triple Self-Sorting in Constitutional Dynamic Networks: Parallel Generation of Imine-Based CuI, FeII, and ZnII Complexes. *Angew. Chem. Int. Ed.* **2020**, *59*, 12484–12492.
- (100) Armao, J. J.; Lehn, J. M. Nonlinear Kinetic Behavior in Constitutional Dynamic Reaction Networks. *J. Am. Chem. Soc.* **2016**, *138*, 16809–16814.
- (101) Kulchat, S.; Chaur, M. N.; Lehn, J. M. Kinetic Selectivity and Thermodynamic Features of Competitive Imine Formation in Dynamic Covalent Chemistry. *Chem. - A Eur. J.* **2017**, *23*, 11108–11118.
- (102) Nitschke, J. R.; Lehn, J.-M. Self-Organization by Selection: Generation of a Metallosupramolecular Grid Architecture by Selection of Components in a Dynamic Library of Ligands. *Proc. Natl. Acad. Sci.* **2003**, *100*, 11970–11974.
- (103) Vantomme, G.; Hafezi, N.; Lehn, J. M. A Light-Induced Reversible Phase Separation and Its Coupling to a Dynamic Library of Imines. *Chem. Sci.* **2014**, *5*, 1475–1483.
- (104) Ingerman, L. A.; Waters, M. L. Photoswitchable Dynamic Combinatorial Libraries: Coupling Azobenzene Photoisomerization with Hydrazone Exchange. *J. Org. Chem.* **2009**, *74*, 111–117.
- (105) Wurtz, A. Aldehyd-Alkohol. 457. *J. für Prakt. Chemie* **1872**, *5*, 457–464.
- (106) Perrin, C. L.; Chang, K. L. The Complete Mechanism of an Aldol Condensation. *J. Org. Chem.* **2016**, *81*, 5631–5635.
- (107) Martínez-Castañeda, Á.; Rodríguez-Solla, H.; Concellón, C.; Del Amo, V. TBD/Al₂O₃: A Novel Catalytic System for Dynamic Intermolecular Aldol Reactions That Exhibit Complex System Behaviour. *Org. Biomol. Chem.* **2012**, *10*, 1976–1981.
- (108) Diels, O.; Alder, K. Synthesen in Der Hydroaromatischen Reihe, V. Mitteilung: Über Δ^4 -Tetrahydro-*o*-Phthalsäure (Stellungnahme Zu Der Mitteilung von E. H. Farmer Und F. L. Warren: Eigenschaften Konjugierter Doppelbindungen (VII) . *Berichte der Dtsch. Chem. Gesellschaft (A B Ser.)* **1929**, *62*, 2087–2090.

- (109) Rickborn, B. The Retro-Diels-Alder Reaction Part I. C=C Dienophiles. *Organic Reactions*. 1998, pp 1–393.
- (110) Reutenauer, P.; Buhler, E.; Boul, P. J.; Candau, S. J.; Lehn, J. M. Room Temperature Dynamic Polymers Based on Diels-Alder Chemistry. *Chem. - A Eur. J.* **2009**, *15*, 1893–1900.
- (111) Jean-Louis, P.; Hérisson Chauvin, Y. Catalyse de Transformation Des Oligomères Par Les Complexes Du Tungstène. *Die Makromol. Chemie* **1970**, *141*, 161–176.
- (112) Otera, J. Transesterification. **1993**.
- (113) Brachvogel, R. C.; Von Delius, M. Orthoester Exchange: A Tripodal Tool for Dynamic Covalent and Systems Chemistry. *Chem. Sci.* **2015**, *6*, 1399–1403.
- (114) Garcia, J. S.; Harbison, R. D. Aldehydes and Ketones. *Hamilt. Hardy's Ind. Toxicol. Sixth Ed.* **2015**, 445–490.
- (115) Ouellette, R. J.; Rawn, J. D. Aldehydes and Ketones: Nucleophilic Addition Reactions. *Org. Chem. Study Guid.* **2015**, 335–360.
- (116) Gregg, B. T.; Golden, K. C.; Quinn, J. F. Indium(III) Trifluoromethanesulfonate as an Efficient Catalyst for the Deprotection of Acetals and Ketals. *J. Org. Chem.* **2007**, *72*, 5890–5893.
- (117) Scheeren, J. W.; Van Melick, J. E. W.; Nivard, R. J. F. The Mechanism of Acetal Formation by Aldehydes or Ketones with Orthoformates. *Anal. Proc.* **1969**, 1175–1176.
- (118) Wedemeyer, W. J.; Welker, E.; Narayan, M.; Scheraga, H. A. Disulfide Bonds and Protein Folding. *Biochemistry* **2000**, *39*, 7032.
- (119) Postma, T. M.; Albericio, F. Disulfide Formation Strategies in Peptide Synthesis. *European J. Org. Chem.* **2014**, *2014*, 3519–3530.
- (120) Witt, D. Recent Developments in Disulfide Bond Formation. *Synthesis (Stuttg.)*. **2008**, No. 16, 2491–2509.
- (121) Mandal, B.; Basu, B. Recent Advances in S-S Bond Formation. *RSC Adv.* **2014**, *4*, 13854–13881.
- (122) Putzu, M.; Gräter, F.; Elstner, M.; Kubař, T. On the Mechanism of Spontaneous Thiol-Disulfide Exchange in Proteins. *Phys. Chem. Chem. Phys.* **2018**, *20*, 16222–16230.
- (123) Alegre-Cebollada, J.; Kosuri, P.; Rivas-Pardo, J. A.; Fernández, J. M. Direct Observation of Disulfide Isomerization in a Single Protein. *Nat. Chem.* **2011**, *3*, 882–887.
- (124) Schiff, H. Mittheilungen Aus Dem Universitätslaboratorium in Pisa: Eine Neue Reihe Organischer Basen. *Justus Liebigs Ann. Chem.* **1864**, *131*, 118–119.
- (125) Donoso, J.; Muñoz, F.; García Del Vado, A.; Echevarría, G.; García Blanco, F. Study of the Hydrolysis and Ionization Constants of Schiff Base from Pyridoxal 5'-Phosphate and n-Hexylamine in Partially Aqueous Solvents. An Application to Phosphorylase B. *Biochem. J.* **1986**, *238*, 137–144.
- (126) Layer, R. W. The Chemistry of Imines. *Chem. Rev.* **1963**, *63*, 489–510.
- (127) Kölmel, D. K.; Kool, E. T. Oximes and Hydrazones in Bioconjugation: Mechanism and Catalysis. *Chem. Rev.* **2017**, *117*, 10358–10376.
- (128) Zhou, Y.; Yuan, Y.; You, L.; Anslyn, E. V. Dynamic Aminal-Based TPA Ligands. *Chem. - A Eur. J.* **2015**, *21*, 8207–8213.
- (129) Kovařiček, P.; Lehn, J. M. Merging Constitutional and Motional Covalent Dynamics in Reversible Imine Formation and Exchange Processes. *J. Am. Chem. Soc.* **2012**, *134*, 9446–9455.

- (130) Kovaříček, P.; Meister, A. C.; Flídrová, K.; Cabot, R.; Kovaříčková, K.; Lehn, J. M. Competition-Driven Selection in Covalent Dynamic Networks and Implementation in Organic Reactional Selectivity. *Chem. Sci.* **2016**, *7*, 3215–3226.
- (131) Giuseppone, N.; Schmitt, J. L.; Schwartz, E.; Lehn, J. M. Scandium(III) Catalysis of Transimination Reactions. Independent and Constitutionally Coupled Reversible Processes. *J. Am. Chem. Soc.* **2005**, *127*, 5528–5539.
- (132) Dirksen, A.; Dirksen, S.; Hackeng, T. M.; Dawson, P. E. Nucleophilic Catalysis of Hydrazone Formation and Transimination: Implications for Dynamic Covalent Chemistry. *J. Am. Chem. Soc.* **2006**, *128*, 15602–15603.
- (133) Ciaccia, M.; Cacciapaglia, R.; Mencarelli, P.; Mandolini, L.; Di Stefano, S. Fast Transimination in Organic Solvents in the Absence of Proton and Metal Catalysts. A Key to Imine Metathesis Catalyzed by Primary Amines under Mild Conditions. *Chem. Sci.* **2013**, *4*, 2253–2261.
- (134) Ciaccia, M.; Di Stefano, S. Mechanisms of Imine Exchange Reactions in Organic Solvents. *Org. Biomol. Chem.* **2015**, *13*, 646–654.
- (135) Aljuhani, M. A.; Barman, S.; Abou-Hamad, E.; Gurinov, A.; Ould-Chikh, S.; Guan, E.; Jedidi, A.; Cavallo, L.; Gates, B. C.; Pelletier, J. D. A.; Basset, J. M. Imine Metathesis Catalyzed by a Silica-Supported Hafnium Imido Complex. *ACS Catal.* **2018**, *8*, 9440–9446.
- (136) Cantrell, G. K.; Meyer, T. Y. Transition-Metal-Catalyzed Imine Metathesis. *Organometallics* **1997**, *16*, 5381–5383.
- (137) Wilhelms, N.; Kulchat, S.; Lehn, J. M. Organocatalysis of C=C/C=C and C=C/C=N Exchange in Dynamic Covalent Chemistry. *Helv. Chim. Acta* **2012**, *95*, 2635–2651.
- (138) Kulchat, S.; Meguellati, K.; Lehn, J. M. Organocatalyzed and Uncatalyzed C=C/C=C and C=C/C=N Exchange Processes between Knoevenagel and Imine Compounds in Dynamic Covalent Chemistry. *Helv. Chim. Acta* **2014**, *97*, 1219–1236.
- (139) Liang, C.; Kulchat, S.; Jiang, S.; Lehn, J. M. Gelation-Driven Selection in Dynamic Covalent C=C/C=N Exchange. *Chem. Sci.* **2017**, *8*, 6822–6828.
- (140) Gu, R.; Flidrova, K.; Lehn, J. M. Dynamic Covalent Metathesis in the C=C/C=N Exchange between Knoevenagel Compounds and Imines. *J. Am. Chem. Soc.* **2018**, *140*, 5560–5568.
- (141) Su, X.; Aprahamian, I. Hydrazone-Based Switches, Metallo-Assemblies and Sensors. *Chem. Soc. Rev.* **2014**, *43*, 1963.
- (142) Gasparini, G.; Dal Molin, M.; Lovato, A. Prins, L. J. Dynamic Covalent Chemistry, *Supramolecular Chemistry: From Molecules to Nanomaterials*, Online 2012 John Wiley & Sons, Ltd.
- (143) Kalia, J.; Raines, R. T. Hydrolytic Stability of Hydrazones and Oximes. *Angew. Chem. Int. Ed.* **2008**, *47*, 7523–7526.
- (144) Abid, O. H.; Ramadan, A. K. Preparation and Identification of Novel 1, 3-Oxazepine Derivatives by Cycloaddition Reactions [2 + 5] of Selected Carboxylic Acid Anhydrides with Imines Derived from 4-Methyl Aniline. *Al-Mustansiriyah J. Sci.* **2018**, *29*, 93.
- (145) Taguchi, K.; Westheimer, F. H. Catalysis by Molecular Sieves in the Preparation of Ketimines and Enamines¹. *J. Org. Chem.* **1971**, *36*, 1570–1572.

- (146) Naeimi, H.; Salimi, F.; Rabiei, K. Mild and Convenient One Pot Synthesis of Schiff Bases in the Presence of P_2O_5 / Al_2O_3 as New Catalyst under Solvent-Free Conditions. *J. Mol. Catal. A Chem.* **2006**, *260*, 100–104.
- (147) Hosseini-sarvari, M. Nano-Tube TiO_2 as a New Catalyst for Eco-Friendly Synthesis of Imines in Sunlight. *Chinese Chem. Lett.* **2011**, *22*, 547–550.
- (148) Ravishankar, L.; Patwe, S. A.; Gosarani, N.; Roy, A. Cerium(III)-Catalyzed Synthesis of Schiff Bases: A Green Approach. *Synth. Commun.* **2010**, *40*, 3177–3180.
- (149) Dalpozzo, R.; De Nino, A.; Nardi, M.; Russo, B.; Procopio, A. Erbium(III) Triflate: A Valuable Catalyst for the Synthesis of Aldimines, Ketimines, and Enaminones. *Synthesis (Stuttg.)* **2006**, No. 7, 1127–1132.
- (150) Chakraborti, A. K.; Bhagat, S.; Rudrawar, S. Magnesium Perchlorate as an Efficient Catalyst for the Synthesis of Imines and Phenylhydrazones. *Tetrahedron Lett.* **2004**, *45*, 7641–7644.
- (151) Liu, G.; Cogan, D. A.; Owens, T. D.; Tang, T. P.; Ellman, J. A. Synthesis of Enantiomerically Pure N-Tert-Butanesulfinyl Imines (Tert- Butanesulfinimines) by the Direct Condensation of Tert-Butanesulfinamide with Aldehydes and Ketones. *J. Org. Chem.* **1999**, *64*, 1278–1284.
- (152) Look, G. C.; Murphy, M. M.; Campbell, D. A.; Gallop, M. A. Trimethylorthoformate: A Mild and Effective Dehydrating Reagent for Solution and Solid Phase Imine Formation. *Tetrahedron Lett.* **1995**, *36*, 2937–2940.
- (153) Hine, J.; Cholod, M. S.; Chess, W. K. Kinetics of the Formation of Imines from Acetone and Primary Amines. Evidence for Internal Acid-Catalyzed Dehydration of Certain Intermediate Carbinolamines. *J. Am. Chem. Soc.* **1973**, *95*, 4270–4276.
- (154) Metzler, D. E. Equilibria between Pyridoxal and Amino Acids and Their Imines. *J. Am. Chem. Soc.* **1957**, *79*, 485–490.
- (155) Duncan, N. C.; Hay, B. P.; Hagaman, E. W.; Custelcean, R. Thermodynamic, Kinetic, and Structural Factors in the Synthesis of Imine-Linked Dynamic Covalent Frameworks. *Tetrahedron* **2012**, *68*, 53–64.
- (156) Cordes, E. H.; Jencks, W. P. General Acid Catalysis of Semicarbazone Formation. *J. Am. Chem. Soc.* **1962**, *84*, 4319–4328.
- (157) Crisalli, P.; Kool, E. T. Water-Soluble Organocatalysts for Hydrazone and Oxime Formation. *J. Org. Chem.* **2013**, *78*, 1184–1189.
- (158) Dirksen, A.; Dawson, P. E. Rapid Oxime and Hydrazone Ligations with Aromatic Aldehydes for Biomolecular Labeling. *Bioconjug. Chem.* **2008**, *19*, 2543–2548.
- (159) Cordes, E. H.; Jencks, W. P. Nucleophilic Catalysis of Semicarbazone Formation by Anilines. *J. Am. Chem. Soc.* **1962**, *84*, 826–831.
- (160) Morales, S.; Guijarro, F. G.; García Ruano, J. L.; Cid, M. B. A General Aminocatalytic Method for the Synthesis of Aldimines. *J. Am. Chem. Soc.* **2014**, *136*, 1082–1089.
- (161) Morales, S.; Luis, J.; Ruano, G.; Cid, M. B. Sustainable Synthesis of Oximes, Hydrazones, and Thiosemicarbazones under Mild Organocatalyzed Reaction Conditions. *J. Org. Chem.* **2016**, *81*, 10016–10022.
- (162) Larsen, D.; Kietrys, A. M.; Clark, S. A.; Park, H. S.; Ekebergh, A.; Kool, E. T. Exceptionally Rapid Oxime and Hydrazone Formation Promoted by Catalytic Amine Buffers with Low Toxicity. *Chem. Sci.* **2018**, *9*, 5252–5259.

- (163) Willi, A. Effect of Substitution on the Acidity Constants of Benzenesulfonamides. *Helv. Chim. Acta.* **1955**, *39*, 46–53.
- (164) Kastening, B.; Holleck, L.; Melkonian, G. A.; *Z. Elektrochem.* **1956**, *60*, 130.
- (165) Jencks, W. P. Studies on the Mechanism of Oxime and Semicarbazone Formation. *J. Am. Chem. Soc.* **1959**, *81*, 475–481.
- (166) Anderson, B. M.; Jencks, W. P. The Effect of Structure on Reactivity in Semicarbazone Formation. *J. Am. Chem. Soc.* **1960**, *82*, 1773–1777.
- (167) Dirksen, A.; Hackeng, T. M.; Dawson, P. E. Nucleophilic Catalysis of Oxime Ligation. *Angew. Chem. Int. Ed.* **2006**, *45*, 7581–7584.
- (168) Crisalli, P.; Kool, E. T. Importance of Ortho Proton Donors in Catalysis of Hydrazone Formation. *Org. Lett.* **2013**, *15*, 1646–1649.
- (169) Larsen, D.; Pittelkow, M.; Karmakar, S.; Kool, E. T. New Organocatalyst Scaffolds with High Activity in Promoting Hydrazone and Oxime Formation at Neutral pH. *Org. Lett.* **2015**, *17*, 274–277.
- (170) Kool, E. T.; Crisalli, P.; Chan, K. M. Fast Alpha Nucleophiles: Structures That Undergo Rapid Hydrazone/Oxime Formation at Neutral PH. *Org. Lett.* **2014**, *16*, 1454–1457.
- (171) Kool, L.; Dekker, F.; Bunschoten, A.; Smales, G. J.; Pauw, B. R.; Velders, A. H.; Saggiomo, V. Gold and Silver Dichroic Nanocomposite in the Quest for 3D Printing the Lycurgus Cup. *Beilstein J. Nanotechnol.* **2020**, *11*, 16–23.
- (172) Thygesen, M. B.; Munch, H.; Sauer, J.; Cló, E.; Jørgensen, M. R.; Hindsgaul, O.; Jensen, K. J. Nucleophilic Catalysis of Carbohydrate Oxime Formation by Anilines. *J. Org. Chem.* **2010**, *75*, 1752–1755.
- (173) Domaille, D. W.; Cha, J. N. Aniline-Terminated DNA Catalyzes Rapid DNA-Hydrazone Formation at Physiological pH. *Chem. Commun.* **2014**, *50*, 3831–3833.
- (174) Blanden, A. R.; Mukherjee, K.; Dilek, O.; Loew, M.; Bane, S. L. 4-Aminophenylalanine as a Biocompatible Nucleophilic Catalyst for Hydrazone Ligations at Low Temperature and Neutral PH. *Bioconjug. Chem.* **2011**, *22*, 1954–1961.
- (175) Drienovská, I.; Mayer, C.; Dulson, C.; Roelfes, G. A Designer Enzyme for Hydrazone and Oxime Formation Featuring an Unnatural Catalytic Aniline Residue. *Nat. Chem.* **2018**, *10*, 946–952.
- (176) Wendeler, M.; Grinberg, L.; Wang, X.; Dawson, P. E.; Baca, M. Enhanced Catalysis of Oxime-Based Bioconjugations by Substituted Anilines. *Bioconjug. Chem.* **2014**, *25*, 93–101.
- (177) Blanden, A. R.; Mukherjee, K.; Dilek, O.; Loew, M.; Bane, S. L. 4-Aminophenylalanine as a Biocompatible Nucleophilic Catalyst for Hydrazone Ligations at Low Temperature and Neutral PH. *Bioconjug. Chem.* **2011**, *22*, 1954–1961.
- (178) Trausel, F.; Fan, B.; van Rossum, S. A. P.; van Esch, J. H.; Eelkema, R. Aniline Catalysed Hydrazone Formation Reactions Show a Large Variation in Reaction Rates and Catalytic Effects. *Adv. Synth. Catal.* **2018**, *360*, 2571–2576.
- (179) Yuen, L. H.; Saxena, N. S.; Park, H. S.; Weinberg, K.; Kool, E. T. Dark Hydrazone Fluorescence Labeling Agents Enable Imaging of Cellular Aldehydic Load. *ACS Chem. Biol.* **2016**, *11*, 2312–2319.
- (180) Rashidian, M.; Mahmoodi, M. M.; Shah, R.; Dozier, J. K.; Wagner, C. R.; Distefano, M. D. A Highly Efficient Catalyst for Oxime Ligation and Hydrazone-Oxime Exchange Suitable for Bioconjugation. *Bioconjug. Chem.* **2013**, *24*, 333–342.

- (181) Wendeler, M.; Grinberg, L.; Wang, X.; Dawson, P. E.; Baca, M. Enhanced Catalysis of Oxime-Based Bioconjugations by Substituted Anilines. *Bioconjug. Chem.* **2014**, *25*, 93–101.
- (182) Crisalli, P.; Kool, E. T. Importance of Ortho Proton Donors in Catalysis of Hydrazone Formation. *Org. Lett.* **2013**, *15*, 1646–1649.
- (183) Larsen, D.; Kietrys, A. M.; Clark, S. A.; Park, H. S.; Ekebergh, A.; Kool, E. T. Exceptionally Rapid Oxime and Hydrazone Formation Promoted by Catalytic Amine Buffers with Low Toxicity. *Chem. Sci.* **2018**, *9*, 5252–5259.
- (184) Morales, S.; Aceña, J. L.; García Ruano, J. L.; Cid, M. B. Sustainable Synthesis of Oximes, Hydrazones, and Thiosemicarbazones under Mild Organocatalyzed Reaction Conditions. *J. Org. Chem.* **2016**, *81*, 10016–10022.
- (185) Armao, J. J.; Lehn, J. M. Nonlinear Kinetic Behavior in Constitutional Dynamic Reaction Networks. *J. Am. Chem. Soc.* **2016**, *138*, 16809–16814.
- (186) Schaufelberger, F.; Hu, L.; Ramström, O. Trans-Symmetric Dynamic Covalent Systems: Connected Transamination and Transimination Reactions. *Chem. - A Eur. J.* **2015**, *21*, 9776–9783.
- (187) Ciaccia, M.; Pilati, S.; Cacciapaglia, R.; Mandolini, L.; Di Stefano, S. Effective Catalysis of Imine Metathesis by Means of Fast Transiminations between Aromatic-Aromatic or Aromatic-Aliphatic Amines. *Org. Biomol. Chem.* **2014**, *12*, 3282–3287.
- (188) koehler, k.; sandstrom, W.; cordes, E. H. Concerning the Mechanism of the Hydrolysis and Aminolysis of Schiff Bases. *J. Am. Chem. Soc.* **1964**, *86*, 2413–2419.
- (189) Hogg, J. L.; Jencks, D. A.; Jencks, W. P. Catalysis of Transimination Through Trapping by Acids and Bases. *J. Am. Chem. Soc.* **1977**, *99*, 4772–4778.
- (190) Fischer, H.; DeCandis, F. X.; Ogden, S. D.; Jencks, W. P. Catalysis of Transimination by Rate-Limiting Proton Transfer to Buffer Bases. *J. Am. Chem. Soc.* **1980**, *102*, 1340–1347.
- (191) Boate, A. R.; Eaton, D. R. The Metal Complex Catalyzed Reactions of Anils. I. The Reaction of Acetone with Anilines. *Can. J. Chem.* **1976**, *54*, 3895–3908.
- (192) Chen, C. W.; Tseng, M. C.; Hsiao, S. K.; Chen, W. H.; Chu, Y. H. Transimination Reactions in [b-3C-Im][NTf₂] Ionic Liquid. *Org. Biomol. Chem.* **2011**, *9*, 4188–4193.
- (193) Ingold, C. K.; Piggot, H. A. The additive formation of four-membered rings. Part II. The conditions which confer stability on the dimethinediazidines *J. Chem. Soc. Trans.* **1923**, *123*, 2745–2752.
- (194) Sugawara, E.; Nikaido, H. Properties of AdeABC and AdeIJK Efflux Systems of *Acinetobacter Baumannii* Compared with Those of the AcrAB-TolC System of *Escherichia Coli*. *Antimicrob. Agents Chemother.* **2014**, *58*, 7250–7257.
- (195) Tóth, G.; Pintér, I.; Messmer, A. Mechanism of the Exchmge Reaction of Aromatic Schiff Bases. *Tetrahedron Lett.* **1974**, *15*, 735–738.
- (196) Kovaříček, P. (2014) Motional, Reactional and Constitutional Dynamics of Imines. [University of Strasbourg]
- (197) Zuckerman, R. L.; Krska, S. W.; Bergman, R. G. Zirconium-Mediated Metathesis of Imines: A Study of the Scope, Longevity, and Mechanism of a Complicated Catalytic System, *J. Am. Chem. Soc.* **2000**, *122*, 751–761.

- (198) Schrock, R. R.; Murdzek, J. S.; Bazan, G. C.; Robbins, J.; Dimare, M.; Regan, M. O. Synthesis of Molybdenum Imido Alkylidene Complexes and Some Reactions Involving Acyclic Olefins. *J. Am. Chem. Soc.* **1990**, *112*, 3875–3886.
- (199) Jencks, W. P. Mechanism and Catalysis of Simple Carbonyl Group Reactions. *Prog. Phys. Org. Chem.* **2007**, *2*, 63–128.
- (200) Bhat, V. T.; Caniard, A. M.; Luksch, T.; Brenk, R.; Campopiano, D. J.; Greaney, M. F. Nucleophilic Catalysis of Acylhydrazone Equilibration for Protein-Directed Dynamic Covalent Chemistry. *Nat. Chem.* **2010**, *2*, 490–497.
- (201) Thygesen, M. B.; Munch, H.; Sauer, J.; Cló, E.; Jørgensen, M. R.; Hindsgaul, O.; Jensen, K. J. Nucleophilic Catalysis of Carbohydrate Oxime Formation by Anilines. *J. Org. Chem.* **2010**, *75*, 1752–1755.
- (202) Domaille, D. W.; Cha, J. N. Aniline-Terminated DNA Catalyzes Rapid DNA–Hydrazone Formation at Physiological PH. *Chem. Commun.* **2014**, *50*, 3831–3833.
- (203) Temme, O.; Laschat, S. Effect of Molecular Sieves on the Formation and Acid-Catalysed Mono- and Bis-Cyclization of N-Arylimines: Easy Entry to Polycyclic Ring Systems by a Novel Cascade Reaction. *J. Chem. Soc. Perkin Trans. 1* **1995**, *2*, 125.
- (204) Cellosolve, M.; Korczynski, A.; Bischoff, C.; Bardach, B. Reduction of Schiff Bases. Benzhydrylamines and Structurally Related. *J. Org. Chem.* **1958**, *23*, 535–539.
- (205) Jennings, W. B.; Lovely, C. J. An Efficient Method for the Preparation of N-Phosphinoyl and N-Sulphonyl Imines Directly from Aromatic Aldehydes. *Tetrahedron Lett.* **1988**, *29*, 3725–3728.
- (206) Jennings, W. B.; Lovely, C. J. The Titanium Tetrachloride Induced Synthesis of N-Phosphinoylimines and N-Sulphonylimines Directly from Aromatic Aldehydes. *Tetrahedron* **1991**, *47*, 5561–5568.
- (207) White, W. A.; Weingarten, H. A Versatile New Enamine Synthesis. *J. Org. Chem.* **1967**, *32*, 213–214.
- (208) Branchaud, B. P. Studies on the Preparation and Reactions of Tritylsuffenimines. *J. Org. Chem.* **1983**, *48*, 3531–3538.
- (209) Clay Catalyzed Synthesis of Imines and Enamines under Solvent-free Conditions using Microwave Irradiation **1997**, *38*, 2039–2042.
- (210) Bhat, V. T.; Caniard, A. M.; Luksch, T.; Brenk, R.; Campopiano, D. J.; Greaney, M. F. Nucleophilic Catalysis of Acylhydrazone Equilibration for Protein-Directed Dynamic Covalent Chemistry. *Nat. Chem.* **2010**, *2*, 490–497.
- (211) Wang, X.; Canary, J. W. Rapid Catalyst-Free Hydrazone Ligation: Protein-Pyridoxal Phosphoramides. *Bioconjugate Chem.* **2012**, *23*, 2329–2334.
- (212) Lindoy, L. F. Metal-Ion Control in the Synthesis of Schiff Base Complexes. *Q. Rev. Chem. Soc.* **1971**, *25*, 379–391.
- (213) Kulchat, S.; Chaur, M. N.; Lehn, J. M. Kinetic Selectivity and Thermodynamic Features of Competitive Imine Formation in Dynamic Covalent Chemistry. *Chem. - Eur. J.* **2017**, *23*, 11108–11118.
- (214) Müller, B.; Vahrenkamp, H. Zinc Complexes of Aldehydes and Ketones, Zinc Complexes of Chelating Aldehydes. *Eur. J. Inorg. Chem.* **1999**, 137–144.
- (215) Hutchinson, D. J.; Cameron, S. A.; Hanton, L. R.; Moratti, S. C. Sensitivity of Silver(I) Complexes of a Pyrimidine-Hydrazone Ligand to Solvent, Counteranion, and Metal-to-Ligand Ratio Changes. *Inorg. Chem.* **2012**, *51*, 5070–5081.

- (216) Njogu, E. M.; Omondi, B.; Nyamori, V. O. Silver(I)-Pyridinyl Schiff Base Complexes: Synthesis, Characterisation and Antimicrobial Studies. *J. Mol. Struct.* **2017**, *1135*, 118–128.
- (217) He, M.; Lehn, J. M. Time-Dependent Switching of Constitutional Dynamic Libraries and Networks from Kinetic to Thermodynamic Distributions. *J. Am. Chem. Soc.* **2019**, *141*, 18560–18569.
- (218) Hamilton, J. M.; Anhorn, M. J.; Oscarson, K. A.; Reibenspies, J. H.; Hancock, R. D. Complexation of Metal Ions, Including Alkali-Earth and Lanthanide(III) Ions, in Aqueous Solution by the Ligand 2,2',6',2''-Terpyridyl. *Inorg. Chem.* **2011**, *50*, 2764–2770.
- (219) Lincoln, S. F. Mechanistic Studies of Metal Aqua Ions: A Semi-Historical Perspective. *Helv. Chim. Acta* **2005**, *88*, 523–545.
- (220) Clegg, J. K.; Harrowfield, J.; Kim, Y.; Lee, Y. H.; Lehn, J. M.; Lim, W. T.; Thuéry, P. Chelation-Controlled Molecular Morphology: Amino to Imine Rearrangements. *Dalt. Trans.* **2012**, *41*, 4335–4357.
- (221) Kölmel, D. K.; Kool, E. T. Oximes and Hydrazones in Bioconjugation: Mechanism and Catalysis. *Chem. Rev.* **2017**, *117*, 10358–10376.
- (222) Capela, M. D.; Mosey, N. J.; Xing, L.; Wang, R.; Petitjean, A. Amine Exchange in Formamidines: An Experimental and Theoretical Study. *Chem. - A Eur. J.* **2011**, *17*, 4598–4612.
- (223) Stadler, A. M. Modulation of the Selectivity of Schiff Base Formation in Mixtures of Two NH₂ Compounds and One Aldehyde or of Two Aldehydes and One Amine. *Isr. J. Chem.* **2013**, *53*, 113–121.
- (224) Larsen, D.; Kietrys, A. M.; Clark, S. A.; Park, H. S.; Ekebergh, A.; Kool, E. T. Exceptionally Rapid Oxime and Hydrazone Formation Promoted by Catalytic Amine Buffers with Low Toxicity. *Chem. Sci.* **2018**, *9*, 5252–5259.
- (225) Dumitru, F.; Legrand, Y. M.; Petit, E.; Van Der Lee, A.; Barboiu, M. Self-Sorting of Metallosupramolecular DCLs via Double-Level Exchange: Amplification in Solution and Solid State Modulation. *Dalt. Trans.* **2012**, *41*, 11860–11865.
- (226) Dhers, S.; Holub, J.; Lehn, J. M. Coevolution and Ratiometric Behaviour in Metal Cation-Driven Dynamic Covalent Systems. *Chem. Sci.* **2017**, *8*, 2125–2130.
- (227) Miller, B. L. *Dynamic Combinatorial Chemistry in Drug Discovery, Bioorganic Chemistry, and Materials Science*; Wiley: Hoboken, NJ, 2010.
- (228) Dirksen, A.; Dirksen, S.; Hackeng, T. M.; Dawson, P. E. Nucleophilic Catalysis of Hydrazone Formation and Transimination: Implications for Dynamic Covalent Chemistry. *J. Am. Chem. Soc.* **2006**, *128*, 15602–15603.
- (229) Stachissini, A. S.; do Amaral, L. Kinetics and Mechanism of Benzaldehyde Girard T Hydrazone Formation. *J. Org. Chem.* **1991**, *56*, 1419–1424.
- (230) Rancan, M.; Tessarolo, J.; Casarin, M.; Zanonato, P. L.; Quici, S.; Armelao, L. Double Level Selection in a Constitutional Dynamic Library of Coordination Driven Supramolecular Polygons. *Inorg. Chem.* **2014**, *53*, 7276–7287.
- (231) Lehn, J. M. Dynamic Combinatorial Chemistry and Virtual Combinatorial Libraries. *Essays Contemp. Chem. From Mol. Struct. Towar. Biol.* **2007**, *9*, 307–326.
- (232) Brisig, B.; Sanders, J. K. M.; Otto, S. Selection and Amplification of a Catalyst from a Dynamic Combinatorial Library. *Angew. Chem. Int. Ed.* **2003**, *42*, 1270–1273.

- (233) Turega, S. M.; Lorenz, C.; Sadownik, J. W.; Philp, D. Target-Driven Selection in a Dynamic Nitron Library. *Chem. Commun.* **2008**, 4076–4078.
- (234) Xu, S.; Giuseppone, N. Self-Duplicating Amplification in a Dynamic Combinatorial Library. *J. Am. Chem. Soc.* **2008**, *130*, 1826–1827.
- (235) Barboiu, M.; Dumitru, F.; Legrand, Y.-M.; Petit, E.; van der Lee, A. Self-Sorting of Equilibrating Metallosupramolecular DCLs via Constitutional Crystallization. *Chem. Commun.* **2009**, No. 16, 2192.
- (236) Barboiu, M. Dynamic Interactive Systems: Dynamic Selection in Hybrid Organic–Inorganic Constitutional Networks. *Chem. Commun.* **2010**, *46*, 7466.
- (237) Miller, B. L. Dynamic Covalent Chemistry: Catalysing Dynamic Libraries. *Nat. Chem.* **2010**, *2*, 433–434.
- (238) Dela Amo, V.; Philp, D. Integrating Replication-Based Selection Strategies in Dynamic Covalent Systems. *Chem. - Eur. J.* **2010**, *16*, 13304–13318.
- (239) Vantomme, G.; Lehn, J.-M. Reversible Adaptation to Photoinduced Shape Switching by Oligomer-Macrocycle Interconversion with Component Selection in a Three-State Constitutional Dynamic System. *Chem. - Eur. J.* **2014**, *20*, 16188–16193.
- (240) Ji, S.; Cao, W.; Yu, Y.; Xu, H. Dynamic Diselenide Bonds: Exchange Reaction Induced by Visible Light without Catalysis. *Angew. Chem. Int. Ed.* **2014**, *53*, 6781–6785.
- (241) Kathan, M.; Kovaříček, P.; Jurissek, C.; Senf, A.; Dallmann, A.; Thünemann, A. F.; Hecht, S. Control of Imine Exchange Kinetics with Photoswitches to Modulate Self-Healing in Polysiloxane Networks by Light Illumination. *Angew. Chem. Int. Ed.* **2016**, *55*, 13882–13886.
- (242) Kassem, S.; Lee, A. T. L.; Leigh, D. A.; Markevicius, A.; Solà, J. Pick-up, Transport and Release of a Molecular Cargo Using a Small-Molecule Robotic Arm. *Nat. Chem.* **2016**, *8*, 138–143.
- (243) Cvrtila, I.; Fanlo-Virgós, H.; Schaeffer, G.; Monreal Santiago, G.; Otto, S. Redox Control over Acyl Hydrazone Photoswitches. *J. Am. Chem. Soc.* **2017**, *139*, 12459–12465.
- (244) Giuseppone, N.; Fuks, G.; Lehn, J. M. Tunable Fluorene-Based Dynamers through Constitutional Dynamic Chemistry. *Chem. - Eur. J.* **2006**, *12*, 1723–1735.
- (245) Zhang, Y.; Barboiu, M. Mechanism Insight into the Constitutional Phase Change Selection of Dynamic Framework Libraries. *ACS Omega* **2018**, *3*, 329–333.
- (246) Klein, J. M.; Saggiomo, V.; Reck, L.; Lüning, U.; Sanders, J. K. M. Dynamic Combinatorial Libraries for the Recognition of Heavy Metal Ions. *Org. Biomol. Chem.* **2012**, *10*, 60–66.
- (247) Tauk, L.; Schröder, A. P.; Decher, G.; Giuseppone, N. Hierarchical Functional Gradients of PH-Responsive Self-Assembled Monolayers Using Dynamic Covalent Chemistry on Surfaces. *Nat. Chem.* **2009**, *1*, 649–656.
- (248) Bracchi, M. E.; Fulton, D. A. Orthogonal Breaking and Forming of Dynamic Covalent Imine and Disulfide Bonds in Aqueous Solution. *Chem. Commun.* **2015**, *51*, 11052–11055.
- (249) Ramström, O.; Lehn, J. M. Drug Discovery by Dynamic Combinatorial Libraries. *Nat. Rev. Drug Discov.* **2002**, *1*, 26–36.
- (250) Mondal, M.; Hirsch, A. K. H. Dynamic Combinatorial Chemistry: A Tool to Facilitate the Identification of Inhibitors for Protein Targets. *Chem. Soc. Rev.* **2015**, *44*, 2455–2488.
- (251) Frei, P.; Hevey, R.; Ernst, B. Dynamic Combinatorial Chemistry: A New Methodology Comes of Age. *Chem. - A Eur. J.* **2019**, *25*, 60–73.

- (252) Schultz, D.; Nitschke, J. R. Kinetic and Thermodynamic Selectivity in Subcomponent Substitution. *Chem. - A Eur. J.* **2007**, *13*, 3660–3665.
- (253) Lao, L. L.; Schmitt, J. L.; Lehn, J. M. Evolution of a Constitutional Dynamic Library Driven by Self-Organisation of a Helically Folded Molecular Strand. *Chem. - A Eur. J.* **2010**, *16*, 4903–4910.
- (254) Orrillo, A. G.; Furlan, R. L. E. Supramolecular Interactions between Library Members Modulate the Behavior of Dynamic Combinatorial Libraries. *J. Org. Chem.* **2010**, *75*, 211–214.
- (255) Simpson, M. G.; Pittelkow, M.; Watson, S. P.; Sanders, J. K. M. Dynamic Combinatorial Chemistry with Hydrazones: Libraries Incorporating Heterocyclic and Steroidal Motifs. *Org. Biomol. Chem.* **2010**, *8*, 1181–1187.
- (256) Solà, J.; Lafuente, M.; Atcher, J.; Alfonso, I. Constitutional Self-Selection from Dynamic Combinatorial Libraries in Aqueous Solution through Supramolecular Interactions. *Chem. Commun.* **2014**, *50*, 4564–4566.
- (257) Schaufelberger, F.; Ramström, O. Kinetic Self-Sorting of Dynamic Covalent Catalysts with Systemic Feedback Regulation. *J. Am. Chem. Soc.* **2016**, *138*, 7836–7839.
- (258) Dhers, S.; Holub, J.; Lehn, J.-M. Coevolution and Ratiometric Behaviour in Metal Cation-Driven Dynamic Covalent Systems. *Chem. Sci.* **2017**, *8*, 2125–2130.
- (259) Polyakov, V. A.; Nelen, M. I.; Nazarpak-Kandlousy, N.; Ryabov, A. D.; Eliseev, A. V. Imine Exchange in O-Aryl and O-Alkyl Oximes as a Base Reaction for Aqueous “dynamic” Combinatorial Libraries. A Kinetic and Thermodynamic Study. *J. Phys. Org. Chem.* **1999**, *12*, 357–363.
- (260) Wendeler, M.; Grinberg, L.; Wang, X.; Dawson, P. E.; Baca, M. Enhanced Catalysis of Oxime-Based Bioconjugations by Substituted Anilines. *Bioconjug. Chem.* **2014**, *25*, 93–101.
- (261) Wang, S.; Gurav, D.; Oommen, O. P.; Varghese, O. P. Insights into the Mechanism and Catalysis of Oxime Coupling Chemistry at Physiological PH. *Chem. - A Eur. J.* **2015**, *21*, 5980–5985.
- (262) Schmidt, P.; Stress, C.; Gillingham, D. Boronic Acids Facilitate Rapid Oxime Condensations at Neutral pH. *Chem. Sci.* **2015**, *6*, 3329–3333.
- (263) Agten, S. M.; Suylen, D. P. L.; Hackeng, T. M. Oxime Catalysis by Freezing. *Bioconjug. Chem.* **2016**, *27*, 42–46.
- (264) Kool, E. T.; Park, D. H.; Crisalli, P. Fast Hydrazone Reactants: Electronic and Acid/Base Effects Strongly Influence Rate at Biological PH. *J. Am. Chem. Soc.* **2013**, *135*, 17663–17666.
- (265) Su, X.; Aprahamian, I. Hydrazone-Based Switches, Metallo-Assemblies and Sensors. *Chem. Soc. Rev.* **2014**, *43*, 1963–1981.
- (266) Su, X.; Aprahamian, I. Zinc(II)-Regulation of Hydrazone Switch Isomerization Kinetics. *Org. Lett.* **2013**, *15*, 5952–5955.
- (267) Van Dijken, D. J.; Kovaříček, P.; Ihrig, S. P.; Hecht, S. Acylhydrazones as Widely Tunable Photoswitches. *J. Am. Chem. Soc.* **2015**, *137*, 14982–14991.
- (268) Gordillo Varela, M. A.; Zuluaga, F.; Chaur Valencia, M. N. Acylhydrazone-Based Dynamic Combinatorial Libraries: Study of the Thermodynamic/Kinetic Evolution, Configurational and Coordination Dynamics. *Rev. Colomb. Química* **2017**, *45*, 39.
- (269) Cordes, E. H.; Jencks, W. P. On the Mechanism of Schiff Base Formation and Hydrolysis. *J. Am. Chem. Soc.* **1962**, *84*, 832–837.

- (270) Vázquez, M. A.; Echevarría, G.; Muñoz, F.; Donoso, J.; Blanco, F. G. Kinetic Study of the Schiff-Base Formation between Glycine and Pyridoxal 5'-Phosphate (PLP), Pyridoxal (PL), and 5'-Deoxypyridoxal (DPL). *J. Chem. Soc. Perkin Trans. 2* **1989**, *11*, 1617–1622.
- (271) Echevarría Gorostidi, G. R.; Basagoitia, A.; Santos Blanco, J. G.; Blanco, F. G. Kinetic Study of the Reaction of Pyridoxal 5'-Phosphate with Hydrazine. *J. Mol. Catal. A Chem.* **1998**, *129*, 173–177.
- (272) Piszkiwicz, D.; Smith, E. L. Bovine Liver Glutamate Dehydrogenase. Equilibria and Kinetics of Imine Formation by Lysine-97 with Pyridoxal 5'-Phosphate. *Biochemistry* **1971**, *10*, 4544–4552.
- (273) Vázquez, M. A.; Muñoz, F.; Donoso, J.; Blanco, F. G. Schiff Bases between Pyridoxal 5'-phosphate and Dodecylamine. Kinetic Study. *Int. J. Chem. Kinet.* **1992**, *24*, 67–78.
- (274) Echevarría-Gorostidi, G. R.; Basagoitia, A.; Pizarro, E.; Goldsmid, R.; Santos Blanco, J. G.; Blanco, F. G. Kinetic Study of the Reaction of Pyridoxal 5'-Phosphate with Hydrazino Compounds of Pharmacological Activity. *Helv. Chim. Acta* **1998**, *81*, 837–844.
- (275) Kirdant, A. S.; Shankarwar, S. G.; Chondhekar, T. K. Kinetic Study and Mechanism of Hydrolysis of N-Salicylidene-m-Chloroaniline. *Int. J. Chem. Sci.* **2010**, *8*, 279–289.
- (276) Wolfenden, R.; Jencks, W. P. The Effect of O-Substituents on Benzaldehyde Semicarbazone Formation. *J. Am. Chem. Soc.* **1961**, *83*, 2763–2768.
- (277) Xu, Y.; Xu, L.; Xia, Y.; Guan, C. J.; Guo, Q. X.; Fu, Y.; Wang, C.; Li, Y. M. Fast and Catalyst-Free Hydrazone Ligation via Ortho-Halo-Substituted Benzaldehydes for Protein C-Terminal Labeling at Neutral pH. *Chem. Commun.* **2015**, *51*, 13189–13192.
- (278) Dilek, O.; Sorrentino, A. M.; Bane, S. Intramolecular Catalysis of Hydrazone Formation of Aryl-Aldehydes via Ortho -Phosphate Proton Exchange. *Synlett* **2016**, *27*, 1335–1338.
- (279) Schmidt, P.; Zhou, L.; Tishinov, K.; Zimmermann, K.; Gillingham, D. Dialdehydes Lead to Exceptionally Fast Bioconjugations at Neutral PH by Virtue of a Cyclic Intermediate. *Angew. Chem. Int. Ed.* **2014**, *53*, 10928–10931.
- (280) Lee, S. H.; Kyung, H.; Yokota, R.; Goto, T.; Oe, T. N-Terminal α -Ketoamide Peptides: Formation and Transamination. *Chem. Res. Toxicol.* **2014**, *27*, 637–648.
- (281) Evangelopoulos, A. E.; Sizer, I. W. Pig Heart Glutamic Aspartic Transaminase Mechanism of Transamination. *Proc. Natl. Acad. Sci.* **1963**, *49*, 638–643.
- (282) Metzler, D. E.; Olivard, J.; Snell, E. E. Transamination of Pyridoxamine and Amino Acids with Glyoxylic Acid. *J. Am. Chem. Soc.* **1954**, *76*, 644–648.
- (283) Abdiseed, F. A.; El-ajaily, M. M. Preparation and Spectroscopic Investigation of a Schiff Base Metal Complexes. *Int. J. PharmTech Res.* **2009**, *1*, 1097–1103.
- (284) Metzler, D. E. Equilibria between Pyridoxal and Amino Acids and Their Imines. *J. Am. Chem. Soc.* **1957**, *79*, 485–490.
- (285) Metzler, D. E.; Ikawa, M.; Snell, E. E. A General Mechanism for Vitamin B6-Catalyzed Reactions. *J. Am. Chem. Soc.* **1954**, *76*, 648–652.
- (286) Chan-Huot, M.; Sharif, S.; Tolstoy, P. M.; Toney, M. D.; Limbach, H. H. NMR Studies of the Stability, Protonation States, and Tautomerism of ¹³C- and ¹⁵N-Labeled Aldimines of the Coenzyme Pyridoxal 5'-Phosphate in Water. *Biochemistry* **2010**, *49*, 10818–10830.

- (287) Toth, K.; Amyes, T. L.; Richard, J. P.; Malthouse, J. P. G.; NiBeilliú, M. E. Claisen-Type Addition of Glycine to Pyridoxal in Water. *J. Am. Chem. Soc.* **2004**, *126*, 10538–10539.
- (288) Robitaille, P. M.; Scott, R. D.; Wang, J.; Metzler, D. E. Schiff Bases and Geminal Diamines Derived from Pyridoxal 5'-Phosphate and Diamines. *J. Am. Chem. Soc.* **1989**, *111*, 3034–3040.
- (289) Blázquez, M.; Pineda, T.; Sevilla, J. M.; Domínguez, M.; García-Blanco, F. The Schiff Base between Pyridoxal-5'-phosphate (PLP) and Hexylamine. Formation of the Unprotonated Form of the Imine by Reaction of the Unprotonated PLP and Free Amine. *J. Phys. Org. Chem.* **1991**, *4*, 372–380.
- (290) Vazquez, M. A.; Munoz, F.; Donoso, J.; Garcia Blanco, F. Spectroscopic Study of the Schiff Bases of Dodecylamine with Pyridoxal 5'-Phosphate and 5'-Deoxypyridoxal. A Model for the Schiff Bases of Pyridoxal 5'-Phosphate in Biological Systems. *Biochem. J.* **1991**, *279*, 759–767.
- (291) Matsuo, Y. Formation of Schiff Bases of Pyridoxal Phosphate. Reaction with Metal Ions. *J. Am. Chem. Soc.* **1957**, *79*, 2011–2015.
- (292) Vázquez, M. A.; Muñoz, F.; Donoso, J.; Blanco, F. G. Amino Acid Catalytic Effect on the Transamination Reaction between Pyridoxal 5'-Phosphate and L-Serine. *J. Mol. Catal.* **1991**, *68*, 105–122.
- (293) del Vado, M. A. G.; Echevarría, G. R.; Blanco, J. G. S.; García Blanco, F. Determination of the Rates of Formation and Hydrolysis of the Schiff Bases Formed by Pyridoxal 5'-Phosphate and Copolypeptides Containing l-Lysine. *J. Mol. Catal.* **1993**, *78*, 379–387.
- (294) Vázquez, M. A.; Echevarría, G.; Muñoz, F.; Donoso, J.; Blanco, F. G. Kinetic Study of the Schiff-Base Formation between Glycine and Pyridoxal 5'-Phosphate (PLP), Pyridoxal (PL), and 5'-Deoxypyridoxal (DPL). *J. Chem. Soc. Perkin Trans. 2* **1989**, *11*, 1617–1622.
- (295) Chan-Huot, M.; Niether, C.; Sharif, S.; Tolstoy, P. M.; Toney, M. D.; Limbach, H. H. NMR Studies of the Protonation States of Pyridoxal-5'-Phosphate in Water. *J. Mol. Struct.* **2010**, *976*, 282–289.
- (296) Sharif, S.; Denisov, G. S.; Toney, M. D.; Limbach, H. H. NMR Studies of Coupled Low- and High-Barrier Hydrogen Bonds in Pyridoxal-5'-Phosphate Model Systems in Polar Solution. *J. Am. Chem. Soc.* **2007**, *129*, 6313–6327.
- (297) Limbach, H. H.; Chan-Huot, M.; Sharif, S.; Tolstoy, P. M.; Shenderovich, I. G.; Denisov, G. S.; Toney, M. D. Critical Hydrogen Bonds and Protonation States of Pyridoxal 5'-Phosphate Revealed by NMR. *Biochim. Biophys. Acta - Proteins Proteomics* **2011**, *1814*, 1426–1437.
- (298) Chan-Huot, M.; Dos, A.; Zander, R.; Sharif, S.; Tolstoy, P. M.; Compton, S.; Fogle, E.; Toney, M. D.; Shenderovich, I.; Denisov, G. S.; Limbach, H. H. NMR Studies of Protonation and Hydrogen Bond States of Internal Aldimines of Pyridoxal 5'-Phosphate Acid-Base in Alanine Racemase, Aspartate Aminotransferase, and Poly- l-Lysine. *J. Am. Chem. Soc.* **2013**, *135*, 18160–18175.
- (299) Wiesinger, H.; Hinz, H. J. Kinetic and Thermodynamic Parameters for Schiff Base Formation of Vitamin B6 Derivatives with Amino Acids. *Arch. Biochem. Biophys.* **1984**, *235*, 34–40.
- (300) Griswold, W. R.; Toney, M. D. Role of the Pyridine Nitrogen in Pyridoxal 5'-Phosphate Catalysis: Activity of Three Classes of PLP Enzymes Reconstituted with Deazapyridoxal 5'-Phosphate. *J. Am. Chem. Soc.* **2011**, *133*, 14823–14830.
- (301) Micellar Effects on Kinetics and Equilibrium of Synthesis and Hydrolysis of Benzylideneaniline: A General Kinetic Conception of Micellar Catalysis. *Tetrahedron* **1973**, *29*, 963–969.

- (302) Godoy-Alcántar, C.; Yatsimirsky, A. K.; Lehn, J. M. Structure-Stability Correlations for Imine Formation in Aqueous Solution. *J. Phys. Org. Chem.* **2005**, *18*, 979–985.
- (303) Fuentes-Martínez, Y.; Godoy-Alcántar, C.; Medrano, F.; Dikiy, A. Kanamycin A: Imine Formation in Aqueous Solution. *J. Phys. Org. Chem.* **2012**, *25*, 1395–1403.
- (304) Meguellati, K.; Fallah-araghi, A.; Baret, J.; Harrak, E. Enhanced Imine Synthesis in Water: From Surfactant-Mediated Catalysis to Host–Guest Mechanisms. *Chem. Commun.* **2013**, 11332–11334.
- (305) Burlingame, R. W.; Love, W. E.; Wang, B. C.; Hamlin, R.; Xuong, N. H.; Moudrianakis, E. N. Crystallographic Structure of the Octameric Histone Core of the Nucleosome at a Resolution of 3.3 Å. *Science* **1985**, *228*, 546–553.
- (306) Luger, K.; Mäder, A. W.; Richmond, R. K.; Sargent, D. F.; Richmond, T. J. Crystal Structure of the Nucleosome Core Particle at 2.8 Å Resolution. *Nature* **1997**, *389*, 251–260.
- (307) Allfrey, V. G.; Faulkner, R.; Mirsky, A. E. Acetylation and Methylation of Histones and Their Possible Role in The. *Proc. Natl. Acad. Sci.* **1964**, *51*, 786–794.
- (308) Vidali, G.; Gershey, E. L.; Allfrey, V. G. Chemical Studies of Histones Acetylation The Distribution of ε-N-Acetyllysine in Calf Thymus Histones. *J. Biol. Chem.* **1968**, *243*, 6361–6366.
- (309) Caldés, C.; Vilanova, B.; Adrover, M.; Donoso, J.; Muñoz, F. The Hydrophobic Substituent in Aminophospholipids Affects the Formation Kinetics of Their Schiff Bases. *Bioorganic Med. Chem. Lett.* **2013**, *23*, 2202–2206.
- (310) Foster, W.; Miyazawa, K.; Fukuma, T.; Kusumaatmaja, H.; Voitchovsky, K. Self-Assembly of Small Molecules at Hydrophobic Interfaces Using Group Effect. *Nanoscale* **2020**, *12*, 5452–5463.
- (311) Pictet, A.; Spengler, T. Über Die Bildung von Isochinolin-derivaten Durch Einwirkung von Methylal Auf Phenyl-äthylamin, Phenyl-alanin Und Tyrosin. *Berichte der Dtsch. Chem. Gesellschaft* **1911**, *44*, 2030–2036.

PUBLICATIONS AND CONFERENCES

Publications

1. Meixia He, Jean-Marie Lehn*. Time-dependent switching of constitutional dynamic libraries and networks from kinetic to thermodynamic distributions. *J. Am. Chem. Soc.* 2019, *141*, 18560-18569.
2. Meixia He, Jean-Marie Lehn.* Catalysis of imine and hydrazone formation by metal salts and synergistic auxiliary amine effect, in preparation for submission.
3. Meixia He, Jean-Marie Lehn.* The C=N formation as a strategy for regulation of gene expression, manuscript in preparation.

Conferences

Oral Presentation:

1. He M., Lehn J.-M.: Adaptation in constitutional dynamic libraries: time-dependent network switching, Journée des Doctorants, Strasbourg, France, 03/12/2019.
2. He M., Lehn J.-M.: Adaptation in constitutional dynamic libraries, XIV Italian Conference on Supramolecular Chemistry (Supramol2019), Lecce, Italy, 07/06/2019.

Poster Presentation:

1. He M., Lehn J.-M.: Adaptation in constitutional dynamic libraries: time-dependent network switching, 50th General Assembly and 47th IUPAC World Chemistry Congress, Paris, France, 10/07/2019.
2. He M., Lehn J.-M.: Adaptation in constitutional dynamic libraries, 14th International Symposium on Macrocyclic and Supramolecular Chemistry (ISMSC 2019), Lecce, Italy, 03/06/2019.
3. He M., Lehn J.-M.: Adaptation in constitutional dynamic libraries, XIV Italian Conference on Supramolecular Chemistry (Supramol2019), Lecce, Italy, 07/06/2019;
4. He M., Lehn J.-M.: Adaptation in constitutional dynamic libraries, Supralyon 2018, Lyon, France, 13/12/2018.

Meixia HE

DYNAMIC COVALENT PROCESS OF C=N BONDS: KINETICS AND THERMODYNAMICS, CATALYSIS AND OUT-OF-EQUILIBRIUM STATES

Résumé

Dans cette thèse, nous avons exploré la formation de composés C=N: la cinétique et la catalyse de la formation C=N, la commutation en fonction du temps de bibliothèques covalentes dynamiques ainsi que la formation d'imine améliorée en phase aqueuse. Premièrement, la formation d'imine et d'hydrazone a été fortement accélérée en présence de sels métalliques comme catalyseurs. Le fonctionnement simultané de l'amine et des sels métalliques a montré une catalyse synergique sur la formation d'hydrazone. Deuxièmement, les [2 × 2] DCL réalisent un passage en fonction du temps de la distribution cinétique à la distribution thermodynamique en criblant les composants à la fois en l'absence et en présence de deux sels métalliques Ag (I) et Zn (II). Troisièmement, du point de vue thermodynamique, la formation d'imine en phase aqueuse a été grandement améliorée en ajustant différents facteurs pour accélérer et stabiliser les produits d'imine générés.

MOTS-CLÉS : Chimie dynamique constitutionnelle, Chimie covalente dynamique, Bibliothèques covalentes dynamiques, États hors équilibre, Commutation cinétique de DCL

Résumé en anglais

In this thesis, we have explored the formation of C=N compounds: the kinetics and catalysis of C=N formation, the time-dependent switching of dynamic covalent libraries as well as the enhanced imine formation in aqueous phase. First, imine and hydrazone formation were greatly accelerated in the presence of metal salts as catalysts. The simultaneous operation of amine and metal salts displayed a synergistic catalysis on hydrazone formation. Second, the [2 × 2] DCL achieve a time-dependent switching from a kinetic distribution to thermodynamic distribution by screening of the components both in the absence and presence of two metal salts Ag(I) and Zn(II). Thirdly, from the thermodynamic point of view, the imine formation in aqueous phase was greatly enhanced through adjusting different factors to accelerate and stabilize the generated imine products.

KEYWORDS: Constitutional dynamic chemistry, Dynamic covalent chemistry, Dynamic covalent libraries, Out-of-equilibrium states, Kinetic switching of DCLs